frontiers | Research Topics

Innovative strategies for enhancing crop resilience against plant viral diseases, 2nd edition

Edited by
Chellappan Padmanabhan and Fuh-Jyh Jan

Published in
Frontiers in Plant Science

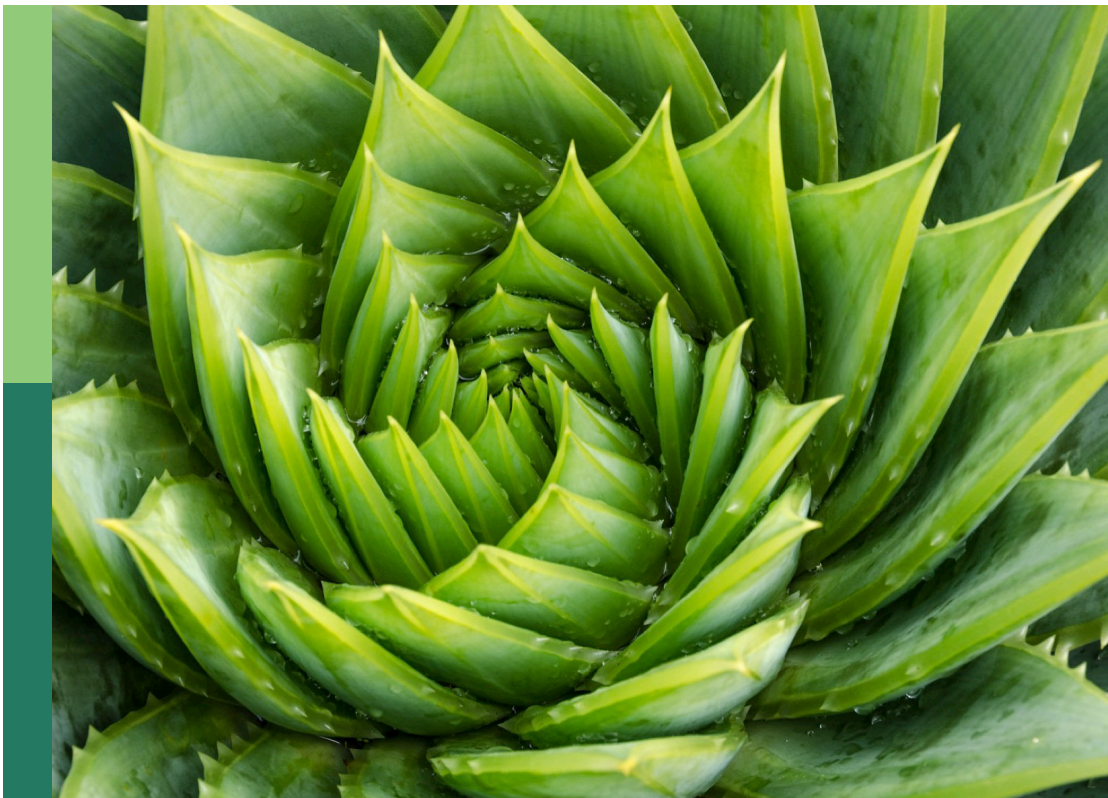

ISSN 1664-8714
ISBN 978-2-8325-6321-2
DOI 10.3389/978-2-8325-6321-2

About Frontiers

Frontiers is more than just an open access publisher of scholarly articles: it is a pioneering approach to the world of academia, radically improving the way scholarly research is managed. The grand vision of Frontiers is a world where all people have an equal opportunity to seek, share and generate knowledge. Frontiers provides immediate and permanent online open access to all its publications, but this alone is not enough to realize our grand goals.

Frontiers journal series

The Frontiers journal series is a multi-tier and interdisciplinary set of open-access, online journals, promising a paradigm shift from the current review, selection and dissemination processes in academic publishing. All Frontiers journals are driven by researchers for researchers; therefore, they constitute a service to the scholarly community. At the same time, the *Frontiers journal series* operates on a revolutionary invention, the tiered publishing system, initially addressing specific communities of scholars, and gradually climbing up to broader public understanding, thus serving the interests of the lay society, too.

Dedication to quality

Each Frontiers article is a landmark of the highest quality, thanks to genuinely collaborative interactions between authors and review editors, who include some of the world's best academicians. Research must be certified by peers before entering a stream of knowledge that may eventually reach the public - and shape society; therefore, Frontiers only applies the most rigorous and unbiased reviews. Frontiers revolutionizes research publishing by freely delivering the most outstanding research, evaluated with no bias from both the academic and social point of view. By applying the most advanced information technologies, Frontiers is catapulting scholarly publishing into a new generation.

What are Frontiers Research Topics?

Frontiers Research Topics are very popular trademarks of the *Frontiers journals series*: they are collections of at least ten articles, all centered on a particular subject. With their unique mix of varied contributions from Original Research to Review Articles, Frontiers Research Topics unify the most influential researchers, the latest key findings and historical advances in a hot research area.

Find out more on how to host your own Frontiers Research Topic or contribute to one as an author by contacting the Frontiers editorial office: frontiersin.org/about/contact

Innovative strategies for enhancing crop resilience against plant viral diseases, 2nd edition

Topic editors

Chellappan Padmanabhan — USDA APHIS PPQ Science and Technology, United States

Fuh-Jyh Jan — National Chung Hsing University, Taiwan

Citation

Padmanabhan, C., Jan, F.-J., eds. (2025). *Innovative strategies for enhancing crop resilience against plant viral diseases, 2nd edition*. Lausanne: Frontiers Media SA. doi: 10.3389/978-2-8325-6321-2

Publisher's note: In this 2nd edition, the following article has been updated:

Padmanabhan C (2025) Editorial: Innovative strategies for enhancing crop resilience against plant viral diseases. Front. Plant Sci. 16:1603589. doi: 10.3389/fpls.2025.1603589

Table of contents

frontiers | Frontiers in Plant Science

TYPE Editorial
PUBLISHED 23 April 2025
DOI 10.3389/fpls.2025.1603589

OPEN ACCESS

EDITED AND REVIEWED BY
Brigitte Mauch-Mani,
Retired, Fribourg, Switzerland

*CORRESPONDENCE
Chellappan Padmanabhan
Chellappan.padmanabhan@usda.gov

RECEIVED 31 March 2025
ACCEPTED 07 April 2025
PUBLISHED 23 April 2025

CITATION
Padmanabhan C (2025) Editorial: Innovative strategies for enhancing crop resilience against plant viral diseases.
Front. Plant Sci. 16:1603589.
doi: 10.3389/fpls.2025.1603589

Editorial: Innovative strategies for enhancing crop resilience against plant viral diseases

Chellappan Padmanabhan*

United States Department of Agriculture, Animal Plant Health Inspection Service, Plant Protection and Quarantine, Science and Technology, Plant Pathogen Confirmatory Diagnostics Laboratory, Laurel, MD, United States

KEYWORDS

artificial intelligence, meta-transcriptomes, virus-pathogenesis, virus-suppressors of silencing, vector transmission, seed pathology, disease resistance

Editorial on the Research Topic
Innovative strategies for enhancing crop resilience against plant viral diseases

This Research Topic covers various subjects related to virus disease detection and translates into plant protection against viruses.

Artificial intelligence

AI for pathogen detection is still in its early stages, and two research articles utilizing the YOLOv4 and PDLM-TK algorithms elegantly described AI-based pathogen detection of plant leaf diseases. To enhance disease prediction systems in agriculture, a large number of images of healthy and diseased leaves of 14 species from the Plant Village dataset were utilized. The YOLOv4 demonstrated high performance with high accuracy on the Plant Village Dataset, including precision, recall, and F1-score. These findings showed that YOLOv4 is an effective tool for accurate disease identification, highlighting significant advances in plant disease detection (Aldakheel et al.). The other article focused on the plant pest and disease lightweight identification model by fusing tensor features and knowledge distillation (PDLM-TK), which represents a further advance in pathogen diagnosis, explicitly addressing the efficiency and accuracy associated with pest and disease identification. This model uses lightweight residual blocks based on spatial tensor (LRB-ST) to obtain enhanced plant image features with a streamlined depth-separable convolution approach with reduced parameter numbers. These results establish PDLM-TK as an alternative to lightweight methods such as MobileViT, providing high efficiency for detecting plant diseases (Zhang et al.).

Meta-transcriptomes

One of the research articles reported on the application of the meta-transcriptome approach for the identification of a virome associated with sugar beets. In addition to detecting known viruses infecting sugar beets, this study identified the spread of the beta

vulgaris satellite virus in new locations, indicating its geographical expansion. In addition, a novel virus, the Erysiphe necator-associated abispo virus, was identified across all libraries and found to originate from different sugar beet growing locations in the United States (Chinnadurai et al.).

Host-susceptibility factors

Understanding the interaction between viral infection and plant cellular mechanisms highlighted the role of the Kunitz peptidase inhibitor-like protein (KPILP) in regulating chloroplast retrograde signaling and facilitating the transport of essential macromolecules during viral infection. Research indicates that viruses such as the Tobacco mosaic virus (TMV) and the crucifer-infecting tobamovirus (crTMV) exploit host factors to enhance their replication and spread by suppressing the plant's defense mechanisms. The results of this study showed reduced levels of KPILP mRNA in systemic infections, indicating its importance for viral survival. The role of the KPILP gene in virus resistance was demonstrated by the fact that the silencing of this gene affected the transport efficiency of both TMV and crTMV. This research provides further strategies for the development of virus control measures for TMV (Ershova et al.).

Virus-pathogenesis

Currently, the *Tomato leaf curl New Delhi virus* (ToLCNDV) is recognized as a significant viral pathogen and poses a threat to tomato, pepper, and cucurbit crops across the world. In this study, coat protein swapping identified a single amino acid in the coat protein coding sequence of ToLCNDV as the pathogenicity factor associated with virus infection in tomato. This research identified a critical molecular factor that can be used for future breeding for resistance against ToLCNDV (Vo et al.).

Virus-suppressors of silencing

The strawberry mottle mosaic virus (SMoV) impacts strawberry productivity. In this article, the authors identified two silencing suppressors, Pro2Glu and P28, from SMoV. Furthermore, Pro2Glu and P28 were found to play a role in increasing the accumulation of potato virus X. This study has implications for formulating strategies to control viral diseases in strawberry and other crops (Fan et al.).

Vector transmission

One of the articles discussed the prevalence and transmission dynamics of the black raspberry necrosis virus (BRNV) and other viruses affecting raspberry in Norway based on three years of data. Infection rates showed that the old raspberry cultivar Veten, including wild raspberry populations, is susceptible to BRNV. Additionally, the known aphid vector, Amphorophora aidaei, is able to acquire the virus within one minute, and transmission can occur within one hour. Understanding the mechanisms behind virus transmission is essential for protecting raspberry crops from these ongoing agricultural threats (Sapkota et al.).

Seed pathology

A study focusing on seed transmission and elimination strategies investigated how viral infections impact the alfalfa (Medicago sativa) industry, specifically targeting six significant viruses: Alfalfa mosaic virus (AMV), Medicago sativa alphapartitivirus1 (MsAPV1), MsAPV2, Medicago sativa deltapartitivirus 1 (MsDPV1), amalgavirus 1(MsAV1), and Cnidium vein yellowing virus 1 (CnVYV1). Virus transmission rates from alfalfa seeds to seedlings were approximately 44% to 88% using PCR assay. The authors tested 16 virus elimination strategies for alfalfa seeds. In conclusion, this research sheds light on critical virus transmission pathways in alfalfa, offers practical methods for managing these diseases, and enhances agricultural productivity (Li et al.).

Disease resistance

Cassava (Manihot esculenta Crantz) is a stable food crop in many countries and has potential as a biodegradable material. In Africa, viral diseases originating from the cassava brown streak virus (CBSV) and the cassava mosaic virus (CMD) challenge cassava production. In this article, quantitative trait loci (QTLs) for CBSD resistance were identified. Two important QTLs on chromosome 4 were linked to resistance against CBSD foliar symptoms, while another QTL on chromosome 11 was linked to root necrosis. The study emphasized key candidate genes, such as phenylalanine ammonia-lyase (PAL) and cinnamoyl-CoA reductase (CCR), which play an essential role in the lignin biosynthesis pathway—critical for plant defense mechanisms against pathogens. This study provides the foundation for breeding strategies to cope with future challenges against viral diseases (Ferguson et al.).

Biocontrol

Biocontrol is important as it is an efficient and safe way to control plant diseases. Pepper veinal mottle virus (PVMV) is a concern for pepper growers. In this study, Bacillus velezensis HN-2, was shown to delay the PVMV infection by its ability colonizing in the intercellular spaces of plants, and induction of the host defense, specifically Jasmonic acid pathway. Accordingly, B. velezensis HN-2 has the potential to provide alternative strategy for virus control (Xuan et al.).

Two review articles focused on virus disease detection and plant protection against viruses. The first article discussed recent advances

in diagnostic technologies and their challenges, in addition to conventional methods such as enzyme-linked immunosorbent assay, polymerase chain reaction and isothermal amplification and biosensor technologies. Sequencing-based diagnostics include next-generation sequencing and portable nanopore sequencing, and CRISPR-Cas assays. These technologies enable faster and more precise detection of plant pathogens (Kanapiya et al.). The other review article focused on plant protection strategies and challenges (Anikina et al.).

In conclusion, all the contributions to this Research Topic highlight the timely translation of plant disease management into major applications.

Author contributions

CP: Writing – original draft, Writing – review & editing.

Acknowledgments

I thank John Bienapfl, Yazmin Rivera, Vessela Mavrodieva, Deshui Zhang, and Catharine Cook for their support. I acknowledge the authors of the studies published in this Research Topic for their valuable contributions and the reviewers for their rigorous reviews. I also thank the editors, editorial board, especially Berna Ustun, for their support.

Conflict of interest

The author declares that the research was conducted in the absence of any commercial or financial relationships that could be construed as a potential conflict of interest.

Generative AI statement

The author(s) declare that no Generative AI was used in the creation of this manuscript.

Publisher's note

frontiers | Frontiers in Plant Science

ORIGINAL RESEARCH
published: 31 May 2022
doi: 10.3389/fpls.2022.786489

Identification of Silencing Suppressor Protein Encoded by Strawberry Mottle Virus

*Lingjiao Fan[1], Chengyong He[1], Dehang Gao[1], Tengfei Xu[1], Fei Xing[2], Jiaqi Yan[1], Binhui Zhan[2], Shifang Li[2] and Hongqing Wang[1]**

[1]*Department of Fruit Science, College of Horticulture, China Agricultural University, Beijing, China,* [2]*State Key Laboratory of Biology of Plant Diseases and Insect Pests, Institute of Plant Protection, Chinese Academy of Agricultural Sciences, Beijing, China*

Strawberry mottle virus (SMoV) is associated with strawberry decline disease, causing losses to fruit yield and quality. In this study, using a screening system that enables detection of both local and systemic plant host (RNA silencing) defense responses, we found that Pro2Glu and P28, encoded by SMoV RNA2 genome, functioned to suppress local and systemic RNA silencing triggered by single- but not double-stranded GFP RNA. Subcellular localization assay revealed that both Pro2Glu and P28 were localized to nucleus and cytoplasm. The deletion of 11 amino acid residues at the C-terminus destabilized Pro2Glu protein, and the disruption of two conserved GW motifs deprived Pro2Glu of ability to suppress RNA silencing. Additionally, SMoV Pro2Glu and P28 enhanced the accumulation of potato virus X (PVX) in *Nicotiana benthamiana* 22 days post-infiltration, and P28 exacerbated significantly the symptoms of PVX. Collectively, these data indicate that the genome of SMoV RNA2 encodes two suppressors of RNA silencing. This is the first identification of a stramovirus suppressor of RNA silencing.

Keywords: strawberry mottle virus, RNA silencing suppressor, subcellular localization, conserved GW motif, symptom determinant

OPEN ACCESS

Edited by:
Giorgio Gambino, Institute for Sustainable Plant Protection (CNR), Italy

Reviewed by:
Hanako Shimura, Hokkaido University, Japan
Ying Zhai, Washington State University, United States
Basudev Ghoshal, Agriculture and Agri-Food Canada, Canada

****Correspondence:***
Hongqing Wang
wanghq@cau.edu.cn

Specialty section:
This article was submitted to Plant Pathogen Interactions, a section of the journal Frontiers in Plant Science

Received: *30 September 2021*
Accepted: *29 April 2022*
Published: *31 May 2022*

Citation:
Fan L, He C, Gao D, Xu T, Xing F, Yan J, Zhan B, Li S and Wang H (2022) Identification of Silencing Suppressor Protein Encoded by Strawberry Mottle Virus. Front. Plant Sci. 13:786489. doi: 10.3389/fpls.2022.786489

INTRODUCTION

Plant viruses are biotrophic pathogens that need living tissue to complete their multiplication cycle, and thus they interfere and/or compete with host for a substantial amount of host resources (Pallas and Garcia, 2011; Mandadi and Scholthof, 2013). To defend against invading viruses, plants employ several layers of immune responses. Among these immune responses, RNA silencing is a conserved eukaryotic gene regulation mechanism that provides sequence-specific antiviral defense (Covey et al., 1997; Baulcombe, 2004; Ding et al., 2004; Gupta et al., 2019). Briefly, the process of RNA silencing is that double-stranded RNA (dsRNA) are cleaved by Dicer-like RNases (DCLs) into 21–24 nucleotides (nt) small interfering RNAs (siRNAs), and then the siRNAs are incorporated into an Argonaute (AGO)-containing RNA-induced silencing complex (RISC) to degrade target RNAs and/or to inhibit its translation (Pallas and Garcia, 2011). In addition, the siRNAs and target RNAs can synthesize dsRNAs in the presence of RNA-dependent RNA polymerases (RDRs), thus amplifying the antiviral silencing signal (Sijen et al., 2001; Parent et al., 2015; Gupta et al., 2019). Furthermore, the siRNAs also can

act as mobile silencing signals that can trigger local silencing by moving from cell to cell *via* plasmodesmata as well as systemic silencing *via* phloem companion cells transport (Melnyk et al., 2011; Pumplin and Voinnet, 2013; Yang et al., 2018).

To counter RNA silencing, viruses encode one or more viral suppressor(s) of RNA silencing (VSR), which function in various steps of the process of RNA silencing (Li and Ding, 2006; Valli et al., 2009; Nakahara and Masuta, 2014; Csorba et al., 2015). The 2b protein of cucumber mosaic virus (CMV) and the p38 protein of turnip crinkle virus (TCV) both interact with AGO1 and inhibit AGO1-mediated gene silencing, but using different mechanisms: 2b through interaction with the PAZ domain and p38 through GW motifs that serve as an Ago "hook" (Danielson and Pezacki, 2013). Concurrently, 2b also binds small RNAs generated upon viral infection by DCLs, and this pathway was considered to be the most relevant in determining the suppressor functionality (González et al., 2010; Danielson and Pezacki, 2013). The P19 protein of tombusviruses, having a high affinity to duplexes 20–22 nucleotides long, functions to sequester small RNA duplexes (Cheng et al., 2011). In addition, P19 also suppresses RNA silencing by inducing the expression of a host miRNA (miR168) that reduces concentration of AGO1, thereby inhibiting RISC formation (Varallyay et al., 2010; Danielson and Pezacki, 2013).

Strawberry mottle virus is the most common virus of strawberry and occurs naturally in the genus *Fragaria* worldwide (Freeman and Mellor, 1962). It is one of the viruses found in association with strawberry decline disease. Its severe strains may reduce vigor and yield by up to 30% in strawberry cultivars (Martin and Tzanetakis, 2006). SMoV has been classified into subgenus *Stramovirus* within the genus *Sadwavirus*, family *Secoviridae* (Sanfaçon et al., 2020). SMoV has two positive-sense RNA genome segments, whereby RNA1 encodes a large polyprotein (about 215 kDa), referred to as P1. The P1 is cleaved in cis by 3C-like protease (3CL-Pro) at five sites to release mature proteins, including a putative RNA helicase (Hel), a 3CL-Pro (Pro), a viral genome-linked protein (Vpg), and an RNA-dependent RNA polymerase (RdRp) at its C-terminus, and two unknown proteins X1 and X2 at its N-terminus. The RNA2 encodes a polyprotein of about 190 kDa, referred to as P2. The P2 is cleaved in cis by glutamic protease (Pro2Glu) to form a 28 kDa unknown function protein (P28) and a Pro2Glu (40 kDa) at its C-terminus; additionally, a movement protein (MP) and a coat protein (CP) at its N-terminus are released with the help of 3CL-Pro (Bhagwat et al., 2016; Mann et al., 2017, 2019). Although the cleavage sites within the polyproteins have been experimentally defined largely, some proteins function is still ill-defined and even unknown.

For the family *Secoviridae*, several VSRs have been identified previously, including the R78 polyprotein of the *waikavirus* maize chlorotic dwarf virus and bellflower vein chlorosis virus (Stewart et al., 2017); the coat protein of the *nepovirus* tomato ringspot virus (Karran and Sanfaçon, 2014); the VP53, VP37 and large capsid protein of the *fabavirus* broad bean wilt virus 2 (Kong et al., 2014); the Vp20 of the *cheravirus* apple latent spherical virus (Yaegashi et al., 2007); and the small coat protein (SCP) of the *comovirus* cowpea mosaic virus (CPMV; Liu et al., 2004). In the present study, we found two suppressors, Pro2Glu and P28, encoded by SMoV RNA2 genome using a screening system that enables detection of both local and systemic plant host RNA silencing. Under the similar experimental conditions, we showed that Pro2Glu and P28 were unable to suppress local RNA silencing triggered by double-stranded GFP RNA. We also reported that Pro2Glu and P28 proteins were localized to nucleus and cytoplasm. Furthermore, G_5W_6 and $G_{116}W_{117}$ motifs of Pro2Glu were indispensable to suppressor activity. Additionally, Pro2Glu and P28 enhanced the accumulation of potato virus X (PVX) in *Nicotiana benthamiana* leaves, and P28 aggravated the symptoms of PVX.

MATERIALS AND METHODS

Plant Materials

Wild type (WT) *N. benthamiana* plants, green fluorescent protein (GFP) transgenic (line 16c) *N. benthamiana* plants and red fluorescent protein (RFP) transgenic *N. benthamiana* plants were used in the present study. They were grown from seeds in an insect-free growth room at 25°C under a 16 h light and 8 h dark photoperiod. The third and fourth leaves from the top were used for infiltration and inoculation experiments when the plants were about 4 weeks old.

Plasmid Construction

Ten SMoV protein coding regions, including X1, X2, Hel, Pro, Vpg, RdRp encoded by RNA1, MP, CP, Pro2Glu, and P28 encoded by RNA2, were individually amplified by polymerase chain reaction (PCR) from the SMoV Chinese isolate DGHY21 (GenBank accession no. MT070753) according to the method described previously (Fan et al., 2021). Specific primers used in this study were listed in **Supplementary Table S1** (containing suitable restriction sites). The PCR products were cloned individually into the pTOPO-Blunt vector (Aidlab, Beijing, China) to generate pTOPO-X1, pTOPO-X2, pTOPO-Hel, pTOPO-Pro, pTOPO-Vpg, pTOPO-RdRp, pTOPO-MP, pTOPO-CP, pTOPO-Pro2Glu, and pTOPO-P28, which were individually digested with specific enzymes for subsequent cloning.

To screen the VSRs, each protein-coding region was subcloned into the pCHF3 vector (Cai et al., 2007) under the control of a 35S promoter and NOS terminator to generate pCHF3-X1, pCHF3-X2, pCHF3-Hel, pCHF3-Pro, pCHF3-Vpg, pCHF3-RdRp, pCHF3-MP, pCHF3-CP, pCHF3-Pro2Glu, and pCHF3-P28. The resulting recombinant pCHF3 constructs were chemically transformed into the *Agrobacterium tumefaciens* strain EHA105.

For the subcellular localization analysis, the full-length fragments of SMoV Pro2Glu and P28 were inserted into, respectively, the *Sma* I/*Kpn* I and *Apa* I/*Kpn* I sites of pCAMBIA1300-GFP vector to produce C1300-Pro2Glu and C1300-P28 that contained GFP fusion protein. The resulting recombinant pCAMBIA1300-GFP constructs were chemically transformed into the *A. tumefaciens* strain GV3101.

For the pathogenicity test, the full-length coding regions of Pro2Glu and P28 were subcloned into the PVX-containing pGR106 vector (a kind gift from David C. Baulcombe, University

of Cambridge, Cambridge, United Kingdom) between the *Cla* I and *Sal* I restriction sites to produce PVX-Pro2Glu and PVX-P28. The *A. tumefaciens* strain GV3101 (pJIC SA_Rep) was transformed with the two plasmids.

To generate the Pro2Glu and P28 derivatives, the $Glu^{dm329-339aa}$ mutant with the 329GVSNRKKHRRG339 motif deleted was amplified by PCR from the plasmid pTOPO-Pro2Glu with primers $Glu^{dm329-339aa}$-F/R. The resulting $Glu^{dm329-339aa}$ was inserted into the *Bam*H I/*Pst* I sites of pCHF3 or *Sma* I/*Kpn* I sites of pCAMBIA1300-GFP to produce pCHF3-$Glu^{dm329-339aa}$ or C1300-$Glu^{dm329-339aa}$, respectively. The GW motifs of Pro2Glu and P28 were disrupted through W_6A (m4Glu), $W_{117}A$ (m1Glu), $W_{172}A$ (m2Glu), and $W_{191}A$ (m3P28) site-directed mutagenesis using gene synthesis by Sangon Biotech (Shanghai, China) Co., Ltd. The resulting mutants were inserted into the *Bam*H I/*Pst* I sites of pCHF3 to produce pCHF3-m4Glu, pCHF3-m1Glu, pCHF3-m2Glu, and pCHF3-m3P28.

Agrobacterium Infiltration and GFP Imaging

Agrobacterium-mediated transient gene expression was carried out based on developed protocols (Hamilton et al., 2002). *Agrobacterium* cultures were pelleted and resuspended to an optical density $OD_{600} = 1.0$ in a solution containing 10 mM $MgCl_2$, 10 mM MES (pH 5.8), and 200 μM acetosyringone, and were incubated at room temperature in dark for 3 h before infiltration. For co-infiltration, equal volumes of *Agrobacterium* cultures harboring 35S-GFP (a 35S promoter-driven construct expressing sense GFP, a kind gift from Prof. Xiuling Yang, Chinese Academy of Agricultural Sciences, Beijing, China) and the tested constructs were mixed, followed by infiltration into fully expanded leaves of 4-week-old 16c or WT *N. benthamiana* plants. A construct pCHF3-P19 to express tomato bushy stunt virus (TBSV) P19 was used as a positive control, and an empty vector pCHF3 was used as a negative control. GFP fluorescence in infiltrated or systemic leaves was monitored under a handheld long-wavelength UV lamp (Black-Ray Model B-100A, San Gabriel, CA, United States) and was photographed with a Canon EOS-M digital camera featuring a 55 mm yellow filter.

Northern Blot Analysis

Total RNA was extracted from *Agrobacterium*-infiltrated leaf patches of *N. benthamiana* line 16c or *N. benthamiana* WT plants by using an E.Z.N.A.® Plant RNA Kit (Omega Bio-tek, Norcross, GA, United States) following the manufacturer's instructions. Then, 2.5 μg of total RNA was separated on 1.5% formaldehyde-agarose gels and was transferred to Hybond N^+ membranes as instructed (GE Healthcare, Buckinghamshire, United Kingdom). The membrane was hybridized with a digoxigenin-labeled GFP probe, which was made using a PCR DIG probe synthesis kit, and was detected using a detection starter kit II according to the manufacturer's instructions (Roche Diagnostic, Basel, Switzerland). GelStain (Transgen, Beijing, China) staining was used to visualize the loading controls for the mRNA.

For siRNA blot assay, total RNA were extracted from infiltrated leaves with Trizol reagent (Transgen, Beijing, China) as recommended by the manufacturer. Low-molecular-mass RNAs were enriched from total RNA by adding equal volume of 10 M lithium chloride and incubating 4 h on ice. The RNA was centrifuged at 13,000 rpm for 15 min. The supernatant was precipitated at −20°C for at least 2 h after adding three volumes of ethanol. The low molecular weight (LMW) RNAs were collected by centrifugation for 15 min at 13,000 rpm. The enriched small RNAs were fractionated on a 15% denaturing polyacrylamide (19:1) gels containing 7 M urea in 0.5 × TBE buffer, then transferred to Hybond N^+ membranes by electroblotting at 20 V for 60 min, and chemically cross-linked *via* 1-ethyl-3-(3-dimethylaminopropyl) carbodiimide (EDC) as described previously (Pall and Hamilton, 2008). The membrane was hybridized with the digoxigenin-labeled GFP probe which was hydrolyzed into about 50 nt long RNA pieces by treatment with sodium carbonate buffer as described by Dalmay et al. (2000) at 40°C overnight, subsequently, washed at 50°C in 2 × SSC (0.3 M and 0.03 M sodium citrate) and 0.2% sodium dodecyl sulfate.

Western Blot Analysis

Total soluble proteins were extracted from *Agrobacterium*-infiltrated leaf patches of *N. benthamiana* WT or *N. benthamiana* line 16c plants by using a Plant Total Protein Lysis Buffer (Sangon Biotech, Shanghai, China). The protein samples were separated by SDS-PAGE. The anti-GFP mouse monoclonal antibody (TransGen Biotech, Beijing, China) was used at 1:5,000 dilution. Western blots were visualized with a goat anti-mouse IgG (H + L) HRP conjugate (TransGen Biotech, Beijing, China) and a chemiluminescence detection system (Tianneng, Shanghai, China). Coomassie blue staining of the large subunit of Rubisco served as loading controls for the Western blot assay.

Protein Interaction Assay

The Y2H experiment was performed using Super Yeast Transformation Kit (Coolaber, Beijing, China) according to the manufacturers. Plasmids of the bait and prey pairs were co-transformed into yeast cells and cultured at 30°C for 72 h on double dropout (−Leu/−Trp) or quadruple dropout (−Ade/-His/−Leu/−Trp) synthetic dextrose (SD) medium, respectively.

Quantitative RT-PCR Analysis

Total RNA was extracted from *N. benthamiana* systemic leaves infected by PVX, PVX-Pro2Glu and PVX-P28 at 22 dpi. Reverse transcription was conducted according to the published method (Fan et al., 2021). The RT-qPCR reactions in the 20 μl volume containing 1 μl cDNA as template were run using GoTaq qPCR Master Mix (Promega, Madison, United States) according to the instructions supplied by the manufacturer on a MyGo Pro real-time PCR instrument (IT-IS Life Science Ltd., Republic of Ireland). Primers G-35 and G-36 were used for determining PVX genomic RNA accumulation as described elsewhere (Gupta et al., 2018). *PP2A* was chosen as the internal control for normalization of virus accumulation in *N. benthamiana* plants. The $2^{-\Delta\Delta CT}$ method was used to analyze the RT-qPCR expression data according to Bustin et al. (2009). GraphPad (GraphPad Software Inc., San Diego, CA, USA) was used to analyze the

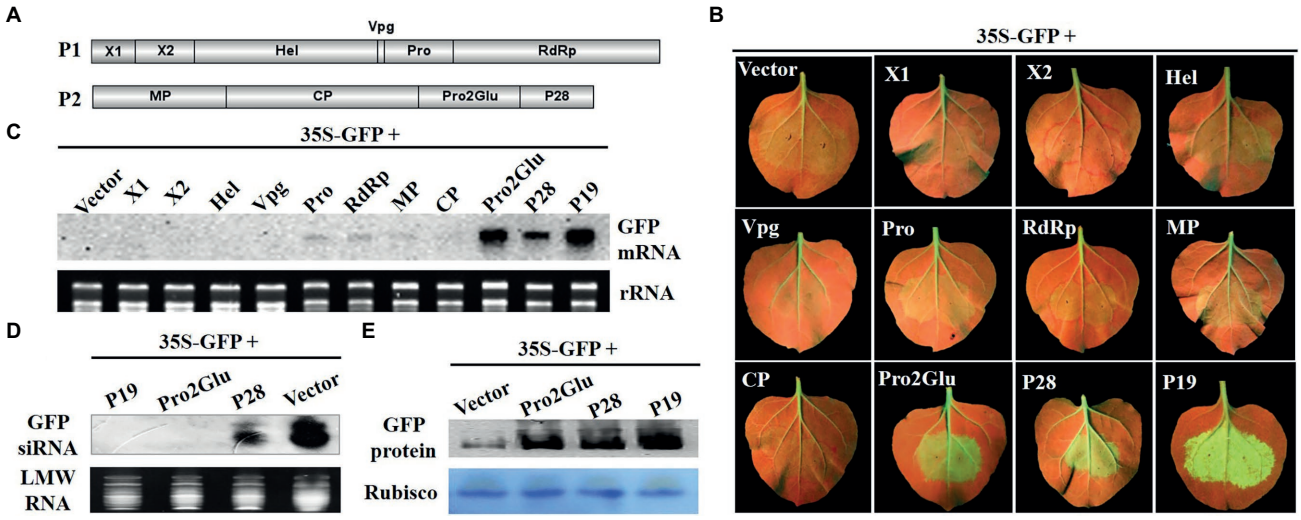

FIGURE 1 | The identification of SMoV silencing suppressor. **(A)** The genomic structure of SMoV. **(B)** The observation of GFP fluorescence in 16c *Nicotiana benthamiana* leaves co-infiltrated by 35S-GFP and pCHF3 vectors expressing individual proteins of SMoV at 5 days post-infiltration (dpi). The plants infiltrated with 35S-GFP and pCHF3 empty vector or pCHF3-P19 were used as negative or positive controls, respectively. **(C)** The analysis of GFP mRNA in infiltrated leaf patches by Northern blot at 5 dpi. DIG-labeled GFP-specific probe was used to detect the GFP mRNA. GelStain (Transgen, Beijing, China) staining was used to visualize the loading controls for the mRNA. The same below. **(D)** Northern blot analysis of low molecular weight (LMW) RNA from infiltrated leaf regions at 5 dpi for GFP-specific siRNA accumulation. DIG-labeled GFP-specific probe after hydrolyzing in sodium carbonate buffer was used to detect the GFP siRNA. GelStain staining was used to visualize the loading controls for the LMW RNA. The same below. **(E)** Western blot analysis of GFP protein in infiltrated leaf regions at 5 dpi using anti-GFP monoclonal antibody. Coomassie blue staining of the large subunit of Rubisco served as loading controls for the Western blot assay. The same below.

experimental data by one-way ANOVA, and multiple comparisons were done using Tukey's test ($p < 0.05$).

Laser-Scanning Confocal Microscopy

Imaging of fluorescent proteins was conducted using a confocal microscopy (LSM880; Carl Zeiss, Jena, Germany) at 60 h post-infiltration. To confirm the nuclei of the leaf epidermal cells, RFP transgenic *N. benthamiana* leaves were infiltrated with *Agrobacterium* cultures harboring the C1300-Pro2Glu or C1300-Glu$^{dm329-339aa}$ construct. For GFP, excitation was performed at 488 nm, and emission was recorded at 500 to 530 nm. For RFP, excitation was done at 561 nm, and emission was recorded at 590 to 630 nm.

Pathogenicity Enhancement Assay

Agrobacterium cultures harboring the PVX-Pro2Glu and PVX-P28 vectors were diluted to approximately $OD_{600} = 0.8$ prior to infiltration into leaves of *N. benthamiana* plants. The infiltrated plants were examined for virus-like symptoms and photographed at various time-points after infiltration.

RESULTS

Pro2Glu and P28 Both Suppress Local RNA Silencing Triggered by Single- but Not Double-Stranded GFP RNA

To identify VSRs of SMoV, a classical GFP-based two-component *Agrobacterium* infiltration assay was used to screen potential VSRs. *Agrobacterium* containing 35S-GFP and plasmids expressing individual proteins (X1, X2, Hel, Vpg, Pro, RdRp, MP, CP, Pro2Glu, and P28) of SMoV (**Figure 1A**) were mixed and co-infiltrated into fully expanded leaves of *N. benthamiana* line 16c. Three days post infiltration (dpi), GFP fluorescence was evident in all *Agrobacterium*-infiltrated leaf patches. By 5 dpi, as a consequence of GFP local silencing, GFP fluorescence became weak in leaves co-infiltrated with 35S-GFP and the empty pCHF3 vector and the tested recombinant pCHF3 vectors expressing X1, X2, Hel, Pro, Vpg, RdRp, MP, and CP. However, GFP fluorescence remained strong in leaves co-infiltrated with 35S-GFP and pCHF3-Pro2Glu or pCHF3-P28, resembling the positive control for silencing suppression (pCHF3-P19) (**Figure 1B**).

The northern blot analysis was carried out using total RNAs (for GFP mRNA) or LMW RNAs (for GFP siRNA) extracted from patches of co-infiltrated leaves. Consistent with the observed GFP fluorescence, GFP mRNA accumulated to higher levels in leaves co-infiltrated with 35S-GFP and pCHF3-P19, pCHF3-Pro2Glu or pCHF3-P28 compared to empty vector (**Figure 1C**), however, GFP siRNA accumulated at significantly reduced levels in plants expressing P28 and was not detected in P19 and Pro2Glu expressing plants (**Figure 1D**). Western blot also showed the accumulation of GFP proteins was higher in the leaves co-infiltrated with Pro2Glu + GFP, P28 + GFP or P19 + GFP than in those co-infiltrated with pCHF3 + GFP (**Figure 1E**). These results indicate that Pro2Glu and P28 encoded by SMoV RNA2 are capable of suppressing local RNA silencing triggered by single-stranded GFP.

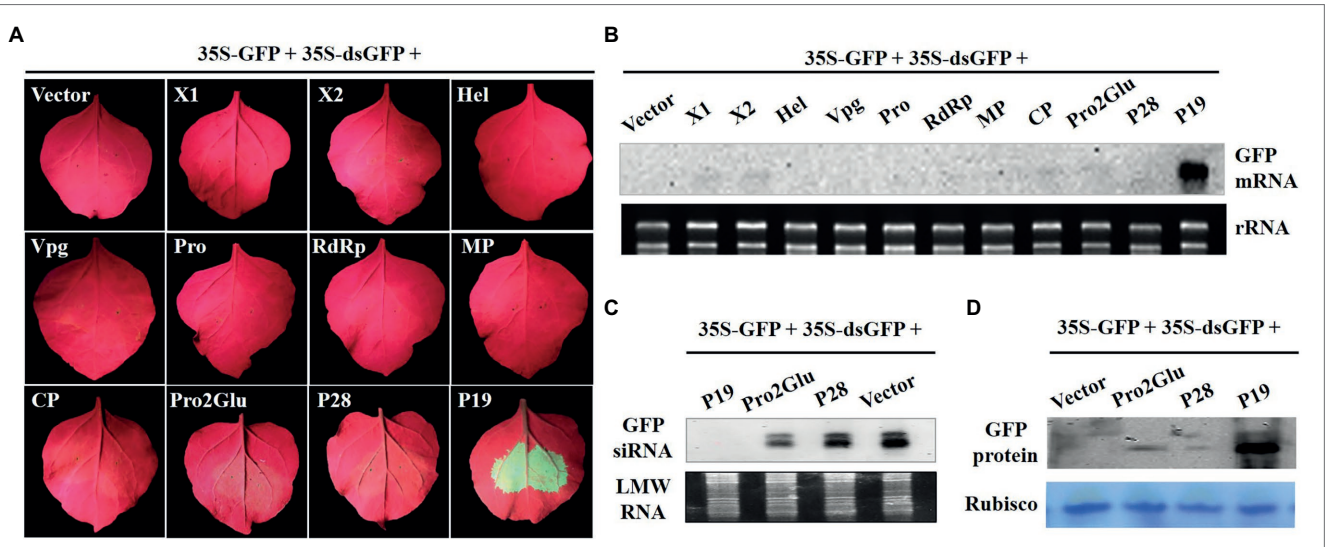

FIGURE 2 | Pro2Glu and P28 failed to suppress local silencing triggered by dsGFP. **(A)** The observation of GFP fluorescence in wild-type *N. benthamiana* leaves co-infiltrated by 35S-GFP, 35S-dsGFP, and pCHF3 vectors expressing individual proteins of SMoV at 3 dpi. The plants co-infiltrated by 35S-GFP, 35S-dsGFP, and pCHF3 empty vector or pCHF3-P19 were designated as negative or positive controls, respectively. **(B)** The analysis of GFP mRNA in infiltrated leaf patches by Northern blot at 3 dpi. **(C)** Northern blot analysis of GFP-specific siRNA in infiltrated leaf regions at 3 dpi. **(D)** Western blot analysis of GFP protein in infiltrated leaf regions at 3 dpi using anti-GFP monoclonal antibody.

To explore whether Pro2Glu and P28 could suppress dsRNA-induced RNA silencing, *Agrobacterium* suspension containing 35S-GFP, 35S-dsGFP (a construct expressing an inverted repeat sequence of GFP, a kind gift from prof. Xiuling Yang, Chinese Academy of Agricultural Sciences, Beijing, China) and plasmids expressing individual proteins X1, X2, Hel, Vpg, Pro, RdRp, MP, CP, Pro2Glu, and P28 were inoculated into fully expanded leaves of *N. benthamiana*. At 3 dpi, only the leaf patches co-inoculated by 35S-GFP, 35S-dsGFP and pCHF3-P19 showed strong GFP fluorescence, whereas leaf patches co-inoculated by 35S-GFP, 35S-dsGFP and empty vector, Pro2Glu, P28 or other eight proteins all showed faded GFP fluorescence (**Figure 2A**). The Northern blot analysis revealed that the leaves co-inoculated with 35S-GFP, 35S-dsGFP and pCHF3-P19 accumulated high levels of GFP mRNA, while GFP siRNA was not detected. Conversely, in other treatments, GFP mRNA remained undetected (**Figure 2B**) and high levels of GFP siRNA were detected (**Figure 2C**). Correspondingly, the western blot analysis revealed that the level of GFP protein expression was stronger in leaf patches co-infiltrated by pCHF3-P19 than in other co-infiltrated treatments (**Figure 2D**). To confirm this observation, we conducted the assay in a leaf of *N. benthamiana*. At 3 dpi, the same results were observed (**Supplementary Figure 1**). These data demonstrate that Pro2Glu and P28 failed to suppress dsGFP-induced RNA silencing.

Pro2Glu and P28 Inhibit Activation of Systemic Host RNA Silencing-Based Defense Responses

To determine whether Pro2Glu and P28 could inhibit activation of systemic host RNA silencing based defense responses, we agroinfiltrated two fully expanded leaves of *N. benthamiana* 16c line with 35S-GFP and empty vector, pCHF3-Pro2Glu, pCHF3-P28 or pCHF3-P19. GFP fluorescence was monitored in the newly emerging leaves of infiltrated plants. The plants with major and minor veins of upper young leaves turning red were assumed to be silenced systemically. At 28 dpi, 95% of plants co-infiltrated with 35S-GFP and empty vector showed systemic silencing, but only 32.4 and 35.3% of plants co-infiltrated with, respectively, 35S-GFP plus pCHF3-Pro2Glu or pCHF3-P28 exhibited systemic silencing (**Figure 3A** and **Supplementary Table 2**). The GFP mRNA and siRNA level of plants upper young leaves were analyzed by Northern blot. The results revealed high accumulation of GFP mRNA and negligible accumulation of GFP siRNA in patches co-infiltrated with 35S-GFP plus pCHF3-Pro2Glu, pCHF3-P28 or pCHF3-P19 (**Figures 3B,C**). These data demonstrate that Pro2Glu and P28 effectively inhibit activation of systemic host RNA silencing-based defense responses.

Some VSRs, such as apple chlorotic leaf spot virus (ACLSV) P50, suppress systemic host RNA silencing without interfering with local silencing. To find out whether SMoV also encodes other suppressor that is unable to suppress local RNA silencing but inhibits systemic RNA silencing, agroinfiltration containing 35S-GFP and the other recombinant plasmids (pCHF3-X1, -X2, -Hel, -Vpg, -Pro, -RdRp, -MP or -CP) into fully expanded leaves of *N. benthamiana* 16c line was done. At 28 dpi, red fluorescence was observed in newly emerging leaves in every treatment with 35S-GFP and pCHF3-X1, -X2, -Hel, -Vpg, -Pro, or –MP. More than 90% of infiltrated plants showed red fluorescence in the other two treatments with 35S-GFP and pCHF3-RdRp or pCHF3-CP (**Figure 3A** and **Supplementary Table 2**). The GFP mRNA

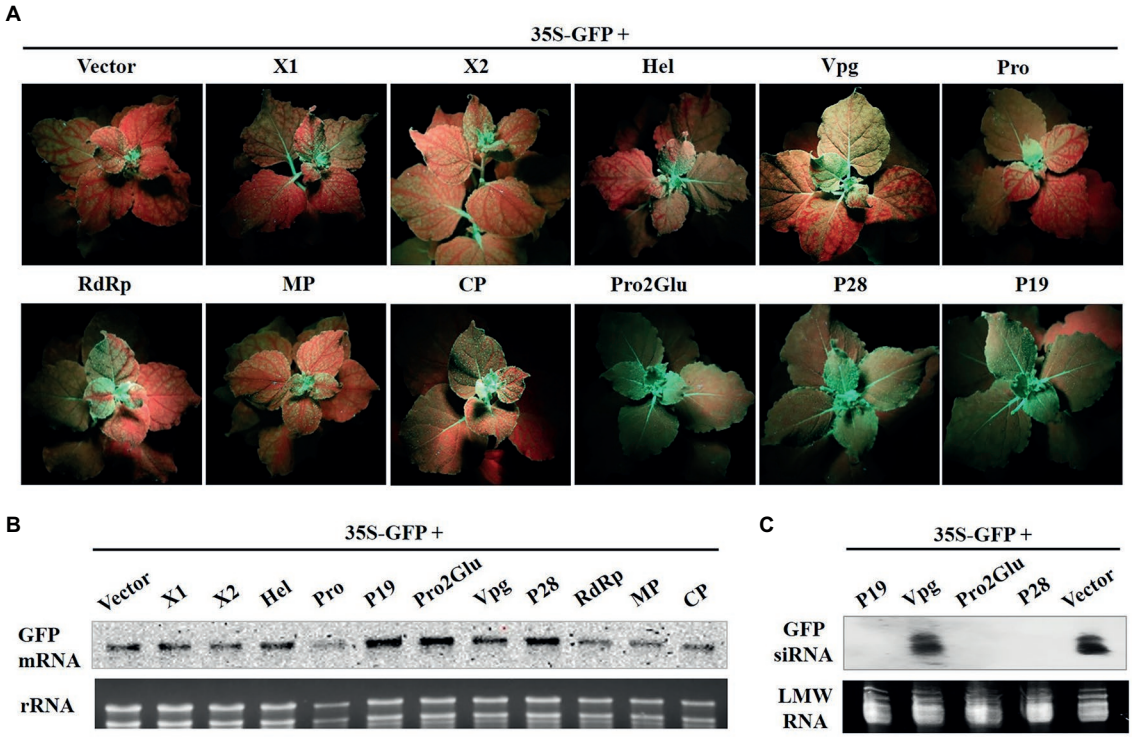

FIGURE 3 | Pro2Glu and P28 inhibited the systemic silencing of GFP in *N. benthamiana* line 16c plants. **(A)** *N. benthamiana* 16c plants infiltrated with 35S-GFP and recombinant plasmids were photographed under UV light at 28 dpi. **(B)** The analysis of GFP mRNA in upper young leaves by Northern blot at 28 dpi. **(C)** The analysis of GFP-specific siRNAs in upper young leaves by Northern blot at 28 dpi.

level of plants upper young leaves was analyzed by Northern blot. The results were consistent with the observed GFP fluorescence (**Figure 3B**). Taken together, these data indicate that X1, X2, Hel, Vpg, Pro, RdRp, MP or CP of SMoV do not efficiently inhibit systemic silencing of GFP.

Deletion of 11 Amino Acids at the C-Terminus Destabilizes Pro2Glu Protein

To determine the subcellular localizations of Pro2Glu and P28, we generated GFP-fused constructs C1300-Pro2Glu and C1300-P28, and individually infiltrated them into *N. benthamiana* leaves. At 60 h post-infiltration, the control leaves expressing GFP showed that GFP protein was localized in the nucleus and cytoplasm. Similarly, Pro2Glu and P28 proteins were observed in the nucleus and cytoplasm (**Supplementary Figure 2**).

Some studies reported that nuclear localization signal (NLS) is required for VSR suppressor activity (Wang et al., 2004; González et al., 2010; Yang et al., 2018). To explore which regions within Pro2Glu and P28 are crucial for their suppressor activity, we analyzed the SMoV Pro2Glu and P28 sequences using cNLS Mapper (Kosugi et al., 2009), and found that the GVSNRKKHRRG motif between amino acids 329 and 339 might be the NLS of the Pro2Glu protein, but the available NLS motif was not predicted in the P28 sequence. Hence, we deleted the 329GVSNRKKHRRG339 motif from Pro2Glu and constructed a cassette (**Figure 4A**; C1300-Glu$^{dm329-339aa}$) to clarify the subcellular localization of the Pro2Glu mutant variant. Parallel with the wild-type Pro2Glu, the fluorescence of C1300-Glu$^{dm329-339aa}$ was generally distributed in the nucleus and cytoplasm (**Figure 4B**). We further confirmed the nuclear localization of Pro2Glu and Glu$^{dm329-339aa}$ in RFP transgenic *N. benthamiana* plants (**Figure 4B**), demonstrating that the region covering aa 329–339 is not required for nuclear localization of Pro2Glu protein.

Furthermore, Glu$^{dm329-339aa}$ was cloned into pCHF3 to evaluate its ability to suppress RNA silencing. Fully expanded leaves of *N. benthamiana* 16c line were co-infiltrated with 35S-GFP and pCHF3-P19, pCHF3 empty vector, pCHF3-Glu$^{dm329-339aa}$ or pCHF3-Pro2Glu, and monitored under UV light. At 4 dpi, strong GFP fluorescence was observed in the leaf patches co-infiltrated with 35S-GFP and pCHF3-Pro2Glu or pCHF3-P19. However, GFP fluorescence was weak in the leaf patches co-infiltrated with 35S-GFP and pCHF3-Glu$^{dm329-339aa}$ or empty vector (**Figure 4C**). This observation was confirmed by the Northern blot analysis that examined the relative GFP mRNA level extracted from the corresponding leaf patches (**Figure 4D**). To determine whether the 329GVSNRKKHRRG339 motif deletion destabilized Pro2Glu protein. Western blot analysis was performed to detect the GFP fusion proteins using anti-GFP antibody. Detection of the expected protein sizes revealed that the deletion of the 329GVSNRKKHRRG339 motif significantly decreased the level of the Pro2Glu protein (**Figure 4E**). Taken together, these results demonstrate that

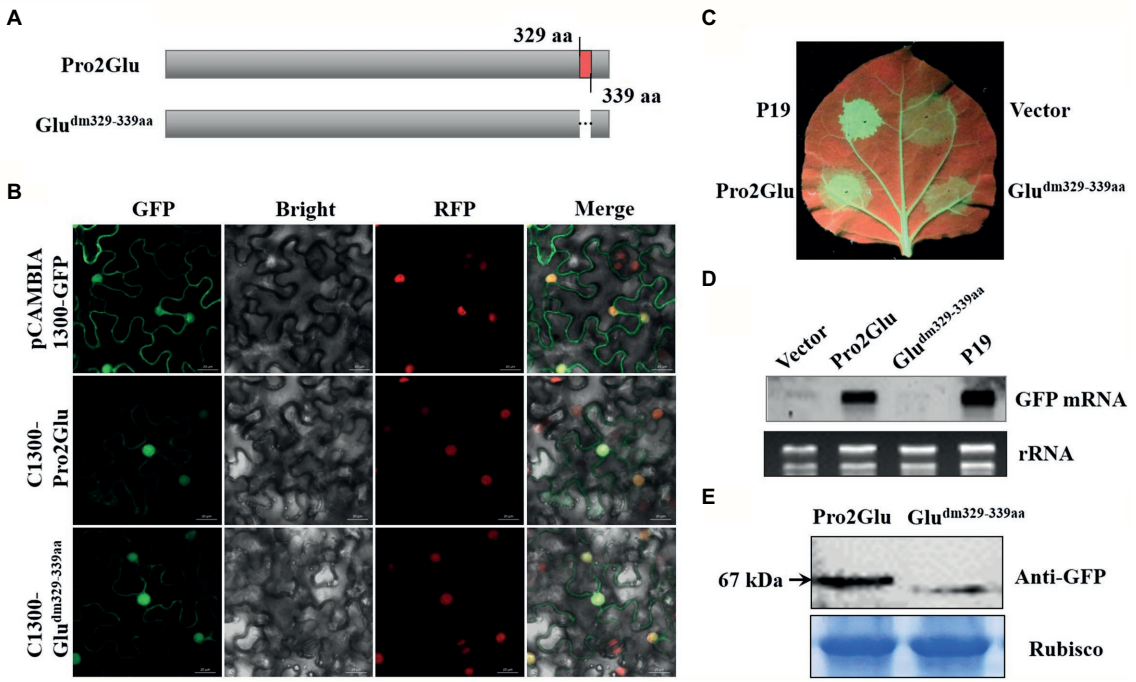

FIGURE 4 | The effect of deletion of 11 amino acids at the C-terminus of Pro2Glu on the subcellular localization and suppressor activity of Pro2Glu. **(A)** Schematic representation of Pro2Glu and its deletion mutant. **(B)** Subcellular localization of Pro2Glu and Glu$^{dm329-339aa}$ variant in leaf epidermal cells of red fluorescent protein transgenic *N. benthamiana*. *Agrobacterium* cultures containing pCAMBIA1300-GFP, C1300-Pro2Glu or C1300-Glu$^{dm329-339aa}$ was infiltrated into leaves of *N. benthamiana*, respectively. Imaging of fluorescent proteins was conducted using a confocal microscopy at 60 h post-infiltrated. **(C)** The observation of GFP fluorescence in leaves of *N. benthamiana* 16c infiltrated with a mixture of *Agrobacterium* cultures containing 35S-GFP and pCHF3-Pro2Glu (bottom left of leaf) or pCHF3-Glu$^{dm329-339aa}$ (bottom right of leaf) at 4 dpi. Expression of 35S-GFP with pCHF3-P19 (upper left of leaf) or pCHF3 vector (upper right of leaf) served as positive or negative controls, respectively. **(D)** The analysis of GFP mRNA in infiltrated leaf patches by Northern blot at 4 dpi. **(E)** Western blot analysis of total proteins from *N. benthamiana* leaf patches infiltrated with GFP-fused constructs C1300-Pro2Glu and C1300-Glu$^{dm329-339}$ at 3 dpi using anti-GFP antibody.

the 329GVSNRKKHRRG339 motif from Pro2Glu is not necessary for Pro2Glu nucleus localization. Since the 11 amino acids deletion makes the Pro2Glu unstable, the role of this motif in RNA silencing remains inconclusive.

Two GW Motifs of Pro2Glu Interfere With Suppressor Activity

The GW motif has been considered to be involved in direct interaction with AGO proteins to inhibit AGO-mediated gene silencing (El-Shami et al., 2007; Lian et al., 2009; Gupta et al., 2019). We analyzed the Pro2Glu and P28 sequences, and identified three conserved GW motifs in Pro2Glu of all available SMoV isolates (**Supplementary Figures 3A–C**) and a conserved GW motif in P28 of Chinese SMoV isolates (**Supplementary Figure 3D**). These GW motifs were disrupted through WA site-directed mutagenesis (**Figures 5A,B**). The resulting mutants were confirmed by Sanger sequencing (**Supplementary Figure 4**). Agroinfiltration of 35S-GFP along with pCHF3-m1Glu or pCHF3-m4Glu into leaves of *N. benthamiana* 16c line showed weak green fluorescence under UV light at 4 dpi compared to leaves co-infiltrated with wild-type pCHF3-Pro2Glu. Concurrently, leaves agroinfiltrated with pCHF3-m2Glu or pCHF3-m3P28 showed green fluorescence similar to wild-type pCHF3-Pro2Glu or pCHF3-P28, respectively (**Figure 5C**).

GFP expression was tested by Northern blot hybridization of total RNA extracted from infiltrated regions at 4 dpi. The results showed that GFP mRNA accumulated at lower levels in pCHF3-m1Glu- or pCHF3-m4Glu-infiltrated leaf patches compared with wild-type pCHF3-Pro2Glu. For pCHF3-m2Glu- or pCHF3-m3P28-infiltrated regions, GFP mRNA accumulation was equivalent to wild-type pCHF3-Pro2Glu or pCHF3-P28, respectively (**Figure 5D**). These data indicate that two GW (G_5W_6 and $G_{116}W_{117}$) motifs of Pro2Glu are indispensable to suppression of local RNA silencing.

Pro2Glu and P28 Enhance Accumulation of PVX RNA, and P28 Is a Putative Symptom Determinant

Most VSRs have been suggested to enhance synergistically the severity of infection when they are expressed from a heterologous virus-based expression vector (Cao et al., 2005; Cañizares et al., 2008; Tatineni et al., 2012; Samuel et al., 2016). To test the hypothesis that Pro2Glu and P28 could enhance pathogenicity of a heterologous virus, we took advantage of the PVX-based heterologous gene expression system to express the Pro2Glu and P28 proteins in WT *N. benthamiana* plants. *Agrobacterium* cultures containing pGR106 empty vector (PVX) or recombinant PVX constructs expressing individual Pro2Glu and P28 were infiltrated

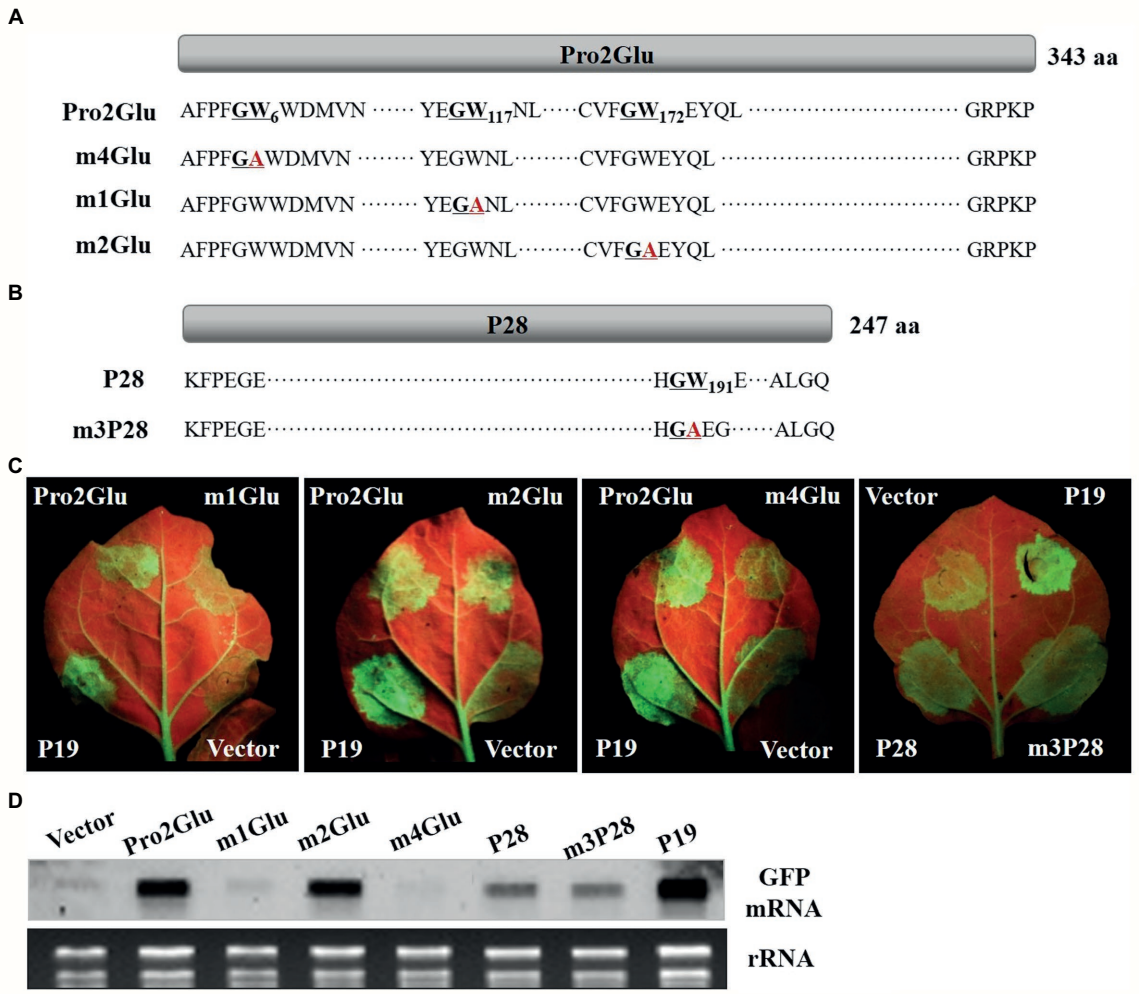

FIGURE 5 | The effect of GW motifs on the suppressor activity of Pro2Glu and P28. **(A)** Schematic representation of Pro2Glu and the mutation sites of its mutants. **(B)** Schematic representation of P28 and the mutation site of its mutant. **(C)** The observation of GFP fluorescence in leaves of *N. benthamiana* 16c infiltrated with *Agrobacterium* cultures containing 35S-GFP, plus pCHF3-Pro2Glu, pCHF3-P28 or their derivatives at 4 dpi. Expression of 35S-GFP with pCHF3-P19 or pCHF3 vector served as positive or negative controls, respectively. **(D)** The analysis of GFP mRNA in infiltrated leaf patches by Northern blot at 4 dpi. The each RNA of lane of Vector, Pro2Glu and P19 is the same as used in **Figure 4D**.

in the third and fourth leaves from top of 4-week-old *N. benthamiana* plants. The inoculated plants were monitored for symptom development. At 10 dpi, non-inoculated systemic leaves exhibited severe mosaic symptoms in *N. benthamiana* plants inoculated with PVX and PVX-P28 (**Supplementary Figure 5**). By 22 dpi, the upper leaves inoculated with PVX-P28 appeared crinkled and had necrotic lesions (**Figure 6A**). However, the plants inoculated with PVX-Pro2Glu showed mild mosaic symptom at 10 dpi (**Supplementary Figure 5**). By 22 dpi, mild mosaic symptoms in the plants inoculated with PVX-Pro2Glu were similar to the control (PVX-inoculated) plants (**Figure 6A**). These observations indicate P28 is a putative symptom determinant, and Pro2Glu does not aggravate the symptoms of PVX.

To determine the genomic RNA copies of PVX, RT-qPCR was performed using total RNA extracted from systemically infected leaves. The result showed that PVX-Pro2Glu and PVX-P28 accumulated with, respectively, 47- and 18-fold increases compared to wild-type PVX at 22 dpi (**Figure 6B**), indicating that Pro2Glu and P28 significantly enhanced heterologous virus PVX accumulation in *N. benthamiana* plants.

DISCUSSION

First recognized as a distinct virus in 1946, SMoV is the most economically important virus infecting strawberries (*Fragaria* spp.) both in terms of its geographic distribution and potential yield losses it can cause (Prentice and Harris, 1946). Its severe strains may reduce vigor and yield of strawberry by up to 30%, and even 80% in mixed infections with strawberry vein banding virus (SVBV), strawberry crinkle virus, and/or strawberry mild yellow edge virus (Thompson et al., 2002; Thompson and Jelkmann, 2003; Fan et al., 2022). However, many attempts to characterize SMoV further had limited success because of difficulties in purifying the virus from

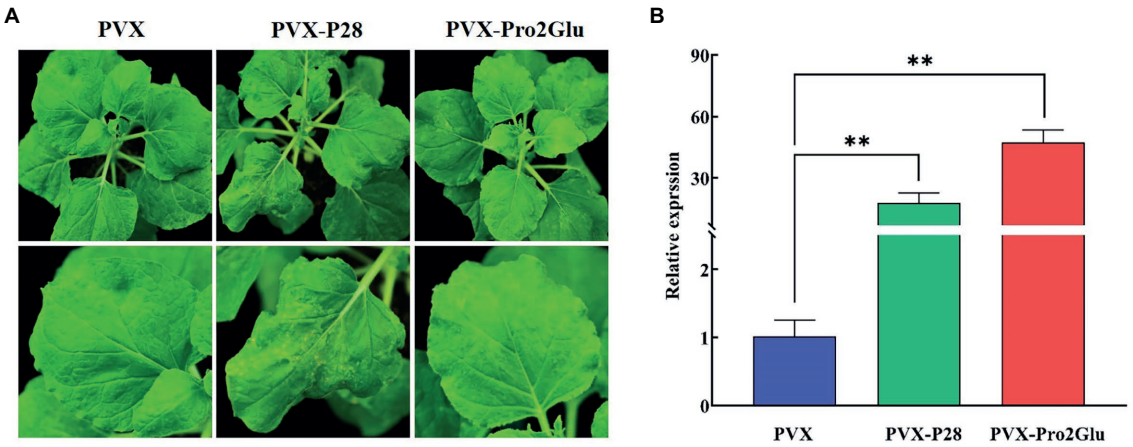

FIGURE 6 | Pro2Glu and P28 enhanced the pathogenicity of potato virus X (PVX) in *N. benthamiana* plants. **(A)** The symptoms on *N. benthamiana* systemic leaves infiltrated by pGR106 empty vector (PVX), PVX-P28 or PVX-Pro2Glu at 22 dpi. **(B)** The relative expression of PVX in *N. benthamiana* systemic leaves at 22 dpi as determined by RT-qPCR. The error bars indicate standard error, $n = 3$. Differences between PVX and PVX-P28 or PVX-Pro2Glu are analyzed by one-way ANOVA and Tukey's test ($p < 0.05$), $^{**}p < 0.01$.

infected plants and its distinct genomic organization. Hence, it remains unclear how SMoV induces disease and interacts and interferes with host components (Bhagwat et al., 2016; Mann et al., 2017, 2019). In the present study, we report that SMoV RNA2 genome encodes two suppressors of RNA silencing. SMoV Pro2Glu and P28 suppressed local and systemic silencing triggered by single- but not double-stranded GFP RNA. Both Pro2Glu and P28 were localized in the nucleus and cytoplasm. We present evidence that Pro2Glu ability to suppress host RNA silencing requires two conserved GW motifs, and deletion of 11 amino acids at the C-terminus destabilizes Pro2Glu protein. Finally, we showed that Pro2Glu and P28 enhanced PVX accumulation in *N. benthamiana* plants, and that P28 is a putative symptom determinant.

Several VSRs have been reported for viruses in *Secoviridae* family (Liu et al., 2004; Yaegashi et al., 2007; Karran and Sanfaçon, 2014; Kong et al., 2014; Stewart et al., 2017). However, our study identified for the first time the virus suppressor of RNA silencing encoded by a stramovirus. Pro2Glu, the first glutamic protease encoded by a positive-strand RNA virus, is unique to a few members of the family *Secoviridae* (Mann et al., 2019). It plays an essential role when SMoV polyprotein was processed into mature proteins (Mann et al., 2019). In our study, we found Pro2Glu acted as a suppressor to counter host RNA silencing. P28, located downstream of Pro2Glu, also suppressed host RNA silencing. Analyses of total RNA, siRNA and soluble proteins from agroinfiltrated leaf patches revealed that Pro2Glu possess a stronger ability to suppress host defense than P28; however, the level of suppression of RNA silencing by Pro2Glu and P28 was weak compared to that of strong VSR P19 of TBSV. This may be because P19 possesses very high affinity to duplexes 20–22 nt siRNA, at the same time, it induces the expression of host miR168 with the result that the formation of RISC is blocked (Danielson and Pezacki, 2013; Kontra et al., 2016).

Pro2Glu shares similarity with CPMV SCP (VSR of CPMV) in genome location (Liu et al., 2004), suggesting that Pro2Glu may suppress host defense in the same manner as SCP of CPMV. Unfortunately, the mechanism of suppression by CPMV SCP is still unclear. Previous studies have reported that the nuclear import was mandatory for some VSRs (Haas et al., 2008; Yang et al., 2011; Perez-Canamas and Hernandez, 2018). We explored the subcellular localization of Pro2Glu and P28 and found they were both localized in nucleus and cytoplasm. Many studies reported that the loss of NLS in VSR abolished the activity of the silencing suppressor, such as 2b of CMV, V2 of mulberry mosaic dwarf-associated virus, P6 of cauliflower mosaic virus (CaMV) and SVBV, and so on (Lucy et al., 2000; Wang et al., 2004; González et al., 2010; Feng et al., 2018; Yang et al., 2018). In the present study, we predicted that the GVSNRKKHRRG motif between amino acids 329 and 339 might be the NLS of the Pro2Glu protein. However, the subcellular localization of $Glu^{dm329\text{-}339aa}$ mutant with the 329GVSNRKKHRRG339 motif deleted was still distributed in the nucleus, indicating that the motif may not be NLS of Pro2Glu. We need a more accurate tool to predict the NLS of Pro2Glu. However, deletion of the 329GVSNRKKHRRG339 motif destabilized Pro2Glu protein, thus the role of this motif in RNA silencing remained inconclusive.

Two conserved GW motifs of Pro2Glu are indispensable to its suppressor activity. The GW motif could "hook up" with AGOs to counteract host RNA silencing-based defenses (Lian et al., 2009; Danielson and Pezacki, 2013). Previous studies also reported that AGO1 localization in the cell appears to be in both cytoplasm and nucleus (González et al., 2010; Gupta et al., 2019). Therefore, we speculate that Pro2Glu protein may suppress the host RNA silencing by interacting directly with AGO1. VSRs may target multiple pathways in host cells, such as CMV 2b, CaMV P6, High Plains wheat mosaic virus (HPWMoV) P7, and so on (Zhang et al., 2006; Feng et al., 2018; Gupta et al., 2019). In our study, Pro2Glu and P28 both failed to suppress local silencing triggered by

dsGFP RNA, demonstrating that they probably target the upstream steps of dsRNA production. It is possible that Pro2Glu and P28 directly interact with suppressor of gene silencing 3 (SGS3) or RNA-dependent RNA polymerase 6 (RDR6), or hinder their function, just like V2 protein of tomato yellow leaf curl virus and beet curly top virus (Glick et al., 2008; Fukunaga and Doudna, 2009; Luna et al., 2017). However, failing in detecting an interaction between Pro2Glu/P28 and SGS3/RDR6 in yeast (**Supplementary Figure 6**) suggests that Pro2Glu and P28 may hinder the function of SGS3 or RDR6 by other pathway. Further study is necessary to clarify the mechanism of Pro2Glu and P28.

VSRs generally are multifunctional. Many VSRs also play a pathogenicity-determining role. The most typical VSR is CMV 2b. Other recently identified VSRs include SVBV P6 (Feng et al., 2018), HPWMoV P7 and P8 (Gupta et al., 2018, 2019), apple geminivirus V2 (Zhan et al., 2018), raspberry bushy dwarf virus 1b (Masamichi et al., 2019), tomato leaf curl Palampur virus AC4 (Kulshreshtha et al., 2019) and so on, all aggravating the pathogenicity of heterologous virus PVX. In our study, we found that P28 exacerbated significantly the symptoms of PVX, indicating that P28 might play an important role in pathogenicity or virulence. Plant miRNAs regulate negatively the expression of mRNA, and involved in symptom development (Wang et al., 2012). Some VSRs could affect the miRNA-induced gene-silencing pathway (Tatineni et al., 2012; Kong et al., 2014). It is possible that P28 has an effect on the miRNA-induced gene-silencing pathway. In contrast, Pro2Glu with PVX caused inconspicuous symptoms compared to PVX, suggesting that Pro2Glu is likely to have little relevance to pathogenicity. Interestingly, RT-qPCR assay showed that Pro2Glu significantly enhanced the accumulation of PVX RNA at 22 dpi, demonstrating that Pro2Glu may help PVX infect plants *via* suppressing host defense responses involving RNA silencing, but may not influence the pathogenicity of PVX.

CONCLUSION

This study increased understanding of the function of Pro2Glu and P28 proteins, which provided a starting point for clarifying the pathogenic mechanism of strawberry mottle virus. In addition, this study identified the stramovirus suppressor of RNA silencing for the first time, which provides a foundation for studying other viruses in the genus *Stramovirus*.

DATA AVAILABILITY STATEMENT

The original contributions presented in the study are included in the article/**Supplementary Material**, further inquiries can be directed to the corresponding author.

AUTHOR CONTRIBUTIONS

LF conducted experiments and wrote the manuscript. CH performed experiments and interpreted data. DG performed experiments and took photos. TX carried out experiments and cultivated experimental plants. FX contributed to experimental design. JY contributed to manuscript revision. BZ contributed to experimental design and data analysis. SL contributed to manuscript revision. HW contributed to experimental design and manuscript review and editing. All authors contributed to the article and approved the submitted version.

FUNDING

The National Key R&D Program of China (2019YFD1001800) funded this study.

ACKNOWLEDGMENTS

We thank Xiuling Yang and Fangfang Li (State Key Laboratory for Biology of Plant Diseases and Insect Pests, Institute of Plant Protection, Chinese Academy of Agricultural Sciences) for kindly providing the 35S-GFP, 35S-dsGFP and pCHF3-P19 constructs, the pCHF3 and pGR106 vectors, the RDR6 plasmid and a handheld long-wavelength UV lamp. We are grateful to Zihao Xia (Plant Protection College, Shenyang Agricultural University) for his valuable advice about siRNA blot assay. In addition, we would like to express our gratitude to EditSprings (https://www.editsprings.cn/) for the expert linguistic services provided.

SUPPLEMENTARY MATERIAL

The Supplementary Material for this article can be found online at: https://www.frontiersin.org/articles/10.3389/fpls.2022.786489/full#supplementary-material

REFERENCES

Baulcombe, D. (2004). RNA silencing in plants. *Nature* 431, 356–363. doi: 10.1038/nature02874

Bhagwat, B., Dickison, V., Ding, X. L., Walker, M., Bernardy, M., Bouthillier, M., et al. (2016). Genome sequence analysis of five Canadian isolates of strawberry mottle virus reveals extensive intra-species diversity and a longer RNA2 with increased coding capacity compared to a previously characterized European isolate. *Arch. Virol.* 161, 1657–1663. doi: 10.1007/s00705-016-2799-6

Bustin, S. A., Benes, V., Garson, J. A., Hellemans, J., Huggett, J., Kubista, M., et al. (2009). The MIQE guidelines: minimum information for publication of quantitative real-time PCR experiments. *Clin. Chem.* 55, 611–622. doi: 10.1373/clinchem.2008.112797

Cai, X. Z., Zhou, X., Xu, Y. P., Joosten, M. H., and de Wit, P. J. (2007). *Cladosporium fulvum* CfHNNI1 induces hypersensitive necrosis, defence gene expression and disease resistance in both host and nonhost plants. *Plant Mol. Biol.* 64, 89–101. doi: 10.1007/s11103-007-9136-0

Cañizares, M. C., Navas-Castillo, J., and Moriones, E. (2008). Multiple suppressors of RNA silencing encoded by both genomic RNAs of the crinivirus, *Tomato chlorosis virus*. *Virology* 379, 168–174. doi: 10.1016/j.virol.2008.06.020

Cao, X., Zhou, P., Zhang, X., Zhu, S., Zhong, X., Xiao, Q., et al. (2005). Identification of an RNA silencing suppressor from a plant double-stranded RNA virus. *J. Virol.* 79, 13018–13027. doi: 10.1128/jvi.79.20.13018-13027.2005

Cheng, J., Danielson, D. C., Nasheri, N., Singaravelu, R., and Pezacki, J. P. (2011). Enhanced specificity of the viral suppressor of RNA silencing protein

P 19 toward sequestering of human micro RNA-122. *Biochemistry* 50, 7745–7755. doi: 10.1021/bi2008273

Covey, S. N., Al-Kaff, N., Lángara, A., and Turner, D. S. (1997). Plants combat infection by gene silencing. *Nature* 385, 781–782. doi: 10.1038/385781a0

Csorba, T., Kontra, L., and Burgyan, J. (2015). Viral silencing suppressors: tools forged to fine-tune host-pathogen coexistence. *Virology* 479–480, 85–103. doi: 10.1016/j.virol.2015.02.028

Dalmay, T., Hamilton, A. J., Mueller, E., and Baulcombe, D. C. (2000). Potato virus X amplicons in *Arabidopsis* mediate genetic and epigenetic gene silencing. *Plant Cell* 12, 369–379. doi: 10.1105/tpc.12.3.369

Danielson, D. C., and Pezacki, J. P. (2013). Studying the RNA silencing pathway with the P19 protein. *FEBS Lett.* 587, 1198–1205. doi: 10.1016/j.febslet.2013.01.036

Ding, S. W., Li, H., Lu, R., Li, F., and Li, W. X. (2004). RNA silencing: a conserved antiviral immunity of plants and animals. *Virus Res.* 102, 109–115. doi: 10.1016/j.virusres.2004.01.021

El-Shami, M., Pontier, D., Lahmy, S., Braun, L., Picart, C., Vega, D., et al. (2007). Reiterated WG/GW motifs form functionally and evolutionarily conserved ARGONAUTE-binding platforms in RNAi-related components. *Genes Dev.* 21, 2539–2544. doi: 10.1101/gad.451207

Fan, L. J., He, C. Y., Wu, M. M., Gao, D. H., Dong, Z. F., Hou, S. F., et al. (2021). Incidence, genomic diversity, and evolution of strawberry mottle virus in China. *Biocell* 45, 1137–1151. doi: 10.32604/biocell.2021.015396

Fan, L. J., Song, D., Khoo, Y. W., Wu, M. M., Xu, T. F., Zhao, X. L., et al. (2022). Effect of strawberry vein banding virus and strawberry mottle virus co-infection on the growth and development of strawberry. *Biocell* 46, 263–273. doi: 10.32604/biocell.2022.016306

Feng, M. F., Zuo, D. P., Jiang, X. Z., Li, S., Chen, J., Jiang, L., et al. (2018). Identification of strawberry vein banding virus encoded P6 as an RNA silencing suppressor. *Virology* 520, 103–110. doi: 10.1016/j.virol.2018.05.003

Freeman, J. A., and Mellor, F. C. (1962). Influence of latent viruses on vigor, yield and quality of British sovereign strawberries. *Can. J. Plant Sci.* 42, 602–610. doi: 10.4141/cjps62-103

Fukunaga, R., and Doudna, J. A. (2009). dsRNA with 5′ overhangs contributes to endogenous and antiviral RNA silencing pathways in plants. *EMBO J.* 28, 545–555. doi: 10.1038/emboj.2009.2

Glick, E., Zrachya, A., Levy, Y., Mett, A., Gidoni, D., Belausov, E., et al. (2008). Interaction with host SGS3 is required for suppression of RNA silencing by tomato yellow leaf curl virus V2 protein. *PNAS* 105, 157–161. doi: 10.1073/pnas.0709036105

González, I., Martínez, L., Rakitina, D. V., Lewsey, M. G., Atencio, F. A., Llave, C., et al. (2010). Cucumber mosaic virus 2b protein subcellular targets and interactions: their significance to RNA silencing suppressor activity. *Mol. Plant-Microbe Interact.* 23, 294–303. doi: 10.1094/MPMI-23-3-0294

Gupta, A. K., Hein, G. L., Graybosch, R. A., and Tatineni, S. (2018). Octapartite negative-sense RNA genome of High Plains wheat mosaic virus encodes two suppressors of RNA silencing. *Virology* 518, 152–162. doi: 10.1016/j.virol.2018.02.013

Gupta, A. K., Hein, G. L., and Tatineni, S. (2019). P7 and P8 proteins of High Plains wheat mosaic virus, a negative-strand RNA virus, employ distinct mechanisms of RNA silencing suppression. *Virology* 535, 20–31. doi: 10.1016/j.virol.2019.06.011

Haas, G., Azevedo, J., Moissiard, G., Geldreich, A., Himber, C., Bureau, M., et al. (2008). Nuclear import of CaMV P6 is required for infection and suppression of the RNA silencing factor DRB4. *EMBO J.* 27, 2102–2112. doi: 10.1038/emboj.2008.129

Hamilton, A., Voinnet, O., Chappell, L., and Baulcombe, D. (2002). Two classes of short interfering RNA in RNA silencing. *EMBO J.* 21, 4671–4679. doi: 10.1093/emboj/cdf464

Karran, R. A., and Sanfaçon, H. (2014). Tomato ringspot virus coat protein binds to ARGONAUTE 1 and suppresses the translation repression of a reporter gene. *Mol. Plant-Microbe Interact.* 27, 933–943. doi: 10.1094/MPMI-04-14-0099-R

Kong, L. F., Wang, Y. Q., Yang, X. L., Sunter, G., and Zhou, X. P. (2014). Broad bean wilt virus 2 encoded VP53, VP37 and large capsid protein orchestrate suppression of RNA silencing in plant. *Virus Res.* 192, 62–73. doi: 10.1016/j.virusres.2014.08.010

Kontra, L., Csorba, T., Tavazza, M., Lucioli, A., Tavazza, R., Moxon, S., et al. (2016). Distinct effects of P19 RNA silencing suppressor on small RNA mediated pathways in plants. *PLoS Pathog.* 12:e1005935. doi: 10.1371/journal.ppat.1005935

Kosugi, S., Hasebe, M., Tomita, M., and Yanagawa, H. (2009). Systematic identification of cell cycle-dependent yeast nucleocytoplasmic shuttling proteins by prediction of composite motifs. *PNAS* 106, 10171–10176. doi: 10.1073/pnas.0900604106

Kulshreshtha, A., Kumar, Y., Roshan, P., Bhattacharjee, B., Mukherjee, S. K., and Hallan, V. (2019). AC4 protein of tomato leaf curl Palampur virus is an RNA silencing suppressor and a pathogenicity determinant. *Microb. Pathog.* 135:103636. doi: 10.1016/j.micpath.2019.103636

Li, F., and Ding, S. W. (2006). Virus counterdefense: diverse strategies for evading the RNA silencing immunity. *Annu. Rev. Microbiol.* 60, 503–531. doi: 10.1146/annurev.micro.60.080805.142205

Lian, S. L., Li, S., Abadal, G. X., Pauley, B. A., Fritzler, M. J., and Chan, E. K. (2009). The C-terminal half of human Ago2 binds to multiple GW-rich regions of GW182 and requires GW182 to mediate silencing. *RNA* 15, 804–813. doi: 10.1261/rna.1229409

Liu, L., Grainger, J., Canizares, M. C., Angell, S. M., and Lomonossoff, G. P. (2004). Cowpea mosaic virus RNA-1 acts as an amplicon whose effects can be counteracted by a RNA-2-encoded suppressor of silencing. *Virology* 323, 37–48. doi: 10.1016/j.virol.2004.02.013

Lucy, A. P., Guo, H. S., Li, W. X., and Ding, S. W. (2000). Suppression of posttranscriptional gene silencing by a plant viral protein localized in the nucleus. *EMBO J.* 19, 1672–1680. doi: 10.1093/emboj/19.7.1672

Luna, A. P., Rodriguez-Negrete, E. A., Morilla, G., Wang, L., Lozano-Duran, R., Castillo, A. G., et al. (2017). V2 from a curtovirus is a suppressor of post-transcriptional gene silencing. *J. Gen. Virol.* 98, 2607–2614. doi: 10.1099/jgv.0.000933

Mandadi, K. K., and Scholthof, K. G. (2013). Plant immune responses against viruses: how does a virus cause disease? *Plant Cell* 25, 1489–1505. doi: 10.1105/tpc.113.111658

Mann, K. S., Chisholm, J., and Sanfaçon, H. (2019). Strawberry mottle virus (family *Secoviridae*, order *Picornavirales*) encodes a novel glutamic protease to process the RNA2 polyprotein at two cleavage sites. *J. Virol.* 93, e01679–e01618. doi: 10.1128/JVI.01679-18

Mann, K. S., Walker, M., and Sanfacon, H. (2017). Identification of cleavage sites recognized by the 3C-like cysteine protease within the two polyproteins of strawberry mottle virus. *Front. Microbiol.* 8:745. doi: 10.3389/fmicb.2017.00745

Martin, R. R., and Tzanetakis, I. E. (2006). Characterization and recent advances in detection of strawberry viruses. *Plant Dis.* 90, 384–396. doi: 10.1094/PD-90-0384

Masamichi, I., Takanori, M., Makoto, I., and Nobuyuki, Y. (2019). The 1b gene of raspberry bushy dwarf virus is a virulence component that facilitates systemic virus infection in plants. *Virology* 526, 222–230. doi: 10.1016/j.virol.2018.10.025

Melnyk, C. W., Molnar, A., and Baulcombe, D. C. (2011). Intercellular and systemic movement of RNA silencing signals. *EMBO J.* 30, 3553–3563. doi: 10.1038/emboj.2011.274

Nakahara, K. S., and Masuta, C. (2014). Interaction between viral RNA silencing suppressors and host factors in plant immunity. *Curr. Opin. Plant Biol.* 20, 88–95. doi: 10.1016/j.pbi.2014.05.004

Pall, G. S., and Hamilton, A. J. (2008). Improved Northern blot method for enhanced detection of small RNA. *Nat. Protoc.* 3, 1077–1084. doi: 10.1038/nprot.2008.67

Pallas, V., and Garcia, J. A. (2011). How do plant viruses induce disease? Interactions and interference with host components. *J. Gen. Virol.* 92, 2691–2705. doi: 10.1099/vir.0.034603-0

Parent, J. S., Bouteiller, N., Elmayan, T., and Vaucheret, H. (2015). Respective contributions of *Arabidopsis* DCL2 and DCL4 to RNA silencing. *Plant J.* 81, 223–232. doi: 10.1111/tpj.12720

Perez-Canamas, M., and Hernandez, C. (2018). New insights into the nucleolar localization of a plant RNA virus-encoded protein that acts in both RNA packaging and RNA silencing suppression: involvement of importins alpha and relevance for viral infection. *Mol. Plant-Microbe Interact.* 31, 1134–1144. doi: 10.1094/MPMI-02-18-0050-R

Prentice, I. W., and Harris, R. V. (1946). Resolution of strawberry virus complexes by means of the aphid vector *Capitophorus fragariae* Theb. *Ann. Appl. Biol.* 33, 50–53. doi: 10.1111/j.1744-7348.1946.tb06273.x

Pumplin, N., and Voinnet, O. (2013). RNA silencing suppression by plant pathogens: defence, counter-defence and counter-counter-defence. *Nat. Rev. Microbiol.* 11, 745–760. doi: 10.1038/nrmicro3120

Samuel, G. H., Wiley, M. R., Badawi, A., Adelman, Z. N., and Myles, K. M. (2016). Yellow fever virus capsid protein is a potent suppressor of RNA silencing that binds double stranded RNA. *PNAS* 113, 13863–13868. doi: 10.1073/pnas.1600544113

Sanfaçon, H., Dasgupta, I., Fuchs, M., Karasev, A. V., Petrzik, K., Thompson, J. R., et al. (2020). Proposed revision of the family *Secoviridae* taxonomy to create three subgenera, *Satsumavirus*, *Stramovirus* and *Cholivirus*, in the genus *Sadwavirus*. *Arch. Virol.* 165, 527–533. doi: 10.1007/s00705-019-04468-7

Sijen, T., Fleenor, J., Simmer, F., Thijssen, K. L., Parrish, S., Timmons, L., et al. (2001). On the role of RNA amplification in dsRNA-triggered gene silencing. *Cell* 107, 465–476. doi: 10.1016/s0092-8674(01)00576-1

Stewart, L. R., Jarugula, S., Zhao, Y. J., Qu, F., and Marty, D. (2017). Identification of a maize chlorotic dwarf virus silencing suppressor protein. *Virology* 504, 88–95. doi: 10.1016/j.virol.2016.11.017

Tatineni, S., Qu, F., Li, R., Morris, T. J., and French, R. (2012). Triticum mosaic poacevirus enlists P1 rather than HC-pro to suppress RNA silencing-mediated host defense. *Virology* 433, 104–115. doi: 10.1016/j.virol.2012.07.016

Thompson, J. R., and Jelkmann, W. (2003). The detection and variation of strawberry mottle virus. *Plant Dis.* 87, 385–390. doi: 10.1094/PDIS.2003.87.4.385

Thompson, J. R., Leone, G., Lindner, J. L., Jelkmann, W., and Schoen, C. D. (2002). Characterization and complete nucleotide sequence of strawberry mottle virus: a tentative member of a new family of bipartite plant picorna-like viruses. *J. Gen. Virol.* 83, 229–239. doi: 10.1099/0022-1317-83-1-229

Valli, A., Lopez-Moya, J. J., and Garcıa, J. A. (2009). *RNA Silencing and its Suppressors in the Plant-Virus Interplay*. Chichester: John Wiley and Sons Ltd..

Varallyay, E., Valoczi, A., Agyi, A., Burgyan, J., and Havelda, Z. (2010). Plant virus mediated induction of miR168 is associated with repression of ARGONAUTE1 accumulation. *EMBO J.* 29, 3507–3519. doi: 10.15252/embj.201797083

Wang, M., Masuta, C., Smith, N., and Shimura, H. (2012). RNA silencing and plant viral diseases. *Mol. Plant-Microbe Interact.* 25, 1275–1285. doi: 10.1094/MPMI-04-12-0093-CR

Wang, Y., Tzfira, T., Gaba, V., Citovsky, V., Palukaitis, P., and Gal-On, A. (2004). Functional analysis of the cucumber mosaic virus 2b protein: pathogenicity and nuclear localization. *J. Gen. Virol.* 85, 3135–3147. doi: 10.1099/vir.0.80250-0

Yaegashi, H., Takahashi, T., Isogai, M., Kobori, T., Ohki, S., and Yoshikawa, N. (2007). Apple chlorotic leaf spot virus 50 kDa movement protein acts as a suppressor of systemic silencing without interfering with local silencing in *Nicotiana benthamiana*. *J. Gen. Virol.* 88, 316–324. doi: 10.1099/vir.0.82377-0

Yang, X., Guo, W., Ma, X., An, Q., and Zhou, X. (2011). Molecular characterization of tomato leaf curl China virus, infecting tomato plants in China, and functional analyses of its associated betasatellite. *Appl. Environ. Microbiol.* 77, 3092–3101. doi: 10.1128/AEM.00017-11

Yang, X. L., Ren, Y. X., Sun, S. S., Wang, D. X., Zhang, F. F., Li, D. W., et al. (2018). Identification of the potential virulence factors and RNA silencing suppressors of mulberry mosaic dwarf-associated geminivirus. *Viruses* 10:472. doi: 10.3390/v10090472

Zhan, B. H., Zhao, W. Y., Li, S. F., Yang, X. L., and Zhou, X. P. (2018). Functional scanning of apple geminivirus proteins as symptom determinants and suppressors of posttranscriptional gene silencing. *Viruses* 10:488. doi: 10.3390/v10090488

Zhang, X. R., Yuan, Y. R., Pei, Y., Lin, S. S., Tuschl, T., Patel, D. J., et al. (2006). Cucumber mosaic virus-encoded 2b suppressor inhibits *Arabidopsis* Argonaute1 cleavage activity to counter plant defense. *Genes Dev.* 20, 3255–3268. doi: 10.1101/gad.1495506

Conflict of Interest: The authors declare that the research was conducted in the absence of any commercial or financial relationships that could be construed as a potential conflict of interest.

Publisher's Note: All claims expressed in this article are solely those of the authors and do not necessarily represent those of their affiliated organizations, or those of the publisher, the editors and the reviewers. Any product that may be evaluated in this article, or claim that may be made by its manufacturer, is not guaranteed or endorsed by the publisher.

frontiers | Frontiers in Plant Science

TYPE Review
PUBLISHED 12 June 2023
DOI 10.3389/fpls.2023.1163270

OPEN ACCESS

EDITED BY
Chellappan Padmanabhan,
USDA APHIS PPQ Science and Technology, United States

REVIEWED BY
Kathleen L Hefferon,
Cornell University, United States
Zishan Ahmad Wani,
Baba Ghulam Shah Badshah University, India
Zahid Ullah,
China University of Geosciences Wuhan, China
Klára Kosová,
Crop Research Institute (CRI), Czechia

*CORRESPONDENCE
Shujaul Mulk Khan
shuja60@gmail.com
Linda Heejung Lho
heeelho@gmail.com
Heesup Han
heesup.han@gmail.com

RECEIVED 10 February 2023
ACCEPTED 25 May 2023
PUBLISHED 12 June 2023

CITATION
Anikina I, Kamarova A, Issayeva K, Issakhanova S, Mustafayeva N, Insebayeva M, Mukhamedzhanova A, Khan SM, Ahmad Z, Lho LH, Han H and Raposo A (2023) Plant protection from virus: a review of different approaches. *Front. Plant Sci.* 14:1163270. doi: 10.3389/fpls.2023.1163270

Plant protection from virus: a review of different approaches

Irina Anikina[1], Aidana Kamarova[2], Kuralay Issayeva[1], Saltanat Issakhanova[1], Nazymgul Mustafayeva[3], Madina Insebayeva[1], Akmaral Mukhamedzhanova[1], Shujaul Mulk Khan[4*], Zeeshan Ahmad[4], Linda Heejung Lho[5*], Heesup Han[6*] and António Raposo[7]

[1]Biotechnology Department, Toraighyrov University, Pavlodar, Kazakhstan, [2]Biology and Ecology Department, Toraighyrov University, Pavlodar, Kazakhstan, [3]Agrotechnology Department, Toraighyrov University, Pavlodar, Kazakhstan, [4]Department of Plant Sciences, Quaid-i-Azam University, Islamabad, Pakistan, [5]College of Business, Division of Tourism and Hotel Management, Cheongju University, Cheongju-si, Chungcheongbuk-do, Republic of Korea, [6]College of Hospitality and Tourism Management, Sejong University, Seoul, Republic of Korea, [7]CBIOS (Research Center for Biosciences and Health Technologies), Universidade Lusófona de Humanidades e Tecnologias, Lisboa, Portugal

This review analyzes methods for controlling plant viral infection. The high harmfulness of viral diseases and the peculiarities of viral pathogenesis impose special requirements regarding developing methods to prevent phytoviruses. The control of viral infection is complicated by the rapid evolution, variability of viruses, and the peculiarities of their pathogenesis. Viral infection in plants is a complex interdependent process. The creation of transgenic varieties has caused much hope in the fight against viral pathogens. The disadvantages of genetically engineered approaches include the fact that the resistance gained is often highly specific and short-lived, and there are bans in many countries on the use of transgenic varieties. Modern prevention methods, diagnosis, and recovery of planting material are at the forefront of the fight against viral infection. The main techniques used for the healing of virus-infected plants include the apical meristem method, which is combined with thermotherapy and chemotherapy. These methods represent a single biotechnological complex method of plant recovery from viruses *in vitro* culture. It widely uses this method for obtaining non-virus planting material for various crops. The disadvantages of the tissue culture-based method of health improvement include the possibility of self-clonal variations resulting from the long-term cultivation of plants under *in vitro* conditions. The possibilities of increasing plant resistance by stimulating their immune system have expanded, which results from the in-depth study of the molecular and genetic bases of plant resistance toward viruses and the investigation of the mechanisms of induction of protective reactions in the plant organism. The existing methods of phytovirus control are ambiguous and require additional research. Further study of the genetic, biochemical, and physiological features of viral pathogenesis and the development of a strategy to increase plant resistance to viruses will allow a new level of phytovirus infection control to be reached.

KEYWORDS

plant virus, resistance genes, PR-proteins, elicitors, method of apical meristems

1 Introduction

Viruses cause various pathological changes, which affect all aspects of plant life. Most viral diseases are characterized by systemic damage, in which the virus moves from the primary site of inoculation to other parts of the plant organism (Ershova et al., 2022; Wang et al., 2022). A virus is usually present until it dies off once the plant is infected, and it is passed to the offspring by vegetative propagation. The viral infection manifests itself in the appearance of plants.

The physiology and biochemistry of the host cells and tissues have changed internally and as a result of the virus (Hull, 2014). The properties of the host plant, the virulence and aggressiveness of the virus strain, the length of the infection, and the environmental factors all affect the disease's diagnostic indications, which can vary greatly (Jones, 2009). These factors also determine the duration of the incubation period. The incubation period is usually a few days or weeks, which can be more than a year for herbaceous plants. Viral, viroid, and mycoplasma diseases are considered very harmful due to their chronic nature. They damage plant species, which leads to plant stress, death, and low crop yields (Table 1). They also change the chemical composition and deteriorate the quality of tubers (Adolf et al., 2020; Kreuze et al., 2020). Viral infection significantly changes the metabolism of plants, which includes a reduction in the photosynthetic activity of plants, which suppresses carbohydrates and other types of metabolism (Anikina and Seitzhanova, 2015). Chloroplasts are destroyed, changed, or aggregated due to viral infection. This leads to the destruction of chlorophyll or its non-participation in synthesis. The degree of photosynthetic suppression depends mainly on the disease development, the characteristics of the virus strain, the disease development phase, the virus strain–disease development phase's characteristics, the host plant, and the environmental conditions (Table 2) (Chen et al., 2019; Akbar et al., 2021).

Almost all viral diseases are characterized by a decreased total carbohydrate content (Handford and Carr, 2007). This occurs due to the destruction of chlorophyll in the mosaic and jaundice lesions. The disruption of the transport of photosynthetic products from the leaves to other plant organs is also affected by viral infections (Akbar et al., 2021). The outflow of starch is disrupted when the phloem is affected, which overloads the parenchyma cells. As a result, the leaves become thicker, leathery, and brittle (Yu, 2015). Changes in the permeability of the parenchyma cell cytoplasm or the carbohydrase activity may also cause delayed starch outflow from the leaves. The study of the histological structure of plants revealed hypertrophy and hyperplasia, which resulted in the formation of tumors and enations. Many viruses affect the vascular system xylem and phloem, which causes the formation of tillers and cell death (Hull, 2014). As a result, the wilting of plants, the delayed outflow of the assimilates from the leaves, and the appearance of necroses on the vegetative plant in tubers and fruits are observed (Gupta N. et al., 2021). The phenomena of hypoplasia and metaplasia accompany the dwarfism of plants and the color changes in the case of virus infection. Many viruses cause changes in the fine structure of infected cells. Vesicles are formed at the periphery of the chloroplasts when they are under the influence of thymoviruses. Chloroplasts in tobacco mosaic virus (TMV)-infected tobacco cells become deformed and often degenerate. The formation of new chloroplasts is also inhibited in these types of cells (Bhattacharyya et al., 2015). These changes are responsible for the chlorosis and mosaic coloration of the affected leaves.

Viral infection causes metabolic abnormalities in the cells of the diseased plant. For example, the water regime is disturbed when it is infected with phytoviruses, which are accompanied by changes in

TABLE 1 Reduction of crop yields under the influence of phytoviruses.

Crop	Decrease in productivity	Source
Sweet potato (*Ipomoea batatas*)	80%–98%	(Mwanga et al., 2001; Clark et al., 2012; Alam et al., 2013)
	30%–50%	(Silva and Fontes, 2022)
Tomatoes (*Solanum lycopersicum*)	42.1%–95.5%	(Hossain et al., 2011; Sevik and Arli-Sokmen, 2012; Farooq et al., 2021)
Okra (*Abelmoschus esculentus* L. Moench)	49%–84%	(Mishra et al., 2017)
	94%	(Dhankhar, 2016)
Potato (*Solanum tuberosum*)	10%–80%	(Mumford et al., 2016; Kreuze et al., 2020)
	10%	(Moses et al., 2017)
	10%–90%	(Salazar, 1996)
	15%–75%	(Gong et al., 2019)
Pepper (*Capsicum annuum*)	70%–80%	(Tolkach et al., 2019)
Watermelon (*Citrullus lanatus*)	10%–75%	(Xu et al., 2004; Tolkach et al., 2019)
Melon (*Cucumis melo* L.)	80%	(Sáez et al., 2022)
	30%–60	(Alonso-Prados et al., 1997)
Wheat (*Triticum*)	80%	(Perry et al., 2000)
	41%–63%	(Cisar et al., 1982)

TABLE 2 Type of overwhelming action under the influence of phytoviruses.

Type of suppression	Source
Plant growth delay	(Fletcher et al., 1998; Jin et al., 2016; Mumford et al., 2016)
Deterioration in the chemical composition and commodity qualities of the crop	(Alonso-Prados et al., 1997; Adolf et al., 2020; Kreuze et al., 2020)
Suppression of photosynthesis and carbohydrate metabolism	(Handford and Carr, 2007; Hull, 2014; Anikina and Seitzhanova, 2015; Chen et al., 2019; Akbar et al., 2021)
Suppression of the hormonal system	(Bari and Jones, 2009; Islam et al., 2019)
Violation of the water balance	(Hull, 2014; Anikina and Seitzhanova, 2015; Gupta N. et al., 2021)

the transpiration intensity and the water inflow due to changes in the vascular system (Anikina and Seitzhanova, 2015). The transpiration flow slows down, and the intensity of transpiration decreases, resulting from changes in the conductive system. In addition, there are changes in leaf transpiration surface due to the development of necroses (stomata malfunction) and the death of a part of the leaf apparatus. The metabolism of the affected plant changes, which can lead to its death due to the water balance disruption (Gupta N. et al., 2021). Almost all viral diseases are characterized by the disruption of nitrogen metabolism. Viruses have no enzymatic activity, but the essential role of the host plant's enzymes is observed with the changes in the nitrogen-containing compounds (Hull, 2014). The proteolytic activity is significantly increased in potato leaves that are affected by the wrinkle mosaic, which can only be attributed to the proteinases of the potato itself. An increased soluble and nitrate nitrogen content is observed in the leaves and tubers of the potatoes that are affected by leaf curl, which is associated with the disruption of the nitrate restoration and protein synthesis processes. The total amount of nitrogen in the plant does not change when tobacco is infected with a mosaic pathogen. A significant portion of it still goes to virion building since the viral protein is formed at the expense of the host plant's protein. The amount of non-protein nitrogen in infected tobacco is greatly reduced under nitrogen deficiency conditions. In contrast, the content of free amino acids increases with excess nitrogen probably due to the increased hydrolysis of the plant proteins (Dyakov et al., 2007).

Studies about the respiration of plants affected by viruses showed that viral infection stimulates the activity of dehydrases, which affect the initial phases of respiration, and the peroxidase activity of the affected plants increases at the same time (Hull, 2014). An increase in the respiration activity in tobacco plants during TMV infection was observed, whereas an increased oxidative activity after the influence of the beets and potatoes' viral infection was also revealed. The activation of respiration is attributed to the protective reactions of the host plant. The peak of the respiration activity and the oxidative enzymes inhibit the reproduction of the virus at the beginning of the infection. The respiration intensity of the infected plant decreases, and the virion synthesis is activated. Many researchers show that viral diseases of plants are accompanied by dwarfism; the appearance of tumors and enations; changes in the shape of the leaves, flowers, and fruits; the formation of excessive buds; and the imbalance of the hormonal metabolism in plants under the influence of viral infection (Ma et al., 2022; Wang et al., 2022). This review aims to analyze and discuss contemporary methods for controlling viral infestation in plants by comparing various methods and taking into account the negative effects of viral diseases as well as the unique difficulties associated with viral pathogenesis. It also aims to identify efficient preventative measures to deal with phytoviruses by examining the molecular and genetic principles underpinning viral pathogenicity. As it focuses on creating strategies to control viral infections in plants, which is crucial for guaranteeing good crop production and addressing issues with food security, this evaluation helps to achieve Sustainable Development Goal 2: Zero Hunger by addressing these objectives.

2 Biotechnological approaches to countering phytoviruses

2.1 Creation of varieties resistant to viruses based on the study of molecular stability mechanisms

The fight against viral infection is complicated due to the rapid evolution of viruses and the obligate parasitic nature of viruses. They penetrate the nucleus of cells, where viruses use the internal reserves of the plant for their reproduction (Tian and Valkonen, 2013; Jones and Naidu, 2019). Promising measures against plant viruses include breeding programs in regard to creating virus-resistant forms, which are in particular based on the marker-assisted selection method to evaluate the genetic defenses of a variety as well as the creation of transgenic varieties with high resistances to viral diseases (Klimenko et al., 2019; Akhter et al., 2021). It has become possible to insert certain genes into the genome of a plant, which is based on genetic engineering, which has resulted in new protective proteins that determine that the resistance to viruses is synthesized in the plant cells. Plant varieties with genes of extreme resistance to certain viruses have already been obtained. For example, a variety of soybean L29 with exceptional resistance to isolates of G5, G6, G7, and G5H strains has been obtained (Tran et al., 2018). R-resistance genes are expressed in plant cells during infection. More than 200 R genes with plant resistance to viruses, bacteria, and fungi have been cloned (Sharipova et al., 2013). Potato R genes are responsible for plant

resistance to the potato virus X (PVX). Tomato SW-5 gene resists tomato spotted wilt virus, and tomato Tm and Tm2 genes resist tomato mosaic virus. Mutational analysis showed that R genes encode translation initiation factors that lead to overcoming the RNA virus infection (Sharipova et al., 2013). Studies about the molecular mechanisms of extreme resistance and their relationship with hypersensitive response concluded that the same NLR genes can trigger both extreme resistance and hypersensitive response. Genes that generally provide the phenotype of extreme resistance can be stimulated in order to induce a hypersensitive response by experimentally increasing cellular levels of derived pathogen proteins (Ross et al., 2021).

Most plant NLR proteins consist of three primary domains, which include the N-terminal helix-helix domain, the Toll/interleukin-1 receptor or divergent helix-helix domain, the central nucleotide-binding domain, and the C-terminal domain rich in leucine repeats (LRR). These proteins function as intracellular immune receptors, and the nucleotide-binding state partially controls their ability to induce an immune response. Inactive NLR proteins are specifically bound to ADP, whereas the recognition and binding of the effector pathogen protein allow the NLR to switch to an active and ATP-bound state that can initiate an immune response (Lolle et al., 2020). A total of 30 genes that are responsible for the resistance of potato plants to viruses X, T, A, and M have currently been identified. Genetic silencing is the deactivation or reduction of one of the plant's genes using RNA interference, which involves the suppression of the gene expression by double-stranded RNA and is also used in order to create genetically modified virus-resistant plants. RNA silencing is an essential antiviral mechanism (Li and Wang, 2022; Lu et al., 2022). A DNA fragment is isolated from the genome and placed in a genetic construct in an inverted (antisense) position to turn off the target gene. Synthesized RNA does not encode anything in this case, but it can bind to the target gene's mRNA. Translation stops and mRNA destruction occurs, and the expression of the target gene is drastically reduced or even completely stopped (Calil and Fontes, 2017; Kochetov and Shumny, 2017). There are currently great expectations for studying the regulatory pathways of plant resistance formation. Signal transduction from external factors leads to the activation of serine/threonine protein kinases, which phosphorylate the threonine or tyrosine residues of other regulatory proteins in this group that is activated by phosphorylation. The coordinated interaction of regulatory signaling pathways occurs during the plant infection, which results in the expression of resistance genes and increased plant defense against pathogens. A study of plant antiviral defense mechanisms revealed that when attacked by an infection, they activate the genes encoding PR proteins, which are pathogenesis-related proteins.

The type and level of PR-protein accumulation depend on the nature and level of the plant damage. Some PR proteins, such as proteinases and β-1,3-glucanases, promote the virus infection of plants. Other PR proteins, such as proteinase inhibitors, ribonucleases, and peroxidases, effectively protect plants against viruses. Signaling systems regulate their coordinated accumulation in plants. Thus, it has been determined that the accumulation of PR-10 proteins around the pathogen introduction or wounding site indicates their participation in plant defense mechanisms (Prasad and Srivastava, 2017). Transgenic plants with increased RNase expression are more resistant to pathogens than the original plants (Kochetov and Shumny, 2017). The disadvantages of the genetically engineered approaches include that the acquired resistance is often specific and short-lived, and there is a *gene silencing* problem (Li and Wang, 2022). The negative factors of cultivating genetically modified plants resistant to certain viruses include the possible redistribution of the virus species structure, which can spread other harmful viral infections. There are restrictions on using genetically modified organisms (GMOs), such as genetically modified potato varieties not being used in Kazakhstan. Modern methods of prevention, as well as the diagnosis and recovery of planting material, are at the forefront of potato virus infection control (Mumford et al., 2016; Kesiraju and Sreevathsa, 2017; Wang et al., 2022).

2.2 Use of genome editing to combat virus infection

Progress in the development of resistant varieties, including those based on transgenic methods, is slow due to the lack of host genes and the duration of the breeding process and the problems associated with the limited use of transgenic plants in many countries (Tiwari et al., 2022). Genome editing technology is a promising approach to control viral pathologies. Breakthroughs in genome editing technology have been made in functional genomics and crop improvement (Zhang et al., 2018; Hofvander et al., 2022). Zinc finger nucleases (ZFNs) and effector nucleases (TALEN) were used as the first available genome-editing tools. These nucleases are chimeric proteins created by fusing their respective DNA-binding domains (DBDs) with the DNA cleavage domain of Fok I restrictase. The method of genome editing based on ZFNs and TALENS has been used for several plant species despite being labor-intensive, and important achievements have been obtained (Shan et al., 2013). However, nowadays, a new genome editing platform has been successfully used, which has surpassed the efficiency of ZFNs and TALEN in plants. According to scientists, CRISPR/Cas is currently the most powerful biological tool for targeted genome modification (Silva and Fontes, 2022; Tiwari et al., 2022). Many researchers consider the CRISPR/Cas-mediated immunity mechanism based on regularly spaced short palindromic repeats (CRISPR) and CRISPR-associated (Cas) proteins crucial in the fight against pathogens. This type of immunity has evolved as an adaptive immune system in archaea and bacteria against an invasion of foreign nucleic acids from viral or plasmid pathogens (Nussenzweig and Marraffini, 2020; Nidhi et al., 2021).

In recent years, there has been growing interest in using various aspects of CRISPR/Cas technologies to create plants resistant to viral pathogens. There are two ways to use CRISPR/Cas systems: the first involves direct targeting of viral genomes, and the second involves introducing targeted mutations into specific host plant genes that encode proteins used by the virus for successful replication and spread in the plant. The first method is the most widespread (Kavuri et al., 2022). Cas class 1 system include types I,

III, and IV with different variants and effector complexes, whereas Cas class 2 systems comprise types II, V, and VI with an effector module containing a single multifunctional protein (Kavuri et al., 2022). Because of their simpler organization, class 2 Cas systems are most widely used as genome-editing tools, with type II and V systems using Cas9 and Cas12 enzymes to edit DNA. Notably, the CRISPR/Cas9 type II class 2 protein is one of the first Cas proteins to be studied, leading to its widespread use for DNA editing in animals, plants, and bacteria (Kavuri et al., 2022). Since the discovery of the CRISPR/Cas9 system in *Streptococcus pyogenes*, related systems have been discovered in many bacterial and archaeal species (Robertson et al., 2022). CRISPR/Cas9 has now produced important advances in plant research because of its simplicity, multiplexing, cost-effectiveness, high efficiency, and minimal target bias. The practical application of the CRISPR/Cas technology faces several bottlenecks whose solution is crucial for plant gene editing, one of which, for example, is the method of delivering components of the Cas9 RNA editing complex into plants. Gene delivery using plasmid DNA and *Agrobacterium* transformation (the main method used) leads to transgenic plants, which is prohibited by the legislation of many countries. The preferred methods are direct (free-associated) delivery of kgRNA and Cas9 protein, which have been actively developed recently (Tiwari et al., 2022). Knowledge of all aspects of CRISPR/Cas systems is constantly expanding.

There are certain limitations in DNA editing using CRISPR, such as the protospacer adjacent motif (PAM) site requirement, non-targeted mutations, and low efficacy against viruses (Ahmad et al., 2020). The recently identified CRISPR/Cas type VI systems can overcome some of these limitations, which use the Cas13 protein to provide sequence-specific cleavage of single-stranded RNA (ssRNA) molecules (Wolter and Puchta, 2018; Kavuri et al., 2022). The discovery of Cas endonucleases targeting RNA molecules marked a new turn in developing CRISPR/Cas technologies. One of the best known is the Cas13 class 2, type VI protein (including Cas13a and Cas13b). Unlike most CRISPR/Cas systems, Cas13 lacks a DNAase motif but contains two RNAase domains (HEPN). RNA manipulations are advantageous over DNA editing because they prevent unwanted pleiotropic effects, and RNA products can be precisely and spatially regulated (Robertson et al., 2022; Sharma et al., 2022). According to the Abudayyeh et al. research, Cas13 cleaves only target RNA molecules and can cleave ssRNA molecules containing sites homologous to cRNA, while, like Cas12a, Cas13 does not need tracrRNA and depends only on cRNA (Abudayyeh et al., 2017). Since most plant viruses contain RNAi genomes, this research opens up new technological possibilities for combating plant viruses. Another widely used RNA editing nuclease is FnCas9 from *Francisella novicida* (Price et al., 2015). This enzyme also works with guide 23 RNA and targets endogenous RNA *in vivo*. However, unlike Cas13, this protein does not contain HEPN domains. It has been suggested that FnCas9 may either recruit endogenous RNAases to cleave the target RNA or possess alternative domains with endonucleolytic activity (Robertson et al., 2022). Like Cas13, FnCas9 has been reprogrammed to target and inhibit RNA-containing human and plant viruses by blocking viral RNA translation and replication (Price et al., 2015; Zhang et al., 2018). Most research on the direct use of the CRISPR/Cas system has been performed on viruses belonging to the family *Geminiviridae*, which cause significant yield losses in economically important crops. The first experiments on CRISPR-mediated resistance to geminiviruses were carried out on the beet severe curly top virus (BSCTV, genus *Curtovirus*) and the bean yellow dwarf virus (BeYDV; genus *Mastervirus*) in *Nicotiana benthamiana* and *Arabidopsis thaliana* plants (Baltes et al., 2014). CRISPR/Cas9 constructs (including kgRNA and Cas9) were targeted to cut coding (such as the replication-related protein gene [Rep]) and non-coding regions in viral genomes (such as Rep binding sites) and an invariant non-coding sequence, the nanonucleotide [TAATATTAC], common to all geminiviruses, contained in the intergenic region [IR]. Plants were transfected with the obtained constructs, and it was shown that the transgenic plants showed a high level of resistance to the target virus, which is manifested by a decrease (up to 87%) in virus accumulation and a reduction of symptom manifestation (Baltes et al., 2014). Zhan et al. showed that the CRISPR/Cas13a system effectively provides a wide range of resistance in transgenic potato plants to potato virus Y (PVY) strains (Zhan et al., 2019). Also, studies by Zhao showed that the LshCas13a system can degrade viral RNA genomes and confer resistance to the RNA virus in monocotyledonous grain plants (Zhao et al., 2020). Transgenic rice plants carrying the CRISPR/Cas13a system were created with three sgRNAs, each targeting the RNA genomes of southern rice black-streaked dwarf virus (SRBSDV) and rice stripe mosaic virus (RSMV). The study confirmed the suppression of viral infection in transgenic rice plants, indicating that CRISPR/Cas13a can also effectively target viral RNA in monocotyledonous plants.

The advantages of this technology include that by working precisely at the gene level, it is possible to bypass the problems of "genetic modification" because genome editing occurs without integrating foreign DNA or RNA into the host genome. Moreover, this method is simple and versatile when compared to other modern breeding technologies (Robertson et al., 2022). Unlike genetically modified organisms, CRISPR/Cas changes the existing genome without introducing foreign genes, particularly site-directed nucleases (SDN1 and SDN2). Consequently, varieties obtained using CRISPR/Cas are expected to be transgenic-free, and biosafety issues will be eliminated. The creation of next-generation systems characterizes the current stage of development of CRISPR methods such as CRISPR-MAD7 and CAS12A nucleases, increasing accuracy, range of possibilities, and applications. The efficiency of the CRISPR-MAD7 system has been proven on mutant rice and wheat plants at 65.6% (Silva and Fontes, 2022). Using MAD7 expands the CRISPR genome-editing toolkit because of its highly efficient target for gene disruption and insertion. According to (Silva and Fontes, 2022), using the new CRISPR/CAS systems (CAS3, CAS12, CAS13, and CAS14) as

multiplexed SGRNAs by targeting them to different sites is a new and more effective strategy for increasing resistance to a wide range of viral infections and disease control in the field.

2.3 Culture of apical meristems to eliminate the virus

One of the main methods used for recovering virus-infected plants is the method of apical meristems. This method uses the apical virus-free zone to obtain an initial healthy plant, which serves as the progenitor of the starting material for primary potato seed production. The effectiveness of this method has been repeatedly confirmed for many plant crops (Bi et al., 2018; Zhang et al., 2019). Many valuable potato varieties have been renewed and used in production for a long time. Potato yields have increased by more than 42% with the implementation of this method (Galeev et al., 2018). An apical meristem is a group of meristematic (formative) cells organized into a growth center, which occupy the terminal position in a shoot or root and form all organs and primary tissues. The upper part of the apical meristem is represented by initials, which are a single cell in horsetails, many ferns, and a multicellular structure in seed plants. The nearest derivatives of the initial cells are often distinguished in the protomeristem zone. There are currently several hypotheses about the reasons for the absence of viral infection in the apical meristem, which are provided below.

1. The absence of a conductive system in the apex slows the spread of viruses from cell to cell. The growth of the apical meristem is faster than viral propagation.
2. The high concentration of auxins in the apex excludes the possibility of virus replication.
3. There are mechanical barriers to the viral infection advancement into the meristematic zone due to the small size of the plasmodesmata.

The apical meristems of the seedlings are isolated at 12–13 plastochrone, which is the time interval between the initiations of two leaf tubercles. Isolated meristems are cultured under aseptic conditions on nutrient media rich in macro-salts and micro-salts with an increased concentration of cytokinins (6-BAP 2 mg/L). The temperature was maintained at 25°C ± 2°C in an air-conditioned culture room, which included 70% humidity, 5 klx illumination, and a photoperiod of 16 h. A small part of the 0.15- to 0.5-mm meristem is usually planted on the nutrient media. The general pattern is provided next. The smaller the size of the meristem, the more likely virus-free plants are obtained. It is isolated under sterile conditions of a laminar box under the magnification of a binocular microscope. On average, 30–45 days pass from planting the meristem on a medium to forming seedlings with five to six leaves, which sometimes takes 2 to 8 months. The media are renewed as they are depleted, and the seedlings are periodically transplanted to new media under sterile conditions. The disadvantages of this method include the difficulty of obtaining the initial virus-free material. The peculiarities of the apical meristem method consist of the complexity of the regeneration of meristems that are 0.1 mm in size. Their engraftment and regenerative ability increase when the size of the meristems increases, but the risk of viruses being present also increases (Moses et al., 2017). It is necessary at this stage to increase the method's effectiveness and suppress the viral pathogenesis in a larger area of the meristem. According to some experts, it is also advisable to use additional procedures, such as treatment with UHF rays with a narrow-band laser as well as thermotherapy, cryotherapy, and chemotherapy (Zhao et al., 2018; Wang et al., 2021; Bettoni et al., 2022).

2.4 Thermotherapy method

The thermotherapy method, which includes heating without lighting, was conducted on the potato tubers and microplants. Exposure modes may vary depending on the varietal characteristics. The efficiency of rehabilitation during the thermal treatment of the potato microplants is 2.4 times higher than for the same method for tubers (Oves and Gaytova, 2016). According to the research by Wang et al. (2021), *in vitro* cultured shallot shoots infected with onion yellow dwarf virus (OYDV) and shallot latent virus (SLV) were thermo-treated at a constant temperature of 36°C for 0, 2, and 4 weeks. The meristems (0.5 mm) that contain one to two leaf primordia were then excised and cultured for shoot regrowth. The meristem culture with thermotherapy produced much higher virus-free plants, which included 70% for OYDV, 80% for SLV, and 50% for both viruses (Wang et al., 2021). Bi et al. (2018) described a droplet-vitrification cryotherapy method for eradicating grapevine leafroll-associated virus-3 (GLRaV-3) from *Vitis* plants' diseased *in vitro* shoots. All the plants recovered after cryotherapy and were free of GLRaV-3 in two wines, which included one table and one rootstock cultivar *Vitis* spp (Bi et al., 2018).

2.5 Method of chemotherapy

The chemotherapy method is based on adding broad-spectrum antiviral drugs, such as virazole, to the nutrient medium where the plant explants are cultivated. The experimental results showed the effectiveness of virazole and amixin for inhibition (78.2%). The high antiviral activity of this drug was found in different cultures, such as against *Odonotoglossum cymbidium* ringspot virus and rose mosaic viruses, but its pronounced toxic effect, which inhibits the differentiation and proliferation processes in plant tissue culture *in vitro*, was also revealed. Substances that are capable of inactivating several viruses have been identified. Particular success in this direction was obtained on potatoes, tobacco, tomatoes, narcissus, and tulips (Sochacki and Podwyszyńska, 2012; Bettoni et al., 2022). Ryabtseva et al. (2015) discovered that for the recovery of the potatoes' *in vitro* culture, the following virus inhibitors

showed a high efficiency, which included chitosan with a dose between 0.1% and 0.01%, interferon with a dose between 0.05% and 0.1%, and virazole with a dose of 0.01%. The percentage of the plants that recovered from viruses was from 25% to 100%, which depended on the variety (Ryabtseva et al., 2015).

The yield of healthy plant regenerants compared to the control was higher by 14.3%–50.0% when antiviral medications, such as interferon, Kagocel, and Arbidol, were used in the nutrient medium in the amount of 50 mg/L. This was revealed in a study on the effect of antiviral drugs in *in vitro* culture on the yield of viable plant explants (Yalovik et al., 2019). Virus inhibitors include chemical nature malonic, oxalic, ascorbic, nucleic acids, antibiotics, gibberellin, heteroauxin, malachite green dye, methylene blue dye, safronin dye, alkalis, formaldehyde, urea, and the salts of heavy metals. The inhibitors of plant viruses were also found in the leaves of currants, forest strawberries, raspberries, pelargonium, parsley, wormwood, apples, cherries, maple, linden, and beets (Anikina and Seitzhanova, 2015). Several groups of synthetic antiviral compounds have also been identified. Most of them are analogs of bases and nucleosides, and their metabolites, such as the purine base derivative 8-azaguanine, which inhibits TMV, PVX, PVY, and 1-β-D-ribofuranosyl-1,2,4-triazole-3-carboxamide (ribavirin), are also active against numerous plant viruses, such as TMV, PVX, and CMV. Their action is based on the inhibition of viral genome replication. Representatives of pyrimidine-like compounds include 2-thiouracil and 5-azadihydrouracil. They inhibit the reproduction of viruses TMV, PVX, PVY, and CMV by inhibiting the biosynthesis of uridine-5-phosphate from orotidine-5′-phosphate by decarboxylase inhibition (Kumar et al., 2001; Sharipova et al., 2013).

The effectiveness of virocides has also been proven with outdoor plant treatments. The limiting factor is the phytotoxicity of virocides and the teratogenic effect of some virocides (Maksimov et al., 2019). In addition, there are still questions about the mutagenic effect of antiviral drugs, and their use also requires control of the identity of the material (Ryabtseva et al., 2015). Both thermotherapy and chemotherapy methods are used as auxiliary tools of the apical meristem method in *in vitro* culture. These methods essentially represent a single biotechnological complex method of plant virus recovery. This method is widely used worldwide, and different plant species have been revitalized with its help (Alam et al., 2013; Moses et al., 2017; Wang et al., 2021). Significant disadvantages of the tissue culture-based rehabilitation method include the possibility of self-clonal variations. These types of plants can deviate from the original variety with their morphological traits and properties, which means that they lose varietal individuality. This is a serious risk for primary seed production because the valuable economic traits of the cultivated variety are still under consideration, and they obtain mutants that they may not have (Oves and Gaytova, 2016; Antonova et al., 2017; Kesiraju and Sreevathsa, 2017). The researchers concluded that regular control of the material for identity is required during the long-term cultivation of plants in the tissue culture. The search for a solution to this problem has led some researchers to propose complementing the apical meristem method with the clonal selection or verifying the genetic identity of the regenerated plants *in vitro* using random amplification of polymorphic DNA (RAPD) (Evstratova et al., 2018). In addition, the cured potatoes can quickly be reinfected in the field.

3 Methods of combating viruses in the field

Virus reservoirs can be weeds along the field edges, birds and insects that travel long distances, and viruses, which can also be transmitted *via* service aggregates. Preventive measures, such as spatial isolation and insecticidal and stimulant treatments, are essential to controlling the spread of plant viruses (Tian and Valkonen, 2013; Wasilewska-Nascimento et al., 2020). These medicines have become important economic factors in regard to increasing the profitability and eco-friendliness of production. They have a beneficial effect on plant product growth, development, yield, and quality, but they are also inducers of resistance to abiotic stress factors and various phytopathogens, which include viruses (Palukaitis et al., 2017). The research for biosafe means of controlling phytopathogens is relevant in light of the increased attention to the ecologization of agricultural crop production. The search for opportunities to stimulate the immune system of plants and build a plant protection system based on pesticide application as well as on the reserve possibilities of the organism itself is essential, which open up new prospects for the development of biotechnology (Maksimov et al., 2019).

Nucleotide-binding proteins with leucine-rich repeats (NLRs), which recognize intracellular proteins of pathogenic origin, often control immune responses to pathogens in plant organisms. Genetic resistance to plant viruses is often phenotypically characterized by programmed cell death at or near the site of infection, which is a hypersensitive reaction. New approaches in order to control viral pathogens are urgently needed (Akhter et al., 2021). One type of approach is plant immunization, which is a process of activating the body's natural defense systems. The possibilities of increasing plant resistance by stimulating their immune system have expanded, which results from the in-depth study of the molecular and genetic bases of plant resistance to viruses and the investigation of the mechanisms of induction of the defense reactions in the plant organism. The key role in the induction of immunity belongs to different substances, which are called elicitors.

The biological immunization of plants involves treating them with weakened cultures of pathogens, non-pathogens, or their metabolites (Kothari and Patel, 2004; Dyakov et al., 2007). Chemical immunization is based on using substances called elicitors, resistance inducers, activators, or immunomodulators, which activate the defense reactions. A cascade of defense reactions is triggered in plants under the action of these drugs, and chemical and physical barriers are formed that prevent pathogen development. Inducers typically send excitatory signals to plant defense genes, which activate a cascade of defense responses and ultimately induced systemic resistance (Calil and Fontes, 2017;

Beris et al., 2018). Elicitors were associated with the induction of phytoalexin synthesis at the beginning of these types of studies, but further studies revealed other protective responses of plants that expanded the list of compounds under the influence of how plants trigger their defense mechanisms (Poliksenova, 2009). Biologically active substances have different characteristics, and many of them are plant growth regulators, which act as elicitors.

Zircon is among the medicines with high elicitor activity, which is obtained based on the plant material of *Echinacea purpurea*. Zircon's efficiency has been proven both as a growth stimulator and as a resistance inducer against various types of diseases, which include viral diseases (Malevannay, 2001). The zircon phytoregulator exhibited an antiviral effect on potato *in vitro* plants when introduced into a Murashige and Skoog culture medium. The application of a zircon phytoregulator at a dose of 0.25 ml/L on potato *in vitro* plants reduced the development of the PVY virus by 10%–70%, which depended on the variety. We show that chlormequat chloride in the Murashige and Skoog culture medium at a dose of 0.3 ml/L exhibited antiviral activity when the antiviral action of the growth regulator chlormequat chloride ($C_5H_{13}Cl_2N$) was analyzed, which belongs to the group of retardants. The percentage of regenerants that are affected by the potato Y virus decreased from 14% to 37.5%, which depended on the variety (Anikina and Seitzhanova, 2015).

The study of the action of plant polyphenols and flavonoids revealed their high effectiveness in suppressing plant virus infection, particularly with the tobacco mosaic virus, the apple stem borer virus, the tomato spot nepovirus, and the potato X-virus (Chojnacka et al., 2021). Evstratova et al. (2018) showed the high elicitor activity of chitosan-based medicine against the potato Y virus (Evstratova et al., 2018). The search for biologically active substances (BASs) that are capable of stimulating plant immune system mechanisms has significantly increased (Prasad and Srivastava, 2017; Gupta AK. et al., 2021). Mandal (2010) investigated the resistance of eggplant under the action of four elicitors, which included salicylic acid, chitosan, methyl salicylate, and methyl jasmonate. The effect of the elicitors resulted in a threefold to fivefold increase in the accumulation of phenols and lignin in the tissues in addition to an increase in the activity level of the main protective enzymes phenylalanine ammonia-lyase peroxidase, polyphenol oxidase, cinnamic alcohol dehydrogenase, and catalase several times, which certainly contribute to the plant's resistance to pathogens (Mandal, 2010). The effectiveness of the steroid glycoside compounds against the tobacco mosaic virus has in particular been illustrated. It was discovered that steroidal glycosides act comprehensively, and under their action *in vitro*, the infectivity of the virus is reduced, and the particle structure and antigenic properties are not violated. They have an elicitor effect on the host plant metabolism. At the same time, RNAase is activated, the formation of new proteins is induced, and the cell ultrastructure is stabilized. Other researchers also confirmed the effectiveness of steroidal glycosides as immunomodulators that increase plant resistance to phytopathogenic viruses (Poliksenova, 2009).

The use of microbial inoculants to induce systemic resistance against viral diseases is of great interest. The researchers showed the high bioprotective potential of microbial inoculants, which included *Pseudomonas fluorescens* and *Bacillus* sp. isolated from banana roots, against the banana virus disease, which was caused by the banana bunchy top virus (BBTV). The banana plants were inoculated with *P. fluorescens* Pf1 and CHA0 strains in combination with endophytic bacterial strains EPB5 and EPB22 (Pf1 + CHA0EP + B5 + EPB22). These plants showed a 60% reduction in the BBTV virus infection compared to untreated plants when grown in soil (Nowak and Shulaev, 2003).

Maksimov et al. (2019) showed that the isolates of *Pseudomonas* spp., which included *P. fluorescens*, *Pseudomonas putida*, *Pseudomonas aeruginosa*, *Pseudomonas taiwanensis*, and *Bacillus* spp., contributed to the protection of papaya plants against the ringspot virus (PRSV). According to studies by Maksimov et al. (2019), the preparation of Phytosporin-M based on *Bacillus subtilis* 26D also showed a high efficiency for plant protection against viral diseases, and the activity of these microorganisms was confirmed against a wide range of diseases, which included bacterial, fungal, and viral ones.

According to Maximov, the biocidal activity of rhizosphere and endophytic bacteria suggests that it indirectly exhibits antiviral activity due to their production of antibiotic substances. Hence, phytopathogenic bacteria, fungi, nematodes, and insect pests can be vectors-transporters of many plant viral infections. One promising approach to creating new antiviral drugs is to use strains of microorganisms with obvious insecticidal or other biocidal effects to control virus vectors. An isolate of *B. subtilis* BS3A25 and its culture filtrate inhibited the development of cucumber mosaic virus in tomato plants by inhibiting the development of the melon aphid *Aphis gossypii*, which is a vector of this disease that may be related to oxidation of surfactants that are produced by the bacteria (Rodríguez et al., 2018) and to the activation of the plant defense mechanisms against the insect and/or the virus that is under the influence of the bacteria (Maksimov et al., 2019). The colonization of internal onion tissues by the endophytic fungus *Hypocrea lixii* (F3ST1) significantly reduced the titer of iris yellow spot virus (IYSV) particles in plants, which reduced their damage by its main transmitter, which is called *Thrips tabaci* Lind (Muvea et al., 2018).

Bettoni et al. (2022) showed high effectiveness in regard to treating potatoes with arachidonic acid against *Phytophthora* and scab as well as against viruses X and M. It is promising to use preparations that are based on bacterial enzymes as elicitors. They became available after the success of genetic engineering in regard to creating highly productive strain producers. Diener (1961) established the antiviral activity of ribonucleases against RNA viruses and showed that the treatment of potato regenerants with RNase resulted in the inactivation of potato virus X and the tobacco mosaic virus in cucumbers.

Using elicitors to control viruses in agricultural plantings is a promising, affordable, and environmentally friendly method of viral disease control. Induced systemic resistance solves many problems with agricultural crop production. It is environmentally friendly and biosafe compared to biocides because it activates the natural plant's defense mechanisms and is simultaneously effective against different phytopathogens under field conditions (Maksimov et al., 2019). The attractiveness of this direction is obvious because preparations with bioregulatory activity are used as immunomodulators, which induce

the protective responses of the plant organism as well as positively affect the yield and quality indicators of plants. The search for virus inhibitors among the preparations with biological activity is of particular practical interest for potato producers because it will greatly simplify the task of obtaining healthy material for seed production (Acharya, 2013; Calil and Fontes, 2017; Somalraju et al., 2022). The proposed approaches for plant protection from phytoviruses are generalized in Table 3.

4 Conclusions and future perspectives

Viral infection in plants is a complex and interdependent process. Viruses are breeding programs to create virus-resistant forms based on genome editing, using the marker-mediated selection method, which makes it possible to evaluate the genetic protection of a variety and use RNA silencing as an important antiviral mechanism. The disadvantages of genetically engineered approaches include that the gained resistance is often specific and short-lived, and there is a problem with "gene silencing". A negative factor of growing genetically changed plants resistant to certain viruses is the possible redistribution of virus species structure, which can provoke the spread of other harmful viral infections. The apical meristem method, combined with other auxiliary methods (thermotherapy and chemotherapy) during the last 50 years, has been the basis for controlling harmful plant viruses. Significant disadvantages of the practice of health improvement based on tissue culture include the possibility of auto-clonal variations because of long-term cultivation of plants under *in vitro* conditions, which are mutant plants genetically different from the original variety. In addition, this technique does not guarantee against rapid reinfection of diseased material under field conditions.

The use of virus inhibitors and elicitors is most justified in the field. At present, several groups of synthetic antiviral compounds have been identified. The efficacy of virocides has been proven in outdoor plant treatments. A limiting factor is the phytotoxicity of virocides, and also the teratogenic effect of some virocides concerning humans has been revealed. Using elicitors to control viruses in agricultural plantings is a promising, affordable, and environmentally friendly approach to preventing viral diseases. Induced systemic resistance is environmentally friendly and biosafe when compared to biocides because it activates natural plant defense mechanisms and is effective simultaneously against different phytopathogens under field conditions. The disadvantages of the method include insufficiently high efficiency. Vector control is a well-known method for preventing the spread of viral infection. The limitations, in this case, are low efficiency and high costs. In

TABLE 3 The proposed approaches to plant protection from phytoviruses.

S. no.	Method	Source
1	Genome editing to combat virus infection	(Shan et al., 2013; Baltes et al., 2014; Price et al., 2015; Abudayyeh et al., 2017; Wolter and Puchta, 2018; Zhang et al., 2018; Zhan et al., 2019; Ahmad et al., 2020; Nussenzweig and Marraffini, 2020; Zhao et al., 2020; Nidhi et al., 2021; Hofvander et al., 2022; Kavuri et al., 2022; Robertson et al., 2022; Sharma et al., 2022; Silva and Fontes, 2022; Tiwari et al., 2022)
2	Apical meristem method	(Zhu-Jun et al., 2011; Hull, 2014; Anikina and Seitzhanova, 2015; Jin et al., 2016; Antonova et al., 2017; Galeev et al., 2018; Zhang et al., 2019)
3	Thermotherapy	(Wu et al., 2015; Oves and Gaytova, 2016; Wang et al., 2022)
4	Combination of thermotherapy methods and the method of apical meristems	(Wang et al., 2006; AlMaarri et al., 2012; Moses et al., 2017)
5	Cryotherapy	(Wang et al., 2006; Yi et al., 2014; Bi et al., 2018; Zhang et al., 2019)
6	Chemotherapy	(AlMaarri et al., 2012; Ryabtseva et al., 2015; Antonova et al., 2017; Yalovik et al., 2019; Bettoni et al., 2022)
7	Combination of thermotherapy and chemotherapy methods	(Fletcher et al., 1998; Yi Lan et al., 2005; Dhital et al., 2007; Nasir et al., 2010; Antonova et al., 2017)
8	Control of viruses vectors	(Jones, 2009; Hull, 2014; Calil and Fontes, 2017; Musidlak et al., 2017; Wei et al., 2018; Jones and Naidu, 2019; Batuman et al., 2020)
9	Creation of transgenic varieties with high resistance to viral diseases	(Rodríguez-Negrete et al., 2009; Sharipova et al., 2013; Wu et al., 2015; Hong and Ju, 2017; Kochetov and Shumny, 2017; Musidlak et al., 2017; Kourelis and van der Hoorn, 2018; Rodríguez et al., 2018; Tran et al., 2018; Yang and Li, 2018; Guo et al., 2019; Klimenko et al., 2019; Lolle et al., 2020; Akhter et al., 2021; Ross et al., 2021; Zhao et al., 2021; Bwalya et al., 2022; Li and Wang, 2022; Lopez-Gomollon and Baulcombe, 2022; Sáez et al., 2022; Liu et al., 2023)
10	Plant immunization	(Kothari and Patel, 2004; Dyakov et al., 2007; Calil and Fontes, 2017; Liu et al., 2017; Beris et al., 2018)
11	The use of biologically active preparations that suppress a viral infection	(French and Towers, 1992; Malhotra et al., 1996; Orazov and Nikitina, 2009; Mandal, 2010; Acharya, 2013; Alazem and Lin, 2017; Prasad and Srivastava, 2017; Maksimov et al., 2019; Chojnacka et al., 2021; Gupta AK. et al., 2021)

addition, considerable damage has been inflicted to the ecology. An alternative direction is the agroecosystem approach based on the study of aspects of multitrophic interactions where the activity of microbial strains with clear insecticidal or other biocidal effects is used to control vector-borne viruses. The antiviral effectiveness of drugs based on microbial enzymes has also been shown. The disadvantages of using microbial preparations include low efficacy. As shown in the literature review, the existing methods of phytovirus control are ambiguous. Further research is needed into plant resistance mechanisms, including the molecular interaction between the host and viral factors. Further study of genetic, biochemical, and physiological features of viral pathogenesis and the development of a strategy for increasing plant resistance to viruses will allow a new level of control of phytovirus infection to be achieved.

Author contributions

All authors listed have made a substantial, direct, and intellectual contribution to the work and approved it for publication.

Funding

This research was funded by Project Erasmus+ (no. 609563-EPP-1-2019-1-DE-EPPKA2-CBHE-JP).

Conflict of interest

The authors declare that the research was conducted in the absence of any commercial or financial relationships that could be construed as a potential conflict of interest.

Publisher's note

All claims expressed in this article are solely those of the authors and do not necessarily represent those of their affiliated organizations, or those of the publisher, the editors and the reviewers. Any product that may be evaluated in this article, or claim that may be made by its manufacturer, is not guaranteed or endorsed by the publisher.

References

Abudayyeh, O. O., Gootenberg, J. S., Essletzbichler, P., Han, S., Joung, J., Belanto, J. J., et al. (2017). RNA Targeting with CRISPR–Cas13. *Nature* 550 (7675), 280–284. doi: 10.1038/nature24049

Acharya, S. (2013). Control of the potato virus X through application of root extracts of chlorophytum nepalense to potato plants and tubers. *Potato Res.* 56 (1), 1–10. doi: 10.1007/s11540-012-9227-4

Adolf, B., Andrade-Piedra, J., Bittara Molina, F., Przetakiewicz, J., Hausladen, H., Kromann, P., et al. (2020). "Fungal, oomycete, and plasmodiophorid diseases of potato," in *The potato crop* (Cham: Springer), 307–350.

Ahmad, S., Wei, X., Sheng, Z., Hu, P., and Tang, S. (2020). CRISPR/Cas9 for development of disease resistance in plants: recent progress, limitations and future prospects. *Briefings Funct. Genomics* 19 (1), 26–39. doi: 10.1093/bfgp/elz041

Akbar, S., Yao, W., Qin, L., Yuan, Y., Powell, C. A., Chen, B., et al. (2021). Comparative analysis of sugar metabolites and their transporters in sugarcane following sugarcane mosaic virus (SCMV) infection. *Int. J. Mol. Sci.* 22 (24), 13574. doi: 10.3390/ijms222413574

Akhter, M., Nakahara, K. S., and Masuta, C. (2021). Resistance induction based on the understanding of molecular interactions between plant viruses and host plants. *Virol. J.* 18 (1), 1–12. doi: 10.1186/s12985-021-01647-4

Alam, I., Sharmin, S. A., Naher, M., Alam, M., Anisuzzaman, M., and Alam, M. F. (2013). Elimination and detection of viruses in meristem-derived plantlets of sweetpotato as a low-cost option toward commercialization. *3 Biotech.* 3 (2), 153–164. doi: 10.1007/s13205-012-0080-6

Alazem, M., and Lin, N.-S. (2017). Antiviral roles of abscisic acid in plants [Review]. *Front. Plant Sci.* 8. doi: 10.3389/fpls.2017.01760

AlMaarri, K., Massa, R., and AlBiski, F. (2012). Evaluation of some therapies and meristem culture to eliminate potato y potyvirus from infected potato plants. *Plant Biotechnol.* 29 (3), 237–243. doi: 10.5511/plantbiotechnology.12.0215a

Alonso-Prados, J., Fraile, A., and Garcia-Arenal, F. (1997). Impact of cucumber mosaic virus and watermelon mosaic virus 2 infection on melon production in central Spain. *J. Plant Pathol.* 79 (2), 131–134. Available at: https://www.jstor.org/stable/41997879.

Anikina, I., and Seitzhanova, D. (2015). *Phytovirusology* (Pavlodar: Kereku), 104.

Antonova, O. Y., Apalikova, O., Ukhatova, Y. V., Krylova, E., Shuvalov, O. Y., Shuvalova, A., et al. (2017). Eradication of viruses in microplants of three cultivated potato species (Solanum tuberosum l., s. phureja juz. & buk., s. stenotomum juz. & buk.) using combined thermo-chemotherapy method. *Agric. Biol.* 52 (1), 95–104. doi: 10.15389/agrobiology.2017.1.95rus

Baltes, N. J., Gil-Humanes, J., Cermak, T., Atkins, P. A., and Voytas, D. F. (2014). DNA Replicons for plant genome engineering. *Plant Cell.* 26 (1), 151–163. doi: 10.1105/tpc.113.119792

Bari, R., and Jones, J. D. (2009). Role of plant hormones in plant defence responses. *Plant Mol. Biol.* 69, 473–488. doi: 10.1007/s11103-008-9435-0

Batuman, O., Turini, T. A., LeStrange, M., Stoddard, S., Miyao, G., Aegerter, B. J., et al. (2020). Development of an IPM strategy for thrips and tomato spotted wilt virus in processing tomatoes in the central valley of California. *Pathogens* 9 (8), 636. doi: 10.3390/pathogens9080636

Beris, D., Theologidis, I., Skandalis, N., and Vassilakos, N. (2018). Bacillus amyloliquefaciens strain MBI600 induces salicylic acid dependent resistance in tomato plants against tomato spotted wilt virus and potato virus y. *Sci. Rep.* 8 (1), 1–11. doi: 10.1038/s41598-018-28677-3

Bettoni, J. C., Mathew, L., Pathirana, R., Wiedow, C., Hunter, D. A., McLachlan, A., et al. (2022). Eradication of potato virus s, potato virus a, and potato virus m from infected *in vitro*-grown potato shoots using *in vitro* therapies. *Front. Plant Sci.* 13, 878733. doi: 10.3389/fpls.2022.878733

Bhattacharyya, D., Gnanasekaran, P., Kumar, R. K., Kushwaha, N. K., Sharma, V. K., Yusuf, M. A., et al. (2015). A geminivirus betasatellite damages the structural and functional integrity of chloroplasts leading to symptom formation and inhibition of photosynthesis. *J. Exp. botany.* 66 (19), 5881–5895. doi: 10.1093/jxb/erv299

Bi, W. L., Hao, X. Y., Cui, Z. H., Pathirana, R., Volk, G. M., and Wang, Q. C. (2018). Shoot tip cryotherapy for efficient eradication of grapevine leafroll-associated virus-3 from diseased grapevine *in vitro* plants. *Ann. Appl. Biol.* 173 (3), 261–270. doi: 10.1111/aab.12459

Bwalya, J., Alazem, M., and Kim, K.-H. (2022). Photosynthesis-related genes induce resistance against soybean mosaic virus: evidence for involvement of the RNA silencing pathway. *Mol. Plant Pathology.* 23 (4), 543–560. doi: 10.1111/mpp.13177

Calil, I. P., and Fontes, E. P. (2017). Plant immunity against viruses: antiviral immune receptors in focus. *Ann. Botany.* 119 (5), 711–723. doi: 10.1093/aob/mcw200

Chen, S., Li, W., Huang, X., Chen, B., Zhang, T., and Zhou, G. (2019). Symptoms and yield loss caused by rice stripe mosaic virus. *Virol. J.* 16 (1), 1–10. doi: 10.1186/s12985-019-1240-7

Chojnacka, K., Skrzypczak, D., Izydorczyk, G., Mikula, K., Szopa, D., and Witek-Krowiak, A. (2021). Antiviral properties of polyphenols from plants. *Foods* 10 (10), 2277. doi: 10.3390/foods10102277

Cisar, G., Brown, C., and Jedlinski, H. (1982). Effect of fall or spring infection and sources of tolerance of barley yellow dwarf of winter wheat 1. *Crop Science.* 22 (3), 474–478. doi: 10.2135/cropsci1982.0011183X002200030009x

Clark, C. A., Davis, J. A., Abad, J. A., Cuellar, W. J., Fuentes, S., Kreuze, J. F., et al. (2012). Sweetpotato viruses: 15 years of progress on understanding and managing complex diseases. *Plant disease.* 96 (2), 168–185. doi: 10.1094/PDIS-07-11-0550

Dhankhar, S. K. (2016). Genetic improvement of okra cultivars for Yellow vein mosaic virus disease resistance using a wild Abelmoschus species. *Acta Hortic.* 1127, 71–74. doi: 10.17660/ActaHortic.2016.1127.13

Dhital, S. P., Sakha, B. M., and Lim, H. T. (2007). Utilization of shoot cuttings for elimination of PLRV and PVY by thermotherapy and chemotherapy from potato (Solanum tuberosum l.). *Nepal J. Sci. Technol.* 7 (0), 1–6. doi: 10.3126/njst.v7i0.528

Diener, T. O. (1961). Virus infection and other factors affecting ribonuclease activity of plant leaves. *Virology* 14 (2), 177–189. doi: 10.1016/0042-6822(61)90193-3

Dyakov, Y. T., Dzhavakhiya, V., and Korpela, T. (2007). Molecular basis of plant immunization. *Compr. Mol. Phytopathology. Elsevier;*, 423–438. doi: 10.1016/B978-044452132-3/50020-1

Ershova, N., Sheshukova, E., Kamarova, K., Arifulin, E., Tashlitsky, V., Serebryakova, M., et al. (2022). Nicotiana benthamiana kunitz peptidase inhibitor-like protein involved in chloroplast-to-nucleus regulatory pathway in plant-virus interaction. *Front. Plant Sci.* 13, 1041867. doi: 10.3389/fpls.2022.1041867

Evstratova, L., Kuznetsova, L., Nikolaeva, E., and Evstratov, I. (2018). Combination of apical meristem and clonal selection in original potato seed production. *Sci. Notes Petrozavodsk State University.* 8 (177), 23–26. doi: 10.15393/uchz.art.2018.245

Farooq, T., Adeel, M., He, Z., Umar, M., Shakoor, N., da Silva, W., et al. (2021). Nanotechnology and plant viruses: an emerging disease management approach for resistant pathogens. *ACS Nano.* 15 (4), 6030–6037. doi: 10.1021/acsnano.0c10910

Fletcher, P. J., Fletcher, J. D., and Cross, R. J. (1998). Potato germplasm: in vitro storage and virus reduction. *New Z. J. Crop Hortic. Sci.* 26 (3), 249–252. doi: 10.1080/01140671.1998.9514060

French, C. J., and Towers, G. H. N. (1992). Inhibition of infectivity of potato virus X by flavonoids. *Phytochemistry* 31 (9), 3017–3020. doi: 10.1016/0031-9422(92)83438-5

Galeev, R. R., Vyshegurov, S. K., Demshina, V. S., Shulga, M. S., and Gumel, M. A. (2018). Efficiency of regenerating potato varieties by the apical meristem method. *J. Pharm. Sci. Res.* 10 (1), 124–128.

Gong, H., Igiraneza, C., and Dusengemungu, L. (2019). Major *in vitro* techniques for potato virus elimination and post eradication detection methods. a review. *Am. J. potato Res.* 96, 379–389. doi: 10.1007/s12230-019-09720-z

Guo, Z., Li, Y., and Ding, S.-W. (2019). Small RNA-based antimicrobial immunity. *Nat. Rev. Immunol.* 19 (1), 31–44. doi: 10.1038/s41577-018-0071-x

Gupta, N., Reddy, K., and Bhattacharyya, D. (2021). Plant responses to geminivirus infection: guardians of the plant immunity. *Virol. J.* 18 (1), 1–25. doi: 10.1186/s12985-021-01612-1

Gupta, A. K., Verma, J., Srivastava, A., Srivastava, S., and Prasad, V. (2021). A comparison of induced antiviral resistance by the phytoprotein CAP-34 and isolate P1f of the rhizobacterium pseudomonas putida. *3 Biotech.* 11 (12), 1–13. doi: 10.1007/s13205-021-03057-3

Handford, M. G., and Carr, J. P. (2007). A defect in carbohydrate metabolism ameliorates symptom severity in virus-infected arabidopsis thaliana. *J. Gen. Virol.* 88 (1), 337–341. doi: 10.1099/vir.0.82376-0

Hofvander, P., Andreasson, E., and Andersson, M. (2022). Potato trait development going fast-forward with genome editing. *Trends Genet.* 38 (3), 218–221. doi: 10.1016/j.tig.2021.10.004

Hong, J. S., and Ju, H. J. (2017). The plant cellular systems for plant virus movement. *Plant Pathol. J.* 33 (3), 213–228. doi: 10.5423/PPJ.RW.09.2016.0198

Hossain, M., Akanda, A., and Hossain, M. (2011). Effect of tomato yellow leaf curl virus (tylcv) on plant growth and yield contributing characters of sixsteen tomato varieteis. *Arab. J. Plant Prot.* 39 (1), 79–83. doi: 10.22268/AJPP-039.1.079083

Hull, R. (2014). *Plant virology. 5th Edition* (London: Academic Press), 854. Available at: https://www.elsevier.com/books/plant-virology/hull/978-0-12-384871-0.

Islam, W., Naveed, H., Zaynab, M., Huang, Z., and Chen, H. Y. (2019). Plant defense against virus diseases; growth hormones in highlights. *Plant Signal. Behav.* 14 (6), 1596719. doi: 10.1080/15592324.2019.1596719

Jin, L., Qin, Q., Wang, Y., Pu, Y., Liu, L., Wen, X., et al. (2016). Rice dwarf virus P2 protein hijacks auxin signaling by directly targeting the rice OsIAA10 protein, enhancing viral infection and disease development. *PloS Pathog.* 12 (9), e1005847. doi: 10.1371/journal.ppat.1005847

Jones, R. A. (2009). Plant virus emergence and evolution: origins, new encounter scenarios, factors driving emergence, effects of changing world conditions, and prospects for control. *Virus Res.* 141 (2), 113–130. doi: 10.1016/j.virusres.2008.07.028

Jones, R. A., and Naidu, R. A. (2019). Global dimensions of plant virus diseases: current status and future perspectives. *Annu. Rev. Virol.* 6, 387–409. doi: 10.1146/annurev-virology-092818-015606

Kavuri, N. R., Ramasamy, M., Qi, Y., and Mandadi, K. (2022). Applications of CRISPR/Cas13-based RNA editing in plants. *Cells* 11 (17), 2665. doi: 10.3390/cells11172665

Kesiraju, K., and Sreevathsa, R. (2017). Apical meristem-targeted in planta transformation strategy: an overview on its utility in crop improvement. *Agri Res. Technol. Open Access J.* 8 (555734), 19080. doi: 10.19080/ARTOAJ.2017.08.555734

Klimenko, N., Antonova, O. Y., Zheltova, V., Fomina, N., Kostina, L., Mamadbokirova, F., et al. (2019). Screening of Russian potato cultivars (Solanum tuberosum l.) with DNA markers linked to the genes conferring extreme resistance to potato virus y. *Sel'skokhozyaistvennaya Biologiya* 54 (5), 958–969. doi: 10.15389/agrobiology.2019.5.958eng

Kochetov, A., and Shumny, V. (2017). Transgenic plants as genetic models for studying functions of plant genes. *Russian J. Genetics: Appl. Res.* 7 (4), 421–427. doi: 10.1134/S2079059717040050

Kothari, I. L., and Patel, M. (2004). Plant immunization [Review]. *Indian J. Exp. Biol.* 42 (3), 244–252. Available at: http://nopr.niscpr.res.in/handle/123456789/23379.

Kourelis, J., and van der Hoorn, R. A. L. (2018). Defended to the nines: 25 years of resistance gene cloning identifies nine mechanisms for r protein function. *Plant Cell.* 30 (2), 285–299. doi: 10.1105/tpc.17.00579

Kreuze, J. F., Souza-Dias, J. A. C., Jeevalatha, A., Figueira, A. R., Valkonen, J. P. T., and Jones, R. A. C. (2020). "Viral diseases in potato," in *The potato crop: its agricultural, nutritional and social contribution to humankind*. Eds. H. Campos and O. Ortiz (Cham: Springer International Publishing), 389–430.

Kumar, R., Sharma, N., Nath, M., Saffran, H. A., and Tyrrell, D. L. J. (2001). Synthesis and antiviral activity of novel acyclic nucleoside analogues of 5-(1-azido-2-haloethyl) uracils. *J. medicinal Chem.* 44 (24), 4225–4229. doi: 10.1021/jm010227k

Li, F., and Wang, A. (2022). Transient expression–mediated gene silencing in plants and suppression of gene silencing with viral suppressors. *Plant Virol. Springer;* 2400, 33–41. doi: 10.1007/978-1-0716-1835-6_4

Liu, J.-Z., Li, F., and Liu, Y. (2017). Editorial: plant immunity against viruses [Editorial]. *Front. Microbiol.* 8. doi: 10.3389/fmicb.2017.00520

Liu, W., Zhang, Z., Li, Y., Zhu, L., and Jiang, L. (2023). Efficient production of d-tagatose via DNA scaffold mediated oxidoreductases assembly in vivo from whey powder. *Food Res. Int.* 166, 112637. doi: 10.1016/j.foodres.2023.112637

Lolle, S., Stevens, D., and Coaker, G. (2020). Plant NLR-triggered immunity: from receptor activation to downstream signaling. *Curr. Opin. Immunol.* 62, 99–105. doi: 10.1016/j.coi.2019.12.007

Lopez-Gomollon, S., and Baulcombe, D. C. (2022). Roles of RNA silencing in viral and non-viral plant immunity and in the crosstalk between disease resistance systems. *Nat. Rev. Mol. Cell Biol.* 23 (10), 645–662. doi: 10.1038/s41580-022-00496-5

Lu, L., Zhai, X., Li, X., Wang, S., Zhang, L., Wang, L., et al (2022). Met1-specific motifs conserved in OTUB subfamily of green plants enable rice OTUB1 to hydrolyse Met1 ubiquitin chains. *Nat. Commun.* 13 (1), 4672. doi: 10.1038/s41467-022-32364-3

Ma, S., Wang, R., Gao, R., Wang, X., Liu, Y., Li, Y, et al. (2022). Antiviral spirooliganones C and D with a unique spiro [bicyclo [2.2. 2] octane-2, 2′-bicyclo [3.1. 0] hexane] carbon skeleton from the roots of Illicium oligandrum. *Chin. Chem. Lett.* 33 (9), 4248–4252. doi: 10.1016/j.cclet.2022.02.050

Maksimov, I., Sorokan, A., Burkhanova, G., Veselova, S., Alekseev, V., Shein, M., et al. (2019). Mechanisms of plant tolerance to RNA viruses induced by plant-growth-promoting microorganisms. *Plants* 8 (12), 575. doi: 10.3390/plants8120575

Malevannay, N. (2001). The explosive temperament of zircon in the service of plants. *New Gardener Farmer.* 1, 45.

Malhotra, B., Onyilagha, J. C., Bohm, B. A., Towers, G. H. N., James, D., Harborne, J. B., et al. (1996). Inhibition of tomato ringspot virus by flavonoids. *Phytochemistry* 43 (6), 1271–1276. doi: 10.1016/S0031-9422(95)00522-6

Mandal, S. (2010). Induction of phenolics, lignin and key defense enzymes in eggplant (Solanum melongena l.) roots in response to elicitors. *Afr. J. Biotechnol.* 9 (47), 8038–8047. doi: 10.5897/AJB10.984

Mishra, GP, Singh, B, Seth, T, Singh, AK, Halder, J, Krishnan, N, et al (2017). Biotechnological Advancements and Begomovirus Management in Okra (Abelmoschus esculentus L.): Status and Perspectives. *Front. Plant Sci.* 8, 360. doi: 10.3389/fpls.2017.00360

Moses, W., Rogers, K., and Mildred, O.-S. (2017). Effect of thermotherapy duration, virus type and cultivar interactions on elimination of potato viruses X and s in infected seed stocks. *Afr. J. Plant Sci.* 11 (3), 61–70. doi: 10.5897/AJPS2016.1497

Mumford, R., Macarthur, R., and Boonham, N. (2016). The role and challenges of new diagnostic technology in plant biosecurity. *Food Secur.* 8 (1), 103–109. doi: 10.1007/s12571-015-0533-y

Musidlak, O., Nawrot, R., and Goździcka-Józefiak, A. (2017). Which plant proteins are involved in antiviral defense? review on *In vivo* and *In vitro* activities of selected plant proteins against viruses. *Int. J. Mol. Sci.* 18 (11), 2300. doi: 10.3390/ijms18112300

Muvea, A. M., Subramanian, S., Maniania, N. K., Poehling, H.-M., Ekesi, S., and Meyhöfer, R. (2018). Endophytic colonization of onions induces resistance against viruliferous thrips and virus replication. *Front. Plant Sci.* 9. doi: 10.3389/fpls.2018.01785

Mwanga, R., Moyer, J., Zhang, D., Carey, E., and Yencho, G. (2001). Nature of resistance of sweetpotato to sweetpotato virus disease. I international conference on sweetpotato. *Food Health Future* 583, 113–119. doi: 10.17660/ActaHortic.2002.583.12

Nasir, I. A., Tabassum, B., Latif, Z., Javed, M. A., Haider, M. S., Javed, M. A., et al. (2010). Strategies to control potato virus y under in vitro conditions. *Pakistan J. Phytopathol.* 22 (1), 63–70.

Nidhi, S., Anand, U., Oleksak, P., Tripathi, P., Lal, J. A., Thomas, G., et al. (2021). Novel CRISPR–cas systems: an updated review of the current achievements, applications, and future research perspectives. *Int. J. Mol. Sci.* 22 (7), 3327. doi: 10.3390/ijms22073327

Nowak, J., and Shulaev, V. (2003). Priming for transplant stress resistance in in vitro propagation. *In Vitro Cell. Dev. Biol. - Plant* 39 (2), 107–124. doi: 10.1079/ivp2002403

Nussenzweig, P. M., and Marraffini, L. A. (2020). Molecular mechanisms of CRISPR-cas immunity in bacteria. *Annu. Rev. Genet.* 54, 93–120. doi: 10.1146/annurev-genet-022120-112523

Orazov, O., and Nikitina, V. (2009). Development of the cucumber plants infected by tobacco mosaic virus after their treatment by flavonoid-bearing concentrates. *Agric. Biol.* 1, 93–98.

Oves, E., and Gaytova, N. (2016). New elements in technology of improvement and obtaining of basic potato clones of promising cultivars and hybrids. *Achievements Sci. Technol. Agro - Ind. Complex.* 30 (11), 60–62.

Palukaitis, P., Yoon, J.-Y., Choi, S.-K., and Carr, J. P. (2017). Manipulation of induced resistance to viruses. *Curr. Opin. Virol.* 26, 141–148. doi: 10.1016/j.coviro.2017.08.001

Perry, K. L., Kolb, F. L., Sammons, B., Lawson, C., Cisar, G., and Ohm, H. (2000). Yield effects of barley yellow dwarf virus in soft red winter wheat. *Phytopathology* 90 (9), 1043–1048. doi: 10.1094/PHYTO.2000.90.9.1043

Poliksenova, V. (2009). Induced plant stability to pathogens and abiotic stress factors. *Bull. BSU.* 2 (1), 48–60.

Prasad, V., and Srivastava, S. (2017). Phytoproteins and induced antiviral defence in susceptible plants: the Indian context. *A century Plant Virol. India. Springer;* p, 689–728. doi: 10.1007/978-981-10-5672-7_28

Price, A. A., Sampson, T. R., Ratner, H. K., Grakoui, A., and Weiss, D. S. (2015). Cas9-mediated targeting of viral RNA in eukaryotic cells. *Proc. Natl. Acad. Sci.* 112 (19), 6164–6169. doi: 10.1073/pnas.1422340112

Robertson, G., Burger, J., and Campa, M. (2022). CRISPR/Cas-based tools for the targeted control of plant viruses. *Mol. Plant Pathol.* 23 (11), 1701–1718. doi: 10.1111/mpp.13252

Rodríguez, M., Marín, A., Torres, M., Béjar, V., Campos, M., and Sampedro, I. (2018). Aphicidal activity of surfactants produced by bacillus atrophaeus L193. *Front. Microbiol.* 9, 3114. doi: 10.3389/fmicb.2018.03114

Rodríguez-Negrete, E. A., Carrillo-Tripp, J., and Rivera-Bustamante, R. F. (2009). RNA Silencing against geminivirus: complementary action of posttranscriptional gene silencing and transcriptional gene silencing in host recovery. *J. Virology.* 83 (3), 1332–1340. doi: 10.1128/JVI.01474-08

Ross, B. T., Zidack, N. K., and Flenniken, M. L. (2021). Extreme resistance to viruses in potato and soybean. *Front. Plant Science.* 12, 658981. doi: 10.3389/fpls.2021.658981

Ryabtseva, T. V., Kulikova, V. I., and Ilkevich, O. G. (2015). Improvement of potatoes by the chemotherapy method in culture of *in vitro*. *Int. Sci. Res. J.* 10 (41), 66–68. doi: 10.18454/IRJ.2015.41.127

Sáez, C., Flores-León, A., Montero-Pau, J., Sifres, A., Dhillon, N. P. S., López, C., et al. (2022). RNA-Seq transcriptome analysis provides candidate genes for resistance to tomato leaf curl new Delhi virus in melon. *Front. Plant Sci.* 12. doi: 10.3389/fpls.2021.798858

Salazar, L. F. (1996). *Potato viruses and their control* (Lima, Peru: International Potato Center).

Sevik, M. A., and Arli-Sokmen, M. (2012). Estimation of the effect of tomato spotted wilt virus (TSWV) infection on some yield components of tomato. *Phytoparasitica* 40, 87–93. doi: 10.1007/s12600-011-0192-2

Shan, Q., Wang, Y., Chen, K., Liang, Z., Li, J., Zhang, Y., et al. (2013). Rapid and efficient gene modification in rice and brachypodium using TALENs. *Mol. Plant* 6 (4), 1365–1368. doi: 10.1093/mp/sss162

Sharipova, M., Balaban, N., Mardanova, A., and Valeeva, L. (2013). Mechanisms of plant resistance to infections. *Sci. Notes Kazan Univ. Natural Sci. Series.* 155 (4), 28–58. Available at: https://repo.btu.kharkov.ua//handle/123456789/1573.

Sharma, V. K., Marla, S., Zheng, W., Mishra, D., Huang, J., Zhang, W., et al. (2022). CRISPR guides induce gene silencing in plants in the absence of cas. *Genome Biol.* 23, 1–24. doi: 10.1186/s13059-021-02586-7

Silva, F. D., and Fontes, E. P. (2022). Clustered regularly interspaced short palindromic repeats-associated protein system for resistance against plant viruses: applications and perspectives. *Front. Plant Sci.* 13. doi: 10.3389/fpls.2022.904829

Sochacki, D., and Podwyszyńska, M. (2012). Virus eradication in narcissus and tulip by chemotherapy. *Floriculture Ornam. Biotechnol.* 6, 114–121.

Somalraju, A., Mccallum, J. L., Main, D., Peters, R. D., and Fofana, B. (2022). Foliar selenium application reduces late blight severity and incidence in potato and acts as a pathogen growth inhibitor and elicitor of induced plant defence. *Can. J. Plant Pathol.* 44 (1), 39–55. doi: 10.1080/07060661.2021.1954093

Tian, Y.-P., and Valkonen, J. P. (2013). Genetic determinants of potato virus y required to overcome or trigger hypersensitive resistance to PVY strain group O controlled by the gene ny in potato. *Mol. Plant-Microbe Interact.* 26 (3), 297–305. doi: 10.1094/MPMI-09-12-0219-R

Tiwari, J. K., Tuteja, N., and Khurana, S. P. (2022). Genome editing (CRISPR-cas)-mediated virus resistance in potato (Solanum tuberosum l.). *Mol. Biol. Rep.*, 1–11. doi: 10.1007/s11033-022-07704-7

Tolkach, V. F., Nadezhda, K., Volkov, Y., and Shchelkanov, M. (2019). "Viruses and their vectors of the vegetable cultures in the russian far east," in *AI Kurentsov's Annual Memorial Meetings*. 200–210. doi: 10.25221/kurentzov.30.19

Tran, P.-T., Widyasari, K., Seo, J.-K., and Kim, K.-H. (2018). Isolation and validation of a candidate Rsv3 gene from a soybean genotype that confers strain-specific resistance to soybean mosaic virus. *Virology* 513, 153–159. doi: 10.1016/j.virol.2017.10.014

Wang, M. R., Hamborg, Z., Blystad, D. R., and Wang, Q. C. (2021). Combining thermotherapy with meristem culture for improved eradication of onion yellow dwarf virus and shallot latent virus from infected *in vitro*-cultured shallot shoots. *Ann. Appl. Biol.* 178 (3), 442–449. doi: 10.1111/aab.12646

Wang, P., Liu, J., Lyu, Y., Huang, Z., Zhang, X., Sun, B., et al. (2022). A review of vector-borne rice viruses. *Viruses* 14 (10), 2258. doi: 10.3390/v14102258

Wang, Q., Liu, Y., Xie, Y., and You, M. (2006). Cryotherapy of potato shoot tips for efficient elimination of potato leafroll virus (PLRV) and potato virus y (PVY). *Potato Res.* 49 (2), 119–129. doi: 10.1007/s11540-006-9011-4

Wasilewska-Nascimento, B., Boguszewska-Mańkowska, D., and Zarzyńska, K. (2020). Challenges in the production of high-quality seed potatoes (Solanum tuberosum l.) in the tropics and subtropics. *Agronomy* 10 (2), 260. doi: 10.3390/agronomy10020260

Wei, J., Jia, D., Mao, Q., Zhang, X., Chen, Q., Wu, W., et al. (2018). Complex interactions between insect-borne rice viruses and their vectors. *Curr. Opin. Virol.* 33, 18–23. doi: 10.1016/j.coviro.2018.07.005

Wolter, F., and Puchta, H. (2018). The CRISPR/Cas revolution reaches the RNA world: Cas13, a new Swiss army knife for plant biologists. *Plant J.* 94 (5), 767–775. doi: 10.1111/tpj.13899

Wu, J., Yang, Z., Wang, Y., Zheng, L., Ye, R., Ji, Y., et al. (2015). Viral-inducible Argonaute18 confers broad-spectrum virus resistance in rice by sequestering a host microRNA. *eLife* 4, e05733. doi: 10.7554/eLife.05733

Xu, Y., Kang, D., Shi, Z., Shen, H., and Wehner, T. (2004). Inheritance of resistance to zucchini yellow mosaic virus and watermelon mosaic virus in watermelon. *J. Heredity.* 95 (6), 498–502. doi: 10.1093/jhered/esh076

Yalovik, A., Fedorova, Y., and Yalovik, L. (2019). The effect of chemotherapy method effect on in vitro potato plants. *Bull. Altai State Agrarian University.* 10 (180), 28–32.

Yang, Z., and Li, Y. (2018). Dissection of RNAi-based antiviral immunity in plants. *Curr. Opin. Virol.* 32, 88–99. doi: 10.1016/j.coviro.2018.08.003

Yi, J.-Y., Lee, G.-A., Jeong, J.-W., Lee, S.-Y., and Lee, Y.-G. (2014). Eliminating potato virus y (PVY) and potato leaf roll virus (PLRV) using cryotherapy of *in vitro*-grown potato shoot tips. *Korean J. Crop Science.* 4 (59), 498–504. doi: 10.7740/kjcs.2014.59.4.498

Yi Lan, F., Shambbu Prasad, D., Kui Hua, L., Dong Man, K., Hae Young, K., Ye Su, S., et al. (2005). Utilization of single nodal cuttings and therapies for eradicating double-infected potato virus (PLRV, PVY) from *In vitro* plantlets of potato (Solanum tuberosum. *). HORTICULTURE Environ. Biotechnol.* 46 (2), 119–125.

Yu, H. (2015). Discussion on the occurrence and control countermeasures of rice yellow dwarf virus. *J. Guangxi Agric.* 30, 15–17. doi: 10.16872/j.cnki.1671-4652.1983.04.008

Zhan, X., Zhang, F., Zhong, Z., Chen, R., Wang, Y., Chang, L., et al. (2019). Generation of virus-resistant potato plants by RNA genome targeting. *Plant Biotechnol. J.* 17 (9), 1814–1822. doi: 10.1111/pbi.13102

Zhang, Z., Wang, Q.-C., Spetz, C., and Blystad, D.-R. (2019). *In vitro* therapies for virus elimination of potato-valuable germplasm in Norway. *Sci. Hortic.* 249, 7–14. doi: 10.1016/j.scienta.2019.01.027

Zhang, T., Zheng, Q., Yi, X., An, H., Zhao, Y., Ma, S., et al. (2018). Establishing RNA virus resistance in plants by harnessing CRISPR immune system. *Plant Biotechnol. J.* 16 (8), 1415–1423. doi: 10.1111/pbi.12881

Zhao, L., Wang, M.-R., Cui, Z.-H., Chen, L., Volk, G. M., and Wang, Q.-C. (2018). Combining thermotherapy with cryotherapy for efficient eradication of apple stem grooving virus from infected in-vitro-cultured apple shoots. *Plant Dis.* 102 (8), 1574–1580. doi: 10.1094/PDIS-11-17-1753-RE

Zhao, S., Wu, Y., and Wu, J. (2021). Arms race between rice and viruses: a review of viral and host factors. *Curr. Opin. Virol.* 47, 38–44. doi: 10.1016/j.coviro.2021.01.002

Zhao, Y., Yang, X., Zhou, G., and Zhang, T. (2020). Engineering plant virus resistance: from RNA silencing to genome editing strategies. *Plant Biotechnol. J.* 18 (2), 328–336. doi: 10.1111/pbi.13278

Zhu-Jun, W., Qiang, Z., and Xin-Huai, Z. (2011). Induced-differentiation of two flavones and two flavonols on a human esophageal squamous cell carcinoma cell line (KYSE-510). *J. Medicinal Plants Res.* 5 (24), 5677–5691. Available at: http://www.academicjournals.org/JMPR.

frontiers | Frontiers in Plant Science

TYPE Original Research
PUBLISHED 10 July 2023
DOI 10.3389/fpls.2023.1206255

OPEN ACCESS

EDITED BY
Chellappan Padmanabhan,
USDA APHIS PPQ Science and Technology,
United States

REVIEWED BY
Ashish Prasad,
Kurukshetra University, India
Wen-Shi Tsai,
National Chiayi University, Taiwan

*CORRESPONDENCE
Giuseppe Parrella
giuseppe.parrella@ipsp.cnr.it
Eui-Joon Kil
viruskil@anu.ac.kr
Sukchan Lee
cell4u@skku.edu

RECEIVED 15 April 2023
ACCEPTED 23 June 2023
PUBLISHED 10 July 2023

CITATION
Vo TTB, Lal A, Nattanong B, Tabassum M, Qureshi MA, Troiano E, Parrella G, Kil E-J and Lee S (2023) Coat protein is responsible for tomato leaf curl New Delhi virus pathogenicity in tomato.
Front. Plant Sci. 14:1206255.
doi: 10.3389/fpls.2023.1206255

Coat protein is responsible for tomato leaf curl New Delhi virus pathogenicity in tomato

Thuy T. B. Vo[1], Aamir Lal[2], Bupi Nattanong[1], Marjia Tabassum[1], Muhammad Amir Qureshi[1], Elisa Troiano[3], Giuseppe Parrella[3]*, Eui-Joon Kil[2,4]* and Sukchan Lee[1]*

[1]Department of Integrative Biotechnology, Sungkyunkwan University, Suwon, Republic of Korea, [2]Agriculture Science and Technology Research Institute, Andong National University, Andong, Republic of Korea, [3]Department of Biology, Agriculture and Food Sciences, Institute for Sustainable Plant Protection of the National Research Council (IPSP-CNR), Portici, Italy, [4]Department of Plant Medicals, Andong National University, Andong, Republic of Korea

Tomato leaf curl New Delhi virus (ToLCNDV), a bipartite *Begomovirus* belonging to the family *Geminiviridae*, causes severe damage to many economically important crops worldwide. In the present study, pathogenicity of Asian (ToLCNDV-In from Pakistan) and Mediterranean isolates (ToLCNDV-ES from Italy) were examined using infectious clones in tomato plants. Only ToLCNDV-In could infect the three tomato cultivars, whereas ToLCNDV-ES could not. Genome-exchange of the two ToLCNDVs revealed the ToLCNDV DNA-A segment as the main factor for ToLCNDV infectivity in tomato. In addition, serial clones with chimeric ToLCNDV-In A and ToLCNDV-ES A genome segments were generated to identify the region determining viral infectivity in tomatoes. A chimeric clone carrying the ToLCNDV-In coat protein (CP) exhibited pathogenic adaptation in tomatoes, indicating that the CP of ToLCNDV is essential for its infectivity. Analyses of infectious clones carrying a single amino acid substitution revealed that amino acid at position 143 of the CP is critical for ToLCNDV infectivity in tomatoes. To better understand the molecular basis whereby CP function in pathogenicity, a yeast two-hybrid screen of a tomato cDNA library was performed using CPs as bait. The hybrid results showed different interactions between the two CPs and Ring finger protein 44-like in the tomato genome. The relative expression levels of upstream and downstream genes and Ring finger 44-like genes were measured using quantitative reverse transcription PCR (RT-qPCR) and compared to those of control plants. This is the first study to compare the biological features of the two ToLCNDV strains related to viral pathogenicity in the same host plant. Our results provide a foundation for elucidating the molecular mechanisms underlying ToLCNDV infection in tomatoes.

KEYWORDS

coat protein, ToLCNDV strain, host interaction, mutant infectious clones, infectivity assay

1 Introduction

Tomatoes (*Solanum lycopersicum* L.) are one of the most important crops in the world, with a high economic value owing to their composition (Hanssen et al., 2010). Many diseases affect tomato production, and approximately half are caused by plant viruses, with at least 312 viruses, satellite viruses, or viroid species associated with tomatoes (Rivarez et al., 2021). Begomoviruses belonging to the *Geminiviridae* family have been identified as prevalent limiting factors for tomato cultivation in many regions (Mabvakure et al., 2016), and tomato leaf curl New Delhi virus (ToLCNDV) is one of the most destructive begomoviruses.

ToLCNDV has a bipartite genome structure (Moriones et al., 2017). In 1995, ToLCNDV was first reported in tomatoes in India (Padidam et al., 1995a) and then spread to cucurbits in the Mediterranean Basin in 2012 (Juárez et al., 2014; Mnari-Hattab et al., 2015; Parrella et al., 2018; Orfanidou et al., 2019). In addition to its wide host range (Srivastava et al., 2016; Jamil et al., 2017; Venkataravanappa et al., 2018; Sharma et al., 2021), this virus also possesses other dangerous characteristics, such as multi-mode transmissibility, including mechanical and seed transmission (López et al., 2015; Kil et al., 2020). Thus, ToLCNDV has emerged as a serious threat to many important crops because of its rapid spread and the extent of the outbreak, even in countries with different geographical locations, thanks mainly to its efficient vector, the *Bemisia tabaci* (Bertin et al., 2018; Bertin et al., 2021). Previous research reported that two strains of ToLCNDV from Indian subcontinent and the Mediterranean Basin presented distinct pathogenicity in tomatoes (Brown et al., 2015; Fortes et al., 2016). Tomato plants infected with the ToLCNDV Indian strain (ToLCNDV-In) exhibited severe symptoms, such as stunted growth, leaflets curled upward and downward, slight chlorosis and yellowing, crumpling, and mosaic/mottling (Singh et al., 2015). Regardless, the ToLCNDV Mediterranean strain (ToLCNDV-ES strain) has primarily adapted to cucurbits, while evolutionary dynamics of this strain observed in Italy, have apparently led to the selection of two subgroups: subgroup I, which is not able to infect the tomato (Vo et al., 2022b; Troiano and Parrella, 2023) and subgroup II which instead infecting tomatoes, although with great difficulty, as evidenced by a low incidence and light symptoms in the field in this plant (Fortes et al., 2016; Ruiz et al., 2017; Yamamoto et al., 2021). Overall, these characteristics indicate that tomato is not a permissive host for ToLCNDV-ES, whereas ToLCNDV isolates from Asia are regarded as a threat to this plant species. However, the causes for these characteristics remain largely unknown. However, to date, there have been no studies comparing the biological characteristics and the molecular mechanisms of different strains of ToLCNDV in the same host species.

In this study, two ToLCNDV isolates, belonging to Asian and Mediterranean strains respectively, were confirmed to have differential infectivity in tomatoes using infectious clones that were successfully constructed previously (Vo et al., 2022a). ToLCNDV isolates from Pakistan, designated as ToLCNDV-In, induced severe symptoms, unlike ToLCNDV-ES isolates from Italy, which are not adapted to tomatoes (Vo et al., 2022b; Troiano and Parrella, 2023). To identify the pathogenicity determinants of ToLCNDV in tomatoes, genomic segments were exchanged between the two isolates and the hybrids were inoculated into different tomato cultivars. After identifying DNA-A as the main factor for ToLCNDV infectivity in tomato, we generated numerous mutant clones by altering six ORFs and the intergenic region (IR) between the two strains. An infectivity assay showed that the clone carrying coat protein (CP) was responsible for ToLCNDV pathogenicity in tomatoes. Site-directed mutagenesis of CP was performed to examine the role of amino acid residues in ToLCNDV infection. The amino acid at position 143 of the CP was found to play a critical role in tomato ToLCNDV-ES infectivity. Yeast two-hybrid screening was performed to examine the interaction between the CP of each ToLCNDV isolate and tomato host proteins. The hybrid assay results showed different interactions between the two ToLCNDV CPs with Ring-finger protein 44-like. This interaction may explain the difference in pathogenicity of the two ToLCNDV strains in tomatoes. This is the first in-depth study that compares biological characteristics of two ToLCNDV strains in the same host plant and identifies the key viral infectivity determinants.

2 Materials and methods

2.1 Virus sources and plant growth condition

A ToLCNDV isolated from Pakistan, belonging to ToLCNDV-India strain group (here designated as ToLCNDV-In) and the Italian isolate 45/16, belonging to subgroup I of ToLCNDV-ES strain group (here designated as ToLCNDV-ES), were used in the present study (Parrella et al., 2018; Vo et al., 2022a).

Infectious clones were successfully generated in a previous study (Vo et al., 2022a). *Nicotiana benthamiana* and three different tomato cultivars including 'San Pedro' from Italy, 'Seogwang' from Korea, and 'Moneymaker' were cultivated in a growth chamber with 16 h light/8 h dark cycles at 22–28 °C

2.2 Construction of chimeric and site-directed mutant clones of two ToLCNDV isolates

Subgenomic components were swapped to form two combinations, ToLCNDV-In DNA-A + ToLCNDV-ES DNA-B and ToLCNDV-ES DNA-A + ToLCNDV-In DNA-B (hereafter designate as ToLCNDV-In-A, ToLCNDV-In-B, ToLCNDV-ES-A and ToLCNDV-ES-B respectively) using an approach similar to other agroinoculations (Vo et al., 2022a). Seven chimeric sequences corresponding to six ORF and the IR of DNA-A components were synthesized by swapping the ToLCNDV-ES sequence on the ToLCNDV-In backbone (Macrogen, Korea) based on the wild-type sequence of the two ToLCNDV isolates with tandem repeat constructs (Figure S1). Plasmids containing swapped sequences were digested with *Hin*dIII/*Spe*I and ligated into the pCAMBIA 1303 vector to generate recombinant plasmids. After transformation of *Agrobacterium tumefaciens* strain GV3101

using the freeze-thaw transformation method (Weigel and Glazebrook, 2006), the infectivity of all the chimeric clones was tested on *N.benthamiana* and tomato plants.

Site-directed mutants of CP were produced using Q5® Site-Directed Mutagenesis Kit (New England Biolabs, Ipswich, MA, USA) following the manufacturer's instructions. Based on the different amino acids in the V1 sequence between the two isolates using multiple alignments, 16-point mutant clones were generated using the designed primer sets (Table S1) with extracted viral DNA from infected leaves as a template. All mutant sequences were confirmed by sequencing, which were then transformed into *Agrobacterium* to generate infectious clones using the same methodology.

2.3 Virus inoculation

A.tumefaciens harboring each viral clone was grown in 20 mL of LB broth medium containing kanamycin (50 μg/mL), rifampicin (50 μg/mL), and gentamycin (50 μg/mL) for 24 h at 28°C with shaking until the optical density (OD) reached 1.0 at 600 nm. Activated cells were pelleted by centrifuging and resuspended in infiltration buffer (10 mM $MgCl_2$, 10 mM MES, 200 μM acetosyringone). *A. tumefaciens* strains containing the recombinant plasmids ToLCNDV-In-A/ToLCNDV-In-B, ToLCNDV-ES-A/ToLCNDV-ES-B, ToLCNDV-In-A/ToLCNDV-ES-B, and ToLCNDV-In-B/ToLCNDV-ES-A were mixed in a 1:1 ratio, and the strains containing chimeric and site-directed mutant clones were mixed in equal proportions. Cell suspensions were used for the infectivity assay of three-week-old tomato plants by pinpricking the main apical shoot.

2.4 Detection of two ToLCNDV isolates accumulation

Inoculated leaf samples were collected 21 days post-inoculation (dpi) to confirm the viral infection. Genomic DNA was extracted and used for PCR amplification with specific primer sets, as described previously (Vo et al., 2022a). To confirm viral replication, Southern blotting was performed as previously described (Southern, 2006). Briefly, after electrophoresis, DNA was transferred to nylon membranes and hybridized with a probe containing [α^{32}P]-dCTP at 65°C for 16 h. The membrane was washed and exposed to an X-ray film.

Quantitative PCR (qPCR) was performed on the agroinoculated plants at 21 dpi to determine the viral titer. Total DNA from different tissues, including new leaves, stems, and roots of the three plants, was extracted and used as a template for qPCR following our previous study (Vo et al., 2022b).

2.5 Yeast two hybrid assay

To identify the interactions between the CPs of each isolate and the host factors, yeast two-hybrid screening of the tomato cDNA library was conducted. For cDNA library construction, total RNA from tomato leaves was isolated using the RNeasy Plant Mini Kit (Qiagen, Hilden, Germany) according to the manufacturer's instructions. The integrity of the total RNA was analyzed using 1% agarose gel electrophoresis and the concentration was determined using a BioTek Epoch Microplate spectrophotometer (BioTek, Winoosku, VT, USA). Then, this RNA was used to construct the Y2H tomato cDNA library by Panbionet (Pohang, Korea). The CP (V1) encoding gene of each isolate was introduced into the pGBKT7 (referred to as In-V1 and ES-V1) vector, which contained a GAL4 DNA-binding domain, kanamycin resistance for selection in *Escherichia coli*, and a TRP1 nutritional marker for selection in yeast. Two plasmids, pGBKT7-In-V1 and pGBKT7-ES-V1, were generated as baits in the GAL4-based two-hybrid system for CPs of ToLCNDV-ES and ToLCNDV-In isolates, respectively. Bait vectors were checked for toxicity and autoactivation in yeast before processing the hybrids. The bait was then hybridized with a cDNA library to identify CP-interaction proteins in tomatoes by Panbionet.

To confirm the interaction between each ToLCNDV CP and the host protein, yeast two-hybrid assays were conducted using a modified lithium acetate yeast transformation (Thompson et al., 1998). Interaction of different host genes including Cathepsin B-like protease 3 (XM_004233173), NAD(P)H-quinone oxidoreductase subunit M (XM_004237313), Ribulose bisphosphate carboxylase small chain 3B (NM_001309210), protein phosphatase 2C (NM_001247571), LOW PSII ACCUMULATION (XM_004247389), NAD(P)H-quinone oxidoreductase subunit M (XM_004237313), and RING finger protein 44- like (XM_004243217) was examined with In-V1 and ES-V1. Prey, including host genes, were cloned into the pGADT7 vector and co-transformed with bait vector pGBKT7 carrying different CPs into *Saccharomyces cerevisiae* strain Y2H Gold. The transformed yeast cells were plated on three nutrient dropout media: SD/-Trp/-Leu (DDO), SD/-Trp/-Leu/-His (TDO), and SD/-Trp/-Leu/-Ade/-His (QDO). The plasmids pGBKT7-53 (Gal4 DNA-BD fused with murine 53) and pGBKT7-Lam (Gal4 BD fused with lamin) were co-transformed with pGADT7-T encoding the Gal4 AD fused with the SV40 large T-antigen and used as positive and negative controls, respectively.

2.6 Relative expression of candidate genes by RT-qPCR

For RT-qPCR, cDNA was synthesized from 1μg of total RNA using Oligo dT primers and Moloney murine leukemia virus (MMLV) reverse transcriptase (Bioneer, Daejeon, Korea). The reaction was performed using TB Green® Premix Ex Taq™ II (Tli RNaseH Plus; TaKaRa Bio, Shiga, Japan) with the primer sets (Table S2). Forty cycles of PCR were performed using a Rotor-Gene Q thermocycler (Qiagen) under the following conditions: 10 s denaturation at 95°C, 15 s annealing at 60°C, and 20 s polymerization at 72°C. Elongation 1α (EF1α) gene was used for internal normalization and each reaction was replicated three times. Data analyses were conducted using the $2^{-\Delta\Delta Ct}$ method (Livak and Schmittgen, 2001). Statistical analyses were performed using the t-

test in the GraphPad Prism software (GraphPad Software, Boston, MA, USA).

3 Results

3.1 Determination of the virulence region using two ToLCNDV infectious clones

Infectivity assays revealed that the ToLCNDV-In infectious clone could infect tomatoes, whereas the ToLCNDV-ES clone was not adapted to this crop (Figure 1). Typical symptoms, including leaf curl, mosaic, and stunting, were induced in ToLCNDV-In-infected tomatoes, whereas a normal phenotype was observed in ToLCNDV-ES-inoculated plants for all the three tomato cultivars (Moneymaker, Seogwang, and San Pedro) (Figure 1A). The PCR detection results were consistent with the appearance of symptoms in the inoculated tomatoes (Figure 1B).

To determine the genomic region responsible for ToLCNDV pathogenicity in tomato, the subgenomes of the two isolates were swapped by mixing DNA components as follows: ToLCNDV-ES-A + ToLCNDV-In-B ($A_{ES}B_{In}$) and ToLCNDV-In-A + ToLCNDV-ES-B ($A_{In}B_{ES}$) and processed, and original ToLCNDV-ES-A/B ($A_{ES}B_{ES}$) and ToLCNDV-In-A/B ($A_{In}B_{In}$) were used as positive and negative control, respectively. The results revealed that only ToLCNDV-In-A supplemented with either ToLCNDV-In-B or ToLCNDV-ES-B could infect tomatoes (Table 1). Infected plants exhibited a typical disease phenotype at 21 dpi (Figure 1A). Furthermore, the viral genome was detected in all symptomatic plants inoculated with $A_{In}B_{In}$ and $A_{In}B_{ES}$ using PCR amplification with specific primers. No infection was observed with $A_{ES}B_{ES}$ or $A_{ES}B_{In}$ (Figure 1B). Virulence was only observed when tomatoes were co-inoculated with ToLCNDV-In-A, demonstrating that the DNA-A component of ToLCNDV-In was responsible for infectivity in tomatoes.

3.2 Coat protein is responsible for ToLCNDV infectivity in tomato

To identify the gene(s) that determine tomato infection by ToLCNDV-In, we synthesized seven chimeric constructs by substituting genomic regions containing C1 (Rep), C2 (TrAP), C3 (REn), C4, V1 (CP), V2, and IR of ToLCNDV-In into the ToLCNDV-ES backbone (abbreviated as $In_{IR}ES$, $In_{C1}ES$, $In_{C2}ES$, $In_{C3}ES$, $In_{C4}ES$, $In_{V1}ES$, and $In_{V2}ES$). After three weeks of inoculation, chimeric construct $In_{V1}ES$ induced moderate leaf curl symptoms, consistent with the PCR amplification results, whereas visible symptoms and viral DNA were not detected in all other constructs in tomatoes (Figure 2A; Table 1). A chimeric clone harboring ToLCNDV-ES V1 in the ToLCNDV-In backbone

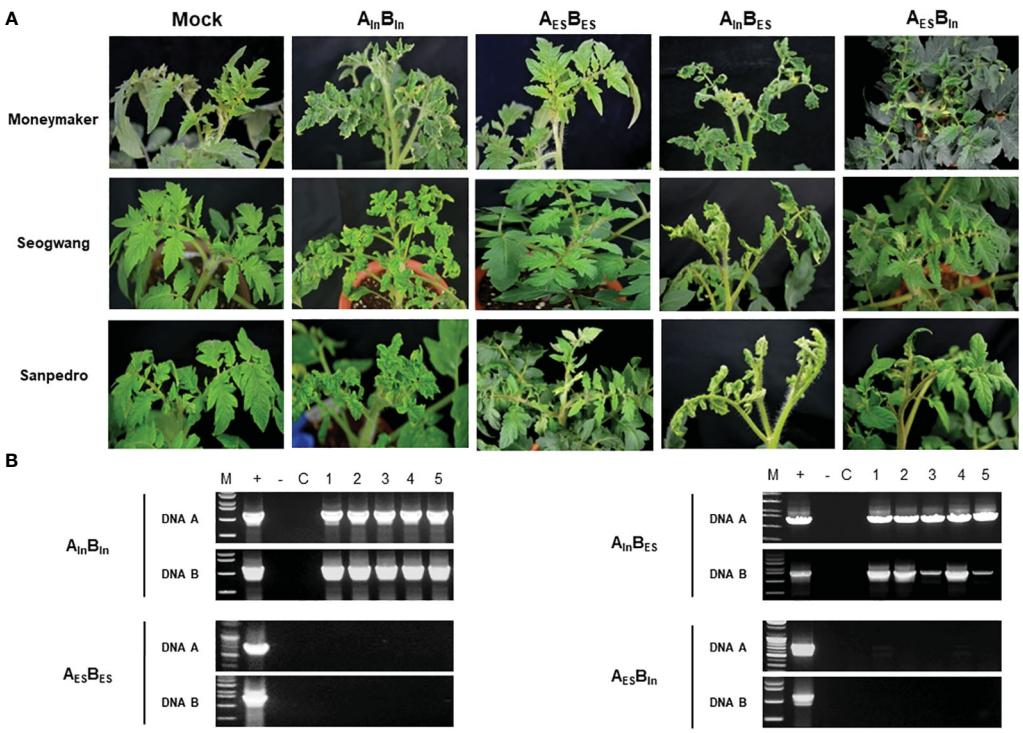

FIGURE 1
Tomato plants infected with swapped ToLCNDV constructs. **(A)** Disease phenotype induced by two ToLCNDV constructs including the original combination (ToLCNDV-ES DNA-A (A_{ES}) + DNA B (B_{ES}) and ToLCNDV-In DNA-A (A_{In}) + DNA B (B_{In}) and swapped subgenome combination ($A_{In}B_{ES}$ or $A_{ES}B_{In}$)at 21 dpi. **(B)** PCR results of viral DNA in systemically infected tomato leaves. Lane M: maker, lane +: positive control, lane −: negative control, lane C: mock plant, lane 1–5: inoculated plants.

10.3389/fpls.2023.1206255

TABLE 1 Infectivity of experiment ToLCNDV clones in *Nicotiana benthamiana* and tomato.

Experiment	IC	*N. benthamiana*		Tomato	
		Infectivity*	Symptoms	Infectivity*	Symptoms
Subgenome swapped	Mock	0/6	–	0/9	–
	$A_{ES}B_{ES}$	6/6	Leaf curl, mosaic, stunting	0/9	–
	$A_{In}B_{In}$	6/6	Leaf curl, mosaic, stunting	9/9	Leaf curl, yellow mosaic, pickering
	$A_{ES}B_{In}$	6/6	Leaf curl, mosaic, stunting	0/9	–
	$A_{In}B_{ES}$	6/6	Leaf curl, mosaic, stunting	9/9	Leaf curl, yellow mosaic, pickering
Chimeric	$In_{IR}ES$	6/6	Leaf curl, mosaic, stunting	0/8	–
	$In_{C1}ES$	6/6	Leaf curl, mosaic, stunting	0/8	–
	$In_{C2}ES$	6/6	Leaf curl, mosaic, stunting	0/8	–
	$In_{C3}ES$	6/6	Leaf curl, mosaic, stunting	0/8	–
	$In_{C4}ES$	6/6	Leaf curl, mosaic, stunting	0/8	–
	$In_{V1}ES$	6/6	Leaf curl, mosaic, stunting	6/8	Moderate leaf curling
	$In_{V2}ES$	6/6	Leaf curl, mosaic, stunting	0/8	–
	$ES_{V1}In$	6/6	Leaf curl, mosaic, stunting	0/8	–

*Infected plants/inoculated plants.

($ES_{V1}In$) was constructed to confirm the role of CP in ToLCNDV infectivity. There was no virus accumulation in symptomless $ES_{V1}In$-inoculated plants, as confirmed by PCR (Figure 2B). According to the Southern hybridization results, open circular and super-coiled forms (double–stranded DNA), as well as a single-stranded form of both DNA components indicated that the chimeric $In_{V1}ES$ clone can replicate in tomato (Figure 2C). Taken together, these results suggest that the CP is responsible for the infectivity in tomatoes of the ToLCNDV-In and of its chimeric construct $In_{V1}ES$.

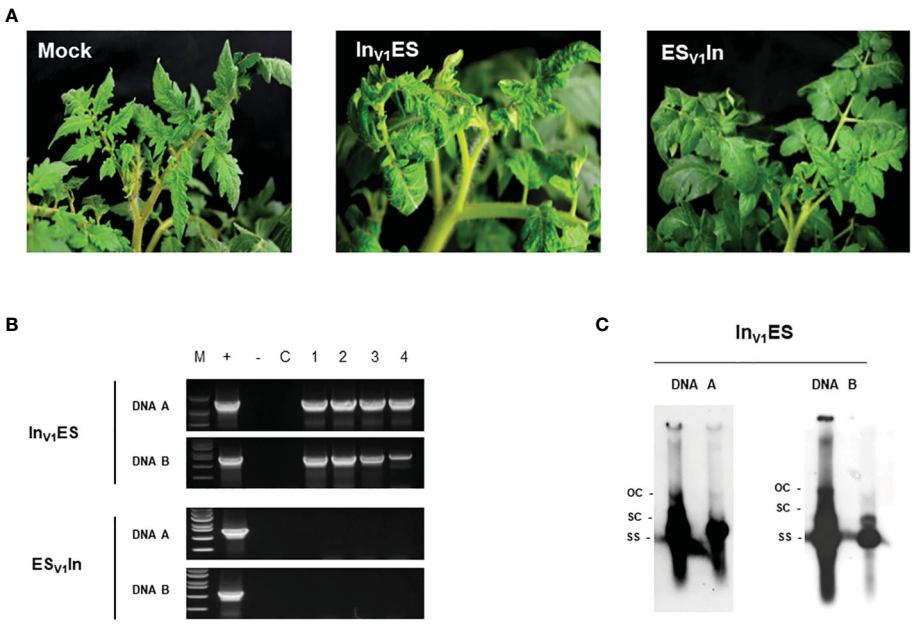

FIGURE 2
Infectivity of AV1 chimeric constructs in tomato. **(A)** Visual symptom of two AV1 constructs ($In_{V1}ES$: ToLCNDV-In CP in ToLCNDV-ES backbone; $ES_{V1}In$: ToLCNDV-ES CP in ToLCNDV-In backbone) at 21 dpi. **(B)** PCR detection of viral DNA in infected tomatoes. Lane M: marker, Lane +: positive control, lane –: negative control, lane C: mock plant, lane 1–4: inoculated plants. **(C)** Southern blot hybridization results of $In_{V1}ES$ chimera clone; the amplicon from PCR detection was used as probe.

3.3 Effect of a single amino acid mutation on coat protein on virus infectivity

To determine the role of different amino acids in the CPs in pathogenicity in tomato, eight site-directed mutant constructs were generated. These included ES-V1^{S2A} (serine residue at amino acid 2 was changed to alanine), ES-V1^{T29A} (threonine residue at amino acid 29 was changed to alanine), ES-V1^{S32V} (serine residue was changed to valine at amino acid 32), ES-V1^{R42K} (arginine residue was changed to lysine at amino acid 42), ES-V1^{W143R} (residue tryptophan at amino acid 143 was changed to arginine), ES-V1^{T148S}, (serine replaced threonine at amino acid 148), ES-V1^{S193C} (cysteine residue replaced serine at amino acid 193), ES-V1^{R194K} (arginine residue was changed to lysine at amino acid 194) based on alignment of V1 full length of ToLCNDV-ES. At contrary, mutants In-V1^{A2S}, In-V1^{A29T}, In-V1^{V32S}, In-V1^{K42R}, In-V1^{R143W}, In-V1^{S148T}, In-V1^{C193S}, and In-V1^{K194R}were generated based on ToLCNDV-In V1 sequence and their infectious clones were constructed (Figure S2). All mutant infectious clones were agroinoculated into tomato plants to confirm their infectivity with the wild-type ToLCNDV clones. A symptomless phenotype was observed in all plants inoculated with either mutant or wild-type ToLCNDV-ES clone after three weeks of inoculation (Figure 3A; Table S3). Nevertheless, viral DNA was only detected in ES-V1^{W143R}-inoculated plants. Three different tissues, upper leaves, stems, and roots of asymptomatic infected plants, were examined for viral presence to determine the movement of the ToLCNDV mutant clone (Figure 3B). PCR results showed that this mutant clone was present in all tested tissues, indicating that ToLCNDV-ES with a single mutation at amino acid 143 position of the CP could replicate and spread systemic infection to other tissues (Figure 3C). In addition, qPCR was performed to quantify the relative viral accumulation of the mutant clone in various tomato tissues after infection. No viral DNA accumulated in the mock-treated plants, whereas there was a high level of mutant ES-V1^{W143R} in all infected tissues, especially in the roots (Figure 3D). In addition, all mutant clones of different amino acids, including amino acid 143 on the ToLCNDV-In CP, showed infectivity and induced typical symptoms in tomatoes. The detectable PCR results (data not shown) and symptomatic phenotype of inoculated plants indicated that the mutation at the amino acid 143 position did not have a major effect on ToLCNDV-In pathogenicity but was essential for ToLCNDV-ES infectivity in tomato, even when no disease symptoms were induced.

In previous reports, some ToLCNDVs isolated from Spain also showed weak adaptation to asymptomatic tomatoes, even though a few plants showed slight vein yellowing only in the lower leaves (Fortes et al., 2016; Yamamoto et al., 2021). Comparison of amino acid sequences among CPs of Spanish ToLCNDV and the two isolates in this study revealed that both isolates from Mediterranean only differ in amino acid 143, suggesting that this amino acid plays an important role in ToLCNDV-ES's ability to infect tomatoes.

3.4 Interaction of ToLCNDV coat protein and host factors

Yeast two-hybrid screening was conducted to determine the interaction between the CP of each ToLCNDV isolate and host proteins. In the screening, only 26 of 53 and 10 of 25 candidates

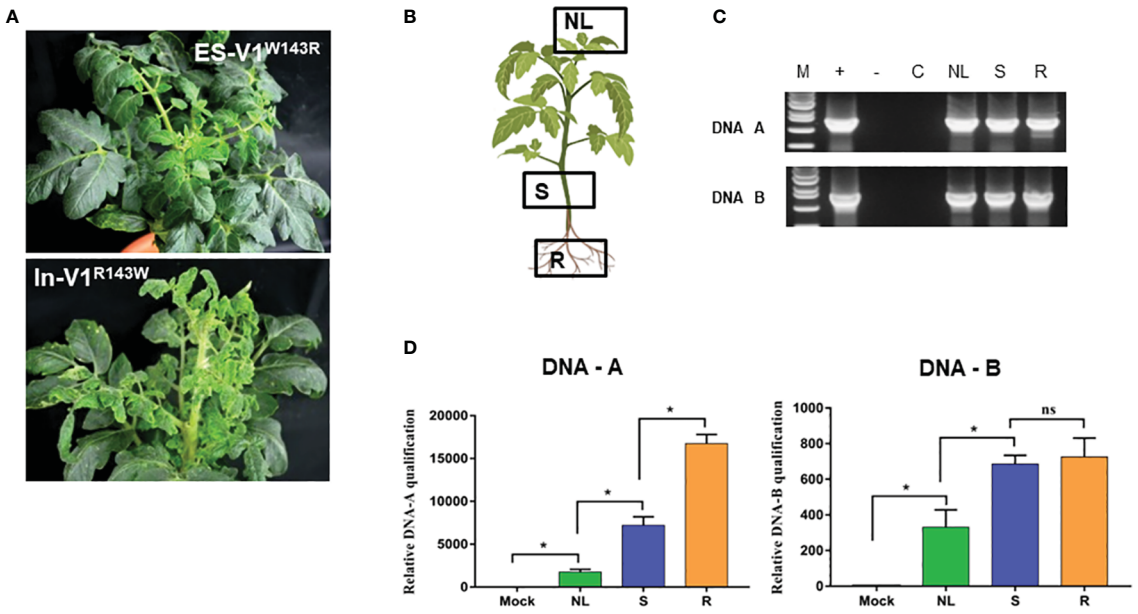

FIGURE 3
Infectivity of amino acid 143 position point mutant clones of coat protein of ToLCNDV. **(A)** Phenotype of point mutant constructs (ES-V1^{W143R}: the residue tryptophan at amino acid 143 was changed to arginine in ToLCNDV-ES CP and In-V1^{R143W}: arginine was changed to tryptophan in ToLCNDV-In CP) in tomato. **(B, C)** Sampling position and PCR results in different tissues, Lane M: positive control, Lane –: negative control, Lane C: mock plant, NL, new leaf; S, stem; R, root. **(D)** Relative viral titer in different tissues. The bar graph indicate the mean ± standard deviation (n = 3). The statistical comparison was performed with the unpaired t-test: *p <0.05, ns, not significant.

truly interacted with ToLCNDV-In CP and ToLCNDV-ES CP, respectively. After sequencing, five host proteins including Cathepsin B-like protease 3, NAD(P)H-quinone oxidoreductase subunit M,Ribulose bisphosphate carboxylase small chain 3B (RBCS4), Protein phosphatase 2C (DIG3), and Protein LOW PSII ACCUMULATION 1 interacted with ToLCNDV-In CP, whereas CP of ToLCNDV-ES interacted with NAD(P)H-quinone oxidoreductase subunit M protein, RING finger protein 44- like, GAGA- binding transcriptional activator, protein CROWDED NUCLEI 4, 1-D-deoxyxylulose 5-phosphate synthase, and thaumatin-like protein 1b (Table 2). Both baits interacted with the same NAD(P)H-quinone oxidoreductase subunit M protein, a flavoenzyme that serves as a quinone reductase, in connection with the conjugation reactions of hydroquinones involved in detoxification pathways (Sellés Vidal et al., 2018).

To verify the interaction between the two CPs and host genes derived from the screening list, baits containing ToLCNDV-In CP and ToLCNDV-ES CP were co-transfected with the prey vector harboring the host genes in the S. *cerevisiae* strain Y2H Gold. Transfected yeasts were grown under different nutrient deficiencies (DDO, TDO, and QDO) with serial dilutions to confirm the interactions. After three days of incubation, the results showed that all captured host proteins interacted with ToLCNDV-In CP and ToLCNDV-ES, except for Ring finger protein 44-like. Interestingly, Ring-finger protein 44- like interacted only with ToLCNDV-ES CP and did not show any binding with ToLCNDV-In CP bait (Figure 4A). The yeast co-transfected with ES CP bait and ring finger prey grew on three nutrient-deficient nutrient media, while yeast co-transfected with ToLCNDV-In CP did not produce any colonies on DDO and QDO media, indicating that there was no interaction between ToLCNDV-In CP and this host protein.

We compared the Ring-finger protein 44-like transcript levels in tomato leaves inoculated with ToLCNDV-In, ToLCNDV-ES and *A. tumefaciens* GV3101 (mock) using RT-qPCR. The relative expression of this protein in ToLCNDV-inoculated leaves was significantly higher than that in GV3101-infiltrated leaves at 21 dpi as shown in Figure 4B, suggesting that the expression of Ring-finger protein 44-like was induced by virus inoculation. However, no significant difference in Ring protein expression between the two ToLCNDV clone-inoculated plants suggests that the infectivity of ToLCNDV in tomato is not related only to the accumulation of Ring-finger protein 44-like. We also assessed the expression of five genes in the upstream and downstream regions under these two conditions (Figure 5; Table S4). RT-qPCR showed increase in expression of cytochrome P450 CYP72A219-like in the upstream region and ATP-dependent zinc metalloprotease FTSH2 in the downstream region with viral infection compared to their expression in mock plants. Expression of upstream genes increased the most in the ToLCNDV-ES-inoculated group. This gene is involved in growth and defense mechanisms by inducing the biosynthesis of defense compounds such as jasmonic acid and flavonoids. These factors also potentially affect ToLCNDV pathogenicity in tomatoes.

4 Discussion

Tomato leaf curl New Delhi virus is a devastating pathogen that causes economic losses to many important crops worldwide (Padidam et al., 1995a; Zaidi et al., 2017). This pathogen shows genetic variability and two main strains, including those from Asia and the Mediterranean region, have been described. In the Indian subcontinent, ToLCNDV has been reported to cause severe symptoms and yield losses, particularly in solanaceous crops (e.g. tomato and aubergine), (Hanssen et al., 2010; Kumar et al., 2015). In the Mediterranean region, however, this virus has caused tremendous damage, mainly to cucurbit crops, while exhibiting low pathogenicity to *Solanaceae* plants. The ToLCNDV outbreak caused losses of over 20% of zucchini and melons in Spain and 80% of pumpkins in Italy (Sáez et al., 2017; Panno et al., 2019; Crespo et al., 2020), whereas no significant losses of tomatoes have been reported in these regions due

TABLE 2 Host proteins interaction with CP of each ToLCNDV isolates, as determined by Y2H screening.

Isolates	Hit *	Host genes	NCBI accession No.
In- CP	14	Cathepsin B-like protease 3	XM_004233173
	1	NAD(P)H-quinone oxidoreductase subunit M	XM_004237313
	1	Ribulose bisphosphate carboxylase small chain 3B, chloroplastic-like (RBCS4)	NM_001309210
	1	Protein phosphatase 2C (DIG3)	NM_001247571
	1	Protein LOW PSII ACCUMULATION 1	XM_004247389
ES-CP	1	NAD(P)H-quinone oxidoreductase subunit M	XM_004237313
	1	RING finger protein 44- like	XM_004243217
	1	GAGA-binding transcriptional activator (BBR/BPC2)	NM_001279314
	1	Protein CROWDED NUCLEI 4 (LOC101246104)	XM_004231905
	1	1-D-deoxyxylulose 5-phosphate synthase (DXS)	NM_001247743
	1	Thaumatin-like protein 1b	XM_004229555

*Number of prey identified independently.

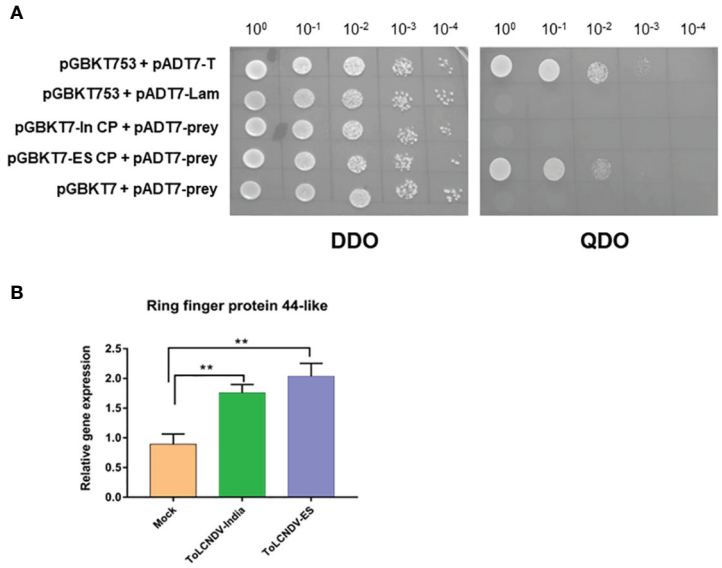

FIGURE 4
Confirmation of Y2H for Ring finger protein 44-like and its expression by RT-qPCR **(A)** Y2H results when each CP is hybridized with Ring finger protein 44-like. CP of each ToLCNDV as bait and Ring finger protein 44-like as prey; pGBKT53 x pADT7-T is positive control, pGBKT53x pADT7-Lam is negative control. Two selection media are DDO (double dropout SD/-Trp/-Leu) and QDO (Quadruple dropout SD/-Trp/-Leu/-His/-Ade). **(B)** Relative expression change of Ring finger protein 44-like in different inoculated leaves at 21 dpi. The statistical comparison was performed with the unpaired t-test: **p <0.01.

to this virus to date. Most studies have focused on different adaptations in susceptible or resistant/tolerant hosts to identify candidate genes against this virus using molecular techniques or high-throughput sequencing (Kushwaha et al., 2015; Romero-Masegosa et al., 2021; Sáez et al., 2022). To date, no studies have been conducted to compare the biological characteristics and reveal the precise molecular mechanisms by which different ToLCNDV strains display distinct adaptations in the same hosts. In our study, two isolates representing Asian and Mediterranean strains showed significant differences in infectivity in agroinoculated tomato, a predominant host for begomoviruses. The infectious clone of ToLCNDV-In isolated from Pakistan exhibited high pathogenicity with severe symptoms, whereas the ToLCNDV-ES clone from Italy showed no pathogenicity in tomatoes. To identify the genomic determinants causing differences in tomato adaptation between the two ToLCNDV strains, many constructs of swapped clones were generated and tested in various tomato cultivars. Genetic evidence indicated that DNA-A of ToLCNDV-In plays a critical role in

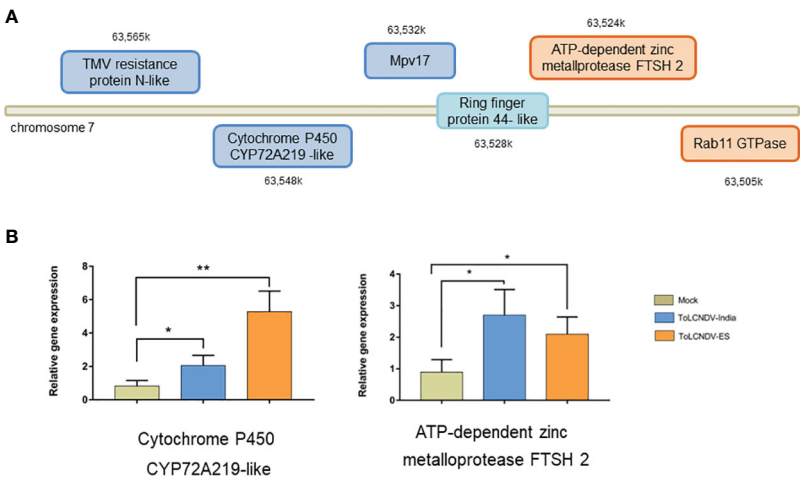

FIGURE 5
Relative expression of upstream and downstream genes for Ring-finger protein 44-like, as determined by RT-qPCR. **(A)** Position of chosen genes in upstream (blue rectangle) and downstream (orange rectangle) region. Their relative expression was checked in plants inoculated with different isolates including mock, ToLCNDV-In, and ToLCNDV-ES; however only one upstream gene and one downstream gene showed significant difference **(B)**. The statistical comparison was performed with the unpaired t-test: *p<0.05, **p <0.01.

infectivity in tomatoes (Figure 1). In addition, the results derived from a series of chimeric viral clones revealed that CP in DNA-A is the key determinant required for the infectivity in tomato. Substituting the CP of ToLCNDV-In within the ToLCNDV-ES backbone resulted in adaptation in tomato, whereas at contrary ToLCNDV-In with the alternative ToLCNDV-ES CP (Figure 2) could not infect tomato. These results complement previous reports indicating that the NSP in DNA B is a symptom determinant of ToLCNDV isolated from Pakistan (Hussain et al., 2005). Both CP and NSP perform their role at different stages of viral invasion. CP is a multifunctional protein that serves to encapsidate the geminate particle, allows the transmission by *B. tabaci*, target the nucleus and export the nuclear viral genome (Harrison et al., 2002). Also, CP is known to be essential for the systemic invasion of monopartite begomoviruses, such as TYLCV, but is not essential for bipartite begomoviruses (Gardiner et al., 1988; Padidam et al., 1995b), indicating that CP plays a more important role in propagation than cell-to-cell movement of viruses inside plants. NSP plays a key role in cell-to-cell movement to spread virus to other tissues in many bipartite begomoviruses (Gafni and Epel, 2002). It is possible that when ToLCNDV-ES CP was restricted in the nascent viral production process for unknown reasons, no infection occurred and NSP could not continue to initiate systemic infection. This theory was also supported by recent field and experimental evidence of complementation between an Italian isolate of ToLCNDV-ES (belonging to subgroup I) and TYLCV, thanks to which ToLCNDV-ES became infectious in tomatoes (Vo et al., 2022b).

On the other hand, Indian isolate CP on ES backbone helped in viral propagation and resulted in systemic infection of tomato through movement proteins. However, the connection with ToLCNDV-ES movement proteins is inefficient compared with original ToLCNDV-In DNA B component, which resulted in the moderate disease phenotype (leaf curling) without severe symptom like wild type ToLCNDV-In. Thus, together with NSP, CP may play a key role in the pathogenicity of ToLCNDV in tomatoes. Moreover, the results revealed that different amino acids are involved in the pathogenicity of CPs. Sequence alignment showed that ToLCNDV-In and ToLCNDV-ES CPs shared 96.8% similarity, differing by only eight amino acids. Analysis of a series of point mutations revealed that alteration of arginine at the 143rd amino acid position in the CP was sufficient for infectivity of ToLCNDV-ES. Point mutations affecting the 2nd, 29th, 32nd, 42nd, 148th, 193rd or 194th amino acid residue had no effect on infectivity of ToLCNDV-ES, which was never detected by PCR. ToLCNDV-ES became infectious in tomato only when tryptophan (W) was substituted by arginine (R) at position 143 in the CP. Sequence alignment revealed that other ToLCNDVs, which can infect tomatoes, also contained arginine at the 143rd position while other amino acid residues were the same as those of ToLCNDV-ES in this study, indicating that this residue was critical for Mediterranean ToLCNDV (data not show). However, a single mutation of amino acid residue at 143-position of ToLCNDV-In CP still induced leaf curling and mosaic symptom, suggesting that the 143rd amino acid residue alone is insufficient to determine the infectivity of ToLCNDV-In. Taken together, the data showed that when viruses of different genotypes were inoculated into the same host, their competence for infection varied, and these genetic variations may be the result of adaptations to new selection pressures during the transmission of ToLCNDV to a new area.

Proving to be a key determinant of ToLCNDV infectivity in tomatoes, the CP of ToLCNDV-ES could be disrupted primarily in the replication process and affect virus viability. The possibility of a virus infecting and inducing symptoms in a specific host plant depends on the expression of specific sets of genes and interactions between the host and virus-encoded proteins (Maule et al., 2002). Thus, yeast two-hybrid screening was performed to identify host proteins that interact with CPs to study the molecular mechanisms involved in the pathogenicity of the two ToLCNDV isolates. Five host proteins were captured as ToLCNDV-In CP bait-interacting partners, while the ToLCNDV-ES bait interacted with the other five host proteins. The binding test using yeast two-hybrid assays showed that all proteins interacted with ToLCNDV-In and ToLCNDV-ES CP. Interestingly, Ring finger protein 44-like, which was identified as an ES CP partner, did not bind to the India CP. Ring finger proteins are widely involved in the regulation of various physiological and biochemical processes, including plant growth and development, stress resistance, and hormone signaling responses (Borden, 2000; Sun et al., 2019). Ring finger proteins, a large family of E3 type, exist widely in eukaryotes and play important roles in ubiquitination, a central process of the ubiquitin/26S proteasome system that plays a role in plant–pathogen interactions (Zeng et al., 2006; Citovsky et al., 2009; Trujillo and Shirasu, 2010). This post-translational modification can affect geminiviral infections. For example, the Tobacco RING E3 Ligase NtRFP1 was reported to mediate the ubiquitination and degradation via the ubiquitin/26S proteasome system of the tomato yellow leaf curl China virus βC1 gene. After viral infection, plants overexpressing NtRFP1 developed attenuated symptoms, whereas plants with silenced expression of NtRFP1 showed severe symptoms (Shen et al., 2016). Therefore, our hypothesis is that the interaction of Ring finger protein 44- like protein with ToLCNDV-ES CP may disrupt the infection of tomatoes by this isolate. Expression of Ring finger protein 44- like in the two ToLCNDV-inoculated leaves did differ, and their upstream and downstream genes showed significantly changed expression levels under the two ToLCNDV-inoculated conditions. In addition to the potential degradation process of the Ring finger protein, the interaction of ToLCNDV-ES CP and Ring finger 44-like protein influences the gene in the upstream region and increases the transcript level, leading to a greater accumulation of defense compounds, suggesting a potential reason for ToLCNDV-ES infectivity in tomato. However, further studies are still required to verify that CP might be a substrate for Ring finger protein, as well as the impact of this protein on ToLCNDV infection in tomatoes.

Our study provides novel insights in understanding the impact of CPs on the difference in the pathogenicity of two ToLCNDV isolates, Asian and Mediterranean strains, in tomatoes. In addition, comparison of amino acids essential for host cell infectivity of ToLCNDV-ES and ToLCNDV-In provides clues of evolutionary conservation. Moreover, based on these data, various strategies can be applied in practice to benefit agriculture, especially for plant protection from plant viruses. Many studies using CPs to produce transgenic plants that show resistance to viruses were reported in the early 1990s. For example, tomato plants transformed with the TYLCV CP were found to be virus resistant (Kunik et al., 1994; Raj

et al., 2005). Although further studies on biological and molecular properties are required, these findings have many advantages in the "breeding for resistance" research to prevent pathogen invasion in different geographical regions.

Data availability statement

The original contributions presented in the study are included in the article/Supplementary Material, further inquiries can be directed to the corresponding author/s.

Author contributions

GP, E-JK and SL conceived and developed the concept, supervised the experiments. TV, AL, BN, MT, MQ and ET performed the experiments. TV, GP, E-JK and SL contributed to the data analysis, interpretation, discussion and write the manuscript. All authors contributed to the article and approved the submitted version.

Funding

This research was supported by the National Research Foundation of Korea grand funded by the Korea government (MSIT) (NRF-2023R1A2C1006882) and by Basic science Research Program through the National Research Foundation of Korea (NRF) funded by the Ministry of Education (NRF-2020R1I1A3071232).

Conflict of interest

The authors declare that the research was conducted in the absence of any commercial or financial relationships that could be construed as a potential conflict of interest.

Publisher's note

Supplementary material

The Supplementary Material for this article can be found online at: https://www.frontiersin.org/articles/10.3389/fpls.2023.1206255/full#supplementary-material

References

Bertin, S., Luigi, M., Parrella, G., Giorgini, M., Davino, S., and Tomassoli, L. J. P. (2018). Survey of the distribution of *Bemisia tabaci* (Hemiptera: Aleyrodidae) in Lazio region (Central Italy): a threat for the northward expansion of tomato leaf curl New Delhi virus (Begomovirus: Geminiviridae) infection. *Phytoparasitica* 46, 171–182. doi: 10.1007/s12600-018-0649-7

Bertin, S., Parrella, G., Nannini, M., Guercio, G., Troiano, E., and Tomassoli, L. J. I. (2021). Distribution and genetic variability of *Bemisia tabaci* cryptic species (Hemiptera: aleyrodidae) in Italy. *Insects* 12, 521. doi: 10.3390/insects12060521

Borden, K. L. (2000). RING domains: master builders of molecular scaffolds? *J. Mol. Biol.* 295, 1103–1112. doi: 10.1006/jmbi.1999.3429

Brown, J. K., Zerbini, F. M., Navas-Castillo, J., Moriones, E., Ramos-Sobrinho, R., Silva, J. C., et al. (2015). Revision of *Begomovirus* taxonomy based on pairwise sequence comparisons. *Arch. Virol.* 6, 1593–1619. doi: 10.1007/s00705-015-2398-y

Citovsky, V., Zaltsman, A., Kozlovsky, S. V., Gafni, Y., and Krichevsky, A. (2009). Proteasomal degradation in plant–pathogen interactions. *Semin. Cell Dev. Biol.* 20, 1048–1054. doi: 10.1016/j.semcdb.2009.05.012

Crespo, O., Robles, C., Ruiz, L., and Janssen, D. (2020). Antagonism of *Cucumber green mottle mosaic virus* against *Tomato leaf curl New Delhi virus* in zucchini and cucumber. *Ann. Appl. Biol.* 176, 147–157. doi: 10.1111/aab.12535

Fortes, I. M., Sánchez-Campos, S., Fiallo-Olivé, E., Díaz-Pendón, J. A., Navas-Castillo, J., and Moriones, E. (2016). A novel strain of tomato leaf curl New Delhi virus has spread to the Mediterranean basin. *Viruses* 8, 307. doi: 10.3390/v8110307

Gafni, Y., and Epel, B. L. (2002). The role of host and viral proteins in intra- and inter-cellular trafficking of geminiviruses. *Physiol. Mol. Plant Pathol.* 60, 231–241. doi: 10.1006/pmpp.2002.0402

Gardiner, W. E., Sunter, G., Brand, L., Elmer, J. S., Rogers, S. G., and Bisaro, D. M. (1988). Genetic analysis of tomato golden mosaic virus: the coat protein is not required for systemic spread or symptom development. *EMBO J.* 7, 899–904. doi: 10.1002/j.1460-2075.1988.tb02894.x

Hanssen, I. M., Lapidot, M., and Thomma, B. P. (2010). Emerging viral diseases of tomato crops. *Mol. Plant Microbe Interact.* 23, 539–548. doi: 10.1094/MPMI-23-5-0539

Harrison, B. D., Swanson, M. M., and Fargette, D. (2002). Begomovirus coat protein: serology, variation and functions. *Physiol. Mol. Plant Pathol.* 60, 257–271. doi: 10.1006/pmpp.2002.0404

Hussain, M., Mansoor, S., Iram, S., Fatima, A. N., and Zafar, Y. (2005). The nuclear shuttle protein of *Tomato leaf curl New Delhi virus* is a pathogenicity determinant. *J. Virol.* 79, 4434–4439. doi: 10.1128/JVI.79.7.4434-4439.2005

Jamil, N., Rehman, A., Hamza, M., Hafeez, A., Ismail, H., Zubair, M., et al. (2017). First report of *Tomato leaf curl New Delhi virus*, a bipartite begomovirus, infecting soybean (*Glycine max*). *Plant Dis.* 101, 845. doi: 10.1094/PDIS-09-16-1267-PDN

Juárez, M., Tovar, R., Fiallo-Olivé, E., Aranda, M., Gosálvez, B., Castillo, P., et al. (2014). First detection of *Tomato leaf curl New Delhi virus* infecting zucchini in Spain. *Plant Dis.* 98, 857. doi: 10.1094/PDIS-10-13-1050-PDN

Kil, E.-J., Vo, T. T. B., Fadhila, C., Ho, P. T., Lal, A., Troiano, E., et al. (2020). Seed transmission of tomato leaf curl new Delhi virus from zucchini squash in Italy. *Plants.* 9, 563. doi: 10.3390/plants9050563

Kumar, R. V., Singh, A. K., Singh, A. K., Yadav, T., Basu, S., Kushwaha, N., et al. (2015). Complexity of *Begomovirus* and betasatellite populations associated with chilli leaf curl disease in India. *J. Gen. Virol.* 96, 3143–3158. doi: 10.1099/jgv.0.000254

Kunik, T., Salomon, R., Zamir, D., Navot, N., Zeidan, M., Michelson, I., et al. (1994). Transgenic tomato plants expressing the tomato yellow leaf curl virus capsid protein are resistant to the virus. *Nat. Biotechnol.* 12, 500–504. doi: 10.1038/nbt0594-500

Kushwaha, N., Singh, A. K., Basu, S., and Chakraborty, S. (2015). Differential response of diverse solanaceous hosts to tomato leaf curl New Delhi virus infection indicates coordinated action of NBS-LRR and RNAi-mediated host defense. *Arch. Virol.* 160, 1499–1509. doi: 10.1007/s00705-015-2399-x

Livak, K. J., and Schmittgen, T. D. (2001). Analysis of relative gene expression data using real-time quantitative PCR and the $2^{-\Delta\Delta c}{}_{T}$ method. *Methods* 25, 402–408. doi: 10.1006/meth.2001.1262

López, C., Ferriol, M., and Picó, M. B. J. E. (2015). Mechanical transmission of *Tomato leaf curl New Delhi virus* to cucurbit germplasm: selection of tolerance sources in *Cucumis melo*. *Euphytica* 204, 679–691. doi: 10.1007/s10681-015-1371-x

Mabvakure, B., Martin, D. P., Kraberger, S., Cloete, L., Van Brunschot, S., Geering, A. D., et al. (2016). Ongoing geographical spread of *Tomato leaf curl New Delhi virus*. *Virology* 498, 257–264. doi: 10.1016/j.virol.2016.08.033

Maule, A., Leh, V., and Lederer, C. (2002). The dialogue between viruses and hosts in compatible interactions. *Curr. Opin. Plant Biol.* 5, 279–284. doi: 10.1016/S1369-5266(02)00272-8

Mnari-Hattab, M., Zammouri, S., Belkadhi, M., Doña, D. B., Ben Nahia, E., and Hajlaoui, M. (2015). First report of *Tomato leaf curl New Delhi virus* infecting cucurbits in Tunisia. *New Dis.Rep.* 31, 2044–0588.2015. doi: 10.5197/j.2044-0588.2015.031.021

Moriones, E., Praveen, S., and Chakraborty, S. (2017). Tomato leaf curl New Delhi virus: an emerging virus complex threatening vegetable and fiber crops. *Viruses* 9, 264. doi: 10.3390/v9100264

Orfanidou, C. G., Malandraki, I., Beris, D., Kektsidou, O., Vassilakos, N., Varveri, C., et al. (2019). First report of tomato leaf curl New Delhi virus in zucchini crops in Greece. *J.Plant Pathol.* 101, 799. doi: 10.1007/s42161-019-00265-y

Padidam, M., Beachy, R. N., and Fauquet, C. M. (1995a). Classification and identification of geminiviruses using sequence comparisons. *J. Gen. Virol.* 76, 249–263. doi: 10.1099/0022-1317-76-2-249

Padidam, M., Beachy, R. N., and Fauquet, C. M. (1995b). Tomato leaf curl geminivirus from India has a bipartite genome and coat protein is not essential for infectivity. *J. Gen. Virol* 76, 25–35. doi: 10.1099/0022-1317-76-1-25

Panno, S., Caruso, A., Troiano, E., Luigi, M., Manglli, A., Vatrano, T., et al. (2019). Emergence of tomato leaf curl New Delhi virus in Italy: estimation of incidence and genetic diversity. *Plant Pathol.* 68, 601–608. doi: 10.1111/ppa.12978

Parrella, G., Troiano, E., Formisano, G., Accotto, G., and Giorgini, M. (2018). First report of *Tomato leaf curl New Delhi virus* associated with severe mosaic of pumpkin in Italy. *Plant Dis.* 102, 459. doi: 10.1094/PDIS-07-17-0940-PDN

Raj, S., Singh, R., Pandey, S., and Singh, B. (2005). *Agrobacterium*-mediated tomato transformation and regeneration of transgenic lines expressing tomato leaf curl virus coat protein gene for resistance against TLCV infection. *Curr. Sci.* 88, 1674–1679. Available at: https://www.jstor.org/stable/24110495

Rivarez, M. P. S., Vučurović, A., Mehle, N., Ravnikar, M., and Kutnjak, D. (2021). Global advances in tomato virome research: current status and the impact of high-throughput sequencing. *Front. Microbiol.* 12, 1064. doi: 10.3389/fmicb.2021.671925

Romero-Masegosa, J., Martínez, C., Aguado, E., García, A., Cebrián, G., Iglesias-Moya, J., et al. (2021). Response of *Cucurbita* spp. to tomato leaf curl New Delhi virus inoculation and identification of a dominant source of resistance in *Cucurbita moschata*. *Plant Pathol.* 70, 206–218. doi: 10.1111/ppa.13268

Ruiz, L., Simon, A., Velasco, L., and Janssen, D. (2017). Biological characterization of *tomato leaf curl New Delhi virus* from Spain. *Plant Pathol.* 66, 376–382. doi: 10.1111/ppa.12587

Sáez, C., Esteras, C., Martínez, C., Ferriol, M., Dhillon, N. P., López, C., et al. (2017). Resistance to tomato leaf curl New Delhi virus in melon is controlled by a major QTL located in chromosome 11. *Plant Cell Rep.* 36, 1571–1584. doi: 10.1007/s00299-017-2175-3

Sáez, C., Flores-León, A., Montero-Pau, J., Sifres, A., Dhillon, N. P. S., López, C., et al. (2022). RNA-Seq transcriptome analysis provides candidate genes for resistance to tomato leaf curl New Delhi virus in melon. *Front. Plant Sci.* 12, 798858. doi: 10.3389/fpls.2021.798858

Sellés Vidal, L., Kelly, C. L., Mordaka, P. M., and Heap, J. T. (2018). Review of NAD (P)H-dependent oxidoreductases: properties, engineering and application. *Biochim. Biophys. Acta-Proteins Proteom.* 1866, 327–347. doi: 10.1016/j.bbapap.2017.11.005

Sharma, J., Lager, P., and Kumar, Y. (2021). First report of *Tomato leaf curl New Delhi virus* infecting *Ricinus communis*. *New Dis.Rep.* 44, e12053. doi: 10.1002/ndr2.12053

Shen, Q., Hu, T., Bao, M., Cao, L., Zhang, H., Song, F., et al. (2016). Tobacco RING E3 ligase NtRFP1 mediates ubiquitination and proteasomal degradation of a geminivirus-encoded βC1. *Mol. Plant* 9, 911–925. doi: 10.1016/j.molp.2016.03.008

Singh, R., Rai, N., Singh, M., Saha, S., and Singh, S. (2015). Detection of tomato leaf curl virus resistance and inheritance in tomato (*Solanum lycopersicum* L.). *J. Agric. Sci.* 153, 78–89. doi: 10.1017/S0021859613000932

Southern, E. (2006). Southern blotting. *Nat. Protoc.* 1, 518–525. doi: 10.1038/nprot.2006.73

Srivastava, A., Kumar, S., Jaidi, M., Raj, S., and Shukla, S. (2016). First report of *Tomato leaf curl New Delhi virus* on opium poppy (*Papaver somniferum*) in India. *Plant Dis.* 100, 232. doi: 10.1094/PDIS-08-15-0883-PDN

Sun, J., Sun, Y., Ahmed, R. I., Ren, A., and Xie, A. M. (2019). Research progress on plant RING-finger proteins. *Genes* 10, 973. doi: 10.3390/genes10120973

Thompson, J. R., Register, E., Curotto, J., Kurtz, M., and Kelly, R. (1998). An improved protocol for the preparation of yeast cells for transformation by electroporation. *Yeast* 14, 565–571. doi: 10.1002/(SICI)1097-0061(19980430)14:6<565::AID-YEA251>3.0.CO;2-B

Troiano, E., and Parrella, G. (2023). First report of *Tomato leaf curl New Delhi virus* in *Lagenaria siceraria* var. *longissima* in Italy. *Phytopathol. Mediterranea* 62, 25-28. doi: 10.36253/phyto-14147

Trujillo, M., and Shirasu, K. (2010). Ubiquitination in plant immunity. *Curr. Opin. Plant Biol.* 13, 402–408. doi: 10.1016/j.pbi.2010.04.002

Venkataravanappa, V., Reddy, C. L., Saha, S., and Reddy, M. K. (2018). Recombinant *Tomato leaf curl New Delhi virus* is associated with yellow vein mosaic disease of okra in India. *Physiol. Mol. Plant Pathol.* 104, 108–118. doi: 10.1016/j.pmpp.2018.10.004

Vo, T. T., Lal, A., Ho, P. T., Troiano, E., Parrella, G., Kil, E.-J., et al. (2022a). Different infectivity of Mediterranean and southern Asian *Tomato leaf curl New Delhi virus* isolates in cucurbit crops. *Plants* 11, 704. doi: 10.3390/plants11050704

Vo, T. T. B., Troiano, E., Lal, A., Hoang, P. T., Kil, E.-J., Lee, S., et al. (2022b). ToLCNDV-ES infection in tomato is enhanced by TYLCV: evidence from field survey and agroinoculation. *Fron. Microb.* 13, 954460. doi: 10.3389/fmicb.2022.954460

Weigel, D., and Glazebrook, J. J. C. P. (2006). Transformation of agrobacterium using the freeze-thaw method. *CSH Protocols* 2006, pdb. prot4666. doi: 10.1101/pdb.prot4666

Yamamoto, H., Wakita, Y., Kitaoka, T., Fujishiro, K., Kesumawati, E., and Koeda, S. (2021). Southeast Asian isolate of the *Tomato leaf curl New Delhi virus* shows higher pathogenicity against tomato and cucurbit crops compared to that of the Mediterranean isolate. *Hortic. J.* 90, 314–325. doi: 10.2503/hortj.UTD-269

Zaidi, S. S. E. A., Martin, D. P., Amin, I., Farooq, M., and Mansoor, S. (2017). *Tomato leaf curl New Delhi virus*: a widespread bipartite *Begomovirus* in the territory of monopartite begomoviruses. *Mol. Plant Pathol.* 18, 901–911. doi: 10.1111/mpp.12481

Zeng, L.-R., Vega-Sánchez, M. E., Zhu, T., and Wang, G.-L. (2006). Ubiquitination-mediated protein degradation and modification: an emerging theme in plant-microbe interactions. *Cell Res.* 16, 413–426. doi: 10.1038/sj.cr.7310053

frontiers | Frontiers in Plant Science

TYPE Original Research
PUBLISHED 18 July 2023
DOI 10.3389/fpls.2023.1224958

OPEN ACCESS

EDITED BY
Chellappan Padmanabhan,
USDA APHIS PPQ Science and Technology, United States

REVIEWED BY
Hanako Shimura,
Hokkaido University, Japan
Katarzyna Otulak-Kozieł,
Warsaw University of Life Sciences, Poland

*CORRESPONDENCE
Tatiana Komarova
t.komarova@belozersky.msu.ru

†These authors have contributed equally to this work

RECEIVED 18 May 2023
ACCEPTED 03 July 2023
PUBLISHED 18 July 2023

CITATION
Ershova N, Kamarova K, Sheshukova E, Antimonova A and Komarova T (2023) A novel cellular factor of *Nicotiana benthamiana* susceptibility to tobamovirus infection.
Front. Plant Sci. 14:1224958.
doi: 10.3389/fpls.2023.1224958

A novel cellular factor of *Nicotiana benthamiana* susceptibility to tobamovirus infection

Natalia Ershova[1†], Kamila Kamarova[1†], Ekaterina Sheshukova[1], Alexandra Antimonova[1] and Tatiana Komarova[1,2*]

[1]Vavilov Institute of General Genetics, Russian Academy of Sciences, Moscow, Russia, [2]Belozersky Institute of Physico-Chemical Biology, Lomonosov Moscow State University, Moscow, Russia

Viral infection, which entails synthesis of viral proteins and active reproduction of the viral genome, effects significant changes in the functions of many intracellular systems in plants. Along with these processes, a virus has to suppress cellular defense to create favorable conditions for its successful systemic spread in a plant. The virus exploits various cellular factors of a permissive host modulating its metabolism as well as local and systemic transport of macromolecules and photoassimilates. The *Nicotiana benthamiana* stress-induced gene encoding Kunitz peptidase inhibitor-like protein (KPILP) has recently been shown to be involved in chloroplast retrograde signaling regulation and stimulation of intercellular transport of macromolecules. In this paper we demonstrate the key role of KPILP in the development of tobamovius infection. Systemic infection of *N. benthamiana* plants with tobacco mosaic virus (TMV) or the closely related crucifer-infecting tobamovirus (crTMV) induces a drastic increase in *KPILP* mRNA accumulation. *KPILP* knockdown significantly reduces the efficiency of TMV and crTMV intercellular transport and reproduction. Plants with *KPILP* silencing become partially resistant to tobamovirus infection. Therefore, KPILP could be regarded as a novel proviral factor in the development of TMV and crTMV infection in *N. benthamiana* plants.

KEYWORDS

tobacco mosaic virus, Kunitz peptidase inhibitor-like protein (KPILP), virus susceptibility genes, intercellular movement, plant-virus interactions, proviral factor

1 Introduction

Due to a limited genome size and hence a limited protein encoding potential, the plant viruses resort to exploiting the cellular factors of their hosts at all stages of infection, creating favorable conditions both for intercellular and systemic transport throughout the plant. Moreover, plant viruses are capable of suppressing the antiviral defense mechanisms

that are activated in response to viral infection (Wu et al., 1994; Wu and Shaw, 1996; Nelson and van Bel, 1998).

Tobacco mosaic virus (TMV) infection starts with a virion penetrating a plant cell, followed by an uncoating and synthesis of the non-structural proteins being essential for viral genome replication and transcription. To ensure a successful infection, three main processes are needed: viral RNA accumulation in the infected cells, intercellular spread of viral genetic material, and, finally, a long-distance transport (Heinlein, 2015; Ishibashi and Ishikawa, 2016). TMV intercellular spread is mediated by a non-structural 30 kDa movement protein (MP). MP interacts with viral and cellular factors, including plasmodesmata-associated proteins (PDAPs) (Ueki and Citovsky, 2014a; Dorokhov et al., 2019), in order to enable cell-to-cell movement of tobamoviral RNA (Liu and Nelson, 2013; Heinlein, 2015; Reagan and Burch-Smith, 2020; Sheshukova et al., 2020). MP binds viral RNA, facilitates its intracellular transport to plasmodesmata (PD) and affects PD permeability *inter alia*, via an indirect regulation of PD callose depositions (Amsbury et al., 2017). MP has been shown to interact with numerous host cell proteins, including the cytoskeletal proteins actin and myosin (Boyko et al., 2007; Guenoune-Gelbart et al., 2008; Hofmann et al., 2009; Amari et al., 2014) as well as myosin-binding protein (Kragler et al., 2003; Curin et al., 2007), cell wall pectin methylesterases (Dorokhov et al., 1999; Chen et al., 2000; Dorokhov et al., 2006), plasma membrane and PD proteins: synaptotagmins (Uchiyama et al., 2014; Yuan et al., 2018; Liu et al., 2020), remorins (Sasaki et al., 2018; Ma et al., 2022), ANK protein (Ueki and Citovsky, 2014b), calreticulin (Chen et al., 2005), etc.

In addition to MP, other TMV proteins were also found to be closely associated with the host factors. For example, TMV 126K component of the replicase was shown to interact with eukaryotic translation elongation factors 1A and 1B (Yamaji et al., 2010; Hwang et al., 2013). Moreover, replication complex components, 126K and 183K, were co-purified with chloroplast proteins, Rubisco activase (RCA) and ATP synthase γ-subunit (AtpC) (Bhat et al., 2013), and shown to interact with the *psbO*-encoded 33 kDa chloroplast protein, a component of the oxygen-evolving complex (Abbink et al., 2002). Another TMV component, the coat protein, was detected in association with chloroplast thylakoid membranes (Reinero and Beachy, 1986). Therefore, viral proteins interact with and exploit various cellular factors, inducing their structural and functional disturbance, thus suppressing or activating defense reactions (Bhattacharyya and Chakraborty, 2017; Rodriguez-Peña et al., 2021). Apart direct interactions between the virus and a host cell, there are multiple indirect effects of the viral infection. For instance, the chloroplast-resident DEAH-box RNA helicase, INCREASED SIZE EXCLUSION LIMIT2 (ISE2), has been implicated in virus-chloroplast interactions. Knockdown of *ISE2* in *Nicotiana benthamiana* plants leads to chlorosis development, activation of chloroplast retrograde signaling (CRS) and intercellular transport of macromolecules, as well as an increased sensitivity to TMV infection (Ganusova et al., 2017). At the same time, transient *ISE2* overexpression also resulted in susceptibility to TMV. The authors explain the increased sensitivity to TMV through the defense reactions activated via jasmonate signaling pathway that suppresses the salicylate-mediated resistance to the viral infection. Overall, these results in the susceptibility of tobacco plants to TMV (Ganusova et al., 2017). This example illustrates the subtle equilibrium between activation and suppression of plant antiviral defense mechanisms (Qiao et al., 2009; Bhat et al., 2013).

The above-mentioned cellular factors do not represent an exhaustive list. They are just a few examples of multiple interactions between the host cell factors and tobamoviral proteins that reflect a complex plant-virus interplay coupled with various ways the virus can exploit the plant cell. Most of these components are essential for the productive and effective viral infection, while not all of them are critical to cellular processes and cell viability. Consequently, these factors could be considered as genetic determinants of plant susceptibility to the virus (Garcia-Ruiz, 2018). The permissive host is characterized by the presence of all cellular factors ensuring a successful infection with a particular virus. Some of these genetic determinants are hardly detectable in the absence of viral infection, because their expression is induced only in response to a viral invasion or any other stress. Research into these virus-induced genes could broaden our knowledge about the plant-virus interaction and give us new opportunities for developing innovative techniques and approaches for antiviral crop protection.

We had previously identified *N. benthamiana* stress-induced gene encoding Kunitz peptidase inhibitor-like protein (KPILP) and showed that its expression is upregulated in response to GFP-encoding viral vector reproduction, prolonged darkness (Sheshukova et al., 2017a) and potato virus X (PVX) infection (Ershova et al., 2022). Recently, KPILP has been shown to be a positive regulator of intercellular macromolecular trafficking and implicated in the regulation of CRS (Ershova et al., 2022).

In this paper we explore the KPILP role in plant-virus interactions, specifically, KPILP functioning during a tobamoviral infection of *N. benthamiana* plants. We hypothesized that KPILP may be a plant susceptibility factor that is not essential for cellular "basic life support" under normal conditions, as it is activated only in response to different stress factors, which include viral infection as well. Viruses, inducing KPILP, could exploit it to modulate the metabolism and create favorable cellular environment for the viral infection. To test this hypothesis, we assessed the reproduction and local transport of GFP-encoding TMV- and crTMV-based viral vectors in plants with up- or downregulated *KPILP* expression and detected significant inhibition of viral intercellular spread, as well as decreased level of viral RNA accumulation in plants with suppressed *KPILP*. In addition, we analyzed the development of systemic TMV and crTMV infection in plants with decreased and increased *KPILP* expression. Symptom monitoring and viability registration during 40 days after inoculation with TMV or crTMV revealed that plants with *KPILP* knockdown acquired a partial resistance to tobamoviral infection, demonstrating less severe and delayed symptom development as well as an increased viability compared to plants with elevated *KPILP* expression. Taken together, these results indicate that KPILP may be a novel susceptibility factor of *N. benthamiana* to tobamovirus infection.

2 Materials and methods

2.1 Plant growth conditions

Wild type *Nicotiana benthamiana* plants were grown in the soil in a controlled environment chamber under a 16 h/8 h day/night cycle.

2.2 Agroinfiltration

Agrobacterium tumefaciens strain GV3101 was transformed with individual binary vectors and grown at 28°C in LB medium supplemented with 50 mg/l rifampicin, 25 mg/l gentamycin and 50 mg/l carbenicillin/kanamycin. *Agrobacterium* overnight culture was diluted with buffer containing 10 mM MES (pH 5.5) and 10 mM $MgSO_4$, and adjusted to final OD_{600} of 0.01 for pPVX or pPVX (frKPILP) plasmids, OD_{600} of 0.3 for TMV:GFP and crTMV:GFP in the experiments with PVX-infected plants and OD_{600} 0.01 in the experiments with 35S-siKPILP. *Agrobacterium* suspension for pCambia1300 and 35S-siKPILP was diluted to OD_{600} of 0.1. Agroinfiltration was performed on almost fully expanded *N. benthamiana* leaves that were still attached to the intact plant. A bacterial suspension was infiltrated into the leaf tissue using a 2-ml syringe. After that the plants were incubated in greenhouse conditions.

2.3 Plant inoculation for systemic infection

N. benthamiana plants were inoculated with pPVX or pPVX (frKPILP) by agroinfiltration of the lower leaves, and in 10-14 days the systemic PVX infection was detected in the upper leaves. To induce TMV systemic infection, lower leaves of *N. benthamiana* plants were inoculated with 300 μg/ml suspension of virus particles in the presence of celite. To obtain plants with crTMV systemic infection, lower leaves were agroinfiltrated with the viral vector encoding crTMV infectious copy.

2.4 GFP imaging and quantification

GFP-containing foci of infection were visualized using a handheld UV lamp (λ = 366 nm). The foci area and fluorescence intensity were measured using open-source ImageJ software (Schneider et al., 2012).

2.5 Quantitative real-time PCR (qRT-PCR) analysis of transcript concentrations

Total RNA was extracted from plant tissues using the ExtractRNA reagent (Evrogen, Russia) according to the manufacturer's instructions. For first strand cDNA synthesis, 0.1 mg of random hexamers and 0.1 mg of oligo-dT primer were added to 2 μg of total RNA, and reverse transcription was performed using Magnus reverse transcriptase (Evrogen, Russia) according to the manufacturer's protocol. Quantitative real-time PCR was carried out using iCycler iQ real-time PCR detection system (Bio-Rad, Hercules, CA, USA). Reference genes were detected using the primers to 18S rRNA gene and protein phosphatase 2A gene (PP2A). The target genes were detected using sequence-specific primers and Eva Green master mix (Syntol, Russia) according to the manufacturer's instructions. Primers used for qRT-PCR are listed in Table S1. Each sample was run three times, and non-template control was added to each run. A minimum of five biological replicates were performed. The results of qRT-PCR were evaluated using the Pfaffl algorithm (Pfaffl, 2001).

2.6 Plasmid constructs

To obtain 35S-siKPILP construct an approach based on the backbone of pKANNIBAL plasmid (Wesley et al., 2001) containing plant intron and multicloning sites for the insertion of sense and antisense fragment of the target sequence was used. 346-nt *KPILP* fragment (from 258 to 603 nt of the coding sequence) was amplified using the corresponding pair of primers to obtain two PCR products: the first (sense orientation) was flanked with XhoI and EcoRI recognition sites and the second (antisense orientation) – with BamHI and XbaI. Oligonucleotides used for PCR are listed in the Table S1. A fragment containing PDK intron was excised from pKANNIBAL using EcoRI and BamHI. At the next step, two abovementioned PCR products digested with the corresponding restriction enzymes (XhoI/EcoRI and BamHI/XbaI, respectively) together with PDK intron flanked with EcoRI/BamHI were ligated in pKANNIBAL plasmid digested with XhoI and XbaI. The obtained intermediate construct contained 35S promoter, sense KPILP fragment, PDK intron, antisense KPILP fragment and OCS terminator. This cassette was excised using PvuII restriction enzyme and transferred to pCambia1300 binary vector digested with PvuII resulting in final 35S-siKPILP construct.

2.7 Statistical analysis

The data was analyzed either by Student's t-test or by one-way ANOVA as indicated in figure captions. The significance of difference between groups was assessed using Tukey honestly significant difference (HSD) test at $p < 0.05$ level or Student's t-test. In all histograms, y-axis error bars represent the standard error of the mean values.

3 Results

3.1 *KPILP* mRNA accumulation drastically increases in response to TMV and crTMV infection

Previously, *KPILP* mRNA levels were shown to increase more than 100-fold during systemic TMV in *Nicotiana tabacum* and crTMV-based viral vector reproduction in *N. benthamiana*

(Sheshukova et al., 2017a). Moreover, we have recently demonstrated that *KPILP* is induced in response to PVX infection. However, it increases only by a factor of 8-12 (Ershova et al., 2022). Here we used *N. benthamiana* as a model plant to study *KPILP* role during tobamovirus infection. First, we obtained plants with TMV and crTMV systemic infection confirmed by visible symptoms as well as viral RNA and coat protein accumulation detected in plant extracts (Figure S1) and analyzed *KPILP* mRNA levels in leaves with TMV (Figure 1A) and crTMV (Figure 1B) systemic infection. The results of qRT-PCR demonstrated that *KPILP* mRNA content was at least by 3 orders of magnitude higher in TMV- and crTMV-infected leaves as compared to the samples from the same plants before inoculation. This indicates that both TMV and crTMV systemic infection leads to a significant increase in *KPILP* expression.

However, such *KPILP* mRNA levels significantly exceed those obtained in experiments with crTMV-based viral vector lacking gene encoding coat protein (CP) (Sheshukova et al., 2017a). To check if this effect could be explained by the absence of one of the viral genes (*CP*) we performed agroinfiltration of *N. benthamiana* leaves with genetic constructs encoding either TMV CP or MP under control of 35S promoter and analyzed *KPILP* mRNA levels 3 days after agroinfiltration. We observed a ~10-fold increase in *KPILP* mRNA in response to *MP* expression and ~14-fold increase induced by *CP* (Figure S2). Thus, the individual viral genes do not stimulate *KPILP* expression in the same extent as systemic TMV and crTMV infection.

3.2 KPILP downregulates expression of nuclear genes encoding chloroplast proteins

N. tabacum TMV infection results in a reduced expression of Rubisco activase gene, *RCA*, and ATP-synthase γ-subunit gene, *AtpC* (Sheshukova et al., 2017b). Both RCA and AtpC are host chloroplast factors that were co-purified with the viral replication complex during TMV infection. They are also important for ensuring a specific plant defense against tobamoviruses but not against PVX (Bhat et al., 2013). Analysis of *RCA* and *AtpC* mRNA levels during TMV and crTMV infection in *N. benthamiana* plants revealed their significant decrease (Figures 2A, B). Considering that *KPILP* was recently demonstrated to downregulate nuclear genes of chloroplast proteins which are regarded as CRS markers (Ershova et al., 2022), and *KPILP* mRNA accumulation showed more than a thousandfold increase in response to tobamovirus infection (Figure 1), we put forward that KPILP could affect *RCA* and *AtpC* genes expression. To test this hypothesis, we agroinfiltrated *N. benthamiana* leaves with 35S-KPILP and assessed *RCA* and *AtpC* mRNA levels in response to transient *KPILP* overexpression (Figure 2C). The results of qRT-PCR indicate that the increased *KPILP* expression leads to halving in *RCA* and *AtpC* mRNA accumulation. As an additional control, we used pCambia1300 binary vector, as agroinfiltration with and the "empty" vector *per se* slightly stimulates *KPILP* expression (Ershova et al., 2022). Indeed, we observed a 20-30% decline in *RCA* and *AtpC* mRNA levels in samples from pCambia1300 agroinfiltrated leaves (Figure 2C).

The nuclear-encoded chloroplast-localized RNA helicase *ISE2* is involved in chloroplast RNA processing and translation. Virus-induced silencing of *ISE2* results in a severe chloroplast dysfunction, suppresses chloroplast gene expression and activates CRS. At early stages of embryogenesis *ISE2* mutations are fatal to embryos (Burch-Smith and Zambryski, 2010; Burch-Smith et al., 2011). We checked whether the tobamovirus infection or *KPILP* overexpression induce any changes in *ISE2* mRNA levels. The results of qRT-PCR analysis revealed no significant difference between the control leaves and the leaves from TMV- (Figure 2A) and crTMV-infected (Figure 2B) plants or leaves with transient *KPILP* expression (Figure 2C). Therefore, the elevated *KPILP* expression induced either by tobamovirus infection or 35S-KPILP agroinfiltration did not affect *ISE2* mRNA accumulation.

To check whether the increase in KPILP, induced by tobamovirus infection affects the other chloroplast proteins encoded by nuclear genes including those associated with CRS, we assessed the expression of CRS marker genes encoding the

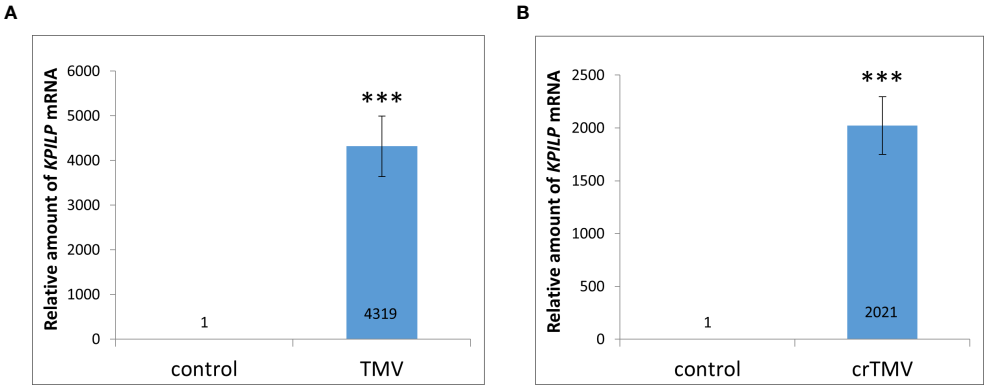

FIGURE 1
Systemic tobamovirus infection drastically stimulates *KPILP* expression. **(A, B)** The relative amount of *KPILP* mRNA in leaves with TMV **(A)** and crTMV **(B)** systemic infection as determined by qRT-PCR. The difference between the control (samples from the same plants before inoculation) and infected leaves is significant at $p<0.001$ (Student's t-test) and marked with ***.

10.3389/fpls.2023.1224958

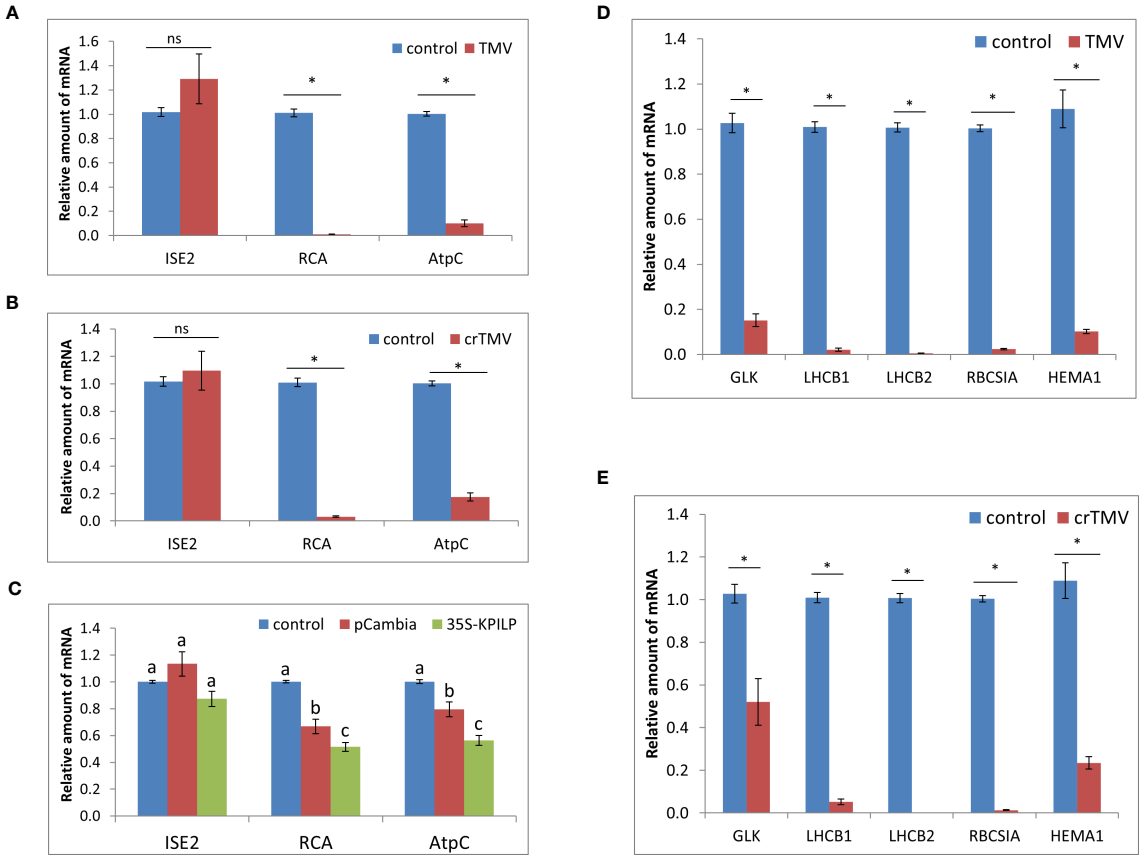

FIGURE 2
Tobamovirus infection downregulates photosynthesis-associated nuclear-encoded genes. Relative amount of mRNA in leaves with TMV **(A)** and crTMV **(B)** systemic infection, as revealed using qRT-PCR. Samples from the same plants before inoculation are taken as 1 (control), *, p<0.001; ns, not significantly different (Student's t-test). **(C)** Relative amount of chloroplast protein encoding mRNA in leaves 3 days after agroinfiltration with "empty" pCambia1300 or 35S-KPILP as determined using qRT-PCR. Values for samples from non-infiltrated leaves are taken as 1 (control). Bars with different letters indicate significant difference at p<0.05 (ANOVA, Tukey HSD), while bars with the same letter are not significantly different. **(D, E)** Relative amount of CRS marker genes mRNA in response to TMV **(D)** or crTMV **(E)** infection as determined using qRT-PCR. The level of mRNA accumulation for each gene in leaves before inoculation was taken as 1. *, p<0.001 (Student's t-test).

components involved in the photosynthetic activity and defining the physiological status of chloroplasts: the transcriptional factor GOLDEN2-LIKE1 (GLK1) (Fitter et al., 2002); the light-harvesting complex antenna proteins LHCB 1 and 2; an isoform of rubisco small subunit (RBCS1A) (Bhat et al., 2013), the glutamyl-tRNA reductase protein (HEMA1) (Schmied et al., 2011). The qRT-PCR analysis revealed that expression of all these genes is downregulated during either TMV (Figure 2D) or crTMV (Figure 2E) systemic infection when *KPILP* expression is significantly increased (Figure 1).

3.3 KPILP stimulates reproduction and intercellular transport of TMV and crTMV

We have recently demonstrated that the increased *KPILP* expression facilitates cell-to-cell movement of 2xGFP reporter molecule and that KPILP *N*-glycosylation is indispensable for its ability to activate the intercellular transport. Moreover, it was shown that the upregulated *KPILP* is associated with decreased PD callose deposition (Ershova et al., 2022). To understand whether KPILP contributes to the viral intercellular movement, we used the previously developed model system for assessing KPILP-mediated effects. It is based on *KPILP* upregulation activated by PVX infection and *KPILP* suppression by virus-induced gene silencing (VIGS) using pPVX and pPVX(frKPILP) viral vectors, respectively (Ershova et al., 2022).

To estimate the efficiency of TMV or crTMV intercellular spread we used TMV:GFP and crTMV:GFP viral vectors, respectively, delivering the corresponding plasmids by agrobacteria into leaves of *N. benthamiana* plants with pPVX or pPVX(frKPILP) systemic infection and confirmed increased or suppressed *KPILP* expression. The control group contained intact plants of the same age. TMV:GFP and crTMV:GFP are capable of only local spread because of a lack of CP. Therefore, monitoring GFP-expressing foci of infection allows assessing the efficiency of infection and intercellular spread.

To obtain the single cells transformed with either TMV:GFP or crTMV:GFP with further development of individual foci, we used the optimized dilutions of argobacterium suspensions. Results shown in Figures 3, 4 demonstrate that the GFP-expressing foci number is much lower in 4 days after agroinfiltration with either

10.3389/fpls.2023.1224958

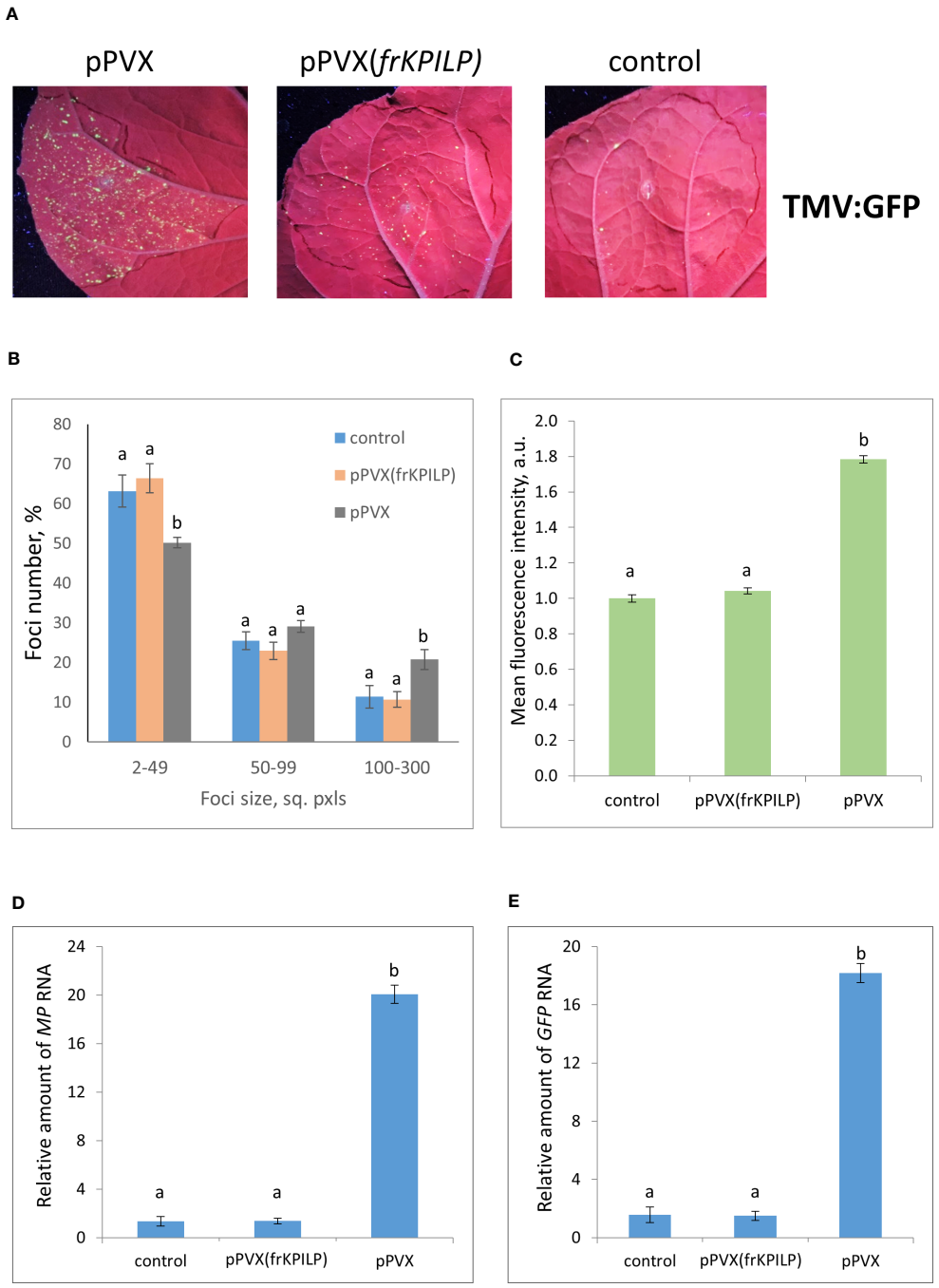

FIGURE 3
Upregulation of *KPILP* expression stimulates TMV:GFP reproduction and intercellular spread. **(A)** GFP-expressing foci visualization under UV light in *N. benthamiana* leaves of control plants (on the right) and plants with up- (on the left, pPVX) and downregulated [in the middle, pPVX(frKPILP)] *KPILP* expression 4 days after agroinfiltration with TMV:GFP. **(B)** Percentage of TMV:GFP-expressing foci of different size. **(C)** Mean GFP fluorescence intensity in analyzed foci. Relative amount of *MP* **(D)** and *GFP* **(E)** RNA in analyzed leaves quantified using qRT-PCR. Mean values and standard error are presented in histograms **(B–E)**. The data was analyzed using ANOVA. Bars without same letters indicate significant differences according to Tukey HSD at $p<0.05$.

TMV:GFP (Figure 3A) or crTMV:GFP (Figure 4A) in control plants and plants with the suppressed *KPILP* expression compared to the plants with an increased *KPILP* level. Notably, *KPILP* mRNA accumulation level is comparable in the control plants and plants with *KPILP* VIGS induced by pPVX(frKPILP) infection (Ershova et al., 2022).

To assess the effect of KPILP on the efficiency of viral intercellular spread and reproduction we quantified the areas of GFP-expressing foci and the intensity of fluorescence in each experimental group. The percentage of larger foci (100-300 square pixels) is the highest in plants with upregulated *KPILP* expression, while the number of small foci (2-49 sq. pxls) is the lowest

10.3389/fpls.2023.1224958

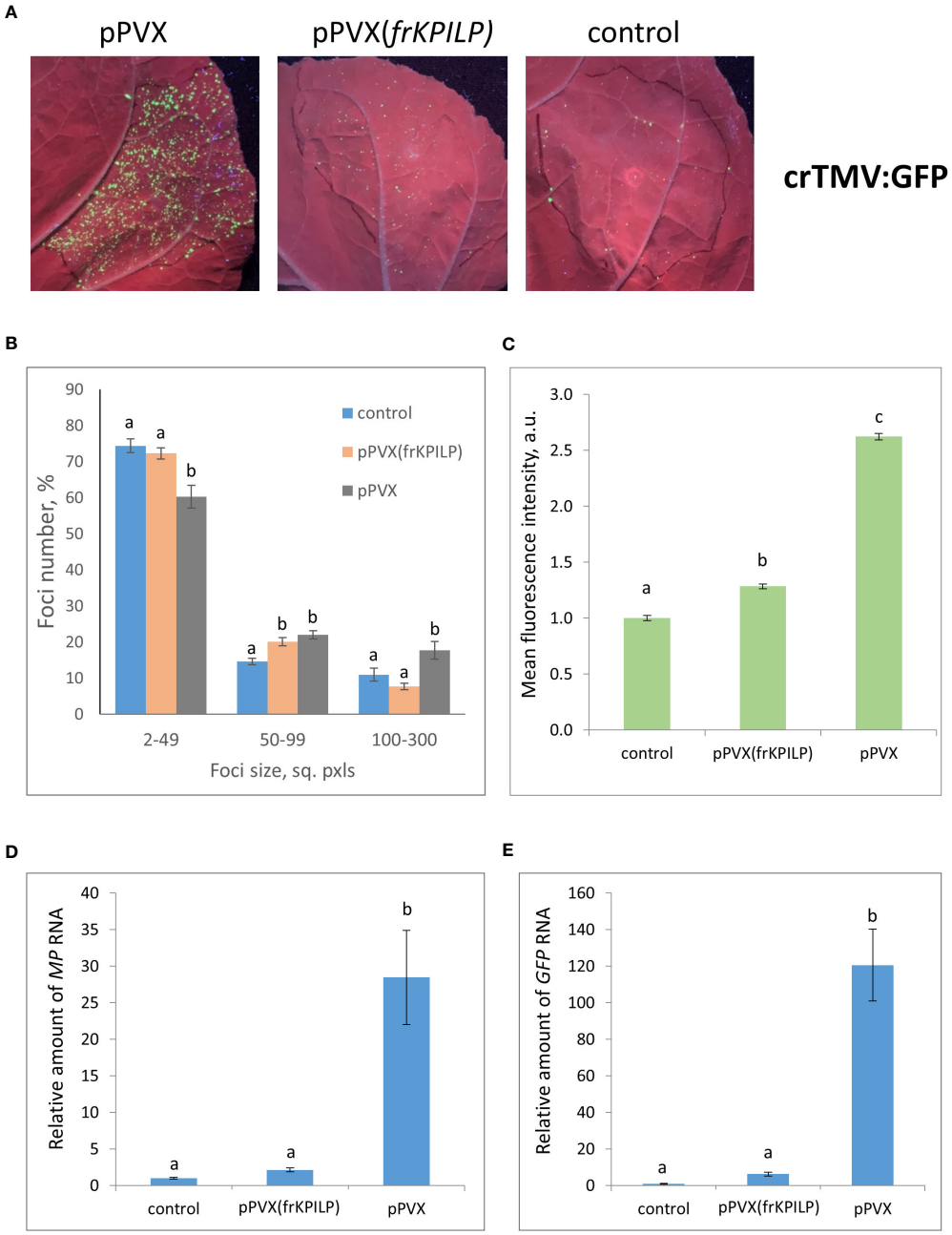

FIGURE 4
Upregulation of *KPILP* expression stimulates crTMV:GFP reproduction and intercellular spread. **(A)** GFP-expressing foci visualization under UV light in *N. benthamiana* leaves of control (on the right) plants and plants with up- (on the left, pPVX) and downregulated [in the middle, pPVX(frKPILP)] KPILP expression 4 days after agroinfiltration with crTMV:GFP. **(B)** Percentage of crTMV:GFP-expressing foci of different size. **(C)** Mean GFP fluorescence intensity in analyzed foci. Relative amount of *MP* **(D)** and *GFP* **(E)** RNA in analyzed leaves quantified by qRT-PCR. Mean values and standard error are presented in histograms **(B–E)**. The data was analyzed using ANOVA. Bars without similar letters indicate significant differences according to Tukey HSD at $p<0.05$.

(Figures 3B, 4B), indicating that the most effective intercellular transport of viral vectors is associated with elevated *KPILP* levels. GFP fluorescence intensity in each focus reflects the level of viral vector reproduction and GFP accumulation. The highest intensity is also observed in plants with upregulated *KPILP* (Figures 3C, 4C).

Viral reproduction efficiency was additionally assessed using qRT-PCR of *MP* and *GFP* RNA in the infiltrated areas. The levels of the corresponding RNA in plants inoculated with TMV:GFP with the increased *KPILP* expression were about 20-fold higher than *MP* and *GFP* RNA levels in plants with silenced *KPILP* and control plants (Figures 3D, E). This indicates that viral reproduction is suppressed when *KPILP* is downregulated. Similar results were obtained in plants inoculated with crTMV:GFP (Figures 4D, E).

Plant agrobacterial transformation efficiency depends on numerous factors and represents a stress factor *per se*. In the abovementioned PVX-based system tobamovirus vectors were delivered via agroinfiltration when *KPILP* expression level was already premodified. Thus, it couldn't be ruled out that this

10.3389/fpls.2023.1224958

potentially led to the different efficiency of plant cells transformation by agrobacteria. To exclude the impact of this putative effect and additionally confirm that *KPILP* silencing negatively affects tobamovirus reproduction we used another experimental system. *KPILP* suppression was performed by the transiently expressed 35S-siKPILP cassette (Figure S3A) encoding 346-nt *KPILP* fragment in sense and antisense orientation separated by a plant intron. The intron was spliced in cells thus forming a hairpin RNA that induced *KPILP* silencing. TMV:GFP or crTMV:GFP vectors were introduced in *N. benthamiana* leaves simultaneously with 35S-siKPILP construct or pCambia1300 as a control (Figures 5A, B). 35S-siKPILP expression was confirmed by qRT-PCR (Figures S3B, C) and was shown to result in a 5-fold downregulation of endogenous *KPILP* levels (Figures 5C, D). An optimized agrobacterial suspension dilution allowed to obtain distinct areas of viral infection – *GFP*-expressing foci the size of which reflected the efficiency of TMV:GFP or crTMV:GFP intercellular spread. The results of foci size quantification (Figures 5E, F) indicate that *KPILP* silencing induced by the expression of 35S-siKPILP led to the increase by 10% of small

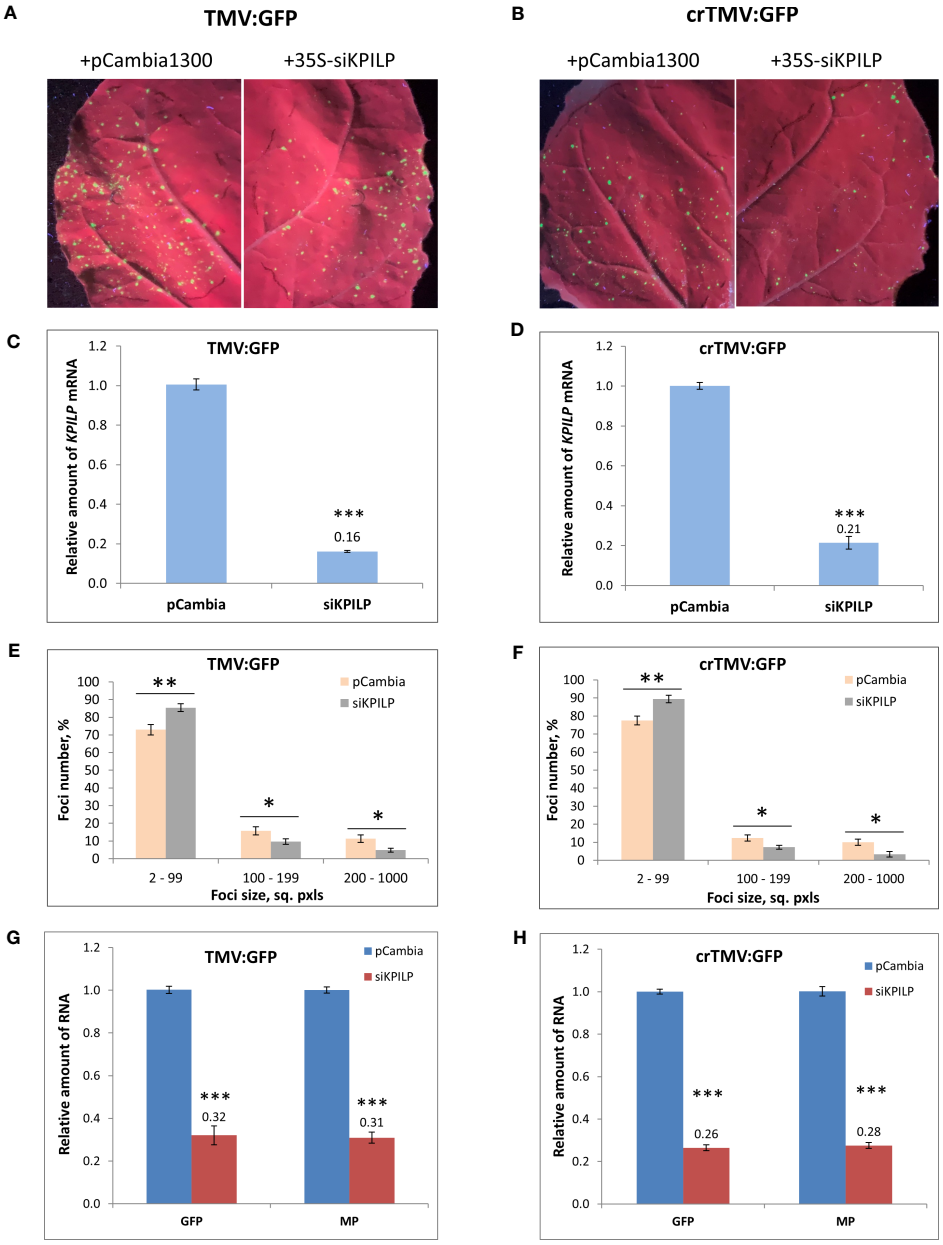

FIGURE 5
KPILP transient downregulation leads to the suppression of tobamovirus intercellular transport and reproduction. **(A, B)** GFP-expressing foci visualization under UV light in *N. benthamiana* leaves agroinfiltrated with TMV:GFP **(A)** or crTMV:GFP **(B)** together with 35S-siKPILP or pCambia1300. **(C, D)** *KPILP* expression 3 days after agroinfiltration in leaves shown in A and B, respectively. **(E, F)** Percentage of TMV:GFP- **(E)** and crTMV:GFP-expressing **(F)** foci of different size. **(G, H)** Relative amount of *MP* and *GFP* RNA in analyzed leaves quantified by qRT-PCR. Mean values and standard error are presented in histograms **(C–H)**. The data was analyzed using Student's t-test. *, p<0.05; **, p<0.01; ***, p<0.001.

foci (2-99 sq. pxls) number and the decrease of larger foci (200-1000 sq. pxls.) amount by 3-fold as compared to the control (viral vectors co-infiltrated with pCambia1300). We also assessed the level of viral RNAs produced from TMV:GFP or crTMV:GFP vectors and encoding MP and GFP in samples from the analyzed infiltrated areas. The results of qRT-PCR demonstrate 3-fold decrease in *MP* and *GFP* RNA accumulation for both viral vectors upon *KPILP* silencing compared to control (Figures 5G, H). Notably, the foci number for both TMV:GFP and crTMV:GFP halved when *KPILP* was downregulated compared to the control areas.

Therefore, we concluded that KPILP is essential for effective tobamovirus infection, reproduction, and intercellular transport.

3.4 *KPILP* silencing leads to increased *N. benthamiana* resistance to TMV and crTMV infection

To assess KPILP role in the development of systemic tobamovirus infection, we used plants with up- and downregulated *KPILP* expression induced by pPVX or pPVX(frKPILP) vectors, respectively, and intact plants of the same age. All three groups were inoculated with TMV or crTMV to obtain the systemic infection. The experiment was repeated twice. We observed the development of symptoms characteristic for tobamovirus infection (Figure S1A) such as lesions on leaves, stem and petiole decay as well as wilting in all groups of plants. Importantly, the systemic TMV and crTMV infection commonly mortal *N. benthamiana* plants, unlike *N. tabacum* plants. During 40 days of monitoring the inoculated plants we documented all changes in the plant appearance and the time of their death. The death ratio of the infected plants by the 40th day is presented in Figure 6. *KPILP* silencing decreases the death rate of TMV-infected plants compared to either the control group or to plants with elevated *KPILP* levels (Figure 6A). However, crTMV infection is not so sensitive to the lack of *KPILP*: 80% of the plants from the *KPILP*-silenced experimental group died by the 40th day after inoculation (Figure 6B). The survivors from the group with downregulated *KPILP* looked the same as plants from the control group (Figure S4). Another parameter that we analyzed was the mean lifespan of plants in each group. Most of the plants with upregulated *KPILP* died in two weeks after TMV inoculation, while plants with silenced *KPILP* had slightly longer lifespan (Figure 6C). In case of crTMV infection, we observed a significant and marked increase in the lifespan of plants with *KPILP* downregulation compared to plants with increased the *KPILP* level (Figure 6D). The results indicate that *KPILP* upregulation induced by pPVX vector shortens the plants' lifespan after inoculation with TMV (Figure 6C) or crTMV (Figure 6D) compared to the control group, where *KPILP* was not upregulated before tobamovirus infection. Plants with silenced *KPILP* demonstrated higher resistance to TMV and crTMV infection compared to plants with increased *KPILP* expression. We concluded that elevated *KPILP* expression stimulates the development of tobamovirus infection and viral reproduction increasing the severity of symptoms, while *KPILP* suppression results in partial resistance to both TMV and crTMV infection.

4 Discussion

Plant viruses exploit a variety of strategies to successfully infect and spread throughout a plant. In this work we have explored the interaction between tobamoviruses and *N. benthamiana*, where the *KPILP* gene plays a regulatory and a potentially decisive role. In mature intact leaves, *KPILP* expression is suppressed. However, when the leaf tissues are infected with TMV, there is a sharp increase in its expression. In the previous paper (Sheshukova et al., 2017a) it was shown that the level of *KPILP* mRNA in roots is much higher than in mature and photosynthetically active leaves. The same paper demonstrated that in a TMV-infected tobacco leaf with mosaic symptoms, the light green zones with altered pigmentation and active virus replication exhibit a considerably higher level of *KPILP* mRNA than in dark green zones with normal pigmentation. This may implicate an inverse correlation between photosynthetic activity of chloroplasts and *KPILP* mRNA levels: (1) *KPILP* expression is active in roots where no photosynthesis occurs; (2) TMV affects functioning of chloroplast probably via activating the *KPILP* expression.

In this paper we demonstrated that the nuclear-encoded chloroplast RNA helicase *ISE2* mRNA accumulation in leaves with systemic tobamovirus infection remained at the same level as before infection. However, it was previously shown that *ISE2* expression increases at early stages of TMV infection by 18 hours after inoculation, and then its level decreases (Ganusova et al., 2017). We could not rule out that *ISE2* expression also changes in our system at earlier stages of infection but then it returns to the initial levels. In the same paper (Ganusova et al., 2017) it was demonstrated that sensitivity to TMV infection increases both in case of transient *ISE2* downregulation and constitutive overexpression. This means that *ISE2* plays an important regulatory role in plant defense response mediated by chloroplast signals. However, we did not find any significant correlation between *ISE2* mRNA levels and increased *KPILP* expression either activated by viral infection or during transient overexpression.

Nevertheless, it was shown that the elevated *KPILP* expression during tobamovirus infection is associated with suppression of genes important for chloroplast functioning including CRS marker genes *LHCB1*, *2*, *RBCSIA* and *HEMA1*. It is in line with the previous results demonstrating KPILP regulatory function toward the above-mentioned CRS marker genes in the transient expression system and during PVX infection (Ershova et al., 2022).

The expression of two other genes encoding chloroplast proteins – RCA and AtpC – was earlier demonstrated to be suppressed during TMV infection in *N. tabacum* but not in response to PVX. The virus-induced silencing of *RCA* and *AtpC* leads to a more efficient TMV spread and accumulation in *N. benthamiana*, which in turn determines the role of these factors in mediating antiviral responses, especially against tobamoviruses (Bhat et al., 2013). In this work we assessed the level of *RCA* and *AtpC* mRNA accumulation during the systemic tobamovirus infection and transient *KPILP* overexpression in *N. benthamiana* leaves. The systemic tobamovirus infection leads to a considerable suppression of these genes, which is in line with the previously

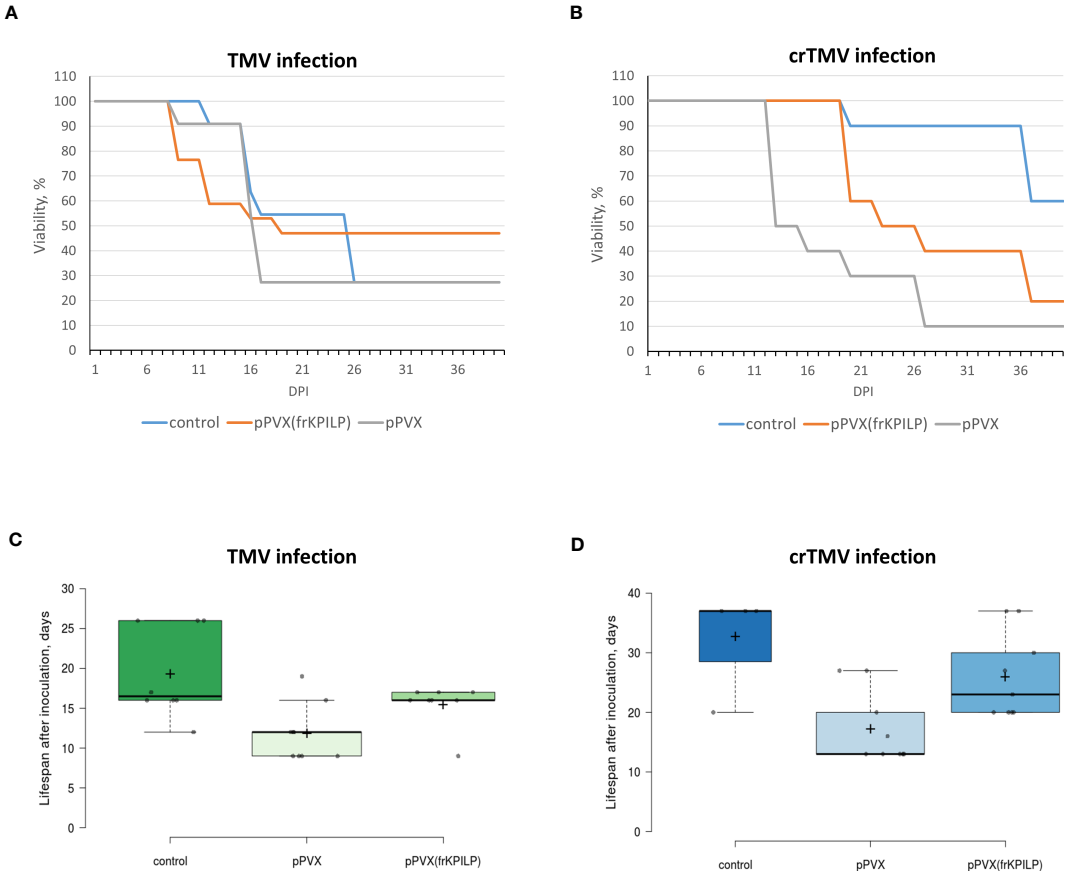

FIGURE 6
KPILP silencing leads to higher resistance of *N. benthamiana* to tobamovirus infection. **(A)** The viability of plants infected with TMV. **(B)** The viability of plants infected with crTMV. **(C)** The lifespan of plants with up- and downregulated *KPILP* inoculated with TMV. **(D)** The lifespan of plants with up- and downregulated *KPILP* inoculated with crTMV. In boxplots **(C, D)** central lines show the medians, and box boundaries indicate the 25th and 75th percentiles as determined by R software, whiskers extend 1.5 times the interquartile range from the 25th and 75th percentiles, outliers are represented by dots, crosses represent sample means, and data points are plotted as circles.

published papers (Bhat et al., 2013; Ganusova et al., 2017; Sheshukova et al., 2017b). We also showed that transient *KPILP* expression halved the levels of *RCA* and *AtpC* mRNA in the intact leaves. The obtained results indicate that KPILP plays an important role in *RCA* and *AtpC* genes expression regulation as well as in regulation of the other examined photosynthesis-associated nuclear-encoded genes during tobamovirus infection.

Suggesting that KPILP could be a proviral host factor exploited by the virus for infecting a plant, we studied how *KPILP* expression affects local spread and reproduction of TMV and crTMV, using TMV:GFP and crTMV:GFP viral vectors, respectively. Inoculating leaves with these vectors enables the quantitative assessment of intercellular transport of the model viral vector by measuring the size of GFP-expressing foci of infection. The intensity of GFP fluorescence in the analyzed foci and the level of *MP* and *GFP* mRNA accumulation reflect the efficiency of virus reproduction.

The obtained results (Figures 3, 4) indicated that there is a positive correlation between *KPILP* expression level and tobamovirus infection efficiency: in plants with upregulated *KPILP* we observed more active local spread of both tobamoviral vectors and higher levels of reproduction while in control group and plants with downregulated *KPILP* expression the viral intercellular transport and reproduction were significantly less efficient. Noteworthy, in this model system the *KPILP* level was modulated prior to agroinfiltration with TMV:GFP or crTMV:GFP. Thus, to properly interpret the obtained results and exclude the influence of *KPILP* on plant cell agrobacterial transformation another experimental set-up was utilized: the simultaneous delivery of plasmid encoding viral vector and the 35S-siKPILP construct that induces *KPILP* silencing. KPILP suppression in these experiments also led to a decreased efficiency of viral vectors' reproduction and intercellular spread (Figure 5) as well as reducing the number of foci of infection. Moreover, using a different experimental set-up we confirmed that KPILP doesn't affect the delivery of genetic material by agrobacteria but has a specific effect on the virus. Together these results allow us to conclude that KPILP plays an important role in tobamovirus infection development.

Using the system with up- and downregulated *KPILP* expression induced by pPVX or pPVX(frKPILP) vectors (Ershova et al., 2022), we assessed the sensitivity of the model plants to the development of systemic tobamovirus infection. We monitored the time in which the most severe symptoms developed, lifespan and viability of plants. Figure 6 shows that plants where *KPILP* is activated have an increased sensitivity to the infection. This

manifests itself in a shorter lifespan and a reduced ratio of the survivors compared to the group of plants with *KPILP* knockdown or the control group. Plants with the downregulated *KPILP* demonstrated an increased resistance to TMV and crTMV infection: the symptoms were less severe, lifespan was longer and the mortality percentage by the 40th day after inoculation was lower. Monitoring the development of infection, we have not observed any significant difference between TMV- and crTMV-infected plants: the symptoms were similar. Moreover, plants with suppressed *KPILP* had similar appearance as the plants from the control group (Figure S4).

In a permissive host, a rapid tobamovirus infection development is possible only in case of favorable conditions for all the infection stages, from virion uncoating to penetration to the vascular system. TMV reaches the vasculature in 16-18 hours after infection (Nilsson-Tillgren et al., 1969). Such a rapid spread within the plant can occur only if the following events are properly synchronized: efficient viral genome expression and replication, synthesis of viral proteins, antiviral response suppression and intercellular transport activation. We can assume that the initial activation of cellular factors exploited by the virus could be induced by the coat protein (CP) which is the first to enter a cell in case of infection as a component of virion, or MP the small amounts of which could be synthesized directly on the template of TMV or crTMV genomic RNA. This remarkable feature of MP was shown for TMV and crTMV (Dorokhov et al., 1993; Dorokhov et al., 1994; Skulachev et al., 1999), whose genome contains internal ribosome entry site (IRES) ($IRES_{MP,75}^{U1}$, and $IRES_{MP,75}^{CR}$, respectively) mediating MP translation directly form genomic RNA.

We could speculate that MP and/or CP can potentially induce *KPILP* expression at the initial stages of infection directly or via other cellular factors. However, *MP* or *CP* overexpression *per se* does not lead to the 1000-fold increase in *KPILP* mRNA accumulation (Figure S2) as it happens in response to systemic TMV infection (Figure 1). Therefore, we could suggest that only in presence of all viral components *KPILP* expression is drastically activated due to the generalized effect of viral reproduction on all cellular components and their functioning. We hypothesize that upon TMV infection we observe a synergetic effect. And at the early steps of infection development KPILP launches irreversible changes in the photosynthetic apparatus and activation of intercellular transport. Although KPILP was not detected in chloroplasts, there is a clear inverse correlation between photosynthesis and *KPILP* expression activated during TMV infection. Moreover, TMV might exploit KPILP for suppression chloroplast activity, thereby influencing the antiviral response and regulating the cell-to-cell and long-distance transport.

Based on the obtained results we could regard KPILP as a proviral cellular factor and one of the susceptibility genetic determinants which is “dormant” in an aerial parts of the intact plant but activated by the viral infection. The question remains unanswered as to whether TMV has a direct effect on *KPILP* expression, suppressing in this way the functional activity of chloroplasts, or whether there are other proteins involved in this regulatory pathway. Therefore, search of potential KPILP partners or cellular factors upstream and downstream of KPILP-based cascade could elucidate the other participants in this interplay and is a subject of further investigation.

Data availability statement

The original contributions presented in the study are included in the article/Supplementary Material. Further inquiries can be directed to the corresponding author.

Author contributions

Conceptualization, NE and TK; design of the experiments and investigation, NE, KK, ES, and AA; data analysis, NE, KK, ES, and TK; writing—original draft preparation, NE and TK; writing—review and editing, NE and TK; funding acquisition, TK. All authors contributed to the article and approved the submitted version.

Funding

The study was supported by the Russian Science Foundation, grant number 19-74-20031, https://rscf.ru/en/project/19-74-20031/.

Acknowledgments

The authors thank Irina Savchenko for technical assistance.

Conflict of interest

The authors declare that the research was conducted in the absence of any commercial or financial relationships that could be construed as a potential conflict of interest.

Publisher’s note

Supplementary material

The Supplementary Material for this article can be found online at: https://www.frontiersin.org/articles/10.3389/fpls.2023.1224958/full#supplementary-material

References

Abbink, T. E. M., Peart, J. R., Mos, T. N. M., Baulcombe, D. C., Bol, J. F., and Linthorst, H. J. M. (2002). Silencing of a gene encoding a protein component of the oxygen-evolving complex of photosystem II enhances virus replication in plants. *Virology* 295, 307–319. doi: 10.1006/viro.2002.1332

Amari, K., Di Donato, M., Dolja, V. V., and Heinlein, M. (2014). Myosins VIII and XI play distinct roles in reproduction and transport of tobacco mosaic virus. *PloS Pathog.* 10, e1004448. doi: 10.1371/journal.ppat.1004448

Amsbury, S., Kirk, P., and Benitez-Alfonso, Y. (2017). Emerging models on the regulation of intercellular transport by plasmodesmata-associated callose. *J. Exp. Bot.* 69, 105–115. doi: 10.1093/jxb/erx337

Bhat, S., Folimonova, S. Y., Cole, A. B., Ballard, K. D., Lei, Z., Watson, B. S., et al. (2013). Influence of host chloroplast proteins on tobacco mosaic virus accumulation and intercellular movement. *Plant Physiol.* 161, 134–147. doi: 10.1104/pp.112.207860

Bhattacharyya, D., and Chakraborty, S. (2017). Chloroplast: the Trojan horse in plant–virus interaction. *Mol. Plant Pathol.* 19, 504–518. doi: 10.1111/mpp.12533

Boyko, V., Hu, Q., Seemanpillai, M., Ashby, J., and Heinlein, M. (2007). Validation of microtubule-associated tobacco mosaic virus RNA movement and involvement of microtubule-aligned particle trafficking. *Plant J. Cell Mol. Biol.* 51, 589–603. doi: 10.1111/j.1365-313X.2007.03163.x

Burch-Smith, T. M., Brunkard, J. O., Choi, Y. G., and Zambryski, P. C. (2011). Organelle–nucleus cross-talk regulates plant intercellular communication via plasmodesmata. *Proc. Natl. Acad. Sci.* 108, E1451–E1460. doi: 10.1073/pnas.1117226108

Burch-Smith, T. M., and Zambryski, P. C. (2010). Loss of INCREASED SIZE EXCLUSION LIMIT (ISE)1 or ISE2 increases the formation of secondary plasmodesmata. *Curr. Biol. CB* 20, 989–993. doi: 10.1016/j.cub.2010.03.064

Chen, M. H., Sheng, J., Hind, G., Handa, A. K., and Citovsky, V. (2000). Interaction between the tobacco mosaic virus movement protein and host cell pectin methylesterases is required for viral cell-to-cell movement. *EMBO J.* 19, 913–920. doi: 10.1093/emboj/19.5.913

Chen, M.-H., Tian, G.-W., Gafni, Y., and Citovsky, V. (2005). Effects of calreticulin on viral cell-to-cell movement. *Plant Physiol.* 138, 1866–1876. doi: 10.1104/pp.105.064386

Curin, M., Ojangu, E.-L., Trutnyeva, K., Ilau, B., Truve, E., and Waigmann, E. (2007). MPB2C, a microtubule-associated plant factor, is required for microtubular accumulation of tobacco mosaic virus movement protein in plants. *Plant Physiol.* 143, 801–811. doi: 10.1104/pp.106.091488

Dorokhov, Y. L., Ershova, N. M., Sheshukova, E. V., and Komarova, T. V. (2019). Plasmodesmata conductivity regulation: a mechanistic model. *Plants* 8, 595. doi: 10.3390/plants8120595

Dorokhov, Y. L., Frolova, O. Y., Skurat, E. V., Ivanov, P. A., Gasanova, T. V., Sheveleva, A. A., et al. (2006). A novel function for a ubiquitous plant enzyme pectin methylesterase: the enhancer of RNA silencing. *FEBS Lett.* 580, 3872–3878. doi: 10.1016/j.febslet.2006.06.013

Dorokhov, Y. L., Ivanov, P. A., Novikov, V. K., Agranovsky, A. A., Morozov, S., Efimov, V. A., et al. (1994). Complete nucleotide sequence and genome organization of a tobamovirus infecting cruciferae plants. *FEBS Lett.* 350, 5–8. doi: 10.1016/0014-5793(94)00721-7

Dorokhov, Y. L., Ivanov, P. A., Novikov, V. K., Yefimov, V. A., and Atabekov, I. G. (1993). Tobamovirus of cruciferous plants: nucleotide sequence of genes of the transport protein, capsid protein, and 3'-terminal untranslated region. *Dokl. Akad. Nauk* 332, 518–522.

Dorokhov, Y. L., Mäkinen, K., Frolova, O. Y., Merits, A., Saarinen, J., Kalkkinen, N., et al. (1999). A novel function for a ubiquitous plant enzyme pectin methylesterase: the host-cell receptor for the tobacco mosaic virus movement protein. *FEBS Lett.* 461, 223–228. doi: 10.1016/S0014-5793(99)01447-7

Ershova, N., Sheshukova, E., Kamarova, K., Arifulin, E., Tashlitsky, V., Serebryakova, M., et al. (2022). Nicotiana benthamiana kunitz peptidase inhibitor-like protein involved in chloroplast-to-nucleus regulatory pathway in plant-virus interaction. *Front. Plant Sci.* 13, 1041867. doi: 10.3389/fpls.2022.1041867

Fitter, D. W., Martin, D. J., Copley, M. J., Scotland, R. W., and Langdale, J. A. (2002). GLK gene pairs regulate chloroplast development in diverse plant species. *Plant J. Cell Mol. Biol.* 31, 713–727. doi: 10.1046/j.1365-313x.2002.01390.x

Ganusova, E., Rice, J. H., Carlew, T. S., Patel, A., Perrodin-Njoku, E., Hewezi, T., et al. (2017). Altered expression of a chloroplast protein affects the outcome of virus and nematode infection. *Mol. Plant-Microbe Interact. MPMI.* 30, 478–488. doi: 10.1094/MPMI-02-17-0031-R

Garcia-Ruiz, H. (2018). Susceptibility genes to plant viruses. *Viruses* 10, 484. doi: 10.3390/v10090484

Guenoune-Gelbart, D., Elbaum, M., Sagi, G., Levy, A., and Epel, B. L. (2008). Tobacco mosaic virus (TMV) replicase and movement protein function synergistically in facilitating TMV spread by lateral diffusion in the plasmodesmal desmotubule of nicotiana benthamiana. *Mol. Plant-Microbe Interact. MPMI* 21, 335–345. doi: 10.1094/MPMI-21-3-0335

Heinlein, M. (2015). Plant virus replication and movement. *Virology* 479–480, 657–671. doi: 10.1016/j.virol.2015.01.025

Hofmann, C., Niehl, A., Sambade, A., Steinmetz, A., and Heinlein, M. (2009). Inhibition of tobacco mosaic virus movement by expression of an actin-binding protein. *Plant Physiol.* 149, 1810–1823. doi: 10.1104/pp.108.133827

Hwang, J., Oh, C.-S., and Kang, B.-C. (2013). Translation elongation factor 1B (eEF1B) is an essential host factor for tobacco mosaic virus infection in plants. *Virology* 439, 105–114. doi: 10.1016/j.virol.2013.02.004

Ishibashi, K., and Ishikawa, M. (2016). Replication of tobamovirus RNA. *Annu. Rev. Phytopathol.* 54, 55–78. doi: 10.1146/annurev-phyto-080615-100217

Kragler, F., Curin, M., Trutnyeva, K., Gansch, A., and Waigmann, E. (2003). MPB2C, a microtubule-associated plant protein binds to and interferes with cell-to-Cell transport of tobacco mosaic virus movement protein. *Plant Physiol.* 132, 1870–1883. doi: 10.1104/pp.103.022269

Liu, Y., Huang, C., Zeng, J., Yu, H., Li, Y., and Yuan, C. (2020). Identification of two additional plasmodesmata localization domains in the tobacco mosaic virus cell-to-cell-movement protein. *Biochem. Biophys. Res. Commun.* 521, 145–151. doi: 10.1016/j.bbrc.2019.10.093

Liu, C., and Nelson, R. S. (2013). The cell biology of tobacco mosaic virus replication and movement. *Front. Plant Sci.* 4. doi: 10.3389/fpls.2013.00012

Ma, T., Fu, S., Wang, K., Wang, Y., Wu, J., and Zhou, X. (2022). Palmitoylation is indispensable for remorin to restrict tobacco mosaic virus cell-to-Cell movement in nicotiana benthamiana. *Viruses* 14, 1324. doi: 10.3390/v14061324

Nelson, R. S., and van Bel, A. J. E. (1998). "The mystery of virus trafficking into, through and out of vascular tissue," in *Progress in botany: genetics cell biology and physiology ecology and vegetation science progress in botany*. Eds. H.-D. Behnke, K. Esser, J. W. Kadereit, U. Lüttge and M. Runge (Berlin, Heidelberg: Springer), 476–533. doi: 10.1007/978-3-642-80446-5_17

Nilsson-Tillgren, T., Kolehmainen-Sevéus, L., and von Wettstein, D. (1969). Studies on the biosynthesis of TMV. *Mol. Gen. Genet. MGG* 104, 124–141. doi: 10.1007/BF00272793

Pfaffl, M. W. (2001). A new mathematical model for relative quantification in real-time RT–PCR. *Nucleic Acids Res.* 29, e45. doi: 10.1093/nar/29.9.e45

Qiao, Y., Li, H. F., Wong, S. M., and Fan, Z. F. (2009). Plastocyanin transit peptide interacts with potato virus X coat protein, while silencing of plastocyanin reduces coat protein accumulation in chloroplasts and symptom severity in host plants. *Mol. Plant-Microbe Interact. MPMI* 22, 1523–1534. doi: 10.1094/MPMI-22-12-1523

Reagan, B. C., and Burch-Smith, T. M. (2020). Viruses reveal the secrets of plasmodesmal cell biology. *Mol. Plant-Microbe Interact. MPMI* 33, 26–39. doi: 10.1094/MPMI-07-19-0212-FI

Reinero, A., and Beachy, R. N. (1986). Association of TMV coat protein with chloroplast membranes in virus-infected leaves. *Plant Mol. Biol.* 6, 291–301. doi: 10.1007/BF00034936

Rodriguez-Peña, R., Mounadi, K. E., and Garcia-Ruiz, H. (2021). Changes in subcellular localization of host proteins induced by plant viruses. *Viruses* 13, 677. doi: 10.3390/v13040677

Sasaki, N., Takashima, E., and Nyunoya, H. (2018). Altered subcellular localization of a tobacco membrane raft-associated remorin protein by tobamovirus infection and transient expression of viral replication and movement proteins. *Front. Plant Sci.* 9. doi: 10.3389/fpls.2018.00619

Schmied, J., Hedtke, B., and Grimm, B. (2011). Overexpression of HEMA1 encoding glutamyl-tRNA reductase. *J. Plant Physiol.* 168, 1372–1379. doi: 10.1016/j.jplph.2010.12.010

Schneider, C. A., Rasband, W. S., and Eliceiri, K. W. (2012). NIH Image to ImageJ: 25 years of image analysis. *Nat. Methods* 9, 671–675. doi: 10.1038/nmeth.2089

Sheshukova, E. V., Ershova, N. M., Kamarova, K. A., Dorokhov, Y. L., and Komarova, T. V. (2020). The tobamoviral movement protein: a "Conditioner" to create a favorable environment for intercellular spread of infection. *Front. Plant Sci.* 11. doi: 10.3389/fpls.2020.00959

Sheshukova, E. V., Komarova, T. V., Ershova, N. M., and Shindyapina, A. V. (2017a). An alternative nested reading frame may participate in the stress-dependent expression of a plant gene. *Front. Plant Sci.* 8. doi: 10.3389/fpls.2017.02137

Sheshukova, E. V., Komarova, T. V., Pozdyshev, D. V., Ershova, N. M., Shindyapina, A. V., Tashlitsky, V. N., et al. (2017b)The intergenic interplay between aldose 1-Epimerase-Like protein and pectin methylesterase in abiotic and biotic stress control (Accessed March 30, 2023).

Skulachev, M. V., Ivanov, P. A., Karpova, O. V., Korpela, T., Rodionova, N. P., Dorokhov, Y. L., et al. (1999). Internal initiation of translation directed by the 5'-untranslated region of the tobamovirus subgenomic RNA I(2). *Virology* 263, 139–154. doi: 10.1006/viro.1999.9928

Uchiyama, A., Shimada-Beltran, H., Levy, A., Zheng, J. Y., Javia, P. A., and Lazarowitz, S. G. (2014). The arabidopsis synaptotagmin SYTA regulates the cell-to-cell movement of diverse plant viruses. *Front. Plant Sci.* 5. doi: 10.3389/fpls.2014.00584

Ueki, S., and Citovsky, V. (2014a). Plasmodesmata-associated proteins. *Plant Signal. Behav.* 9, e27899. doi: 10.4161/psb.27899

Ueki, S., and Citovsky, V. (2014b). Plasmodesmata-associated proteins: can we see the whole elephant? *Plant Signal. Behav.* 9, e27899. doi: 10.4161/psb.27899

Wesley, S. V., Helliwell, C. A., Smith, N. A., Wang, M. B., Rouse, D. T., Liu, Q., et al. (2001). Construct design for efficient, effective and high-throughput gene silencing in plants. *Plant J. Cell Mol. Biol.* 27, 581–590. doi: 10.1046/j.1365-313x.2001.01105.x

Wu, X., and Shaw, J. (1996). Bidirectional uncoating of the genomic RNA of a helical virus. *Proc. Natl. Acad. Sci. U. S. A.* 93, 2981–2984. doi: 10.1073/pnas.93.7.2981

Wu, X., Xu, Z., and Shaw, J. G. (1994). Uncoating of tobacco mosaic virus RNA in protoplasts. *Virology* 200, 256–262. doi: 10.1006/viro.1994.1183

Yamaji, Y., Sakurai, K., Hamada, K., Komatsu, K., Ozeki, J., Yoshida, A., et al. (2010). Significance of eukaryotic translation elongation factor 1A in tobacco mosaic virus infection. *Arch. Virol.* 155, 263–268. doi: 10.1007/s00705-009-0571-x

Yuan, C., Lazarowitz, S. G., and Citovsky, V. (2018). The plasmodesmal localization signal of TMV MP is recognized by plant synaptotagmin SYTA. *mBio* 9, e01314–e01318. doi: 10.1128/mBio.01314-18

frontiers | Frontiers in Plant Science

TYPE Original Research
PUBLISHED 03 November 2023
DOI 10.3389/fpls.2023.1270963

OPEN ACCESS

EDITED BY
Yi-Hong Wang,
University of Louisiana at Lafayette,
United States

REVIEWED BY
Yinhua Chen,
Hainan University, China
Wanwisa Siriwan,
Kasetsart University, Thailand

*CORRESPONDENCE
Morag E. Ferguson
m.ferguson@cgiar.org

†PRESENT ADDRESSES
Rodney P. Eyles,
Instituto Gulbenkian de Ciência, Oeiras, Portugal
Ana Luísa Garcia-Oliveira,
Breeding Resources, International Maize and Wheat Improvement Center (CIMMYT), Nairobi, Kenya; Department of Molecular Biology, Chaudhary Charan Singh Haryana Agricultural University, Haryana, India
Teddy Amuge,
Department of Agro-Industrial Technology, Masinde Muliro University of Science and Technology, Kakamega, Kenya
Steve Rounsley,
Product Development, Inari Agriculture, West Lafayette, IN, United States
Geoffrey Mkamilo,
Tanzania Agricultural Research Institute Headquarters, Makutupora, Tanzania

RECEIVED 01 August 2023
ACCEPTED 09 October 2023
PUBLISHED 03 November 2023

CITATION
Ferguson ME, Eyles RP, Garcia-Oliveira AL, Kapinga F, Masumba EA, Amuge T, Bredeson JV, Rokhsar DS, Lyons JB, Shah T, Rounsley S and Mkamilo G (2023) Candidate genes for field resistance to cassava brown streak disease revealed through the analysis of multiple data sources.
Front. Plant Sci. 14:1270963.
doi: 10.3389/fpls.2023.1270963

Candidate genes for field resistance to cassava brown streak disease revealed through the analysis of multiple data sources

Morag E. Ferguson[1*], Rodney P. Eyles[1†], Ana Luísa Garcia-Oliveira[1†], Fortunus Kapinga[1,2], Esther A. Masumba[1,3], Teddy Amuge[1,4†], Jessen V. Bredeson[5], Daniel S. Rokhsar[5], Jessica B. Lyons[5], Trushar Shah[6], Steve Rounsley[7†] and Geoffrey Mkamilo[2†]

[1]Cassava Breeding, International Institute of Tropical Agriculture (IITA), Nairobi, Kenya, [2]Cassava Breeding, Naliendele Agricultural Research Institute, Mtwara, Tanzania, [3]Cassava Breeding, Sugarcane Research Institute, Kibaha, Tanzania, [4]Cassava Breeding, National Crops Resources Research Institute (NaCRRI), Namulonge, Uganda, [5]Molecular and Cell Biology Department, University of California, Berkeley, Berkeley, CA, United States, [6]Bioinformatics, International Institute of Tropical Agriculture (IITA), Nairobi, Kenya, [7]Seeds & Traits R&D, Dow AgroSciences, Indianapolis, IN, United States

Cassava (*Manihot esculenta* Crantz) is a food and industrial storage root crop with substantial potential to contribute to managing risk associated with climate change due to its inherent resilience and in providing a biodegradable option in manufacturing. In Africa, cassava production is challenged by two viral diseases, cassava brown streak disease (CBSD) and cassava mosaic disease. Here we detect quantitative trait loci (QTL) associated with CBSD in a biparental mapping population of a Tanzanian landrace, Nachinyaya and AR37-80, phenotyped in two locations over three years. The purpose was to use the information to ultimately facilitate either marker-assisted selection or adjust weightings in genomic selection to increase the efficiency of breeding. Results from this study were considered in relation to those from four other biparental populations, of similar genetic backgrounds, that were phenotyped and genotyped simultaneously. Further, we investigated the co-localization of QTL for CBSD resistance across populations and the genetic relationships of parents based on whole genome sequence information. Two QTL on chromosome 4 for resistance to CBSD foliar symptoms and one on each of chromosomes 11 and 18 for root necrosis were of interest. Of significance within the candidate genes underlying the QTL on chromosome 4 are Phenylalanine ammonia-lyase (PAL) and Cinnamoyl-CoA reductase (CCR) genes and three PEPR1-related kinases associated with the lignin pathway. In addition, a CCR gene was also underlying the root necrosis-resistant QTL on chromosome 11. Upregulation of key genes in the cassava lignification pathway from an earlier transcriptome study, including PAL and CCR, in a CBSD-resistant landrace compared to a susceptible landrace suggests a higher level of basal lignin deposition in the CBSD-resistant landrace. Earlier RNAscope® *in situ* hybridisation imaging experiments demonstrate that cassava brown streak virus (CBSV) is restricted to phloem vessels in CBSV-

resistant varieties, and phloem unloading for replication in mesophyll cells is prevented. The results provide evidence for the involvement of the lignin pathway. In addition, five eukaryotic initiation factor (eIF) genes associated with plant virus resistance were found within the priority QTL regions.

KEYWORDS

lignin, phenylalanine ammonia-lyase, cinnamoyl-CoA reductase, eIF, PEPR1-related kinases, quantitative trait loci

Introduction

Cassava, a clonally propagated starchy root crop, is an important staple food and the third most important source of starch globally (Expert Market Research, 2023). Its relevance to the changing global environment with an increasing need for resilience against unpredictable and extreme weather patterns and the requirement to move away from plastics to more biodegradable solutions make cassava a crop for the future. Cassava and its products were estimated to provide on average 250 kcal/capita/day to the population in Africa in 2020 (FAOSTAT, 2023) making it an extremely important food source and trade commodity with tremendous potential for the future in Africa. Cassava is well adapted to the challenges of climate change, being naturally resilient to drought, high temperatures and low soil fertility. In Africa, two viral diseases, cassava mosaic disease (CMD), and cassava brown streak disease (CBSD), ravage cassava. These diseases are spread through the distribution of infected cuttings used as planting material and by whitefly (*Bemisia tabaci*) transmission (Maruthi et al., 2005). Resistance to these diseases is now among the highest breeding priorities, particularly in hotspot areas (Legg et al., 2014).

A relatively new viral disease, CBSD, caused by two species of Ipomovirus (Winter et al., 2010; Mbanzibwa et al., 2011), was, until 2003, restricted geographically to the East Africa coastal region where it was first reported by Storey (1936). After 2003, the disease began to spread in the Great Lakes region of East Africa (Alicai et al., 2007). The western frontier of the CBSD pandemic is now in eastern DR Congo, covering approximately 14% of the country (approx. 321,000 km^2) with Haut-Katanga and Sud-Kivu being the latest provinces where CBSD has been detected (Casinga et al., 2021). CBSD is an important threat to West Africa (Legg et al., 2014). CBSD generally shows mild foliar symptoms but causes a brown corky necrosis in the storage roots, rendering them unusable. Nichols (1950) provides an excellent description of symptom expression.

Breeding for high levels of resistance is the priority approach for managing the impacts of CBSD. The first sustained effort in breeding for resistance to CMD and CBSD started in 1937 in Amani, northern Tanzania by the East African Agriculture and Forestry Research Organisation (EAAFRO) where crosses involving landraces and wild species were undertaken for addressing both CMD, as a priority, and CBSD (Jennings, 2003). Work on breeding for CBSD resistance continued from 1966, from the Naliendele Agriculture Research Institute, Tanzania after the Amani program closed in 1956 (Hillocks and Jennings, 2003). Here, sources of tolerance to CBSD focused on landraces from Tanzania and northern Mozambique, of which Nachinyaya, used in this study, is one. Since that time, new sources of resistance and even immunity to CBSV and Ugandan CBSV (UCBSV) have been uncovered in germplasm from South America (Sheat et al., 2019).

Phenotyping for CBSD is a challenging and expensive endeavour. Symptom expression can vary depending on growing conditions, as well as within and between roots (Hillocks and Jennings, 2003). Continued recycling of planting material over several years can lead to degeneration from the cumulative effects of disease (Shirima et al., 2019). All of these extends the time taken for accurate phenotyping. Locating quantitative trait loci (QTL) associated with CBSD resistance to facilitate either marker-assisted selection or adjust weightings in genomic selection has been a goal. Four bi-parental breeding populations, based on Tanzanian germplasm and conducted simultaneously, have been reported (Kapinga, 2017; Masumba et al., 2017; Nzuki et al., 2017; Garcia-Oliveira et al., 2020). Kayondo et al. (2018) and Somo et al. (2020) applied a Genome Wide Association Mapping (GWAS) approach to investigate the genetic architecture of CBSD and the potential of genomic selection through the assessment of genomic prediction in breeding for CBSD resistance.

Here we report on a fifth bi-parental mapping population, Nachinyaya × AR37-80, which was developed and phenotyped at the same time as four other populations; Namikonga × Albert (Masumba et al., 2017), NDL06/132 × AR37-80 (Kapinga, 2017), Kiroba × AR37-80 (Nzuki et al., 2017) and AR40-6 × Albert (Garcia-Oliveira et al., 2020). We compare the results with these populations and identify co-locating QTL for CBSD. This is viewed in relation to genetic relationships between the resistant parents gained from re-sequencing data (Bredeson et al., 2016), gene expression data from transcriptomic analysis of resistant and susceptible parents (Amuge et al., 2017), and imaging data from RNAscope® *in situ* hybridisation (Sheat et al., 2020; Sheat et al., 2021) to identify candidate genes for CBSD resistance.

Materials and methods

Development of Nachinyaya × AR37-80 (NCAR) population

The CBSD-tolerant parent used to develop the NCAR population, Nachinyaya, is a landrace from northern Mozambique and south-eastern Tanzania. Its tolerance to CBSD

root necrosis symptoms is well known, although it can show quite severe foliar symptoms. It is also susceptible to CMD (Hillocks et al., 1996; Hillocks et al., 2001; Thresh, 2003). The pollen parent, AR37-80, is a cross between a CMD-resistant line (C33) from IITA and CW259-42, the latter of which is a backcross of MTAI 8 (Rayong 60) and an interspecific cross between *M. flabellifolia* and CM 2766-5. It was developed through simple sequence repeat (SSR) marker-assisted selection, being positively selected for the CMD2 resistance locus and cassava green mite (CGM) resistance. It is, however, susceptible to CBSD (Blair et al., 2007; Okogbenin et al., 2012).

Pollinations were made by hand around midday according to Masumba et al. (2017) at the Sugarcane Research Institute (SRI) at Kibaha, Tanzania (6°46'52.22"S, 38°58'25.05"E). A flotation test was used to discard hollow seeds and select viable seeds which were then germinated in seed trays on benches in a screen house where temperatures were generally between 20°C to 30°C. Seedlings were transplanted into a field at Makutupora Agricultural Research Station (5°58'36.87"S, 35°46'00.00"E) in central Tanzania, an isolated, disease-free location. After one year the plants were ratooned and planted as the first phenotyping trial.

Phenotyping

Phenotyping was conducted over three consecutive seasons, 2013/14, 2014/15 and 2015/16 in two CBSD hotspot locations in coastal Tanzania, Naliendele in the south (10°23'00.60"S, 40° 09'50.58"E) and Chambezi (6°33'21.29"S, 38°54'44.10"E) on the central coast. Stakes were obtained from the disease-free multiplication site in Makutupora for the first year, then subsequently replanted from the harvested trial in each location for the second and third years, to facilitate the accumulation of viral load. Planting was done in January of each year to maximise disease pressure (Shirima et al., 2019). The site–season combinations were designated as experiments N1, N2 and N3 for Naliendele for 2013/14, 2014/15 and 2015/16 respectively, and experiments C1, C2 and C3 for Chambezi for the same seasons. Due to the large number of entries, an Alpha lattice design was used with incomplete blocks (Kashif et al., 2011). Five clonal plants were planted per plot at a spacing of 1 x 1 m in two replications. To increase the intensity and even distribution of disease pressure, CBSD-susceptible and infected plants with clear symptoms from surrounding farms were planted around each incomplete block. After data cleaning, a final population of 186 genotypes was used for analysis.

Scoring of foliar symptoms for CBSD was performed at 3 and 6 months after planting (MAP) in each experiment, on an individual plant basis, using the 1–5 scale (Hillocks and Thresh, 2000; Masumba et al., 2017). CBSD root necrosis was scored in N1, N2, C1, and C2 immediately after harvest (12 MAP), to avoid post-harvest physiological deterioration (Ravi et al., 1996). Root necrosis was not scored in C3 or N3. A maximum of seven randomly sampled roots per plant were assessed. Roots were cut using a knife or root-cutter (Kapinga, 2017) at equal intervals of 5 cm to expose the cross-section areas for CBSD severity assessment. A scale of 1–5 was used where 1 is no root necrosis, and 5 is over approximately 40% root necrosis (Masumba et al., 2017).

Shapiro-Wilk normality (SWILK) (Shapiro and Wilk, 1965), incorporated in the Genetic Analysis of Clonal F1 and Double Cross population (GACD v1.1) mapping software (Zhang et al., 2015), was used to determine the normality of the trait frequency distributions across the locations in both seasons.

Genotyping

As cassava is an outcrossing species and parental stakes were partly derived from farmers' fields, the integrity of the F1s was assessed for 'off-types' and 'selfs' (which are synonymous with outcross progeny between two clonal genotypes) using simple sequence repeat (SSR) markers. Leaf material from young plantlets was sampled for genomic DNA extraction according to a miniprep protocol modified from Dellaporta et al. (1983) based on Kapinga (2017). Initially 55 SSR primer pairs were used to screen the parents to identify polymorphic markers. Ultimately 14 of these, which produced unambiguous amplification products (NS911, SSRY100, -12, -151, -169, -171, -19, -38, -5, -51, -52 and -63) (Mba et al., 2001) were used to screen the entire population. Reaction conditions were according to Kawuki et al. (2013) and amplification products were resolved using capillary electrophoresis on an ABI 3730 and scored using GeneMapper v4.1 software. Results were used to identify true crosses.

DNA from true crosses were sent to UC Berkeley for genotyping-by-sequencing (GBS) (Elshire et al., 2011) with modifications (International Cassava Genetic Map Consortium, 2015; Masumba et al., 2017). Single-nucleotide polymorphisms (SNPs) were called against reference genome sequence version 5.1 (v5.1) and filtered for segregating loci as described by International Cassava Genetic Map Consortium (2015).

Genetic linkage mapping and QTL analysis

A genetic linkage map was constructed from SNP data of true cross progeny in JoinMap® v4.1. (van Ooijen, 2006). Initially, markers and individuals with more than 20% missing data were excluded, as were tetra-allelic loci and those with identical (ie. genetically redundant) segregation patterns. SNP marker data were coded according to the CP option in JoinMap v4.1 manual for outcrossing species. Bi-allelic SNPs provided segregation types 'lmxll', 'nnxnp' and 'hkxhk'; and tri-allelic SNPs 'efxfg'. The maximum-likelihood algorithm for cross-pollinated (CP) was used as is appropriate for outcrossing species in which both parents are heterozygous and the linkage phase is unknown.

A one-step genetic linkage map was generated with groups defined using a minimum Logarithm of Odds (LOD) of 5.0 with marker order being defined using the regression mapping algorithm (Wu et al., 2014) and Kosambi's mapping function (van Ooijen, 2009). The linkage groups were named according to the corresponding chromosome as determined by the International Cassava Genetic Map Consortium (2015).

The mean trait score for each genotype across the replicates in each year and site was calculated and used for QTL mapping using inclusive composite interval mapping (ICIM) in Integrated Genetic Analysis Software of Clonal F1 and Double Cross Populations (GACD) version 1.1 (Yu et al., 2006; Zhang et al., 2015). Traits were CBSD foliar (3 and 6 MAP) and CBSD root necrosis. Based on the actual number of identified alleles in the two parents each marker locus was classified into four categories as described for GACD (Garcia-Oliveira et al., 2020). A significance threshold of LOD 3.0 was assigned manually. A LOD score of 3.0 or more is generally accepted as evidence of linkage as this implies that the likelihood in favour of linkage is 1000 times greater than the alternative. A QTL was considered 'real' when flanking markers of a significant QTL were consistent in two or more sites/seasons in any one population. Flanking markers, LOD scores, and adjusted percentage phenotypic variance explained (PVE%) are reported from the .QIC file.

QTL identifiers are prefixed with 'q' for 'QTL' followed by the trait abbreviation, 'c' for 'chromosome' and the number of the chromosome. If more than one trait QTL was identified per chromosome, then a point followed by a sequential number was used. A suffix 'NC' was added to specify that the QTL was identified in Nachinyaya. All QTL and marker positions are given in 5.1 of the cassava genome sequence, unless indicated.

Comparisons were made with QTL detected in four previously published bi-parental mapping populations, which were genotyped and phenotyped at the same time as the NCAR population (Kapinga, 2017; Masumba et al., 2017; Nzuki et al., 2017; Garcia-Oliveira et al., 2020), and QTL consistent across populations were highlighted. Candidate genes influencing resistance were selected from annotations from the Panther Classification System in combination with an extensive literature review of genes underlying the genomic positions of selected consistent QTL. This information was considered together with the gene expression data of these and related candidate genes from a time course transcriptomic experiment of UCBSV infected and uninfected Namikonga and Albert (Amuge et al., 2017).

Results

Controlled pollination resulted in 1,216 seeds of which 49% (600 seeds) germinated after three months of storage to break dormancy. Of these, only 271 established well in the field at Makutupora. Initial quality control, to ensure the integrity of the population, did not reveal any selfs, but 11 off-types.

After excluding loci with significant deviation from Mendelian segregation as well as individuals and loci with a large amount of missing data, a data set of 199 individuals remained for genetic linkage mapping. A total of 2,887 SNPs were detected, of which 2,289 were mapped onto 18 linkage groups with a cumulative map length of 1802 centiMorgans (cM). The highest marker density was on chromosome 15 (average 0.47 cM between markers) and the lowest was on chromosome 13 (average 1.38 cM between markers) (Supplementary File S1). The average marker density was 1.27 SNPs per cM (Supplementary File S1). The genetic linkage maps of these populations formed the basis of the first high-resolution linkage map for cassava, which in turn formed the basis of the first physical map organized into chromosomes (International Cassava Genetic Map Consortium, 2015).

After consolidation and cleaning of genotyping and phenotyping data across sites and the removal of individuals with a large amount of missing data, 186 F1 individuals remained for QTL analysis. Overall mean scores for CBSD foliar symptoms, across both 3 and 6 MAP scores and all three growing seasons were higher in Chambezi (2.16) than Naliendele (1.19) (Table 1). Indeed, overall mean root necrosis scores were also higher in Chambezi (2.27) than in Naliendele (1.68). The same situation is reflected within years, with mean severity scores for CBSD root necrosis in Naliendele of 1.72 (N1) and 1.64 (N2) and Chambezi 2.2 (C1) and 2.34 (C2). For CBSD foliar symptoms, an increasing trend over the years in Naliendele 1.06 (N1), 1.18 (N2) and 1.34 (N3), and higher mean severity score in Chambezi, but not consistently increasing across years 2.4 (C1), 1.93 (C2) and 2.16 (C3). CBSD foliar severity scores were consistently higher at 6 MAP than 3 MAP in both locations (1.21 (6 MAP) compared to 1.18 (3 MAP) in Naliendele, and 2.51 (6 MAP) compared to 1.81 (3 MAP) in Chambezi) (Table 1).

QTL associated with CBSD resistance

In the NCAR population, three consistent QTL associated with CBSD root necrosis resistance were detected on chromosomes 7, 11 and 12, all detected from data from C1 and C2 under high disease pressure (Table 2). A fourth region was detected on chromosome 18 in C1 only, characterised by two QTL, one quite specific (chrXVIII:6,327,979 to 6,801,336), the other encompassing the first (chrXVIII:4,212,438 to 8,916,735) (Table 2). Flanking markers, and distances between flanking markers, in the current version of the cassava reference genome assembly (v8.1; NCBI GenBank accession GCA_001659605.2, https://phytozome-next.jgi.doe.gov/info/Mesculenta_v8_1) (Bredeson et al. in preparation) can be found in Supplementary File S2. Logarithm of Odds (LOD) scores ranged from 2.64 (on chromosome 18) to 8.38 (on chromosome 11) from C2. The percentage of variance explained (PVE) ranged from 6.3 (on chromosome 7) to 32.4 (on chromosome 11).

Seventeen QTL that occurred in one or more site/season or scoring time-point were identified for foliar symptoms in the NCAR population. These occurred on 11 different chromosomes, i.e., 1, 4, 5, 6, 7, 8, 10, 11, 14, 17, and 18 (Table 3), with six QTL on chromosome 1. Data for individual sites/seasons can be found in Supplementary File S3. It is interesting to note that LOD and PVE scores were very high for Naliendele season 1 (2013/14). This may be due to the low disease pressure and non-normality of the data.

Comparison of QTL for CBSD across populations

QTL for both root necrosis and foliar symptoms, discovered in the NCAR population, were considered in relation to four other populations that were developed and phenotyped simultaneously

10.3389/fpls.2023.1270963

TABLE 1 Basic statistics for CBSD root necrosis (CBSDRN) and CBSD foliar symptoms (CBSDF) from three seasons of phenotyping trials in Naliendele (N) and Chambezi (C).

Trait[a]	Experiment[b]	Mean (1–5 scale)	Variance	StdError	Skewness	Kurtosis	SWILK test	P-value
CBSDRN	N1	1.7182	0.4361	0.6604	1.3666	2.1902	0.8661	0.000***
	N2	1.6360	0.1510	0.3885	1.1347	2.7825	0.9112	0.000***
	C1	2.1962	0.3831	0.6189	0.9186	3.5837	0.8362	0.000***
	C2	2.3413	0.5797	0.7614	0.6587	1.4959	0.9171	0.000***
CBSDF	N1-3	1.0155	0.0082	0.0903	8.2033	78.119	0.1989	0.000***
	N1-6	1.1113	0.1506	0.3880	6.6301	56.3559	0.3476	0.000***
	N2-3	1.1777	0.1168	0.3418	4.0402	24.9493	0.5810	0.000***
	N2-6	1.1793	0.0693	0.2632	1.9729	3.8787	0.7097	0.000***
	N3-3	1.3527	0.1998	0.4470	2.0145	4.3965	0.7135	0.000***
	N3-6	1.3324	0.2094	0.4576	2.6699	8.8964	0.6705	0.000***
	C1-3	1.6361	0.1891	0.4348	0.3646	-0.4403	0.9478	0.000***
	C1-6	3.1625	0.9306	0.9647	-0.0122	-0.4980	0.9600	0.001**
	C2-3	2.0179	0.4060	0.6372	0.5850	0.7373	0.9376	0.000***
	C2-6	1.8401	0.6009	0.7752	1.3342	2.4359	0.8667	0.000***
	C3-3	1.7872	0.2590	0.5089	0.6328	1.5607	0.9159	0.000***
	C3-6	2.5242	0.3505	0.5921	-1.1533	1.1999	0.8476	0.000***

[a]CBSDRN—CBSD root necrosis, CBSDF—CBSD foliar symptoms.
[b]N1 = Naliendele 2013/14, N2 = Naliendele 2014/15, C1 = Chambezi 2013/14, C2 = Chambezi 2014/15, -3 = 3MAP, and -6 = 6MAP,
StdError = standard error, ** P ≤ 0.01; *** P ≤ 0.001.

i.e.: NDL06/132 AR37-80 (NDLAR) (Kapinga, 2017), Namikonga × Albert (NxA) (Masumba et al., 2017), Kiroba × AR37-80 (KAR) (Nzuki et al., 2017) and AR40-6 × Albert (ARAL) (Garcia-Oliveira et al., 2020). A total of 42 QTL were defined across populations for CBSD tolerance (Supplementary File S4); 10 for root necrosis, 29 for foliar symptoms and four for both, including one QTL on chromosome 8 from NCAR which covers a large region and encompasses four other QTL associated with either foliar symptoms or root necrosis and is thus not counted as a separate QTL. A schematic comparison of QTL for CBSD root necrosis and foliar symptoms can be found in Figure 1 and compiled in Supplementary File S4. There are four chromosomal regions that are striking when viewing information across populations:

1. QTL on both arms of chromosome 4 appear important for resistance to CBSD foliar symptoms (Table 4 and Figure 1). On the left arm, QTL from KAR (C1, C2) and NCAR (N1, N2) overlap from 2.4 to 3.4 Mbp and a QTL from NDLAR overlaps with NCAR (N1, N2) from 2.4 to 3.8 Mbp (C1, N1). This QTL has been designated qCBSDFc4_L.

TABLE 2 Consistent QTL identified in Nachinyaya × AR37-80 population for resistance to CBSD-induced root necrosis.

QTL name	Chr	Position (cM)	Trials in which the QTL was identified	Flanking markers (v5.1) (bp)		Parental effects			LOD	Adjusted PVE (%)
				Left marker	Right marker	F	M	FM		
qCBSDRNc7NC	7	26	C1	chrVII:4,715,293	chrVII:4,813,810	-0.1920	0.1275	0.1056	3.47	8.3
qCBSDRNc7NC	7	26	C2	chrVII:4,715,293	chrVII:4,813,810	-0.1995	0.1346	0.1336	3.48	6.3
qCBSDRNc11NC	11	27	C1	chrXI:4,383,294	chrXI:4,527,454	0.2605	-0.3863	-0.3637	4.41	31.7
qCBSDRNc11NC	11	27	C2	chrXI:4,383,294	chrXI:4,527,454	0.3384	-0.5399	-0.3221	8.38	32.4
qCBSDRNc12NC	12	37	C1	chrXII:6,934,834	chrXII:10,102,374	-0.0880	-0.0960	0.1203	3.04	7.5
qCBSDRNc12NC	12	40	C2	chrXII:6,934,834	chrXII:10,102,374	-0.1516	-0.1189	0.1116	3.85	7.8
qCBSDRNc18NC*	18	7	C1	chrXVIII:4,212,438	chrXVIII:8,916,735	-0.1024	-0.1063	0.1019	2.64	8.6
qCBSDRNc18NC*	18	28	C1	chrXVIII:6,327,979	chrXVIII:6,801,336	-0.0728	-0.1584	0.1767	2.84	12.2

* Although the LOD score is not above 3.0, due to consistencies with QTL in other populations (see below), this is worthy of inclusion.

TABLE 3 QTL associated with CBSD foliar symptoms, scored at 3 and 6 MAP in Chambezi and Naliendele in three seasons, C1–3 and N1–3.

QTL name	Chr	Trials in which the QTL was identified*	Position (cM)	Flanking markers (v5.1) (bp)		LOD	Adjusted PVE (%)
				Left marker	Right marker		
qCBSDFc1NCa	1	C2^{6}, N3^{6}	30	chrI:3,985,072	chrI:4,383,262	9.39	44.4
qCBSDFc1NCb	1	N2^{3}, C1^{6}, N2^{6}	33	chrI:4,658,167	chrI:4,815,462	13.06	37.4
qCBSDFc1NCc	1	N1^{6}, N2^{3}, N3^{6}	57	chrI:9,703,189	chrI:10,030,347	25.28	61.2
qCBSDFc1NCd	1	N2^{3}, N2^{6}, C2^{6}, N3^{3}, N3^{6}	74	chrI:13,330,388	chrI:14,450,997	10.14	37.6
qCBSDFc1NCe	1	N1^{6}, N3^{3}	102	chrI:19,342,967	chrI:19,919,971	19.58	62.6
qCBSDFc1NCf	1	N2^{6}, N2^{3}, C2^{6}	106	chrI:21,287,026	chrI:21,864,131	4.39	28.8
qCBSDFc4NCa	4	N1^{3}, N3^{3}	82	chrIV:2,421,127	chrIV:2,421,144	22.56	70.9
qCBSDFc4NCb	4	N2^{3}, N3^{3}	4	chrIV:19,678,070	chrIV:20,065,474	9.17	41.5
qCBSDFc5NC	5	C1^{6}, C2^{3}	106	chrV:19,675,325	chrV:20,779,139	3.59	7.6
qCBSDFc6NC	6	C2^{3}, C2^{6}	73	chrVI:8,507,878	chrVI:8,507,925	6.17	16.6
qCBSDFc7NC	7	N1^{6}, C2^{6}, N3^{3,6}	7	chrVII:261,026	chrVII:1,796,230	29.19	61.3
qCBSDFc8NC	8	C3^{3}, N1^{6}, N3^{3}, N2^{3}, N3^{3}, C3^{6}	37	chrVIII:12,759,725**	chrVIII:17,587,092	24.37	60.7
qCBSDFc10NC	10	C1^{3}, N3^{6}, N3^{6}	66	chrX:14,023,601	chrX:14,620,013	9.49	40.3
qCBSDFc11NC	11	N3^{3}, N3^{3}, N1^{3}	75	chrXI:13,715,995	chrXI:14,393,447	24.76	67
qCBSDFc14NC	14	N1^{3}, C2^{6}	70	chrXIV:14,795,105	chrXIV:14,835,447	25.36	70.9
qCBSDFc17NC	17	N3^{6}, N1^{6}, C2^{3}	89	chrXVII:69,840	chrXVII:364,832	8.21	41.6
qCBSDFc18NC***	18	C2^{3}, C3^{3}	9	chrXVIII:4,212,438	chrXVIII:8,916,735	3.38	13.1

* The superscript denotes the time of scoring: ^{3}, 3 MAP; ^{6}, 6 MAP.
**QTL across the six trials indicated each had a QTL within this range, although the flanking markers were not consistent.
*** This QTL was significant for resistance to CBSD root necrosis in C1.
The LOD and PVE are reported for the trial which is underlined in the 'Trial' field.

2. On the right arm of chromosome 4, a QTL from NDLAR (N1) (19.4 to 19.5 Mbp) is very close to a QTL from NCAR (N2, N3) (19.7 to 20.1 Mbp) and has been designated as qCBSDFc4_R.
3. A series of QTL for CBSD-induced root necrosis from three populations (NDLAR, NCAR and NxA) between 3.6 and 7.3 Mbp on chromosome 11 are either overlapping, in series or close to one another and are here grouped as qCBSDRNc11 (Figure 1 and Table 5). The first QTL from NCAR (N1 and N2) is from 3.6 to 4.3 Mbp with a second adjoining QTL from C2 from 4.3 to 5.3 Mbp. Encompassed within this second QTL is a QTL from NCAR (C1 and C2) and NxA (C1, C2). Adjoining this from 5.3 to 7.3 Mbp is another QTL from NDLAR in C1 and N1. The maximum amount of phenotypic variation explained is 32% in NCAR (C2).
4. The left arm of chromosome 18 is associated with resistance to CBSD foliar symptoms from around 4.2 to 8.9 Mbp in Nachinyaya, 5.8 to 6.0 Mbp in Kiroba and 10.0 to 10.9 Mbp in AR40-6 (Table 6 and Figure 1). This region is designated qCBSDRNFc18.
5. For root necrosis resistance on chromosome 18, it appears there may be two QTL which are quite close to each other. Nachinyaya, Namikonga and AR40-6 all have QTL from 6.3 to 6.8 Mbp. NDL06/132 has a QTL for root necrosis overlapping this (from 6.7 to 9 Mbp) and Namikonga has a further QTL for root necrosis within this region from 8.6 to 8.9 Mbp (Table 6 and Figure 1). These two overlapping QTL here are designated qCBSDRNc18a (6.3 - 6.8 Mbp) and qCBSDRNc18b (8.6 - 9.0 Mbp).

Candidate genes associated with CBSD resistance

The QTL prioritised for selecting potential candidate genes were qCBSDFc4_L (2.4 - 3.8 Mbp), qCBSDFc4_R (19.4 - 20.1 Mbp), qCBSDRNc11 (3.6 - 7.3 Mbp) and qCBSDRNc18a (6.3 - 6.8 Mbp) and qCBSDRNc18b (8.6 - 9.0 Mbp) and contained 1,168 genes (Supplementary File S5). It was decided not to look further into foliar symptoms of Chromosome 18, as the QTL defined here was less precise and consistent. Gene families underlying these QTL with known association with viral resistance were selected from annotations from the Panther Classification System in combination with an extensive literature review (Table 7). Interestingly cinnamoyl-CoA reductase (CCR) genes involved in lignin synthesis were found within QTL regions on both chromosomes 4 and 11. These were also found to be highly upregulated in both

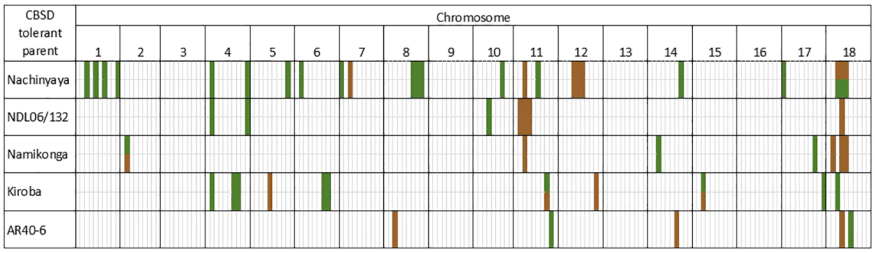

FIGURE 1
Schematic presentation of the positions of QTL in five bi-parental mapping populations developed for mapping resistance to CBSD foliar (green) and root necrosis (brown). Details of QTL can be found in Supplementary File S4.

infected and uninfected Namikonga compared to Albert in the study by Amuge et al. (2017). In fact, several genes in the lignin biosynthesis pathway were found to be upregulated in resistant Namikonga, compared to Albert (Supplementary File S6).

Discussion

A bi-parental mapping population was constructed from Nachinyaya (a landrace from northern Mozambique and southern Tanzania, known to have tolerance to CBSD root necrosis that has been durable for several decades, and susceptible to CMD) and AR37-80 (selected for the CMD2 gene and CGM resistance, but susceptible to CBSD (Blair et al., 2007; Okogbenin et al., 2012)). The final population size used for QTL analysis was 186 individuals. This population was phenotyped for CBSD root necrosis and CBSD foliar symptoms over three seasons (2013/14, 2014/15, and 2015/16) in two hotspot locations, Naliendele and Chambezi, Tanzania.

QTL and candidate genes associated with CBSD resistance

A total of 42 QTL have been defined for tolerance to CBSD (Supplementary File S4) across five populations developed, phenotyped and genotyped at the same time as this population (NDL06/132 × AR37-80 (NDLAR) (Kapinga, 2017), Namikonga × Albert (NxA) (Masumba et al., 2017), Kiroba × AR37-80 (KAR) (Nzuki et al., 2017) and AR40-6 × Albert (ARAL) (Garcia-Oliveira et al., 2020). To prioritise QTL results for further investigation, they are considered in conjunction with other information (1) co-localisation across populations; (2) identity by descent (IBD) analysis of parents based on whole genome sequence information (Bredeson et al., 2016) and (3) introgression segments from *M. glaziovii* (Bredeson et al., 2016). Viewing results across populations, particularly with a knowledge of the relatedness of parents, and identifying QTL that occur in more than one population provides confidence in the validity of QTL.

Identity-by-descent analysis reveals the close relationship between the CBSD tolerance donor parents (Nachinyaya, Namikonga and NDL06/132) of three of the populations (NCAR, NxA and NDLAR), whereas the CBSD tolerant donors (Kiroba and AR40-6) of the other two populations are more independent (Bredeson et al., 2016; Nzuki et al., 2017). This has implications for interpreting the results. NDL06/132 and Nachinyaya appear to be full siblings, with Nachinyaya a full sibling of Albert, which in turn is a full sibling of TMEB117 (Bredeson et al., 2016). Namikonga is also closely related, with a parent–offspring relationship with TMEB117. TMEB117 is a Nigerian landrace that has been widely used in the IITA breeding program for

TABLE 4 Details of two regions with overlapping or closely positioned QTL on chromosome 4 for foliar symptoms across five populations phenotyped in the same sites and years.

QTL name‡	Resistant parent	Site/season (MAP*)	Flanking markers (v5.1) (bp)	LOD	PVE (%)
Composite QTL name qCBSDFc4_L					
qCBSDFc4KR	Kiroba	C1 & C2(3)	2,397,127–3,389,179	2.51–2.78	6.00–10.93
qCBSDFc4NCa	Nachinyaya	N2 & N1(3)	2,421,127–2,421,144	4.86–22.56	9.00–70.90
qCBSDFLc4a	NDL06/132	C1(9) & N1(6)	2,768,314–3,766,228	3.43–15.99	6.50–35.72
Composite QTL name qCBSDFc4_R					
qCBSDFLc4b	NDL06/132	C1(9)	16,481,626–17,222,649	2.77	5.10
qCBSDFLc4c		N1(3)	19,421,153–19,503,605	3.31	8.78
qCBSDFc4NCb	Nachinyaya	N3(6) & N2(3)	19,678,070–20,065,474	5.22–9.17	26.70–41.50

‡From original publication.
*Months after planting.

TABLE 5 Details of one region with overlapping or closely positioned QTL on chromosome 11 for CBSD-induced root necrosis (qCBSDRNc11) across five populations phenotyped in the same sites and years.

QTL name	Resistant parent	Site/season	Flanking markers (v5.1) (bp)	LOD	PVE (%)
Composite QTL name qCBSDRNc11_R					
qCBSDRNc11NDb*	NDL06/132	N1 & N2	3,559,047–4,301,373	3.19–5.6	11.52–11.93
qCBSDRNc11NDc*		C2	4,301,373–5,325,558	4.63	12.72
qCBSDRNc11NDa*		C1 & N1	5,325,558–7,316,171	2.86–12.65	14.75–17.8
qCBSDRNc11NC	Nachinyaya	C1 & C2	4,383,294–4,527,454	4.41–8.38	31.7–32.4
qCBSDRNc11Na	Namikonga	C1 & C2	4,502,175–4,527,454	3.35–3.81	5.2–7.6
qCBSDRNc11Nb		C2	4,527,454–4,617,294	7.5	17.8
qCBSDRNc11Nc		C1	4,617,294–4,760,631	3.6	5.3

*The names of the QTL have been modified from their original designation with an ND included after c11, to indicate the NDLAR population.

poundability characteristics. TMEB117 was almost identical to TMEB693 (apart from CMD resistance) (Ferguson et al., 2019) and appeared to be widely distributed in Africa. This variety is possibly an early introduction to East Africa (Ferguson et al., 2019) and a parent in the Amani breeding program. This would explain the relationship between Nachinyaya, Albert and Namikonga. Namikonga is the Amani hybrid 46106/27, a third backcross of *M. glaziovii*, and mentioned by Hillocks and Jennings (2003) as one the best Amani hybrids. In Kenya, it is also known as Kaleso (Amuge et al., 2017). Interestingly NDL06/132 was thought to be a cross from female parent NDL90/34 and likely male parent Nachinyaya that was selected from a crossing block in Naliendele, southern Tanzania, although Bredeson et al. (2016) shows NDL06/132 and Nachinyaya to be full siblings. There was no *M. glaziovii* wild species introgression segment detected in either NDL06/132 or Nachinyaya (Bredeson et al., 2016). Many years ago, TMEB117 was reported to be 'highly resistant' (immune) to CBSV and, thus, maybe a source of CBSD resistance/tolerance (Stephan Winter, per. comm.).

In contrast, Kiroba is a landrace from around Dar es Salaam, which occasionally shows severe leaf symptoms of CBSV but no root symptoms, even under high disease pressure. The results from whole genome re-sequencing data, suggest Kiroba has a parent–offspring relationship with tree cassava (an *M. esculenta* – *M. glaziovii* hybrid) and is more related to West African and South American germplasm than East African germplasm (Nzuki et al., 2017). Introgression segments from *M. glaziovii* were identified by Nzuki et al. (2017) on chromosomes 1, 17 and 18. This, together with the fact that it has good yield and vigour, suggests it may be derived from the Amani breeding program. AR40-6 is a cross between a CMD-resistant line from West Africa and South American/Asian breeding lines. It clusters with the South American and West African germplasm (Nzuki et al., 2017) as opposed to East African germplasm.

TABLE 6 Details of regions with overlapping or closely positioned QTL on Chromosome 18 for CBSD-induced root necrosis (qCBSDRNc18) and foliar symptoms (qCBSDFc18) across five populations phenotyped in the same sites and years.

QTL name	Resistant parent	Site/season	Flanking markers (v5.1) (bp)	LOD	PVE (%)
Composite QTL name qCBSDRNc18a and b					
qCBSDRNFc18NC	Nachinyaya	N2(6)	4,212,438–7,761,534	2.96	8.25
		C2(3), C3(3)	4,212,438–8,916,735	2.53–3.38	6.26–13.08
qCBSDRNFc18NC		C1(RN)	4,212,438–8,916,735	2.64	8.6
		C1(RN)	6,327,979–6,801,336	2.84	12.2
qCBSDFc18K	Kiroba	C2(6)	5,764,853–6,089,207	2.79	9.6
qCBSDRNc18Na	Namikonga	N2(RN)	6,320,754–6,502,253	3.31	8.21
		C1(RN)	6,327,979–6,801,336	2.84	12.2
qCBSDRNc18Nb		C2(RN)	8,650,285–8,943,971	5.1	6.49
qCBSDRNc18AR	AR40-6	N1(RN), C2(RN)	6,433,344–6,501,916	6.68–11.49	2.13–3.05
qCBSDFc18AR		C1(6), C2(6)	10,068,641–10,924,641	3.21–3.35	12–13
qCBSDRNc18ND	NDL06/132	C2(RN), N2(RN)	6,795,075–9,002,167	4.63–11.52	8.3–18.3

10.3389/fpls.2023.1270963

TABLE 7 Genes considered to have the highest likelihood of contributing to CBSD resistance contained within QTL on chromosomes 4, 11 and 18.

Trait	Right flanking (v5.1)	Left flanking (v8.1)	Right flanking (v8.1)	Gene ID (v8.1)	Region	Annotation
Chromosome 4						
Foliar	3,389,179	2,756,162	3,913,060	Manes.04G026700	3,132,187–3,137,031 (–)	Mitogen-activated protein kinase 3 (MAPK3)
Foliar	2,252,300	1,933,035	2,252,300	Manes.04G018000	2,203,816–2,207,282 (–)	Phenylalanine ammonia-lyase (PAL)
Foliar	15,734,008	30,208,991	31,029,727	Manes.04G103200	30,780,920–30,784,436 (–)	cinnamoyl-CoA reductase (CCR)
Foliar	3,766,228	3,195,542	4,403,548	Manes.04G028600	3,381,000–3,386,365 (–)	ribonuclease P/MRP protein subunit RPP1
Foliar	15,734,008	30,208,991	31,029,727	Manes.04G099100 Manes.04G099066 Manes.04G099300	30,355,304–30,362,981 (+) 30,365,861–30,377,729 (+) 30,379,086–30,383,919 (+)	Leucine-rich repeat receptor-like kinase PEPR1-related
Foliar	19,678,070	33,800,870	34,209,641	Manes.04G141500	34,006,333–34,010,108 (–)	Translation initiation factor 4A (EIF4A)
Foliar	15,734,008	30,208,991	31,029,727	Manes.04G102600	30,718,979–30,718,979 (–)	WRKY 40 transcription factor
Chromosome 11						
Root necrosis	5,325,558	6,600,507	8,959,420	Manes.11G063000	8,755,246–8,758,965 (–)	HOPW1-1-interacting1
Root necrosis	5,325,558	8,959,420	11,729,302	Manes.11G066500	9,469,194–9,471,365 (+)	WRKY 40 transcription factor
Root necrosis	4,527,454	6,600,507	8,959,420	Manes.11G064002	901,788–8,905,954 (+)	double strand RNA binding domain from dead end protein 1 DCL-4
Root necrosis	4,301,373	4,987,387	6,600,507	Manes.11G048500	5,229,033–5,235,934 (+)	Translation initiation factor 4A (EIF4AIII)
Root necrosis	4,617,294	6,984,296	7,146,789	Manes.11G058800	7,135,381–7,148,175 (+)	Translation initiation factor 3 (EIF3)
Root necrosis	4,527,454	6,861,781	6,886,880	Manes.11G056100	6,861,620–6,863,275 (+)	F18B13.21 protein-related
Root necrosis	4,617,294	6,886,880	6,984,296	Manes.11G056600	6,895,728–6,898,010 (–)	PPR repeat
Root necrosis	7,316,171	8,959,420	11,729,302	Manes.11G070900	10,223,822–10,236,933 (+)	Mitogen-activated kinase/threonine-protein kinase OSR1
Root necrosis	4,760,631	6,984,296	7,146,789	Manes.11G058000	7,005,871–7,014,518 (+)	Molecular chaperone HSP40/DNAJ-like protein
Root necrosis	7,316,171	8,959,420	11,729,302	Manes.11G065500	9,127,715–9,131,631 (+)	Cinnamoyl-CoA reductase (CCR)
Root necrosis	7,316,171	8,959,420	11,729,302	Manes.11G073900	10,660,113–10,667,824 (–)	DEAD BOX HELICASE-RELATED
Chromosome 18						
Root necrosis	6,801,336	8,032,346	8,535,185	Manes.18G091400	8,399,198–8,401,243 (–)	U6 snRNA-associated Sm-like protein LSm3 (LSM3)
Root necrosis	9,002,167	11,169,084	11,185,913	Manes.18G111600	11,169,084–11,185,913 (–)	Translation initiation factor 2D (EIF2D)

(Continued)

TABLE 7 Continued

Trait	Right flanking (v5.1)	Left flanking (v8.1)	Right flanking (v8.1)	Gene ID (v8.1)	Region	Annotation
Root necrosis	8,916,735	5,339,282	11,217,402	Manes.18G072500	6,486,039–6,487,930 (–)	Translation initiation factor 5 (EIF5)
Root necrosis	8,916,735	5,339,282	11,217,402	Manes.18G071100	6,394,596–6,407,441 (–)	E3 ubiquitin Rab5/6 GTPase effector

In the NCAR population reported here, consistent QTL associated with resistance to CBSD root necrosis were detected on chromosomes 7, 11 and 12, all of which were identified within data from C1 and C2, cultivated under high disease pressure (Table 2). A fourth region was detected on chromosome 18 in C1 only, characterised by two QTL, one quite specific (chrXVIII:6,327,979–6,801,336), the other encompassing the first (chrXVIII:4,212,438–8,916,735) (Table 2). This also co-locates with QTL for foliar symptoms from this population. In addition, 17 significant QTL were associated with foliar symptoms. Here, we initially highlight QTL and chromosomal regions which are found in more than one population and provide possible explanations for this based on the relatedness of parents. We then highlight QTL that occur in only one population but either occur in many sites/seasons or, for other reasons, appear to warrant further investigation.

Two QTL on chromosome 4 are of interest; qCBSDFc4_L was associated with resistance to foliar symptoms in KAR (C1, C2) and NCAR (N1, N2) populations overlapping from 2.4 to 3.4 Mbp. This is noteworthy even though the donor parents of these populations are not particularly closely related. Of possibly greater interest is the QTL qCBSDFc4_R associated with foliar symptoms from NCAR and NDLAR (with CBSD tolerant donor parents Nachinyaya and NDL06/132, respectively). These parents are likely full sibs with an identity by descent (IBD) of 0.5411 based on whole genome sequence information (Bredeson et al., 2016). Neither Nachinyaya nor NDL06/132 have *M. glaziovii* introgression segments in their genome (Bredeson et al., 2016), implying that these QTL regions are derived from the *M. esculenta* genome.

Kayondo et al. (2018) using GWAS found many SNPs in high linkage disequilibrium, defining a QTL covering both arms of chromosome 4. This supports the evidence presented here. In contrast, Kayondo et al. (2018) suggest that this QTL is derived from an introgression segment from *M. glaziovii* and confirmed the presence and segregation of the introgressed genome segment in both panels using a set of diagnostic markers from *M. glaziovii*. Due to the high level of linkage disequilibrium at the QTL location, they do not highlight a single locus or loci as candidate gene(s) associated with CBSD foliar severity. Interestingly Somo et al. (2020), also using GWAS, detected a QTL on chromosome 4 (*QTL-cbsd4|cmd-1*), tagged by marker S4_24670203, which showed significant associations with both CBSD foliar symptoms and CMD resistance in the K4_cluster1 dataset. This is relatively close to the qCBSDFc4_R region (16,481,626–20,065,474 bp (v5.1).

Three populations with closely related CBSD donor parents (Namikonga, Nachinyaya and NDL06/132) all mapped the qCBSDRNc11 locus (Figure 1 and Table 5). This locus is supported by evidence from 11 site/season combinations. The locus currently stretches over 3.7 Mbp from positions 3.6–7.3 Mbp, although the regions around 4.5 Mbp seem to be well supported with NCAR having a QTL covering only 144 kbp from 4,383,294 to 4,527,454 bp (6,683,896–6,886,880 bp in v8.1, a distance of 202,984 bp) from C1 and C2 and accounting for 32% of the variation in each site. In addition, NxA has a QTL covering just 25 kbp from 4,502,175 to 4,527,454 bp (6,861,782–6,886,880 bp in v8.1, 25,098 bp) from the same site/seasons but, in this case, accounts for an average of 6.4% of the phenotypic variation. There are no *M. glaziovii* introgression regions on chromosome 11 (Bredeson et al., 2016), so qCBSDRNc11 is likely to be derived from the *M. esculenta* genome. Given these data, we believe this region warrants further investigation.

In contrast to the study here, Kayondo et al. (2018) found 83 significant SNP markers on chromosome 11 associated with foliar symptoms at 3 MAP and 33 SNPs at 6 MAP, but around ~23 Mbp. They could not identify SNPs surpassing the Bonferroni threshold for CBSD root severity across two panels. However, analysis of the multi-location data for Panel 1 identified significant regions of CBSD association on chromosomes 5, 11 and 18 (−log10(P-value) > 6.5), which explained 8, 6 and 10% of the phenotypic variance, respectively. This supports the observations reported here regarding QTL on chromosome 11 and their association with CBSD root necrosis. In addition, Somo et al. (2020) identified a QTL associated with CBSD foliar symptoms, similar to that of Kayondo et al. (2018), but again these do not coincide with the QTL identified for root necrosis here.

A third region on chromosome 18 is more complex. A QTL occurs across a large region from 4.2 to 8.9 Mbp in NCAR and is associated with both foliar symptoms (C2, C3 and N2) and root necrosis (C1). The only other population showing a QTL associated with foliar symptoms within this region is KAR in C2 from 5.7–6.0 Mbp, albeit with a low LOD score of 2.79 with a PVE of 9.6%. It seems that there is more evidence for QTL associated with root necrosis in this region (qCBSDRNc18). Within the QTL region of NCAR (4.2–8.9 Mbp), there are two, more specific, regions defined by other populations. NxA, NCAR and the population ARAL with the unrelated donor parent AR40-6 have QTL from 6.3–6.8 Mbp, all associated with root necrosis in a total of five site/season environments. A neighbouring QTL from 6.8–9.0 Mbp in a further two populations (NDLAR (6.8–9.0 Mbp) and NxA (8.6–8.9 Mbp)) is associated with root necrosis in a total of three sites/seasons. Thus, all three related CBSD tolerant parents (NDL06/132, Nachinyaya and Namikonga) with good levels of tolerance to root

necrosis have QTL for root necrosis between 6.3–9.0 Mbp on chromosome 18 (Table 6 and Figure 1). Although this region is large, it appears to be genuine. ARAL shows a QTL for foliar symptoms from 10 to 10.9 Mbp in both C1 and C2, which may be of additional interest. There are no *M. glaziovii* introgression regions on chromosome 18 (Bredeson et al., 2016), so the QTL described here are likely to be derived from the *M. esculenta* genome. Kayondo et al. (2018) identified significant regions of CBSD root severity association from multi-location data for Panel 1 on 18 (−log10 (P-value) > 6.5), in addition to chromosomes 5 and 11, which explained 10% of the phenotypic variance.

Some QTL, not shared across populations, are worthy of mention and further investigation. The NCAR population, with donor parent Nachinyaya, apart from possessing the important qCBSDFc4_L, qCBSDFc4_R and qCBSDFc18 loci, contain other important QTL associated with foliar symptoms, including six QTL distributed across chromosome 1 and on chromosomes 5, 6, 7, 8, 10, 11, 14 and 17 (Table 3). Chromosome 1 has a large *M. glaziovii* introgression segment in some Amani-derived varieties (Bredeson et al., 2016), but interestingly *M. glaziovii* introgression segments were not found in Nachinyaya, and QTL associated with foliar symptoms were not found on chromosome 1 of other varieties with introgression segments. This indicates that foliar symptom resistance on chromosome 1 comes from the cultivated *M. esculenta*. In addition, QTL on chromosomes 7 (qCBSDRNc7NC) and 12 (qCBSDRNc12NC) were associated with root necrosis in C1 and C2 under high disease pressure, although these did have slightly lower PVEs compared to qCBSDRNc11NC and qCBSDRNc18NC. Somo et al. (2020) detected two QTL associated with both CMD and CBSD foliar symptoms on chromosome 12 (QTL-cbsd12|cmd-1 and QTL-cbsd12|cmd-2), the latter SNP tag S12_7929439 which is close to the QTL detected here for CBSD root necrosis 6,934,834–10,102,374 bp (v5.1), 8,250,631–12,995,530 bp (v8.1). It also overlaps with another QTL for CMD severity detected by Somo et al. (2020) at 6.3–8.7 Mbp (v5.1).

In Namikonga, a QTL on chromosome 2 named qCBSDRNFc2Nm from 3.5–3.6 Mbp (v5.1) was associated with foliar symptoms in all site/season combinations and root necrosis in both years in Naliendele and should be of particular interest. Somo et al. (2020) detected a QTL for root necrosis in the Tanzanian Ukiriguru GWAS population with SNP tagged at S2_9258334.

As Kiroba and AR40-6 are more distantly related to the other CBSD donor parents, they may possess unique QTL. For CBSD root necrosis and foliar symptoms, a small region (15.7–15.8 Mbp which corresponds with 26.956–27.058 Mbp in v8.1) on the other arm of chromosome 11 to the QTL from the Nachinyaya-NDL06/132-Naminkonga group, is implicated in the KAR population (qCBSDRNFc11KR). It is significant in C1, N1 and N2 and is worthy of further investigation (Nzuki et al., 2017). Somo et al. (2020) detected a QTL for CBSD foliar symptoms from between 22.88 and 22.94 Mbp in an Ukiriguru population.

In addition, a QTL on chromosome 15 (qCBSDRNFc15K) (4.2–4.7 Mbp) in the KAR population is significant for root necrosis in N2 and foliar symptoms in N1 and N2, but interestingly this was not detected under the higher disease pressure of Chambezi. Two further QTL related solely to root necrosis from the KAR population are also interesting; qCBSDRNc12K on chromosome 12 (16.4–17.3 Mbp), which is significant in C1, N1 and N2 and qCBSDRNc5K, although this is less consistent (Nzuki et al., 2017). The QTL found here does not coincide with that detected by Somo et al. (2020) for CMD and CBSD foliar symptoms. In ARAL, a QTL on chromosome 14 for root necrosis was detected when scoring was done using a 1–5 scale (qCBSDRNSc14AR) (12.1–13.9 Mbp) in N1, N2 and C2 and by area of necrosis (qCBSDRNAc14AR) (12.9–13.6 Mbp) in the same environments. This is worthy of further investigation and, for convenience, is designated here as qCBSDRNc14AR.

In summary, the polygenic nature of tolerance to CBSD root necrosis and foliar symptoms in the populations studied here is evident, as is their instability across environments. This was also noted by Kayondo et al. (2018). It appears that although tolerance to foliar symptoms and root necrosis are largely under different genetic controls, there are some regions of the genome which may influence both. It is recommended that the following two QTL are targeted, as first priority, for marker development for use in marker-assisted breeding for foliar symptom resistance; qCBSDFc4_L and qCBSDFc4_R; four for CBSD-induced root necrosis qCBSDRNc11, qCBSDRNc18 (which may also confer some tolerance to foliar symptoms), qCBSDRNc12K and qCBSDRNc14AR; and three QTL for both root necrosis and foliar symptom resistance: qCBSDRNFc2Nm, qCBSDRNFc11KR and qCBSDRNFc15K. Due to the large number of QTL detected across various mapping populations and panels, it is important that QTL should be mapped onto the most recent version of the cassava reference genome (Mbanjo et al., 2021).

Candidate genes associated with CBSD resistance

A literature survey was carried out on the 1,168 genes contained within the priority QTL regions on chromosomes 4, 11 and 18 (Supplementary File S5) to determine those most likely to contribute to CBSD resistance (Table 7). Those considered the most significant are discussed below.

PAL and CCR

Of particular relevance are two genes, phenylalanine ammonia-lyase (PAL) (Manes.04G018000) and cinnamoyl-CoA reductase (CCR) (Manes.04G103200), found in QTL regions for foliar symptoms (chromosome 4). A second CCR (Manes.11G065500) is found within the QTL for root necrosis on chromosome 11. A second PAL gene (Manes.10G047500) was also identified on chromosome 10 (5,218,254–5,221,121 bp (v8.1)). CCR proteins operate downstream of PAL within the lignin biosynthetic pathway (Wadenbäck et al., 2008) and catalyse the production of several of its components (Yadav et al., 2020). We examined key genes of the cassava lignification pathway (Wang et al., 2023) using previously published transcriptomic data from Amuge et al. (2017). We found these to be strongly upregulated in the CBSD-resistant landrace Namikonga compared to the susceptible landrace Albert (Supplementary File S6) throughout the lignification pathway. This was the case in both uninfected and infected plants, strongly

suggesting Namikonga has a higher level of basal lignin deposition. Wild cassava species, or those with introgression segments, tend to have more fibrous storage roots, commensurate with greater lignin content. Manes.11G065500 was upregulated 2.4x to 14.3x and 1.6x to 11.8x in Namikonga-infected and uninfected plants, respectively.

For long-distance and systemic infection, CBSVs, like other plant viruses, are translocated through the plant in both external and internal phloem vessels with the source-sink flow of photoassimilates (Graciano-Ribeiro et al., 2009; Nassar et al., 2010; Hipper et al., 2013; Sheat et al., 2021). Virus particles then pass from sieve elements of the phloem into the companion cells (SE–CC complex) to translocate to parenchyma and mesophyll cells, where they replicate. Resistance to long-distance movement is achieved either by preventing the virus from entering (loading) or exiting (unloading) the SE–CC complex (Rajamäki and Valkonen, 2009; Vuorinen et al., 2011). Sheat et al. (2021) demonstrated the extensive distribution of U/CBSV virus particles in phloem and non-phloem cells in leaves, stems and roots in CBSD susceptible varieties using RNAscope® *in situ* hybridisation. In contrast, in a highly resistant variety from South America they demonstrated very few virus particles in the external phloem cells of the stem, with no accumulation, and an absence of viral particles in the parenchyma tissue. This indicates a restriction of movement, most likely in the unloading, of CBSV from the SE–CC to surrounding cells, thus preventing the virus from reaching sites of replication. In other clones, the virus was restricted to stems and roots or roots only, with organ-specific, variable phloem uploading implicated. This supports the observation here of different QTL for root and foliar CBSD symptoms implying that different mechanisms or conditions may exist for virus restriction in these tissues. Sheat et al. (2021) suggest that phloem restriction is a specific resistance response of the host since the viruses otherwise move and replicate extensively in susceptible cassava varieties.

CCR-mediated lignin synthesis and its contribution to pathogen resistance are reported in the case of fungal (Xu et al., 2011), bacterial (Liu et al., 2021) and viral resistance (tomato yellow leaf curl virus, Sade et al., 2015). It is thought that the increase in lignin deposition contributes to cell wall thickening, which acts as a physical barrier to unloading from the phloem to parenchyma cells at the onset of infection in resistant lines. However, the upregulation of components of the lignification pathway does not necessarily correlate with increased lignification (Kofalvi and Nassuth, 1995), suggesting further function of components of this pathway. CCR has also been shown to be an effector of Rac1, a small GTPase operating within plant defence signalling pathways and is an elicitor of the hypersensitive response to infection by Tobacco mosaic virus (Moeder et al., 2005; Kawasaki et al., 2006). The value of plant-derived lignin as an antiviral agent in non-plants has been an area of substantial research (reviewed in Ullah et al. (2022)). These studies have shown that lignin-derived material effectively inactivate a range of viral pathogens. The precise mechanism by which this is achieved is yet to be fully understood. However, mutants or overexpression lines within the lignin pathway suggest it performs an important role in pathogen resistance, both as a passive or active regulatory component of the immune response (Xu et al., 2011).

Although PAL operates upstream of CCR in the lignification pathway (thus polymorphisms within PAL are more likely to account for its up-regulation than CCR) the known functions and increased basal expression of CCR in Namikonga, seen in the Amuge et al. (2017) data, suggest it is a strong candidate for CBSD resistance

eIF

We identified eukaryotic initiation factor (eIF) genes within QTL on chromosomes 4 (eIF4A), 11 (eIF4AIII, eIF3) and 18 (eIF5 and eIF2D). eIFs protein complexes or subunits are required to recruit mRNA to ribosomes for translation. This process can be co-opted by viruses for their own replication (Zhang et al., 2015). eIF4F complexes contain a 5′cap recognition subunit required for the correct placement of mRNA within the ribosome. Many viral transcripts, including those from members of *Potyviridae*, lack a 5′ cap but can utilise eIF complexes for translation through the binding of a cap-independent translation element (CITE) to an eIF4F subunit, eIF4G (Kneller et al., 2006). eIF4A functions as an RNA helicase, removing tertiary structures from mRNA prior to translation and is also likely to contribute to efficient viral RNA translation by substantially increasing the binding affinity of eIF4F to the CITE (Zhao et al., 2017). eIF4 and eIF5 genes are known to be major contributors to plant virus recessive resistance, as minor sequence changes can prevent viral translation. This protection can be broad-ranging and mutations as minor as a single nucleotide have been shown to confer protection (Ling et al., 2009; Rodríguez-Hernández et al., 2012). While eIF4 has been a major focus of eIF contribution to viral resistance (including the poly-A binding protein eIF4E in CBSD resistance (Shi et al., 2017)), more recently, eIF3 has been shown to be involved in barley yellow dwarf virus replication by facilitating binding viral 5′ UTR to the 40S subunit (Powell et al., 2022). We also note Manes.11G073900 within a QTL region on chromosome 11. This is annotated as a DEAD BOX HELICASE but has very high homology with other eIF4 proteins and may represent a third eIF on chromosome 11. A possible role of eIF2D in viral resistance has recently been proposed (Kim et al., 2023). It has been suggested that, upon viral infection, translation can be switched from the standard 5′cap dependent mechanism to one using non-AUG codons facilitated by eIF2A and/or eIF2D (Green et al., 2022). The cell uses this switch to prevent viral replication through interaction with eIF4 in the manner described above. However, positive-stranded RNA viruses are also able to utilise this mechanism and continue replication.

PEPR1

Chromosome 4 contains a cluster of three PEPR1-related kinase genes. PEPR1/2 proteins act as peptide receptors as part of an innate immunity activation network. *Arabidopsis* plants with disruptions in this pathway show reduced root callose and lignin deposition and are more susceptible to infection by *Pseudomonas syringae* (Jing et al., 2023). AtPEPR1 is one of several proteins which can act as co-receptors within this network with BRASSINOSTEROID INSENSITIVE 1-associated receptor kinase 1 (BAK1). Mutant forms of AtBAK1 show increased susceptibility to a range of viral infections, while AtPEPR1 mutants do not show variation in viral load (Yang et al., 2010; Kørner

et al., 2013). AtPEPR1/2 gene expression is linked with increased salicylic acid (SA) production, a major factor in plant viral defence (reviewed in Alazem and Lin, 2015). Additionally, AtPEPR1 is induced upon wounding by feeding insects, including whitefly (Wang et al., 2019), presumably to prime the immune response against invasive microbes. PEPR1 studies have been largely restricted to *Arabidopsis*, and a role in viral defence in other species should not be ruled out.

WRKY

The data contained a single WRKY 40 transcription factor gene underlying the QTL on chromosome 4 and two WRKY 25 transcription factor genes on chromosome 18. The WKRY gene family is manifold, performing a variety of functions, including regulation of biotic stress response (Chen et al., 2017; Jiang et al., 2017). In *Arabido*psis, WKRY40 and WKRY25 proteins are negative regulators of key resistance genes and mutants show decreased susceptibility to *P. syringae* infection (Zheng et al., 2007; Pandey et al., 2010). Notably, transcriptional profiling indicates a possible role for another WKRY40 homologue in resistance to the South African cassava mosaic virus (Freeborough et al., 2021).

MAPK3

We identified a mitogen-activated protein kinase 3 (MAPK3) gene on chromosome 4 (Manes.04G026700). MAPK proteins are a component of signalling cascades with several known functions, including being strongly associated with SA and jasmonic acid (JA) mediated immunity. In tomato, SlMAPK3 enhances tolerance to tomato yellow leaf curl virus (TYLCV) and is upregulated in infected plants (Li et al., 2017). Although cassava contains multiple MAPK3 genes, Manes.04G026700 has the highest peptide similarity (84%) to SlMAPK3. In a variety of plant species, endogenous application of JA increases resistance to viral infection and increases transcription of MAPK genes (Shang et al., 2011).

HOPW1-1

M. esculenta HOPW1-1-interacting1 (MeWIN1) protein is a member of the plant-specific AP2/EREBP transcription factor family. MeWIN1 is a homologue of AtSHN1/WIN1, which contributes to infection resistance by various fungi by regulating the induction of pathogenesis-related and redox-related genes (Sela et al., 2013). Besides, WIN1 possibly regulates SA in Arabidopsis through interaction with hopW1-1 effector proteins in response to *Pseudomonas syringae* infection (Lee et al., 2008). In cotton, GhWIN2 positively regulates JA biosynthesis but negatively influences SA biosynthesis (Li et al., 2019). WIN1 is strongly linked with cuticle formation, and increased expression has been shown to enhance the physical barrier against leaf-feeding insects and, by extension, their viral load. Beyond this function, WIN1 has been shown to perform multiple roles including pathogen defence and hormone regulation.

DCL-4

Manes.11G064002, annotated as a DICER-LIKE 4 (DLC-4) protein-encoding gene, was strongly up-regulated in Namikonga, five days post-infection, compared to Albert (Amuge et al., 2017). DCL-4 proteins form part of the plant RNAi immunity system and are involved in virus-induced RNA silencing (VIGS) by mediating the biogenesis, at the site of viral infection, of small interfering RNAs. These can be triggered upon infection and act non-cell autonomously to enable viral defence mechanisms in uninfected tissue (Garcia-Ruiz et al., 2010).

LSM3

Members of the LSM family of proteins are involved in eukaryotic mRNA turnover through de-adenylation and de-capping mechanisms. Positive-stranded RNA viruses require host translation to produce RNA replication proteins which, in turn, replicate viral RNA by recruiting it from the host translation mechanism (Chen and Ahlquist, 2000; Schwartz et al., 2002). To distinguish viral from host RNA, Brome mosaic virus has been shown to utilise the mRNA processing function of LSM proteins, and LSM deficiency blocks viral RNA translation (Noueiry et al., 2003).

Rab5/6 GTPase effector protein

Rab GTPases are present on the surface of organelles where they act as recognition and binding platforms for intracellular proteins but are also widely involved in viral infection (reviewed in Spearman, 2018). Positive-stranded RNA virus replication utilises membrane-bound viral replication proteins as well as host membrane proteins, including Rab5 and Rab5 effectors (Stone et al., 2007).

LRR

The most frequent class of plant resistance genes (R genes) are denoted as NBS-LRR, which usually contain both a nucleotide-binding site domain and a leucine-rich repeat domain (McHale et al., 2006). The LRR domain is thought to be a major determinant of pathogen recognition specificity (Collier and Moffett, 2009). A total of 228 NBS-LRR type genes and 99 partial genes (without the NBS domain) were located on v4.1 of the casava genome sequence (Lozano et al., 2015). There were several LRR proteins underlying all target QTL investigated here, with 11 such genes within a 1.28 Mbp region underlying the QTL on chromosome 11. Although Kayondo et al. (2018) identified a cluster of NBS-LRR genes on chromosome 11 through genome-wide associated mapping and genomic selection, this region was outside of the QTL region investigated here. Neither Maruthi et al. (2014) nor Lozano et al. (2015) found any significant differential expression of NBS-LRR genes in cassava infected with CBSV; however, NBS-LRR genes were implicated in resistance to cassava anthracnose disease (Utsumi et al., 2016). Zhang et al. (2022) selected four NBS-LRR genes from the transcriptome databases of Lozano et al. (2015) and Utsumi et al. (2016) for further investigation and found that they were significantly induced by *Xanthomonas axonopodis* pv. *manihotis* (Xam) and salicylic acid treatment. Of these, the MeLRR1 gene (Manes. 11G053000.1) is within the QTL region on chromosome 11 investigated here.

Conclusions

A total of 42 QTL have been defined across five bi-parental mapping populations, developed, genotyped and phenotyped predominantly to detect QTL associated with tolerance to CBSD in largely Tanzanian germplasm. This indicates that this source of tolerance to CBSD root necrosis and foliar symptoms is quantitative. Most QTL are specific for either root necrosis or foliar symptoms, indicating they are largely independently controlled and explaining field (Kayondo et al., 2018; Garcia-Oliveira et al., 2020) and imaging (Sheat et al., 2021) observations. Four QTL are highly supported by cross-population evidence; two on chromosome 4 associated with foliar symptoms, and two on chromosomes 11 and 18 associated with root necrosis. Tolerance to root necrosis does not appear to come from wild species but from TME117 or a similar genotype. Additional population-specific QTL were highlighted for further investigation in four populations. This provides opportunities for QTL stacking. Evidence from the co-location of QTL, parental relationships, gene expression from transcriptome analysis and imaging reports highlight several candidate genes for CBSD resistance. These include PAL and CCR genes involved in the lignin synthesis pathway, in resistance to both foliar CBSD symptoms (chromosome 4) and root necrosis (chromosome 11) and the PEPR1-related kinases shown to be involved with lignin synthesis and virus resistance. The involvement of the lignin pathway can explain, in part, the previously reported restriction of virus particles to phloem tissues in resistant varieties. Further research should endeavour to validate these results and determine whether they are applicable to other resistant varieties, particularly those of South American origin. The presence of eIF underlying QTL should be of interest in the case of Potyvirus resistance. These genes provide good candidates for validation and the development of molecular markers for marker-assisted breeding. Alternatively, due to the polygenic nature of these traits, a genomic selection approach to breeding may be more appropriate.

Data availability statement

The original contributions presented in the study are included in the article/Supplementary Material. Further inquiries can be directed to the corresponding author.

Author contributions

MEF: Conceptualization, Data curation, Formal Analysis, Funding acquisition, Investigation, Methodology, Project administration, Supervision, Writing – original draft, Writing – review & editing. RPE: Data curation, Formal Analysis, Investigation, Methodology, Writing – review & editing. AL-O: Data curation, Formal Analysis, Investigation, Writing – review & editing. FK: Data curation, Formal Analysis, Investigation, Writing – review & editing. EM: Investigation, Writing – review & editing. TA: Investigation, Writing – review & editing. JB: Investigation, Writing – review & editing. DR: Conceptualization, Funding acquisition, Project administration, Supervision, Writing – review & editing. JL: Investigation, Writing – review & editing. TS: Formal Analysis, Writing – review & editing. SR: Conceptualization, Funding acquisition, Methodology, Writing – review & editing. GM: Conceptualization, Funding acquisition, Project administration, Writing – review & editing.

Funding

The author(s) declare financial support was received for the research, authorship, and/or publication of this article. This work was partially funded by the Bill and Melinda Gates Foundation under Project OPPGD1016, 'Biotechnology Applications to Combat Cassava Brown Streak Disease' and partially through the NEXTGEN Cassava project, through a grant to Cornell University by the Bill & Melinda Gates Foundation (Grant INV-007637 http://www.gatesfoundation.org) and the UK's Foreign, Commonwealth & Development Office (FCDO).

Conflict of interest

Author SR was employed by the company Dow AgroSciences.

The remaining authors declare that the research was conducted in the absence of any commercial or financial relationships that could be construed as a potential conflict of interest.

Publisher's note

Supplementary material

The Supplementary Material for this article can be found online at: https://www.frontiersin.org/articles/10.3389/fpls.2023.1270963/full#supplementary-material

References

Alazem, M., and Lin, N. (2015). Roles of plant hormones in the regulation of host–virus interactions. *Mol. Plant Pathol.* 16, 529–540. doi: 10.1111/mpp.12204

Alicai, T., Omongo, C. A., Maruthi, M. N., Hillocks, R. J., Baguma, Y., Kawuki, R., et al. (2007). Re-emergence of cassava brown streak disease in Uganda. *Plant Dis.* 91, 24–29. doi: 10.1094/PD-91-0024

Amuge, T., Berger, D. K., Katari, M. S., Myburg, A. A., Goldman, S. L., and Ferguson, M. E. (2017). A time series transcriptome analysis of cassava (*Manihot esculenta* Crantz) varieties challenged with Ugandan cassava brown streak virus. *Sci. Rep.* 7, 9747. doi: 10.1038/s41598-017-09617-z

Blair, M. W., Fregene, M. A., Beebe, S. E., and Ceballos, H. (2007). "Chapter 7 Marker-assisted selection in common beans and cassava," in *Marker-assisted selection: Current status and future perspectives in crops, livestock, forestry and fish*. Ed. E. P. Guimarães (Rome: FAO), 81–115.

Bredeson, J. V., Lyons, J. B., Prochnik, S. E., Wu, G. A., Ha, C. M., Edsinger-Gonzales, E., et al. (2016). Sequencing wild and cultivated cassava and related species reveals extensive interspecific hybridization and genetic diversity. *Nat. Biotechnol.* 34, 562–570. doi: 10.1038/nbt.3535

Casinga, C. M., Shirima, R. R., Mahungu, N. M., Tata-Hangy, W., Bashizi, K. B., Munyerenkana, C. M., et al. (2021). Expansion of the cassava brown streak disease epidemic in eastern Democratic Republic of Congo. *Plant Dis.* 105 (8), 2177–2188. doi: 10.1094/PDIS-05-20-1135-RE

Chen, F., Hu, Y., Vannozzi, A., Wu, K., Cai, H., Qin, Y., et al. (2017). The WRKY transcription factor family in model plants and crops. *Crit. Rev. Plant Sci.* 36, 311–335. doi: 10.1080/07352689.2018.1441103

Chen, J., and Ahlquist, P. (2000). Brome mosaic virus polymerase-like protein 2a is directed to the endoplasmic reticulum by helicase-like viral protein 1a. *J. Virol.* 1, 74 (9):4310–8. doi: 10.1128/jvi.74.9.4310-4318.2000

Collier, S. M., and Moffett, P. (2009). NB-LRRs work a "bait and switch". *pathogens. Trends Plant Sci.* 14, 521–529. doi: 10.1016/j.tplants.2009.08.001

Dellaporta, S. L., Wood, J., and Hicks, J. B. (1983). A plant DNA minipreparation: version II. *Plant Mol. Biol. Rep.* 1, 19–21. doi: 10.1007/BF02712670

Elshire, R. J., Glaubitz, J. C., Sun, Q., Poland, J. A., Kawamoto, K., Buckler, E. S., et al. (2011). A robust, simple genotyping-by-sequencing (GBS) approach for high diversity species. *PloS One* 6, e19379. doi: 10.1371/journal.pone.0019379

Expert Market Research. (2023). *Global cassava starch market price, size, report & Forecast 2023-2028*. Available at: https://www.expertmarketresearch.com/reports/cassava-starch-market (Accessed 25th April 2023).

FAOSTAT. (2023). Available at: https://www.fao.org/faostat/en/#data.

Ferguson, M. E., Shah, T., Kulakow, P., and Ceballos, H. (2019). A global overview of cassava genetic diversity. *PloS One* 14 (11), e0224763. doi: 10.1371/journal.pone.0224763

Freeborough, W., Gentle, N., and Rey, M. E. (2021). WRKY transcription factors in cassava contribute to regulation of tolerance and susceptibility to cassava mosaic disease through stress responses. *Viruses* 13, 1820. doi: 10.3390/v13091820

Garcia-Oliveira, A. L., Kimata, B., Kasele, S., Kapinga, F., Masumba, E., Mkamilo, G., et al. (2020). Genetic analysis and QTL mapping for multiple biotic stress resistance in cassava. *PloS One* 15 (8), p.e0236674. doi: 10.1371/journal.pone.0236674

Garcia-Ruiz, H., Takeda, A., Chapman, E. J., Sullivan, C. M., and Fahlgren, N. (2010). Arabidopsis RNA-dependent RNA polymerases and dicer-like proteins in antiviral defense and small interfering RNA biogenesis during Turnip Mosaic Virus infection. *Plant Cell* 22, 481–496. doi: 10.1105/tpc.109.073056

Graciano-Ribeiro, D., Hashimoto, D., Nogueira, L., Teodoro, D., Miranda, S., and Nassar, N. (2009). Internal phloem in an interspecific hybrid of Cassava, an indicator of breeding value for drought resistance. *Genet. Mol. Res.* 8, 1139–1146. doi: 10.4238/vol8-3gmr629

Green, K. M., Miller, S. L., Malik, I., and Todd, P. K. (2022). Non-canonical initiation factors modulate repeat-associated non-AUG translation. *Hum. Mol. Genet.* 31 (15), 2521–2534. doi: 10.1093/hmg/ddac021

Hillocks, R. J., and Jennings, D. L. (2003). Cassava brown streak disease: A review of present knowledge and research needs. *Int. J. Pest Manage.* 49, 225–234. doi: 10.1080/0967087031000101061

Hillocks, R. J., Raya, M. D., Mtunda, K., and Kiozia, H. (2001). Effects of cassava brown streak virus disease on yield and quality of cassava in Tanzania. *J. Phytopathol.* 149, 389–394. doi: 10.1111/j.1439-0434.2001.tb03868.x

Hillocks, J., Raya, M., and Thresh, J. M. (1996). The association between root necrosis and above-ground symptoms of brown streak virus infection of cassava in southern Tanzania. *Int. J. Pest Manage.* 42 (4), 285–289. doi: 10.1080/09670879609372008

Hillocks, R. J., and Thresh, J. M. (2000). Cassava mosaic and cassava brown streak virus diseases in Africa: a comparative guide to symptoms and aetiologies. *Roots* 7 (1), 1–8.

Hipper, C., Brault, V., Ziegler-Graff, V., and Revers, F. (2013). Viral and cellular factors involved in phloem transport of plant viruses. *Front. Plant Sci.* 4, 154. doi: 10.3389/fpls.2013.00154

International Cassava Genetic Map Consortium (2015). High-resolution linkage map and chromosome-scale genome assembly for cassava (*Manihot esculenta* Crantz) from 10 populations. *G3: Genes|Genomes|Genetics* 5, 133–144. doi: 10.1534/g3.114.015008

Jennings, D. L. (2003). "Historical perspective on breeding for resistance to cassava brown streak disease," in *Cassava brown streak virus disease: past, present and future*, 27–30.

Jiang, J., Ma, S., Ye, N., Jiang, M., Cao, J., and Zhang, J. (2017). WRKY transcription factors in plant responses to stresses. *J. Integr. Plant Biol.* 59, 86–101. doi: 10.1111/jipb.12513

Jing, Y., Zou, X., Sun, C., Qin, X., and Zheng, X. (2023). Danger-associate peptide regulates root immunity in Arabidopsis. *Biochem. Biophys. Res. Commun* 663, 163-170. doi: 10.1016/j.bbrc.2023.04.091

Kapinga, F. A. (2017). *Development of new tools for cassava brown streak disease resistance breeding* (Bloemfontein, South Africa: PhD Thesis. University of the Free State).

Kashif, M., Khan, M. I., Arif, M., Answer, M., and Ijaz, M. (2011). Efficiency of alpha lattice design in rice field trials in Pakistan. *J. Sci. Res.* 3 (1), 91. doi: 10.3329/jsr.v3i1.4773

Kawasaki, T., Koita, H., Nakatsubo, T., Hasegawa, K., Wakabayashi, K., Takahashi, H., et al. (2006). Cinnamoyl-CoA reductase, a key enzyme in lignin biosynthesis, is an effector of small GTPase Rac in defense signaling in rice. *Proc. Natl. Acad. Sci.* 103 (1), pp.230–pp.235. doi: 10.1073/pnas.0509875103

Kawuki, R. S., Herselman, L., Labuschagne, M. T., Nzuki, I., Ralimanana, I., Bidiaka, M., et al. (2013). Genetic diversity of cassava (*Manihot esculenta* Crantz) landraces and cultivars from southern, eastern and central Africa. *Plant Genet. Resour.* 11 (2), 170–181. doi: 10.1017/S1479262113000014

Kayondo, S. I., Pino Del Carpio, D., Lozano, R., Ozimati, A., Wolfe, M., Baguma, Y., et al. (2018). Genome-wide association mapping and genomic prediction for CBSD resistance in *Manihot esculenta*. *Sci. Rep.* 8 (1), 1549. doi: 10.1038/s41598-018-19696-1

Kim, H., Aponte-Diaz, D., Sotoudegan, M. S., Shengjuler, D., Arnold, J. J., and Cameron, C. E. (2023). The enterovirus genome can be translated in an IRES-independent manner that requires the initiation factors eIF2A/eIF2D. *PloS Biol.* 21 (1), e3001693. doi: 10.1371/journal.pbio.3001693

Kneller, E. L. P., Rakotondrafara, A. M., and Miller, W. A. (2006). 'Cap-independent translation of plant viral RNAs'. *Virus Res.* 119 (1), 63–75. doi: 10.1016/j.virusres.2005.10.010

Kofalvi, S. A., and Nassuth, A. (1995). Influence of wheat streak mosaic virus infection on phenylpropanoid metabolism and the accumulation of phenolics and lignin in wheat. *Physiol. Mol. Plant Pathol.* 47 (6), 365–377. doi: 10.1006/pmpp.1995.1065

Kørner, C. J., Klauser, D., Niehl, A., Domínguez-Ferreras, A., Chinchilla, D., Boller, T., et al. (2013). The immunity regulator BAK1 contributes to resistance against diverse RNA viruses. *Mol. Plant-Microbe Interact.* 26, 1271–1280. doi: 10.1094/MPMI-06-13-0179-R

Lee, M. W., Jelenska, J., and Greenberg, J. T. (2008). Arabidopsis proteins important for modulating defense responses to *Pseudomonas syringae* that secrete HopW1-1. *Plant J.* 54 (3), pp.452–pp.465. doi: 10.1111/j.1365-313X.2008.03439.x

Legg, J., Somado, E. A., Barker, I., Beach, L., Ceballos, H., Cuellar, W., et al. (2014). A global alliance declaring war on cassava viruses in Africa. *Food Security.* 6 (2), 231–248. doi: 10.1007/s12571-014-0340-x

Li, X., Liu, N., Sun, Y., Wang, P., Ge, X., Pei, Y., et al. (2019). The cotton GhWIN2 gene activates the cuticle biosynthesis pathway and influences the salicylic and jasmonic acid biosynthesis pathways. *BMC Plant Biol.* 19 (1), 1–13. doi: 10.1186/s12870-019-1888-6

Li, Y., Qin, L., Zhao, J., Muhammad, T., Cao, H., Li, H., et al. (2017). SlMAPK3 enhances tolerance to tomato yellow leaf curl virus (TYLCV) by regulating salicylic acid and jasmonic acid signaling in tomato (*Solanum lycopersicum*). *PloS One* 12 (2), e0172466. doi: 10.1371/journal.pone.0172466

Ling, K.-S., Harris, K. R., Meyer, J. D., Levi, A., Guner, N., Wehner, T. C., et al. (2009). Non-synonymous single nucleotide polymorphisms in the watermelon eIF4E gene are closely associated with resistance to Zucchini yellow mosaic virus. *Theor. Appl. Genet.* 120, 191–200. doi: 10.1007/s00122-009-1169-0

Liu, D., Wu, J., Lin, L., Li, P., Li, S., Wang, Y., et al. (2021). Overexpression of Cinnamoyl-CoA Reductase 2 in *Brassica napus* increases resistance to *Sclerotinia sclerotiorum* by affecting lignin biosynthesis. *Front. Plant Sci.* 12, 732733. doi: 10.3389/fpls.2021.732733

Lozano, R., Hamblin, M. T., Prochnik, S., and Jannink, J. L. (2015). Identification and distribution of the NBS-LRR gene family in the Cassava genome. *BMC Genomics* 16 (1), 1–4. doi: 10.1186/s12864-015-1554-9

Maruthi, M. N., Bouvaine, S., Tufan, H. A., Mohammed, I. U., and Hillocks, R. J. (2014). Transcriptional response of virus-infected cassava and identification of putative sources of resistance for cassava brown streak disease. *PloS One* 9, e96642. doi: 10.1371/journal.pone.0096642

Maruthi, M. N., Hillocks, R. J., Mtunda, K., Raya, M. D., Muhanna, M., Kiozia, H., et al. (2005). Transmission of Cassava brown streak virus by *Bemisia tabaci* (Gennadius). *J. Phytopathol.* 153, 307–312. doi: 10.1111/j.1439-0434.2005.00974.x

Masumba, E. A., Kapinga, F., Mkamilo, G., Salum, K., Kulembeka, H., Rounsley, S., et al. (2017). QTL associated with resistance to cassava brown streak and cassava

mosaic diseases in a bi-parental cross of two Tanzanian farmer-varieties, Namikonga and Albert. *Theor. Appl. Genet.* 130 (10), 2069–2090. doi: 10.1007/s00122-017-2943-z

Mba, R. E. C., Stephenson, P., Edwards, K., Melzer, S., Nkumbira, J., Gullberg, U., et al. (2001). Simple sequence repeat (SSR) markers survey of the cassava (*Manihot esculenta* Crantz) genome: towards an SSR-based molecular genetic map of cassava. *Theor. Appl. Genet.* 102, 21–31. doi: 10.1007/s001220051614

Mbanjo, E. G., Rabbi, I. Y., Ferguson, M. E., Kayondo, S. I., Eng, N. H., and Tripathi, L. (2021). Technological innovations for improving cassava production in sub-Saharan Africa. *Front. Genet.* 11, 1829. doi: 10.3389/fgene.2020.623736

Mbanzibwa, D. R., Tian, Y. P., Tugume, A. K., Patil, B. L., Yadav, J. S., Bagewadi, B., et al. (2011). Evolution of cassava brown streak disease-associated viruses. *J. Gen. Virol.* 92, 974–987. doi: 10.1099/vir.0.026922-0

McHale, L., Tan, X., Koehl, P., and Michelmore, R. W. (2006). Plant NBS-LRR proteins: adaptable guards. *Genome Biol.* 7, 212. doi: 10.1186/gb-2006-7-4-212

Moeder, W., Yoshioka, K., and Klessig, D. F. (2005). Involvement of the small GTPase Rac in the defense responses of tobacco to pathogens. *Mol. Plant-Microbe Interact.* 18 (2), 116–124. doi: 10.1094/MPMI-18-0116

Nassar, N. M. A., Abreu, L. F. A., Teodoro, D. A. P., and Graciano-Ribeiro, D. (2010). Drought tolerant stem anatomy characteristics in *Manihot esculenta* (Euphorbiaceae) and a wild relative. *Genet. Mol. Res.* 9, 1023–1031. doi: 10.4238/vol9-2gmr800

Nichols, R. F. J. (1950). The brown streak disease of cassava: distribution, climatic effects and diagnostic symptoms. *East Afr. Agric. J.* 15, 154–160. doi: 10.1080/03670074.1950.11664727

Noueiry, A. O., Diez, J., Falk, S. P., Chen, J., and Ahlquist, P. (2003). Yeast Lsm1p-7p/Pat1p deadenylation-dependent mRNA-decapping factors are required for brome mosaic virus genomic RNA translation. *Mol. Cell. Biol.* 23 (12), 4094–4106. doi: 10.1128/MCB.23.12.4094-4106.2003

Nzuki, I., Katari, M. S., Bredeson, J. V., Masumba, E., Kapinga, F., Salum, K., et al. (2017). QTL mapping for pest and disease resistance in cassava and coincidence of some QTL with introgression regions derived from *Manihot glaziovii*. *Front. Plant Sci.* 8, 1168. doi: 10.3389/fpls.2017.01168

Okogbenin, E., Egesi, C. N., Olasanmi, B., Ogundapo, O., Kahya, S., Hurtado, P., et al. (2012). Molecular marker analysis and validation of resistance to cassava mosaic disease in elite cassava genotypes in Nigeria. *Crop Sci.* 52, 2576–2586. doi: 10.2135/cropsci2011.11.0586

Pandey, S. P., Roccaro, M., Schön, M., Logemann, E., and Somssich, I. E. (2010). Transcriptional reprogramming regulated by WRKY18 and WRKY40 facilitates powdery mildew infection of Arabidopsis. *Plant J.* 64, 912–923. doi: 10.1111/j.1365-313X.2010.04387.x

Powell, P., Bhardwaj, U., and Goss, D. (2022). Eukaryotic initiation factor 4F promotes a reorientation of eukaryotic initiation factor 3 binding on the 5′ and the 3′ UTRs of barley yellow dwarf virus mRNA. *Nucleic Acids Res.* 50 (9), 4988–4999. doi: 10.1093/nar/gkac284

Rajamäki, M.-L., and Valkonen, J. P. (2009). Control of nuclear and nucleolar localization of nuclear inclusion protein a of picorna-like potato virus A in *Nicotiana species*. *Plant Cell* 21, 2485–2502. doi: 10.1105/tpc.108.064147

Ravi, V., Aked, J., and Balagopalan, C. (1996). Review on tropical root and tuber crops I. Storage methods and quality changes. *Crit. Rev. Food Sci. Nutr.* 36, 661–709. doi: 10.1080/10408399609527744

Rodríguez-Hernández, A. M., Gosalvez, B., Sempere, R. N., Burgos, L., Aranda, M. A., Truniger, V., et al. (2012). Melon RNA interference (RNAi) lines silenced for Cm-eIF4E show broad virus resistance. *Mol. Plant Pathol.* 13, 755–763. doi: 10.1111/j.1364-3703.2012.00785.x

Sade, D., Shriki, O., Cuadros-Inostroza, A., Tohge, T., Semel, Y., Haviv, Y., et al. (2015). Comparative metabolomics and transcriptomics of plant response to Tomato yellow leaf curl virus infection in resistant and susceptible tomato cultivars. *Metabolomics* 11, 81–97. doi: 10.1007/s11306-014-0670-x

Schwartz, M., Chen, J., Janda, M., Sullivan, M., den Boon, J., and Ahlquist, P. (2002). A positive-strand RNA virus replication complex parallels form and function of retrovirus capsids. *Mol. Cell* 9 (3), 505–514. doi: 10.1016/S1097-2765(02)00474-4

Sela, D., Buxdorf, K., Shi, J. X., Feldmesser, E., Schreiber, L., Aharoni, A., et al. (2013). Overexpression of AtSHN1/WIN1 provokes unique defense responses. *PloS One* 8 (7), e70146. doi: 10.1371/journal.pone.0070146

Shang, J., Xi, D. H., Xu, F., Wang, S. D., Cao, S., Xu, M. Y., et al. (2011). A broad-spectrum, efficient and nontransgenic approach to control plant viruses by application of salicylic acid and jasmonic acid. *Planta* 233, 299–308. doi: 10.1007/s00425-010-1308-5

Shapiro, S. S., and Wilk, M. B. (1965). An analysis of variance test for normality (complete samples). *Biometrika* 52 (3/4), 591–611. doi: 10.1093/biomet/52.3-4.591

Sheat, S., Fuerholzner, B., Stein, B., and Winter, S. (2019). Resistance against cassava brown streak viruses from Africa in cassava germplasm from South America. *Front. Plant Science.* 10, 567. doi: 10.3389/fpls.2019.00567

Sheat, S., Margaria, P., and Winter, S. (2021). Differential tropism in roots and shoots of resistant and susceptible cassava (*Manihot esculenta* Crantz) infected by Cassava brown streak viruses. *Cells* 10 (5), 1221. doi: 10.3390/cells10051221

Sheat, S., Winter, S., and Margaria, P. (2020). Duplex in situ hybridization of virus nucleic acids in plant tissues using RNAscope®. *Methods Mol. Biol.* 2148, 203–215. doi: 10.1007/978-1-0716-0623-0_13

Shi, S., Zhang, X., Mandel, M. A., Zhang, P., Zhang, Y., Ferguson, M., et al. (2017). Variations of five eIF4E genes across cassava accessions exhibiting tolerant and susceptible responses to cassava brown streak disease. *PloS One* 12 (8), e0181998. doi: 10.1371/journal.pone.0181998

Shirima, R. R., Maeda, D. G., Kanju, E. E., Tumwegamire, S., Ceasar, G., Mushi, E., et al. (2019). Assessing the degeneration of cassava under high-virus inoculum conditions in coastal Tanzania. *Plant Disease.* 103 (10), 2652–2664. doi: 10.1094/PDIS-05-18-0750-RE

Somo, M., Kulembeka, H., Mtunda, K., Mrema, E., Salum, K., Wolfe, M. D., et al. (2020). Genomic prediction and quantitative trait locus discovery in a cassava training population constructed from multiple breeding stages. *Crop Sci.* 60 (2), 896–913. doi: 10.1002/csc2.20003

Spearman, P. (2018). Viral interactions with host cell Rab GTPases. *Small GTPases* 9, 192–201. doi: 10.1080/21541248.2017.1346552

Stone, M., Jia, S., Heo, W. D., Meyer, T., and Konan, K. V. (2007). Participation of rab5, an early endosome protein, in hepatitis C virus RNA replication machinery. *J. Virology.* 81 (9), 4551–4563. doi: 10.1128/JVI.01366-06

Storey, H. H. (1936). Virus diseases on East African plants. VI. A progress report on the studies of the diseases of cassava. *East Afr. Agric. J.* 2, 34–39.

Thresh, J. M. (2003). "Brief history of cassava brown streak virus disease," in *Cassava brown streak virus disease: past present and future. Proceedings of an international workshop, mombasa, Kenya, 27-30 october 2002*. Eds. J. P. Legg. and R. J. Hillocks (Aylesford, UK: Natural Resources International Limited), 100pp.

Ullah, I., Chen, Z., Xiea, Y., Khan, S. S., Singh, S., Yu, C., et al. (2022). Recent advances in biological activities of lignin and emerging biomedical applications: a short review. *Int. J. Biol. Macromolecules* 208, 819-832. doi: 10.1016/j.ijbiomac.2022.03.182

Utsumi, Y., Tanaka, M., Kurotani, A., Yoshida, T., Mochida, K., Matsui, A., et al. (2016). Cassava (Manihot esculenta) transcriptome analysis in response to infection by the fungus Colletotrichum gloeosporioides using an oligonucleotide-DNA microarray. *Journal of plant research* 129, pp.711-726. doi: 10.1016/j.ijbiomac.2022.03.182

van Ooijen, J. W. (2006). *JoinMap 4: software for the calculation of genetic linkage maps in experimental populations*. (Netherlands: Kyazma B. V. Wageningen).

van Ooijen, J. W. (2009). *MapQTL ® 6: Software for the mapping of quantitative trait loci in experimental populations of diploid*. Ed. B. V. Kyazma (Netherlands: Kyazma B. V. Wageningen), 1–60.

Vuorinen, A. L., Kelloniemi, J., and Valkonen, J. P. (2011). Why do viruses need phloem for systemic invasion of plants? *Plant Sci.* 181, 355–363. doi: 10.1016/j.plantsci.2011.06.008

Wadenbäck, J., von Arnold, S., Egertsdotter, U., Walter, M. H., Grima-Pettenati, J., Goffner, D., et al. (2008). Lignin biosynthesis in transgenic Norway spruce plants harboring an antisense construct for cinnamoyl CoA reductase (CCR). *Transgenic Res.* 17, 379–392. doi: 10.1007/s11248-007-9113-z

Wang, R., Xie, M., Zhao, W., Yan, P., Wang, Y., Gu, Y., et al. (2023). WGCNA reveals genes associated with lignification in the secondary stages of wood formation. *Forests* 14 (1), 99. doi: 10.3390/f14010099

Wang, N., Zhao, P., Ma, Y., Yao, X., Sun, Y., Huang, X., et al. (2019). A whitefly effector Bsp9 targets host immunity regulator WRKY33 to promote performance. *Philos. Trans. R. Soc. B* 374, 20180313. doi: 10.1098/rstb.2018.0313

Winter, S., Koerbler, M., Stein, B., Pietruszka, A., Paape, M., and Butgereitt, A. (2010). Analysis of cassava brown streak viruses reveals the presence of distinct virus species causing cassava brown streak disease in East Africa. *J. Gen. Virol.* 91, 1365–1372. doi: 10.1099/vir.0.014688-0

Wu, J., Li, L.-T., Li, M., Khan, M. A., Li, X.-G., Chen, H., et al. (2014). High-density genetic linkage map construction and identification of fruit-related QTLs in pear using SNP and SSR markers. *J. Exp. Bot.* 65 (20), 5771–5781. doi: 10.1093/jxb/eru311

Xu, L., Zhu, L., Tu, L., Liu, L., Yuan, D., Jin, L., et al. (2011). Lignin metabolism has a central role in the resistance of cotton to the wilt fungus Verticillium dahliae as revealed by RNA-Seq-dependent transcriptional analysis and histochemistry. *J. Exp. Bot.* 62 (15), 5607–5621. doi: 10.1093/jxb/err245

Yadav, V., Wang, Z., Wei, C., Amo, A., Ahmed, B., Yang, X., et al. (2020). Phenylpropanoid pathway engineering: An emerging approach towards plant defense. *Pathogens* 9 (4), 312. doi: 10.3390/pathogens9040312

Yang, H., Gou, X., He, K., Xi, D., Du, J., Lin, H., et al. (2010). BAK1 and BKK1 in Arabidopsis thaliana confer reduced susceptibility to turnip crinkle virus. *Eur. J. Plant Pathol.* 127, 149–156. doi: 10.1007/s10658-010-9581-5

Yu, Y., Zhang, J., Shi, Y., Song, Y., Wang, T., and Li, Y. (2006). QTL analysis for plant height and leaf angle by using different populations of maize. *J. Maize Sci.* 14, 88–92.

Zhang, J., Roberts, R., and Rakotondrafara, A. M. (2015). The role of the 5′ untranslated regions of Potyviridae in translation. *Virus Res.* 206, 74–81. doi: 10.1016/j.virusres.2015.02.005

Zhang, H., Ye, Z., Liu, Z., Sun, Y., Li, X., Wu, J., et al. (2022). The cassava NBS-LRR genes confer resistance to cassava bacterial blight. *Front. Plant Sci.* 13. doi: 10.3389/fpls.2022.790140

Zhao, P., Liu, Q., Miller, W.A., and Goss, D.J. (2017). 'Eukaryotic translation initiation factor 4G (eIF4G) coordinates interactions with eIF4A, eIF4B, and eIF4E in binding and translation of the barley yellow dwarf virus 3′ cap-independent translation element (BTE)'. *J. Biol. Chem.* 292 (14), 5921–5931. doi: 10.1074/jbc.M116.764902

Zheng, Z., Mosher, S. L., Fan, B., Klessig, D. F., and Chen, Z. (2007). Functional analysis of Arabidopsis WRKY25 transcription factor in plant defense against *Pseudomonas syringae*. *BMC Plant Biol.* 7 (1), 1–3. doi: 10.1186/1471-2229-7-2

frontiers | Frontiers in Plant Science

TYPE Original Research
PUBLISHED 22 April 2024
DOI 10.3389/fpls.2024.1355941

OPEN ACCESS

EDITED BY
Chellappan Padmanabhan,
USDA APHIS PPQ Science and Technology,
United States

REVIEWED BY
Nagaraju Yalavarthi,
Central Silk Board, India
Jonathan Shao,
United States Department of Agriculture,
United States

*CORRESPONDENCE
Eman Abdullah Aldakheel
eaaldakheel@pnu.edu.sa

RECEIVED 14 December 2023
ACCEPTED 27 March 2024
PUBLISHED 22 April 2024

CITATION
Aldakheel EA, Zakariah M and Alabdalall AH (2024) Detection and identification of plant leaf diseases using YOLOv4.
Front. Plant Sci. 15:1355941.
doi: 10.3389/fpls.2024.1355941

Detection and identification of plant leaf diseases using YOLOv4

Eman Abdullah Aldakheel[1]*, Mohammed Zakariah[2] and Amira H. Alabdalall[3]

[1]Department of Computer Sciences, College of Computer and Information Sciences, Princess Nourah bint Abdulrahman University, Riyadh, Saudi Arabia, [2]Department of Computer Science, College of Computer and Information Science, King Saud University, Riyadh, Saudi Arabia, [3]Department of Biology, College of Science, Imam Abdulrahman Bin Faisal University, Dammam, Saudi Arabia

Detecting plant leaf diseases accurately and promptly is essential for reducing economic consequences and maximizing crop yield. However, farmers' dependence on conventional manual techniques presents a difficulty in accurately pinpointing particular diseases. This research investigates the utilization of the YOLOv4 algorithm for detecting and identifying plant leaf diseases. This study uses the comprehensive Plant Village Dataset, which includes over fifty thousand photos of healthy and diseased plant leaves from fourteen different species, to develop advanced disease prediction systems in agriculture. Data augmentation techniques including histogram equalization and horizontal flip were used to improve the dataset and strengthen the model's resilience. A comprehensive assessment of the YOLOv4 algorithm was conducted, which involved comparing its performance with established target identification methods including Densenet, Alexanet, and neural networks. When YOLOv4 was used on the Plant Village dataset, it achieved an impressive accuracy of 99.99%. The evaluation criteria, including accuracy, precision, recall, and f1-score, consistently showed high performance with a value of 0.99, confirming the effectiveness of the proposed methodology. This study's results demonstrate substantial advancements in plant disease detection and underscore the capabilities of YOLOv4 as a sophisticated tool for accurate disease prediction. These developments have significant significance for everyone involved in agriculture, researchers, and farmers, providing improved capacities for disease control and crop protection.

KEYWORDS

plant leaf disease, leaf disease detection, object detection, deep-learning, YOLO v4, darknet

Abbreviations: PLF, Plant Leaf Disease; SVM, Support Vector Machine; CNN, Convolution Neural Network; RPN, Region Proposal Networks; DL, Deep Learning; SSCNN, Self-Structured CNN; SPP, Spatial Pyramid Pooling; RS, Remote Sensing; ANN, Artificial Neural Network; ML, Machine Learning; RCNN, Region Convolution Neural Network; YOLO, You Only Look Once; PDDNN, Plant Disease Detection Neural Network; KNN, K-Nearest Neighbour; DNN, Deep Neural Network.

1 Introduction

Plant diseases present a crucial obstacle to the growth of agriculture in every country, resulting in significant yearly financial losses (Mitra, 2021). Plant disease detection has developed into a substantial area of study in pattern recognition and contemporary agricultural development due to developments in machine learning technology (Roy and Bhaduri, 2021; Albattah et al., 2022; Sanida et al., 2023). Early plant disease identification approaches used a support vector machine (SVM) (Rahman et al., 2023; Thangavel et al., 2023), artificial neural network (ANN) (Attallah, 2023), and SVM method for disease diagnosis under segmented plant disease spots. These techniques are used to manually isolate the affected area of an image, after which the K-means clustering method is implemented (Javidan et al., 2023).

With the advancement of AI technology, agricultural detection based on AI is now widely utilized for tasks including predicting crop production, processing weed identification, and finding plant diseases (Albattah et al., 2022). Moreover, the process of machine learning-based disease detection involves several steps. Firstly, the dataset undergoes preprocessing to ensure its suitability for analysis. Following this, feature extraction algorithms are employed to identify and extract relevant features from regions of interest in the images, specifically focusing on disease-affected areas of plant leaves. Subsequently, the extracted feature information is transmitted to the classifier, where model parameters are derived. Finally, the system accepts the identified categories of diseases, along with their respective severity levels, integrating this crucial information into the output for further analysis or action. Moreover, leveraging image recognition through machine learning methodologies holds significant promise for enhancing the generalization ability of models. Specifically, in the domain of detecting and identifying plant leaf diseases using YOLOv4, the term "model generalization ability" pertains to the model's proficiency in accurately identifying and categorizing diseases in plant leaves across a broad spectrum of scenarios, including instances not encountered during training. This capability enables the model to effectively discern subtle patterns and characteristics indicative of various leaf diseases, thereby contributing to more reliable and robust disease detection systems (Singh et al., 2017). When there are fewer classes, it is easier to distinguish between their characteristics. Moreover, the categories can only be identified within minimal visual settings. Researching a fast, end-to-end plant disease detection system is vital since it will be necessary to meet the demands of large-scale planting.

Further, early identification and management of plant diseases is an essential part of crop harvesting, since it helps to minimize development problems and lowers the need for pesticides. As a result, the environmental damage brought on by pesticide use is reduced, supporting sustainable agricultural practices (Perveen et al., 2023). Many ML techniques have been used for plant and disease categorization and detection.Where such approaches, however, perform less well and more slowly when detecting diseases in real time (Peng and Wang, 2022), likely due to the problematic image preprocessing and feature extraction stages. The fact that classic ML methods are unsuitable for real-world detection scenarios with complex backgrounds and non-uniform surfaces is another major disadvantage of these methods. With several applications, deep learning has lately achieved a substantial breakthrough in this area of computer vision (Wang et al., 2021).

Additionally, it has been used for picture segmentation, crop recognition, and automated agriculture technology, including the classification of crops and fruits (Dhinesh et al., 2019). Models based on convolutional neural networks (CNNs) have gained popularity due to their improved accuracy in object detection (Sangeetha et al., 2022). CNNs can save time on preprocessing because they automatically extract features from the input images. The ability to identify crop diseases has made great strides in recent years (Dhinesh et al., 2019; Sangeetha et al., 2022). There are now two distinct kinds of CNN-based object detectors: those with a single detection stage and those with two. One of the most popular two-stage detectors is the region convolution neural network (RCNN), which consists of the fast/faster RCNN and the mask-RCNN (Sangeetha et al., 2022). These models have had significant effects on automated agriculture management (Chen et al., 2022), crop and fruit detection (Eunice et al., 2022), and yield and growth assessment (Hassan et al., 2021). Although these models cannot recognize high-resolution images in real-time, faster R-CNN, consisting of region proposal networks (RPN) (Chen and Wu, 2023) and classification networks, considerably decrease detection time. By combining target categorization and localization into a regression problem, the recently suggested You Only Look Once (YOLO) (Soeb et al., 2023) method simplifies the problem. Due to its lack of RPN, YOLO employs regression to directly locate targets in the image, significantly improving its detection speed. High precision, accuracy, and detection speed are hallmarks of modern object detection technologies like YOLOv4 (Xinming and Tang, 2023), which can perform several real-time object recognition applications.

This work (Chuanlei et al., 2017) concentrates on rust and scab detection in apple leaves, which are susceptible to two dangerous and prevalent fungal infections. Real-time early disease identification of apple leaves is challenging due to factors such as the fine-grained multi-scale distribution, the similarity of colour texture between illnesses and background, the diversity of diseases' morphology, and the occurrence of many diseases on the same leaf. A significant gap exists between the current model and real-time illness diagnosis on mobile computing devices since existing disease detection algorithms pay off accuracy for real-time detection speed (Arathi and Dulhare, 2023).

Plant leaves have many different features, such as differences in size, shape, color, and growth conditions, but effectively identifying and categorizing diseases is still quite difficult. Brightness fluctuations that occur during the process of capturing leaf image aggravate this issue and challenge detection strategies. This paper presents a novel approach that leverages the YOLOv4 architecture to achieve remarkable accuracy on the Plant Village dataset. It is shown that the used methodology is robust against a range of input sample distortions, including noise, blurring, rotation, contrast changes, lighting adjustments, color inconsistencies, and brightness swings. The outcomes highlight how well the recommended approach works to improve plant leaf disease identification and detection.

To create a framework for plant disease detection and classification, the following processes must be completed: data collection, model training, and multiple-class categorization of plant leaf disease. Figure 1 provides an overview of the proposed framework. Leaf disease items can be found and identified with the Yolov4 method.

The following are the primary contributions of this research paper:

- This study applies YOLOv4, a cutting-edge object detection framework, to plant pathology. The work improves plant leaf disease identification accuracy and efficiency by seamlessly incorporating YOLOv4, providing a fresh method to address agricultural concerns.
- The study achieves high precision in recognizing and classifying various plant leaf diseases through thorough image annotation and data preprocessing. The suggested methodology's robustness provides accurate disease diagnosis, assisting farmers and researchers in timely intervention and crop management.
- The study uses the widely accepted Plant Village dataset, which helps validate and benchmark the proposed model. This dataset selection improves the generalizability of the findings, allowing for more excellent applications in plant pathology research.
- The research provides valuable insights into the practical implementation of the YOLOv4 architecture for detecting plant leaf disease. The precise methodology can help researchers and practitioners implement and adapt this technology in real-world agricultural contexts.

The fundamental structure of this paper is as follows: An overview of the topic is given in the first part. The literature on diagnosing leaf diseases is reviewed in the section 2. The dataset structure and the evaluation criteria for the experiments are presented in the 3 section. The methodology portion is covered in section 4, and a comparison of the findings is covered in section 5. The discussion portion is covered under Section 6. Finally, a summary concludes in section 7, where the paper is closed up.

2 Literature review

In the context of precision agriculture, there is a strong need for sophisticated techniques that improve detection efficiency because plant diseases pose significant risks to crop health and the field (Attallah, 2023; Rahman et al., 2023; Thangavel et al., 2023). In computer vision for plant disease identification, deep learning—specifically, the YOLOv4 architecture—has proven to be a potent tool. Deep learning holds great potential to overcome obstacles associated with various illness kinds and environmental variables (Javidan et al., 2023). Previous research has demonstrated the drawbacks of standard approaches. The release of YOLOv4 improves object identification speed and accuracy, which makes it an excellent option for applications in plant pathology (Singh et al., 2017). An in-depth analysis of the current research environment is provided by this literature review, which sets the stage for a later investigation into the use of YOLOv4 in identifying and detecting plant leaf diseases (Perveen et al., 2023).

By addressing the fundamental restrictions that are present in the approaches that are currently in use, Peng et al (Peng and Wang, 2022). have made great achievements in the advancement of plant disease identification. Predefined recognition categories and the significant demand for image annotation are two examples of these restrictions that are particularly difficult to overcome. The authors have methodically separated the PlantVillage dataset into two sub-datasets, which they have referred to as PlantVillage-A and PlantVillage-B. This allowed them to use the PlantVillage dataset as a solid foundation for training and evaluation. Remarkable accuracy rates of 98% for YOLOv5 and 97.84% for ResNet were achieved by their proposed strategy, which indicates a significant change from the standard approaches that have been historically utilized. Not only does this achievement serve as a testimonial to the effectiveness of the

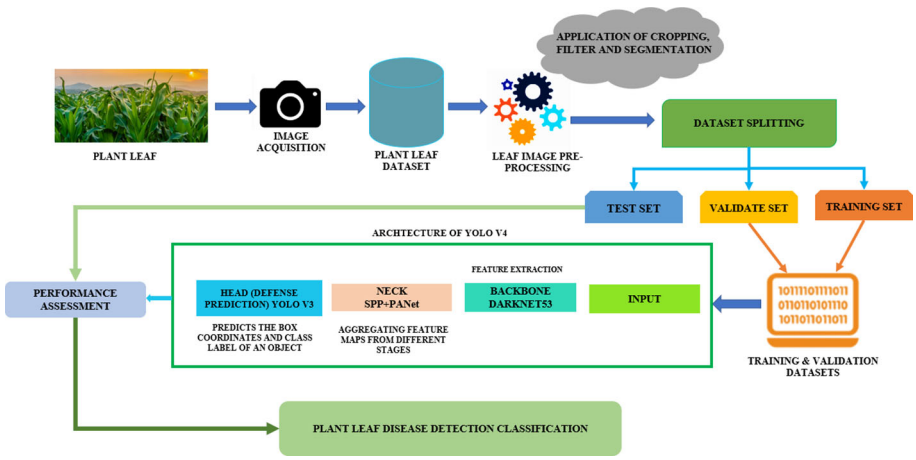

FIGURE 1
Implementing the Yolov4 disease detection and identification framework in plant leaves.

technique in minimizing the inadequacies of previous methodologies, but it also serves to enhance the precision and adaptability of leaf disease identification. A full re-evaluation of recognition categories and an improved method to picture annotation are both components of the strategy that has been presented.

Further, Chen et al. (2022) introduced an improved model based on the YOLOv5 network to precisely identify diseases in the difficult conditions of various natural habitats, significantly contributing to plant disease recognition and using the PlantVillage dataset—especially the rubber tree disease database with 2375 images—the suggested model targets anthracnose and powdery mildew. The model achieves an impressive 86.5% accuracy rate, highlighting its usefulness in improving methods for identifying plant diseases.

Moreover, Eunice et al. (2022) address the critical imperative of early plant disease diagnosis for optimizing food production and reducing economic losses. Leveraging the advancements in deep learning, the study introduces a robust leaf disease detection model for agricultural applications. The focus lies on utilizing CNN-based pre-trained models, specifically DenseNet-121 and VGG-16, with meticulous hyperparameter fine-tuning. The PlantVillage dataset, comprising 54,305 samples, serves as the comprehensive foundation partitioned for training, validation, and testing. Impressively, the proposed model achieves an exceptional accuracy of 99.81%, underscoring its effectiveness in enhancing plant disease identification accuracy and its potential for substantial impact on agricultural practices and crop management strategies (Hassan et al., 2021; Chen and Wu, 2023; Soeb et al., 2023; Xinming and Tang, 2023).

Likewise, Chuanlei et al. (2017) contributed to the critical domain of apple leaf disease identification within computer vision, addressing the challenge of adequate representation of diseased leaf images. Leveraging the PlantVillage dataset, comprising ninety images, the study employs a methodology centred on a Support Vector Machine (SVM) classifier. Impressively, the proposed model achieves an accuracy surpassing 95% on the PlantVillage dataset, showcasing the efficacy of the developed apple leaf disease recognition method (Arathi and Dulhare, 2023; Bin Naeem et al., 2023; Xu et al., 2023). This work holds substantial promise for advancing computer vision applications in precision agriculture and plant health monitoring (Vengaiah and Konda, 2023; Terentev et al., 2023; Liu et al., 2023).

Further, Kaur et al. (2022) contributed significantly to the imperative task of plant disease identification for sustainable agriculture. Acknowledging the challenges of manual monitoring, the research focuses on grapevines, targeting four prevalent diseases: Leaf blight, Black rot, stable, and Black measles (Taheri-Garavand et al., 2021; Sharma et al., 2023). With the overarching need for automated disease characterization in agriculture, the study utilizes the PlantVillage dataset, emphasizing grapevine health with 2115 images. The proposed Hybrid Convolutional Neural Network emerges as a robust solution, achieving a remarkable accuracy of 98.7%. This work stands at the forefront of precision agriculture, offering a comprehensive approach to automatic and accurate leaf disease recognition in grape plants (Mustafa et al., 2020).

Moreover, Jasim et al (Jasim and Al-Tuwaijari, 2020). contributed to precision agriculture with their research using Image Processing and Deep Learning Techniques. The study leverages the comprehensive Plant Village dataset comprising 20,636 images to address the critical task of detecting and classifying plant leaf diseases. Further, it Employs deep-learning techniques, particularly Convolutional Neural Networks (CNN), where the research advances the state-of-the-art in disease identification (Liu and Wang, 2021). Using CNN allowed for the classification of 15 distinct classes, encompassing various diseases such as bacteria and fungi, along with a category for healthy leaves. The proposed model attained an accuracy of 90.029%, underscoring its efficacy in the automated detection and classification of plant leaf diseases, thereby contributing significantly to advancing precision agriculture methodologies.

To sum up, this study has advanced plant pathology significantly. The study effectively solves the crucial need for precise and effective plant leaf disease detection and classification using the YOLOv4 architecture. The research shows that picture annotation, data preparation, and model training, that is used to diagnose various diseases through creative integration and rigorous methods reliably. High precision is achieved with the help of the YOLOv4 model, demonstrating the model's potential for practical application in agriculture. This approach facilitates prompt interventions and sustainable crop management practices, contributing to the evolving field of precision agriculture.

Table 1 contains a list of previous references along with plant types, techniques, limitations and outcomes.

The review concludes by highlighting the development of plant disease identification approaches and highlighting the usefulness and accessibility of YOLOv4 in addressing the drawbacks of conventional methods. Molecular techniques, hyperspectral imaging, and traditional computer vision have all been necessary. However, YOLOv4 presents a viable path toward precise and effective illness detection. Its versatility and intuitive interface offer prospects for broad implementation in farming environments. With the advancement of technology, crop health monitoring can be improved by incorporating YOLOv4 into plant disease control strategies, which will increase agricultural output and sustainability.

3 Data collection

Over 50,000 images of healthy and diseased plant leaves from 14 distinct plant species are included in the publicly accessible image resource called "Plant Village." The dataset was produced to help develop computer vision algorithms for plant disease identification on an automated basis.

Each image in the dataset is annotated with the corresponding plant species and whether a disease is present. The pictures in the collection were taken using a smartphone camera, and they come in various lighting, backgrounds, and orientations.

The Plant Village dataset, compiled by scholars at Pennsylvania State University, is accessible for download on the official website. Utilized in a number of programs and studies to identify plant diseases, the dataset has contributed to the advancement of research in this field.

TABLE 1 List of past references with datasets, methodology, and results.

References	Datasets	Methodology	Limitations	Results
(Peng and Wang, 2022)	- The Plant Village dataset is used. - It consists of around thirty-eight thousand and thirty-five images for Plant Village-A dataset and sixteen thousand two-hundred and seventy images for Plant Village-B.	YOLO V5, ResNet-50	The research paper's limitation is its potential for generalizability, as the performance of the proposed picture retrieval system may vary across different datasets and environments.	The resNet model has an accuracy of 97.84% for the Plant Village dataset.
(Wang et al., 2021)	PlantVillage dataset consists of images of 14 plants with around 3000 images.	Squeeze-and-excitation SSD (Se_SSD), deep block SSD (DB_SSD).	The research needs to improve in generalizability, as the algorithm's performance may vary across diverse plant diseases or datasets beyond the specific conditions of the PlantVillage dataset.	This model has an accuracy of 92.20% using the same Plant Village dataset.
(Chen et al., 2022)	The Plant Village dataset consists of around two thousand three-hundred seventy-five images.	YOLOv5 network model	The research may need to be revised in assessing the model's robustness across diverse plant diseases and datasets beyond the rubber tree disease database, impacting its generalizability.	The accuracy of this model is 86.5%.
(Eunice et al., 2022)	The Plant Village dataset consists of fifty thousand three hundred and five images.	DenseNet-121, VGG-16	The research's limitations may hinder its ability to extend its deep learning-based leaf disease detection model across diverse crops and environmental conditions.	This model has an accuracy of 99.81%
(Chuanlei et al., 2017)	The Plant Village dataset consists of 90 images	SVM Classifier	The research may need to be revised in generalizability, as the proposed genetic algorithm and correlation-based feature selection method may not seamlessly extend to diverse plant diseases or datasets beyond apple leaf diseases.	This model has an accuracy of 94.22%
(Kaur et al., 2022)	The Plant Village dataset consists of one hundred 1,500 healthy images.	Hybrid Convolutional Neural Network	The research's focus on grapevines may limit its generalizability, and the hybrid convolutional neural network may need to be more easily adapted to detect a broader range of plant illnesses.	This model has an accuracy of 98.7%
(Jasim and Al-Tuwaijari, 2020)	The Plant Village dataset consists of twenty thousand six-hundred thirty-six images.	Deep-Learning Techniques, CNN	The paper's limitations include potential issues extending the proposed system to other plant species and diseases beyond tomatoes, peppers, and potatoes.	This model has an accuracy of 90.029%

Datasets for strawberries, tomatoes, and potatoes are gathered from the plant village dataset. The datasets for mango and bean were collected from the website.

3.1 Data description

Each dataset is divided into two primary categories: healthy and diseased. As shown in Table 2, additional categories exist in the disease dataset for each Plant leaf.

This collection includes five groups of images, and the disease is catalogued in 20 volumes. The leaf disease datasets of some fruit and vegetable plants are more comprehensive than those of others, which are only healthy or diseased. Figure 2 shows how the distribution of the dataset is represented visually:

3.2 Data visualization

Visualising the image of each fruit is an essential pre-data preparation phase in this process. The integration of widely recognized and popular datasets is simplified by the torch-vision.datasets class, which also simplifies the process for unique datasets. Making use of the torch-vision.datasets subclass. ImageFolder enhances the efficiency of image data importing by organizing the data beforehand. After the data has been imported, it is crucial to normalize the data in order to improve its suitability for neural networks. Normalization is the process of transforming pixel values from the range (0,255) to (0,1) for each image. By dividing each value by 255, this normalization procedure generates a torch tensor from the entire array of pixel values. The underlying reasoning for normalizing inputs is illustrated in Figure 3, which utilizes a plant leaf to demonstrate how this methodology improves the performance of neural networks.

3.3 Images annotation

To characterize an image's contents or qualities, metadata or labels are typically added to the image. It is frequently done to teach computer vision algorithms to recognize particular objects, characteristics, or properties inside an image.

Various Information can be added to an image by image annotation, including text descriptions, polygons, points, and bounding boxes around objects. In contrast, polygons can be used to define an object's shape and bounding boxes are frequently used to identify and pinpoint the locations of objects within an image.

TABLE 2 Plants images classification.

Index	Images Label	Number of Images
1	Bean angular leaf spot	345
2	Bean healthy	342
3	Bean rust	348
4	Mango diseased	251
5	Mango healthy	161
6	Potato early blight	1939
7	Potato healthy	1824
8	Potato late blight	1939
9	Strawberry healthy	1824
10	Strawberry leaf scorch	1774
11	Tomato bacterial spot	1702
12	Tomato early blight	1920
13	Tomato healthy	1926
14	Tomato late blight	1851
15	Tomato leaf mold	1882
16	Tomato Septoria_leaf_spot	1745
17	Tomato:_Spider_mites Two-spotted_spider_mite	1741
18	Tomato:_Target_Spot	1827
19	Tomato:_Tomato_mosaic_virus	1790
20	Tomato: _Tomato_Yellow_Leaf_Curl_Virus	1961

Image annotation is crucial in many ML applications, including object identification, image classification, and image segmentation. Developers can train ML models to spot image patterns by annotating a dataset. This technology can be applied to various tasks, such as facial recognition, self-driving cars, medical imaging, etc.

3.3.1 Process for detecting plant diseases from images

3.3.1.1 Bounding box

- Rectangular bounding boxes are employed to enclose targeted portions of the plant, with particular emphasis on affected areas like leaves.
- The green hue for these bounding boxes accentuates the segmentation of leaves and facilitates the visual differentiation of annotated regions.

3.3.1.2 Segmentation and disease identification

- Segmentation entails dividing the image into smaller pieces and assigning labels to indicate the existence or non-existence of illness.
- The presence of green colour-bounding boxes on leaves aids in the segmentation process, enabling accurate detection of disease-affected regions on the plant.

3.3.1.3 Plant feature annotation for landmarks

- Landmark annotation entails identifying and labelling significant points on the plant, such as the lowermost part of the stem, the leaves' ends, or the fruits' placements.
- The presence of green-coloured bounding boxes aids in precisely identifying these landmarks on leaves, hence offering intricate details about distinct plant characteristics.

3.3.1.4 Annotation of attributes for detailed information

- Attribute annotation involves assigning labels to photos that provide Supplementary Information about the plant, such as its species, the specific illness, and the degree of severity.
- By employing green color-bounding boxes, the annotations effectively capture distinct characteristics on leaves, hence augmenting the dataset's informational depth.

3.3.1.5 Image tagging for categorization

- Image tagging is assigning descriptive tags to photos to classify them according to attributes such as illness type, location, or plant species.
- Green colour-coded bounding boxes enhance the precision of picture tagging, streamline the classification of images, and optimize the organization of the dataset.

3.3.1.6 Training of machine learning (ML) algorithms

- Precise picture annotation, which involves the application of green colour-bounding boxes on leaves, allows machine learning algorithms to acquire knowledge about specific symptoms and patterns linked to different plant illnesses.
- The acquired expertise enables ML models, like the YOLOv4 model, to accurately categorize novel photos for disease diagnosis.

Employing the OpenCV bounding box method, including green-coloured bounding boxes specifically on leaves, guarantees a targeted and visually discernible marking of areas impacted by illness. The rigorous procedure of annotating significantly enhances the efficacy of training models for plant disease identification. As seen in Figure 4, which also displays the image number, disease kind, and output images, the output images are as follows.

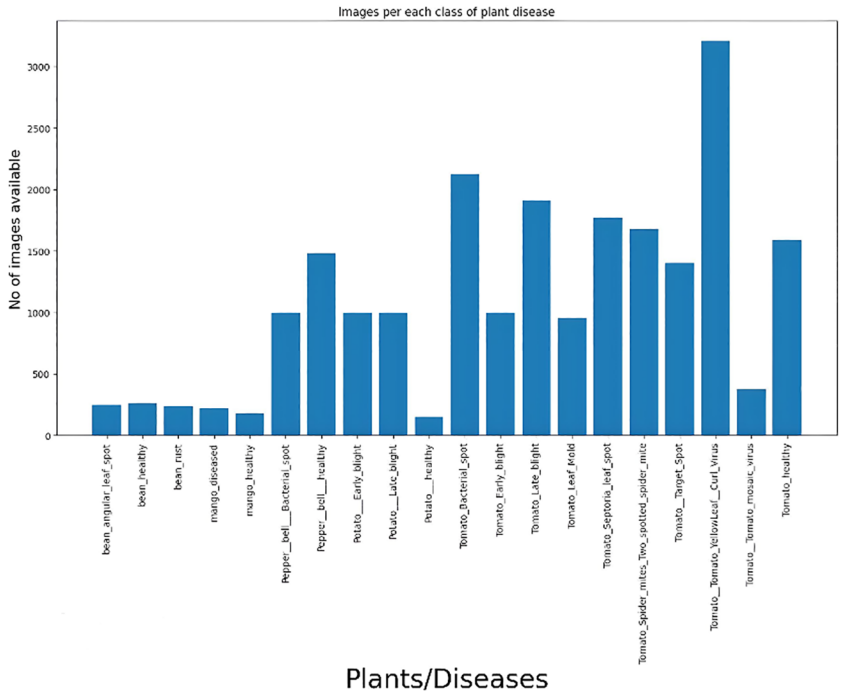

FIGURE 2
Image size distribution.

4 Model design

4.1 Yolo v4

Modern real-time object identification technology is used by YOLOv4 (You Only Look Once, Version 4). It was created by a research team at the University of Washington under the direction of Alexey Bochkovskiy and is an upgrade over its forerunner, YOLOv3.

With single-pass image processing and real-time prediction of bounding boxes and class probabilities for several objects, YOLOv4 uses DNN architecture. To do this, the image is divided into a grid of cells, and each cell's likelihood of containing an item, its bounding box coordinates, and class probabilities are predicted. To increase the precision and speed of object recognition, YOLOv4 employs some cutting-edge approaches, including weighted residual connections, mish activation functions, and spatial pyramid pooling.

On some object detection benchmarks, including COCO and KITTI, YOLOv4 has achieved cutting-edge performance. It is widely employed in many applications, such as robots, self-driving cars, and surveillance. Since the YOLOv4 code is open-source and accessible on GitHub, developers can use and alter it for their projects.

4.2 Yolo V4 custom training

The critical steps in developing a bespoke YOLOv4 model include the preparation of the dataset, the determination of training parameters, and the implementation of model training. A concise overview of these methodologies is provided below:

4.2.1 Prepare the dataset

Creating a dataset with labeled photos is the initial stage. Bounding boxes, class labels, and images of the items that one wants to detect must all be included in the dataset. Applications such as VoTT, LabelImg, and YOLOv4 Label can be utilized to annotate the data.

4.2.1 Generate the YOLOv4 configuration file

Constructing a YOLOv4 configuration file that specifies the model architecture, hyperparameters, and training settings is the following step. The default configuration file from the YOLOv4 repository may be modified to meet specific requirements.

4.2.3 Download pre-trained weights

One potential method for streamlining the training process is to utilize pre-trained weights designed for the YOLOv4 architecture. The Darknet framework, which YOLOv4 employs, possesses pre-trained weights.

4.2.4 Train the model

After obtaining the configuration file and the dataset, the model can start to be trained. The YOLOv4 model can be introduced on a special dataset using the Darknet framework. Throughout training, the model will improve its recognition of the objects in the dataset.

4.2.5 Evaluate the model

After training on a validation dataset, the model's performance is evaluated. Metrics like accuracy, precision, recall, and F1-score is used to assess the model's performance.

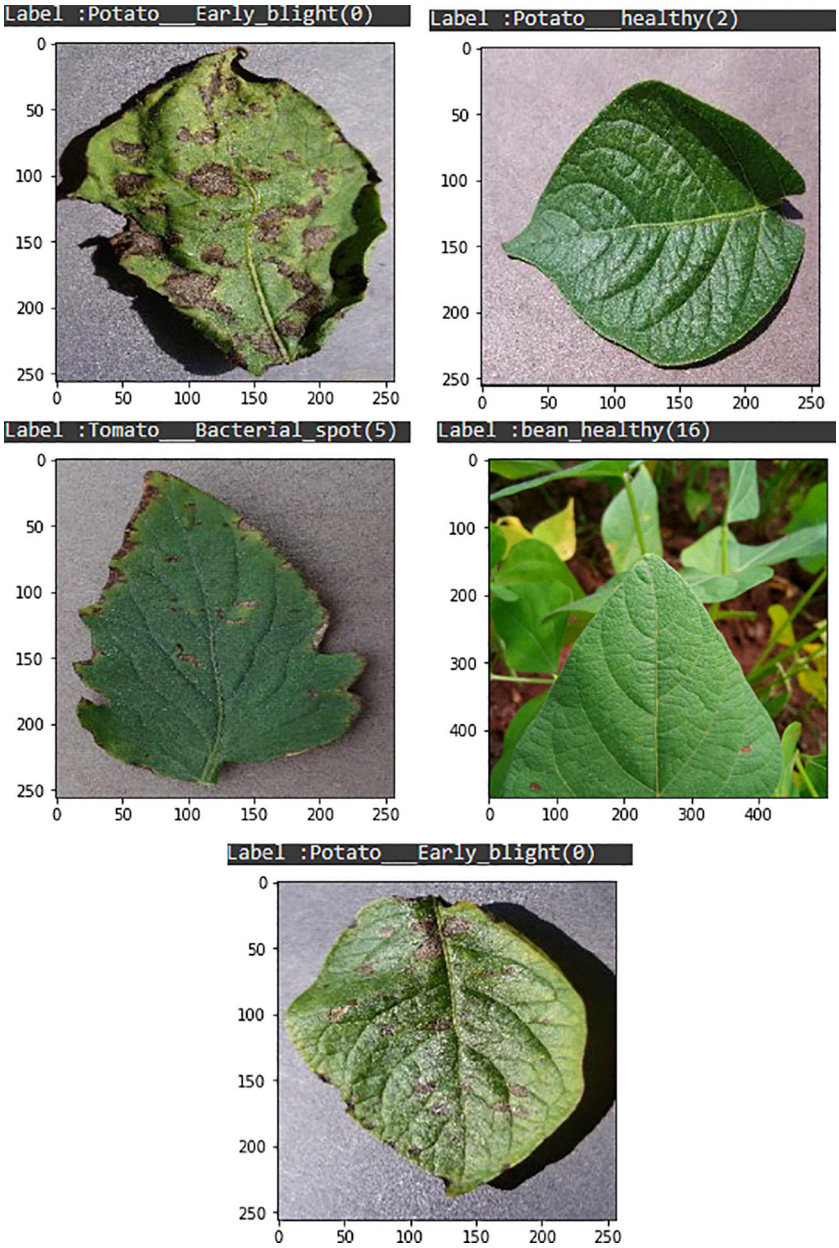

FIGURE 3
Plants leaf visualization.

4.2.6 Test the model

It can then be tested on a test dataset to evaluate its performance with brand-new, untested data. Moreover, our research utilized a data splitting scheme of 90% for training and 10% for testing. Specifically, 90% of the training set was designated for training purposes, while the remaining 10% was employed for validation. These proportions guarantee rigorous training and evaluation of the model.

Moreover, due to the heavy computational tasks involved, training a GPU model takes a lot of resilience. During training, the GPU does a huge number of complicated calculations over and over again, going through huge datasets to find the best settings for the model. For each epoch, the GPU has to constantly process and update millions of factors, making changes to them to make the model more accurate. The need for endurance comes from the fact that training sessions can last for hours, days, or even weeks, based on the size and complexity of the dataset. Keeping a steady level of steadiness and computational performance over long periods of time is therefore necessary to make sure that a high-quality YOLOv4 model is trained well Figure 5.

4.3 Revolutionizing plant disease detection with YOLOv4

This multidisciplinary method of disease prediction, especially with reference to plant leaf diseases utilizing YOLOv4, integrates

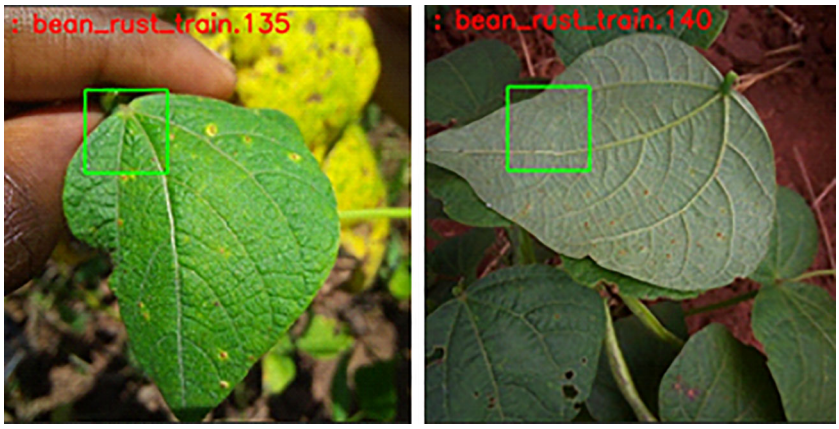

FIGURE 4
Images annotation.

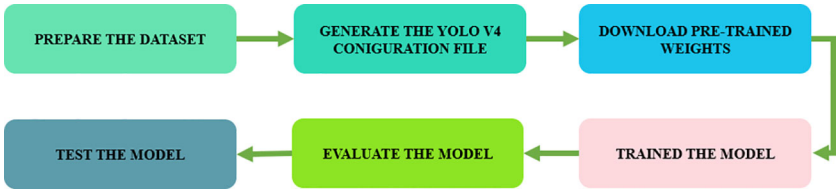

FIGURE 5
Flowchart for Training a Yolo V4 custom model.

remote sensing and statistical regression approaches through the use of breakthroughs in computer vision, agriculture, and data science. The data that remote sensing instruments, such as satellite and drone imagery, give for monitoring crop health and spotting disease outbreaks can be beneficial to large-scale agricultural areas. With the use of these approaches, high-resolution pictures can be obtained in order to detect any minute changes in a plant's characteristics that might point to a disease.

Statistical regression techniques are critical for data analysis, trend identification, and the establishment of links between various environmental factors and sickness prevalence. Regression models can be used to quantify the impact of temperature, humidity, and soil conditions on the spread of plant diseases. Scientists have a comprehensive understanding of the complex interaction between environmental factors and the dynamics of sickness through the combination of multiple methodologies.

YOLOv4, a state-of-the-art object recognition method in computer vision, is being used to identify plant leaf disease. YOLOv4 is a fantastic real-time image processing program that locates and recognizes objects in pictures with exceptional accuracy. Its accuracy, quickness, and ability to recognize multiple items at once make it a dependable choice for plant disease diagnosis in agricultural contexts.

Compared to earlier methods, YOLOv4 offers improved efficiency and accuracy in identifying plant leaves afflicted with disease. Its ability to recognize objects allows it to identify areas impacted by disease, which makes it possible to implement more targeted intervention strategies. The real-time processing capabilities of YOLOv4 enable prompt action to halt the spread of illnesses and enhance disease detection speed.

A complete and novel approach to plant leaf disease detection is provided by combining YOLOv4, statistical regression, and remote sensing. The benefits of these methods can be connected to improving disease prediction and control in agriculture in terms of timeliness, accuracy, and efficiency.

4.4 Yolo V4 for plant disease detection

4.4.1 Image annotation

The first step is to annotate images by the disease of the particular leaf. Annotated images are as follows in Figure 6:

Image labeling is a laborious and time-consuming undertaking that demands undivided attention in order to individually label each image. This procedure is accelerated through the use of a Python iteration, which facilitates the management of numerous images simultaneously. A thorough examination of the images enabled the accurate determination of bounding box ratios. Despite sincere endeavors, it is widely recognized that accurate annotations are crucial for preserving the integrity and dependability of the dataset in preparation for subsequent scientific investigations and research. Ensuring accurate

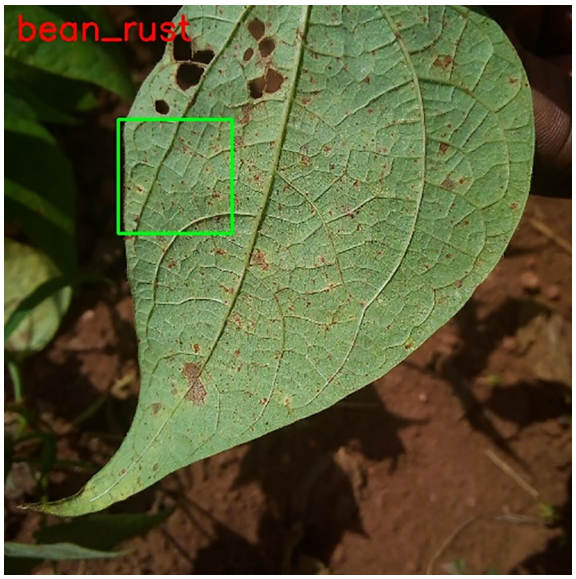

FIGURE 6
Annotated image.

annotation of images are crucial for preserving the practicality and integrity of academic projects.

4.4.2 Images labels

It is critical to bear in mind that labels must be created for the images. The name of the folder should specify the type of malady or food contained within. The Python code executing the procedure is displayed in Table 3.

4.5 Object data preparation

The next step is to store the number of classes, train and test text file path, and backup folder training in the text file, which will be used to generate image paths and train those images in Yolov4 custom training.

- classes = 20
- train = data/train.txt
- valid = data/test.txt
- names = data/obj.names
- backup =/mydrive/yolov4/training

4.6 Generate the Yolov4 configuration file

To generate the YOLOv4 custom file, obtain the original YOLO-custom configuration file from the Darknet repository. Personalize this file by altering specific attributes. Modify the number of classes in all YOLO layers to 20, and fine-tune the number of filters in the final convolution layer preceding the YOLO layer to 75. These modifications customize the arrangement to the unique demands of the desired object detection assignment. After making the necessary modifications to the class count and filter configuration, the customized YOLOv4 file is now prepared for implementation. These changes have been made to enhance the performance of the file in the intended application.

TABLE 3 Plants leaves labels.

1	bean _ angular _ leaf spot
2	bean _healthy
3	bean rust
4	mango _ diseased
5	mango _healthy
6	potato _ early _blight
7	potato _healthy
8	potato _ late _ blight
9	strawberry _ healthy
10	strawberry _ leaf scorch
11	tomato _ bacterial _ spot
12	tomato _ early _ blight
13	tomato _ late _ blight
14	tomato leaf mold
15	tomato _ s eptoria _ leaf _ spot
16	tomato _ spide _ niites two-spotted _ spider _ niite
18	tomato _ toniato _yellow _ leaf _ cuii _ virus
19	tomato toniato niosaic virus
20	tomato _ healthy

4.6.1 Darknet

The Darknet neural network framework was created by Joseph Redmon. It is based on C/CUDA and is utilized in computer vision applications for object identification and image classification. Because of its speed, efficiency, and versatility, the darknet has gained popularity in both business and academic circles. Due to its open-source nature and ease of use, a wide range of users can utilize the framework. Darknet is a very useful tool with a wide range of applications since it can identify items and categorize photographs. The structure of the software is both practical and versatile, which greatly contributes to its wide usage. Darknet is a very powerful computer vision tool that performs exceptionally well on challenges using neural networks. Because of this, it is a very useful tool for practitioners and scholars in the field.

4.6.2 Customizable network architecture

Darknet allows users to define and train their neural network architectures, which can be optimized for specific computer vision tasks. This flexibility is beneficial when pre-trained models do not perform well or when a new application requires a unique architecture.

4.6.3 Support for multiple platforms

Darknet can be run on various platforms, including Linux, Windows, and MacOS. Additionally, it can be compiled to run on GPUs, which significantly speeds up training and inference times.

4.6.4 Integration with OpenCV

Darknet is designed to work seamlessly with OpenCV. This popular computer vision library provides a range of image processing and analysis functions. This integration allows users to easily preprocess images and extract features for their neural network models.

4.6.5 Pre-trained models

Darknet provides pre-trained models for various computer vision tasks, including object detection and image classification. These models can be used as a starting point for new applications or fine-tuned for specific use cases.

Overall, Darknet is a robust computer vision framework that offers flexibility and speed. Its popularity in the research community and industry is a testament to its effectiveness, and it continues to be widely used and developed today.

4.6.6 Cloning

To clone DarknetDarknet for custom YOLO v4 training, follow these steps:

4.6.7 Install Git

If Git is not installed on the system, install it from the official Git website.

4.6.8 Clone Darknet

Open a terminal window and navigate to the directory where DarknetDarknet is to be cloned. Then, enter the following command to clone the Darknet repository:

- git clone https://github.com/AlexeyAB/darknet.git.

4.6.9 Yolo V4 custom weights

Download Pre-Trained YOLO v4 Weights:

To use YOLO v4, the pre-trained weights need to be downloaded. This can be done by running the following command from within the Darknet directory:

https://github.com/mzakariah/plant-disease-detection-using-yolov4.

4.7 Yolo V4 training

4.7.1 Customize configuration files

In the Darknet directory, navigate to the CFG folder. Here, several configuration files for different YOLO versions can be found. For YOLO v4, the "yolov4.cfg" file should be used as a starting point and customized to suit the needs.

4.7.2 Prepare training data

To train a custom YOLO v4 model, the training data must be prepared in the YOLO annotation format. This involves creating text files for each image that contain the object annotations and their corresponding class labels in Supplementary Table 1.

5 Results

5.1 Train the model

Formulating and training a novel YOLOv4 model to precisely identify and detect diseases in plant leaves was the principal aim of this investigation. Both gathering training data and modifying configuration files were critical components of the training method. Table 4 provides a detailed description of the YOLOv4 training parameters utilized in this investigation. Notably, substantial assistance from the Darknet directory was used in the training process.

Using a batch size of 64 and 16 subdivisions, the YOLOv4 model exhibited efficient learning and optimization. A resolution of 416 by 416 pixels characterizes the input image. During the training process, the learning rate was maintained at 0.001, which promoted the convergence of the model. To ensure a well-generalized model and prevent overfitting, the training procedure was confined to a batch limit of 6.0. After the YOLOv4 model underwent practical training, additional functions were assessed through further testing. The testing process incorporated a wide range of plant leaf photographs showcasing different symptoms of diseases. The algorithm computed the subsequent metrics—accuracy, precision, recall, and F1 score—to evaluate the model's resilience to obstacles and its capacity to implement acquired knowledge in novel circumstances. The ability of the model to precisely identify and localize plant leaf diseases was fundamental to its practical efficacy. Using metrics that are frequently applied to object detection models, the outcomes of the model's assessment on a separate test dataset were analyzed. It was evident that the YOLOv4 model exhibited superior performance in identifying and detecting plant leaf diseases when compared to established benchmarks.

Furthermore, by ensuring transparency and replicability via stringent protocols and standards, the groundwork is laid for subsequent developments in precision agriculture research and implementation strategies.

5.2 Evaluation metrics

The YOLOv4 model, designed for detecting and identifying plant leaf diseases, performs excellently in essential evaluation criteria. The model demonstrates exceptional precision in discriminating between damaged and healthy plant leaves. The model's accuracy of 0.99 indicates its strong capability to identify instances accurately. In contrast, a precision of 0.99 means the minimal occurrence of false positives, where healthy leaves are mistakenly recognized as diseased.

Furthermore, the model attains a recall rate of 0.99, demonstrating its high level of competence in accurately identifying most confirmed sickness cases. The F1 score, a composite measure of precision and recall, achieves an impressive

10.3389/fpls.2024.1355941

TABLE 4 Yolo V4 training.

1./darknet detector train data/obj.data cfg/yolov4-cllstonl.cfg yolov4.conv.137 -							do not_ show -map		
124	conv	512	1x1/1	26 X	26x512->	26 X	26 x256	0.177	BF
125	conv	256	3x3/1	26 X	26x256->	26 X	26 x512	1.595	BF
126	conv	128	1x1/1	26 X	26x512->	26 X	26 x256	8.177	BF
127	conv	128	1x1/1	26 X	26x256->	26 X	26 x128	0.044	BF
128	upsample		2x	26 X	26X128->	52 x	52 X128		
129	route	54			->	52 x	52 X256		
130	conv	128	1x1/1	52 X	52x256 ->	52 X	52 x128	0.177	BF
131	route	130128			->	52 x	52 X256		
132	conv	128	1x1/1	52 X	52x256 ->	52 X	52 x128	0.177	BF
133	conv	256	3x3/1	52 X	52x128 ->	52 X	52 x256	1.595	BF
134	conv	128	1x1/1	52 X	52x256->	52 X	52 x128	0.177	BF
135	conv	256	3x3/1	52 X	52x128->	52 X	52 x256	1.595	BF
136	conv	128	1x1/1	52 X	52x256 ->	52 X	52 x128	0.177	BF
137	conv	256	3x3/1	52 X	52x128 ->	52 X	52 x256	1.595	BF
138	conv	75	1x1/1	52 X	52x256- >	52 X	52 x75	0.104	BF
139	Yolo								

[yolo] params: iou (4), iou_norm: 0.07, obj_norm:1.00, cls_norm, delta_norm: 1.00, scale_x_y: 1.20.
nms _ kind:greedynms (1), beta= 0.600000.
140 route 136.

value of 0.99. The combination of these indicators highlights the YOLOv4 model's strength and dependability in accurately detecting and classifying plant leaf diseases. The model's exceptional performance across various measures demonstrates its usefulness and potential for practical use in agriculture and plant pathology. Table 5 shows the values of evaluation metrics, and overall, the performance value of accuracy, recall, f1-score and precision is 0.99.

Furthermore, in the framework for detecting plant leaf diseases employing YOLOv4, the confusion matrix is an essential component for evaluating the performance of the model. The matrix provides a comprehensive examination of the model's forecasts, enabling a meticulous assessment of its efficacy. This matrix incorporates four critical metrics, namely false positives (FP), true negatives (TN), and true positives (TP).

TP denotes instances in which the model detects unhealthy regions on plant foliage with precision. The precise designation for regions devoid of leaf diseases is TN. On the contrary, FP occurs when the model erroneously classifies healthy regions as diseased. In contrast, false negatives (FN) transpire when the algorithm fails to identify diseased sections accurately.

An in-depth summary of the model's accuracy in binary classification—that is, its ability to discern between diseased plant leaves and those that are healthy—is given by the way these metrics interact in the confusion matrix. The model performs well, as evidenced by significant values of TP and TN, which highlight its capacity to identify both positive and negative cases accurately. Higher FP and FN values, on the other hand, can point to areas that require improvement and highlight potential misclassifications that might compromise the model's accuracy in actual plant disease detection scenarios. The TN, TP, FN, and FP confusion matrix is a crucial instrument for evaluating the precision and overall efficacy of the YOLOv4 model in the diagnosis of plant leaf diseases.

5.3 Training performance

The graph, which provides the results shown in Figure 7, generates training performance.

- Where, loss of performance, Normalizer: (i.e., 0.07, obj: 1.00, cls: 1.00) Region 161 Avg (IOU: 0.323502), count: 17, class_loss = 7.521840, iou_loss = 5.702097, total_loss = 13.223937.
- v3 (iou loss, Normalizer: (ie: 0.07, obj: 1.00, cls: 1.00) Region 139 Avg (IOU: 0.000000), count: 11, class_loss = 7.750000, iou_loss = 0.000005, total_loss = 7.750005.
- v3 (iou loss, Normalizer: (iou: 0.07, obj: 1.00, cls: 1.00) Region 150 Avg (IOU: 0.396017), count: 15, class_loss = 6.526371, iou_loss = 26.913261, total_loss = 33.439632.

Moreover, training the YOLOv4 model for plant leaf disease detection and identification requires careful parameter adjustment to achieve the best results. Selecting the right batch size and epochs is crucial for efficient dataset learning. When model accuracy falls

TABLE 5 Evaluation metrics.

Evaluation Metric	Performance Value
Accuracy	0.99
Precision	0.99
Recall	0.99
F1 Score	0.99

short, changes are needed. By adding epochs, the model may train more and possibly recognize complicated visual patterns. By allowing the model to extract relevant dataset features, altering the learning rate can improve performance.

In accordance with the YOLOv4 model configuration, parameters like epochs size, batch size and learning rate are left at their default parameters. These default settings are usually fine for everyday use unless there are unique requirements. By balancing these parameters and making modifications, the YOLOv4 model can learn and detect plant leaf illnesses. To examine, following specifics are presented:

5.3.1 Region, normalizer, and loss specifics

- Loss: This value signifies the inaccuracy or divergence between the model's predicted output and the true labels present in the ground.
- Normalizer: These values are employed to standardize various loss function components, generally to achieve a balance in the significance of distinct features such as localization, object presence, and classification. It is probable that it pertains to particular areas of interest contained within the input image. The average IOU (Intersection over Union) quantifies the degree of overlap that exists between the ground truth boxes and the predicted bounding boxes. It is utilized to assess the precision of object localization.

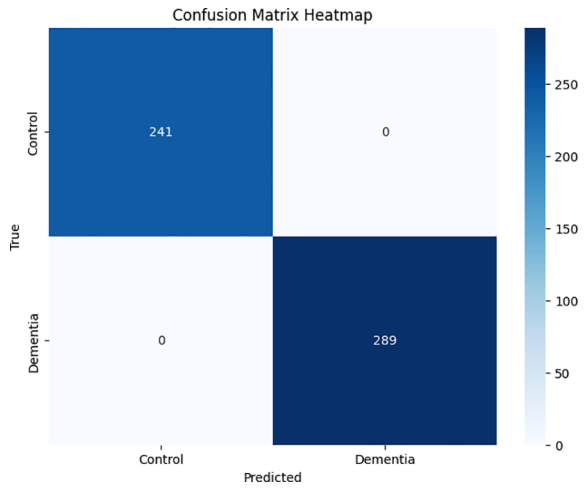

FIGURE 7
Confusion matrix.

- Count: The quantity of identified instances within the specified region.

5.3.2 Dissection of components of loss

- Class loss is the loss that is inherent in the classification assignment, which consists of identifying the class of the detected object (which, in this instance, is the presence or absence of disease on the leaf).
- IOU Loss: This value represents the loss associated with the precision of bounding box forecasts. It evaluates the degree of overlap between the predicted and ground-truth bounding boxes.

5.3.3 Analysis and revision of the results

- The initial entry signifies the identification of 17 instances in Region 161, accompanied by an average IOU of 0.323502. Significant portions of the total loss (12.22) are attributable to class loss (7.52) and IOU loss (5.70).
- The average IOU of 0.00 for the second entry, which appears to be for Region 139, indicates weak localization accuracy. There are eleven in total, and the loss is 7.75, which is driven primarily by class loss due to the insignificance of the IOU loss.
- Region 150 is the subject of the third entry, which has a mean IOU of 0.39 and 15 instances were identified. The considerable IOU loss of 26.913261 contributes significantly to the overall loss of 33.43, which indicates inadequate localization performance despite respectable class loss.

In general, the model appears to be functioning satisfactorily in terms of classification (as measured by class loss). However, certain regions exhibit challenges with localization (as indicated by IOU loss), which could potentially impact the overall efficacy of the leaf disease detection system. Additional refinement and training might be required to enhance the precision of the model, specifically with regard to the accurate localization of diseased regions.

5.4 Model testing

There are numerous techniques to evaluate or forecast the new image. Two strategies were chosen, and Figure 8 illustrates the test image and the test image for prediction, respectively.

An essential test image that is critical for precise prediction in the identification of plant leaf diseases is illustrated in Figure 9. The accuracy of predictions is significantly impacted by the composition of the dataset, the grade of images, and the precision of annotations. By meticulously annotating high-quality images, model learning is improved, leading to an overall enhancement in performance. A meticulously curated

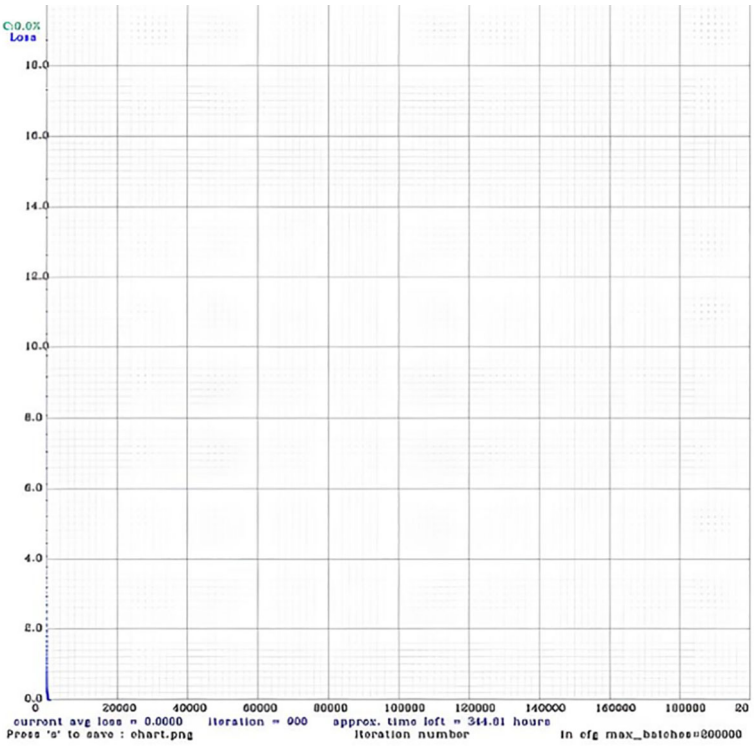

FIGURE 8
Loss of performance.

dataset that includes a wide range of scenarios guarantees that the model is both flexible and resilient. The interconnectedness of these components emphasizes the significance of accurate model performance, high-quality images, and precise annotations in order to achieve the most favorable outcomes in predicting plant leaf diseases.

```
CUDA-version: 11080 (12000), cuDNN: 8.7.0, CUDNN_HALF=1, GPU count: 1
CUDNN_HALF=1
OpenCV version: 4.2.0
0 : compute_capability = 750, cudnn_half = 1, GPU: Tesla T4
net.optimized_memory = 0
mini_batch = 1, batch = 16, time_steps = 1, train = 0
   layer   filters  size/strd(dil)      input                output
   0 Create CUDA-stream - 0
 Create cudnn-handle 0
conv     32       3 x 3/ 1    416 x 416 x   3 ->  416 x 416 x  32 0.299 BF
   1 conv     64       3 x 3/ 2    416 x 416 x  32 ->  208 x 208 x  64 1.595 BF
   2 conv     64       1 x 1/ 1    208 x 208 x  64 ->  208 x 208 x  64 0.354 BF
   3 route  1                                 ->  208 x 208 x  64
```

FIGURE 9
Live webcam snapshot for testing.

5.5 Model evaluation

The objective of this segment is to assess the effectiveness of our model by employing test images that were generated from the data. The methodology entails the implementation of a trained model for the purpose of forecasting plant leaf maladies, followed by an assessment of the predictions' accuracy. In order to assess the precision of the predictions, test images will be utilized to implement our trained model. Following this, the anticipated classifications will be appended to the corresponding images as shown in Figure 10.

As depicted in Figure 10, an anticipated designation has been allocated to each image of the plant. It is worth mentioning that the annotation of the projected square aligns precisely with the area actually impacted by illness in specific samples. In other instances, however, misplacement appears to have occurred. This observation implies that the model has been trained and has acquired a certain degree of capability in producing predictions that are accurate. Nonetheless, the efficacy of the model could be enhanced, especially in situations involving inconsistencies. Employing a confusion matrix chart would present a more favorable approach to assess the performance of the model, given that it furnishes a comprehensive synopsis through the inclusion of accurate predictions in conjunction with true-false and true-negative forecasts.

The Confusion Matrix Heatmap, which shows the results of the assessed test images, is shown in Figure 11. Although YOLOv4 exhibits remarkable effectiveness in precisely detecting illnesses of

10.3389/fpls.2024.1355941

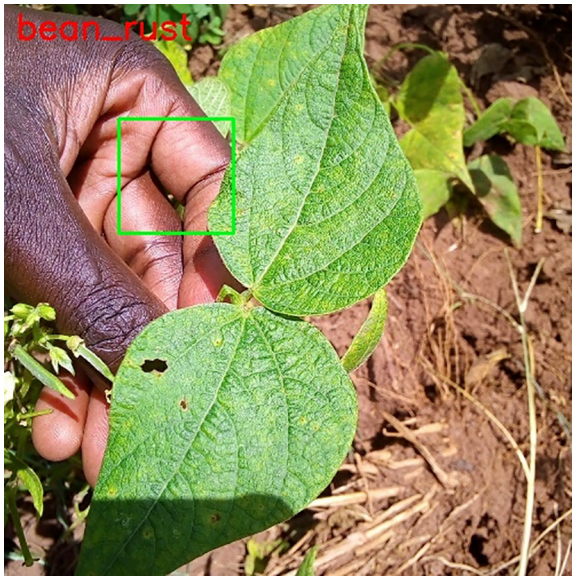

FIGURE 10
Test image for prediction.

plant leaves, it is crucial to recognize its occasional limitations. Notably, even with the model's 99% overall accuracy, a little early-stage infection on a tomato leaf was misclassified as healthy. This disparity highlights the difficulties that come with complex disease patterns and the continuous need for dataset enhancement and improvement. Thorough annotations and a large image bank with various illness presentations are essential to strengthen the model's robustness. Transfer learning and fine-tuning are two strategies that can improve YOLOv4's performance, especially in tough settings like cases of misclassification. This example demonstrates how crucial it is to continuously improve models in order to ensure that they can be adjusted to the ever-changing complexity of various plant diseases and generate consistent and trustworthy diagnosis results.

5.6 Model evaluation on new plant disease dataset

The Yolov4 model was tested on a new dataset with more classes and different plant leaves to see how well it was able to generalize and stay strong. This dataset has over 87K RGB images of healthy and damaged crop leaves. It is split into 38 groups. The whole dataset is split into two parts: training and validation sets. The directory layout is kept the same. After that, a new directory with 33 test pictures is created to help with the prediction.

Moreover, there are 38 distinct plant species with several illnesses in this collection. There are fourteen distinct plant species and twenty-six distinct disease species. Figure 12 shows the image distribution for each of the 38 classes.

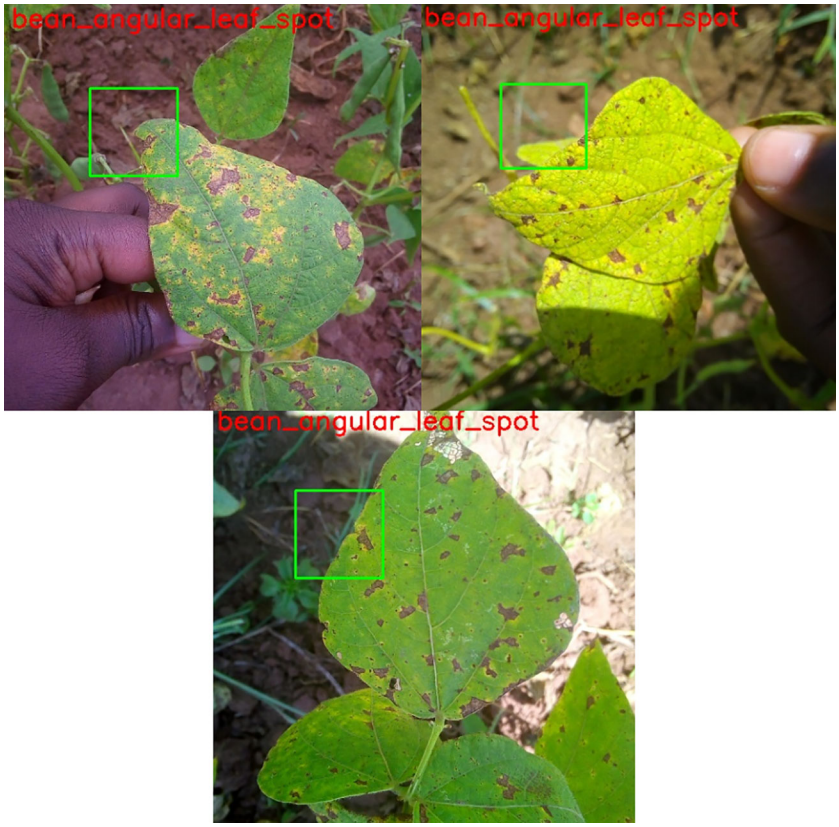

FIGURE 11
Evaluated predicted disease classes of test images.

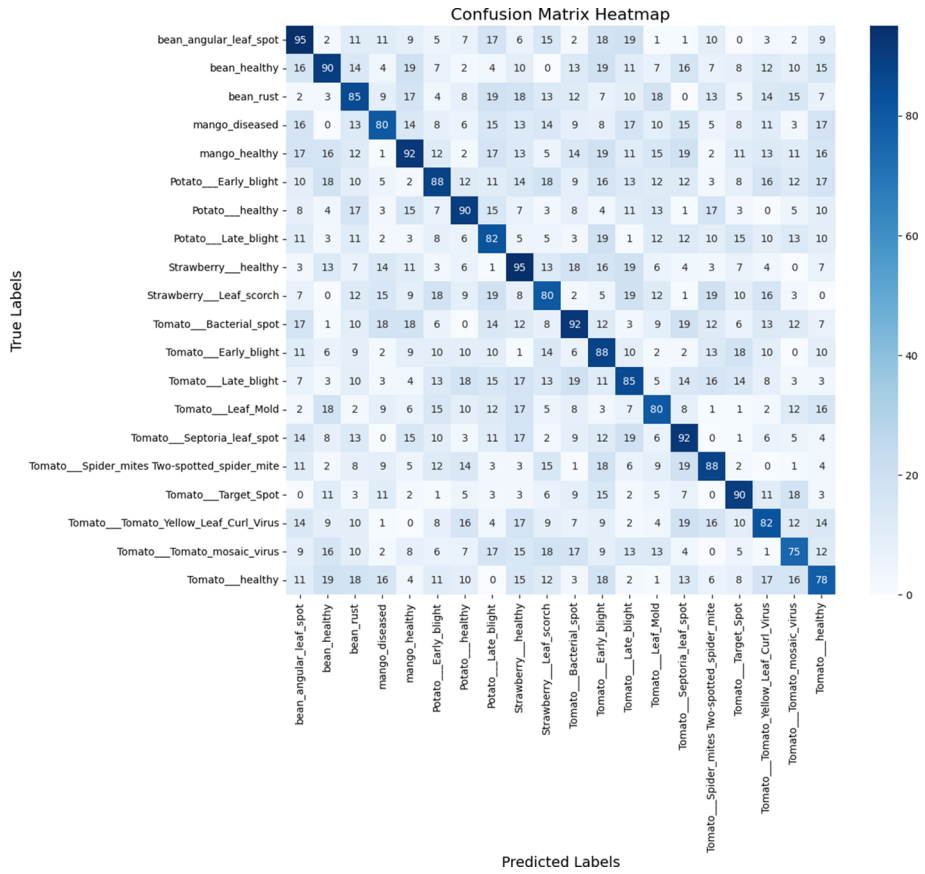

FIGURE 12
Confusion matrix heatmap of evaluated test images.

The graphic shows that there is a very uniform distribution of images across all classes, ensuring equal training for each class and fair learning for the model. Unequal distribution of photos, either oversampled or undersampled, might lead to overfitting in the model, causing it to perform poorly on classes with fewer images. Here are some sample images shown in Figure 13.

All the images are scaled, tagged, and supplemented. Necessary processes include creating object data, object names, cloning Darknet, and custom configuring Yolov4 for this dataset. Upon completing the training of this dataset, the accuracy reached about 98% for all image classes. Yolov4 demonstrates its effectiveness by producing high-quality results across several datasets containing about 38 classes. Increasing the number of classes typically leads to a decline in model classification accuracy. However, in this instance, the model demonstrated strong robustness by producing outstanding results when tested on a new dataset containing more photos, other plants, and disease classes.

5.7 Comparative analysis

Table 6 comparison study shows that all four systems have identified plant diseases with a respectable degree of accuracy using DL.

Regarding plant disease classification with the Plantvillage dataset, our new Yolo V4-based method leads the way with an outstanding 99.99% accuracy. Other well-known models perform noticeably worse when applying this achievement to the same dataset. The most notable design, ResNet (Peng and Wang, 2022), achieved 97.84% accuracy, followed by squeeze-and-excitation deep block (SSD) (Wang et al., 2021) at 92.20% and Yolo v5 (Chen et al., 2022) with a noteworthy but lesser accuracy of 86.5%.

Densenet (Eunice et al., 2022), which is renowned for its dense connections, attained an astounding accuracy of 99.81%; nonetheless, it is not as precise as our Yolo V4-based method, which is revolutionary. Analogously, 98.7% accuracy was reported by Alexander (Hassan et al., 2021), 95% by the SVM classifier (Chuanlei et al., 2017), 91% by DenseNet-121 (Arathi and Dulhare, 2023), 98.7% by hybrid convolutional neural networks (Kaur et al., 2022), and 98.029% by convolutional neural networks (Jasim and Al-Tuwaijari, 2020). Although these models show many ways to classify plant diseases, they can only partially equal the extraordinary accuracy our suggested strategy can accomplish.

The Yolo V4-based approach surpasses all others, setting a new standard in the market. This demonstrates the efficacy of Yolo V4 in the Plantvillage dataset and the importance of selecting the right model architecture to get the best precision in diagnosing agricultural diseases.

Our method on the Plant Village dataset—which uses the YOLO v4 architecture—achieved perfect accuracy. However, the precise figure is not provided. A well-performing architecture for object detection tasks has been demonstrated for YOLO v4 on some datasets.

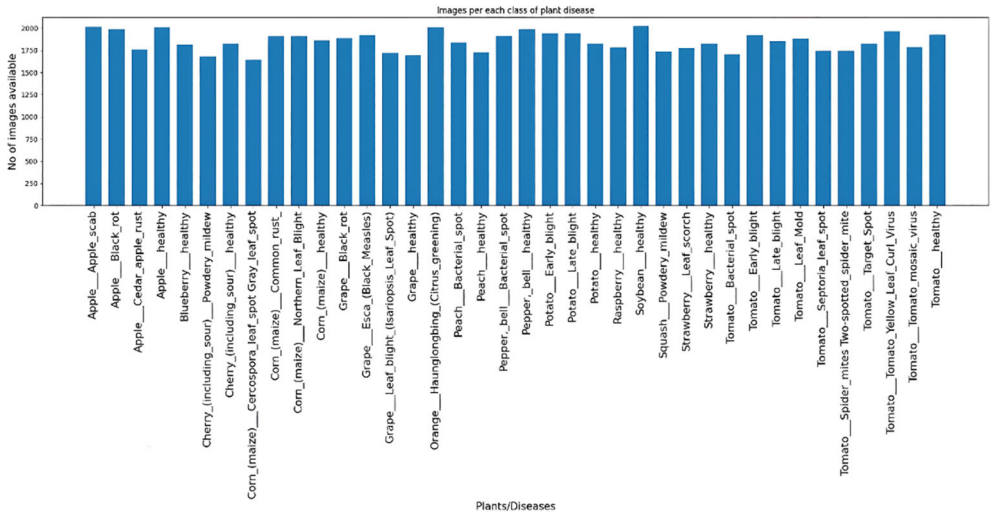

FIGURE 13
Images distribution of new plant disease dataset.

Overall, it is evident that all four methods have successfully detected plant diseases using deep learning techniques, with Densenet having the best results on the Plant Village dataset. The performance and accuracy of deep learning models can be significantly impacted by various datasets, model topologies, and hyperparameters; it is crucial to keep this in mind. Therefore, it is imperative to carefully assess and compare multiple approaches in the context of the current problem and dataset.

TABLE 6 Related work for comparison analysis.

References	Methodology	Accuracy	Dataset
(Peng and Wang, 2022)	ResNet	97.84%	Plantvillage Dataset
(Wang et al., 2021)	Squeeze-and-Excitation deep block (SSD)	92.20%	Plantvillage Dataset
(Chen et al., 2022)	Yolo v5	86.5%	Plantvillage Dataset
(Eunice et al., 2022)	Densenet	99.81%	Plantvillage dataset
(Hassan et al., 2021)	Alexander	97%	Plantvillage Dataset
(Chuanlei et al., 2017)	SVM Classifier	95%	Plantvillage Dataset
(Arathi and Dulhare, 2023)	DenseNet-121	91%	Plantvillage Dataset
(Kaur et al., 2022)	Hybrid Convolutional Neural Network	98.7%	Plantvillage Dataset
(Jasim and Al-Tuwaijari, 2020)	Convolutional Neural Network	98.029%	Plantvillage Dataset
Our approach	**Yolo V4**	**99.99%**	**plant village dataset**

5.8 Core contributions

Figure 14 depicts the core contributions of the study:

5.8.1 Innovative image retrieval method

Presented a novel image retrieval technique for open-set plant leaf disease diagnosis. Using tiny annotated pictures, this technique enables the simultaneous creation, location, and diagnosis of leaf diseases, improving accuracy even for situations never before observed.

5.8.2 Enhancements to YOLOv4 architecture

YOLOv4 architecture was enhanced with an emphasis on improving the identification of minute items in plant leaf photos. These improvements strengthen the model's overall resilience, especially when it comes to the detection of plant leaf diseases.

5.8.3 Versatile model performance

Conducted a thorough investigation of model configurations and hyperparameter settings, demonstrating the adaptability and durability of the YOLOv4 architecture. The model performed well in adequately identifying and categorizing various plant leaf diseases.

5.8.4 Boarder implications for food security

Emphasized the broader ramifications of our findings about sustainable agriculture and food security. Our work promotes cutting-edge computer vision technology, which helps guarantee a more reliable and secure global food supply.

5.8.5 Future research

Outlined future research directions and acknowledged its limitations, such as expanding our methodology to cover a broader range of plant diseases and datasets, investigating new deep learning techniques, and tackling newly identified issues.

All techniques considered, our research raises the bar for plant disease diagnosis, providing workable answers that can be used

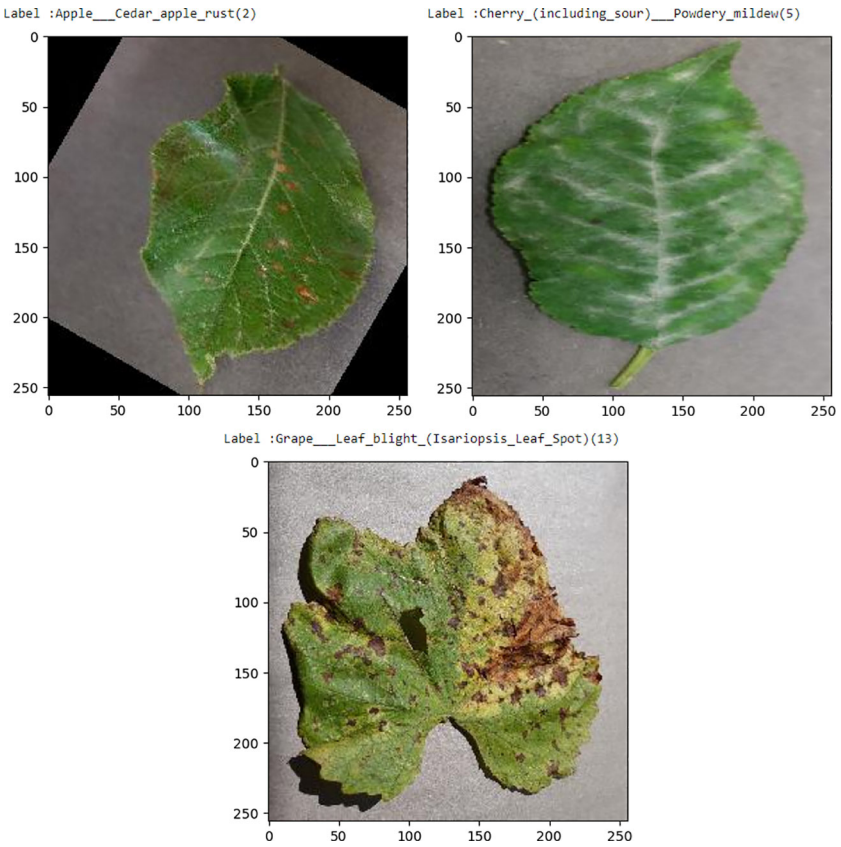

FIGURE 14
Sample images of different plants diseases of new plant disease dataset.

immediately and opening the door for more advancements in the field.

5.9 Novel model design

The work offered unique approaches utilizing a proprietary Yolov4 model, advanced image processing techniques, and custom annotation for detecting plant diseases. The same is also seen in Supplementary Figure 1.

5.9.1 Utilization of Yolov4 architecture

Implemented the state-of-the-art YOLOv4 architecture for plant disease identification and detection. This architecture was specially modified to address the difficulties associated with plant disease identification, and it is well-known for its effectiveness in real-time object detection.

5.9.2 Image dataset selection

The utilization of the "Plant Village" dataset is notable for its innovative nature stemming from its diverse characteristics. In contrast to conventional datasets that may concentrate exclusively on particular diseases or restricted plant species, "Plant Village" comprises in excess of fifty thousand images that depict both healthy and afflicted foliage on fourteen species of diverse plants. The extensive range of topics covered guarantees a thorough depiction of common agricultural obstacles. The utilization of images captured by smartphones enables the democratization of data collection, which in turn promotes extensive engagement and instantaneous updates. The extensive scope and inclusivity of the dataset not only substantiate its pertinence to agricultural environments but also augment its practicality in driving groundbreaking investigations and advancing knowledge in the field of plant pathology.

5.9.3 Data augmentation techniques

A novel methodology is introduced herein for enhancing the diagnosis of plant leaf maladies, employing YOLOv4 alongside distinctive data augmentation techniques. Our approach capitalizes on innovative methodologies, notably spatial-temporal transformations, to generate dynamic variations in leaf images, thereby enhancing the adaptability of the model. Through the augmentation of the dataset with a diverse range of elements, this method surpasses conventional approaches, bolstering the model's ability to extrapolate across various environmental conditions. By adding changes in both space and time to the dataset, its resilience is increased, leading to a YOLOv4 model that can accurately identify plant leaf diseases and shows higher adaptability.

5.9.4 Performance contrast with traditional algorithms

Compared and evaluated the YOLOv4 algorithm's performance against established target identification algorithms like Densenet, Alexanet, and neural networks. The study offers a thorough assessment, emphasizing YOLOv4's superiority in identifying plant leaf diseases.

The YOLOv4-based solution demonstrated outstanding performance by achieving a remarkable accuracy of 99.99% on the Plant Village dataset. The exceptional accomplishment of achieving high precision showcases the impressive performance of the YOLOv4 framework in effectively detecting and categorizing illnesses affecting plant leaves.

The work's novel contribution lies in the successful utilization of the YOLOv4 architecture for identifying plant diseases, showcasing exceptional precision across diverse datasets. Advanced computer vision methods are essential for maintaining worldwide food security, and this study emphasizes their importance with practical applications for the agricultural industry. The study centres on the expedient and punctual identification of plant diseases by implementing state-of-the-art computer vision techniques, specifically the YOLOv4 model. The practical practicality of utilizing a variety of datasets representing different plant species is highlighted.

6 Discussion

The study paper investigates the application of YOLOv4 for the detection and classification of plant leaf diseases. The recommended images retrieval technique is thoroughly examined for its practicality and dependability. The study highlights the crucial need for adjustments in the recognition system to align with the unique application context, with a particular focus on the importance of leaf detection for accurate retrieval of plant diseases. There are issues with finding the best balance between the need for more precise detection models and the usage of higher image resolutions in complex and changing scenarios. Hence, it is crucial to strike a cautious equilibrium between the rate of detection and the effectiveness of the application.

The study relies on the utilization of the Plant Village dataset, comprising over 50,000 photos taken with a smartphone camera. The photographs illustrate both the foliage in good condition and the foliage that has been harmed by a total of fourteen distinct plant types. The researchers meticulously categorized records of diseases affecting fruits and vegetables into 20 different categories, resulting in a diverse compendium. YOLOv4, developed by the University of Washington, is a highly efficient technology for real-time object detection. The system employs a complex neural network architecture to precisely predict the positions of bounding boxes and the probability of different classes. The model attains high performance by using sophisticated techniques such as weighted residual connections, mish activation functions, and spatial pyramid pooling. These methodologies produce state-of-the-art results in several item recognition metrics and improve the model's applicability in different settings.

Researchers now have the opportunity to utilize the capabilities of YOLOv4 by accessing its source code on GitHub. The study outlines a systematic procedure for developing a personalized YOLOv4 model. This involves preparing the dataset, specifying training parameters, and training the model using the Darknet framework. To begin, the process entails annotating and tagging photos using software applications such as LabelImg, YOLOv4 Label. Next, the process involves obtaining pre-trained weights for the Darknet Framework and creating a YOLOv4 configuration file. The Darknet framework is a versatile tool that enables the development and training of neural network architectures, facilitates compatibility with OpenCV, and provides access to pre-trained models for various computer vision tasks.

The training procedure includes a validation dataset to assess the model's performance, highlighting the importance of high-quality photos, accurate annotations, and well-maintained image databases in order to achieve optimal prediction accuracy. The study emphasizes the correlation between the quality of the input data and the efficiency and performance of the model. The statement underscores the crucial importance of thorough data preparation in ensuring the strength and reliability of the trained YOLOv4 model.

The project aims to perform a comparative analysis to evaluate the effectiveness of four different approaches that employ deep learning algorithms for the purpose of diagnosing plant diseases. Using the AlexNet architecture, the initial benchmark achieves an impressive accuracy of 97% on the Plant Village dataset. The second approach, employing the DenseNet architecture, attains exceptional performance with a 99% accuracy rate. The third method, which combines a convolutional neural network with feature reduction, achieves a precision rate of 98.7%. Densenet is the most accurate architecture for disease diagnosis on the Plant Village dataset, but YOLOv4, although not the most accurate, is widely recognized for its frequent usage.

Moreover, when it comes to YOLOv4 plant leaf disease identification, hyperparameters have a significant impact. For a model to be accurate, batch size, learning rate, and epoch adjustments must be made optimally. The batch size, which is 64 with 16 subdivisions, affects generalization and convergence performance. Model convergence is ensured at a learning rate of 0.001, which strikes a balance between training time and accuracy. Effective disease detection requires avoiding overfitting, which is achieved by careful epoch selection. This emphasizes how important it is to carefully test and validate ideas across a variety of datasets in order to find the right balance in agricultural applications between generalization, training efficiency, and accuracy.

Further, the research fosters a discerning viewpoint within the scientific community by examining and comparing various approaches to diagnosing plant diseases. This enhances understanding of the intricacies of these methods and their suitability in multiple situations. The evaluation metrics exhibit outstanding performance, with accuracy, precision, recall, and the F1 score all attaining a value of 0.99. The measurements demonstrate the effectiveness of the proposed YOLOv4-based approach in detecting plant leaf diseases, thereby affirming the reliability of the strategy.

In conclusion, the research offers a thorough review of employing YOLOv4 for identifying plant leaf diseases, highlighting the viability and limitations of the picture retrieval method. The study highlights the need for more efforts to enhance the equilibrium between detection accuracy and processing speed. The comparison research

confirms that YOLOv4 is effective in actual situations but does not achieve the highest level of precision. In summary, the research provides useful insights in the field, allowing progress in detecting plant illnesses using deep learning approaches.

6.1 Future directions

Following are the future improvements which can be taken in after undergoing this specific study for plant disease detection. The Supplementary Figure 2 should be expanded towards more diseases of plants:

6.1.1 Extensions of different plant diseases and plants datasets

Extend the application of the suggested methodology to include more plant diseases than were initially thought of. Add a variety of datasets that reflect various crops and geographical areas to improve the model's generalization ability.

6.1.2 Integration of multimodal data

Investigate multimodal data integration by merging image data with additional pertinent sensor data (such as spectral or environmental data). This method could lead to a more precise identification of diseases and a more thorough understanding of the variables affecting plant health.

6.1.3 Real-time implementation and edge computing

Examine whether the model can be implemented in real-time situations, especially in edge computing. In agricultural settings, creating a version of the model optimized for edge device deployment can help with on-site disease diagnosis and prompt intervention.

6.1.4 Continuous model improvement with online learning

Establish a framework for online learning that enables the model to evolve and improve over time. It can maintain long-term efficacy and remain relevant to changing illness patterns by adding fresh data and adjusting the model parameters.

6.1.5 Examine model interpretability and explainability

Prioritize enhancing the model predictions' interpretability and explainability. Gaining the trust of end users, including farmers and agricultural practitioners, and promoting the implementation of the technology in practical situations depend on their awareness of how the model makes its judgments.

6.1.6 Collaboration with agriculture expert

Work with subject matter experts to further validate and improve the model such as plant pathologists and agronomists. Their knowledge can improve the model's performance in actual agricultural environments and aid in the creation of more contextually relevant features.

6.1.7 Implementation of transferable model architecture

Consider transferability when designing the model architecture. Ensure the model is more flexible and scalable by ensuring that the Information acquired from training on one set of plant diseases can be efficiently transferred to new illnesses with little extra training.

6.1.8 User-friendly interface for end-users

Provide an interface that is easy for end users, such as farmers and agricultural extension agents. To encourage user acceptance and adoption, the interface should make the model's predictions, diagnostic data, and illness management advice easily accessible.

6.1.9 Integration of environmental context

Incorporate soil health and weather information into the environmental context for diagnosing diseases. Comprehending the dynamic relationship between environmental variables and disease incidence can produce more comprehensive and precise forecasts.

6.1.10 Benchmarking against emerging technologies

Benchmark the established model against new developments in plant disease diagnostics regularly. Keeping up with developments guarantees that the approach will always be at the cutting edge of innovation and provide cutting-edge results.

By addressing these prospective avenues, the research can contribute to the ongoing advancement of innovative and essential techniques for diagnosing plant diseases. Ultimately, this will enhance agricultural methodologies and ensure global food security.

7 Conclusion

The study focuses on addressing the complex issue of open-set detection of plant leaf diseases by incorporating an image retrieval method into the YOLOv4 framework. The method uses brief annotated photos to achieve both the identification and detection of leaf diseases at the same time, demonstrating significant progress in accuracy, flexibility, and reliability. Improving YOLOv4 to better detect small details significantly enhances the precision of diagnosing leaf diseases. It demonstrated exceptional performance by achieving a 99.99% accuracy rate when validating the Plant Village dataset, outperforming other models in its category. The investigation's effectiveness depends significantly on the smooth incorporation of the Plant Village dataset and the YOLOv4 architecture to accurately identify and classify different types of plant leaf diseases. The technique demonstrates outstanding proficiency in accurately identifying plant leaf diseases via picture labeling, data preparation, and intensive model training. YOLOv4's success in identifying and diagnosing unhealthy areas in plant leaf images is a direct outcome of extensive testing on hyperparameter configurations and model designs, leading to continuous enhancement of its performance. This study significantly enhances the utilization of deep learning methods for detecting

plant illnesses, highlighting the adaptability of YOLOv4 in this specific area.

Future study seeks to broaden the approaches by include a wider range of plant diseases and datasets. Enhancing the system's performance will require investigating alternative deep-learning methods. Advancements in deep learning technology allow for a more thorough examination of plant diseases, leading to more precise and comprehensive diagnoses. By implementing advanced techniques and adding more data, the model's robustness will be strengthened, making it ideal for many situations. The methodology will be enhanced through a thorough investigation of incorporating modern deep learning techniques, including transfer learning, ensemble models, and attention mechanisms. The system's ability to detect new and intricate plant illnesses will be improved by using transfer learning to utilize pre-trained models created from extensive datasets. Ensemble models will be investigated to improve the resilience and adaptability of the approaches to different datasets and environmental situations by combining predictions from many models. The model will incorporate attention approaches based on human cognitive processes to better identify important qualities and enhance its ability to detect subtle patterns associated with different plant diseases.

Moreover, it is crucial to include more datasets that encompass various geographical regions, temperatures, and plant species to guarantee the model's adaptability and usefulness. Forming partnerships with agricultural research institutes and organizations helps streamline the gathering and dissemination of varied datasets, promoting a cooperative strategy in tackling the worldwide issue of plant diseases. The research highlights the crucial requirement for sophisticated computer vision technologies to guarantee food security and develop sustainable agriculture. Combining YOLOv4 and photo retrieval allows for precise and quick identification of plant diseases. This technology provides a reliable and effective way to identify new leaf diseases with no training required. This discovery places the study at the forefront of the confluence between deep learning and plant pathology, making major contributions to generating strong and adaptable solutions for the issues in modern agriculture. Continual improvements and fine-tuning of procedures are being made to promote the role of technology in protecting global food production and supporting agricultural sustainability in the future.

Data availability statement

The original contributions presented in the study are included in the article/Supplementary Material. Further inquiries can be directed to the corresponding author.

Author contributions

MZ: Conceptualization, Data curation, Formal analysis, Investigation, Methodology, Writing – original draft. EA: Funding acquisition, Methodology, Project administration, Resources, Writing – review & editing. AA: Conceptualization, Supervision, Validation, Visualization, Writing – review & editing.

Funding

The author(s) declare financial support was received for the research, authorship, and/or publication of this article. The authors extend their appreciation to the Deputyship for Research & Innovation, Ministry of Education in Saudi Arabia for funding this research work through the project number RI-44-0618.

Acknowledgments

The authors extend their appreciation to the Deputyship for Research & Innovation, Ministry of Education in Saudi Arabia for funding this research work through the project number RI-44-0618.

Conflict of interest

The authors declare that the research was conducted in the absence of any commercial or financial relationships that could be construed as a potential conflict of interest.

Publisher's note

Supplementary material

The Supplementary Material for this article can be found online at: https://www.frontiersin.org/articles/10.3389/fpls.2024.1355941/full#supplementary-material

References

Albattah, W., Nawaz, M., Javed, A., Masood, M., and Albahli, S. (2022). A novel deep learning method for detection and classification of plant diseases. *Complex Intelligent Syst.*, 1–18. doi: 10.1007/s40747-021-00536-1

Arathi, B., and Dulhare, U. N. (2023). "Classification of cotton leaf diseases using transfer learning-denseNet-121," in *Proceedings of Third International Conference on Advances in Computer Engineering and Communication Systems: ICACECS 2022*. (Hyderabad, India) 393–405.

Attallah, O. (2023). Tomato leaf disease classification via compact convolutional neural networks with transfer learning and feature selection. *Horticulture* 9, 149. doi: 10.3390/horticulturae9020149

Bin Naeem, A., Senapati, B., Chauhan, A. S., Kumar, S., Gavilan, J. C. O., and Abdel-Rehim, W. M. F. (2023). Deep learning models for cotton leaf disease detection with VGG-16. *Int. J. Intelligent Syst. Appl. Eng.* 11, 550–556.

Chen, Y., and Wu, Q. (2023). Grape leaf disease identification with sparse data via generative adversarial networks and convolutional neural networks. *Precis Agric.* 24, 235–253. doi: 10.1007/s11119-022-09941-z

Chen, Z., Ruhui, W., Yiyan, L., Chuyu, L., Siyu, C., Zhineng, Y., et al. (2022). Plant disease recognition model based on improved YOLOv5. *Agronomy* 12, 365. doi: 10.3390/agronomy12020365

Chuanlei, Z., Shanwen, Z., Jucheng, Y., Yancui, S., and Jia, C. (2017). Apple leaf disease identification using genetic algorithm and correlation-based feature selection method. *Int. J. Agric. Biol. Eng.* 10, 74–83.

Dhinesh, E., Jagan, A., et al. (2019). "Detection of leaf disease using principal component analysis and linear support vector machine," in *2019 11th International Conference on Advanced Computing (ICoAC)*. (Chennai, India) 350–355.

Eunice, J., Popescu, D. E., Chowdary, M. K., and Hemanth, J. (2022). Deep learning-based leaf disease detection in crops using images for agricultural applications. *Agronomy* 12, 2395.

Hassan, S. M., Maji, A. K., Jasiński, M., Leonowicz, Z., and Jasińska, E. (2021). Identification of plant-leaf diseases using CNN and transfer-learning approach. *Electron. (Basel)* 10, 1388. doi: 10.3390/electronics10121388

Jasim, M. A., and Al-Tuwaijari, J. M. (2020). "Plant leaf diseases detection and classification using image processing and deep learning techniques," in *2020 International Conference on Computer Science and Software Engineering (CSASE)*. (Duhok, Iraq) 259–265.

Javidan, S. M., Banakar, A., Vakilian, K. A., and Ampatzidis, Y. (2023). Diagnosis of grape leaf diseases using automatic K-means clustering and machine learning. *Smart Agric. Technol.* 3, 100081. doi: 10.1016/j.atech.2022.100081

Kaur, P., Shilpi, H., Rajeev, T., Shuchi, U., Surbhi, B., Arwa, M., et al. (2022). Recognition of leaf disease using the hybrid convolutional neural network by applying feature reduction. *Sensors* 22, 575. doi: 10.3390/s22020575

Liu, G., Peng, J., and El-Latif, A. A. A. (2023). SK-mobileNet: A lightweight adaptive network based on complex deep transfer learning for plant disease recognition. *Arab J. Sci. Eng.* 48, 1661–1675. doi: 10.1007/s13369-022-06987-z

Liu, J., and Wang, X. (2021). Plant diseases and pests detection based on deep learning: a review. *Plant Methods* 17, 1–18. doi: 10.1186/s13007-021-00722-9

Mitra, D. (2021). Emerging plant diseases: research status and challenges. *Emerging Trends Plant Pathol.* 1–17.

Mustafa, M. S., Husin, Z., Tan, W. K., Mavi, M. F., and Farook, R. S. M. (2020). Development of an automated hybrid intelligent system for herbs plant classification and early herbs plant disease detection. *Neural Comput. Appl.* 32, 11419–11441. doi: 10.1007/s00521-019-04634-7

Peng, Y., and Wang, Y. (2022). Leaf disease image retrieval with object detection and deep metric learning. *Front. Plant Sci.* 13, 963302. doi: 10.3389/fpls.2022.963302

Perveen, K., Sanjay, K., Sahil, K., Mukesh, S., Najla, A. A., Shanzeh, B., et al. (2023). Multidimensional attention-based CNN model for identifying apple leaf disease. *J. Food Qual* 2023, 1–12. doi: 10.1155/2023/9504186

Rahman, S. U., Alam, F., Ahmad, N., and Arshad, S. (2023). Image processing based system for the detection, identification and treatment of tomato leaf diseases. *Multimed Tools Appl.* 82, 9431–9445. doi: 10.1007/s11042-022-13715-0

Roy, A. M., and Bhaduri, J. (2021). A deep learning enabled multi-class plant disease detection model based on computer vision. *Ai* 2, 413–428. doi: 10.3390/ai2030026

Sangeetha, K., Rima, P., Kumar, P., and Preethees, S. (2022). "Apple leaf disease detection using deep learning," in *2022 6th International Conference on Computing Methodologies and Communication (ICCMC)*. (Erode, India) 1063–1067.

Sanida, M. V., Sanida, T., Sideris, A., and Dasygenis, M. (2023). An efficient hybrid CNN classification model for tomato crop disease. *Technol. (Basel)* 11, 10. doi: 10.3390/technologies11010010

Sharma, R. P., Dharavath, R., and Edla, D. R. (2023). IoFT-FIS: Internet of farm things based prediction for crop pest infestation using optimized fuzzy inference system. *Internet Things* 21, 100658. doi: 10.1007/978-3-031-33808-3

Singh, M. K., Chetia, S., and Singh, M. (2017). Detection and classification of plant leaf diseases in image processing using MATLAB. *Int. J. Life Sci. Res.* 5, 120–124.

Soeb, M. J. A., Fahad, J., Tahmina, A., Muhammad, R., Fahim, M., Aney, P., et al. (2023). Tea leaf disease detection and identification based on YOLOv7 (YOLO-T). *Sci. Rep.* 13, 6078, 2023. doi: 10.1038/s41598-023-33270-4

Taheri-Garavand, A., Nasiri, A., Fanourakis, D., Fatahi, S., Omid, M., and Nikoloudakis, N. (2021). Automated in situ seed variety identification via deep learning: a case study in chickpea. *Plants* 10, 1406. doi: 10.3390/plants10071406

Terentev, A., Vladimir, B., Ekaterina, S., Dmitriy, E., Danila, E., Dmitriy, K., et al. (2023). Hyperspectral remote sensing for early detection of wheat leaf rust caused by puccinia triticina. *Agriculture* 13, 1186. doi: 10.3390/agriculture13061186

Thangavel, K. D., Seerengasamy, U., Palaniappan, S., and Sekar, R. (2023). Prediction of factors for Controlling of Green House Farming with Fuzzy based multi-class Support Vector Machine. *Alexandria Eng. J.* 62, 279–289.

Vengaiah, C., and Konda, S. R. (2023). Improving tomato leaf disease detection with denseNet-121 architecture. *Int. J. Intelligent Syst. Appl. Eng.* 11, 442–448.

Wang, J., Yu, L., Yang, J., and Dong, H. (2021). Dba_ssd: A novel end-to-end object detection algorithm applied to plant disease detection. *Information* 12, 474. doi: 10.3390/info12110474

Xinming, W., and Tang, S. (2023). Comparative study on Leaf disease identification using Yolo v4 and Yolo v7 algorithm. *AgBioForum*, 25, 1.

Xu, L., Cao, B., Ning, S., Zhang, W., and Zhao, F. (2023). Peanut leaf disease identification with deep learning algorithms. *Mol. Breed.* 43, 25. doi: 10.1007/s11032-023-01370-8

frontiers | Frontiers in Plant Science

TYPE Original Research
PUBLISHED 06 June 2024
DOI 10.3389/fpls.2024.1330219

OPEN ACCESS

EDITED BY
Brigitte Mauch-Mani,
Université de Neuchâtel, Switzerland

REVIEWED BY
Liying Sun,
Northwest A&F University, China
Katarzyna Otulak-Koziel,
Warsaw University of Life Sciences, Poland
Marcio Sanches,
Brazilian Agricultural Research Corporation (EMBRAPA), Brazil

*CORRESPONDENCE
Liping Ban
liping_ban@163.com

RECEIVED 30 October 2023
ACCEPTED 21 May 2024
PUBLISHED 06 June 2024

CITATION
Li J, Shang Q, Luo Y, Wei S, Zhao C and Ban L (2024) Transmission from seed to seedling and elimination of alfalfa viruses.
Front. Plant Sci. 15:1330219.
doi: 10.3389/fpls.2024.1330219

Transmission from seed to seedling and elimination of alfalfa viruses

Jin Li[1,2], Qiaoxia Shang[3,4], Yingning Luo[1], Shuhua Wei[5], Chaoyang Zhao[6] and Liping Ban[1]*

[1]College of Grassland Science and Technology, China Agricultural University, Beijing, China, [2]Sanya Institute, China Agricultural University, Sanya, China, [3]College of Bioscience and Resource Environment, Beijing University of Agriculture, Beijing, China, [4]Key Laboratory of Urban Agriculture in North China, Ministry of Agriculture and Rural Affairs, Beijing University of Agriculture, Beijing, China, [5]Institute of Plant Protection, Ningxia Academy of Agriculture and Forestry Sciences, Yinchuan, China, [6]Center for Medical, Agricultural and Veterinary Entomology, United States Department of Agriculture- Agricultural Research Service (USDA-ARS), Gainesville, FL, United States

Introduction: Viral diseases have become a vital factor limiting the development of the alfalfa (*Medicago sativa*) industry. Six viruses infecting alfalfa with a high incidence rate are Alfalfa mosaic virus (AMV), Medicago sativa alphapartitivirus 1 (MsAPV1), Medicago sativa alphapartitivirus 2 (MsAPV2), Medicago sativa deltapartitivirus 1 (MsDPV1), Medicago sativa amalgavirus 1 (MsAV1), and Cnidium vein yellowing virus 1 (CnVYV1). The purpose of this study was to develop preventive measures against these viruses by investigating their transmission through alfalfa seeds.

Methods: In this study, we investigated the transmission rate of alfalfa viruses from seed to seedling by PCR, determined the location of viruses in seed by dissecting seed embryos and seed coat, tracked the changes of viruses in seedlings, and finally discover effective elimination measures for alfalfa viruses from 16 measures.

Results and discussion: Our results demonstrated that all these six viruses could be transmitted from alfalfa seeds to seedlings with the transmission rate ranging from 44.44% to 88.89%. For AMV, MsAPV2, and MsAV1, the viral load was significantly higher in the seed coats than in the seed embryos; however, it did not show significant differences between these two parts of the seeds for MsAPV1, MsDPV1, and CnVYV1. Dynamic accumulation analysis of AMV and MsAPV2 indicated that the viral load in plants increased continuously in the early growth stage, making it important to inactivate these viruses prior to their seed-to-seedling transmission. Sixteen treatments including physical, chemical, and combinations of physical and chemical measures were compared in terms of their elimination efficiency on AMV and MsAPV2 and impacts on seed germination. The results showed that soaking alfalfa seeds in sterile distilled water for 2h + 2% NaClO for 1h or 2% NaClO for 1h were more promisingly applicable because it could significantly reduce AMV and MsAPV2 particles in both seeds and seedlings. Our data revealed a route of virus transmission in alfalfa and shed light on the discovery of a highly efficient method for the management of alfalfa viral diseases.

KEYWORDS

alfalfa viruses, transmission from seed to seedling, alfalfa mosaic virus (AMV), Medicago sativa alphapartitivirus 2 (MsAPV2), viruses elimination

1 Introduction

Viral diseases are one of the most significant biological threats to alfalfa (*Medicago sativa*). Currently, more than 50 viral species have been reported that can infect alfalfa, causing severe symptoms such as enation, streak, yellowing, and mosaic, and inhibiting the normal growth and development of the alfalfa (Han et al., 2019; Jiang et al., 2019; Li et al., 2021; Guo et al., 2022; Li et al., 2022). Viral diseases have become a vital factor hindering the development of the alfalfa industry. Seeds are an important source for dissemination of plant diseases, and provide an route for virus infection in plants at their early stage (Ban et al., 2021). Also, seeds may serve as the initially infected source for plant viruses to be further transmitted to other plants through insect vectors (Li et al., 2021; Liu et al., 2021; McNeill et al., 2021), resulting in the rapid epidemic of viral diseases in the field.

At present, twenty-one species of alfalfa viruses have been detected in China (Guo et al., 2022; Li et al., 2022). In our previous study, we found six viruses with a high incidence rate and virus loads in alfalfa were alfalfa mosaic virus (AMV), Medicago sativa alphapartitivirus 1 (MsAPV1), Medicago sativa alphapartitivirus 2 (MsAPV2), Medicago sativa deltapartitivirus 1 (MsDPV1), Medicago sativa amalgavirus 1 (MsAV1), and cnidium vein yellowing virus 1 (CnVYV1) (Li et al., 2022). As a worldwide spread vital alfalfa virus that has drawn extensive attention, AMV may cause alfalfa biomass loss by up to 30% (Han et al., 2019). AMV particles are attached to the seed coats in a stable form, highly resistant to potential damages caused by storage temperature and location changes (Frosheiser, 1964, Frosheiser, 1974). By contrast, the other five viruses, MsAPV1, MsAPV2, MsDPV1, MsAV1, and CnVYV1, were recently detected in the main alfalfa cultivation region in China (Li et al., 2022), but whether and how they were transmitted by seeds remained to be investigated. Moreover, virus accumulation in plants and the dynamic process vary among different viral species (Ryabinina et al., 2020; Xu et al., 2023). Exploring the dynamics and understanding the virus replication process in the early stage of plant development may provide insights into early virus diagnosis and viral disease management.

Effective management of viral diseases in plants relies on the prevention of virus spread given that little can be done to restore the health of plants once they are infected by viruses. For seed-borne plant viruses, prevention of their spreading includes the removal of infection sources by virus elimination in seeds. For example, seeds may be treated with dry heat or microwave, or soaked in a solution of trisodium phosphate (Na_3PO_4), hydrochloric acid (HCl), or sodium hypochlorite (NaClO) (Herrera-Vásquez et al., 2009; Ren et al., 2017; Davino et al., 2020; Samarah et al., 2021). Viruses attached to seed surfaces could be eradicated or inactivated markedly with these protocols, which are economical and effective ways to reduce viral infections. Studies have shown that Melon necrotic spot virus (MNSV) could be eradicated from melon seeds after 144h of heat treatment at 70°C (Herrera-Vásquez et al., 2009), and that heat treatment was also effective to eradicate simultaneously three main viruses, Cucumber mosaic virus (CMV), Watermelon mosaic virus (WMV), and Zucchini yellow mosaic virus (ZYMV), that co-parasite in zucchini seeds (Ren et al., 2017). Treating alfalfa seeds using 2000 mg/L of calcium hypochlorite or aqueous ozone has been shown to be effective, with an inactivation efficiency ranging from 66.03% to 82.78%, to decontaminate human viruses such as Human norovirus, Murine norovirus, and Tulane virus, all of which can cause human gastroenteritis (Qing and Kalmia, 2014; Wang et al., 2015).

In spite of numerous studies on treating seeds for virus elimination, little has been known regarding elimination against plant viruses on alfalfa seeds. Therefore, in this study, we set forth to investigate the transmission of six important alfalfa viruses via seeds and discover effective elimination measures for the control of these viral diseases on alfalfa seeds.

2 Materials and methods

2.1 Plant materials

The twelve alfalfa cultivars widely cultivated throughout China and analyzed in this study were “Caribou”, “Sanditi”, “Zhongmu No.1”, “Zhongmu No.2”, “Gannong No.3”, “Gannong No.5”, “Zhaodong”, “Juneng 601”, “WL343HQ”, “310SC”, “42IQ”, and “4030”. The seeds of these varieties are further used to extract seed total RNA, as well as to detect the six alfalfa viruses in seeds. Nine replicates per cultivar, each replicate consisting of ten randomly selected seeds, were used for virus load detection.

2.2 Seed dissection

Prior to separating seed coats from embryos, the seeds were soaked in sterile, deionized water for four hours. To prevent cross-contamination of viruses between different tissues, the tweezers used to handle the seeds were sterilized by 75% ethanol spraying and burning. The seed coats and embryos after dissection are further used to extract total RNA and to detect the six alfalfa viruses loads. Each replicate of sample consisted of twenty seed coats or embryos, and five replicates were prepared for each sample.

2.3 Seed germination

The alfalfa seeds cv. “Zhongmu No.1” was soaked in sterile deionized water for four hours, then transferred on moist filter paper in 150mm Petri dishes, which were then placed in a growth chamber (Ningbo Jiangnan Instrument Factory, Zhejiang, China) at a temperature of 26°C and a humidity of 60%. To evaluate virus transmission via seeds, seedlings were collected for virus quantification on day seven post-germination. This test comprised a total of 90 seedlings, with ten seedlings per replicate for a total of nine replicates.

To determine the germination energy and germination rate which were both used to characterizing seed germination, the progress of the germinated seeds during the germination process was observed and recorded daily. Fifty seeds were placed in a Petri

dish for germination, which was repeated three times. Germination energy used to determine the germination speed was calculated as the number of seeds that germinated within the first four days divided by the total number of seeds. The germination rate was calculated as the number of seeds that germinated within the first seven days divided by the total number of seeds (Xiang et al., 2022).

2.4 Dynamic of viral load accumulation

To investigate the dynamic changes in the loads of AMV and MsAPV2, seeds of alfalfa cv. "Zhongmu No.1" was planted individually in a 10 cm x 10 cm pot filled with sterile nutrient substrates. The pots were then placed in a growth chamber with a photoperiod of 14 hours of light and an air temperature of 26°C. Leaves from germinated seedlings were harvested every three days for five weeks, starting when the second leaves appeared. Each replicate consisted of leaves collected from five plants with five replicates prepared. The collected leaves were stored at -80°C for RNA extraction.

2.5 Comparison of viruses elimination protocols in seeds

The seeds of alfalfa cv. "Zhongmu No.1" were treated using 16 different treatments (Table 1) to compare their efficacy of disinfecting AMV and MsAPV2. These treatments included nine physical-based treatment, four chemical-based treatment, and three combined physical and chemical treatments (Table 1). Untreated seeds were used as control. For each treatment experiment, a seed batch of 300 seeds was used.

2.5.1 Physical-based treatment on alfalfa seeds

Seeds submerged in sterile distilled water for 2h (T1), seeds submerged in 60°C sterile distilled water for 2h (T2), and microwave at 600W for 1min (T3) were used separately on alfalfa seeds. Six different thermal-based treatments were applied on alfalfa seeds, according to the protocols: seeds heated at 70°C for 24 h (T4), 48h (T5), 72h (T6); seeds heated 80°C for 24 h (T7), 48h (T8), 72h (T9) (Córdoba-Sellés et al., 2007; Herrera-Vásquez et al., 2009; Davino et al., 2020; Samarah et al., 2021).

2.5.2 Chemical-based treatment on alfalfa seeds

Four different chemical-based treatments were tested to evaluate the possibility of eradicating viruses from seeds, according to the following protocols: seeds submerged in 10% trisodium phosphate solution (Na_3PO_4) for 4h (T10), seeds submerged in 75% ethanol solution for 1h (T11), seeds submerged in 2% hydrochloric acid (HCl) for 1h (T12), seeds submerged in 2% sodium hypochlorite (NaClO) for 1h (T13) (Herrera-Vásquez et al., 2009; Davino et al., 2020; Samarah et al., 2021). At the end of each treatment the seeds were washed three times for 5 min with sterile distilled water and dried on sterile absorbent paper.

TABLE 1 Sixteen seed elimination treatments (T1-T16).

No.	Treatment
Physical Only	
T1	Sterile distilled water for 2h
T2	60°C water for 1h
T3	Microwave at 600W for 1min
T4	Dry heat at 70°C for 24 h
T5	Dry heat at 70°C for 48 h
T6	Dry heat at 70°C for 72 h
T7	Dry heat at 80°C for 24 h
T8	Dry heat at 80°C for 48 h
T9	Dry heat at 80°C for 72 h
Chemical Only	
T10	10% Na_3PO_4 for 4h
T11	75% Ethanol solution for 1h
T12	2% HCl for 1h
T13	2% NaClO for 1h
Physical and Chemical	
T14	Sterile distilled water for 2h +10% Na_3PO_4 for 1h
T15	Sterile distilled water for 2h + 2% HCl for 1h
T16	Sterile distilled water for 2h + 2% NaClO for 1h

2.5.3 Combined physical and chemical treatments

Three different combined physical and chemical treatments were applied on seeds, according to the following protocols: seeds submerged in sterile distilled water for 2h + 10% Na_3PO_4 for 1h (T14), seeds submerged in sterile distilled water for 2h + 2% HCl for 1h (T15), seeds submerged in sterile distilled water for 2h + 2% NaClO for 1h (T16).

When dealing with treatments that require soaking, for each replicate of the treatment, seeds were immersed in 45 ml of the treatment solution in a 50-ml beaker and placed on a horizontal shaker (Huxi, Shanghai, China) for slow agitation at a speed of 150 rpm/min for the specified treatment durations. After immersion, seeds were rinsed and air-dried to their original moisture content on filter papers at ambient room conditions (25 ± 3°C) for 3 days.

The treated and untreated seeds were pre-germinated in Petri dishes on moist tissue paper at 26°C after the different treatments to understand if each treatment affects seed germination, in terms of percentage and time. Treated seeds and the seedlings germinated from treated seeds were then subject to virus quantification using qRT-PCR. Seed germination experiments were also performed as described in *2.3*. We conducted three times of elimination for each protocol, with each time including five replicates and each replicate consisting of 10 seeds or seedlings. Seeds or seedlings were ground individually in liquid nitrogen in 2 ml microcentrifuge tubes with a

5mm diameter and two 3mm diameter zirconia beads using a grinding machine (FOCUCY, Hunan, China).

2.6 RNA extraction and virus detection

Total RNA was extracted from the whole seeds, seed coats, or embryos following Chang's protocol (Chang et al., 1993) using TRIzol Reagent (Invitrogen, Carlsbad, CA, USA). Then, 1 μg of RNA was reverse transcribed to cDNA using the PrimeScript RT reagent Kit including a gDNA Eraser treatment (TaKaRa, Dalian, China) according to the manufacturer's instructions.

The qRT-PCR analysis was carried out using GS AntiQ qRT-PCR SYBR Green Master Mix (Genesand, Beijing, China) on the qTOWER3 system (Analytik Jena AG, Jena, Germany). The primers for the viral genes are listed in Supplementary Table 1, and the absolute quantification was measured as described by Li et al. (2022). Each reaction mixture (25 μL) contained 0.5 μL (10 mM) of forward and reverse primers each, 12.5 μL of GS AntiQ qRT-PCR SYBR Green Master Mix (Genesand, China), and 1 μL cDNA (10ng RNA). The PCR conditions were set as 95°C for 5 min, followed by 40 cycles of 95°C for 10 s and 60°C for 30 s. At the end of the reaction, the melting curve of each gene was recorded, and the absolute gene expression was analyzed using the standard curve method based on the geometric mean of threshold cycle (Ct) values. Samples without a Ct value indicated negative qRT-PCR results.

2.7 Statistical analysis

Data were analyzed by analysis of variance (ANOVA) of SPSS Statistics v. 26.0 (IBM, Armonk, NY, USA). Fisher's least significant difference (LSD; $P \leq 0.05$) was calculated to compare means with significant F-test results.

3 Results

3.1 Transmission of viruses from seeds to seedlings

To determine whether the six predominant alfalfa viruses, i.e., AMV, MsAPV2, MsAPV1, MsDPV1, MsAV1 and CnVYV1, could be transmitted via alfalfa seeds, we conducted qRT-PCR analyses on the seeds of 12 alfalfa cultivars commonly grown in China. The results showed that all six viruses were detected in the seeds of at least eight alfalfa cultivars (Figure 1). All 12 cultivars were found to be positive for AMV and MsAPV2, which had higher viral accumulation than the other four viruses in the seeds of ten cultivars except the low amounts of AMV in the cultivars "Juneng 601" and "Zhongmu No. 2" (Figure 1). In this test, CnVYV1 was not detected in three cultivars ("310SC", "WL343HQ", and "Gannong No.5"), and neither was MsAV1 in "Zhaodong" (Figure 1).

To further determine whether these viruses could be transmitted from seeds to seedlings, we quantified these viruses in

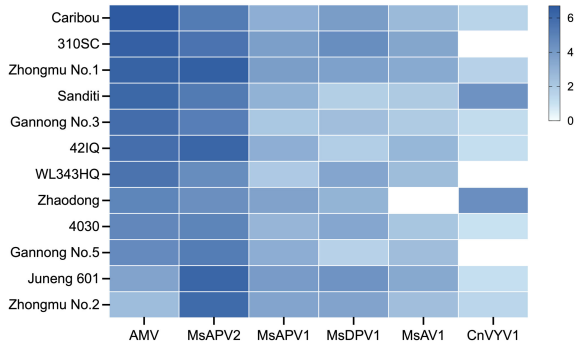

FIGURE 1
Heat map of the absolute amounts of six viruses detected in the seeds of 12 alfalfa cultivars. Virus copies were quantified by qRT-PCR. The logarithm of detected virus copies to base 10 is color coded according to the scale as shown. To ensure the representation of all samples, a value of 0.01 was assigned as the Ct value for the samples with no virus detected.

the seven-day-old alfalfa seedlings (*cv*. "Zhongmu No.1") germinated from virus-carrying seeds by qRT-PCR and found that all six viruses were present in seedlings in spite that their copy numbers varied (Table 2; Supplementary Figure 1). Among these viruses, MsAPV2 was detected in 88.89% of seedlings, followed by AMV which was detected in 77.78% of seedlings. MsAPV1, MsDPV1, MsAV1, and CnVYV1 were found in 44.44%, 55.56%, 66.67%, and 66.67% of seedlings, respectively (Table 2; Supplementary Figure 1). We also found that the copy number of AMV in seedlings (3.75×10^2 copies) was significantly lower (~ 5,000 times) than in seeds (2.04×10^6 copies). On the other hand, MsAPV2 and CnVYV1 had significantly higher copy numbers in seedlings (4.73×10^7 copies for MsAPV2, and 6.23×10^2 copies for CnVYV1) than in seeds (2.89×10^6 copies for MsAPV2, and 4.19×10^1 copies for CnVYV1), while MsAPV1, MsDPV1, and MsAV1 had almost the same (no significance) number of viruses in seeds and seedlings (Table 2). These results indicated that alfalfa seeds may serve as a source for the six alfalfa viruses' transmission to seedings, however, the transmission rate may vary in different viruses.

3.2 Distribution of viruses in seed tissues

To understand how the six viruses were transmitted from seeds to seedlings, we aimed to discover which part of the seeds, the external (seed coats) or internal part (embryos), carried the viruses. All six viruses were detected in both parts of the seeds, however, their quantities differed (Figure 2). For AMV, MsAPV2, and MsAV1 (Figure 2), viral accumulation in seed coats was significantly higher than in embryos. It is worth noting that AMV in seed coats was 9209.27 times of the amount in embryos, however, MsAPV2 and MsAV1 in seed coats were only 19.24 and 5.48 times the amounts in embryos, respectively. No significant differences in virus amounts were found between coats and embryos for MsAPV1, MsDPV1, and CnVYV1, although MsAPV1 and CnVYV1

TABLE 2 Virus transmission from seeds to seedlings assessed by qRT-PCR.

Virus species	Seed infection rate (%)	Seed virus accumulation (copies)	Seedling infection rate (%)	Seedling virus accumulation (copies)	Significance
AMV	100	$2.04\times10^{6}\pm 4.85\times10^{5}$	77.78	$3.75\times10^{2}\pm 1.79\times10^{1}$	**
MsAPV2	100	$2.89\times10^{6}\pm 4.23\times10^{5}$	88.89	$4.73\times10^{7}\pm 3.82\times10^{6}$	**
MsAPV1	100	$6.97\times10^{3}\pm 9.07\times10^{2}$	44.44	$1.05\times10^{4}\pm 6.12\times10^{2}$	ns
MsDPV1	100	$5.00\times10^{3}\pm 4.89\times10^{2}$	55.56	$8.18\times10^{3}\pm 1.08\times10^{3}$	ns
MsAV1	100	$2.01\times10^{3}\pm 2.68\times10^{2}$	66.67	$3.13\times10^{3}\pm 2.66\times10^{2}$	ns
CnVYV1	100	$4.19\times10^{1}\pm 1.02\times10^{1}$	66.67	$6.23\times10^{2}\pm 6.02\times10^{1}$	*

Statistical analysis was based on nine replicates of seeds and seedlings examined. Asterisks indicate significant differences of virus accumulation between seed and seedling (* $p< 0.05$, ** $p< 0.01$, ns: not significant). Data are mean ± SE.

appeared more abundant in coats than in embryos, while MsDPV1 appeared more abundant in embryos than in coats (Figure 2).

3.3 Dynamics of viruses in seedlings

To better understand the dynamic accumulation of viruses in seedlings, we quantified AMV and MsAPV2, the two viruses with the highest seed-to-seedling transmission rates (Table 2), every three days for five weeks, starting from the appearance of the first true leaf. The amount of AMV showed an upward trend at first but a downward trend later (Figure 3A). The initial copy numbers of AMV in seedlings were low (only 74.81 copies), but reached a peak at 8.85×10^{3} copies (with a 117-fold increase) after three weeks, and decreased to 6.69×10^{2} copies on day 34, the last day of virus monitoring. In contrast, MsAPV2 showed an overall upward trend yet with fluctuation during the whole test period (Figure 3B). Its initial detected copy numbers were 5.39×10^{6} copies while reaching the maximum amount of 2.48×10^{7} copies on day 31, a 4.6-fold increase compared to the initial (Figure 3B).

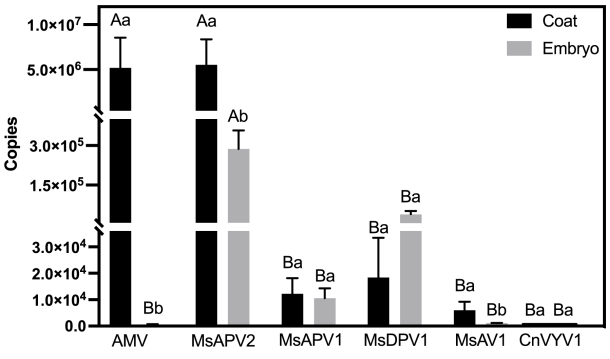

FIGURE 2
Virus titers comparison between the seed coats and embryos of alfalfa cv. "Zhongmu No.1". Bar indicate the SE of virus concentration in four replicates, and letters "(A, B) and (a, b)" marks on the bar indicate significant differences between six treatments of coat and embryo, respectively ($p < 0.05$).

3.4 Elimination efficacy and effect on germination of 16 seed treatments

Based on the high incidence of virus load for AMV and MsAPV2 on alfalfa in the field (Li et al., 2022), we attempted to optimize the elimination protocol for these two viruses in this study. We tested 16 different treatments, namely T1 ~ T16 (Table 1), on alfalfa seeds, and then quantified AMV and MsAPV2 independently in both the treated seeds and the seedlings germinated from the treated seeds.

The results showed that all 16 treatments reduced AMV accumulation in seeds significantly ($p < 0.01$) from 1.89×10^{7} copies (control) to 8.41×10^{4} ~ 5.11×10^{6} copies, with a elimination efficiency of 72.93% ~ 99.55% (Supplementary Figure 2A, Supplementary Table 1). Among these, T7 (Dry heat at 80°C for 24 h), T15 (Sterile distilled water for 2h + 2% HCl for 1h), T13 (2% NaClO for 1h) and T2 (60°C water for 1h) tend to have a higher elimination efficiencies of 99.08%, 99.40%, 99.52%, and 99.55%, respectively (Figure 4A; Supplementary Figure 2A, Supplementary Table 1).

Virus quantification in the seedlings germinated from the treated seeds showed that eight methods significantly decreased ($p < 0.01$) AMV copies in seedlings from 1298.49 to a range of 145.79 ~ 758.06, with elimination efficiencies ranging from 41.62% to 88.77% (Figure 4A). Among these, the four most efficient methods were T10, T16, T13, and T12, with elimination efficiencies of 81.84%, 84.64%, 85.01%, and 88.77%, respectively (Figure 4A; Supplementary Table 1). Interestingly, seven physical methods (T4, T5, T6, T7, T8, T9, and T11) did not reduce AMV copy numbers in seedlings, instead, they increased the latter by 1.43 to 10.45 times (Supplementary Figure 2A, Supplementary Table 1).

Regarding the elimination effect on MsAPV2, all 16 protocols significantly ($p < 0.01$) decreased MsAPV2 accumulation in seeds from 3.6×10^{7} copies (control) to 2.78×10^{5} ~ 6.54×10^{6} copies, with elimination efficiencies ranging from 81.84% to 99.23% (Figure 4B. Supplementary Figure 2B, Supplementary Table 1). Fifteen protocols except T3 were also able to decrease MsAPV2 accumulation in the seedlings germinated from the treated seeds significantly ($p < 0.01$), from 8.88×10^{7} (control) to a range of 2.40×10^{6} ~ 4.32×10^{7} copies, with elimination efficiencies of

10.3389/fpls.2024.1330219

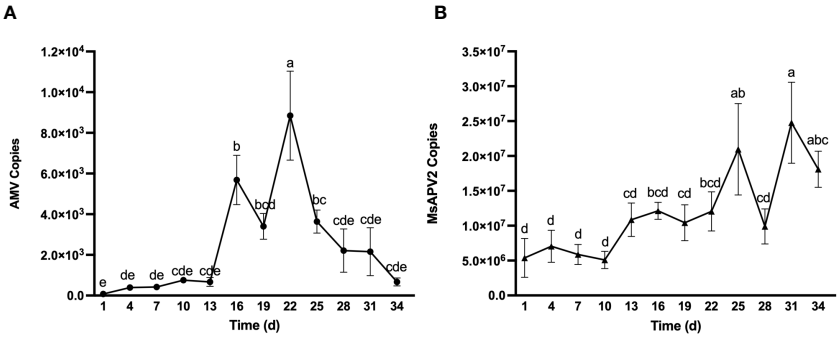

FIGURE 3
Dynamic accumulation of AMV **(A)** and MsAPV2 **(B)** in seedlings. Sampling time (X-axis) started from Day 1 when the first true leaves were unfolded. Different letters on top of error bars indicate significant ($p < 0.5$) differences of virus copy numbers.

48.28% ~ 97.30% (Figure 4B; Supplementary Figure 2B, Supplementary Table 1). The six more efficient methods (elimination efficiency > 90%) were T10, T16, T5, T9, T8, and T13, which had elimination efficiencies of 97.30%, 93.72%, 92.02%, 91.85%, 91.77%, and 91.55%, respectively (Figure 4B; Supplementary Table 1).

We also assessed the treatment effects on alfalfa seed germination rate and found that eleven out of sixteen methods had no significant impact on germination energy or rate compared to the control (CK). However, three methods (T10, T14, and T15) decreased the germination rate significantly ($p < 0.05$), and two

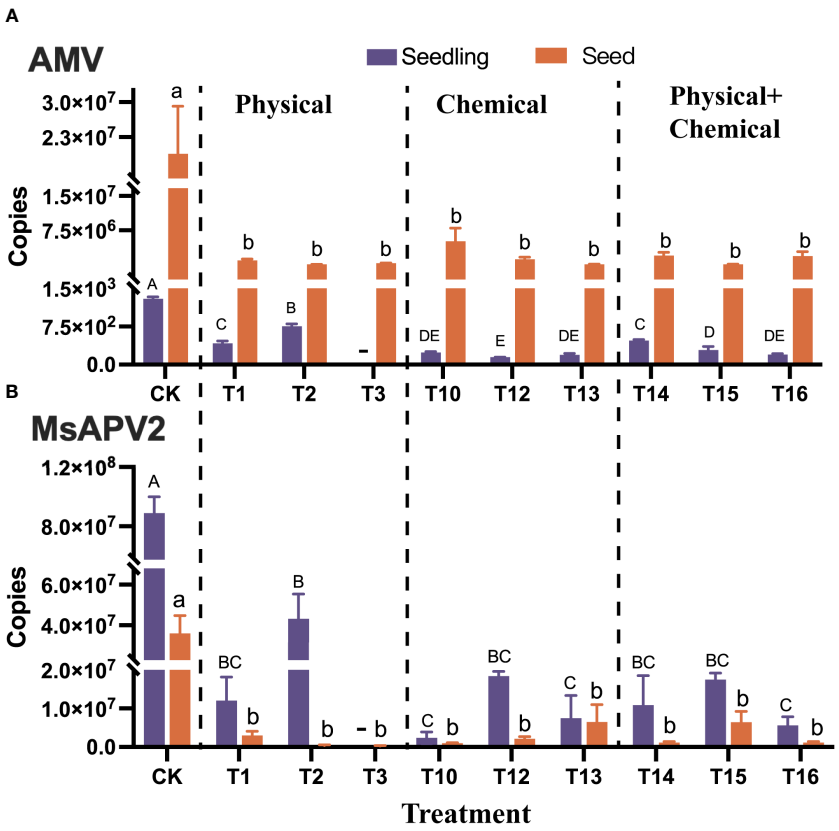

FIGURE 4
Elimination of AMV **(A)** and MsAPV2 **(B)** from alfalfa seeds using nine different treatments (T1-T3, T10, T12-T16, refer to Table 2 for details) which effectively eliminated the viruses from alfalfa seeds and seedlings. Detected virus copies in the seedlings germinated from the treated seeds and in the treated seeds are shown on the left and right, respectively. Different uppercase or lowercase letters next to error bars indicate significant ($p < 0.05$) differences in viruses in seedling or seeds, respectively. "-" indicated the data unavailable in this treatment.

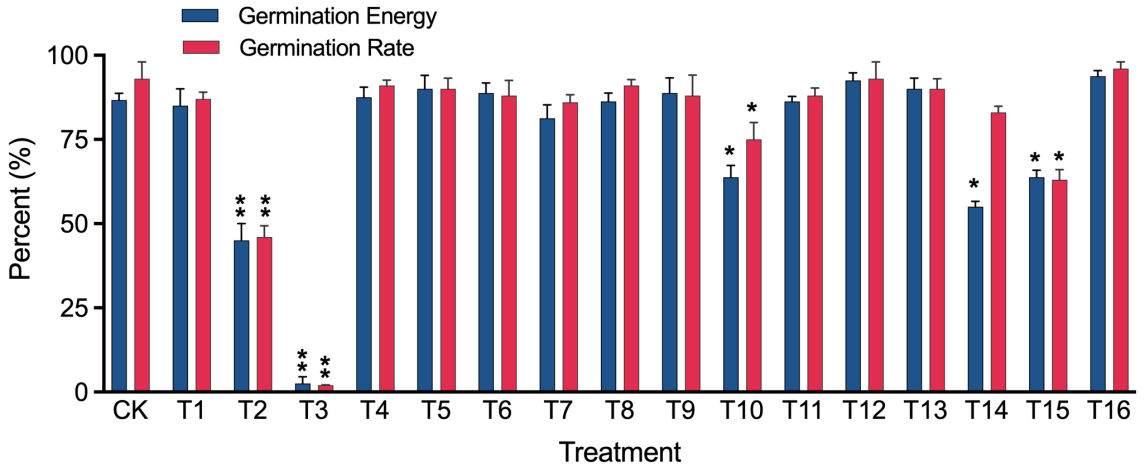

FIGURE 5
Germination energy and germination rate of alfalfa cv. "Zhongmu No.1" seeds disinfected using 16 different treatments (T1-T16, refer to Table 2 for details). Significant ($p < 0.05$) and extremely significant ($p < 0.01$) differences from the untreated seeds (CK) are indicated by single and double asterisks, respectively, shown on top of error bars.

methods (T2 and T3) decreased the germination rate extremely significantly ($p < 0.01$) (Figure 5).

4 Discussion

Seed transmission is one of the vital routes for viruses to infect their host plants, and more than 20 viral species have been found to infect alfalfa in China (Guo et al., 2022; Li et al., 2022). However, the distribution and transmission of these viruses via seeds have been rarely reported. To understand the prevalence and distribution of these viruses and select local disease-resistant/tolerant alfalfa cultivars, it is important to understand whether seeds serve as a transmission route for these viruses. This study found that all six main alfalfa viruses investigated were seed-borne viruses. We also compared 16 seed elimination protocols regarding their virus elimination efficiency and effect on seed germination for the selection of an effective protocol that can be field applied.

By performing qRT-PCR analyses, we found that the rate of AMV transmission from seeds to seedlings in alfalfa was 77.78% (Table 2), which was much higher than a previously reported rate (< 10%) (Frosheiser, 1964). This difference could be owing to a higher seed viral survival rate and seed transmission rate today resulting from the increase in temperature and light intensity caused by global warming (Roossinck, 2015; Bueso et al., 2017; Pagán, 2022). It is also likely owing to the highly improved sensitivity by using qRT-PCR in our work for virus detection and quantification – studies have shown that qRT-PCR is 100 ~ 1,000 times more sensitive than traditional virus quantification treatments (Torre et al., 2020; Li et al., 2022). Alternatively, there is the possibility that alfalfa cultivar may affect the seed transmission rate of the virus, such as 2.1% for alfalfa cv. Vernal and 0.8% for cv. California Common (Frosheiser, 1974). Of course, the strain of virus also affects its ability to spread (Klose et al., 1996).

Distribution analysis demonstrated that AMV copy numbers in seed coats (> 99%) were 9209.27 times of those in seed embryos (< 1%) (Figure 2), in alignment with a previous report which also showed that AMV was more frequently detected in seed coats than in embryos (Pesic and Hiruki, 1986). This might account for its low seed-to-seedling transmission rate because viruses on seed coats tend to be transmitted to seedlings passively through mechanical abrasion (Broadbent, 1965; Johansen et al., 1994) and become less active during the process of plant development (Johansen et al., 1994). In contrast, MsAPV2, which had a similar total quantity of virus copies in seeds (2.89×10^6 copies, including those in both coats and embryos) as AMV (2.04×10^6 copies) but appeared to be more enriched in embryos (2.87×10^5 copies) than AMV (5.62×10^2 copies), was also more abundantly detected in seedlings (4.73×10^7 copies) than the latter (3.75×10^2 copies). This further supports that seed embryos, rather than seed coats, may play an important role in the transmission of plant viruses from seeds to seedlings. Previous studies have demonstrated that virus-infected seed embryos could produce diseased seedlings (Uyemoto and Grogan, 1977; Wang and Maule, 1992), and seed embryos may serve as a main route of seed-to-seedling transmission because viruses that invade/infect embryos can proragate actively via replication with the development of plants from seeds to seedlings (Johansen et al., 1994).

In this study, we report for the first time that five alfalfa viruses (MsAPV2, MsAPV1, MsDPV1, MsAV1, and CnVYV1) can be transmitted from seeds to seedlings and found that their transmission rates were relatively high (44.44% ~ 88.89%). There is also a shortcoming in our study, that is, we only studied the transmission rate of the virus from seed to seedling in the market, not maternal transmission. Some of the viruses we studied have reported maternal transmission rates in the same family. The viruses of Partiviridae and Amalgavirdae are unlikely to be transmitted by vectors due to the absence of movement proteins, therefore, their spread among plants mainly relied on pollens or seeds, a means with a relatively high transmission rate (Nibert et al., 2014). For example, white clover cryptic virus-1 (WCCV-1) of

Partitiviridae had a transmission rate of 48% (Guy and Gerard, 2016), and southern tomato virus (STV) and blueberry latent virus (BBLV) of Amalgavirdae had the transmission rate of 86% and 100%, respectively (Fukuhara et al., 2020; Martin et al., 2011). Unlike Partiviridae and Amalgavirdae viruses, Secoviridae viruses could be transmitted in a variety of ways, by seeds, pollens, and arthropod vectors, with varying transmission rates (Thompson et al., 2017). However, The exact maternal transmission rates of these viruses we studied is still uncertain and remains to be investigated.

We also observed that AMV and MsAPV2 demonstrated distinct dynamic accumulation patterns in alfalfa seedlings. AMV accumulation accelerated in the first three weeks of monitoring but dropped afterward until the end of observation (Figure 3), a pattern like the accumulation of tomato spotted wilt virus (TSWV) in infected pepper plants (Xu et al., 2023). TSWV accumulation was reported to display an increasing trend until reaching its peak at the end of the second week after inoculation, approximately 50 times higher than the amount detected on the first day, and then decrease in the following three weeks (Xu et al., 2023). This suggested that early diagnosis and elimination of plant viruses is critical for the management of these viral diseases. The decrease of viral load in plants following an increasing trend might be attributed to the activation of plant immune mechanisms as responses to mitigate viral infection. In contrast, MsAPV2, which was transmitted from seeds to seedlings at a substantial amount, demonstrated an increasing trend of viral accumulation in seedlings until the end of observation (Figure 3), likely as a result of continuous virus replication and accountable for the high prevalence of MsAPV2 in the field (Li et al., 2022). This resembled cucumber green mottle mosaic virus (CGMMV), whose copy numbers on the infected cucumber plants could increase continuously by ten times within five weeks (Ryabinina et al., 2020), suggesting that elimination measures must be taken in the early growth stages of alfalfa to minimize viral load on the plants and prevent MsAPV2 outbreak in the field.

To mitigate and even eradicate the infection of seed-borne viruses in alfalfa, seed treatments shall be conducted using physical and/or chemical treatments for the preparation of virus-free seeds. We compared 16 methods (T1-T16) regarding their efficacy of virus elimination and effects on seed germination and found that both T13 (2% NaClO for 1 h) and T16 (soaking in sterile water for 2h + 2% NaClO for 1h) reduced the load of AMV and MsAPV2 effectively, meanwhile improving seed germination rate, though not significantly. Similar protocols have been successfully employed to eliminate other plant viruses, such as tomato brown rugose fruit virus (TBRFV) and pepino mosaic virus (PepMV), without impairing seed germination (Córdoba-Sellés et al., 2007; Davino et al., 2020; Samarah et al., 2021). Thermal treatment has been used to eliminate viruses such as MNSV (Herrera-Vásquez et al., 2009), CMV, WMV, and ZYMV (Ren et al., 2017) by heating seeds at a minimum of 65°C. In our study, thermal methods (70°C and 80°C) did not reduce AMV copy numbers in seedlings, instead, they increased the latter. These suggested that heat treatment may not be suitable for AMV elimination. It should be noted that all 16 treatments were only able to reduce, but not eradicate AMV and MsAPV2 infection, because these viruses existed not only on the seed coats but also in the embryos (Herrera-Vásquez et al., 2009) and these treatments might only be able to inactivate virus particles attached to the seed coats or embryo surface but not to those that have already infected the embryo tissues inside. Therefore, these methods should be used together with other measures to better control these virus diseases.

Seed trade is becoming more frequent across the globe. The circulation of infected seeds will rapidly increase the spread of the virus in the world. Our study confirmed that six important alfalfa viruses can be transmitted through alfalfa seeds. Therefore, in order to prevent the spread of the virus, virus inspection and quarantine in the importing country and virus elimination in seeds in the exporting country are crucial. Further, in order to more effectively verify the elimination effect in our experiment, field experiments could be used to verify the effect, and then promoted to a larger area.

Data availability statement

The original contributions presented in the study are included in the article/Supplementary Material. Further inquiries can be directed to the corresponding author.

Author contributions

JL: Conceptualization, Formal analysis, Methodology, Writing – original draft, Writing – review & editing. QS: Methodology, Writing – review & editing. YL: Formal analysis, Methodology, Writing – original draft. SW: Formal analysis, Writing – review & editing. CZ: Formal analysis, Writing – review & editing. LB: Conceptualization, Project administration, Writing – original draft, Writing – review & editing.

Funding

The author(s) declare financial support was received for the research, authorship, and/or publication of this article. This research was funded by the Fund of Key Laboratory of Urban Agriculture In North China, Ministry of Agriculture and Rural Affairs, P.R.China, Beijing University of Agriculture, Beijing 102206, P.R. China, grant number kf202401, the Beijing Food Crops Innovation Consortium, grant number BAIC02–2024, the National Natural Science Foundation of China (NSFC), grant number 31971759, and jointly supported by the Ningxia Province Sci-Tech Innovation Demonstration Program of High-Quality Agricultural Development and Ecological Conservation, grant number NGSB-2021–15-04.

Acknowledgments

We are grateful to Professor Xuemin Wang of Institute of Animal Science of Chinese Academy of Agricultural Sciences for her support and provide the alfalfa seeds.

Conflict of interest

The authors declare that the research was conducted in the absence of any commercial or financial relationships that could be construed as a potential conflict of interest.

Publisher's note

All claims expressed in this article are solely those of the authors and do not necessarily represent those of their affiliated organizations, or those of the publisher, the editors and the reviewers. Any product that may be evaluated in this article, or claim that may be made by its manufacturer, is not guaranteed or endorsed by the publisher.

Supplementary material

The Supplementary Material for this article can be found online at: https://www.frontiersin.org/articles/10.3389/fpls.2024.1330219/full#supplementary-material

References

Ban, L., Li, J., Yan, M., Gao, Y., Zhang, J., Moural, T. W., et al. (2021). Illumina sequencing of 18S/16S rRNA reveals microbial community composition, diversity, and potential pathogens in 17 turfgrass seeds. *Plant Dis.* 105, 1328–1338. doi: 10.1094/PDIS-06-18-0946-RE

Broadbent, L. (1965). The epidemiology of tomato mosaic. *Ann. Appl. Biol.* 56, 177–205. doi: 10.1111/j.1744-7348.1965.tb01227.x

Bueso, E., Serrano, R., Pallás, V., and Sánchez-Navarro, J. A. (2017). Seed tolerance to deterioration in arabidopsis is affected by virus infection. *Plant Physiol. Biochem.* 116, 1–8. doi: 10.1016/j.plaphy.2017.04.020

Chang, S., Puryear, J., and Cairney, J. (1993). A simple and efficient method for isolating RNA from pine trees. *Plant Mol. Biol. Rep.* 11, 113–116. doi: 10.1007/BF02670468

Córdoba-Sellés, M., García-Rández, A., Alfaro-Fernández, A., and Jordá-Gutiérrez, C. (2007). Seed transmission of Pepino mosaic virus and efficacy of tomato seed disinfection treatments. *Plant Dis.* 91, 1250–1254. doi: 10.1094/PDIS-91-10-1250

Davino, S., Caruso, A. G., Bertacca, S., Barone, S., and Panno, S. (2020). *Tomato brown rugose fruit virus*: Seed transmission rate and efficacy of different seed disinfection treatments. *Plants* 9, 1615. doi: 10.3390/plants9111615

Frosheiser, F. I. (1964). *Alfalfa mosaic virus* transmitted through alfalfa seed. *Phytopathology* 54, 893.

Frosheiser, F. (1974). *Alfalfa mosaic virus* transmission to seed through alfalfa gametes and longevity in alfalfa seed. *Phytopathology* 64, 102–105. doi: 10.1094/Phyto-64-102

Fukuhara, T., Tabara, M., Koiwa, H., and Takahashi, H. (2020). Effect of asymptomatic infection with aouthern tomato virus on tomato plants. *Arch. Virol.* 165 (1), 11–20. doi: 10.1007/s00705-019-04436-1

Guo, Z., Zhang, T., Chen, Z., Niu, J., Cui, X., Mao, Y., et al. (2022). Occurrence, distribution, and genetic diversity of alfalfa (*Medicago sativa* L.) viruses in four major alfalfa-producing provinces of China. *Front. Microbiol.* 12. doi: 10.3389/fmicb.2021.771361

Guy, P. L., and Gerard, P. J. (2016). White clover cryptic virus 1 in new zealand and eastern australia. *Ann. Appl. Biol.* 168 (2), 225–231. doi: 10.1111/aab.12258

Han, Y., Hu, H., Yu, Y., Zhang, Z., and Fan, Z. (2019). Effects of alfalfa mosaic disease on photosynthetic performance, growth, and forage quality of *Medicago sativa*. *Pratacultural Sci.* 36, 2061–2068. doi: 10.11829/j.issn.1001-0629.2018-0705

Herrera-Vásquez, J. A., Córdoba-Sellés, M. C., Cebrián, M. C., Alfaro-Fernández, A., and Jordá, C. (2009). Seed transmission of Melon necrotic spot virus and efficacy of seed-disinfection treatments. *Plant Pathol.* 58, 436–442. doi: 10.1111/j.1365–3059.2008.01985.x

Jiang, P., Shao, J., and Nemchinov, L. G. (2019). Identification of emerging viral genomes in transcriptomic datasets of alfalfa (*Medicago sativa* L.). *Virol. J.* 16, 153. doi: 10.1186/s12985-019-1257-y

Johansen, E., Edwards, M. C., and Hampton, R. O. (1994). Seed transmission of viruses - current perspectives. *Annu. Rev. Phytopathol.* 32, 363–386. doi: 10.1146/annurev.py.32.090194.002051

Klose, M. J., Sdoodee, R., Teakle, D. S., Milne, J. R., Greber, R. S., and Walter, G. H. (1996). Transmission of three strains of tobacco streak ilarvirus by different thrips species using virus-infected pollen. *J. Phytopathol.* 144, 281–284. doi: 10.1111/j.1439-0434.1996.tb01530.x

Li, J., Gu, H., Liu, Y., Wei, S., Hu, G., Wang, X., et al. (2021). RNA-seq reveals plant virus composition and diversity in alfalfa, thrips, and aphids in Beijing, China. *Arch. Virol.* 166, 1711–1722. doi: 10.1007/s00705-021-05067-1

Li, J., Shang, Q., Liu, Y., Dai, W., Li, X., Wei, S., et al. (2022). Occurrence, distribution, and transmission of alfalfa viruses in China. *Viruses* 14, 1519. doi: 10.3390/v14071519

Liu, Y., Li, J., and Ban, L. (2021). Morphology and distribution of antennal sensilla in three species of Thripidae (Thysanoptera) infesting alfalfa *Medicago sativa*. *Insects* 12, 81. doi: 10.3390/insects12010081

Martin, R. R., Zhou, J., and Tzanetakis, I. E. (2011). Blueberry latent virus: an amalgam of the partitiviridae and totiviridae. *Virus Res.* 155 (1), 175–180. doi: 10.1016/j.virusres.2010.09.020

McNeill, M. R., Tu, X., Ferguson, C. M., Ban, L., Hardwick, S., Rong, Z., et al. (2021). Diversity and impacts of key grassland and forage arthropod pests in China and New Zealand: an overview of IPM and biosecurity opportunities. *NeoBiota* 65, 137–168. doi: 10.3897/neobiota.65.61991

Nibert, M. L., Ghabrial, S. A., Maiss, E., Lesker, T., Vainio, E. J., Jiang, D., et al. (2014). Taxonomic reorganization of family partitiviridae and other recent progress in partitivirus research. *Virus Res.* 188, 128–141. doi: 10.1016/j.virusres.2014.04.007

Pagán, I. (2022). Transmission through seeds: The unknown life of plant viruses. *PLoS Pathog.* 18, e1010707. doi: 10.1371/journal.ppat.1010707

Pesic, Z., and Hiruki, C. (1986). Differences in the incidence of *Alfalfa mosaic virus* in seed coat and embryo of alfalfa seed. *Can. J. Plant Pathol.* 8, 39–42. doi: 10.1080/07060668609501839

Qing, W., and Kalmia, E. K. (2014). Effectiveness of Calcium Hypochlorite on viral and bacterial contamination of alfalfa seeds. *Foodborne Pathog. Dis.* 11, 759–768. doi: 10.1089/fpd.2014.1766

Ren, C., Zhou, D., Dou, Y., and Xiang, B. (2017). Detection of viruses in seeds of seed-zuchini and evaluation of heat treatment on virus elimination. *Plant Prot.* 43, 122–128. doi: 10.3969/j.issn.0529-1542.2017.02.020

Roossinck, M. J. (2015). Plants, viruses and the environment: ecology and mutualism. *Virology* 479–480, 271–277. doi: 10.1016/j.virol.2015.03.041

Ryabinina, V., Pashkovsky, S., Plotnikov, K., and Gordienko, E. (2020). "Dynamics of cucumber green mottle mosaic virus accumulation and its association to the disease manifestation," in *Proceedings of the International Scientific Conference The Fifth Technological Order: Prospects for the Development and Modernization of the Russian Agro-Industrial Sector (TFTS 2019)*. 70–72 (French: Atlantis Press). doi: 10.2991/assehr.k.200113.141

Samarah, N., Sulaiman, A., Salem, N. M., and Turina, M. (2021). Disinfection treatments eliminated *Tomato brown rugose fruit virus* in tomato seeds. *Eur. J. Plant Pathol.* 159, 153–162. doi: 10.1007/s10658-020-02151-1

Thompson, J. R., Dasgupta, I., Fuchs, M., Iwanami, T., Karasev, A. V., Petrzik, K., et al. (2017). ICTV virus taxonomy profile: Secoviridae. *J. Gen. Virol.* 98 (4), 529–531. doi: 10.1099/jgv.0.000779

Torre, C., Agüero, J., Gómez-Aix, C., and Aranda, M. A. (2020). Comparison of DAS-ELISA and qRT-PCR for the detection of cucurbit viruses in seeds. *Ann. Appl. Biol.* 176, 158–169. doi: 10.1111/aab.12543

Uyemoto, J., and Grogan, R. (1977). Southern bean mosaic virus: evidence for seed transmission in bean embryos. *Phytopathology* 67 (10), 1190–1196. doi: 10.1094/Phyto-67-1190

Wang, Q., Markland, S., and Kniel, K. E. (2015). Inactivation of human norovirus and its surrogates on alfalfa seeds by aqueous ozone. *J. Food Prot.* 78, 1586–1591. doi: 10.4315/0362-028X.JFP-15-029

Wang, D., and Maule, A. J. (1992). Early embryo invasion as a determinant in pea of the seed transmission of pea seed-borne mosaic virus. *J. Gen. Virol.* 73 (7), 1615–1620. doi: 10.1099/0022-1317-73-7-1615

Xiang, S., Wang, H., Tian, L., Chen, Y., Sun, W., and Zhou, Q. (2022). Effect of temperature on germination characteristics of different alfalfa varieties. *Grassland Turf* 42, 74–82. doi: 10.13817/j.cnki.cyycp.2022.02.011

Xu, Y., Jia, Z., Gao, X., Chen, Z., Li, Y., and Liu, Y. (2023). Dynamic changes of virus accumulation in pepper infected by *Tomato spotted wilt virus*. *Mol. Plant Breed* 21 (05), 1603–1609. doi: 10.13271/j.mpb.021.001603

frontiers | Frontiers in Plant Science

TYPE Original Research
PUBLISHED 10 July 2024
DOI 10.3389/fpls.2024.1403202

OPEN ACCESS

EDITED BY
Brigitte Mauch-Mani,
Université de Neuchâtel, Switzerland

REVIEWED BY
Susheel Kumar Sharma,
Indian Agricultural Research Institute (ICAR), India
Orlando Borras-Hidalgo,
Qilu University of Technology, China

*CORRESPONDENCE
Pengfei Jin
jinpengfei@hainanu.edu.cn

†These authors have contributed equally to this work

RECEIVED 19 March 2024
ACCEPTED 13 June 2024
PUBLISHED 10 July 2024

CITATION
Xuan Z, Wang Y, Shen Y, Pan X, Wang J, Liu W, Miao W and Jin P (2024) *Bacillus velezensis* HN-2: a potent antiviral agent against pepper veinal mottle virus. *Front. Plant Sci.* 15:1403202. doi: 10.3389/fpls.2024.1403202

Bacillus velezensis HN-2: a potent antiviral agent against pepper veinal mottle virus

Zhe Xuan[1,2†], Yu Wang[1†], Yuying Shen[1†], Xiao Pan[1], Jiatong Wang[1], Wenbo Liu[1], Weiguo Miao[1] and Pengfei Jin[1*]

[1]College of Plant Protection, Hainan University/Key Laboratory of Green Prevention and Control of Tropical Plant Diseases and Pests (Hainan University), Ministry of Education, Haikou, China, [2]School of Life and Health Sciences, Hainan University, Haikou, China

Background: Pepper veinal mottle virus (PVMV) belongs to the genus *Potyvirus* within the family Potyviridae and is a major threat to pepper production, causing reduction in yield and fruit quality; however, efficient pesticides and chemical treatments for plant protection against viral infections are lacking. Hence, there is a critical need to discover highly active and environment-friendly antiviral agents derived from natural sources. *Bacillus* spp. are widely utilized as biocontrol agents to manage fungal, bacterial, and viral plant diseases. Particularly, *Bacillus velezensis* HN-2 exhibits a strong antibiotic activity against plant pathogens and can also induce plant resistance.

Methods: The experimental subjects employed in this study were *Bacillus velezensis* HN-2, benzothiadiazole, and dufulin, aiming to evaluate their impact on antioxidant activity, levels of reactive oxygen species, activity of defense enzymes, and expression of defense-related genes in Nicotiana benthamiana. Furthermore, the colonization ability of *Bacillus velezensis* HN-2 in Capsicum chinense was investigated.

Results: The results of bioassays revealed the robust colonization capability of *Bacillus velezensis* HN-2, particularly in intercellular spaces, leading to delayed infection and enhanced protection against PVMV through multiple plant defense mechanisms, thereby promoting plant growth. Furthermore, *Bacillus velezensis* HN-2 increased the activities of antioxidant enzymes, thereby mitigating the PVMV-induced ROS production in *Nicotiana benthamiana*. Moreover, the application of *Bacillus velezensis* HN-2 at 5 dpi significantly increased the expression of JA-responsive genes, whereas the expression of salicylic acid-responsive genes remained unchanged, implying the activation of the JA signaling pathway as a crucial mechanism underlying *Bacillus velezensis* HN-2-induced anti-PVMV activity. Immunoblot analysis revealed that HN-2 treatment delayed PVMV infection at 15 dpi, further highlighting its role in inducing plant resistance and promoting growth and development.

Conclusions: These findings underscore the potential of *Bacillus velezensis* HN-2 for field application in managing viral plant diseases effectively.

KEYWORDS

biocontrol agent, PVMV, antiviral, induced systemic resistance, plant immune, *Bacillus velezensis*, *Potyvirus*, pepper veinal mottle virus

1 Introduction

The pepper cultivar *Capsicum chinense* is a local germplasm of the domesticated species, cultivated exclusively in Hainan Island, China (Hu et al., 2020). *C. chinense* is widely utilized for preparing canned sauce, a favorite commercial product among tourists. The increased production of *C. chinense* in Hainan has led to numerous plant disease outbreaks. Notably, five plant viral diseases, including the chilli veinal mottle virus (ChiVMV, *Potyvirus*), pepper veinal mottle virus (PVMV, *Potyvirus*), chilli ringspot virus (ChiRSV, *Potyvirus*), tobacco mosaic virus (TMV, *Tobamovirus*), and cucumber mosaic virus (CMV, *Cucumovirus*), are prevalent in the Hainan province fields, causing considerable economic losses over the last decade. PVMV was initially identified in Eastern Ghana in 1971 (Brunt and Kenten, 1971) and belongs to the genus *Potyvirus*, family Potyviridae, sharing characteristics with other potyviruses (Alegbejo and Abo, 2002; Ha et al., 2008; Matsumoto et al., 2016). PVMV infects a variety of hosts, such as pepper, tomato, tobacco, eggplant, petunia, *Solanum nigrum* L., *S. integrifolim* Poir., *Datura metel*, *D. stramonium*, *Physalis angulata*, and *P. micrantha* (Brunt et al., 1978; Givord, 1982; Atiri and Ligan, 1986; Alegbejo, 1999). Liang et al. (2015) reported a PVMV infection incidence of 74.07% in Wenchang and Wanning, Hainan, which significantly impacts pepper production and fruit quality (Fajinmi and Odebode, 2010). Despite its prevalence, effective pesticides and chemical treatments against PVMV are limited, necessitating the development of novel antiviral agents and resistant varieties.

Currently, effectively controlling the virus once a plant has been infected remains a challenge for farmers. The primary methods for virus control involve cultivating resistant varieties, developing and utilizing natural products, and using chemicals and synthetic compounds. The potential concept of chemically mediated plant virus control relies on compounds that activate the plant immune system. When locally infected with a necrotizing pathogen or non-pathogen, plants often develop long-lasting, broad-spectrum "immunity" against subsequent infection (Kunz et al., 1997). Benzo(1,2,3)-thiadiazole-7-carbothioic acid S-methyl ester (BTH) is a synthetic compound capable of inducing disease resistance in several dicotyledonous and monocotyledonous plant species (Friedrich et al., 1996). Friedrich et al. (1996) found that BTH cannot cause the accumulation of salicylic acid (SA) but can induce disease resistance and *nahG* gene expression, thus activating the SAR signal transduction pathway at the site or downstream of SA accumulation. These results demonstrate the disease control mechanism of BTH by which it activates SAR. Dufulin is a novel antiviral agent that is highly effective against plant viruses and is widely used to prevent and control viral diseases in tobacco and rice in China (Song et al., 2009). Chen et al. (2012) found that HrBP1 is a target protein of dufulin, which can also activate the SA signaling pathway to induce host plants to generate antiviral responses.

However, in recent decades, plant growth-promoting rhizobacteria (PGPRs) have been shown to interact symbiotically and synergistically and effectively colonize the rhizosphere (Ongena and Jacques, 2008). They represent a mutually helpful plant–microbe interaction. Plant growth is enhanced by PGPR through antibiosis, the induction of systemic resistance, and competitive multiplication. The most crucial biocontrol trait of PGPR is their ability to trigger an immune reaction in plant tissues, leading to a systemically expressed resistance state that renders the host less susceptible to subsequent infection (induced systemic resistance, ISR) (Mariuotto and Ongena, 2015; Pršić and Ongena, 2020). PGPR can be beneficial to plants and can perform the same function as chemical fertilizers, pesticides, and elicitors do. *Bacillus* is an important and well-characterized model organism of plant growth-promoting rhizobacteria. *Bacillus subtilis* belongs to a new class of MAMPs. It can effectively inhibit plant activity and ISR, which act as elicitors of plant immunity (Boutrot and Zipfel, 2017; Radhakrishnan et al., 2017). *Bacillus* also produces various metabolites such as lipopeptides, hydrolytic enzymes, and bacterial volatile compounds (BVCs) (Cazorla et al., 2007; Wang et al., 2018; Rajaofera et al., 2019; Jin et al., 2020a, b). Notably, *Bacillus* spp. synthesize antibiotic lipopeptides, including surfactin, iturin, and fengycin (Hashem et al., 2019). Fengycin and surfactin can interact with plant cells as bacterial determinants to turn on an immune response through the stimulation of the induced systemic resistance phenomenon. García-Gutiérrez et al. (2013) showed that ISR is activated by *Bacillus* spp. through the induction of the synthesis of jasmonic acid, ethylene, and *NPR1* regulatory genes in plants. Some studies have indicated that *Bacillus* spp. produce secondary metabolites, such as lipopeptides, which can stimulate and initiate the activities of key enzymes of the oxylipin pathway in tomatoes (Blée, 2002). The phenolic or phenylpropanoid metabolic pathway is also well known to be stimulated concomitantly by the activation of plant defense reactions (Dixon et al., 2002). Ongena et al. (2005) found that when potato tuber cells were treated with fengycins produced by *Bacillus*, the accumulation of plant phenolics was involved in or derived from phenylpropanoid metabolism. Jayaraj et al. (2004) reported that phenylalanine ammonia-lyase, peroxidase, and *de novo* protein synthesis in plants was activated; these enzymes were produced when *Bacillus* was applied to plants. Furthermore, *Bacillus* and BVCs exhibit potent antiviral activities against various plant viruses, including cucumber mosaic cucumovirus (CMV), tomato mottle virus (TMV), pepper mottle virus (PepMoV), tomato yellow leaf curl virus (TYLCV), and tomato spotted wilt virus (TSWV) (Ongena and Jacques, 2008; Kong et al., 2018). In addition, Wu et al. (2017) found that *B. amyloliquefaciens* FZB42 strains produce two types of cyclodipeptides that can induce resistance against TMV infection in *N. benthamiana* by activating the SA-mediated plant defense pathway. *Bacillus* spp. are promising candidates for broad-spectrum antiviral therapy (Ongena and Jacques, 2008). However, despite significant advances made over the past few decades in understanding the regulation of hormonal modulation by PGPR and the induction of acquired systemic resistance in plants (Pieterse et al., 2012, 2014; Köhl et al., 2019), we are still far from having a clear picture of the intricate immune-related molecular events and resistance pathways induced by biocontrol microorganisms.

In a previous study, the cyclic lipopeptide C_{15} surfactin, isolated from *Bacillus velezensis* HN-2, was shown to induce systemic resistance to pathogens in plants, thereby contributing to their biocontrol activity. Here we present a novel approach wherein *Bacillus velezensis* HN-2 is capable of eliciting an immune

response in plant tissues, resulting in systemic resistance against PVMV and exhibiting strong colonization. This suggests potential for future field applications in managing plant viral diseases.

2 Materials and methods

2.1 Bacterial strains' culture conditions and chemical compounds

B. velezensis strain HN-2, which was stored at CCTCC (ID.CCTCC M 2018382) and cultured in lysogeny broth (LB) medium, was centrifuged at 200 rpm for 48 h at 28°C to separate bacterial cells, remove supernatants, and collect cultures, which were adjust to the desired optical density at 600 nm (OD600 = 0.9) and irrigated on soil and plant root. *B. velezensis* strain HN-2-GFP was cultured in chloramphenicol (5 μg mL^{-1}) LB medium. Then, 50 mg mL^{-1} benzothiadiazole and dufulin solution was smeared on whole leaves. Benzothiadiazole (99% purity; Aladdin Co., China) and dufulin (99% purity; Tianyuan Co., China) were used as positive controls, and sterile water (CK) was used as the blank control, respectively.

2.2 Plant materials

Tobacco seeds (*Nicotiana benthamiana L.*) were surface-sterilized for 3 min in 75% ethanol, rinsed with sterile water for five times, and then germinated in 1/2 MS medium in a growth chamber maintained at 25°C (24 h in the dark). Following germination, the seedlings were transferred as plantlets, filled with autoclaved soil consisting of 1:1 (v/v) high-nutrient soil and vermiculite in pots, and then cultured in a growth chamber at 25°C/25°C (14-h light/10-h dark) with 70% relative humidity and observed daily for symptom development recording [Pepper (*capsicum chinense*): Cooperative 903 Big Red Pepper (Shanghai Pepper Institute)].

2.3 Agroinfiltration

Similarly, *N. benthamiana* plants at the seventh leaf stage were carefully selected and subjected to infiltration with *Agrobacterium tumefaciens* (GV3101 + PVMV) cultures containing the relevant plasmids. The cultures were adjusted to the desired optical density at 600 nm (final OD600 = 1) and infiltrated into the leaf tissues of *N. benthamiana* plants essentially (Cui and Wang, 2017). The leaves were inoculated with the virus after 48 h and cultivated in a greenhouse. Five treatments were adopted: sterile water, sterile water + pHNu-GFP, sterile water + benzothiadiazole + pHNu-GFP, sterile water + dufulin + pHNu-GFP, and sterile water + HN-2 + pHNu-GFP, respectively.

2.4 Diaminobenzidine staining and enzyme activity determination

Superoxide dismutase (SOD), peroxidase (POD), catalase (CAT), and malondialdehyde (MDA) activities were determined according to the protocol provided by the manufacturer (Nanjing Jiancheng Biology Institution, Nanjing, China). The diaminobenzidine (DAB) (BBI Life Sciences, China) test was used to detect reactive oxygen species (ROS) production, and the method is as described previously (Liu et al., 2020). Tissue samples were collected at 1, 3, 5, 7, and 15 days after the inoculation treatment for assays on defensive enzyme activities and observation by DAB staining. All of the measurements were performed in triplicate.

2.5 Phytohormone content measurements

The concentration of salicylic acid (SA) was determined using a previously established method with minor modifications (Nakano and Mukaihara, 2018). Tissue samples were collected at 1, 3, 5, 7, and 15 days after inoculation treatment and extracted twice at 4°C for 1 h using 400 μL of an extraction solvent (10% methanol and 1% acetic acid). The standard salicylic acid was purchased from Sigma. A subsequent analysis was conducted using high-performance liquid chromatography on an Agilent 1260 Infinity II LC system equipped with a C18 column. Chromatographic separation utilized solvent A (0.1% formic acid in water) and solvent B (0.1% formic acid in acetonitrile) following a gradient elution: starting at 10% solvent B for 1 min, 95% solvent B for 10 min, maintaining at this level for 2 min, returning to the initial conditions with 10% solvent B for 0.1 min, and finally equilibrating for 2 min at 10% solvent B condition with a constant flow rate of 0.3 mL min^{-1}.

2.6 RNA extraction and RT-PCR

Tissue samples were collected at 1, 3, 5, 7, and 15 days after inoculation treatment and frozen in liquid nitrogen for subsequent RNA isolation. The quality of extracted RNA should be given following the RNAprep pure KIT (Tiangen), and complementary DNA (cDNA) was synthesized with the Prime Script RT-PCR kit (TaKaRa, Japan). For the qRT-PCR assay, each biological treatment was carried out in three replicates using the SYBR Premix EX Taq kit (TaKaRa) in 20 μL on the ABI Prism 7500 system. The program consisted of a HotStart activation step at 95°C for 14 s, followed by 40 cycles of 95°C for 15 s, 59°C for 30 s, and 72°C for 30 s. The $2^{-\triangle\triangle CT}$ method (Livak and Schmittgen, 2001) was used to precisely quantify and calculate the relative transcriptional level of each tested gene. All of the measurements were performed in triplicate. The expressions of eight target genes (*Cat1*, *Rboh*, *PAL*, *Ja*, *PR-1b*, *PR3*, *PR5*, and *NPR1* gene) were monitored with qRT-PCR. The *ACT1* gene was used as the internal reference. The gene primers are listed in Supplementary Table S1.

2.7 Western blotting analysis

Total protein collection and western blotting analysis were performed using a previously reported method (Cui and Wang, 2016). The total proteins were extracted from fresh leaf tissues of *N. benthamiana* plants which were collected at 1, 3, 5, and 15 days after inoculation treatment, and fresh plant leaves were ground to a fine powder in liquid nitrogen. Briefly, protein samples were subjected to electrophoresis on 12% sodium dodecylsulfate–polyacrylamide gel electrophoresis (SDS-PAGE) and electroblotting onto a polyvinylidene difluoride membrane (Immobilon), followed by Western blotting assays using anti-GFP antibodies. Goat anti-rabbit immunoglobulin antibody (Abcam) conjugated to horseradish peroxidase was used as the secondary antibody. The hybridization signals in the blotted membranes were detected with the substrates of enhanced chemiluminescence detection reagents (Thermo Fisher Scientific) and visualized under an ImageQuant LAS 4000 mini biomolecular imager (GE Healthcare).

2.8 *B. velezensis* HN-2 colonization assay in *Capsicum chinense*

Identical *Capsicum chinense* seeds were selected for the colonization assay. The colonization assay was performed using a previously reported method (Deng et al., 2019). The plants were kept in square pots (5 × 5 cm), at one plant per pot with nutrition soil, in a greenhouse at a consistent temperature of 30°C. Then, 10 mL of sterile water containing 10^6 colony-forming units (CFUs) g^{-1} of *B. velezensis* strain HN-2-GFP with Cm (chloramphenicol) label was inoculated into the soil of 1-month generated *C. chinense* seedlings. A total of 300 plants were set for the treatment. After inoculation for 3, 5, 15, 30, and 45 days, nine plants were harvested each time for investigation of *B. velezensis* strain HN-2-GFP colonization. The collected roots with rhizosphere soil were put into 50-mL tubes with 10 mL of sterile water and sonicated three times at 30 s $cycle^{-1}$. The washing buffer during the three times was subjected to low-speed centrifugation (1,000 × *g*, 10 min). The pellets were set as a rhizosphere soil sample. The roots were transferred into a new tube containing 10 mL of sterile water. The roots were sonicated for another three rounds of 30 s $cycle^{-1}$. After the roots were put into another 10-mL tube with fresh sterile water, the roots were ground using an electric pestle. The homogenate was set as root sample. The samples were used to spread the plates with 5 μg mL^{-1} chloramphenicol after properly diluting. CFUs were calculated. The CFU of the rhizosphere soil samples and roots was normalized by using the corresponding root fresh weight with rhizosphere soil from each plant.

2.9 Antivirus tests in the field

To test the protective effect of *B. velezensis* HN-2 on plant protection and antiviral function, after 60 days of growth, a total of 300 *Capsicum chinense* with the same growth trend were transplanted in the field. The strain HN-2 (OD600 = 0.9) was irrigated on the soil of *C. chinense*. Benzothiadiazole, dufulin, and sterile water were sprayed on the leaves of *C. chinense*. The sterile water served as a blank control, and the plants that were inoculated with PVMV-GFP is the negative control. Benzothiadiazole and dufulin were used as positive controls. At 2 days after spraying or irrigation, the plants were inoculated with PVMV. The accumulation of PVMV-GFP protein was detected by Western blotting at 60 days post-inoculation (dpi). The infection of PVMV-GFP in *C. chinense* was observed at 180 dpi. Five samples per treatment were collected for further virus detection. The above-mentioned experiments were repeated five times, with nine plants each time.

2.10 Statistical analyses

All experiments and data presented here involved at least three repeats. The statistical analyses were all performed using SPSS (version 19.0; SPSS Inc). All data were expressed as means ± SD. Different letters indicate statistically significant differences between treatments according to Duncan's multiple-range test at $P < 0.05$, and the independent-samples test was used to test the significance of the difference.

3 Results

3.1 Effect of *B. velezensis* HN-2 in defense against PVMV

To evaluate the resistance of *B. velezensis* HN-2 against PVMV, sterile water (CK) served as the blank control, and pHNu-GFP was used as the negative control. Benzothiadiazole and dufulin were used as positive controls. We pretreated *N. benthamiana* leaves with water, benzothiadiazole, dufulin, and *B. velezensis* HN-2 (Figure 1A). Subsequently, pHNu-GFP was inoculated through *Agrobacterium* infection (agroinfiltration) at 48 h post-pretreatment. The subsequent infection of pHNu-GFP was visualized at 1, 3, and 5 dpi (that is, at 3, 5, and 7 dpi of the experimental treatments) under UV light and DAB staining. As shown in Figures 1A, B, no damage was observed and no green fluorescence was detected in *N. benthamiana* leaves at 1 and 3 dpi. Figures 1C, D show that the GFP fluorescent signals visualized in the inoculated leaves treated with HN-2 were much lower than those of the negative control and positive controls at 5 and 7 dpi. At 7 dpi, GFP fluorescence was detected in the young leaves of the positive and negative plants due to the systemic movement of PVMV-GFP. However, in the young leaves of HN-2-treated plants, slightly expanded GFP signals were visualized at 7 dpi (Figure 1D). In addition, we measured the accumulation of PVMV-GFP protein by using Western blotting in the inoculated leaves at 15 dpi. The expression level of PVMV-GFP in both adult and young leaves of the plants treated with *B. velezensis* HN-2 was pronouncedly lower than that of the other treatment groups, with a particularly pronounced effect observed in young leaves (Figures 2A, B). This is in line with the fluorescence signals observed under UV light. Furthermore, in comparison to

10.3389/fpls.2024.1403202

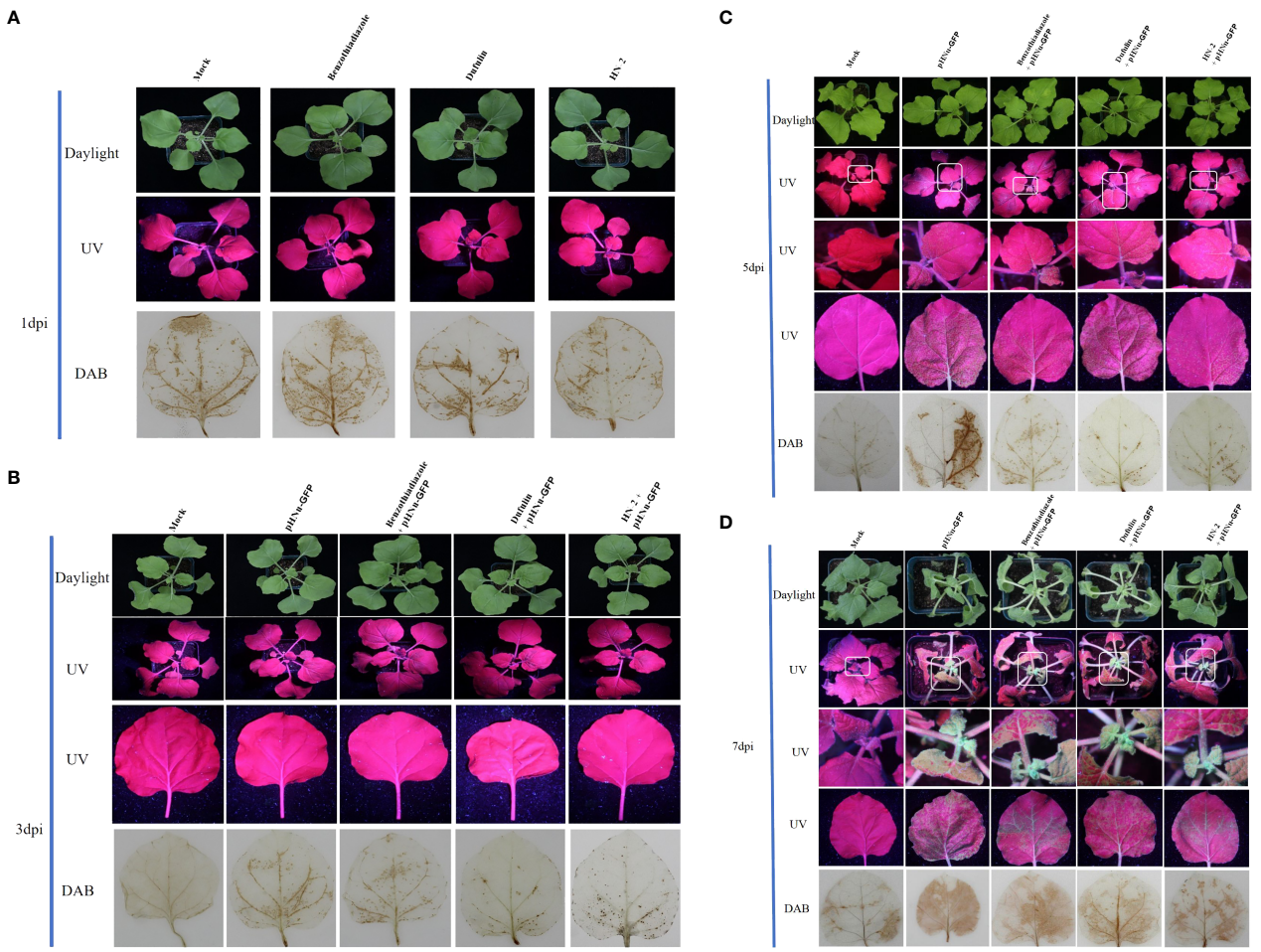

FIGURE 1
Persistent antiviral effect of benzothiadiazole, dufulin, and *B. velezensis* HN-2 on *N. benthamiana*; each treatment group was inoculated with PVMV-GFP on 3, 5, and 7 days, respectively. The leaves of *N. benthamiana* were treated with sterile water, benzothiadiazole, and dufulin at a concentration of 50 mg mL^{-1}, while *B. velezensis* strain HN-2-GFP irrigation on soil and plant root was at a concentration of 5 μg mL^{-1}. After 48 h of pretreatment, *N. benthamiana* plants at the seventh leaf stage with a similar growth were infiltrated with *Agrobacterium tumefaciens* (GV3101 + PVMV) cultures containing the relevant plasmid and cultivated in a greenhouse environment. DAB staining was used to detect the production of H_2O_2 on *N. benthamiana*. **(A)** Green GFP fluorescence signals (under UV light) and DAB staining were observed after benzothiadiazole, dufulin, HN-2, and sterile water treatments for 1 dpi (that is, representing 24 h of pretreatment). **(B)** Green GFP fluorescence signals (under UV light) and DAB staining were observed after benzothiadiazole, dufulin, HN-2, and sterile water treatments for 3 dpi and friction inoculation of PVMV-GFP at 1 dpi. **(C)** Green GFP fluorescence signals (under UV light) and DAB staining were observed after benzothiadiazole, dufulin, HN-2, and sterile water treatments for 5 dpi and friction inoculation of PVMV-GFP at 3 dpi. **(D)** Green GFP fluorescence signals (under UV light) and DAB staining were observed after benzothiadiazole, dufulin, HN-2, and sterile water treatments for 7 dpi and friction inoculation of PVMV-GFP at 5 dpi. "Mock" means sterile water treatment.

therapeutic efficacy against PVMV achieved by treatments involving benzothiadiazole and dufulin, the results strongly indicated that *B. velezensis* HN-2 exhibits a significant therapeutic effect on *N. benthamiana* plants following PVMV infection.

3.2 *B. velezensis* HN-2 alleviates PVMV-induced oxidative damage

DAB is oxidized by hydrogen peroxide in the presence of some haem-containing proteins, which was performed to generate a dark brown precipitate. This precipitate is used as a stain to detect the presence and distribution of hydrogen peroxide in plant cells (Daudi and O'Brien, 2012). Upon treatment with benzothiadiazole, dufulin, and *B. velezensis* HN-2, which can induce plants to produce peroxide, black precipitates were produced after staining using DAB. To observe the continuous induction of ROS by five treatments, the accumulation of H_2O_2 was detected in the leaves at 1, 3, 5, and 7 dpi after spraying for 2 days (Figure 1). The results revealed the appearance of dark brown precipitates along the leaf veins across all treatment groups. Figure 1A demonstrates that uninfected *N. benthamiana* plants did not exhibit the spontaneous formation of dark brown precipitates. From the first day after PVMV inoculation, that is, at 3 dpi, an increasing number of dark spots was observed exclusively in pHNu-GFP-treated plants due to the combined effects of PVMV infection and pharmaceutical treatments. There was an increase in benzothiadiazole- and dufulin-treated plants, but they were significantly different from plants which were only treated with pHNu-GFP. Additionally, *B. velezensis* HN-2

10.3389/fpls.2024.1403202

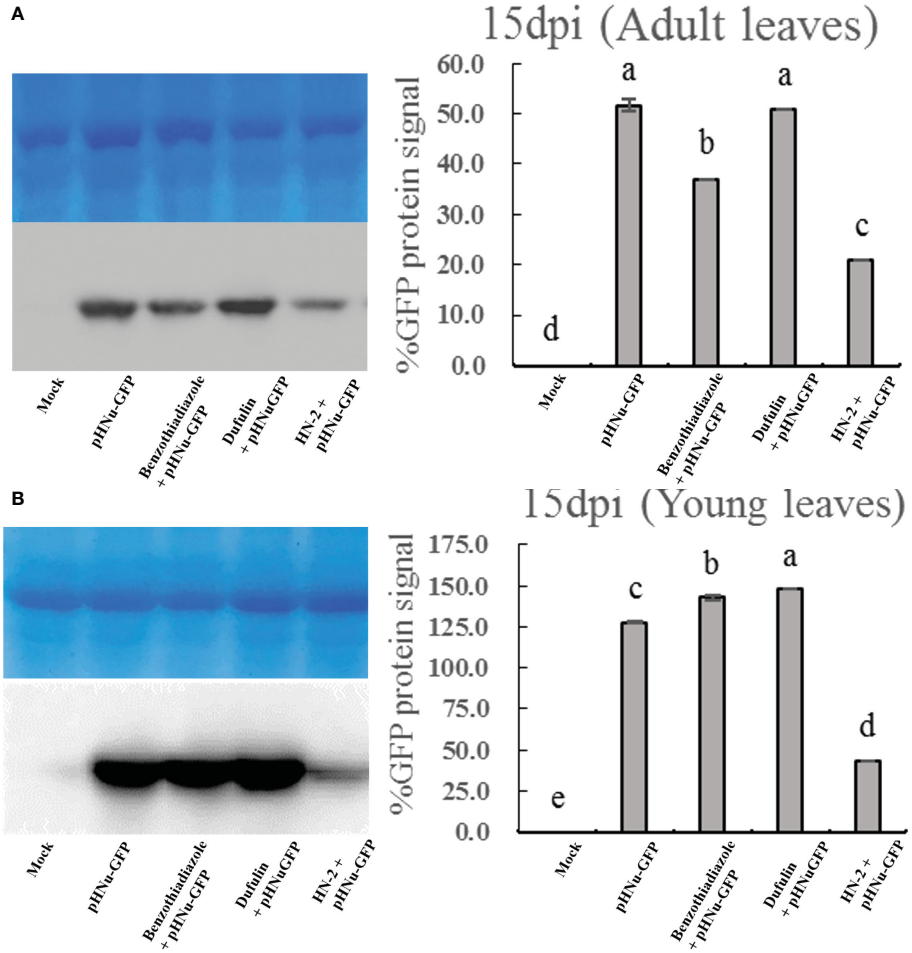

FIGURE 2
Western blotting analysis showing the level of the PVMV-GFP protein in the adult leaves **(A)** and young leaves **(B)** of *N. benthamiana* at 15 dpi, which were treated with sterile water (mock), pHNu-GFP, benzothiadiazole-, dufulin-, and *B. velezensis* HN-2-pHNu-GFP. Values represent means standard deviations (SDs) from three independent experiments; different lowercase letters indicate a highly significant difference ($P < 0.05$).

treatment resulted in a significantly fewer black spots than the other treatments. The dark brown precipitates exhibited similar patterns between benzothiadiazole-treated *N. benthamiana* leaves inoculated with pHNu-GFP at 3, 5, and 7 dpi compared to dufulin-treated plants (Figures 1B–D), where at 7 dpi they accounted for approximately two-thirds of the leaf area covered by precipitation. Furthermore, as treatment time increased substantially, so did the amount of dark brown precipitates; notably at 7 dpi, they were detected throughout *N. benthamiana* leaves treated only with pHNu-GFP. Figure 1D illustrates that adult leaves treated with HN-2 showed less accumulation of dark brown precipitates than young leaves as indicated by decreased staining at 5 dpi, suggesting that HN-2 can reduce the oxidative damage in leaves caused by PVMV. The oxidative damage effects of the plants were significantly weaker than those of BTH and dufulin treatments.

3.3 Determination of defense enzyme activities and SA accumulation

Due to the crucial role of antioxidant enzymes in plant defense mechanisms against various plant pathogens, the current work aimed to evaluate the activities of antioxidant enzymes, including superoxide dismutase, peroxidase, catalase, and malondialdehyde. The objective was to determine whether there were induced antioxidant activities after inoculation with pHNu-GFP in the five treatments, which were clearly differentiated by HN-2 treatments (Figure 3). SOD enzymes play a major role in detoxifying reactive superoxide (O^{2-}) species into H_2O_2, which is subsequently degraded by catalases (El-Gendi et al., 2022). As depicted in Figure 3A, the results indicated a slight enhancement of approximately 1.07-fold (409.85 unit mg^{-1} FW) in SOD activity following PVMV treatment, which was not significantly different from the positive controls and HN-2-treated plants after PVMV-GFP inoculation compared to the blank control at 1 dpi. This observation could be attributed to an initial response of the plant defense system to oxidative stress. However, at 3 dpi, HN-2-treated plants exhibited the highest SOD activity with a peak value of 421.13 unit mg-1 FW, representing increases of 1.10-, 1.33-, and 1.04-fold when compared to BTH-treated, dufulin-treated, and blank control samples, respectively. Subsequently, there was a decline in SOD activity at 5 dpi.

Antioxidant enzymes, such as peroxidase, play a pivotal role in the conversion of H_2O_2 to H_2O (Gill and Tuteja, 2010). The results of

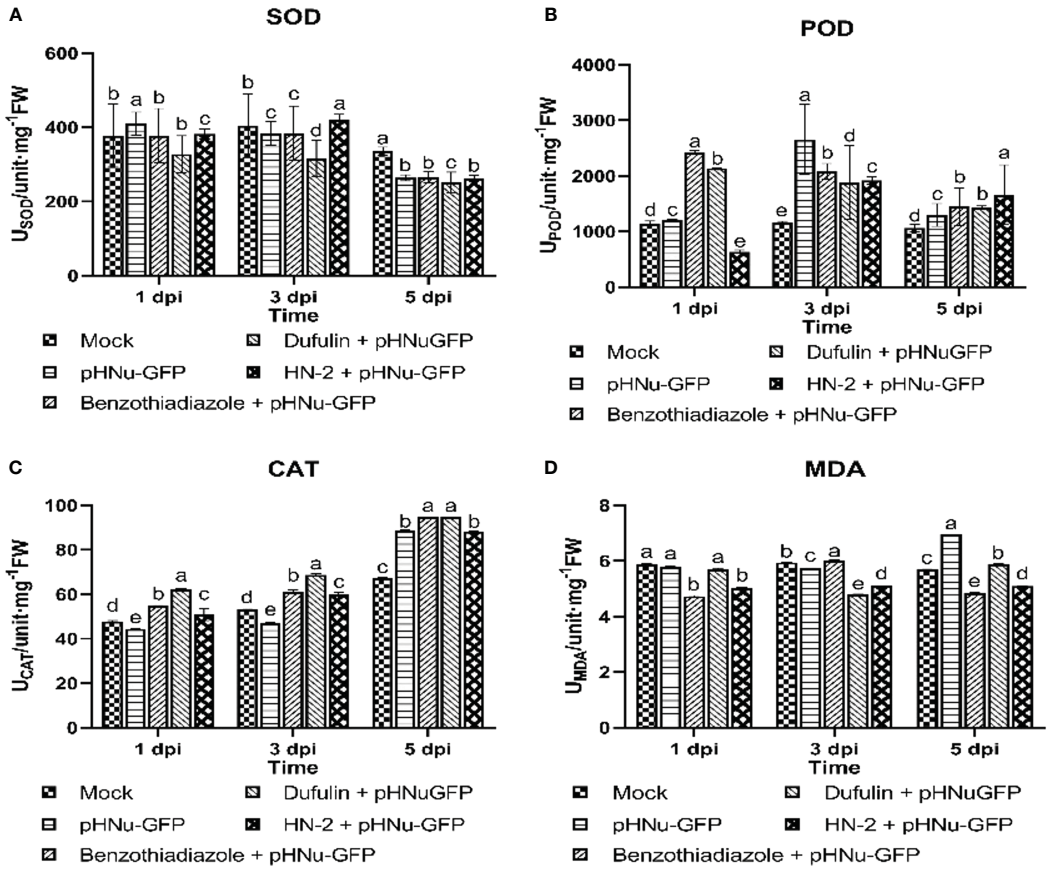

FIGURE 3
Antioxidant-related enzyme activaties in *N. benthamiana*. Tissue samples were collected after sterile water (mock), pHNu-GFP, benzothiadiazole-, dufulin-, and *B. velezensis* HN-2-pHNu-GFP treatments at 1, 3, and 5 dpi (that is, cultures were incubated for 3, 5, and 7 dpi) for assays on defensive enzyme activity assays. **(A)** Superoxide dismutase (SOD), **(B)** peroxidase (POD), **(C)** catalase (CAT), and **(D)** malondialdehyde (MDA). All experiments were repeated three times, and similar results were obtained. Data are presented as the means ± SD from three independent experiments. Values represent means standard deviations (SDs) from three independent experiments; different lowercase letters indicate a highly significant difference ($P < 0.05$).

the enzyme activity assay revealed a significant reduction in POD activities by 80.09% in the HN-2 treatment plants (635.62 unit mg^{-1} FW) compared to the blank control (1,144.68 unit mg^{-1} FW) at 1 dpi. Following inoculation of *N. benthamiana* with pHNu-GFP for 3 days, the highest POD activity was observed in the PVMV treatment (2,655.43 unit mg^{-1} FW), followed by BTH treatment (2,078.14 unit mg^{-1} FW), HN-2 treatment (1,916.74 unit mg^{-1} FW), and dufulin treatment (1,884.14 unit mg^{-1} FW) when compared to the blank control (Figure 3B). Furthermore, contrasting patterns were observed in changes of POD activity at 5 dpi; the HN-2 treatment demonstrated the highest level at 1,660.31 unit mg^{-1} FW, indicating a 1.15-, 1.16-, and 1.57-fold increase in activity compared to the BTH treatment (1,447.06 unit mg^{-1} FW), dufulin treatment (1,430.72 unit mg^{-1} FW), and blank control (1,060.72 unit mg^{-1} FW), respectively.

The activity of the antioxidant enzyme CAT gradually increased in all treatments and reached its peak at 5 dpi. Remarkably, the BTH-treated and dufulin-treated groups exhibited significantly higher levels of CAT content, with a significant increase of 1.07- and 1.08-fold compared to HN-2 treatments, respectively. Additionally, there was a slight but insignificant increase in CAT activity values exhibited in HN-2 treatments (50.79 and 60.00 unit mg^{-1} FW, respectively) by 1.06- and 1.13-fold compared to the blank control (47.75and 53.24 unit mg^{-1} FW, respectively) at 1 and 3 dpi. Meanwhile, it increased by 1.31-fold compared with the blank control at 5 dpi (Figure 3C).

Malondialdehyde (MDA), as a marker for oxidative stress, could be a great indicator of membrane disruption in plants attacked by pathogens (Loreto and Velikova, 2001; Lv et al., 2020). Interestingly, we found that MDA activity remained relatively stable with prolonged HN-2 treatment (5.03 unit mg^{-1} FW, 5.12 unit mg^{-1} FW, and 5.10 unit mg^{-1} FW, respectively), exhibiting a significant reduction in MDA content compared to PVMV treatment (5.80 unit mg^{-1} FW, 5.74 unit mg^{-1} FW, and 6.94 unit mg^{-1} FW, respectively) and the blank control (5.87 unit mg^{-1} FW, 5.94 unit mg^{-1} FW, and 5.69 unit mg^{-1} FW, respectively), representing decreases of approximately 13.28%, 10.80%, and 26.60% and reductions of approximately 14.31%, 13.80%, and 10.37%, respectively. In addition, HN-2 treatments on *N. benthamiana* resulted in a considerable reduction in MDA content when compared to both PVMV treatment and blank control. Furthermore, BTH treatments (4.73 unit mg^{-1} FW at 1 dpi and 4.86 unit mg^{-1} FW at 5 dpi) and dufulin treatment (4.80 unit mg^{-1} FW at 3 dpi) showed a minimal buildup of MDA activity compared to HN-2 treatments, respectively. On the contrary, dufulin treatment exhibited an increase of approximately 1.17-fold at 3 dpi, while dufulin treatment showed an

increase of 1.13- and 1.16-fold at 1 and 5 dpi, respectively, in comparison with HN-2 treatment (Figure 3D).

Salicylic acid (SA), a crucial signaling molecule involved in plant disease resistance and playing a central role in orchestrating induced plant defense by activating several defense-related genes, leading to SAR-induced signal transduction in plants, was quantified using high-performance liquid chromatography (HPLC). In *N. benthamiana* leaves inoculated with HN-2, the SA content gradually increased and peaked at 3dpi, reaching the highest levels of 0.322 μg g^{-1} FW among five treatments, which represented a slight enhancement of approximately 1.08- and 1.12-fold when compared to BTH-treated (0.297μg g^{-1} FW) and dufulin-treated (0.287μg g^{-1} FW). Moreover, there was no significant difference between the SA content in HN-2 treatment (0.237 μg g^{-1} FW) and those treated with dufulin (0.220 μg g^{-1} FW), but compared to BTH treatment and PVMV treatment and blank control, decreases of 26.97%, 40.52%, and 24.93%, respectively, were shown (Figure 4).

3.4 Effect of HN-2 on the expression of defense-related genes and jasmonic acid

To further validate the mechanism underlying resistance after HN-2 treatment, we quantified the expression of jasmonic acid (JA), resistance-related genes (*Rboh*, *PAL*, and *Cat1* gene) and PR protein genes (*NPR1*, *PR-1b*, *PR3*, and *PR5* gene) in *N. benthamiana* using RT-PCR. We investigated the viral suppression mechanism in response to HN-2 treatment by examining the expression of *JA*, a key regulatory factor of induced systemic resistance (ISR) (Zhou and Wang, 2018). As depicted in Figure 5A, *JA* expression gradually increased from 1 to 3 dpi and peaked at 5 dpi within HN-2-treated plants. Notably, the fold change was significantly higher compared to the blank control samples as well as BTH and dufulin treatments with values of 7.81-, 2.22-, and 4.29-fold, respectively.

Respiratory burst oxidase homology (*Rboh*)-mediated H_2O_2 generation plays a crucial role in plant growth, development, and response to adverse environmental conditions (Chen and Yang, 2020). In the current study, we observed a significant increase in the expression of Rboh in dufulin-treated plants at 1 and 3 dpi, while BTH treatment exhibited the highest expression among all treatments at 5 dpi. However, compared to the blank control, HN-2 treatment resulted in a modest increase of *Rboh* expression by 1.89-, 1.18-, and 1.34-fold at 1, 3, and 5 dpi, respectively, albeit lower than that of the positive controls (Figure 5B). Phenylalanine ammonia-lyase (*PAL*) is a key regulator enzyme involved in the phenylpropanoid pathway for polyphenolic compound production. In comparison to mock-inoculated plants in the present study, the expression of *PAL* was significantly upregulated in HN-2-treated leaves, with the relative expression levels peaking at 24 h and reaching a level 32.61-fold higher than the blank control before returning to near-normal levels within 72 h. Subsequently, there was an increase by 25.58-, 15.33-, and 6.47-fold compared with BTH- and dufulin-treated controls at 5 dpi, respectively (Figure 5C). Figure 5D demonstrated a similar expression of *Cat1* across all treated plants at 1 and 3 dpi. Furthermore, *Cat1* expression was markedly increased in HN-2-treated leaves, reaching its peak level at 5 dpi with 49.84-, 58.27-, and 9.69-fold higher expressions than those observed for blank control, BTH-treated plants, and Dufulin-treated plants, respectively.

Following viral infection, the expression levels of *NPR1*, *PR-1b*, *PR3*, and *PR5* genes gradually increased over time in the leaves of *N. benthamiana* treated with HN-2. We quantitatively analyzed the gene

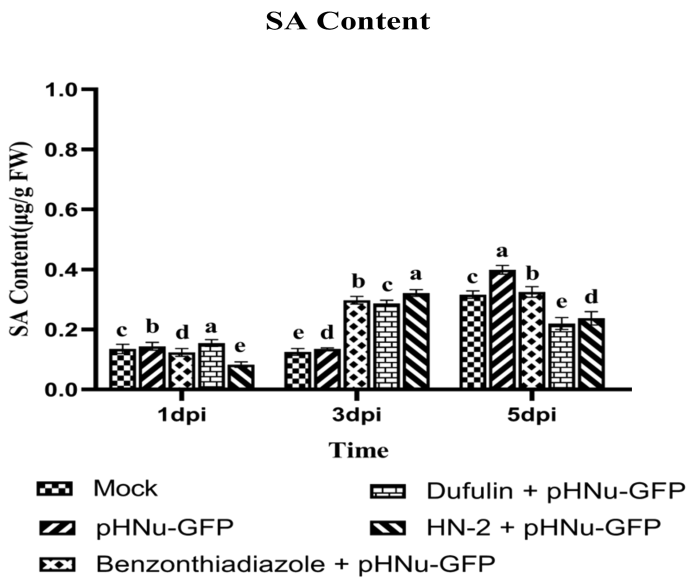

FIGURE 4
Persistent SA activation effects of sterile water (mock), pHNu-GFP, benzothiadiazole-, dufulin-, and HN-2-pHNu-GFP on *N. benthamiana*. PVMV-GFP in the inoculated leaves of *N. benthamiana* at 1, 3, and 5 dpi at the same time—that is, cultures were incubated for 3, 5, and 7 dpi. Data are presented as the means ± SD from three independent experiments. Values represent means standard deviations (SDs) from three independent experiments; different lowercase letters indicate a highly significant difference ($P < 0.05$).

10.3389/fpls.2024.1403202

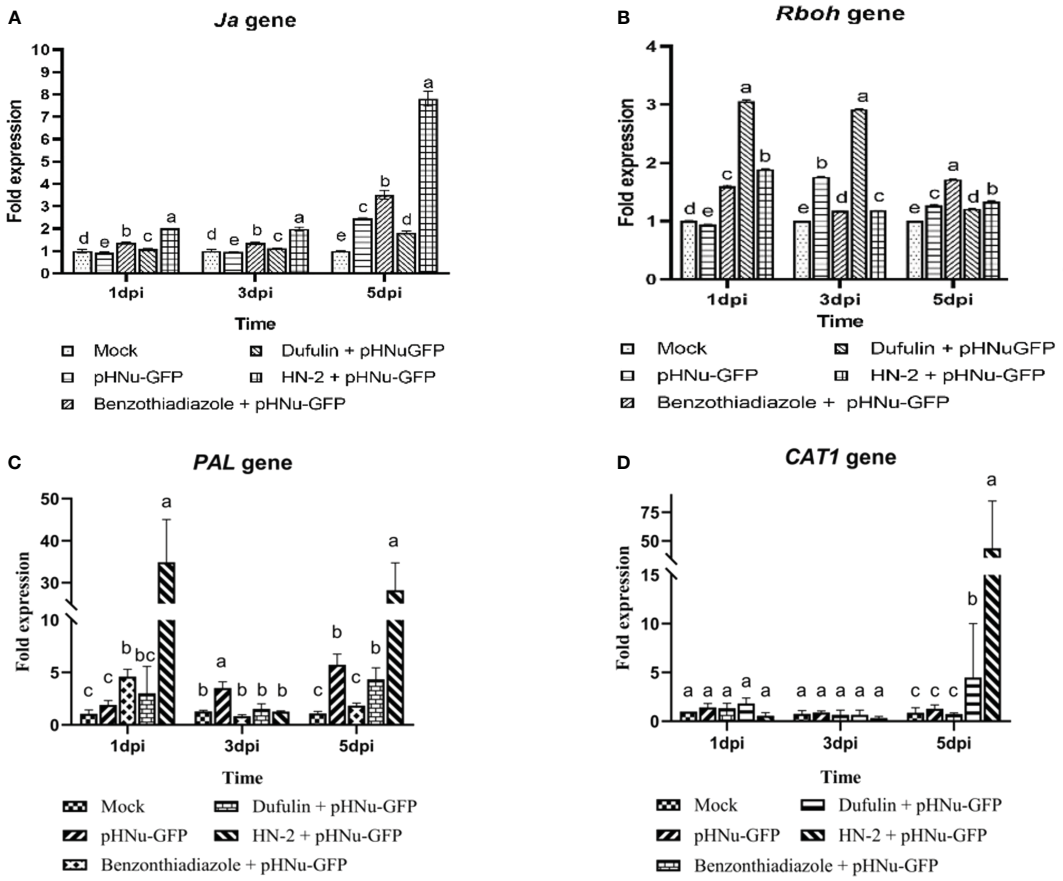

FIGURE 5
Expression of defense-related genes and jasmonic acid *(Ja)* in *N. benthamiana*. PVMV-GFP in the inoculated leaves of *N. benthamiana* at 1, 3, and 5 dpi at the same time—that is, cultures were incubated for 3, 5, and 7 dpi. **(A)** qRT-PCR analysis showing the expression profile of *Ja* in the inoculated leaves of *N. benthamiana* and treated in sterile water, pHNu-GFP, benzothiadiazole, dufulin, and HN-2, and expression levels were represented as a fold change and normalized to the actin gene. Effects of *B. velezensis* HN-2 on the expression of defense-related enzyme genes in the leaves of *N. benthamiana*. Tissue samples were collected for qRT-PCR analysis and the expression of *N. benthamiana* in sterile water (mock), pHNu-GFP, benzothiadiazole-, dufulin-, and HN-2-pHNu-GFP treatments at 1, 3, and 5 dpi (that is, cultures were incubated for 3, 5, and 7 dpi). Expression levels (means ± SD) were represented as a fold change and normalized to the actin gene. **(B)** Respiratory burst oxidase homolog (*Rboh*), **(C)** phenylalanine ammonia-lyase (*PAL*), and **(D)** catalase1 (*CAT1*). The experiment was repeated three times, and the data were normalized according to the $2^{-\triangle\triangle CT}$ method. Different letters indicate statistically significant differences between treatments according to Duncan's multiple-range test at $P < 0.05$. Values represent means standard deviations (SDs) from three independent experiments; different lowercase letters indicate a highly significant difference ($P < 0.05$).

expression at 1, 3, and 5 dpi. In the present study, *NPR1* and *PR-1b* exhibited a gradual increase in the HN-2-treated plants and peaked at 5 dpi. The expression of *NPR1* gene was found to be significantly higher (2.87-, 2.24-, and 2.35-fold) compared to the blank control as well as BTH-treated and dufulin-treated plants (Figure 6A). Similarly, the expression levels of the *PR-1b* gene showed significant increases of 22.26-, 1.45-, and 1.50-fold compared to the blank control, BTH-treated plants, and dufulin-treated plants (Figure 6B). Interestingly, the result showed that the expression levels of *PR3* and *PR5* genes were significantly upregulated at 1 dpi, followed by a subsequent decrease and eventual peak at 5 dpi. At both time points (1 and 5 dpi), there was a substantial increase in *PR3* gene expression in HN-2-treated plants compared to all three controls: blank control (287.00-fold), BTH-treated (95.32-fold), and dufulin-treated (281.00-fold), respectively (Figure 6C). Similarly for *PR5* gene, the expression levels remained significantly higher in HN-2-treated plants than the blank control and BTH- and dufulin-treated plants with a respective fold increase of 312.44-, 45.52-, and 31.88-fold, respectively, at 1 dpi and 285.14-, 5.40-, and 12.30-fold increase at 5 dpi (Figure 6D). These findings indicate that HN-2 treatment substantially enhanced PR gene expression in PVMV-infected *N. benthamiana*.

3.5 Effect of colonization in *C. chinense* by *B. velezensis* strain HN-2

One-month generated *C. chinense* seedlings were then cultivated in nutrition potting soil mixed with sterile water containing 10^6 CFU mL^{-1} of *B. velezensis* strain HN-2-GFP under controlled greenhouse conditions to confirm the number of colonies in *C. chinense* rhizosphere soil and root interior soil at 3, 5, 15, 30, and 45 dpi. Our results showed that rhizosphere soil colonization initially increased and then decreased over time, reaching its highest level at 15 dpi before gradually declining at

10.3389/fpls.2024.1403202

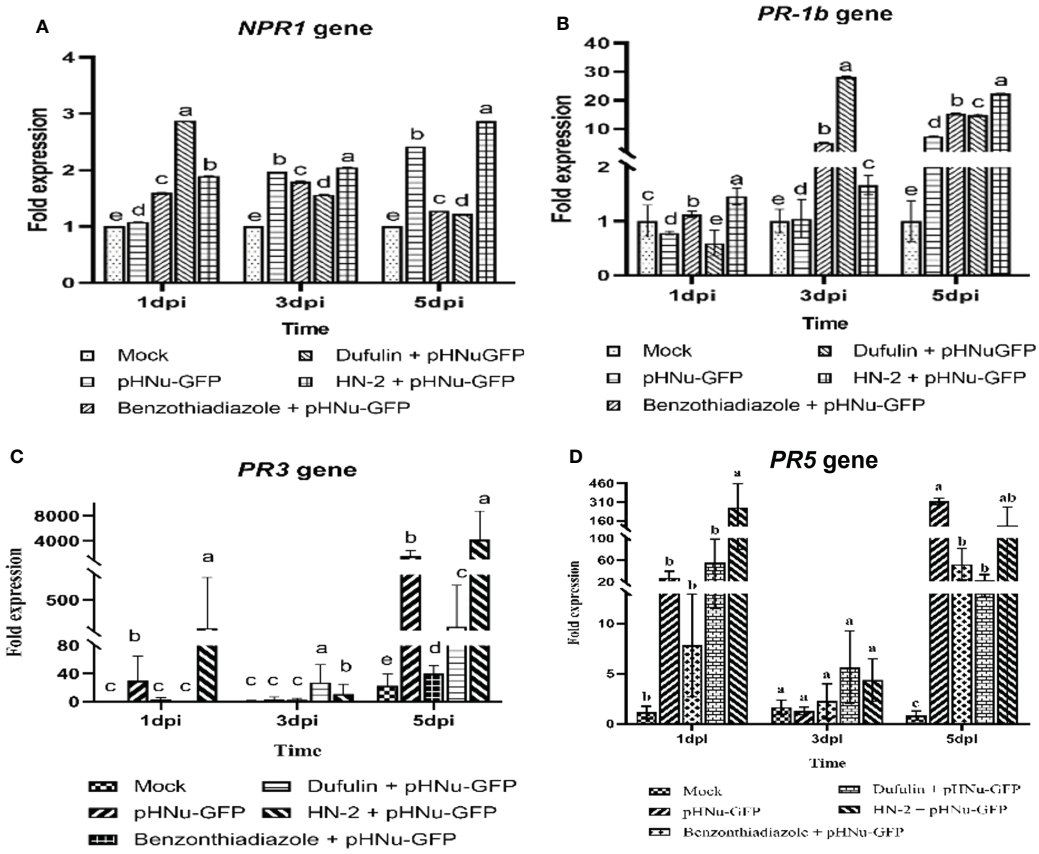

FIGURE 6
Expression of pathogenesis-related protein genes of *N. benthamiana*. qRT-PCR analysis showing the transcript levels (means ± SD) of PR protein genes in sterile water (mock), pHNu-GFP, benzothiadiazole-, dufulin-, and HN-2-pHNu-GFP treatments of *N. benthamiana* at 1, 3, and 5 dpi (that is, cultures were incubated for 3, 5, and 7 dpi). The expression levels were represented as a fold change and normalized to the actin gene. **(A)** Nonexpressor of pathogenesis-related genes 1 (*NPR1*), **(B)** pathogenesis-related proteins 1b (*PR1b*), **(C)** pathogenesis-related proteins 3 (*PR3*), and **(D)** pathogenesis-related proteins 5 (*PR5*). The experiment was repeated three times, and the data were normalized according to the $2^{-\triangle\triangle CT}$ method. Values represent means standard deviations (SDs) from three independent experiments; different lowercase letters indicate a highly significant difference ($P < 0.05$).

both 30 and 45 dpi. In contrast, root colonization was lower than rhizosphere colonization at the early stage (3 dpi), but it gradually increased with prolonged treatment duration and surpassed rhizosphere colonization by 5 dpi. Subsequently, root interior soil exhibited a high level of colonization at 45 dpi (Figure 7A).

3.6 Effect of *C. chinense* by *B. velezensis* strain HN-2 on resistance to PVMV in the field

To evaluate the PVMV resistance function of *B. velezensis* HN-2 under field conditions, we subjected field-grown *C. chinense* plants to irrigation with strain HN-2 in soil. Additionally, the leaves of *C. chinense* were sprayed with benzothiadiazole, dufulin, and sterile water, respectively. At 2 days after spraying or irrigation, the plants were inoculated with PVMV. At 60 and 180 dpi after planting, leaf samples were collected, and quantitative analysis was performed for five treatments: sterile water, pHNu-GFP, benzothiadiazole + pHNu-GFP, dufulin + pHNu-GFP, and HN-2 + pHNu-GFP. Western blotting was used to detect the accumulation of PVMV-GFP protein in 60 dpi after inoculation. The results showed that high levels of GFP protein were only detected in pHNu-GFP treatment. GFP protein was almost undetectable in plants treated with benzothiadiazole, dufulin, and *B. velezensis* HN-2 (Figure 7B). We observed that the growth of *C. chinense* treated with HN-2 exhibited a significant improvement compared to those treated with pHNu-GFP as well as BTH and dufulin treatments, similar to the blank control at 180 dpi (Figure 7C). According to a statistical analysis of morbidity rates, no morbidity was observed in the group receiving only water treatment, almost 100% incidence rate was observed in the group receiving only PVMV (pHNu-GFP), and incidences for BTH and dufulin treatments were at 80% and 75%, respectively, whereas the HN-2 treatment group showed a significantly lower incidence rate of only 60%.

4 Discussion

PVMV stands as a prominent plant viral ailment in Hainan province's fields, causing substantial economic losses since its recent emergence. Limited effective pesticides and chemical treatments

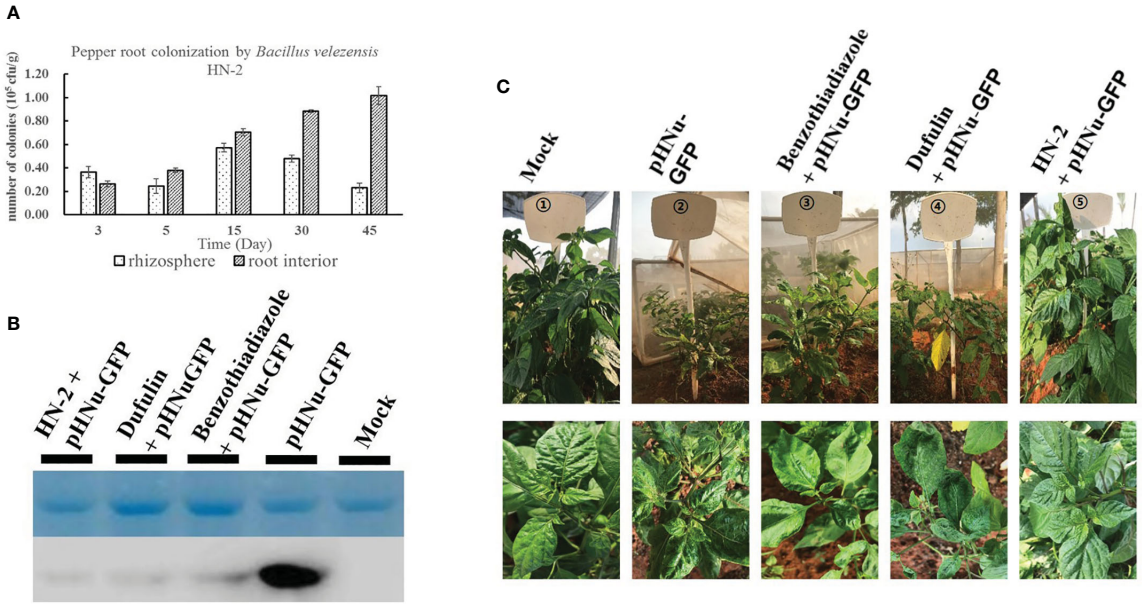

FIGURE 7
Colonization of *B. velezensis* HN-2 in *Capsicum chinense*. **(A)** *B. velezensis* HN-2 colonization experiment in the rhizosphere and root interior of *C. chinense* against PVMV infection. The 3, 5, 15, 30, and 45 dpi post-inoculation were set for observation. **(B)** The accumulation of pHNu-GFP protein was detected by western blotting at 60 dpi. **(C)** The strain HN-2 (OD600 = 0.9) was irrigated in the soil of *C. chinense*. Benzothiadiazole, dufulin, and sterile water were sprayed on the leaves of *C. chinense* 48 h after spraying or irrigation, and then these were inoculated with PVMV. The infection of PVMV-GFP in *C. chinense* was observed at 180 dpi. All experiments were repeated three times with three independent plants per time.

exist to combat PVMV infection. Previous studies have shown that *Bacillus* spp. can promote plant growth, and its metabolites can significantly inhibit the effects of plant pathogens, which are commonly used in plant disease management (Fira et al., 2018; Abdelkhalek et al., 2020). These metabolites offer a wide range of secondary compounds that may stimulate plant ISR while impeding pathogen growth (Fira et al., 2018; Vurukonda et al., 2018). Although ISR using *Bacillus* has shown promise against various plant viruses, such as TMV, CMV, and PVY (Murphy et al., 2000, 2003; Wang et al., 2009), its efficacy against PVMV remains unexplored. In this study, we assessed the antiviral properties of *Bacillus velezensis* HN-2 and its chemical counterparts. Our study revealed that treatment with *B. velezensis* strain HN-2 reduced the PVMV infection rates, symptoms, and disease severity in *Capsicum chinense*, correlating with reduced virus quantities in the leaves. These findings underscore the potent control efficacy of *B. velezensis* HN-2 against PVMV infection in *C. chinense*, further affirming its role as a plant growth-promoting rhizobacterium capable of inducing plant-induced systemic resistance against PVMV by eliciting JA production.

Benzothiadiazole and dufulin are exogenous chemical small molecule plant disease activators that lack antimicrobial activity *in vitro* but induce the accumulation of reactive oxygen and phenolics, enhance defense enzyme activity, induce disease-course-related protein expression in plants, activate the SA signaling pathway, and prompt SAR antiviral immune mechanisms to improve the inhibition of viral infection (Chen et al., 2012; Song et al., 2014; Zhou and Wang, 2018; Huang et al., 2020; Wang et al., 2021). While chemical elicitors effectively manage viral diseases, they often result in significant growth penalties in many cases (Heil and Baldwin, 2002). Previous studies by Azami-Sardooei et al. (2013) observed no changes in plant size or yield of tomatoes treated with BTH relative to that in the controls, except for low-level leaf stunting and slight leaf scorching at high concentrations (1,000 mg L^{-1}). However, in cucumbers and beans, 100 mg L^{-1} BTH treatment reduced the plant size, growth rate, and flower and fruit numbers. Spychalski et al. (2021) demonstrated that BTH-mediated induction of SAR may alter plant resource allocation, leading to a growth–immunity trade-off and potentially reducing yield. Furthermore, Yu et al. (2021) found that dufulin exposure affected the fatty acid transport involved in carnitine formation, altering free fatty acid concentrations and Tubifex's oxidative damage response. Moreover, dufulin may act on the urea cycle by inhibiting ASL, causing urea cycle disorder. However, the long-term toxic effects of BTH and dufulin on plants and the environment remain unclear. Conversely, *B. velezensis* is recognized as an important biocontrol strain capable of triggering disease resistance across various plant species while being environment friendly, as it completely degrades in soil without residue (Ye et al., 2018).

Recent studies have emphasized that *B. velezensis* can induce plant disease resistance through various cluster genes involved in the synthesis of non-ribosomal and ribosomal secondary metabolites, volatile compounds, and cyclic lipopeptides with antimicrobial properties; these genes also act as stimulators of ISR (Ye et al., 2018; Borriss et al., 2019). A previous study revealed the potent inhibitory effect of *B. velezensis* strain PEA1 against *F. oxysporum* and CMV infections, suggesting its potential as a biocontrol agent (Abdelkhalek et al., 2020). Vinodkumar et al.

(2018) reported the effective reduction of TSV incidence by *B. amyloliquefaciens* (VB7) under field and glasshouse conditions. Similarly, Lee and Ryu (2016) observed no reduction in fruit yield with *Bacillus amyloliquefaciens* strain 5B6 treatment compared to that in water-treated control plants. However, BTH treatment consistently reduced fruit yield in pepper. Moreover, few studies have directly compared the efficacy of biological controls and chemical inducers of plant immunity (such as dufulin and BTH) against plant viruses. In the present study, we selected BTH and dufulin as positive controls and revealed that the primary mechanism of *B. velezensis* HN-2 resistance to PVMV is the induction of systemic resistance. Under greenhouse conditions, soil and plant root irrigation with *B. velezensis* strain HN-2-GFP, combined with foliar application of benzothiadiazole and dufulin 48 h before viral inoculation, significantly ($P < 0.05$) reduced the disease symptoms and PVMV accumulation levels in treated tobacco plants compared to those in the PVMV-, BTH-, or dufulin-treated plants at 7 dpi. Visualization of green fluorescent signals in the inoculated leaves treated with *B. velezensis* HN-2 revealed much lower intensities at 5 and 7 dpi compared to those in negative and positive controls. This reduction was accompanied by mosaic patterns and severe shrivel symptoms in the negative and positive controls, while no evident symptoms were observed in the mock or *B. velezensis* HN-2 extract-treated tobacco plants.

In DAB staining, 3,3-diaminobenzidine was used to visually detect H_2O_2, as ROS generation is often associated with plant cell death (Zhu et al., 2013). Oxidized DAB precipitates as a brown color at the peroxidase site and is observable via light microscopy (Hans et al., 1997; Liu et al., 2014; Zhu et al., 2016). Furthermore, with increasing processing time, the leaves of plants treated with PVMV, BTH, and dufulin gradually darkened. By the 7th day, the PVMV-treated leaves exhibited substantial browning, whereas those treated with BTH and dufulin displayed dark brown precipitates covering approximately two-thirds of the leaf area. Conversely, HN-2-treated leaves showed the least browning compared to the negative and positive controls, with water-treated leaves appearing almost transparent. These DAB staining results were consistent with the results of green fluorescence analysis. Western blot analysis of young leaves at 15 dpi also showed similar results. These results strongly suggest that *B. velezensis* HN-2 not only exerts a strong antiviral effect but also exhibits sustained efficacy. This may be attributed to the *B. velezensis* HN-2-mediated induction of plant ISR, conferring robust resilience in *N. benthamiana* against PVMV-GFP infection and sustaining its antiviral effects over time.

Plants exhibit specific resistance mechanisms when faced with adverse conditions. HR refers to programmed cell death triggered by an exaggerated response at the infection site. Various reports have indicated that HR causes rapid death of plant cells, which can effectively limit pathogen growth at the infection site, thereby preventing further spread to the surrounding healthy tissues and activating plant resistance responses (Guo et al., 2020; Wang et al., 2021). Viral infections can induce a burst of ROS in host plants, resulting in oxidative stress (Yang et al., 2018). Notably, H_2O_2, a type of ROS, serves as an early mediator of plant resistance (Wu et al., 2015). Accordingly, the rapid generation of ROS is a preliminary process by which plants respond to pathogen challenges, with H_2O_2 being capable of initiating cell death during the HR response (Delledonne et al., 2001). Plant cells defend themselves against the oxidative damage caused by ROS through the production of antioxidant enzymes, such as SOD, POD, CAT, MDA, and PAL, which play important roles in plant defense against pathogens and counteract viral infection (Zhang et al., 2016; Lv et al., 2020). Guo et al. (2019) found that following viral infection, POD, PPO, and PAL activities increased more rapidly in the leaves of Ba13-treated plants than in those of the controls. The antiviral activity of *Bacillus velezensis* PEA1 induces systemic resistance to CMV, with significantly elevated transcriptional levels of *PAL*, *CHS*, *HQT, PR-1*, and *POD* (Abdelkhalek et al., 2020). Lv et al. (2020) reported that an increase in SOD, POD, CAT, and MDA activities leads to the activation of the plant immune system to combat TMV infection. Similarly, our study revealed that HN-2 treatment reduced PVMV-induced oxidative damage by increasing SOD, POD, and CAT activities compared to those in the blank and negative controls, thereby achieving antiviral effects. These results suggest that SOD, POD, and CAT eliminate excess peroxides, thereby preventing oxidative damage. In contrast, the activity of MDA after HN-2 treatment was lower than that of the blank and negative controls, with no significant difference in activity observed from 1 to 5 dpi following pHNu-GFP inoculation. Following stress exposure, the upregulation of CAT can minimize oxidative stress, which plays a critical role in preventing oxidative damage and protecting plant cells from the oxidative damage caused by ROS (Blackman and Hardham, 2008; Abdelkhalek et al., 2021). In our experiments, the expression of *Cat1* remained consistent across all treatments at 1 and 3 dpi, with rapid accumulation observed in the HN-2-treated plants at 5 dpi, aligning with changes in CAT enzyme activities, demonstrating the efficacy of *B. velezensis* HN-2 in protecting cells from ROS-induced damage, and inducing long-lasting systemic resistance in *N. benthamiana* following primary inoculation.

SAR and ISR are two major forms of plant defense, wherein the plant hormones SA, JA, ABA, and ET play key roles in regulating the signaling networks associated with plant defense against pathogens. SA is essential for SAR activation in tissues distal to the infection site, whereas jasmonate and ethylene are required for ISR (Zhu et al., 2016). Abdelkhalek et al. (2020) demonstrated that SAR induced *B. velezensis* PEA1 against CMV-activated gene expression and enzyme activity related to systemic resistance while inhibiting infection. ISR is recognized as an effective biological control method for inducing plant defense against a broad range of pathogens (Nie et al., 2017). JA serves as a regulatory factor of ISR (Zhou and Wang, 2018); previous studies have shown that *B. amyloliquefaciens* Ba13 can enhance plant resistance against TYLCV disease by directly inducing systemic resistance and increasing the number of beneficial microbes in the rhizosphere (Guo et al., 2019). In the present study, the simultaneous determination of JA and SA revealed that the SA content under the HN-2 treatment gradually increased, reaching a peak at 3 dpi, and subsequently decreased. At 5 dpi, the blank control and BTH-treated groups had 1.33- and 1.37-folds higher SA contents than the HN-2-treated group, respectively. Meanwhile, the expression of JA rapidly increased after 3 dpi and peaked at 5 dpi in

the HN-2-treated plants; it was 7.81-, 2.22-, and 4.29-folds higher than that in the blank control and BTH- and dufulin-treated groups, respectively. These results indicate that *B. velezensis* HN-2 treatment significantly elevated JA expression, potentially activating resistance-related gene expression and defense enzyme activity to enhance plant-induced systemic resistance, thereby aiding in the control of PVMV infection.

Rbohs are key enzymes responsible for ROS production in response to hormonal and environmental signals in plants and play crucial roles in plant growth, development, and stress responses (Suzuki et al., 2011; Sun et al., 2015). ROS levels are elevated by Rboh enzymes in response to multiple biotic and abiotic stresses (He et al., 2017; Liu et al., 2017; Zhai et al., 2018; Chapman et al., 2019). In the present study, the expression of *Rboh* under the HN-2 treatment increased by 1.89-, 1.18-, and 1.34-folds at 1, 3, and 5 dpi, respectively, compared to that in the blank control group but remained lower than that in the BTH- and dufulin-treated groups. These results suggest that *B. velezensis* strain HN-2 may potentially maintain *Rboh* in a low-expression state to restrict ROS production and consequently reduce PVMV-induced oxidative damage. *PAL* is a key regulatory enzyme of the phenylpropanoid pathway and is involved in the production of polyphenolic compounds (Guo et al., 2020). POD and *PAL* play important roles in plant defenses against pathogens. Wang et al. (2012) observed that tobacco plants with excessive expression of the *PAL* enzyme exhibited strong resistance to TMV infection, whereas plants with inhibited enzyme activity were more susceptible to TMV. Interestingly, in the present study, *PAL* expression was significantly increased under the HN-2 treatment, peaking at 24 h before reducing to near-normal levels at 3 dpi, and subsequently increased by 25.58-, 15.33-, and 6.47-fold compared with BTH- and dufulin-treated controls at 5 dpi, respectively. Conversely, POD activity was lowest at 1 dpi and increased rapidly at 3 dpi, which indicated that *PAL* expression was induced in advance following virus infection and continued to be induced at 5 dpi, thereby enabling sustained POD activity after 3 dpi. At 5 dpi, the HN-2 treatment demonstrated the highest level at 1,660.31 unit mg^{-1} FW, indicating 1.15-, 1.16-, and 1.57-fold increase in activity compared to the BTH treatment, dufulin treatment, and blank control, respectively. This increase in POD activity may activate the plant immune system to combat PVMV infection.

PR proteins are produced in plants during pathogen attacks and constitute vital components of the plant defense mechanism (Sels et al., 2008). Numerous studies have shown that PGPRs boost plant health by improving defense against various pathogens, often associated with JA and ET pathway induction (Beneduzi et al., 2012; Pieterse et al., 2014; Rahman et al., 2015). In tobacco, ISR triggered by non-pathogen PGPR strains is accompanied by the upregulation of PR genes encoding pathogenesis-related proteins, as evidenced by RT-PCR analysis results indicating an increased expression of PR genes upon treatment with *B. velezensis* (Wang et al., 2009). SAR, demonstrated across many plant species, involves the accumulation of PR proteins (*PR-1*, *PR-2*, and *PR-5*) and SA as its molecular basis (Gao et al., 2014). Niu et al. (2011) found that ISR simultaneously activates the SA- and JA/ET-dependent signaling pathways, leading to the induced expressions of *PR1*, *PR2*, *PR5*, and *PDF1.2*. *NPR1* acts as a regulator of SAR and ISR, mediating the SA–JA crosstalk (Pieterse et al., 2014). The *NPR1* (nonexpresser of PR genes) protein serves as a key regulator in transmitting SA and JA/ethylene signals, thus triggering acquired resistance responses (Spoel et al., 2003). Previous studies suggest that the induction of *PR1* gene synthesis may be associated with increased *NPR1* gene expression and conformational changes in the *NPR1* protein (Mou et al., 2003). Nie et al. (2017) showed that root-drench application of *Bacillus cereus* AR156 significantly reduced disease incidence by activating ISR through a mechanism dependent on *NPR1*, leading to the expression of downstream defense-related genes, such as *PR1*, *PR2*, *PR5*, and *PDF1.2*, and activation of cellular defense responses. Similarly, inoculation with *B. amyloliquefaciens* Ba13 improved the defense ability of tomato plants against TYLCV infection by activating the expression of genes and enzymes related to systemic resistance in tomato—for example, by increasing the expression of the resistance-related genes *PR1*, *PR2*, and *PR3* (Guo et al., 2019). The expression of *PR-1b*, *PR3*, *PR5*, and *NPR1* gradually increased over time in the leaves of HN-2-treated *N. benthamiana* after PVMV inoculation; we quantitatively analyzed the gene expression at 1, 3, and 5 dpi. Consistent with previous findings, *B. velezensis* HN-2 treatment significantly increased the transcriptional levels of *NPR1*, *PR-1b*, *PR3*, and *PR5*, with *PR3* and *PR5* showing the most significant upregulation compared to those in the blank control. Our experimental results indicated that *B. velezensis* HN-2 treatment significantly increased PR gene expression and activated plant-induced systemic resistance, thus highlighting the antiviral properties of this strain. From an agronomic perspective, the ISR triggered by PGPR is interesting, given its long-lasting and broad-spectrum protection without growth costs and its minimal potential to promote pathogen resistance (Köhl et al., 2019). In a previous study, *Arabidopsis* plants were root-drenched with *Bacillus cereus* AR156 at 5×10^8 CFU mL^{-1}, with 10 inoculated plants for each genotype. The results showed that AR156 only colonized the roots and significantly reduced disease incidence through the activation of ISR (Nie et al., 2017). Guo et al. (2019) watered tomato plants with a *Bacillus amyloliquefaciens* Ba13 suspension at 10^6 CFU mL^{-1}; after 3 weeks, post-bacterial inoculation performed viral infection, wherein 65 replicates were sampled for systemic resistance-related assays and virus quantification. It was found that the number and distribution of rhizosphere-dominant bacteria were changed by Ba13 application and can enhance plant resistance against TYLCV disease through the direct induction of systemic resistance. To elucidate the relationship between the colonization of *B. velezensis* HN-2 in *C. chinense* roots and its role in plant virus resistance, a total of 600 plants were subjected to root drenches with *B. velezensis* strain HN-2 at 10^6 CFU g^{-1} under greenhouse cultivation conditions. The results demonstrated that *B. velezensis* HN-2 rapidly colonized the rhizosphere within 72 h, and with the extension of treatment time, HN-2 mainly colonized the root interior after 5 dpi. Subsequently, the number of colonies in *C. chinense* root interior increased by fivefold compared to that in the rhizosphere. Western blotting of PVMV-GFP protein accumulation after 60

days of inoculation showed that high levels of GFP protein were detected only in pHNu-GFP treatment, while when treated with benzothiadiazole, dufulin, and *B. velezensis* HN-2, GFP protein was almost undetectable in plants. Simultaneously, at 60 days after PVMV-GFP inoculation, a comparative experiment was conducted on the antiviral effect of *B. velezensis* HN-2 on *C. chinense* plants grown in soil that was irrigated under field conditions. We observed that the growth of *C. chinense* treated with HN-2 was significantly superior to that of PVMV-infected plants treated with BTH and dufulin, resembling that of the blank control at 180 dpi in the field.

In a word, the data presented in this study indicate that *B. velezensis* HN-2 functions as a PGPR, rapidly colonizing *C. chinense* roots and activating the expression of genes and enzymes associated with systemic resistance. When plants were infected with PVMV and treated with *B. velezensis* HN-2, the JA signaling pathway was activated, leading to increased *JA* content and the simultaneous activation of the *NPR1*-dependent mechanism, resulting in the significant upregulation of *PR-1b*, *PR3*, and *PR5*. Moreover, cellular defense responses, including CAT, POD, *Rboh*, *PAL*, and *CAT1* activities, exhibited a more rapid and significant increase. Furthermore, the increased expression of JA pathway genes suggests the activation of ISR under *Bacillus velezensis* HN-2 treatment. However, there was no significant increase in SA content, indicating that systemic acquired resistance (SAR) pathway was not induced by this treatment (Figure 8). In conclusion, *B. velezensis* HN-2 can effectively induce plant ISR-mediated defense responses and enhances plants' immunity (including *C. chinense*) by activating the JA signaling pathway, thereby mitigating symptoms caused by PVMV and safeguarding the plants against pathogenic infections.

5 Conclusions

In summary, *Bacillus velezensis* HN-2 is a new antiviral agent against plant viruses and plays significant roles in ISR by activating gene expression and enzyme activity related to systemic resistance, thus inhibiting infection. The strain HN-2 may be considered a promising source of plant growth promotion, with highly effective antiviral substances for plant protection and for development against PVMV diseases. This study provides theoretical basis for the green prevention and control of plant virus diseases.

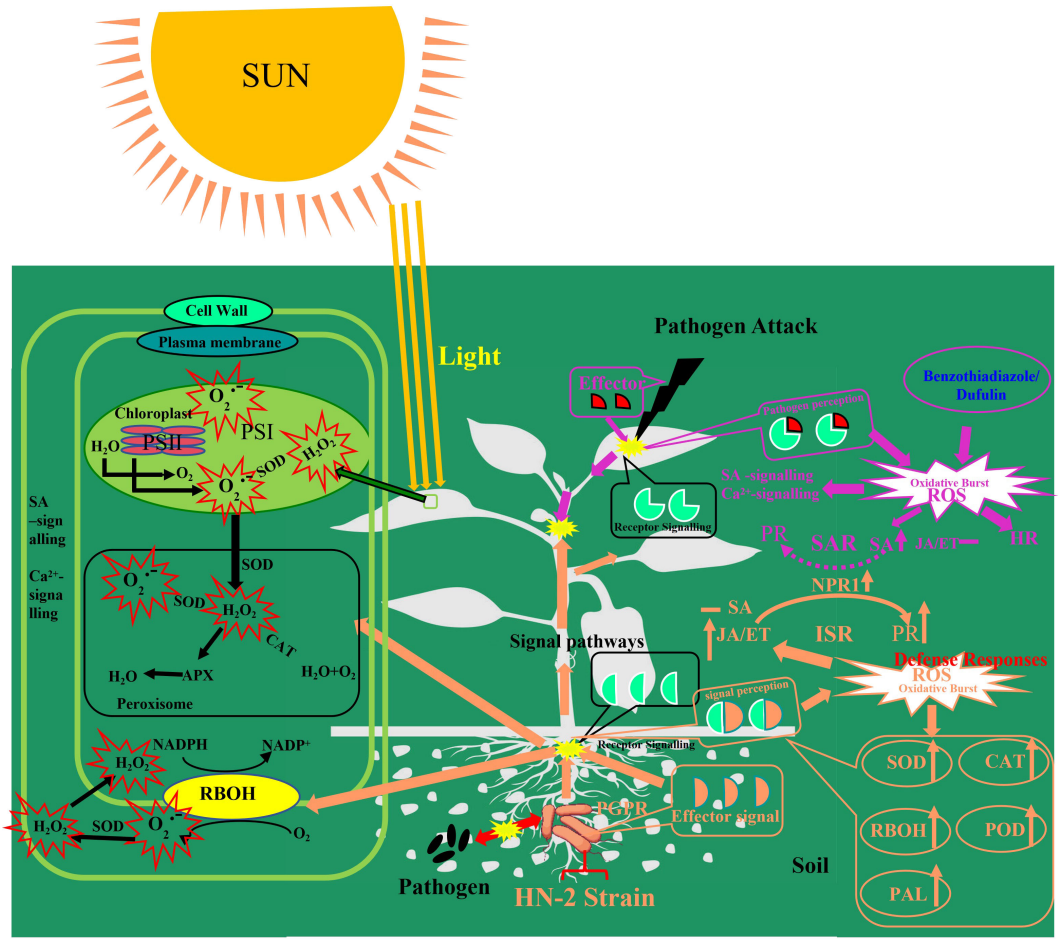

FIGURE 8
Conceptual model depicting the mechanisms illustrating how symbiosis and convocation probiotics by *B. velezensis* on the rhizosphere and soil ultimately inhibit plant pathogens (plant disease and virus).

Data availability statement

The datasets presented in this study can be found in online repositories. The names of the repository/repositories and accession number(s) can be found in the article/Supplementary Material.

Author contributions

PJ: Formal analysis, Funding acquisition, Supervision, Writing – review & editing. ZX: Data curation, Investigation, Writing – original draft. YW: Data curation, Investigation, Writing – original draft. YS: Data curation, Methodology, Writing – original draft. XP: Data curation, Investigation, Writing – original draft. JW: Data curation, Investigation, Writing – original draft. WL: Formal analysis, Resources, Writing – review & editing. WM: Supervision, Writing – review & editing.

Funding

The author(s) declare financial support was received for the research, authorship, and/or publication of this article. This work was supported by grants from Hainan Provincial Natural Science Foundation-the Scientific Research Foundation for Advanced Talents (Grant No. 2019RC163; 324RC455), the National Natural Science Foundation of China (Grant No. 31960552; 32260698), the Collaborative Innovation Center of Nanfan and High Efficiency Tropical Agriculture of Hainan University (XTCX2022NYA01).

Acknowledgments

We would like to thank Prof. Xianchao Sun (Southwest University, Chongqing, China) for technical support. We would like to thank Prof. Hongguang Cui (Hainan University, Haikou, China) for providing the pHNu-GFP (PVMV-GFP) vectors.

Conflict of interest

The authors declare that the research was conducted in the absence of any commercial or financial relationships that could be construed as a potential conflict of interest.

Publisher's note

Supplementary material

The Supplementary Material for this article can be found online at: https://www.frontiersin.org/articles/10.3389/fpls.2024.1403202/full#supplementary-material

References

Abdelkhalek, A., Al-Askar, A. A., Alsubaie, M. M., and Behiry, S. I. (2021). First Report of Protective Activity of Paronychia argentea Extract against Tobacco Mosaic Virus Infection. *Plants.* 10, 2435. doi: 10.3390/plants10112435

Abdelkhalek, A., Behiry, S. I., and Al-Askar, A. A. (2020). *Bacillus velezensis* PEA1 Inhibits Fusarium oxysporum Growth and Induces Systemic Resistance to Cucumber Mosaic Virus. *Agronomy.* 10, 1312. doi: 10.3390/agronomy10091312

Alegbejo, M. D. (1999). Physalis micrantha L., a weed host of pepper veinal mottle virus. *J. Vegetable Crop Production.* 5, 59–66. doi: 10.1300/J068v05n01_06

Alegbejo, M. D., and Abo, M. E. (2002). Ecology, epidemiology and control of pepper veinal mottle virus (PVMV), genus potyvirus, in West Africa. *J. Sustain. Agriculture.* 20, 5–16. doi: 10.1300/J064v20n02_03

Atiri, G. I., and Ligan, D. (1986). Effects of pyrethroids (Cypermethrin and deltamethrin) on the disease expression of cowpea aphid-borne mosaic virus. *Agric. Ecosyst. Environment.* 15, 31–37. doi: 10.1016/0167-8809(86)90111-8

Azami-Sardooei, Z., Seifi, H. S., and De Vleesschauwer, D. (2013). Benzothiadiazole (BTH)-induced resistance against *Botrytis cinerea* is inversely correlated with vegetative and generative growth in bean and cucumber, but not in tomato. *Australas. Plant Pathology.* 42, 485–490. doi: 10.1007/s13313-013-0207-1

Beneduzi, A., Ambrosini, A., and Passaglia, L. M. P. (2012). Plant growth-promoting rhizobacteria (PGPR): Their potential as antagonists and biocontrol agents. *Genet. Mol. Biol.* 35 (4 Suppl), 1044–1051. doi: 10.1590/S1415-47572012000600020

Blackman, L. M., and Hardham, A. R. (2008). Regulation of catalase activity and gene expression during Phytophthora nicotianae development and infection of tobacco. *Mol. Plant Pathol.* 9, 495–510. doi: 10.1111/j.1364-3703.2008.00478.x

Blée, E. (2002). Impact of phyto-oxylipins in plant defense. *Trends Plant Sci.* 7, 315–322. doi: 10.1016/S1360-1385(02)02290-2

Borriss, R., Wu, H., and Gao, X. (2019). *Secondary metabolites of the plant growth promoting model rhizobacterium* bacillus velezensis *FZB42 are involved in direct suppression of plant pathogens and in stimulation of plant-induced systemic resistance* (Singapore: Springer). doi: 10.1007/978-981-13-5862-3_8

Boutrot, F., and Zipfel, C. (2017). Function, discovery, and exploitation of plant pattern recognition receptors for broad-spectrum disease resistance. *Annu. Rev. Phytopathology.* 55, 257–286. doi: 10.1146/annurev-phyto-080614-120106

Brunt, A. A., and Kenten, R. H. (1971). Pepper veinal mottle virus-a new member of the potato virus Y group from peppers (*Capsicum annuum* L. and *C. frutescens* L.) in Ghana. *Ann. Appl. Biol.* 69, 235–243. doi: 10.1111/j.1744-7348.1971.tb04676.x

Brunt, A. A., Kenten, R. H., and Phillips, S. (1978). Symptomatologically distinct strains of pepper veinal mottle virus from four West African solanaceous crops. *Ann. Appl. Biol.* 88, 115–119. doi: 10.1111/j.1744-7348.1978.tb00685.x

Cazorla, F. M., Romero, D., Pérez-García, A., Lugtenberg, B. J. J., de Vicente, A., and Bloemberg, G. (2007). Isolation and characterization of antagonistic *Bacillus subtilis* strains from the avocado rhizoplane displaying biocontrol activity. *J. Appl. Microbiol.* 103, 1950–1959. doi: 10.1111/j.1365-2672.2007.03433.x

Chapman, J. M., Muhlemann, J. K., Gayomba, S. R., and Muday, G. K. (2019). *Rboh*-dependent ROS synthesis and ROS scavenging by plant specialized metabolites to modulate plant development and stress responses. *Chem. Res. toxicology.* 32, 370–396. doi: 10.1021/acs.chemrestox.9b00028

Chen, Q., and Yang, G. (2020). Signal function studies of ROS, especially *rboh*-dependent ROS, in plant growth, development and environmental stress. *J. Plant Growth Regulation.* 39, 157–171. doi: 10.1007/s00344-019-09971-4

Chen, Z., Zeng, M., Song, B., Hou, C., Hu, D., Li, X., et al. (2012). Dufulin activates hrBP1 to produce antiviral responses in tobacco. *PloS One* 7, e37944. doi: 10.1371/journal.pone.0037944

Cui, H. G., and Wang, A. M. (2016). Plum pox virus6K1 protein is required for viral replication and targets the viral replication complex at the early stage of infection. *J. Virology.* 90, 5119–5131. doi: 10.1128/JVI.00024-16

Cui, H. G., and Wang, A. M. (2017). An efficient viral vector for functional genomic studies of Prunus fruit trees and its induced resistance to Plum pox virus via silencing of a host factor gene. *Plant Biotechnol. J.* 15, 344–356. doi: 10.1111/pbi.12629

Daudi, A., and O'Brien, J. A. (2012). Detection of hydrogen peroxide by DAB staining in arabidopsis leaves. *Bio-protocol.* 2, e263. doi: 10.21769/BioProtoc.263

Delledonne, M., Zeier, J., Marocco, A., and Lamb, C. (2001). Signal interactions between nitric oxide and reactive oxygen intermediates in the plant hypersensitive disease resistance response. *Proc. Natl. Acad. Sci.* 98, 13454–13459. doi: 10.1073/pnas.231178298

Deng, Y., Chen, H., Li, C., Xu, J., Qi, Q., and Xu, Y. (2019). Endophytebacillus subtilisevade plant defense by producing lantibiotic subtilomycin to mask self-produced flagellin. *Commun. Biol.* 2, 368. doi: 10.1038/s42003-019-0614-0

Dixon, R. A., Achnine, L., Kota, P., Liu, C. J., Reddy, M. S., and Wang, L. (2002). The phenylpropanoid pathway and plant defence-a genomics perspective. *Mol. Plant pathology.* 3, 371–390. doi: 10.1046/j.1364-3703.2002.00131.x

El-Gendi, H., Al-Askar, A. A., Király, L., Samy, M. A., Moawad, H., and Abdelkhalek, A. (2022). Foliar Applications of *Bacillus subtilis* HA1 Culture Filtrate Enhance Tomato Growth and Induce Systemic Resistance against Tobacco mosaic virus Infection. *Horticulturae.* 8, 301. doi: 10.3390/horticulturae8040301

Fajinmi, A. A., and Odebode, C. A. (2010). Evaluation of maize/pepper intercropping model in the management of pepper veinal mottle virus, genus Potyvirus, family Potyviridae on cultivated pepper (*Capsicum annuum* L.) in Nigeria. *Arch. Phytopathol. Plant Protection.* 43, 1524–1533. doi: 10.1080/03235400802583677

Fira, D., Dimkić, I., Berić, T., Lozo, J., and Stanković, S. (2018). Biological control of plant pathogens by Bacillus species. *J. Biotechnol.* 285, 44–55. doi: 10.1016/j.jbiotec.2018.07.044

Friedrich, L., Lawton, K. A., and Ruess, W. (1996). A Benzothiadiazole derivative induces systemic acquired resistance in tobacco. *Plant J.* 10, 61–70. doi: 10.1046/j.1365-313X.1996.10010061.x

Gao, Q. M., Kachroo, A., and Kachroo, P. (2014). Chemical inducers of systemic immunity in plants. *J. Exp. botany.* 65, 1849–1855. doi: 10.1093/jxb/eru010

García-Gutiérrez, M. S., Ortega-Álvaro, A., Busquets-García, A., Pérez-Ortiz, J. M., Caltana, L., Ricatti, M. J., et al. (2013). Synaptic plasticity alterations associated with memory impairment induced by deletion of CB2 cannabinoid receptors. *Neuropharmacology.* 73, 388–396. doi: 10.1016/j.neuropharm.2013.05.034

Gill, S. S., and Tuteja, N. (2010). Reactive oxygen species and antioxidant machinery in abiotic stress tolerance in crop plants. *Plant Physiol. biochemistry: PPB.* 48, 909–930. doi: 10.1016/j.plaphy.2010.08.016

Givord, L. (1982). Pepper veinal mottle virus in the weed Physalis angulata in the Ivory Coast. *Plant Disease.* 66, 1081–1082. doi: 10.1094/PD-66-1081

Guo, Q., Li, Y., and Lou, Y. (2019). *Bacillus amyloliquefaciens* Ba13 induces plant systemic resistance and improves rhizosphere microecology against tomato yellow leaf curl virus disease. *Appl. Soil Ecology.* 137, 154–166. doi: 10.1016/j.apsoil.2019.01.015

Guo, W., Yan, H., Ren, X., Tang, R., Sun, Y., Wang, Y., et al. (2020). Berberine induces resistance against tobacco mosaic virus in tobacco. *Pest Manage. science.* 76, 1804–1813. doi: 10.1002/ps.5709

Ha, J. H., Hong, J. S., Kim, T. S., and Ryu, K. H. (2008). Complete genome sequence of an isolate of Pepper veinal mottle virus and phylogenetic relationship with other potyviruses. *Arch. virology.* 153, 2315–2318. doi: 10.1007/s00705-008-0245-0

Hans, T.-C., Zhang, Z., and Wei, Y. (1997). Subcellular localization of H_2O_2 in plants. H_2O_2 accumulation in papillae and hypersensitive response during the barley—powdery mildew interaction. *Plant J.* 11, 1187–1194. doi: 10.1046/j.1365-313X.1997.11061187.x

Hashem, A., Tabassum, B., and Fathi Abd Allah, E. (2019). *Bacillus subtilis*: A plant-growth promoting rhizobacterium that also impacts biotic stress. *Saudi J. Biol. Sci.* 26, 1291–1297. doi: 10.1016/j.sjbs.2019.05.004

He, H., Yan, J., Yu, X., Liang, Y., Fang, L., Scheller, H. V., et al. (2017). The NADPH-oxidase At*Rboh*I plays a positive role in drought-stress response in Arabidopsis thaliana. *Biochem. Biophys. Res. Commun.* 491, 834–839. doi: 10.1016/j.bbrc.2017.05.131

Heil, M., and Baldwin, I. T. (2002). Fitness costs of induced resistance: emerging experimental support for a slippery concept. *Trends Plant science.* 7, 61–67. doi: 10.1016/S1360-1385(01)02186-0

Hu, W., Qin, L., Yan, H., Miao, W., Cui, H., and Liu, W. (2020). Use of an Infectious cDNA Clone of Pepper Veinal Mottle Virus to Confirm the Etiology of a Disease in Capsicum chinense. *Phytopathology.* 110, 80–84. doi: 10.1094/PHYTO-08-19-0307-FI

Huang, L., Wang, S., and Zhang, Z. (2020). The effect and mechanism of Dufulin in controlling tomato yellow leaf curl virus on tomato plants. *Res. Square*. doi: 10.21203/rs.3.rs-44135/v1

Jayaraj, J., Yi, H., and Liang, G. H. (2004). Foliar application of *Bacillus subtilis* AUBS1 reduces sheath blight and triggers defense mechanisms in rice. *Z. fur Pflanzenkrankheiten und Pflanzenschutz.* 2), 111. doi: 10.1007/BF03356138

Jin, P. F., Wang, H., Tan, Z., Xuan, Z., Dahar, G. Y., Li, Q. X., et al. (2020a). Antifungal mechanism of bacillomycin D from *Bacillus velezensis* HN-2 against *Colletotrichum gloeosporioides* Penz. *Pesticide Biochem. Physiol.* 163, 102–107. doi: 10.1016/j.pestbp.2019.11.004

Jin, P. F., Wang, Y., Tan, Z., Liu, W. B., and Miao, W. G. (2020b). Antibacterial activity and rice-induced resistance, mediated by C_{15}surfactin A, in controlling rice disease caused by *Xanthomonas oryzae* pv. *oryzae*. *Pesticide Biochem. Physiol.* 169, 104669. doi: 10.1016/j.pestbp.2020.104669

Köhl, J., Kolnaar, R., and Ravensberg, W. J. (2019). Mode of action of microbial biological control agents against plant diseases: relevance beyond efficacy. *Front. Plant science.* 10. doi: 10.3389/fpls.2019.00845

Kong, H. G., Shin, T. S., Kim, T. H., and Ryu, C. M. (2018). Stereoisomers of the bacterial volatile compound 2,3-butanediol differently elicit systemic defense responses of pepper against multiple viruses in the field. *Front. Plant science.* 9. doi: 10.3389/fpls.2018.00090

Kunz, W., Schurter, R. D., and Maetzke, T. (1997). The chemistry of benzothiadiazole plant activators. *Pesticide Science.* 50, 275–282. doi: 10.1002/(SICI)1096-9063(199708)50:43.0.CO;2-7

Lee, G. H., and Ryu, C. M. (2016). Spraying of Leaf-Colonizing *Bacillus amyloliquefaciens* Protects Pepper from Cucumber mosaic virus. *Plant disease.* 100, 2099–2105. doi: 10.1094/PDIS-03-16-0314-RE

Liang, J., Wang, J. H., Zhang, S. Y., Yu, N. T., Zhang, Y. L., Wang, X., et al. (2015). Identification and detection of pepper veinal mottle virus in hainan. *Chin. J. Trop. Crops.* 36 (5), 966–971.

Liu, Y. H., Offler, C. E., and Ruan, Y. L. (2014). A simple, rapid, and reliable protocol to localize hydrogen peroxide in large plant organs by DAB-mediated tissue printing. *Front. Plant science.* 5. doi: 10.3389/fpls.2014.00745

Liu, C., Peang, H., Li, X., Liu, C., Lv, X., Wei, X., et al. (2020). Genome-wide analysis of NDR1/HIN1-like genes in pepper (*Capsicum annuum* L.) and functional characterization of *CaNHL*$_4$ under biotic and abiotic stresses. *Horticulture Res.* 7, 93. doi: 10.1038/s41438-020-0318-0

Liu, B., Sun, L., Ma, L., and Hao, F. (2017). Both At*Rboh*D and At*Rboh*F are essential for mediating responses to oxygen deficiency in Arabidopsis. *Plant Cell Rep.* 36, 947–957. doi: 10.1007/s00299-017-2128-x

Livak, K. J., and Schmittgen, T. D. (2001). Analysis of relative gene expression data using real-time quantitative PCR and the 2(-Delta Delta C(T)) Method. *Methods (San Diego Calif.).* 25, 402–408. doi: 10.1006/meth.2001.1262

Loreto, F., and Velikova, V. (2001). Isoprene produced by leaves protects the photosynthetic apparatus against ozone damage, quenches ozone products, and reduces lipid peroxidation of cellular membranes. *Plant Physiol.* 127, 1781–1787. doi: 10.1104/pp.010497

Lv, X., Xiang, S., Wang, X., Wu, L., Liu, C., Yuan, M., et al. (2020). Synthetic chloroinconazide compound exhibits highly efficient antiviral activity against tobacco mosaic virus. *Pest Manage. science.* 76, 3636–3648. doi: 10.1002/ps.5910

Mariuotto, M., and Ongena, M. (2015). Molecular patterns of rhizobacteria involved in plant immunity elicitation. *Adv. Botanical Res.* 75, 21–56. doi: 10.1016/bs.abr.2015.07.002

Matsumoto, K., Yasaka, R., and Setoyama, T. (2016). Chilli pepper rugose mosaic disease caused by Pepper veinal mottle virus occurs on Ishigaki Island, Japan[J]. *J. Gen. Plant Pathology.* 82, 57–60. doi: 10.1007/s10327-015-0634-7

Mou, Z., Fan, W., and Dong, X. (2003). Inducers of plant systemic acquired resistance regulate *NPR1* function through redox changes. *Cell.* 113, 935–944. doi: 10.1016/S0092-8674(03)00429-X

Murphy, J. F., Reddy, M. S., Ryu, C. M., Kloepper, J. W., and Li, R. (2003). Rhizobacteria-Mediated Growth Promotion of Tomato Leads to Protection Against Cucumber mosaic virus. *Phytopathology.* 93, 1301–1307. doi: 10.1094/PHYTO.2003.93.10.1301

Murphy, J. F., Zehnder, G. W., Schuster, D. J., Sikora, E. J., Polston, J. E., and Kloepper, J. W. (2000). Plant Growth-Promoting Rhizobacterial Mediated Protection in Tomato Against Tomato mottle virus. *Plant disease.* 84, 779–784. doi: 10.1094/PDIS.2000.84.7.779

Nakano, M., and Mukaihara, T. (2018). Ralstonia solanacearum type III effector ri*PAL* targets chloroplasts and induces jasmonic acid production to suppress salicylic acid-mediated defense responses in plants. *Plant Cell Physiol.* 59, 2576–2589. doi: 10.1093/pcp/pcy177

Nie, P., Li, X., Wang, S., Guo, J., Zhao, H., and Niu, D. (2017). Induced Systemic Resistance against *Botrytis cinerea* by *Bacillus cereus* AR156 through a JA/ET- and *NPR1*-Dependent Signaling Pathway and Activates PAMP-Triggered Immunity in *Arabidopsis*. *Front. Plant science.* 8. doi: 10.3389/fpls.2017.00238

Niu, D. D., Liu, H. X., Jiang, C. H., Wang, Y. P., Wang, Q. Y., Jin, H. L., et al. (2011). The plant growth-promoting rhizobacterium *Bacillus cereus* AR156 induces systemic resistance in Arabidopsis thaliana by simultaneously activating salicylate- and jasmonate/ethylene-dependent signaling pathways. *Mol. Plant-Microbe interactions: MPMI.* 24, 533–542. doi: 10.1094/MPMI-09-10-0213

Ongena, M., and Jacques, P. (2008). Bacillus lipopeptides: versatile weapons for plant disease biocontrol. *Trends Microbiol.* 16, 115–125. doi: 10.1016/j.tim.2007.12.009

Ongena, M., Jacques, P., Touré, Y., Destain, J., Jabrane, A., and Thonart, P. (2005). Involvement of fengycin-type lipopeptides in the multifaceted biocontrol potential of Bacillus subtilis. *Appl. Microbiol. Biotechnol.* 69, 29–38. doi: 10.1007/s00253-005-1940-3

Pieterse, C. M., van der Does, D., Zamioudis, C., Leon-Reyes, A., and Van Wees, S. C. (2012). Hormonal modulation of plant immunity. *Annu. Rev. Cell Dev. Biol.* 28, 489–521. doi: 10.1146/annurev-cellbio-092910-154055

Pieterse, C. M., Zamioudis, C., Berendsen, R. L., Weller, D. M., Van Wees, S. C., and Bakker, P. A. (2014). Induced systemic resistance by beneficial microbes. *Annu. Rev. phytopathology.* 52, 347–375. doi: 10.1146/annurev-phyto-082712-102340

Pršić, J., and Ongena, M. (2020). Elicitors of plant immunity triggered by beneficial bacteria. *Front. Plant science.* 11. doi: 10.3389/fpls

Radhakrishnan, R., Hashem, A., and Abd Allah, E. F. (2017). *Bacillus*: A biological tool for crop improvement through bio-molecular changes in adverse environments. *Front. Physiol.* 8. doi: 10.3389/fphys

Rahman, A., Uddin, W., and Wenner, N. G. (2015). Induced systemic resistance responses in perennial ryegrass against *Magnaporthe oryzae* elicited by semi-purified surfactin lipopeptides and live cells of *Bacillus amyloliquefaciens*. *Mol. Plant pathology.* 16, 546–558. doi: 10.1111/mpp.12209

Rajaofera, M. J. N., Wang, Y., Dahar, G. Y., Jin, P., Fan, L., Xu, L., et al. (2019). Volatile organic compounds of *Bacillus atrophaeus* HAB-5 inhibit the growth of *Colletotrichum gloeosporioides*. *Pesticide Biochem. Physiol.* 156, 170–176. doi: 10.1016/j.pestbp.2019.02.019

Sels, J., Mathys, J., De Coninck, B. M., Cammue, B. P., and De Bolle, M. F. (2008). Plant pathogenesis-related (PR) proteins: a focus on PR peptides. *Plant Physiol. biochemistry: PPB.* 46, 941–950. doi: 10.1016/j.plaphy.2008.06.011

Song, H., Liu, Y., Liu, Y., Wang, L., and Wang, Q. (2014). Synthesis and antiviral and fungicidal activity evaluation of β-carboline, dihydro-β-carboline, tetrahydro-β-carboline alkaloids, and their derivatives. *J. Agric. Food Chem.* 62, 1010–1018. doi: 10.1021/jf404840x

Song, B. A., Yang, S., Jin, L. H., and Bhadury, S. (2009). *). Environment friendly anti-plant viral agent* (Berlin: Springer press), 234–253. doi: 10.1007/978-3-642-03692-7

Spoel, S. H., Koornneef, A., Claessens, S. M., Korzelius, J. P., Van Pelt, J. A., Mueller, M. J., et al. (2003). *NPR1* modulates cross-talk between salicylate- and jasmonate-dependent defense pathways through a novel function in the cytosol. *Plant Cell.* 15, 760–770. doi: 10.1105/tpc.009159

Spychalski, M., Kukawka, R., Krzesiński, W., Spiżewski, T., Michalecka, M., Poniatowska, A., et al. (2021). Use of new BTH derivative as supplement or substitute of standard fungicidal program in strawberry cultivation. *Agronomy.* 11, 1031. doi: 10.3390/agronomy11061031

Sun, X. D., Hu, X. Y., and Yang, Y. P. (2015). Molecular and functional comparisons of reactive burst oxygen species gene family in arabidopsis. *Plant Diversity Resources.* 37, 463–471. doi: 10.7677/ynzwyj201514148

Suzuki, N., Miller, G., Morales, J., Shulaev, V., Torres, M. A., and Mittler, R. (2011). Respiratory burst oxidases: the engines of ros signaling. *Curr. Opin. Plant Biol.* 14, 691–699. doi: 10.1016/j.pbi.2011.07.014

Vinodkumar, S., Nakkeeran, S., Renukadevi, P., and Mohankumar, S. (2018). Diversity and antiviral potential of rhizospheric and endophytic *Bacillus* species and phyto-antiviral principles against tobacco streak virus in cotton. *Agriculture Ecosyst. Environment.* 267, 42–51. doi: 10.1016/j.agee.2018.08.008

Vurukonda, S. S. K. P., Giovanardi, D., and Stefani, E. (2018). Plant growth promoting and biocontrol activity of streptomyces spp. as endophytes. *Int. J. Mol. Sci.* 19, 952. doi: 10.3390/ijms19040952

Wang, D., Liu, B., Ma, Z., Feng, J., and Yan, H. (2021). Reticine A, a new potent natural elicitor: isolation from the fruit peel of Citrus reticulate and induction of systemic resistance against tobacco mosaic virus and other plant fungal diseases. *Pest Manage. science.* 77, 354–364. doi: 10.1002/ps.6025

Wang, S., Wu, H., Qiao, J., Ma, L., Liu, J., Xia, Y., et al. (2009). Molecular mechanism of plant growth promotion and induced systemic resistance to tobacco mosaic virus by Bacillus spp. *J. Microbiol. Biotechnol.* 19, 1250–1258. doi: 10.4014/jmb.0901.008

Wang, X. Q., Zhao, D. L., Shen, L. L., Jing, C. L., and Zhang, C. S. (2018). "Application and mechanisms of Bacillus subtilis in biological control of plant disease." in Role of Rhizospheric Microbes in Soil, ed. Meena, V (Singapore: Springer), 225–250. doi: 10.1007/978-981-10-8402-7_9

Wang, J., Zhu, Y., Wang, H., Zhang, H. S., and Wang, K. (2012). Inhibitory effects of esterified whey protein fractions by inducing chemical defense against tobacco mosaic virus (TMV) in tobacco seedlings. *Ind. Crops Products* 37, 207–212. doi: 10.1016/j.indcrop.2011.11.023

Wu, D., Chu, H., Jia, L., Chen, K., and Zhao, L. (2015). A feedback inhibition between nitric oxide and hydrogen peroxide in the heat shock pathway in Arabidopsis seedlings. *Plant Growth Regulation.* 75, 503–509. doi: 10.1007/s10725-014-0014-x

Wu, L., Wu, H., Chen, L., Zhang, H., and Gao, X. (2017). Induction of systemic disease resistance in Nicotiana benthamiana by the cyclodipeptides cyclo (l-Pro-l-Pro) and cyclo (d-Pro-d-Pro). *Mol. Plant pathology.* 18, 67–74. doi: 10.1111/mpp.12381

Yang, T., Zhu, L. S., Meng, Y., Lv, R., Zhou, Z., Zhu, L., et al. (2018). Alpha-momorcharin enhances Tobacco mosaic virus resistance in tobacco^{NN} by manipulating jasmonic acid-salicylic acid crosstalk. *J. Plant Physiol.* 223, 116–126. doi: 10.1016/j.jplph.2017.04.011

Ye, M., Tang, X., Yang, R., Zhang, H., Li, F., Tao, F., et al. (2018). Characteristics and application of a novel species of *bacillus: bacillus velezensis*. *ACS Chem. Biol.* 13, 500–505. doi: 10.1021/acschembio.7b00874

Yu, Y., Zhu, Y., Yang, J., Zhu, W., Zhou, Z., and Zhang, R. (2021). Effects of dufulin on oxidative stress and metabolomic profile of tubifex. *Metabolites.* 11, 381. doi: 10.3390/metabo11060381

Zhai, L., Sun, C., Feng, Y., Li, D., Chai, X., Wang, L., et al. (2018). Atrop6 is involved in reactive oxygen species signaling in response to iron-deficiency stress in arabidopsis thaliana. *FEBS Letters.* 592, 3446–3459. doi: 10.1002/1873-3468.13257

Zhang, G., Feng, J., Han, L., and Zhang, X. (2016). Antiviral activity of glycoprotein GP-1 isolated from *Streptomyces kanasensis* ZX01. *Int. J. Biol. macromolecules.* 88, 572–577. doi: 10.1016/j.ijbiomac.2016.04.038

Zhou, M., and Wang, W. (2018). Recent advances in synthetic chemical inducers of plant immunity. *Front. Plant science.* 9. doi: 10.3389/fpls.2018.01613

Zhu, F., Yuan, S., Zhang, Z. W., Qian, K., Feng, J. G., and Yang, Y. Z. (2016). Pokeweed antiviral protein (PAP) increases plant systemic resistance to Tobacco mosaic virus infection in Nicotiana benthamiana. *Eur. J. Plant Pathol.* 146, 541–549. doi: 10.1007/s10658016-0938-2

Zhu, F., Zhang, P., Meng, Y. F., Xu, F., Zhang, D. W., Cheng, J., et al. (2013). Alpha-momorcharin, a RIP produced by bitter melon, enhances defense response in tobacco plants against diverse plant viruses and shows antifungal activity *in vitro*. *Planta.* 237, 77–88. doi: 10.1007/s00425-012-1746-3

frontiers | Frontiers in Plant Science

TYPE Review
PUBLISHED 13 August 2024
DOI 10.3389/fpls.2024.1451790

OPEN ACCESS

EDITED BY
Chellappan Padmanabhan,
USDA APHIS PPQ Science and Technology,
United States

REVIEWED BY
Carla M. R. Varanda,
Research Centre for Natural Resources,
Environment and Society (CERNAS), Portugal
Ho-jong Ju,
Jeonbuk National University,
Republic of Korea

*CORRESPONDENCE
Kazbek Dyussembayev
Dyussembayev@biocenter.kz

RECEIVED 19 June 2024
ACCEPTED 24 July 2024
PUBLISHED 13 August 2024

CITATION
Kanapiya A, Amanbayeva U, Tulegenova Z, Abash A, Zhangazin S, Dyussembayev K and Mukiyanova G (2024) Recent advances and challenges in plant viral diagnostics.
Front. Plant Sci. 15:1451790.
doi: 10.3389/fpls.2024.1451790

Recent advances and challenges in plant viral diagnostics

Aizada Kanapiya[1], Ulbike Amanbayeva[2], Zhanar Tulegenova[1,2], Altyngul Abash[1], Sayan Zhangazin[1], Kazbek Dyussembayev[1,2]* and Gulzhamal Mukiyanova[2,3]

[1]Department of Biotechnology and Microbiology, L.N. Gumilyov Eurasian National University, Astana, Kazakhstan, [2]Laboratory of Biodiversity and Genetic Resources, National Center for Biotechnology, Astana, Kazakhstan, [3]Scientific Center "Agrotechnopark", Shakarim University, Semey, Kazakhstan

Accurate and timely diagnosis of plant viral infections plays a key role in effective disease control and maintaining agricultural productivity. Recent advances in the diagnosis of plant viruses have significantly expanded our ability to detect and monitor viral pathogens in agricultural crops. This review discusses the latest advances in diagnostic technologies, including both traditional methods and the latest innovations. Conventional methods such as enzyme-linked immunosorbent assay and DNA amplification-based assays remain widely used due to their reliability and accuracy. However, diagnostics such as next-generation sequencing and CRISPR-based detection offer faster, more sensitive and specific virus detection. The review highlights the main advantages and limitations of detection systems used in plant viral diagnostics including conventional methods, biosensor technologies and advanced sequence-based techniques. In addition, it also discusses the effectiveness of commercially available diagnostic tools and challenges facing modern diagnostic techniques as well as future directions for improving informed disease management strategies. Understanding the main features of available diagnostic methodologies would enable stakeholders to choose optimal management strategies against viral threats and ensure global food security.

KEYWORDS

plant virus, disease diagnostics, biosensor, sequencing technologies, CRISPR-Cas

1 Introduction

Plant pathogens are diverse groups of microorganisms that cause various diseases in plants, which can result in serious economic losses in agriculture. After fungi, viruses are the second most prevalent plant pathogens (Wang et al., 2023). These microscopic parasites are composed of small particles containing nucleic acid (either RNA or DNA) encased in a protein shell. Typically, viruses measure just a few nanometers in size and infect plants, causing a range of diseases and crop damage (Kovalskaya and Hammond, 2014; Manjunatha et al., 2022; Huang et al., 2023).

Viruses can infect all kinds of plants leading to huge economic damage worth many billions of dollars annually. They are the main pathogens causing both new and recurrent plant diseases worldwide, and cause damage to both natural vegetation and cultivated plants (Ghorbani et al., 2023; Huang et al., 2023). For instance, it was revealed the spread and emergence of *Potato virus Y* strains, including strains that cause economically important diseases of tobacco, tomatoes, and peppers, as well as the fact that the virus continues to develop with the relatively recent emergence of new damaging recombinant strains (Torrance and Talianksy, 2020). This evolution of *Potato virus Y* strains presents significant challenges for disease management and highlights the importance of continuous monitoring and adaptation of control strategies. Plant viruses affect plant life processes such as photosynthesis, metabolism and growth, which can ultimately lead to characteristic symptoms of the disease, such as yellowness of the leaves, deformations of plants, the formation of spots and blisters on the leaves, as well as tissue death (Jiang and Zhou, 2023).

As part of plant science, the study of plant viral diagnostics helps to develop disease control strategies, such as selecting resistant plant varieties, applying chemical and biological preparations to prevent the spread of viruses. Chemical control of plant viruses has been a significant aspect of integrated disease management programs. Particularly, insecticides are mostly employed for their convenience and effectiveness in preventing virus transmission by vectors, and this is also because direct control measures are usually unsuccessful against viruses (Garzo et al., 2020). However, it poses environmental and health risks despite its occasional effectiveness (Pandit et al., 2022). These risks underline the need to find alternative methods to combat viral diseases of plants. Accurate identification of pathogens is a key component of controlling plant diseases, as early detection allows for effective measures to control and prevent their spread (Kalimuthu et al., 2022). Conventional diagnostic systems include various methods such as selective cultural, immunological (Edwards and Cooper, 1985) and molecular (Olmos et al., 2007). In addition to detecting viruses, these methods determine their type and quantity, which is useful for developing management strategies and controlling plant diseases. Furthermore, there are high-performance next-generation sequencing platforms that provide powerful tools for the identification and surveillance of viral infections.

2 Conventional methods for detection of plant viruses

In order to develop and apply protective agents against viral infections of plants, it is necessary to have detection methods with high sensitivity and specificity that will be available for practical use in agricultural conditions (Devi et al., 2024). Conventional methods for detecting plant viruses can achieve a balance between the reliability of the results and the practicality of their application. The main tools for routine screening and diagnosis of viral infections are enzyme-linked immunosorbent assay (ELISA) and amplification-based molecular approaches.

2.1 Enzyme-linked immunosorbent assay

ELISA is a convenient and sensitive tool for detecting the presence of viral agents and their quantification in plant tissues (Bramhachari et al., 2019). The method is based on the specific interaction of antibodies with proteins, in case of viral detection, mainly with the capsid protein of the target virus. If the target virus is present in the sap of the plant, it will interact with primary antibodies. After removing the unrelated primary antibodies, a reporter molecule, usually an enzyme, is added to the secondary antibodies, which allows the virus to be detected by forming a chromogenic product on the substrate (Nascimento et al., 2017).

Secondary antibodies target the permanent region of the primary antibody. For example, for primary antibodies derived from rabbits and directed against a viral antigen, enzyme-linked anti-rabbit IgG obtained from other mammals such as cattle, horse and goat can be used. In case with plant viral detection, plant juice extract is added to the wells of the microtiter tablet, then antibodies are added after incubation, followed by rinsing. If the virus of interest is present in the plant, it will bind to antibodies. Any unbound extract is washed off before adding a secondary antibody that recognizes the primary antibody (Abd El-Aziz, 2019).

According to the method of binding antibodies and antigens, as well as the level of sensitivity and specificity, several main types of ELISA have been developed (Figure 1). Direct ELISA uses one type of antibodies associated with the enzyme, therefore it is convenient and fast, but may be less sensitive. Indirect ELISA offers increased sensitivity and specificity using two antibodies, as well as sandwich ELISA, which is the best choice for complex antigens with multiple epitopes. Competitive ELISA is effective for the accurate quantification of antigens, especially in the case of low concentrations or small sizes, since it is based on competition between labeled and unlabeled antigens for binding to an antibody (Khan et al., 2023).

ELISA-based methods, such as direct tissue blot immunoassay, double antibody sandwich ELISA, and tissue-print ELISA are the most popular in viral identification (Abd El-Aziz, 2019). There are also several modifications of ELISA that offer improved methodologies and diverse applications in various fields. The plate-trapped antigen ELISA demonstrated high sensitivity and specificity for detecting viruses that cause significant economic losses in important Brazilian crops. The kit was able to detect six viral species from the genera *Comovirus*, *Cucumovirus*, *Potyvirus*, and *Sobemovirus* in infected plant tissues (Nascimento et al., 2017). A few examples of ELISA techniques developed for plant viral diagnostics are summarized in Table 1.

ELISA is recognized as the world standard for detecting viruses in crops due to a number of advantages such as ease of implementation and sensitivity, which allows detecting low concentrations of viral samples. Moreover, it also offers versatility, which allows adapting to detect a wide range of plant viruses through the use of various antibodies (Mehetre et al., 2021). However, despite its many advantages, ELISA also has a few disadvantages that may limit its use in certain situations. The specificity of ELISA depends on the quality of the antibodies used

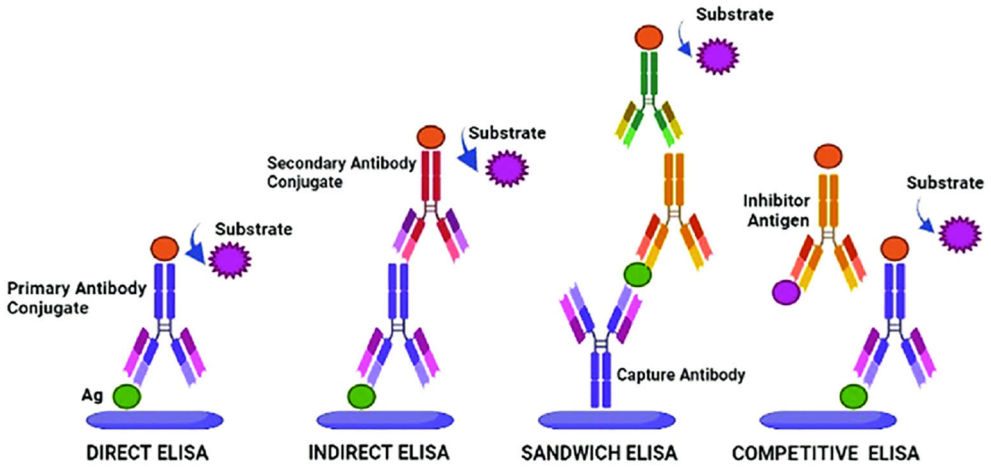

FIGURE 1
ELISA types and their working principles. Adopted with permission from Khan et al. (2023).

in the analysis. Insufficient purity or specificity of antibodies can lead to false positive or false negative results, which reduces the reliability of diagnosis. The production of high-quality antibodies also requires significant costs and time (Tabatabaei et al., 2021). Despite this, ELISA remains the main method for routine screening and diagnosis of viral diseases in agriculture due to its balance between sensitivity, specificity, cost and ease of use.

2.2 Polymerase chain reaction

Molecular methods are one of the most promising approaches to the diagnosis of plant viruses. These methods are based on the analysis of nucleic acids of viruses, such as DNA and RNA, using various techniques of molecular biology (Mehetre et al., 2021). One of the key molecular methods is PCR, which allows to increase the number of

TABLE 1 ELISA tests developed for plant viral disease diagnostics.

Technique	Crop	Pathogen	Ref.
Dot-ELISA	Sugarcane Maize Potato Tomato	*Sorghum mosaic virus* *Maize chlorotic mottle virus* *Maize dwarf mosaic virus* *Potato virus S* *Potato virus M* *Tomato mottle mosaic virus*	Faccioli and Colombarini (1996) Chen et al. (2020) Li et al. (2021) Javaran et al. (2021)
Plate-trapped antigen ELISA	Squash Cucumber Cowpea Zucchini Papaya	*Squash mosaic virus* *Cowpea severe mosaic virus* *Cucumber mosaic virus* *Cowpea aphidborne mosaic virus* *Zucchini yellow mosaic virus* *Papaya lethal yellowing virus* *Zucchini lethal chlorosis virus*	Nascimento et al. (2017) Ramos et al. (2018)
Triple antibody sandwich ELISA	Cucumber Pepper Tobacco Tomato Potato Canary Carrizo citrange Cassava	*Cucumber mosaic virus* *Pepper mild mottle virus* *Tobacco mosaic virus* *Odontoglossum ringspot virus* *Tomato mosaic virus* *Ribgrass mosaic virus* *Potato mop-top virus* *Barley yellow dwarf virus* *Cereal yellow dwarf virus* *Citrus psorosis virus* *Sri Lankan cassava mosaic virus*	Arif et al. (1994) Martín et al. (2004) Yu et al. (2005) Ilbagi et al. (2008) Phatsaman et al. (2020) Charoenvilaisiri et al. (2021)
Double antibody sandwich ELISA	Potato Peanut Chrysanthemum Sorghum	*Potato virus Y* *Potato virus S* *Tomato spotted wilt virus* *Tomato black ring virus`* *Sugarcane streak mosaic virus*	Hema et al. (1999) Lai et al. (2021) Chinnaiah et al. (2022) Tessema et al. (2024)

certain DNA or RNA fragments. The PCR have been used for detection of many plant viruses such as *Banana bunchy top virus* (Wang et al., 2022), *Tobacco ringspot virus* (Lee et al., 2015), *Bean common mosaic virus* (Xu and Hampton, 1996), *Apple mosaic virus* (Nabi et al., 2023), *Papaya ringspot virus* (Hamim et al., 2018) and more (Table 2). Based on PCR, many modifications were developed, including reverse transcription PCR (RT-PCR), quantitative PCR (qPCR), nested PCR and multiplex PCR (Wang et al., 2022).

PCR can detect infectious agents at the earliest stages of infection, which significantly increases the effectiveness of measures to combat plant diseases. It is also versatile, as it can be used to diagnose a wide range of viruses, bacteria and fungi, unlike ELISA, which requires different sets of antibodies for each individual pathogen. The high sensitivity of PCR makes it possible to detect low concentrations of DNA, which has a risk of leading to false positives (Venbrux et al., 2023).

Particularly, qPCR is more sensitive in detecting small concentrations of target viruses while significantly reducing detection time compared to other PCR methods. Its swifter pace is attributed to the elimination of the gel electrophoresis step required for confirmation, thereby lowering the risk of contamination (Hema and Konakalla, 2021). The qPCR, also known as real-time PCR, allows for the amplification and simultaneous quantification of specific DNA or RNA sequences. This method leverages the sensitivity and specificity of PCR, coupled with real-time measurement of the amplified product using fluorescent dyes or probes. Furthermore, the ability to quantify viral load precisely in infected plants makes qPCR particularly valuable for understanding the dynamics of virus infection and for making informed decisions in plant disease management.

qPCR is increasing its applications in plant virus diagnostics with many reported assays to detect viruses. Based on SYBR Green I, the qPCR and a nested RT-PCR were developed to detect *Potato mop-top virus*. The detection sensitivity was several times higher than in dot-blot hybridization and standard PCR analysis (Zhou et al., 2019). In another study, a SYBR Green-based RT-qPCR assay was developed for the detection of *Indian citrus ringspot virus* (Kokane et al., 2021a). The assay was highly specific to *Indian citrus ringspot virus*, showing no cross-reactivity with other citrus pathogens, and was about 100 times more sensitive than conventional RT-PCR. SYBR Green is based on the use of a fluorescent dye that binds to double-stranded DNA, whereas another TaqMan qPCR technique uses fluorescent probes to specifically identify target sequences. Real-time analysis of TaqMan qPCR was performed using a newly designed primer pair, and the assay was reproducible and could specifically detect *Banana streak virus* without cross-reaction with *Cucumber mosaic virus* and *Banana terminal virus* at the same time showing higher sensitivity than Endpoint PCR (Jie et al., 2017). Overall, qPCR offers several advantages over traditional PCR, including increased sensitivity, specificity, and the ability to quantify DNA in real-time (Venbrux et al., 2023).

2.3 Isothermal amplification methods

There is an increasing trend in the rapid development of molecular technologies, which have demonstrated effective advancements for diagnostics. PCR is the golden standard in molecular diagnostics due to its high sensitivity and specificity. However, PCR methods require three different temperature

TABLE 2 Application of PCR-based molecular approaches in plant virus diagnostics.

Technique	Pathogen	Crop	References
qPCR	*Tobacco mosaic virus* *Cucumber mosaic virus* *Sugarcane bacilliform virus* *Sugarcane bacilliform IM virus* *Sugarcane bacilliform MO virus*	Tobacco Sugarcane	Feng et al. (2006) Sun et al. (2018) Ellis et al. (2020)
RT-qPCR	*Citrus tristeza virus* *Citrus leaf blotch virus* *Tobacco Mosaic Virus* *Barley yellow dwarf virus* *Cereal yellow dwarf virus*	Citrus plants Tobacco Barley	Balaji et al. (2003) Ruiz-Ruiz et al. (2007) Ruiz-Ruiz et al. (2009) Kokane et al. (2021b)
Nested PCR	*Prune dwarf virus*, *Prunus necrotic ringspot virus* *Apple mosaic virus* *Lettuce mosaic virus* *Squash vein yellowing virus*	Prune Apple Lettuce Squash	Moreno et al. (2007) Maliogka et al. (2010)
Multiplex PCR	*Banana streak Mysore virus* *Banana bunchy top virus* *Capsicum chlorosis orthotospovirus* *Chilli veinal mottle virus* *Large cardamom chirke virus* *Cucumber mosaic virus* *Pepper mild mottle virus* *Chilli leaf curl virus* *Artichoke Italian latent virus*	Banana Chili Cucumber Pepper Artichoke	Selvarajan et al. (2011) Minutillo et al. (2012) Devi et al. (2022)

regimes, necessitating expensive equipment. Additionally, the complexity and stringent laboratory requirements limit the use of PCR in field conditions. As a result, several alternative isothermal amplification methods have been emerged. Many methods of isothermal amplification have been developed, the most well-known loop-mediated isothermal amplification (LAMP) and recombinase polymerase amplification (RPA) have widely been used for plant pathogen detection (Moon et al., 2022).

The LAMP is widely recognized for its simplicity, high specificity and sensitivity, as well as the ability to rapidly increase target sequences without the need for expensive equipment, such as thermocycles (Soroka et al., 2021). The LAMP process uses several primers that target different areas within the nucleic acid sequence. These primers include internal primers (FIP and BIP), external primers (F3 and B3) and loop primers (LF and LB), which initiate DNA synthesis with displacing activity (Notomi et al., 2015) (Figure 2).

The reaction proceeds at a constant temperature (typically between 60°C and 65°C), eliminating the need for thermal cycling. This allows the use of simple equipment that does not require complex settings and temperature control, which makes the LAMP simple and suitable for in-field use (Zanoli and Spoto, 2012). The operating principle is based on the cyclic amplification of target sequences of DNA or RNA using specially developed primers and unique enzymes. LAMP begins with the external primers binding to the target DNA or RNA sequence. The inner primers then form loops at complementary sites and initiate the synthesis of new strands. This produces characteristic D-loops and stem-loop structures (Park, 2022). As a result, the display of the synthesis of new strands continues cyclically, resulting in an exponential increase in the specific target sequence.

RT-LAMP assay was developed recently for detection of *Yam mosaic virus* using newly designed YMV1-OPT primers (Festus et al., 2023). The assay detected 0.1 fg/μL of purified RNA with a sensitivity equivalent to RT-PCR, developed in the same study. In contrast, other similar studies claimed that RT-LAMP had a higher sensitivity and specificity than the RT-PCR method (Hua et al., 2023; Kimura et al., 2023). In another study, Caruso et al. (2023) developed the design of six LAMP primers that showed high level of efficiency, sensitivity and selectivity to detect *Tomato leaf curl New Delhi virus*. Notably, this assay showed 1000 times more sensitivity than traditional PCR with comparable specificity. An important feature of LAMP is that it can be successfully carried out using a crude extract of an infected plant (Panno et al., 2020). This in turn would reduce the overall assay performance time as well as making it more efficient for development of a potential on-site detection tool due to its simplicity of sample preparation.

The RPA is an isothermal method of nucleic acid amplification, which is used for the rapid and specific diagnosis of various infectious diseases, including viral infections in plants. The system operates at a constant temperature (usually between 37-42°C) and does not require complex equipment, which makes this method especially useful for use in field conditions and/or in resource-limited environments. The RPA process is based on the use of recombinant proteins that recognize and bind to the target DNA. Recombinant proteins (recombinases) bind to primers, then recombinase-primer complexes are recognized and bind to complementary sequences on the target DNA. They are embedded in the target DNA, replacing the original chains. Stabilizing proteins protect the single-stranded sections of DNA that are formed. After that, the polymerase synthesizes a new DNA chain starting with primers, which leads to an exponential increase in the number of copies of the target sequence (Ivanov et al., 2021). The method is rapid operating at a constant temperature, which simplifies the technical equipment. It can detect low amounts of target DNA or RNA, and specificity is provided by recombinant proteins and specific primers. It also could be used for multiplex

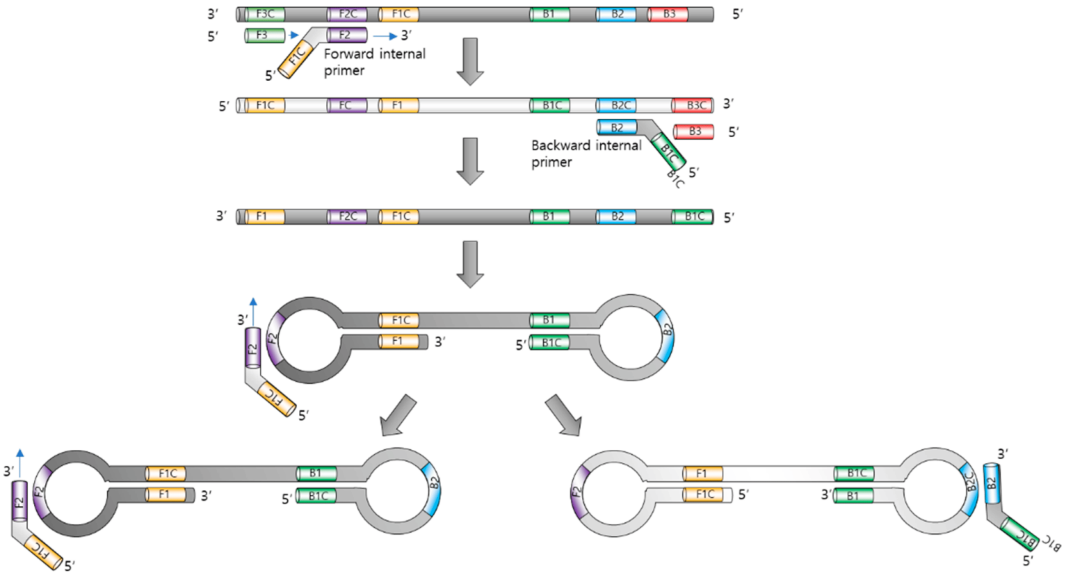

FIGURE 2
Loop-mediated isothermal amplification. Adopted with permission from Park (2022).

detection such as the PCR method. For instance, an RPA analysis was developed to detect DNA and RNA viruses of *Cucurbit leaf crumple virus*, *Cucurbit yellow stunting disorder virus* and *Cucurbit chlorotic yellows virus* (Jailani and Paret, 2023). The assay time was 80 minutes with the ability to process several mixed plant DNA and RNA viruses simultaneously. RPA was also used for simultaneous detection of *Maize chlorotic mottle virus* and *Sugarcane mosaic virus* in maize (Gao et al., 2021). The detection limit of the RPA method was 102 copies/μL, while conventional PCR showed sensitivity 10 times less. The analysis was carried out in only 30 minutes and was specific for the simultaneous detection of two viruses, since no cross-reaction was detected with three other viruses infecting maize. In another study, fast and sensitive RPA was created in combination with analysis using a lateral flow dipstick (LFD) to detect *Bean common mosaic virus* (Qin et al., 2021). The sensitivity of this RPA-LFD assay was 1000 times higher than conventional PCR assay and no cross-reaction was detected with other *Potyviruses*.

In comparison with other conventional diagnostic methods, LAMP can amplify DNA at detectable levels within 30-60 minutes, which is significantly faster than any PCR-based approaches. RPA is even faster, often achieving results in only 10-20 minutes (Bhat et al., 2022). In terms of sensitivity, isothermal methods can achieve detection limits that are comparable to, if not better than, those of PCR. For instance, LAMP can detect a few to several tens of copies of a target sequence, making it highly sensitive. However, isothermal amplification is limited by the species level, while primers have been developed for the PCR method can detect viruses at various taxonomic levels (Rubio et al., 2020). In contrast, their ease of use and minimal equipment requirements make them particularly attractive for field diagnostics and use in resource-limited settings. However, the choice of method should be guided by specific diagnostic needs, considering factors such as speed, simplicity, and sensitivity.

3 Biosensor technologies

Biosensors are innovative tools that have been developed with the purpose of determining the presence and quantification of target biological components within testing samples. The working principle of biosensor techniques is based on the ability of biological elements such as antibodies or nucleic acids to bind specifically to targeted analytes. This interaction changes any physical or chemical properties, which can then be measured by a sensor (Naresh and Lee, 2021). These devices provide multiple advantages including exceptional performance, possibility to integrate natural or synthetic antibodies, rapid response, high sensitivity and specificity, portability, miniaturization capability, and real-time analysis (Saylan et al., 2019; Dyussembayev et al., 2021). In addition, they offer an affordable and accessible means to swiftly detect plant pathogens in-field. In fact, most of the infectious agents detected by biosensors are human pathogens, including *Human immunodeficiency virus* (Babamiri et al., 2018), Hepatitis B (Tam et al., 2017), Ebola infections (Baca et al., 2015), *Norovirus* (Hwang et al., 2017). However, over the previous two decades, biosensors have been employed in a wide range of applications including detection of plant viruses such as *Cowpea mosaic virus*, *Tobacco mosaic virus*, *Salad mosaic virus* (Fang and Ramasamy, 2015).

Biosensors are usually classified according to their signal transduction and biorecognition principles. The transduction system can include electrochemical, optical, piezoelectric, and thermal sensors (Martinelli et al., 2015). However, the biosensors are more often divided into two large groups according to their biorecognition elements: antibody- and nucleic acid-based biosensors. The antibody-based biosensors have distinctive signs of binding antibodies to target molecules, which ensures high detection accuracy (Figure 3). These antibodies can be directly attached to the surface of the sensor or to contacts with magnetic beads for immunomagnetic separation and subsequent detection (Byrne et al., 2009; Patel, 2021).

A method for detecting the *Maize chlorotic mottle virus* has been developed using a quartz crystal microwave (QCM) immunosensor with a special gold piece (Huang et al., 2014). The assay includes using quartz microweights, which can change their frequency depending on the mass adsorbed on their surface. This frequency change is used to quantify the presence of the virus. Gold surfaces of QCM crystals serve as the basis for subsequent binding of antibodies. As a result, the detection limit was approximately 250 ng/mL, which is comparable to the existing ELISA method. The QCM sensor has shown high specificity and sensitivity to both purified *Maize chlorotic mottle virus* and crude extracts from maize leaf samples. Another type of biosensor based on surface plasmon resonance system employing monoclonal antibodies was developed to detect *Potato virus Y*. The ability of the biosensor to detect and quantify *Potato virus Y* particles was compared with ELISA and RT-qPCR. The detection limit of the biosensor assay was 0.31 mg/mL,

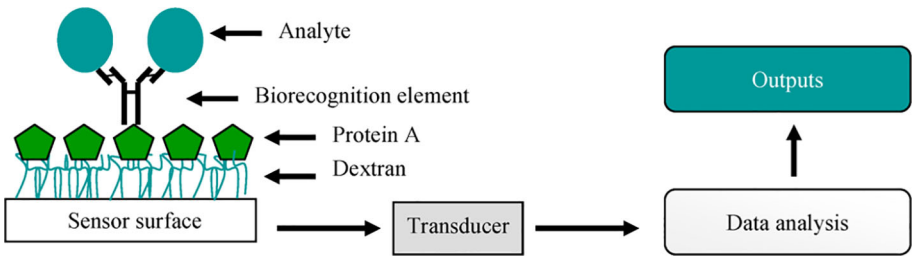

FIGURE 3
A simple representation of a biosensor. Adopted with permission from Byrne et al. (2009).

which is much less sensitive than the 0.019 mg/mL of ELISA (Gutiérrez-Aguirre et al., 2014). A biosensor utilizing surface plasmon resonance was used for the specific detection of *Maize chlorotic mottle virus* (Zeng et al., 2013). In lower concentrations assay enabled the detection in 30 minutes that faster than ELISA assay and with a detection limit of approximately 1 ppb (parts per billion). A similar surface plasmon resonance biosensor has been successfully developed for detection of the *Potato virus Y*, *Apple stem pitting virus*, *Maize chlorotic mottle virus*, *Barley stripe mosaic virus*, and *Cowpea mosaic virus* (Hong and Lee, 2018). The bioelectronic biosensor has been developed based on an electrolyte-gated organic field-effect transistor for the specific detection of *Plum pox virus* in *Nicotiana benthamiana* plant extracts (Berto et al., 2019). The working principle relies on specific binding of viral particles to anti-viral antibodies in plant extracts with a sub ng/mL detection limit. Notably, the authors claimed that the novel electronic sensor could potentially be manufactured using cost-effective methods and easily adapted into a portable device suitable for use in field conditions.

In contrast, nucleic acid-based biosensors represent another important class of analytical tools. Particularly, DNA biosensors are mainly used for diagnostic purposes and the principle is often based on a simple hybridization process where DNA probes bind specifically to target complementary sequences, allowing the detection and quantification of specific target sequences through a DNA (Carvajal Barbosa et al., 2021). Briefly, in the presence of targeted analyte, hybridization occurs between the DNA probe and the analyte, resulting in altered physical or chemical properties of the sensor. These DNA-based biosensors, also called genosensors, have been used for plant viral diagnostics. For example, Malecka et al. (2014) proposed a DNA biosensor for detection of specific oligonucleotides sequences of *Plum pox virus* in plant extracts. The sensor demonstrated a selectivity in discriminating between healthy and infected plants with a detection limit of 12.8 pg/mL.

Another example of DNA biosensor is QCM-based piezoelectric sensor based on DNA/RNA hybridization developed by Eun et al. (2002) for detection of two orchid viruses: *Cymbidium mosaic virus* and *Odontoglossum ring spot virus*. The specific nucleotide probe-coated DNA sensor was able to detect both viruses in quantities as low as approximately 1 ng in purified RNA preparations and 10 ng in the crude sap of infected orchids. In general, nucleic acids are often chosen as a tool to mediate various physico-chemical interactions in biosensors due to their specificity and sensitivity. This allows nucleic acids to interact more accurately and efficiently with target molecules than protein components such as antibodies. Thus, nucleic acid-based biosensors can detect significantly lower concentrations of target molecules, making them more sensitive and therefore potentially more useful in various applications where high precision and sensitivity are required (Hong and Lee, 2018).

DNA Microarray biosensors have been also developed for detection of several plant viral pathogens (Zherdev et al., 2018). This method is based on the use of virus-specific oligonucleotides that bind to a membrane or glass. After the total RNA is converted to cDNA and increased by PCR using pathogen-specific primers labeled with markers suitable for detecting molecules, the amplified and labeled products are applied to the array and DNA hybridization process is performed. After cleaning, the array will show the result depending on the marker used (Bhat et al., 2020).

A DNA microarray has been developed by Krawczyk et al. (2017) and it is designed for simultaneous identification of five pathogens of maize: *Pantoea ananatis*, *Pantoea agglomerans*, *Enterobacter cloacae* subsp., *Maize dwarf mosaic virus* and *Sugarcane mosaic virus*. Two more similar assays have been effectively developed for simultaneous detection of various potato viruses (Bystricka et al., 2003; Agindotan and Perry, 2008). Generally, comparing microarray-based and other biosensors in plant viral diagnostics, it can be noted that microarrays can simultaneously analyze many molecules, which increases the effectiveness of pathogen screening (Govindarajan et al., 2012). While other biosensors are usually easier to use and require a smaller sample volume, which makes them more convenient for field research. However, the combination of their advantages would lead to even more effective and innovative diagnostic platforms.

4 Sequencing-based diagnostics

Several sequencing-based diagnostic techniques have been applied for detecting plant viruses, including next-generation sequencing. These approaches allow the detection and identification of viral pathogens in various plant samples (Pecman et al., 2017). By sequencing the entire nucleic acid content in the sample, researchers can simultaneously detect known and new viruses, identify genetic variants and characterize viral populations in the sample (Qin, 2019). One of the main advantages of sequential diagnostics is their ability to provide comprehensive information about the virus community present in the sample (Hadidi et al., 2016), unlike traditional diagnostic methods that target specific viruses or virus families (Avila-Quezada et al., 2022).

Sequencing-based technologies are widely used for detecting plant viruses due to high performance, sensitivity and scalability. In addition, high-throughput sequencing allows for a faster transition from virus discovery to the development of specific detection methods such as PCR or LAMP. It also contributes to the improvement of existing methods by identifying sequence variations within viral populations (Maree et al., 2018). These platforms allow researchers to quickly and cost-effectively generate massive sequences of action data, facilitating large-scale viral surveys, epidemiological research and outbreak investigations.

4.1 Next-generation sequencing

Next-Generation Sequencing (NGS) refers to advanced sequencing technologies that allow for rapid and high-throughput sequencing of DNA or RNA (Qin, 2019). With this new generation of sequencing methods, it is possible to obtain detailed information about the genetic composition of viruses in a timely and accurate manner, which makes them a valuable tool in the fight against

infectious diseases (Nafea et al., 2024). By overcoming the limitations of traditional methods, NGS provides more accurate and complete analysis. In plant virology, NGS has been instrumental in discovering and isolating numerous plant viruses such as the *Pepino mosaic virus* (Prabha et al., 2013), *Grapevine leafroll-associated virus 1* (Morán et al., 2023), *Citrus leaf blotch virus isolate mulberry alba 2* (Chen et al., 2022), *Cherry mottle leaf virus*, *Cherry virus A* (Rott et al., 2017) etc.

Apart from the discovering of new viruses, NGS can also detect complete nucleotide sequences of viruses. For example, a complete sequence of the *Artichoke latent virus* was obtained, and it identified the virus to the genus *Macluravirus* (Minutillo et al., 2015). Consequently, this allowed refutation of the fact that *Artichoke latent virus* was originally proposed as a member of the genus *Potyvirus*. In fact, it is important to not only detect known viral isolates but also ensure that the diagnostic assay is reproducible across testing viral population. For example, NGS analysis was able to identify 14 distinct isolates of *Apple stem spot virus* and five variants of *Apple leaf chlorotype virus* (Singhal et al., 2021). Similarly, seven species of plant viruses have been detected using metagenomic analysis via NGS in symptomatic and asymptomatic tea plants collected from the field, along with two novel viral species that were latent pathogens: *Tea plant necrotic ring blotch virus* and *Tea plant line pattern virus* (Hao et al., 2018). Mwaipopo et al. (2021) used NGS technology to identify common bean viruses in wild plants, and as a result, a wide range of virus species has been identified due to high throughput of NGS. In addition, RT-PCR was used for validation of results, and the study identified viruses from at least 25 different genera, highlighting the complexity of virus interactions within the studied ecosystems.

Among the various sequencing technologies, there are three main approaches: Illumina, Ion Torrent and PacBio. Each of these technologies has advantages and operating principles, making them suitable for different research tasks. Illumina is ideal for research requiring high precision and performance, especially for short DNA fragments. Ion Torrent is a more accessible and faster method, which makes it attractive for routine sequencing where high accuracy is not critical, while PacBio offers the unique advantage of long reads, which is important for high-complexity genome research, including the detection of structural variations and the assembly of new genomes. All these techniques have been used for studying various plant viruses (Table 3).

4.2 Portable nanopore sequencing

Portable nanopore sequencing technology has great potential to bring plant viral diagnostics to a whole new level by offering fast and accurate early diagnosis of viral pathogens directly in the field or at the point of need. It also provides rapid and efficient DNA/RNA sequencing, which makes it significantly advantageous over most conventional diagnostics (MacKenzie and Argyropoulos, 2023). The principle of sequencing technology is based on the transmission of single-stranded DNA or RNA through microscopic nanopores. During the process of passing through the nucleotides in the sample, the nucleotides act on the electrical field, resulting in changes in the current. These changes in the current can be fixed and analyzed by computer software to determine the sequence of nucleotides (Sun et al., 2022) (Figure 4).

MinION technology developed by Oxford Nanopore Technology (ONT) (Maliogka et al., 2018) is a portable single-molecule genome sequencing device (Bronzato Badial et al., 2018). The platform sequences both short and long reads as well as detect modified bases (i.e. methylation) in both DNA and RNA in real time (Garcia-Pedemonte et al., 2023). Javaran et al. (2023) recently used ONT based on direct-cDNA sequencing from dsRNA to detect multiple grapevine viruses. As a result, it was possible using this technology to detect as low concentrations of 20 common viruses as standard Illumina MiSeq sequencing was capable, which confirms its reliability and effectiveness. The ONT has also been used to detect a few yam viruses such as *Dioscorea bacilliform virus*, *Yam mild mosaic virus* and *Yam chlorotic necrosis virus* (Filloux et al., 2018). In another study, MinION was used for identification of *Cucumber Bulgarian latent virus*, which threatens cucumbers grown in greenhouses (Dong et al., 2022). Although MinION sequencing and real-time analysis using ONT EPI2ME WIMP reduced the assay performance time to 48 h, the read accuracy was low – around 83-98% identical to the reference genome. Also, too many gaps make the reads impossible to assemble. Consequently, this technology is still not as accurate as Sanger sequencing when it comes to analyzing viral whole genome sequences. Phannareth et al. (2020) performed detection of *Plum pox virus* in tobacco using MinION technology with two different kits: cDNA PCR Sequencing kit (SQK-PCS108) and Direct RNA Sequencing kit (SQK-RNA001). The results demonstrated the effectiveness of both kits in identifying

TABLE 3 Next-Generation Sequencing technologies used for plant viral diagnostics.

Technique	Pathogen	Main advantages	Read length	References
Illumina	*Carrot yellow leaf virus*, *Grapevine redblotch virus* *Citrus leprosis viroid* *Tomato apical stunt viroid* *Barley yellow dwarf virus* *Sugarcane yellow leaf virus*	High throughput Low error rate Cost effectiveness	100-300 bp	Villamor et al. (2019) Pecman et al. (2022) Lee et al. (2023)
Ion Torrent sequencing	*Citrus tristeza virus* *Tomato mottle mosaic virus* *Little cherry virus 1*	Cost effectiveness	200-400 bp	Fillmer et al. (2015) Katsiani et al. (2018) Bester et al. (2021)
Pacific Biosciences (PacBio) sequencing	*Cryphonectria hypovirus 1* *Barley yellow dwarf virus-GAV*	Long reads High accuracy Reproducibility	10-20 kb	Shen et al. (2020) Leigh et al. (2021)

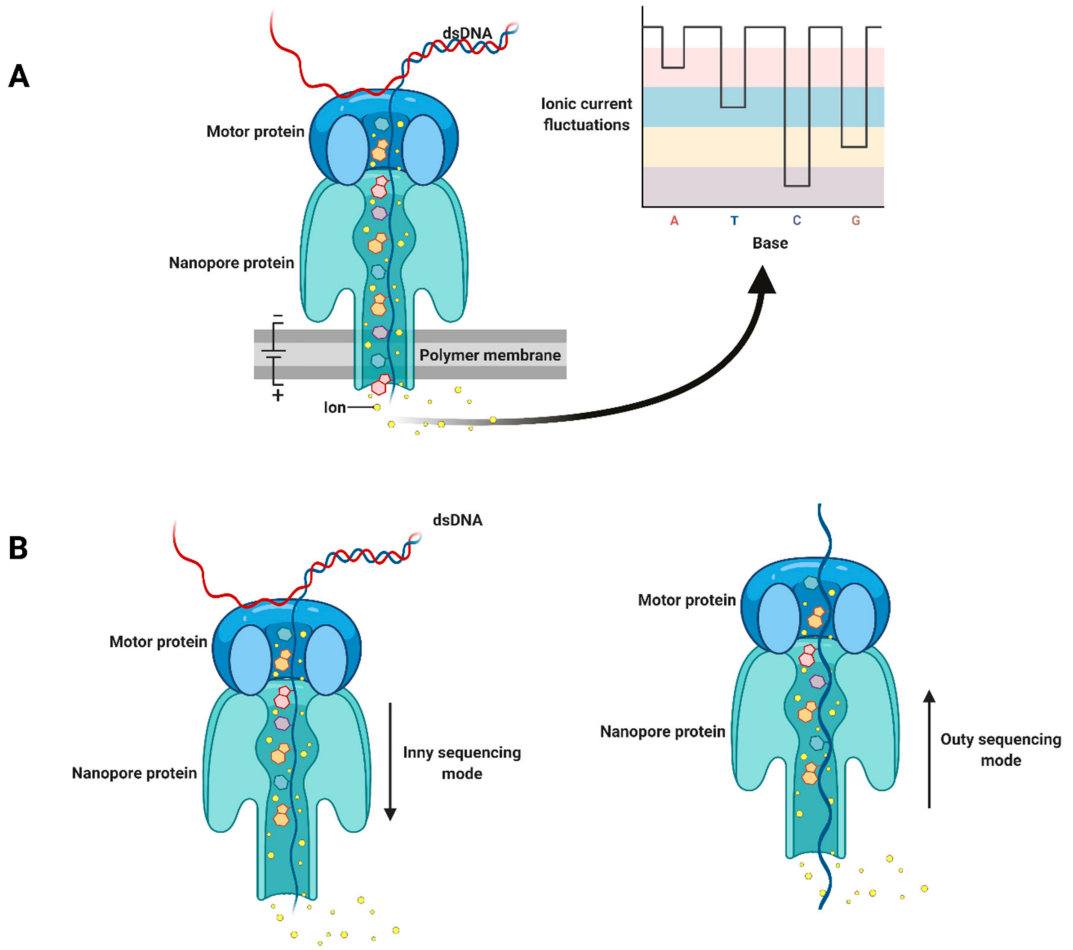

FIGURE 4
Schematic illustration of nanopore sequencing technology: **(A)** double-stranded DNA is unwound by a motor protein; **(B)** inny and outy sequencing modes. Adapted with permission from Javaran et al. (2021).

plant viruses in tobacco samples. Moreover, for rapid identification of *Jasmine virus H* in *Ixora coccinea* plants, complete genome sequencing was performed using the ONT MinION platform only within 48 hours (Kim et al., 2023).

Compared with the other sequencing platforms, Nanopore sequencing can acquire entire viral genomes without assembly algorithms, thereby minimizing errors. Nanopore sequencing is widely available and allows long-read sequencing, and the simplicity of these long-lasting sequencing systems makes these devices attractive (MacKenzie and Argyropoulos, 2023). This technology allows direct sequencing of DNA or RNA samples and provides fast and real-time dynamic monitoring of sequencing data in the field (Chen et al., 2023).

4.3 CRISPR-Cas

The CRISPR-Cas system, discovered as part of the adaptive immune response of bacteria to viruses, has become an effective tool for genetic engineering as well as for plant pathogen diagnostics. Recently, it has also found application in the detection of plant viruses, offering accurate, sensitive and fast assays for diagnosing viral infections. Various approaches have been used to analyze nucleic acids, including Specific High-sensitivity Enzymatic Reporter Unlocking (SHERLOCK) and DNA Endonuclease-Targeted CRISPR Trans Reporter (DETECTR). SHERLOCK combines CRISPR-Cas 13a with isothermal amplification to detect specific RNA or DNA sequences of plant viruses, when DETECTR is based on CRISPR-Cas12a and targets DNA endonuclease (Fang et al., 2023). The basic principle is that the CRISPR-Cas system can be programmed to specifically detect by binding to specific sequences within viral genomes. When the CRISPR-Cas system detects a virus, a cascade of reactions is activated that effectively mark the viral sequence or even inactivate the virus (Cao et al., 2020; Lou et al., 2022).

Marqués et al. (2022) used CRISPR-Cas12a and CRISPR-Cas13a/d systems to detect three different viruses - *Tobacco mosaic virus*, *Tobacco etch virus*, and *Potato virus X* in tobacco plants. The results demonstrated that the use of these systems makes it possible to carry out simultaneous detection of multiple viruses accurately and quickly, which is important for on-site use. Another simple and fast diagnostic test was developed using

CRISPR/Cas12a for the simultaneous detection of four RNA viruses and one viroid in apple (Jiao et al., 2021). Aman et al. (2020) also demonstrated RT-RPA single-step diagnostic assay employing CRISPR/Cas12a system for the detection of *Potato virus X*, *Potato virus Y* and *Tobacco mosaic virus*. The developed assay takes less than 30 minutes to perform and uses an inexpensive fluorescence visualizer, which makes it suitable for in-field diagnostics. Another CRISPR-Cas12a assay has been recently developed for detection of *Beet necrotic yellow vein virus* in sugar beet (Ramachandran et al., 2021). Notably, the assay involves RT-PA that allows the amplification of viral RNA at a constant temperature. This simplifies the process and eliminates the need for complex equipment. At the same time, the assay used a minimum number of primers as well as showing high level of sensitivity.

In general, CRISPR-Cas systems have not only been used in the diagnosis of plant viruses, but also been utilized for antiviral purposes in plants. CRISPR-Cas9 system has been shown promising results in conferring resistance to plant DNA and RNA viruses. The study by Ali et al. (2015) showed that the system introduced mutations into the target sequences of the *Tomato yellow leaf curl virus*. There was applied systemic delivery of sgRNAs aimed at coding and non-coding sequences of the virus. As a result, tobacco plants expressing CRISPR/Cas9 showed a decrease in the accumulation of viral DNA, which led to the elimination or significant reduction of infection symptoms. Recently, it has been developed CRISPR/Cas9-based banana genome editing, which can be used to create disease-resistant varieties (Tripathi et al., 2021). Similar strategy has also been used for inactivation of endogenous *Banana streak virus* by editing virus sequences (Tripathi et al., 2019). The results showed that multiplexing CRISPR/Cas9 technology is very effective for creating precise deletions in banana genome. Seventy-five percent of the edited events remained asymptomatic compared to the unedited control plants under water stress, which confirms the inactivation of the virus into infectious viral particles.

CRISPR-Cas-based pathogen detection systems have been attributed several advantages. Overall, they show great potential for on-site diagnostics due to their high sensitivity and specificity, and minimal requirement for advanced equipment (Wang et al., 2020; Venbrux et al., 2023). The system detects viral RNA without reverse transcription or amplification, which means the process becomes simpler, faster and more cost-effective (Devi et al., 2024). Traditional methods of virus diagnosis often require a long time to obtain results, while CRISPR-Cas analysis detection of the viral genome takes within a few hours. Moreover, it is possible to create tests based on paper strips using CRISPR-Cas that allow to quickly and conveniently determine the presence of viruses in plant tissues even without special equipment (Tsou et al., 2019).

5 Commercially available devices

Commercially available devices for the diagnosis of plant viruses are an invaluable tool for agronomists, gardeners and biologists. They provide the ability to quickly and accurately detect viruses in real time, which allows to quickly take measures to control the spread of infection. For the rapid detection of targeted analytes, tests are usually carried out using paper test strips, side-flow and vertical-flow immunoassay (Singh et al., 2018).

Paper sensors are considered as a new alternative technology that are being used as simple, inexpensive, portable and disposable analytical devices for many applications, including clinical diagnosis, food quality control and environmental monitoring. Furthermore, only a small number of samples and reagents are required for analysis on the paper substrate, making it ideal for application in disease diagnostics (Chailapakul et al., 2020). Typically, paper substrates are used that are pre-processed to apply bioreceptors or chemical reagents specifically related to the targeted analytes. The sample containing the analyte is applied to a paper strip, after which it migrates through the capillaries along the surface of the paper. During the migration of the sample, there is an interaction between the bioreceptors on the paper surface and the target analytes. This interaction leads to the formation of analyte-bioreceptor complexes that can be detected both visually and with special equipment (Yao et al., 2022).

Another example of commercially available diagnostic devices is a lateral flow immunoassay method (LFA), which is a rapid and simple test that can be carried out in field conditions. This method is based on the interaction of antigen and antibody, resulting in the formation of a visible signal, usually in the form of a color band, making it convenient to use (Byzova et al., 2018). LFA stripes have been developed that can distinguish *Tobacco mosaic virus*, *Tobacco vein banding mosaic virus* and *Potato virus Y* from mixed infection samples within minutes. The developed LFA strip can be widely used for the diagnosis of pathogens in the field as it already demonstrated the ability to accurately identify different strains of *Potato virus Y* (Guo et al., 2022). Other studies also pointed out the efficiency of this technique for accurate and rapid detection of *Grapevine leafroll-associated virus* (Byzova et al., 2018) and *Banana bract mosaic virus* (Selvarajan et al., 2020).

Agristrip technology is based on immunochromatographic assay principles, commonly known as lateral flow immunoassays utilizing monoclonal antibodies that are highly specific to the pathogen. Multiple detection methods such as Agristrip, microscopy, ELISA, PCR and PCR revealed infection of S. subterranea (Bouchek-Mechiche et al., 2011). The Agristrip developed for S. subterranea detection was as sensitive as DAS-ELISA, with a detection limit of 1-10 sponsors per mL of buffer. Also, Sss AgriStrip provides results within a very short timeframe, typically starting to show bands after 1 to 2 minutes, with maximum intensity reached after about 10 to 15 minutes. This test allows for quick and easy on-site detection, making it suitable for routine identification of powdery scab symptoms on tubers. This rapid response is essential in field settings, where timely identification of infected tubers can significantly impact disease management strategies and prevent the spread of the pathogen. Its design allows for on-site testing, which is invaluable during potato inspections at farms. By facilitating quick and accurate detection, the Sss AgriStrip plays a vital role in protecting potato crops and ensuring the sustainability of potato production (Bouchek-Mechiche et al., 2011).

6 Challenges and future directions

With the development of technologies and methods in molecular biology, the level of accuracy, sensitivity and availability of diagnostics for plant viral diseases has increased significantly. Consequently, recent advances in the diagnosis of plant viruses represent a significant breakthrough, opening new opportunities to control and prevent viral epidemics in agriculture. Despite these achievements, there are several challenges that may affect the obtainment of accurate and reliable results. One of the main problems is working with crude extracts from plant tissues, which often contain various contaminants and inhibitors that may affect subsequent molecular analysis. Crude extracts typically contain nucleic acids of both host and virus, which may result in false positives. Moreover, the presence of polysaccharides, polyphenols and other secondary metabolites in plant tissues may hinder DNA recovery procedures, resulting in low yields and poor DNA quality. In addition, the diversity of plant virus genomes makes the nucleic acid extraction difficult. Plant viruses may contain single-stranded RNA, double-stranded RNA, or single-stranded DNA genomes, each requiring special extraction techniques to effectively isolate viral nucleic acids. Standard DNA extraction protocols often include long steps such as shredding plant tissues, cell lysis and nucleic acid purification. However, these techniques may not be appropriate for all plant species or virus strains, resulting in inconsistencies in the efficiency and reliability of DNA extraction. Furthermore, the choice of extraction method may affect both the sensitivity and specificity of subsequent diagnostic tests. Some extraction methods can selectively lead to co-purification of inhibitors or destruction of viral nucleic acids, resulting in false negative results or reduced sensitivity of the analysis.

In contrast, recent advances in sequencing technologies have revolutionized the field of plant virology, offering powerful tools for comprehensive and high-performance virus detection, characterization and surveillance. In fact, some biosensors are compact devices that can provide rapid on-site detection of plant viruses, making them ideal for point-of-care diagnostics. NGS, on the other hand, offers a comprehensive and high-throughput approach to plant virus diagnostics. By sequencing the entire viral genome present in testing samples, NGS can identify multiple viruses simultaneously and even detect novel or emerging viral strains. This deep sequencing capability in turn allows a detailed characterization of the plant virome. Moreover, integrating CRISPR-Cas systems into plant virus diagnostics presents exciting opportunities for targeted and precise virus detection and manipulation. Additionally, CRISPR-Cas systems can be utilized for genome editing to confer resistance to specific viruses in plants, offering a sustainable solution to combat viral infections. Each of these approaches offers unique advantages and capabilities, making them valuable assets in the field of plant virology.

Nowadays, one of the most important concerns of growers is the availability of portable diagnostic devices when it comes to combating plant pathogens including viruses, which will allow quicker measures to control plant diseases. In fact, this could substantially improve informed disease management overall. As technology continues to evolve, drones could also be used to further enhance their ability to detect and monitor the condition of plants (Abbas et al., 2023).

7 Conclusion

Economic losses are estimated to exceed several billion dollars per year worldwide due to lack of timely conducted management strategies. Plant diseases caused by viruses can be effectively controlled if control agents are used at the initial stage of the development of viral diseases or by planting virus-free crops. Therefore, rapid and accurate disease diagnostics is needed. Symptomatic diagnosis is still useful, but often provides erroneous results due to confusion related to the high variability of symptoms caused by interactions between the host and the virus or abiotic stresses. On the other hand, conventional lab-based detection methods require trained personnel and substantial amount of time to provide results. Therefore, reliable and portable diagnostic platforms are required that could be useful for timely decision making.

Author contributions

AK: Writing – original draft. UA: Writing – original draft. ZT: Writing – original draft. AA: Writing – original draft. SZ: Writing – original draft. KD: Writing – original draft, Writing – review & editing. GM: Supervision, Writing – review & editing.

Funding

The author(s) declare financial support was received for the research, authorship, and/or publication of this article. This work was supported by Ministry of Science and Higher Education of the Republic of Kazakhstan (Grant No. AP14872087).

Conflict of interest

The authors declare that the research was conducted in the absence of any commercial or financial relationships that could be construed as a potential conflict of interest.

Publisher's note

References

Abbas, A., Zhang, Z., Zheng, H., Alami, M. M., Alrefaei, A. F., Abbas, Q., et al. (2023). Drones in plant disease assessment, efficient monitoring, and detection: A way forward to smart agriculture. *Agronomy* 13, 1524. doi: 10.3390/agronomy13061524

Abd El-Aziz, M. H. (2019). Three modern serological methods to detect plant viruses. *J. Of Plant Sci. And Phytopathol.* 3, 101–106. doi: 10.29328/journal.jpsp

Agindotan, B., and Perry, K. L. (2008). Macroarray detection of eleven potato-infecting viruses and potato spindle tuber viroid. *Plant Dis.* 92, 730–740. doi: 10.1094/PDIS-92-5-0730

Ali, Z., Abulfaraj, A., Idris, A., Ali, S., Tashkandi, M., and Mahfouz, M. M. (2015). Crispr/cas9-mediated viral interference in plants. *Genome Biol.* 16, 1–11. doi: 10.1186/s13059-015-0799-6

Aman, R., Mahas, A., Marsic, T., Hassan, N., and Mahfouz, M. M. (2020). Efficient, rapid, and sensitive detection of plant rna viruses with one-pot rt-rpa–crispr/cas12a assay. *Front. In Microbiol.* 11, 610872. doi: 10.3389/fmicb.2020.610872

Arif, M., Torrance, L., and Reavy, B. (1994). Improved efficiency of detection of potato mop-top furovirus in potato tubers and in the roots and leaves of soil-bait plants. *Potato Res.* 37, 373–381. doi: 10.1007/BF02358351

Avila-Quezada, G. D., Golinska, P., and Rai, M. (2022). Engineered nanomaterials in plant diseases: can we combat phytopathogens? *Appl. Microbiol. And Biotechnol.* 106, 117–129. doi: 10.1007/s00253-021-11725-w

Babamiri, B., Salimi, A., and Hallaj, R. (2018). A molecularly imprinted electrochemiluminescence sensor for ultrasensitive hiv-1 gene detection using eus nanocrystals as luminophore. *Biosensors And Bioelectron.* 117, 332–339. doi: 10.1016/j.bios.2018.06.003

Baca, J. T., Severns, V., Lovato, D., Branch, D. W., and Larson, R. S. (2015). Rapid detection of ebola virus with A reagent-free, point-of-care biosensor. *Sensors* 15, 8605–8614. doi: 10.3390/s150408605

Balaji, B., Bucholtz, D. B., and Anderson, J. M. (2003). Barley yellow dwarf virus and cereal yellow dwarf virus quantification by real-time polymerase chain reaction in resistant and susceptible plants. *Phytopathology* 93, 1386–1392. doi: 10.1094/PHYTO.2003.93.11.1386

Berto, M., Vecchi, E., Baiamonte, L., Condò, C., Sensi, M., Di Lauro, M., et al. (2019). Label free detection of plant viruses with organic transistor biosensors. *Sensors And Actuators B: Chem.* 281, 150–156. doi: 10.1016/j.snb.2018.10.080

Bester, R., Cook, G., Breytenbach, J. H., Steyn, C., De Bruyn, R., and Maree, H. J. (2021). Towards the validation of high-throughput sequencing (Hts) for routine plant virus diagnostics: measurement of variation linked to hts detection of citrus viruses and viroids. *Virol. J.* 18, 1–19. doi: 10.1186/s12985-021-01523-1

Bhat, A. I., Aman, R., and Mahfouz, M. (2022). Onsite detection of plant viruses using isothermal amplification assays. *Plant Biotechnol. J.* 20, 1859–1873. doi: 10.1111/pbi.13871

Bhat, A. I., Rao, G. P., Bhat, A. I., and Rao, G. P. (2020). "DNA microarray for detection of plant viruses," in Eds. A. I. Bhat and G. P. Rao *Characterization of plant viruses: Methods and protocols*. (Springer US), 357–367. doi: 10.1007/978-1-0716-0334-5_37

Bouchek-Mechiche, K., Montfort, F., and Merz, U. (2011). Evaluation of the sss agristrip rapid diagnostic test for the detection of spongospora subterranea on potato tubers. *Eur. J. Of Plant Pathol.* 131, 277–287. doi: 10.1007/s10658-011-9807-1

Bramhachari, P. V., Mohana Sheela, G., Prathyusha, A., Madhavi, M., Satish Kumar, K., Reddy, N. N. R., et al. (2019). Advanced immunotechnological methods for detection and diagnosis of viral infections: current applications and future challenges. In: *Dynam. Of Immune Activ. In Viral Dis.* (Springer, Singapore), 261–275. doi: 10.1007/978-981-15-1045-8_17

Bronzato Badial, A., Sherman, D., Stone, A., Gopakumar, A., Wilson, V., Schneider, W., et al. (2018). Nanopore sequencing as A surveillance tool for plant pathogens in plant and insect tissues. *Plant Dis.* 102, 1648–1652. doi: 10.1094/PDIS-04-17-0488-RE

Byrne, B., Stack, E., Gilmartin, N., and O'kennedy, R. (2009). Antibody-based sensors: principles, problems and potential for detection of pathogens and associated toxins. *Sensors* 9, 4407–4445. doi: 10.3390/s90604407

Bystricka, D., Lenz, O., Mraz, I., Dědic, P., and Sip, M. (2003). Dna microarray: parallel detection of potato viruses. *Acta Virol.* 47, 41–44.

Byzova, N. A., Vinogradova, S. V., Porotikova, E. V., Terekhova, U. D., Zherdev, A. V., and Dzantiev, B. B. (2018). Lateral flow immunoassay for rapid detection of grapevine leafroll-associated virus. *Biosensors* 8, 111. doi: 10.3390/bios8040111

Cao, Y., Zhou, H., Zhou, X., and Li, F. (2020). Control of plant viruses by crispr/cas system-mediated adaptive immunity. *Front. In Microbiol.* 11, 593700. doi: 10.3389/fmicb.2020.593700

Caruso, A. G., Ragona, A., Bertacca, S., Montoya, M. A. M., Panno, S., and Davino, S. (2023). Development of an in-field real-time lamp assay for rapid detection of tomato leaf curl New Delhi virus. *Plants* 12, 1487. doi: 10.3390/plants12071487

Carvajal Barbosa, L., Insuasty Cepeda, D., León Torres, A. F., Arias Cortes, M. M., Rivera Monroy, Z. J., and Garcia Castaneda, J. E. (2021). Nucleic acid-based biosensors: analytical devices for prevention, diagnosis and treatment of diseases. *Vitae* 28, 1–27. doi: 10.17533/udea.vitae.v28n3a34725

Chailapakul, O., Siangproh, W., Jampasa, S., Chaiyo, S., Teengam, P., Yakoh, A., et al. (2020). Paper-based sensors for the application of biological compound detection. *Compr. Anal. Chem.* 89, 31–62. doi: 10.1016/bs.coac.2020.03.002

Charoenvilaisiri, S., Seepiban, C., Kumpoosiri, M., Rukpratanporn, S., Warin, N., Phuangrat, B., et al. (2021). Development of A triple antibody sandwich enzyme-linked immunosorbent assay for cassava mosaic disease detection using A monoclonal antibody to Sri Lankan cassava mosaic virus. *Virol. J.* 18, 100. doi: 10.1186/s12985-021-01572-6

Chen, H., Ali, N., Lv, W., Shen, Y., Qing, Z., Lin, Y., et al. (2020). Comparison of ic-rt-pcr, dot-elisa and indirect-elisa for the detection of sorghum mosaic virus in field-grown sugarcane plants. *Sugar Tech* 22, 122–129. doi: 10.1007/s12355-019-00738-5

Chen, L., Xu, Z.-L., Liu, P.-G., Zhu, Y., Lin, T.-B., Li, T.-Y., et al. (2022). Identification of three viruses infecting mulberry varieties. *Viruses* 14, 2564. doi: 10.3390/v14112564

Chen, P., Sun, Z., Wang, J., Liu, X., Bai, Y., Chen, J., et al. (2023). Portble nanopore-sequencing technology: trends in development and applications. *Front. In Microbiol.* 14, 1043967. doi: 10.3389/fmicb.2023.1043967

Chinnaiah, S., Ganesan, M. V., Sevugapperumal, N., Mariappan, S., Uthandi, S., and Perumal, R. (2022). A sequel study on the occurrence of tomato spotted wilt virus (Tswv) in cut-chrysanthemum by das-elisa using recombinant nucleocapsid protein to produce polyclonal antiserum. *J. Of Virol. Methods* 300, 114410. doi: 10.1016/j.jviromet.2021.114410

Devi, B. M., Guruprasath, S., Balu, P., Chattopadhyay, A., Thilagar, S. S., Dhanabalan, K. V., et al. (2024). Dissecting diagnostic and management strategies for plant viral diseases: what next? *Agriculture* 14, 284. doi: 10.3390/agriculture14020284

Devi, O. P., Sharma, S. K., Sanatombi, K., Devi, K. S., Pathaw, N., Roy, S. S., et al. (2022). A simplified multiplex pcr assay for simultaneous detection of six viruses infecting diverse chilli species in India and its application in field diagnosis. *Pathogens* 12, 6. doi: 10.3390/pathogens12010006

Dong, Z.-X., Lin, C.-C., Chen, Y.-K., Chou, C.-C., and Chen, T.-C. (2022). Identification of an emerging cucumber virus in Taiwan using oxford nanopore sequencing technology. *Plant Methods* 18, 143. doi: 10.1186/s13007-022-00976-x

Dyussembayev, K., Sambasivam, P., Bar, I., Brownlie, J. C., Shiddiky, M. J. A., and Ford, R. (2021). Biosensor technologies for early detection and quantification of plant pathogens. *Front. In Chem.* 9. doi: 10.3389/fchem.2021.636245

Edwards, M., and Cooper, J. (1985). Plant virus detection using A new form of indirect elisa. *J. Of Virol. Methods* 11, 309–319. doi: 10.1016/0166-0934(85)90024-2

Ellis, M. D., Hoak, J. M., Ellis, B. W., Brown, J. A., Sit, T. L., Wilkinson, C. A., et al. (2020). Quantitative real-time pcr analysis of individual flue-cured tobacco seeds and seedlings reveals seed transmission of tobacco mosaic virus. *Phytopathology* 110, 194–205. doi: 10.1094/PHYTO-06-19-0201-FI

Eun, A. J.-C., Huang, L., Chew, F.-T., Li, S. F.-Y., and Wong, S.-M. (2002). Detection of two orchid viruses using quartz crystal microbalance (Qcm) immunosensors. *J. Of Virol. Methods* 99, 71–79. doi: 10.1016/S0166-0934(01)00382-2

Faccioli, G., and Colombarini, A. (1996). Correlation of potato virus S and virus M contents of potato meristem tips with the percentage of virus-free plantlets produced *in vitro*. *Potato Res.* 39, 129–140. doi: 10.1007/BF02358213

Fang, Y., and Ramasamy, R. (2015). Current and prospective methods for plant disease detection. *Biosensors* 5, 537–561. doi: 10.3390/bios5030537

Fang, L., Yang, L., Han, M., Xu, H., Ding, W., and Dong, X. (2023). Crispr-cas technology: A key approach for sars-cov-2 detection. *Front. In Bioeng. And Biotechnol.* 11, 1158672. doi: 10.3389/fbioe.2023.1158672

Feng, J.-L., Chen, S.-N., Tang, X.-S., Ding, X.-F., Du, Z.-Y., and Chen, J.-S. (2006). Quantitative determination of cucumber mosaic virus genome rnas in virions by real-time reverse transcription-polymerase chain reaction. *Acta Biochim. Et Biophys. Sin.* 38, 669–676. doi: 10.1111/j.1745-7270.2006.00216.x

Festus, R. O., Seal, S. E., Prempeh, R., Quain, M. D., and Silva, G. (2023). Improved reverse transcription loop-mediated isothermal amplification (Rt-lamp) for the rapid and sensitive detection of yam mosaic virus. *Viruses* 15, 1592. doi: 10.3390/v15071592

Fillmer, K., Adkins, S., Pongam, P., and D'elia, T. (2015). Complete genome sequence of A tomato mottle mosaic virus isolate from the United States. *Genome Announce.* 3, 10.1128. doi: 10.1128/genomeA.00167-15

Filloux, D., Fernandez, E., Loire, E., Claude, L., Galzi, S., Candresse, T., et al. (2018). Nanopore-based detection and characterization of yam viruses. *Sci. Rep.* 8, 17879. doi: 10.1038/s41598-018-36042-7

Gao, X., Chen, Y., Luo, X., Du, Z., Hao, K., An, M., et al. (2021). Recombinase polymerase amplification assay for simultaneous detection of maize chlorotic mottle virus and sugarcane mosaic virus in maize. *ACS Omega* 6, 18008–18013. doi: 10.1021/acsomega.1c01767

Garcia-Pedemonte, D., Carcereny, A., Gregori, J., Quer, J., Garcia-Cehic, D., Guerrero, L., et al. (2023). Comparison of nanopore and synthesis-based next-generation sequencing platforms for sars-cov-2 variant monitoring in wastewater. *Int. J. Of Mol. Sci.* 24, 17184. doi: 10.3390/ijms242417184

Garzo, E., Moreno, A., Plaza, M., and Fereres, A. (2020). Feeding behavior and virus-transmission ability of insect vectors exposed to systemic insecticides. *Plants* 9, 895. doi: 10.3390/plants9070895

Ghorbani, A., Astaraki, S., Rostami, M., and Pakdel, A. (2023). Unleashing the power of colloidal gold immunochromatographic assays for plant virus diagnostics. *Methodsx* 12, 102498. doi: 10.1016/j.mex.2023.102498

Govindarajan, R., Duraiyan, J., Kaliyappan, K., and Palanisamy, M. (2012). Microarray and its applications. *J. Of Pharm. And Bioallied Sci.* 4, S310–S312. doi: 10.4103/0975-7406.100283

Guo, Y., Wu, W., Zhang, X., Ding, M., Yu, J., Zhang, J., et al. (2022). Triplex lateral flow immunoassay for rapid diagnosis of tobacco mosaic virus, tobacco vein banding mosaic virus, and potato virus Y. *Plant Dis.* 106, 3033–3039. doi: 10.1094/PDIS-08-21-1756-RE

Gutiérrez-Aguirre, I., Hodnik, V., Glais, L., Rupar, M., Jacquot, E., Anderluh, G., et al. (2014). Surface plasmon resonance for monitoring the interaction of potato virus Y with monoclonal antibodies. *Anal. Biochem.* 447, 74–81. doi: 10.1016/j.ab.2013.10.032

Hadidi, A., Flores, R., Candresse, T., and Barba, M. (2016). Next-generation sequencing and genome editing in plant virology. *Front. In Microbiol.* 7, 217578. doi: 10.3389/fmicb.2016.01325

Hamim, I., Borth, W., Melzer, M., and Hu, J. (2018). Ultra-sensitive detection of papaya ringspot virus using single-tube nested pcr. *Acta Virol.* 62, 379–385. doi: 10.4149/av_2018_405

Hao, X., Zhang, W., Zhao, F., Liu, Y., Qian, W., Wang, Y., et al. (2018). Discovery of plant viruses from tea plant (Camellia sinensis (L.) O. Kuntze) by metagenomic sequencing. *Front. In Microbiol.* 9, 2175. doi: 10.3389/fmicb.2018.02175

Hema, M., Joseph, J., Gopinath, K., Sreenivasulu, P., and Savithri, H. (1999). Molecular characterization and interviral relationships of A flexuous filamentous virus causing mosaic disease of sugarcane (Saccharum officinarum L.) in India. *Arch. Of Virol.* 144, 479–490. doi: 10.1007/s007050050519

Hema, M., and Konakalla, N. C. (2021). Recent developments in detection and diagnosis of plant viruses. Recent developments. *Appl. Microbiol. And Biochem.* 2, 163–180. doi: 10.1016/B978-0-12-821406-0.00016-3

Hong, S., and Lee, C. (2018). The current status and future outlook of quantum dot-based biosensors for plant virus detection. *Plant Pathol. J.* 34, 85. doi: 10.5423/PPJ.RW.08.2017.0184

Hua, Y., Feng, C., Gu, T., Chen, H., Liu, D., Xu, K., et al. (2023). Development of polyclonal antibodies and A serological-based reverse-transcription loop-mediated isothermal amplification (S-rt-lamp) assay for rice black-streaked dwarf virus detection in both rice and small brown planthopper. *Viruses* 15, 2127. doi: 10.3390/v15102127

Huang, M., Wu, Z., Li, J., Ding, Y., Chen, S., and Li, X. (2023). Plant protection against viruses: an integrated review of plant immunity agents. *Int. J. Of Mol. Sci.* 24, 4453. doi: 10.3390/ijms24054453

Huang, X., Xu, J., Ji, H.-F., Li, G., and Chen, H. (2014). Quartz crystal microbalance based biosensor for rapid and sensitive detection of maize chlorotic mottle virus. *Anal. Methods* 6, 4530–4536. doi: 10.1039/C4AY00292J

Hwang, H. J., Ryu, M. Y., Park, C. Y., Ahn, J., Park, H. G., Choi, C., et al. (2017). High sensitive and selective electrochemical biosensor: label-free detection of human norovirus using affinity peptide as molecular binder. *Biosensors And Bioelectron.* 87, 164–170. doi: 10.1016/j.bios.2016.08.031

Ilbagi, H., Rabenstein, F., Habekuss, A., Ordon, F., Citir, A., Cebeci, O., et al. (2008). Molecular, serological and transmission electron microscopic analysis of the barley yellow dwarf virus-pav and the cereal yellow dwarf virus-rpv in canary seed (Phalaris canariensis L.). *Cereal Res. Commun.* 36, 225–234. doi: 10.1556/CRC.36.2008.2.3

Ivanov, A. V., Safenkova, I. V., Zherdev, A. V., and Dzantiev, B. B. (2021). The potential use of isothermal amplification assays for in-field diagnostics of plant pathogens. *Plants* 10, 2424. doi: 10.3390/plants10112424

Jailani, A. A. K., and Paret, M. L. (2023). Development of A multiplex rt-rpa assay for simultaneous detection of three viruses in cucurbits. *Mol. Plant Pathol.* 24, 1443–1450. doi: 10.1111/mpp.13380

Javaran, V. J., Moffett, P., Lemoyne, P., Xu, D., Adkar-Purushothama, C. R., and Fall, M. L. (2021). Grapevine virology in the third-generation sequencing era: from virus detection to viral epitranscriptomics. *Plants* 10, 2355. doi: 10.3390/plants10112355

Javaran, V. J., Poursalavati, A., Lemoyne, P., Ste-Croix, D. T., Moffett, P., and Fall, M. L. (2023). Nanovirseq: dsrna sequencing for plant virus and viroid detection by nanopore sequencing. *Biorxiv*, 524564. doi: 10.1101/2023.01.18.524564

Jiang, T., and Zhou, T. (2023). Unraveling the mechanisms of virus-induced symptom development in plants. *Plants* 12, 2830. doi: 10.3390/plants12152830

Jiao, J., Kong, K., Han, J., Song, S., Bai, T., Song, C., et al. (2021). Field detection of multiple rna viruses/viroids in apple using A crispr/cas12a-based visual assay. *Plant Biotechnol. J.* 19, 394–405. doi: 10.1111/pbi.13474

Jie, S. U. N., Wan, W., Xue-Qin, R. A. O., and Hua-Ping, L. I. (2017). Development of taqman real-time pcr assay for investigating transmission of banana streak virus in micropropagated banana. *Acta Phytopathol. Sin.* 47, 187–196. doi: 10.13926/j.cnki.apps.000091

Kalimuthu, K., Arivalagan, J., Mohan, M., Christyraj, J. R. S. S., Arockiaraj, J., Muthusamy, R., et al. (2022). Point of care diagnosis of plant virus: current trends and prospects. *Mol. And Cell. Probes* 61, 101779. doi: 10.1016/j.mcp.2021.101779

Katsiani, A., Maliogka, V. I., Katis, N., Svanella-Dumas, L., Olmos, A., Ruiz-García, A. B., et al. (2018). High-throughput sequencing reveals further diversity of little cherry virus 1 with implications for diagnostics. *Viruses* 10, 385. doi: 10.3390/v10070385

Khan, M., Shah, S. H., Salman, M., Abdullah, M., Hayat, F., and Akbar, S. (2023). Enzyme-linked immunosorbent assay versus chemiluminescent immunoassay: A general overview. *Global J. Of Medical Pharma. And Biomed. Update* 18, 1–5. doi: 10.25259/GJMPBU_77_2022

Kim, S. W., Lee, H. J., Choi, S., Cho, I. S., and Jeong, R. D. (2023). Rapid identification of jasmine virus H infecting ixora coccinea by nanopore metatranscriptomics. *Plant Pathol. J.* 39, 303–308. doi: 10.5423/PPJ.NT.03.2023.0037

Kimura, K., Miyazaki, A., Suzuki, T., Yamamoto, T., Kitazawa, Y., Maejima, K., et al. (2023). A reverse-transcription loop-mediated isothermal amplification technique to detect tomato mottle mosaic virus, an emerging tobamovirus. *Viruses* 15, 1688. doi: 10.3390/v15081688

Kokane, A. D., Lawrence, K., Kokane, S. B., Gubyad, M. G., Misra, P., Reddy, M. K., et al. (2021a). Development of A sybr green-based rt-qpcr assay for the detection of Indian citrus ringspot virus. *3 Biotech.* 11, 359. doi: 10.1007/s13205-021-02903-8

Kokane, S. B., Misra, P., Kokane, A. D., Gubyad, M. G., Warghane, A. J., Surwase, D., et al. (2021b). Development of A real-time rt-pcr method for the detection of citrus tristeza virus (Ctv) and its implication in studying virus distribution in planta. *3 Biotech.* 11, 431. doi: 10.1007/s13205-021-02976-5

Kovalskaya, N., and Hammond, R. W. (2014). Molecular biology of viroid–host interactions and disease control strategies. *Plant Sci.* 228, 48–60. doi: 10.1016/j.plantsci.2014.05.006

Krawczyk, K., Uszczyńska-Ratajczak, B., Majewska, A., and Borodynko-Filas, N. (2017). Dna microarray-based detection and identification of bacterial and viral pathogens of maize. *J. Of Plant Dis. And Prot.* 124, 577–583. doi: 10.1007/s41348-017-0098-4

Lai, P.-C., Abney, M. R., Chen, Y.-J., Bag, S., and Srinivasan, R. (2021). Discrepancies in serology-based and nucleic acid-based detection and quantitation of tomato spotted wilt orthotospovirus in leaf and root tissues from symptomatic and asymptomatic peanut plants. *Pathogens* 10, 1476. doi: 10.3390/pathogens10111476

Lee, H.-J., Kim, S.-M., and Jeong, R.-D. (2023). Analysis of wheat virome in Korea using illumina and oxford nanopore sequencing platforms. *Plants* 12, 2374. doi: 10.3390/plants12122374

Lee, S., Lee, G., Choi, I., and Rho, J. (2015). Development of pcr diagnostic system for detection of the seed-transmitted tobacco ringspot virus in quarantine. *Indian J. Of Microbiol.* 55, 231–233. doi: 10.1007/s12088-015-0518-8

Leigh, D. M., Peranić, K., Prospero, S., Cornejo, C., Ćurković-Perica, M., Kupper, Q., et al. (2021). Long-read sequencing reveals the evolutionary drivers of intra-host diversity across natural rna mycovirus infections. *Virus Evol.* 7, 1–14. doi: 10.1093/ve/veab101

Li, X., Guo, L., Guo, M., Qi, D., Zhou, X., Li, F., et al. (2021). Three highly sensitive monoclonal antibody-based serological assays for the detection of tomato mottle mosaic virus. *Phytopathol. Res.* 3, 1–9. doi: 10.1186/s42483-021-00100-2

Lou, J., Wang, B., Li, J., Ni, P., Jin, Y., Chen, S., et al. (2022). The crispr-cas system as A tool for diagnosing and treating infectious diseases. *Mol. Biol. Rep.* 49, 11301–11311. doi: 10.1007/s11033-022-07752-z

MacKenzie, M., and Argyropoulos, C. (2023). An introduction to nanopore sequencing: past, present, and future considerations. *Micromachines* 14, 459. doi: 10.3390/mi14020459

Malecka, K., Michalczuk, L., Radecka, H., and Radecki, J. (2014). Ion-channel genosensor for the detection of specific dna sequences derived from plum pox virus in plant extracts. *Sensors* 14, 18611–18624. doi: 10.3390/s141018611

Maliogka, V., Charou, A., Efthimiou, K., Katsiani, A., Chatzivassiliou, E., and Katis, N. (2010). Identification of ilarviruses in almond and cherry fruit trees using nested pcr assays. *Julius-Kühn-Archiv* 427.

Maliogka, V. I., Minafra, A., Saldarelli, P., Ruiz-García, A. B., Glasa, M., Katis, N., et al. (2018). Recent advances on detection and characterization of fruit tree viruses using high-throughput sequencing technologies. *Viruses* 10, 436. doi: 10.3390/v10080436

Manjunatha, L., Rajashekara, H., Uppala, L. S., Ambika, D. S., Patil, B., Shankarappa, K. S., et al. (2022). Mechanisms of microbial plant protection and control of plant viruses. *Plants* 11, 3449. doi: 10.3390/plants11243449

Maree, H. J., Fox, A., Al Rwahnih, M., Boonham, N., and Candresse, T. (2018). Application of hts for routine plant virus diagnostics: state of the art and challenges. *Front. In Plant Sci.* 9, 401885. doi: 10.3389/fpls.2018.01082

Marqués, M.-C., Sánchez-Vicente, J., Ruiz, R., Montagud-Martínez, R., Márquez-Costa, R., Gómez, G., et al. (2022). Diagnostics of infections produced by the plant viruses tmv, tev, and pvx with crispr-cas12 and crispr-cas13. *ACS Synth. Biol.* 11, 2384–2393. doi: 10.1021/acssynbio.2c00090

Martín, S., Alioto, D., Milne, R. G., Garnsey, S. M., Laura García, M., Grau, O., et al. (2004). Detection of citrus psorosis virus by elisa, molecular hybridization, rt-pcr and immunosorbent electron microscopy and its association with citrus psorosis disease. *Eur. J. Of Plant Pathol.* 110, 747–757. doi: 10.1023/B:EJPP.0000041570.28825.29

Martinelli, F., Scalenghe, R., Davino, S., Panno, S., Scuderi, G., Ruisi, P., et al. (2015). Advanced methods of plant disease detection. A review. *Agron. For Sustain. Dev.* 35, 1–25. doi: 10.1007/s13593-014-0246-1

Mehetre, G. T., Leo, V. V., Singh, G., Sorokan, A., Maksimov, I., Yadav, M. K., et al. (2021). Current developments and challenges in plant viral diagnostics: A systematic review. *Viruses* 13, 412. doi: 10.3390/v13030412

Minutillo, S. A., Marais, A., Mascia, T., Faure, C., Svanella-Dumas, L., Theil, S., et al. (2015). Complete nucleotide sequence of artichoke latent virus shows it to be A member of the genus macluravirus in the family potyviridae. *Phytopathology* 105, 1155–1160. doi: 10.1094/PHYTO-01-15-0010-R

Minutillo, S. A., Mascia, T., and Gallitelli, D. (2012). A dna probe mix for the multiplex detection of ten artichoke viruses. *Eur. J. Of Plant Pathol.* 134, 459–465. doi: 10.1007/s10658-012-0032-3

Moon, Y. J., Lee, S. Y., and Oh, S. W. (2022). A review of isothermal amplification methods and food-origin inhibitors against detecting food-borne pathogens. *Foods* 11, 322. doi: 10.3390/foods11030322

Morán, F., Olmos, A., Glasa, M., Silva, M. B. D., Maliogka, V., Wetzel, T., et al. (2023). A novel and highly inclusive quantitative real-time rt-pcr method for the broad and efficient detection of grapevine leafroll-associated virus 1. *Plants* 12, 876. doi: 10.3390/plants12040876

Moreno, A., Bertolini, E., Olmos, A., Cambra, M., and Fereres, A. (2007). Estimation of vector propensity for lettuce mosaic virus based on viral detection in single aphids. *Spanish J. Of Agric. Res.* 3, 376–384. doi: 10.5424/sjar/2007053-5343

Mwaipopo, B., Rajamäki, M.-L., Ngowi, N., Nchimbi-Msolla, S., Njau, P. J., Valkonen, J. P., et al. (2021). Next-generation sequencing-based detection of common bean viruses in wild plants from Tanzania and their mechanical transmission to common bean plants. *Plant Dis.* 105, 2541–2550. doi: 10.1094/PDIS-07-20-1420-RE

Nabi, S. U., Mir, J. I., Yasmin, S., Din, A., Raja, W. H., Madhu, G., et al. (2023). Tissue and time optimization for real-time detection of apple mosaic virus and apple necrotic mosaic virus associated with mosaic disease of apple (Malus domestica). *Viruses* 15, 795. doi: 10.3390/v15030795

Nafea, A. M., Wang, Y., Wang, D., Salama, A. M., Aziz, M. A., Xu, S., et al. (2024). Application of next-generation sequencing to identify different pathogens. *Front. In Microbiol.* 14, 1329330. doi: 10.3389/fmicb.2023.1329330

Naresh, V., and Lee, N. (2021). A review on biosensors and recent development of nanostructured materials-enabled biosensors. *Sensors* 21, 1109. doi: 10.3390/s21041109

Nascimento, A. K. Q., Lima, J. A. A., and Barbosa, G. D. S. (2017). A simple kit of plate-trapped antigen enzyme-linked immunosorbent assay for identification of plant viruses1. *Rev. Ciec. Agron.* 48, 216–220. doi: 10.5935/1806-6690.20170025

Notomi, T., Mori, Y., Tomita, N., and Kanda, H. (2015). Loop-mediated isothermal amplification (Lamp): principle, features, and future prospects. *J. Of Microbiol.* 53, 1–5. doi: 10.1007/s12275-015-4656-9

Olmos, A., Capote, N., Bertolini, E., Cambra, M., Punja, Z., and Boer, S. (2007). Molecular diagnostic methods for plant viruses. In: Z. K. Punja, S. H. Boer and H. Sanfacon II Eds. *Biotechnol. And Plant Dis. Manage.* (Oxfordshire, UK: CABI), 227–249. doi: 10.1079/9781845932886.0227

Pandit, M. A., Kumar, J., Gulati, S., Bhandari, N., Mehta, P., Katyal, R., et al. (2022). Major biological control strategies for plant pathogens. *Pathogens* 11, 273. doi: 10.3390/pathogens11020273

Panno, S., Matić, S., Tiberini, A., Caruso, A. G., Bella, P., Torta, L., et al. (2020). Loop mediated isothermal amplification: principles and applications in plant virology. *Plants* 9, 461. doi: 10.3390/plants9040461

Park, J.-W. (2022). Principles and applications of loop-mediated isothermal amplification to point-of-care tests. *Biosensors* 12, 857. doi: 10.3390/bios12100857

Patel, P. (2021). A review on plant disease diagnosis through biosensor. *Int. J. Of Biosensors Bioelectron.* 7, 50–52. doi: 10.15406/IJBSBE

Pecman, A., Adams, I., Gutiérrez-Aguirre, I., Fox, A., Boonham, N., Ravnikar, M., et al. (2022). Systematic comparison of nanopore and illumina sequencing for the detection of plant viruses and viroids using total rna sequencing approach. *Front. In Microbiol.* 13, 883921. doi: 10.3389/fmicb.2022.883921

Pecman, A., Kutnjak, D., Gutiérrez-Aguirre, I., Adams, I., Fox, A., Boonham, N., et al. (2017). Next generation sequencing for detection and discovery of plant viruses and viroids: comparison of two approaches. *Front. In Microbiol.* 8, 1998. doi: 10.3389/fmicb.2017.01998

Phannareth, T., Nunziata, S. O., Stulberg, M. J., Galvez, M. E., and Rivera, Y. (2020). Comparison of nanopore sequencing protocols and real-time analysis for phytopathogen diagnostics. *Plant Health Prog.* 22, 31–36. doi: 10.1094/PHP-02-20-0013-RS

Phatsaman, T., Hongprayoon, R., and Wasee, S. (2020). Monoclonal antibody-based diagnostic assays for pepper mild mottle virus. *J. Of Plant Pathol.* 102, 327–333. doi: 10.1007/s42161-019-00421-4

Prabha, K., Baranwal, V., and Jain, R. (2013). Applications of next generation high throughput sequencing technologies in characterization, discovery and molecular interaction of plant viruses. *Indian J. Of Virol.* 24, 157–165. doi: 10.1007/s13337-013-0133-4

Qin, D. (2019). Next-generation sequencing and its clinical application. *Cancer Biol. Med.* 16, 4. doi: 10.20892/j.issn.2095-3941.2018.0055

Qin, J., Yin, Z., Shen, D., Chen, H., Chen, X., Cui, X., et al. (2021). Development of A recombinase polymerase amplification combined with lateral flow dipstick assay for rapid and sensitive detection of bean common mosaic virus. *Phytopathol. Res.* 3, 3. doi: 10.1186/s42483-021-00080-3

Ramachandran, V., Weiland, J. J., and Bolton, M. D. (2021). Crispr-based isothermal next-generation diagnostic method for virus detection in sugarbeet. *Front. In Microbiol.* 12, 679994. doi: 10.3389/fmicb.2021.679994

Ramos, V. C., Spadotti, D. M., Bampi, D., and Rezende, J. A. (2018). Resistance of cucurbita maxima 'Exposição'to zucchini lethal chlorosis virus is likely associated with restriction to the systemic movement of the virus. *Trop. Plant Pathol.* 43, 433–438. doi: 10.1007/s40858-018-0235-z

Rott, M., Xiang, Y., Boyes, I., Belton, M., Saeed, H., Kesanakurti, P., et al. (2017). Application of next generation sequencing for diagnostic testing of tree fruit viruses and viroids. *Plant Dis.* 101, 1489–1499. doi: 10.1094/PDIS-03-17-0306-RE

Rubio, L., Galipienso, L., and Ferriol, I. (2020). Detection of plant viruses and disease management: relevance of genetic diversity and evolution. *Front. In Plant Sci.* 11, 1092. doi: 10.3389/fpls.2020.01092

Ruiz-Ruiz, S., Ambrós, S., Del Carmen Vives, M., Navarro, L., Moreno, P., and Guerri, J. (2009). Detection and quantitation of citrus leaf blotch virus by taqman real-time rt-pcr. *J. Of Virol. Methods* 160, 57–62. doi: 10.1016/j.jviromet.2009.04.012

Ruiz-Ruiz, S., Moreno, P., Guerri, J., and Ambrós, S. (2007). A real-time rt-pcr assay for detection and absolute quantitation of citrus tristeza virus in different plant tissues. *J. Of Virol. Methods* 145, 96–105. doi: 10.1016/j.jviromet.2007.05.011

Saylan, Y., Erdem, Ö., Ünal, S., and Denizli, A. (2019). An alternative medical diagnosis method: biosensors for virus detection. *Biosensors* 9, 65. doi: 10.3390/bios9020065

Selvarajan, R., Kanichelvam, P. S., Balasubramanian, V., and Subramanian, S. S. (2020). A rapid and sensitive lateral flow immunoassay (Lfia) test for the on-site detection of banana bract mosaic virus in banana plants. *J. Of Virol. Methods* 284, 113929. doi: 10.1016/j.jviromet.2020.113929

Selvarajan, R., Sheeba, M. M., and Balasubramanian, V. (2011). Simultaneous detection of episomal banana streak mysore virus and banana bunchy top virus using multiplex rt–pcr. *Curr. Sci.* 100, 31–34. www.jstor.org/stable/24069708.

Shen, C., Wei, C., Li, J., Zhang, X., and Wu, Y. (2020). Integrated single-molecule long-read sequencing and illumina sequencing reveal the resistance mechanism of psathyrostachys huashanica in response to barley yellow dwarf virus-gav. *Phytopathol. Res.* 2, 1–15. doi: 10.1186/s42483-020-00057-8

Singh, A. T., Lantigua, D., Meka, A., Taing, S., Pandher, M., and Camci-Unal, G. (2018). Based sensors: emerging themes and applications. *Sensors* 18, 2838. doi: 10.3390/s18092838

Singhal, P., Nabi, S. U., Yadav, M. K., and Dubey, A. (2021). Mixed infection of plant viruses: diagnostics, interactions and impact on host. *J. Of Plant Dis. And Prot.* 128, 353–368. doi: 10.1007/s41348-020-00384-0

Soroka, M., Wasowicz, B., and Rymaszewska, A. (2021). Loop-mediated isothermal amplification (Lamp): the better sibling of pcr? *Cells* 10, 1931. doi: 10.3390/cells10081931

Sun, S.-R., Ahmad, K., Wu, X.-B., Chen, J.-S., Fu, H.-Y., Huang, M.-T., et al. (2018). Development of quantitative real-time pcr assays for rapid and sensitive detection of two badnavirus species in sugarcane. *BioMed. Res. Int.* 2018, 8678242. doi: 10.1155/2018/8678242

Sun, K., Liu, Y., Zhou, X., Yin, C., Zhang, P., Yang, Q., et al. (2022). Nanopore sequencing technology and its application in plant virus diagnostics. *Front. In Microbiol.* 13, 939666. doi: 10.3389/fmicb.2022.939666

Tabatabaei, M. S., Islam, R., and Ahmed, M. (2021). Applications of gold nanoparticles in elisa, pcr, and immuno-pcr assays: A review. *Anal. Chimica Acta* 1143, 250–266. doi: 10.1016/j.aca.2020.08.030

Tam, Y. J., Zeenathul, N. A., Rezaei, M. A., Mustafa, N. H., Azmi, M. L. M., Bahaman, A. R., et al. (2017). Wide dynamic range of surface-plasmon-resonance-based assay for hepatitis B surface antigen antibody optimal detection in comparison with elisa. *Biotechnol. And Appl. Biochem.* 64, 735–744. doi: 10.1002/bab.1528

Tessema, L., Kakuhenzire, R., Seid, E., Tafesse, S., Tadesse, Y., Negash, K., et al. (2024). Detection of six potato viruses using double antibody sandwich elisa from *in vitro*, screen house and field grown potato crops in Ethiopia. *Discover Appl. Sci.* 6, 79. doi: 10.1007/s42452-023-05619-x

Torrance, L., and Talianksy, M. E. (2020). Potato virus Y emergence and evolution from the andes of South America to become a major destructive pathogen of potato and other solanaceous crops worldwide. *Viruses* 12, 1430. doi: 10.3390/v12121430

Tripathi, J. N., Ntui, V. O., Ron, M., Muiruri, S. K., Britt, A., and Tripathi, L. (2019). CRISPR/Cas9 editing of endogenous banana streak virus in the B genome of Musa spp. overcomes a major challenge in banana breeding. *Commun Biol.* 2, 46. doi: 10.1038/s42003-019-0288-7

Tripathi, L., Ntui, V. O., Tripathi, J. N., and Kumar, P. L. (2021). Application of crispr/cas for diagnosis and management of viral diseases of banana. *Front. In Microbiol.* 11, 609784. doi: 10.3389/fmicb.2020.609784

Tsou, J.-H., Leng, Q., and Jiang, F. (2019). A crispr test for detection of circulating nuclei acids. *Trans. Oncol.* 12, 1566–1573. doi: 10.1016/j.tranon.2019.08.011

Venbrux, M., Crauwels, S., and Rediers, H. (2023). Current and emerging trends in techniques for plant pathogen detection. *Front. In Plant Sci.* 14, 1120968. doi: 10.3389/fpls.2023.1120968

Villamor, D., Ho, T., Al Rwahnih, M., Martin, R., and Tzanetakis, I. (2019). High throughput sequencing for plant virus detection and discovery. *Phytopathology* 109, 716–725. doi: 10.1094/PHYTO-07-18-0257-RVW

Wang, Y. M., Ostendorf, B., Gautam, D., Habili, N., and Pagay, V. (2022). Plant viral disease detection: from molecular diagnosis to optical sensing technology—A multidisciplinary review. *Remote Sens.* 14, 1542. doi: 10.3390/rs14071542

Wang, X., Shang, X., and Huang, X. (2020). Next-generation pathogen diagnosis with crispr/cas-based detection methods. *Emerg. Microbes Infect.* 9, 1682–1691. doi: 10.1080/22221751.2020.1793689

Wang, L., Zhang, W., Shen, W., Li, M., Fu, Y., Li, Z., et al. (2023). Integrated transcriptome and microrna sequencing analyses reveal gene responses in poplar leaves infected by the novel pathogen bean common mosaic virus (Bcmv). *Front. In Plant Sci.* 14, 1163232. doi: 10.3389/fpls.2023.1163232

Xu, L., and Hampton, R. (1996). Molecular detection of bean common mosaic and bean common mosaic necrosis potyviruses and pathogroups. *Arch. Of Virol.* 141, 1961–1977. doi: 10.1007/BF01718207

Yao, Z., Coatsworth, P., Shi, X., Zhi, J., Hu, L., Yan, R., et al. (2022). Based sensors for diagnostics, human activity monitoring, food safety and environmental detection. *Sensors Diagnost.* 1, 312–342. doi: 10.1039/D2SD00017B

Yu, C., Wu, J., and Zhou, X. (2005). Detection and subgrouping of cucumber mosaic virus isolates by tas-elisa and immunocapture rt-pcr. *J. Of Virol. Methods* 123, 155–161. doi: 10.1016/j.jviromet.2004.09.014

Zanoli, L. M., and Spoto, G. (2012). Isothermal amplification methods for the detection of nucleic acids in microfluidic devices. *Biosensors* 3, 18–43. doi: 10.3390/bios3010018

Zeng, C., Huang, X., Xu, J., Li, G., Ma, J., Ji, H.-F., et al. (2013). Rapid and sensitive detection of maize chlorotic mottle virus using surface plasmon resonance-based biosensor. *Anal. Biochem.* 440, 18–22. doi: 10.1016/j.ab.2013.04.026

Zherdev, A. V., Vinogradova, S. V., Byzova, N. A., Porotikova, E. V., Kamionskaya, A. M., and Dzantiev, B. B. (2018). Methods for the diagnosis of grapevine viral infections: A review. *Agriculture* 8, 195. doi: 10.3390/agriculture8120195

Zhou, H., Lei, Y., Wang, P., Liu, M., and Hu, X. (2019). Development of sybr green real-time pcr and nested rt-pcr for the detection of potato mop-top virus (Pmtv) and viral surveys in progeny tubers derived from pmtv infected potato tubers. *Mol. And Cell. Probes* 47, 101438. doi: 10.1016/j.mcp.2019.101438

frontiers | Frontiers in Plant Science

TYPE Original Research
PUBLISHED 30 August 2024
DOI 10.3389/fpls.2024.1429402

OPEN ACCESS

EDITED BY
Brigitte Mauch-Mani,
Université de Neuchâtel, Switzerland

REVIEWED BY
Beatriz Xoconostle-Cázares,
Center for Research and Advanced Studies, National Polytechnic Institute of Mexico (CINVESTAV), Mexico
Despoina Beris

*CORRESPONDENCE
Vanitharani Ramachandran
vanitharani.ramachandran@usda.gov

RECEIVED 08 May 2024
ACCEPTED 29 July 2024
PUBLISHED 30 August 2024

CITATION
Chinnadurai C, Wyatt NA, Weiland JJ, Neher OT, Hastings J, Bloomquist MW, Chu C, Chanda AK, Khan M, Bolton MD and Ramachandran V (2024) Meta-transcriptomic analysis reveals the geographical expansion of known sugarbeet-infecting viruses and the occurrence of a novel virus in sugarbeet in the United States.
Front. Plant Sci. 15:1429402.
doi: 10.3389/fpls.2024.1429402

Meta-transcriptomic analysis reveals the geographical expansion of known sugarbeet-infecting viruses and the occurrence of a novel virus in sugarbeet in the United States

Chinnaraja Chinnadurai[1], Nathan A. Wyatt[2], John J. Weiland[2], Oliver T. Neher[3], Joe Hastings[4], Mark W. Bloomquist[5], Chenggen Chu[2], Ashok K. Chanda[6,7], Mohamed Khan[1], Melvin D. Bolton[1,2] and Vanitharani Ramachandran[1,2]*

[1]Department of Plant Pathology, North Dakota State University, Fargo, ND, United States, [2]United States Department of Agriculture, Agricultural Research Service, Edward T. Schafer Agricultural Research Center, Fargo, ND, United States, [3]Sugarbeet Research, Amalgamated Sugar Company, Boise, ID, United States, [4]Agriculture Department, American Crystal Sugar Company, Moorhead, MN, United States, [5]Agriculture Department, Southern Minnesota Beet Sugar Cooperative, Renville, MN, United States, [6]Department of Plant Pathology, University of Minnesota, St. Paul, MN, United States, [7]Northwest Research and Outreach Center, University of Minnesota, Crookston, MN, United States

In this study, meta-transcriptome sequencing was conducted on a total of 18 sugarbeet (*Beta vulgaris* L. subsp. *vulgaris*) sample libraries to profile the virome of field-grown sugarbeet to identify the occurrence and distribution of known and potentially new viruses from five different states in the United States. Sugarbeet roots with symptoms resembling rhizomania caused by beet necrotic yellow vein virus (BNYVV), or leaves exhibiting leaf-curling, yellowing to browning, or green mosaic were collected from the sugarbeet growing areas of California, Colorado, Idaho, Minnesota, and North Dakota. *In silico* analysis of *de novo* assembled contigs revealed the presence of nearly full-length genomes of BNYVV, beet soil-borne virus (BSBV), and beet soil-borne mosaic virus (BSBMV), which represent known sugarbeet-infecting viruses. Among those, BNYVV was widespread across the locations, whereas BSBV was prevalent in Minnesota and Idaho, and BSBMV was only detected in Minnesota. In addition, two recently reported *Beta vulgaris* satellite virus isoforms (BvSatV-1A and BvSatV-1B) were detected in new locations, indicating the geographical expansion of this known virus. Besides these known sugarbeet-infecting viruses, the bioinformatic analysis identified the widespread occurrence of a new uncharacterized *Erysiphe necator*-associated abispo virus (En_abispoV), a fungus-related virus that was identified in all 14 libraries. En_abispoV contains two RNA components, and nearly complete sequences of both RNA1 and RNA2 were obtained from RNASeq and were further confirmed by primer-walking RT-PCR and Sanger sequencing.

Phylogenetic comparison of En_abispoV isolates obtained in this study showed varying levels of genetic diversity within RNA1 and RNA2 compared to previously reported isolates. The undertaken meta-transcriptomic approach revealed the widespread nature of coexisting viruses associated with field-grown sugarbeet exhibiting virus disease-like symptoms in the United States.

KEYWORDS

RNA sequencing, virome, rhizomania, meta-transcriptomic, sugarbeet, *Beta vulgaris*

1 Introduction

Sugarbeet (*Beta vulgaris* L. subsp. *vulgaris*), a sucrose-accumulating root crop that contributes one-fourth of the world's sugar, is cultivated in Europe, Asia, Mediterranean countries, and parts of North America (Biancardi et al., 2010). In the United States (U. S.), sugarbeet is grown in four regions covering 11 states viz., the Great Lakes region (Michigan) to the east of the Mississippi River, the upper Midwest (Minnesota and North Dakota), the Great Plains (Colorado, Montana, Nebraska, and Wyoming), and the Far West (California, Idaho, Oregon, and Washington), where approximately 1.5 million acres are grown annually (https://www.ers.usda.gov). Sugarbeet production is affected by a number of viral diseases. Among the viral diseases of sugarbeet, rhizomania, caused by the *Beet necrotic yellow vein virus* (BNYVV, genus *Benyvirus*), is a leading global virus disease of sugarbeet (Tamada, 1999; Tamada and Baba, 1973; Rush et al., 2006). In the U. S., rhizomania was first reported in California in 1983, and shortly after, had spread to all sugarbeet-growing regions of the U. S (Duffus et al., 1984; Weiland et al., 2019; Wisler et al., 1997). BNYVV is transmitted by *Polymyxa betae*, a plasmodiophoromycete vector that can survive long periods in the soil under favorable conditions (Fujisawa and Sugimoto, 1977). The same *P. betae* vector also transmits three other soil-borne viruses *Beet soil-borne mosaic virus* (genus *Benyvirus*), Beet soil-borne virus (genus *Pomovirus*), and *Beet virus Q* (genus *Pomovirus*) in sugarbeet (Meunier et al., 2003). Curly top is another yield-limiting viral disease of sugarbeet. The disease is caused by ssDNA *Beet curly top virus* (genus *Curtovirus*). Beet curly top virus (BCTV) is transmitted by the beet leafhopper, *Circulifer tenellus*, and there are 11 strains of BCTV reported that cause curly top disease in sugarbeet (Strausbaugh et al., 2017; Teng et al., 2010). Virus yellows is caused by a complex of viruses including *Beet mild yellowing virus* (genus *Polerovirus*), *Beet chlorosis virus* (genus *Polerovirus*), and *Beet yellows virus* (genus *Closterovirus*). Beet mild yellowing virus (BMYV) and Beet chlorosis virus (BChV) are typically transmitted by the green peach aphid *Myzus persicae* (100%), and also by *Macrosiphum euphorbiae* (83 - 98%) (Hossain et al., 2021; Kozłowska-Makulska et al., 2009). BYV has been reported to be transmitted by more than 20 aphid species, with *Myzus persicae* and *Aphis fabae* emerging as the primary natural carriers (German-Retana et al., 1999). *Beet mosaic virus* (BtMV) is an aphid-transmissible potyvirus causing mosaic symptoms on leaves and can exacerbate virus yellows disease when co-infecting sugarbeet with that complex (Wintermantel, 2005).

The advent of next-generation high-throughput sequencing (HTS) technologies has offered the opportunity to discover an unprecedented number of viruses that have advanced our knowledge of virus diversity in many agricultural crop plants. Prior to the HTS era, etiological investigations of economically important virus-like diseases led to the discovery of new viruses in crops. One approach to HTS-enabled virus discovery exploits RNA-silencing, which is an anti-viral defense mechanism that operates in plants to combat viruses. Viruses can activate the plant RNA silencing defense system and become targets of virus-derived small RNAs (vsiRNAs), a hallmark of the RNA silencing phenomenon (Kwon et al., 2020; Vanitharani et al., 2005; Saumet and Lecellier, 2006). In the past, HTS of vsiRNAs enabled the identification of new viruses; however, virus assembly was tedious due to the short-read size of small RNA. With the advancement of HTS technology, RNA-Seq with an increased read length is being widely used to capture the 'virome' in a wide range of environmental and biological samples (Kamitani et al., 2019; Lai et al., 2022). In this way, researchers can understand at greater depth the virus spectrum in plants, which in turn facilitates new ways to study mixed infections and understand the possible synergistic or antagonistic interactions that might lead to disease.

The study of viromes has gained increasing attention in virus research, and it has been documented in various crops and fruits (Jo et al., 2017, 2018, 2020a, b; Pecman et al., 2017). RNA-Seq of rhizomania-infected sugarbeet roots led to the isolation of a U. S. strain of BNYVV, a novel *B. vulgaris* alphanecrovirus (BvANV-1) and a putative *B. vulgaris* satellite virus (BvSatV) in addition to the known soil-borne viruses BSBMV, BSBV, beet black scorch virus (BBSV), and BVQ (Weiland et al., 2020). Recently, using meta-transcriptomic sequencing of sugarbeet with stunted growth, Ramachandran and co-workers identified the presence of *Tomato bushy stunt virus* that

belongs to the genus *Tombusvirus*, and BNYVV (Ramachandran et al., 2023a). Further, a study on table beet with hairy roots and shorter petiole symptoms revealed the occurrence of the *Pepper yellow dwarf* strain of BCTV and *Spinach curly top Arizona virus* (Ramachandran et al., 2023b). Despite these investigations, the thorough examination of viromes related to sugarbeet roots and leaves is limited.

In this study, we explored the natural diversity of viruses in 18 field-grown sugarbeet samples collected from five U.S. states that were symptomatic for rhizomania, root diseases, or other virus-like foliar diseases that resembled curly top and virus yellows by subjecting them to HTS. The analysis of HTS data revealed the occurrence and distribution of known sugarbeet-infecting soil-borne and foliar viruses such as BNYVV, BSBMV, BSBV, and BCTV. Interestingly, the newly reported BvSatV from Minnesota (Weiland et al., 2020) was found nearly nationwide and was identified in Colorado, Idaho, and North Dakota, indicating a larger distribution within the U.S. The number of co-infections and differences in virus titers revealed through RNA-Seq was further confirmed using RT-PCR analysis and Sanger sequencing, adding a measurable component to our analysis. Our HTS analysis resulted in the identification of a virus related to a fungus-infecting virus, *Erysiphe necator*-associated abispo virus (En_abispoV), for the first time in sugarbeet. Furthermore, this virus was detected in multiple sugarbeet growing locations within the U. S. The nearly full-length genome sequences of RNA1 and RNA2 of the En_abispoV were determined using primer walking, RT-PCR, and sequence confirmation by Sanger sequencing which validated the HTS results. The identification of this mycovirus-related virus in sugarbeet in multiple locations suggests an association of a fungal host with sugarbeet across the nation.

2 Materials and methods

2.1 Sample collection

Field-grown sugarbeet roots samples with rhizomania symptoms and leaf samples with varying virus disease-like symptoms of leaf-curling, yellowing to browning, or green mosaic were collected from the production fields of five different states in the U. S. (California, Colorado, Idaho, Minnesota, and North Dakota). Sample details as described in Table 1. Each beet sample represents a pool of hairy roots obtained from four to eight beets with rhizomania symptoms. Each leaf sample represents portions of leaves obtained from four to eight sugarbeet plants exhibiting leaf symptoms resembling virus diseases. The samples from Minnesota and North Dakota were obtained in coordination with the agriculturalists of the American Crystal Sugar Company (Moorhead, MN), Minn-Dak Farmers' Cooperative (Wahpeton, ND), and Southern Minnesota Beet Sugar Cooperative (Renville, MN). The agriculturalists of Amalgamated Sugar Company (Boise, Idaho) and Spreckels Sugar Company (Brawley, CA) provided the samples from Idaho and the Imperial Valley of California, respectively, and leaf samples were collected from Colorado.

2.2 High-throughput sequencing and data analysis

Total RNA was extracted from the hairy-root tissue of beet samples or from the symptomatic leaf samples obtained from the harvested sugarbeet plants using the RNeasy plant mini kit (Qiagen, USA) according to the manufacturer's instructions. For RNA-Seq, 18 libraries were constructed using the Illumina Ribo-Zero Plus rRNA Depletion Kit (Illumina, CA) and sequenced on the Illumina NovaSeq 6000 platform at Novogene Corporation Inc (Sacramento, California). Paired-end reads of each sample were collected from Novogene Corporation Inc. Adapter sequences were trimmed, and low-quality reads (Q<30) were filtered using Trimmamotic v0.39 (Bolger et al., 2014). Quality filtering eliminated 1.12% to 14.64% of raw reads, and approximately 75.2% to 98.35% of clean reads (Table 1) were mapped against RefBeet-1.2.2 (GCA_00511025.2), a reference sugarbeet genome retrieved from GenBank, for host genome mapping using Bowtie2 v2.5.1. Samtools v1.17 was used to produce mapping statistics. Bamtools v2.5.2 was used to convert BAM files into FASTQ files. The remaining unmapped reads from RefBeet-mapping were *de novo* assembled to generate contigs using SPAdes genome assembler v3.15.5 (Bankevich et al., 2012). Assembled contigs were subjected to BLASTn search with an E-value cutoff of set to 1e-10 using blast+ v2.13.0. Geneious Prime 2023.1.1 was used to construct complete genome fragments of beet viruses using contigs larger than 150 nts in size generated from *de novo* assembly. The genome coverage percentage was obtained after mapping the reads to each of the RNA components of individual viruses (Figure 1) using the Burrows-Wheeler transform algorithm (Li and Durbin, 2009). The raw sequencing data for each sample were deposited in the National Centre for Biotechnology Information (NCBI)-Sequence Read Archive (SRA) database with accession numbers under the BioProject number PRJNA1107161.

2.3 RT-PCR analysis and validation of HTS results

To validate the obtained HTS results, RT-PCR was performed using a one-step RT-PCR kit (Qiagen, MA, USA) for individual samples to confirm the presence of sugarbeet infecting viruses using primers to amplify target regions on the various genomic RNA components for each virus. The primer details used for the amplification of each virus are given in Supplementary Table 1 with primer numbers as follows: BNYVV, 1 to 8; BSBV, 9-14; BSBMV, 15-22; BvSatV, 23 to 24; BvANV-1, 25 to 26; and En_abispoV, RNA1 (27 to 28) and RNA2 (39 to 40). The RT-PCR mix contained 4 µl of 5x one-step RT-PCR buffer, 1 µl of 10

10.3389/fpls.2024.1429402

TABLE 1 Sample details are given with corresponding RNA sequencing read counts, reads mapped with sugarbeet genome and the number of known and new viruses identified in each sample.

Sample ID	Plant material	Location	Symptoms	Raw reads	Cleaned reads	RefBeet mapped reads	Major viral hits (known)	New virus (This study)
LS-1	Sugarbeet leaf	Minnesota	Leaf curling	90845002	82438928	73554506	No hit	En_abispoV
LS-2	Sugarbeet leaf	Minnesota	Leaf curling	78246166	68054502	63837831	BNYVV, BSBMV, BSBV, BvSatV	En_abispoV
LS-3	Sugarbeet leaf	Minnesota	Leaf browning	52053897	50416306	47541014	No hit	En_abispoV
LS-4	Sugar beet leaf	Minnesota	Pale yellow leaf	74067691	71694196	70513376	BvSatV	En_abispoV
LS-5	Sugar beet leaf	Colorado	Virus yellows like	55453681	53058786	49119145	BNYVV, BSBV, BvSatV	None
LS-6	Sugar beet leaf	Colorado	Virus yellows like	61434972	57460862	50003927	BNYVV, BSBV, BvSatV	En_abispoV
LS-7	Sugar beet leaf	Colorado	Virus yellows like	57982821	54835076	52751266	BNYVV	En_abispoV
LS-8	Sugar beet leaf	Colorado	Virus yellows like	92781163	89363196	78220865	BNYVV	En_abispoV
LS-9	Sugar beet leaf	Minnesota	Green mosaic	61067543	57557070	57079361	BvSatV	None
BS-1	Sugar beet root	California	Rhizomania-like	77286055	76421130	66304588	BNYVV	None
BS-2	Sugar beet root	Minnesota	Rhizomania-like	95343104	91104798	87562039	BNYVV, BSBMV, BSBV, BvSatV	En_abispoV
BS-3	Sugar beet root	Minnesota	Rhizomania-like	96269692	87728010	83004296	BNYVV, BSBMV, BvSatV, BvANV-1	En_abispoV
BS-4	Sugar beet root	Minnesota	Rhizomania-like	131704187	113079702	108888832	BNYVV, BSBMV, BSBV, BvSatV	En_abispoV
BS-5	Sugar beet root	Minnesota	Rhizomania-like	111323704	98611082	74156692	BNYVV, BSBMV, BSBV, BvSatV	En_abispoV
BS-6	Sugar beet root	Minnesota	Rhizomania-like	71429229	60972252	53756433	BNYVV, BSBMV, BSBV, BvSatV	En_abispoV
BS-7	Sugar beet root	North Dakota	Rhizomania-like	99144096	84626106	72707202	BNYVV, BSBMV, BSBV, BvSatV	En_abispoV
BS-8	Sugar beet root	Minnesota	Rhizomania-like	77043522	67745390	64567582	BNYVV, BvSatV	En_abispoV
BS-9	Sugar beet root	Idaho	Rhizomania-like	74691654	65889374	59504029	BNYVV, BSBV, BvSatV, BCTV	None

mM dNTP mix, 1 µl of 10 mM each forward and reverse primers, 20 U of RNase inhibitor (Invitrogen, USA), 1 µl of one-step RT-PCR enzyme mix, and 100 ng of total RNA and adjusted with nuclease-free water to a final volume of 20 µl. The PCR conditions differed in annealing temperature with a range between 52-58°C for each virus fragment based on the Tm values of the primer pairs. PCR conditions were as follows: 50°C for 60 mins, 95°C for 15 mins, followed by 35 cycles of 95°C for 40 sec, 52-58°C for 40 sec, and 72°C for 45 sec, and then final primer extension at 72°C for 15 mins. All PCR amplicons were gel purified using a QIAquick Gel Extraction kit (Qiagen, MA, USA) and Sanger sequenced from both ends (Eurofins Genomics, KY, USA). A BLASTn search on NCBI was used to confirm the presence of viruses using sequencing results.

2.4 Genome characterization of *Erysiphe necator*-associated abispo virus

In addition to the contigs extracted from *de novo* assembly, primer walking strategies were followed using RT-PCR to amplify the complete genome of En_abispoV. Four samples BS-2, LS-1, LS-2 (Minnesota), and LS-6 (Colorado) were selected to obtain the

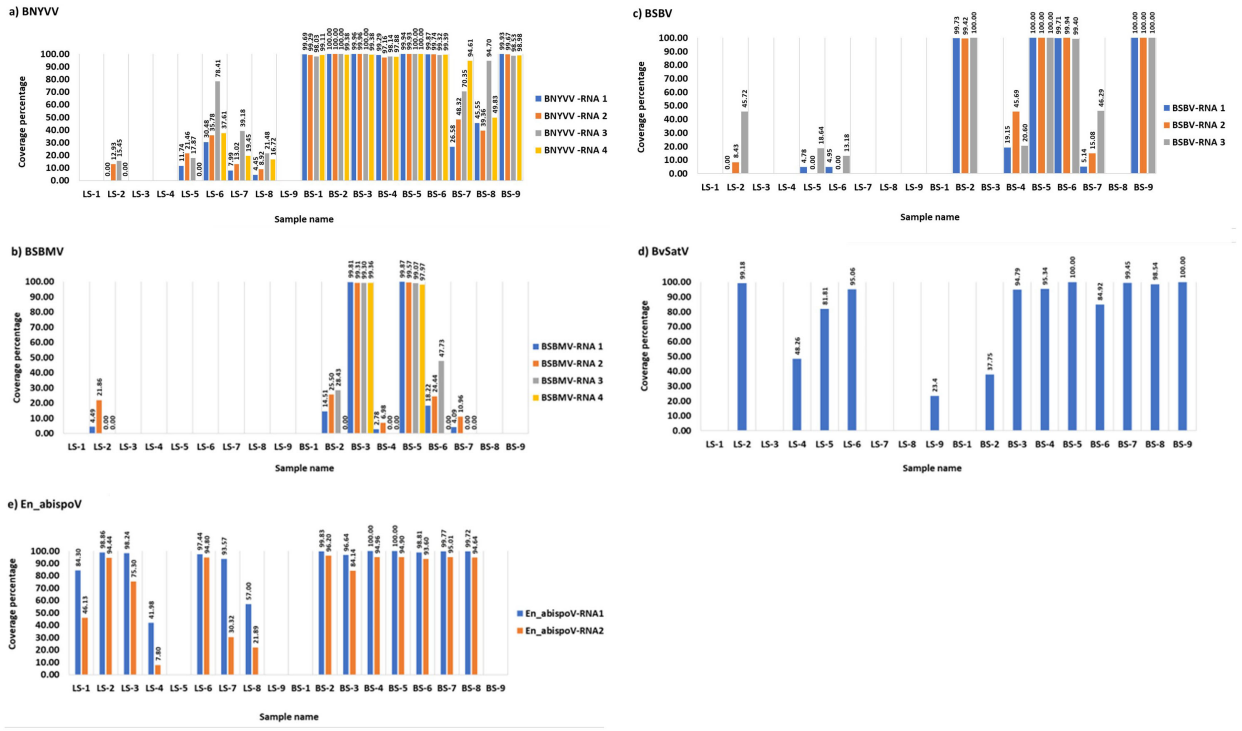

FIGURE 1
The coverage percentage in the bar diagram represents the total length of RNA segments obtained from bowtie2 mapping for major known and newly identified viruses. Seven root libraries for BNYVV **(A)**, two for BSBMV **(B)**, four for BSBV **(C)**, eight for BvSatV **(D)**, and eight for En_abispoV **(E)** were found with more than 90% genome coverage in their RNA segments. Reads mapped to BCTV in beet sample BS-9 (Idaho) covered 37.04% of the genome and beet sample BS-3 (Minnesota) was found to have 62.02% coverage for BvANV-1.

complete genome sequences. Six primer pairs targeting contiguous overlapping genome fragments of RNA1 (Primer numbers 27 to 38; Supplementary Table 1) and five primer pairs for RNA2 (Primer numbers 39 to 48; Supplementary Table 1) were designed using a Multiple Primer Analyzer (ThermoFisher Scientific, USA) based on closely matched reference genome sequences (MN611695.1 and MN611694.1) retrieved from BLASTn analysis. A one-step RT-PCR assay (Qiagen, MA, USA) was performed in Pro-Flex PCR systems (Applied Biosystems, USA). The PCR mix contained 4 µl of 5x one-step RT-PCR buffer, 1 µl of 10 mM dNTP mix, 1 µl of 10 mM forward and reverse primers, 20 U of RNase inhibitor (Invitrogen, USA), 1 µl of one-step RT-PCR enzyme mix, and nuclease-free water to a final volume of 20 µl. The PCR conditions were as follows; 50°C for 60 mins, 95°C for 15 mins, followed by 35 cycles of 95°C for 40 sec, 52-56°C for 40 sec, and 72°C for 45 sec, and then final primer extension at 72°C for 10 mins. All PCR amplicons were gel purified using a QIAquick Gel Extraction kit (Qiagen, MA, USA) and the sequence was confirmed using Sanger sequencing from both directions (Eurofins Genomics, KY, USA). Geneious Prime 2023.1.1 was used to assemble the full genome sequences of RNA1 and RNA2 obtained through the Sanger sequencing.

ORF finder from the NCBI was used to find the candidate open reading frames in the two RNA sequences. The Conserved Domain Database (CDD)-NCBI, Pfam 35.0, and InterPro 91.0 at the European Molecular Biology Laboratory- European Bioinformatics Institute (EMBL-EBI) were used to confirm the conserved domain of protein sequences. The genome annotation transfer utility (GATU) (Tcherepanov et al., 2006) was used to annotate the RNA1 and RNA2 of newly identified virus isolates in this study with *Erysiphe necator*-associated abispo virus 8 isolate PMS7_214 segment RNA1, complete sequence (MN611695.1) and *Erysiphe necator*-associated abispo virus 7 isolate PMS5_242 segment RNA2, complete sequence (MN611694.1) as reference sequences, respectively.

2.5 Phylogenetic analysis

Phylogenetic analysis was performed for BvSatV and En_abispoV. For BvSatV, RNA sequences from five beet samples from Minnesota (BS-3, BS-4, BS-5, BS-6, and BS-8), one beet sample each from North Dakota (BS-7) and Idaho (BS-9), and two leaf samples from Colorado (LS-5 and LS-6), and one leaf sample from Minnesota (LS-2) were used. For the newly identified En_abispoV, RNA1 and RNA2 sequences from six beet samples from Minnesota (BS-2, BS-3, BS-4, BS-5, BS-6, and BS-8), one beet sample from North Dakota (BS-7), three leaf samples from Minnesota (LS-1, LS-2, and LS-3), and two leaf samples from Colorado (LS-6 and LS-7) were used in phylogenetic analysis. For En_abispoV, virus isolates that matched En_abispoV, including Grapevine-associated RNA virus 4 (GVRV), *Sclerotinia sclerotiorum* virga-like virus 1, and *Agaricus bisporus* virus 16

were used in the analysis. In total, 14 isolates related to En_abispoV covering the entire ORF region from different geographical regions, and all three available BvSatV isolates reported from the U.S. were retrieved from the NCBI GenBank and used in the phylogenetic analysis. Sequence alignment was performed using the ClustalW multiple alignment tool and the sequence identity matrix was obtained using BioEdit Sequence Alignment Editor 7.2.5 software (Hall et al., 2011). All the aligned sequences were trimmed to equal length and used for the phylogenetic tree construction. Maximum-likelihood phylograms were constructed following LG with the Freq.(+F) substitution model and the Nearest-Neighbor-Interchange (NNI) ML Heuristic method with 1000 bootstrap replications using MEGA 11.0.13 software (Tamura et al., 2021).

3 Results

3.1 Identification and geographical expansion of known sugarbeet-infecting viruses

Meta-transcriptomic analysis of total RNA isolated from sugarbeet leaf samples exhibiting virus disease-like symptoms of leaf-curling, yellowing to browning, or green mosaic, and root samples with rhizomania symptoms yielded 52 to 131 million raw reads across the 18 libraries. Among the libraries, the known and historically most commonly occurring sugarbeet-infecting viruses, BNYVV, BSBV, and BSBMV were identified as the major viral hits (Table 1). Overall, the virus-specific contigs were found more in the beet root samples than in the leaf samples. The number of virus-associated contigs ranked higher for BNYVV compared to BSBV and BSBMV (Figure 2). BNYVV-specific contigs were found in 14 out of 18 libraries, and among these nine libraries constructed from root samples had contigs specific to BNYVV RNA1, RNA2, RNA3, and RNA4 (Supplementary Table 2). Although BNYVV was detected in five leaf-derived samples, overall, the number of contigs was low and did not represent all four RNA components of BNYVV except in one sample, LS-6. None of the 14 libraries revealed contigs matching to RNA5 of BNYVV which is consistent with the previously observed absence of RNA5 in the U.S. The highest number of BNYVV-specific contigs was found in BS-2, 13919 from Minnesota, while BS-9 from Idaho had 1875 contigs, and BS-1 from California recorded 147 contigs (Figure 2). The genome coverage of BNYVV on RNA1 through RNA4 was observed to be more than 97% in seven root libraries originating from Minnesota, Idaho, and California (Figure 1). Details of BLAST results of the assembled consensus sequences obtained for major viruses from each library are provided in Supplementary Table 3.

The contigs specific to BSBV were found in nine (six beet root and three leaf) samples. The maximum number of contigs corresponding to BSBV was found in BS-9 (5534) from Idaho, followed by BS-5 (1842) and BS-6 (289) from Minnesota (Figure 2;

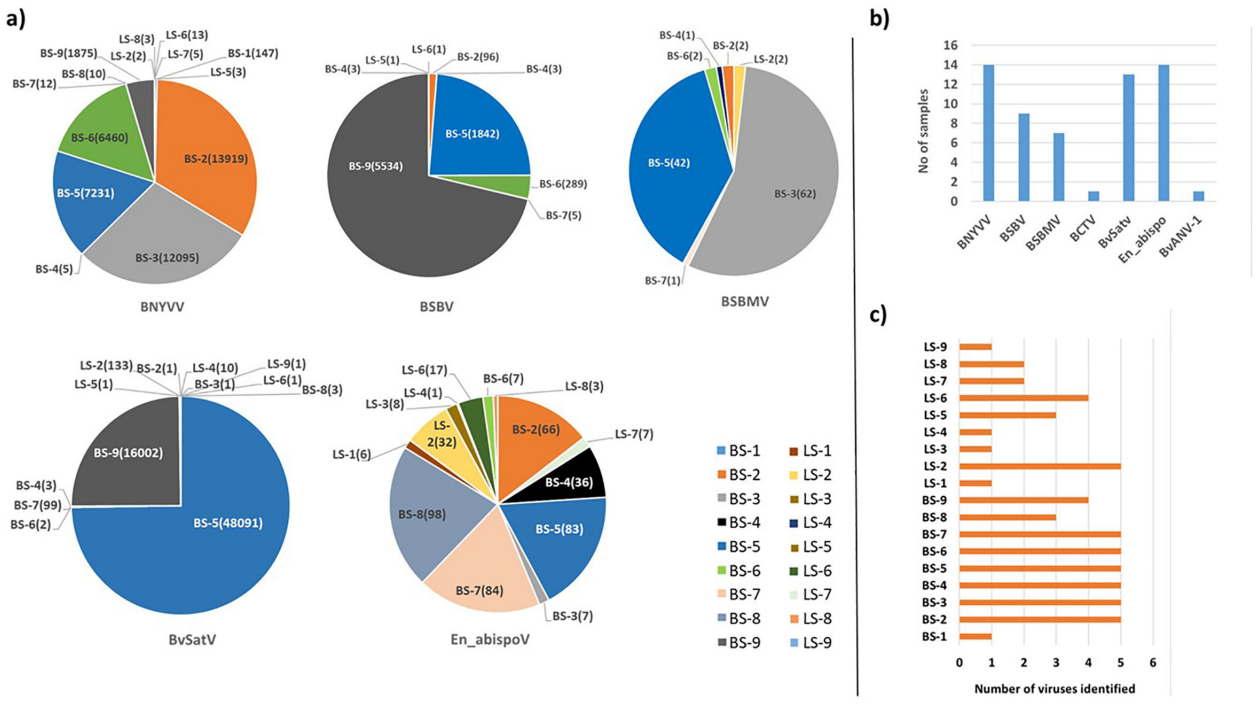

FIGURE 2
(A) The total number of contigs obtained in RNA sequencing for major known and newly detected viruses in root and leaf samples of sugar beet from five different states in the U.S. Contig numbers are given in parentheses (). **(B)** Number of samples found with each virus. **(C)** Number of viruses identified in each sample. In 14 libraries, BNYVV and En_apispoV emerged as prevalent viruses, while in 13 libraries, BvSatV was identified as the second most common. BCTV was identified only in beet sample BS-9 from Idaho with 3 contigs and BvANV-1 was identified in beet sample BS-3 from Minnesota with 4 contigs.

Supplementary Table 2). Mapping of BSBV-specific reads representing all three genomic RNAs in all three libraries resulted in more than 99% genome coverage of the viral segments (Figure 1). In the case of BSBMV, which is only reported in the U. S., contigs representing all four BSBMV RNA segments were identified in two root libraries, BS-3 and BS-5, from Minnesota with genome coverage ranging from 97.97% to 99.87% (Figure 1). A reduced number of contigs representing partial sequences of BSBMV was found in the BS-2, BS-4, BS-6, and BS-7 libraries, and in the leaf-derived one (Supplementary Table 2). Among the major sugarbeet-infecting foliar viruses, BCTV, which is commonly found in the western region of the U.S. was detected in BS-9 from Idaho; however, the coverage was only 37%, representing the partial genome of BCTV.

The recently reported BvSatV from Minnesota (Weiland et al., 2020) was detected in 13 out of 18 libraries. BS-5 from Minnesota was found to possess a large number of contigs, 48091 for this virus, and the second largest was in the library BS-9 from Idaho with 16002 contigs (Figure 2). BvSatV was detected in the leaf sample libraries, LS-5 and LS-6, from Colorado, and LS-2, LS-4, and LS-9 from Minnesota. The BvSatV isoform BvSatV-1B was found only in two libraries, BS-9 from Idaho and LS-2 from Minnesota, and the remaining 11 libraries mainly possessed the isoform BvSatV-1A. Overall, more than 80% genome coverage for BvSatV was found in seven root- and three leaf-libraries (Figure 1). The identification of BvSatV for the first time in Idaho and Colorado shows the presence of the virus in sugarbeet growing areas other than Minnesota. Another recently discovered BvANV-1 (Weiland et al., 2020) was detected only in BS-3 from Minnesota with 62% genome coverage. In addition to these significant known sugarbeet-infecting viruses, contigs representing *Beta vulgaris* mitovirus and beet cryptic virus were observed in many beet root and leaf samples. Additionally, a previously reported *Lettuce chlorosis virus* (Wisler et al., 1997) was detected in library BS-1, a sample originating from California.

Altogether, BNYVV was detected in samples originating from all the locations of California, Colorado, Idaho, Minnesota, and North Dakota, and BSBV was detected in four locations except California, whereas BSBMV presence was found only in the Minnesota and North Dakota areas. Interestingly, BvSatV isoforms (BvSatV-1A and BvSatV-1B), which were recently found in Minnesota, were detected in the samples obtained from Colorado, Idaho, and North Dakota, indicating the expanded occurrence of BvSatV in new sugarbeet growing areas in addition to Minnesota. Comparative analysis revealed less sequence diversity for BNYVV, BSBV, BSBMV, and BvSatV. The corresponding RNA components shared greater than 95% sequence identity with the reference genomes and hence these previously characterized sugarbeet-infecting viruses were not subjected to detailed analysis in this study.

3.2 Identification of a putative mycovirus-related virus naturally occurring in sugarbeet

Other than the known sugarbeet-infecting viruses, a relatively large number of contigs related to the fungus-associated viruses such as *Erysiphe necator*-associated abispo virus, *Erysiphe necator*-associated narnavirus, *Erysiphe necator*-associated ourmia-like virus, and *Plasmopara viticola* lesion-associated ourmia-like virus were detected in both beet root and leaf sample libraries. Among these mycoviruses, contigs related to *Erysiphe necator*-associated abispo virus (designated En_abispoV) were taken into detailed genome characterization and phylogenetic analysis since En_abispoV is an understudied virus and no publications are available on this virus other than GenBank sequence information. The contigs that were closely related to En_abispoV were detected in 14 out of 18 libraries including both leaf and root samples (Figure 2; Supplementary Table 2). BLASTn search analysis identified contigs matching to *Erysiphe necator*-associated abispo virus 8 isolate PMS7_214 segment RNA1, complete sequence (MN611695.1), with 95.4% to 97.18% nucleotide identity, and *Erysiphe necator*-associated abispo virus 7 isolate PMS5_242 segment RNA2, complete sequence (MN611694.1), with 93.2% to 96.87% nucleotide identity. The genome coverage of both En_abispoV RNA1 and RNA2 was greater than 90% in all root samples that were positive for En_abispoV except BS-3, which showed 84% coverage for RNA2, and all these root samples originated from Minnesota and North Dakota (Figure 1). The contigs corresponding to En_abispoV were undetectable in samples BS-1 and BS-9 which represented California and Idaho, respectively. The contigs matching En_abispoV RNA1 and RNA2 were identified in seven out of nine leaf samples that originated from the Minnesota and Colorado regions; however, the overall degree of genome coverage was variable (Figure 1). Unlike the major known sugarbeet-infecting viruses, the En_abispoV RNA1 and RNA2 specific contigs were detected both in the leaf and root samples of sugarbeet plants. Further, this study revealed the existence of En_abispoV RNA1 and RNA2 in Minnesota, North Dakota, and Colorado. It is worth noting that contigs representing En_abispoV RNA1 and RNA2 were not detected in the samples obtained from California and Idaho (Table 1).

Among the identified viruses, the well-known BNYVV, and the newly identified, En_abispoV were widespread as they were represented in 14 of the 18 libraries. BvSatV represents the second most prevalent viral pathogen detected (13 libraries) followed by BSBV (detected in nine libraries), and BSBMV being found in seven libraries (Figure 2). Overall, these results indicate the existence of multiple viruses in field samples and were more prevalent in the roots compared to the leaves of sugarbeet plants (Figure 2).

3.3 Validation of HTS-identified viruses using RT-PCR

To validate the meta-transcriptomic results, RT-PCR analysis was carried out to confirm the presence of three common infecting viruses, BNYVV, BSBMV, and BSBV; the two recently discovered BvSatV isoforms and BvANV-1; and the newly identified En_abispoV (Figure 3). Using RT-PCR, the target genome fragments were amplified for BNYVV RNA1 to RNA4 in all nine root samples, BS-1 through BS-9, as described in Table 1. Although contigs representing BNYVV were detectable in leaf samples, amplification of the genome using RT-PCR was difficult due to low coverage. For example, in sample LS-6, RT-PCR amplified RNA2, 3, and 4, but was unable to amplify RNA1.

For BSBMV, target genome fragments were amplified for RNA1 to RNA4 in two root samples from Minnesota, and for the BSBV target regions were amplified for RNA1-RNA3 in four root samples, of which three samples were from Minnesota and one from Idaho (Figure 3). BvSatV was amplified in seven root (BS-3 to BS-9) and four leaf samples (LS-2, LS-4 to LS-6) (Table 1). RT-PCR failed to amplify BvSatV in BS-2 due to low coverage. BvANV-1 was detected only in BS-3 from Minnesota, and in that sample, the target fragment of BvANV-1 was amplified (Figure 3). Due to low coverage, BCTV was not subjected to PCR-based confirmation in sample BS-9. En_abispoV RNA1 and RNA2 were successfully amplified from seven root samples, BS-2 to BS-8, and in seven leaf samples, LS-1 to 4 and LS-6 to 8, except for LS-1 and LS-4 from Minnesota and LS-8 from Colorado where mild amplification was encountered for RNA2 (Figure 3).

The RT-PCR products were confirmed by Sanger sequencing and BLASTn analysis of the obtained sequences revealed the presence of the corresponding viral target sequences (Supplementary Table 4). The nucleotide sequence identity for BNYVV was obtained as follows: BNYVV-RNA1 (99.56-99.85%), BNYVV-RNA2 (99.35-99.67%), BNYVV-RNA3 (99.36-100%), and BNYVV-RNA4 (99.81-100%). For BSBMV, the sequence identities are as follows: BSBMV-

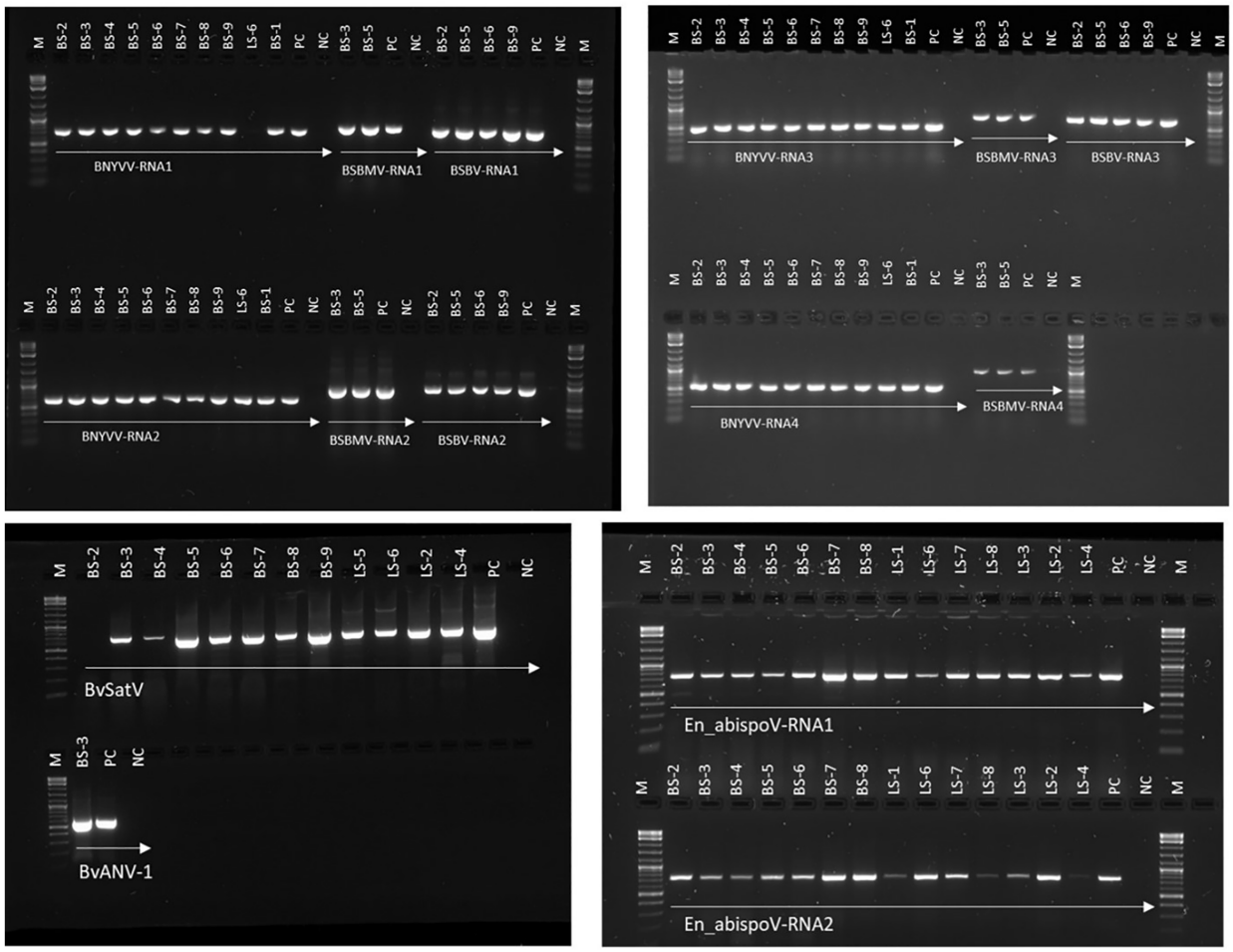

FIGURE 3
RT-PCR-based validation for major sugar beet infecting viruses identified in RNA sequencing from sugar beet samples. Target genome sizes: BNYVV-RNA1, 729 bp; BNYVV-RNA2, 628 bp; BNYVV-RNA3, 504 bp; BNYVV-RNA4, 567 bp; BSBMV-RNA1, 828 bp; BSBMV-RNA2, 912 bp; BSBMV-RNA3, 738 bp; BSBMV-RNA4, 962 bp; BSBV-RNA1,772 bp; BSBV-RNA2,922 bp; BSBV-RNA3,704 bp; BvSatV, 706 bp; BvANV-1,644 bp; En_abispoV-RNA1,773 bp; and En_abispoV-RNA2, 766 bp. M, 1kb plus DNA ladder; PC, positive control; NC, negative control. BNYVV-RNA1 in LS-6 and BvSatV in BS-2 failed to amplify in the RT-PCR reaction and a low coverage might be the reason behind the failure of amplification.

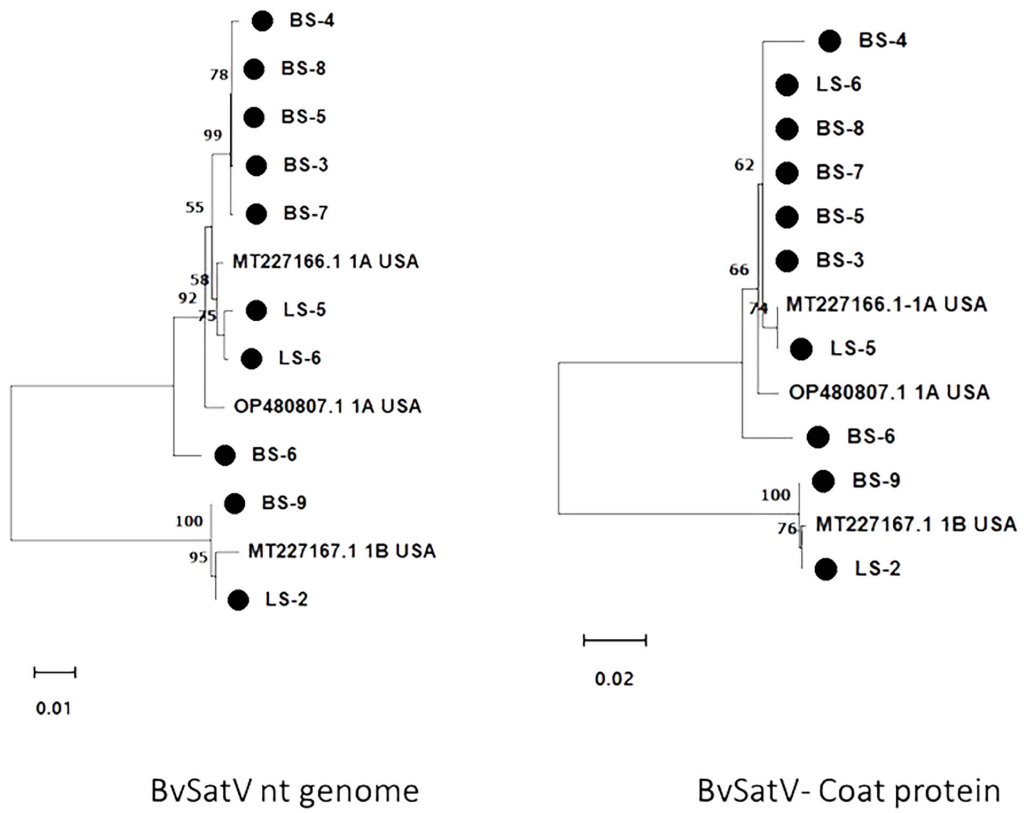

FIGURE 4
Maximum likelihood phylogram constructed with 1000 bootstrap replications for BvSatV nt genome and the deduced amino acid (aa) sequence of coat protein with previously reported isolates. Nucleotide sequences were trimmed to equal lengths of 911 nt, and complete amino acid (215 aa) sequences of coat protein were used. Two clusters were formed in phylogram with two isoforms of BvSatV where one cluster represented isolates closely matching with BvSatV-1A isoform and the other cluster represented isolates matching with BvSatV-1B isolate. • Marks denote isolates from this study.

RNA1 (99.36-99.47%), BSBMV-RNA2 (98.87-99.09%), BSBMV-RNA3 (98.13-99.54%), and BSBMV-RNA4 (98.93-99.54%). Sequence identity for BSBV: BSBV-RNA1 (99.03-99.72%), BSBV-RNA2 (99.21-99.34%), and BSBV-RNA3 (98.78-99.84%). In the case of BvSatV, BLASTn search identified two isoforms, BvSatV-1A and BvSatV-1B, among the samples. A primer sequence conserved between the two variants of BvSatV was used to amplify both the isoforms of BvSatV. Sequencing of the RT-PCR amplicons obtained for BvSatV revealed that the BS-9 root sample from Idaho and the leaf sample LS-2 from Minnesota were found to match with BvSatV-1B with 98.06%-98.21% identity. The rest of the samples that were positive for BvSatV matched to BvSatV-1A with 98.62%-98.79% identity (Figures 3, 4).

3.4 Genome characterization of *Erysiphe necator*-associated abispo virus

In addition to RNASeq-aided extraction of the complete genome sequence of En_abispoV in 14 libraries, we used contiguous overlapping regions of RNA1 and RNA2 to validate the HTS results. Using RT-PCR and primer walking strategies, the near-complete sequences of En_abispoV RNA1 and RNA2 were obtained in one of the root samples (BS-2) and two leaf samples (LS-1 and LS-2) originating from Minnesota, and a leaf sample from Colorado (LS-6) (Figure 5). All the specific sizes of PCR amplicons were gel-purified and sequenced. Among the four samples, LS-1 showed very mild amplification for a few fragments of RNA1 and RNA2 where RT-PCR amplicons were used as templates to reamplify the regions. BLASTn analysis with overlapping sequences of RNA1 showed 94.12% to 97.01% identity with *Erysiphe necator*-associated abispo virus-8 (MN611695.1), and RNA 2 sequences showed 94.36% to 95.36% identity with *Erysiphe necator*-associated abispo virus-7 isolate (MN611694.1). The nearly complete genomes of RNA1 and RNA2 were constructed using the overlapping sequences obtained through RT-PCR and Sanger sequencing and the reconstructed sequences matched to the corresponding reference sequences. The near-complete genome of RNA1 and RNA2, compared in all four samples, showed a range of 1691 to 1704 nts for RNA1 and 1790 to 1799 nts for RNA2.

These RNA1 and RNA2 genome sequences that were obtained from all four samples harbored the full-length open-reading frame (ORF). The ORF finder from the NCBI showed a single open reading frame in RNA1 and RNA2 for all four samples that was 1653 bp and 1731 bp in size, respectively. CDD-NCBI, Pfam 35.0,

10.3389/fpls.2024.1429402

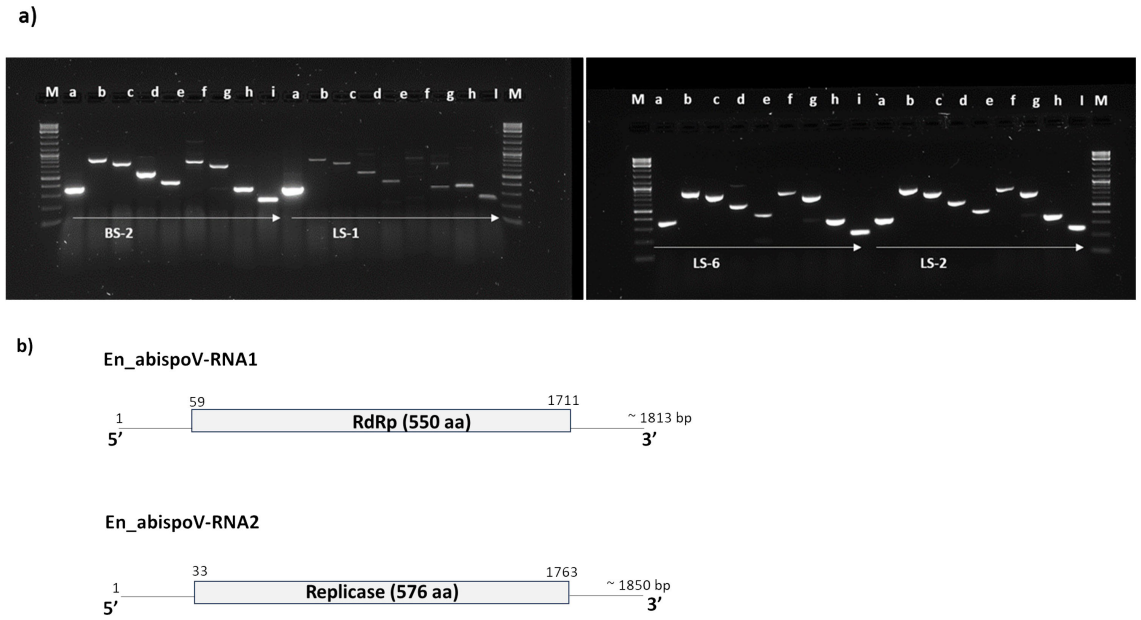

FIGURE 5
(A) Overlapping genome fragments of En_abispoV RNA1 and RNA2 were amplified in RT-PCR following primer walking strategies. Lane: M, 1 kb plus DNA ladder; a through e, overlapping genome fragments of RNA1 (a, 364 bp; b, 863 bp; c, 769 bp; D, 575 bp; and e, 439 bp); f through i, overlapping genome fragments of RNA2 (f, 819 bp,;g, 712 bp; h, 369bp; and i, 258 bp). Primer details are given in Supplementary Table 1. In LS-1, the target genome fragments e and f showed mild amplification and these amplicons were subjected to reamplification in RT-PCR reactions and the target regions obtained. **(B)** Graphical representation of the genome organization of En_abispoV and the RNA1 and RNA2 components. The numbers on the genome indicate the nucleotide positions of the genome and the deduced ORFs are indicated in open boxes with annotation.

and InterPro 91.0 from the EMBL-EBI identified a conserved domain in the ORF of RNA1, which was 550 amino acid residues in size and belonged to the ps-ssRNAv-RdRp-like superfamily (cl40470). The ORF in RNA2 had 576 amino acid residues and contained a Vmethyltransf superfamily (cl03298) conserved domain. RNA1 and RNA2 of all four samples were annotated using GATU and submitted to GenBank and accession numbers were obtained (PP747086 - PP747093).

3.5 Full genome assembly of viruses and phylogenetic analysis of BvSatV and En_abispoV

The complete and nearly complete genome sequences of the major sugarbeet-infecting viruses BNYVV, BSBMV, and BSBV were obtained from the HTS results. BNYVV was the most widespread and its genome sequence was extracted in seven root libraries wherein the assembled genome for RNA1 ranged from 6749 to 6698 nt, for RNA2 from 4576 to 4620 nt, for RNA3 from 1740 to 1780 nt, and for RNA4 from 1437 to 1543 nt. The BNYVV isolates obtained in this study showed 98.62% – 99.98% nucleotide sequence identities in RNA1 through RNA4 to the previously reported BNYVV U.S. isolate. The *de novo* assembled BSBMV genome sequences from two root libraries revealed the complete sequence of RNA1 (6656 to 6668 nt), RNA2 (4583 to 4594 nt), RNA3 (1697 to 1713 nt), and RNA4 (1702 to 1769 nt). Comparison of the BSBMV RNA sequences revealed 98.23%-99.88% identities to the U.S. isolate of BSBMV. The near-complete sequences of BSBV genome RNA1 (5818 to 5834 nt), RNA2 (3427 to 3453 nt), and RNA3 (3002 to 3006 nt) were obtained in four root libraries. Sequence comparison at the nucleotide level revealed 98.23%-99.88% similarities to the previously reported BSBV. GenBank accession numbers are provided for each of the viruses used in the analysis (Supplementary Table 4).

The genome sequence of BvSatV was assembled in seven roots and three leaf libraries using HTS data that ranged from 1118 to 1210 nt, and were submitted to GenBank, and accession numbers were obtained (PP739046 - PP739055). Phylogenetic analysis showed two clusters, each specific to isoform BvSatV-1A and BvSatV-1B, respectively. Among the two isoforms, BvSatV-1A was widespread and detected in eight libraries, and BvSatV-1B was found only in two libraries (LS-2 and BS-9). BvSatV-1A identified in this study revealed 97.58% – 99.28% nt identity with the previously reported BvSatV-1A strain MT227166.1, while the BvSatV-1B is closely related to the 1B isolate MT227167.1 with 99.32% - 99.45% nt identities. Overall, the isolates from the BvSatV-1A cluster shared 89.6% to 90.66% identity at genome sequence level; however, it shared slightly less homology at the amino acid sequence in the coat protein coding region with 84.18% to 85.58% to the isolates of BvSatV-1B cluster (Supplementary Table 5; Figure 4).

Using HTS data, the En_abispoV genome sequence was assembled in 12 libraries. The size of RNA1 ranged from 1796 to 1813 nts, and the RNA2 range from 1572 to 1850 nts. The obtained sequences were submitted to GenBank, and obtained accession

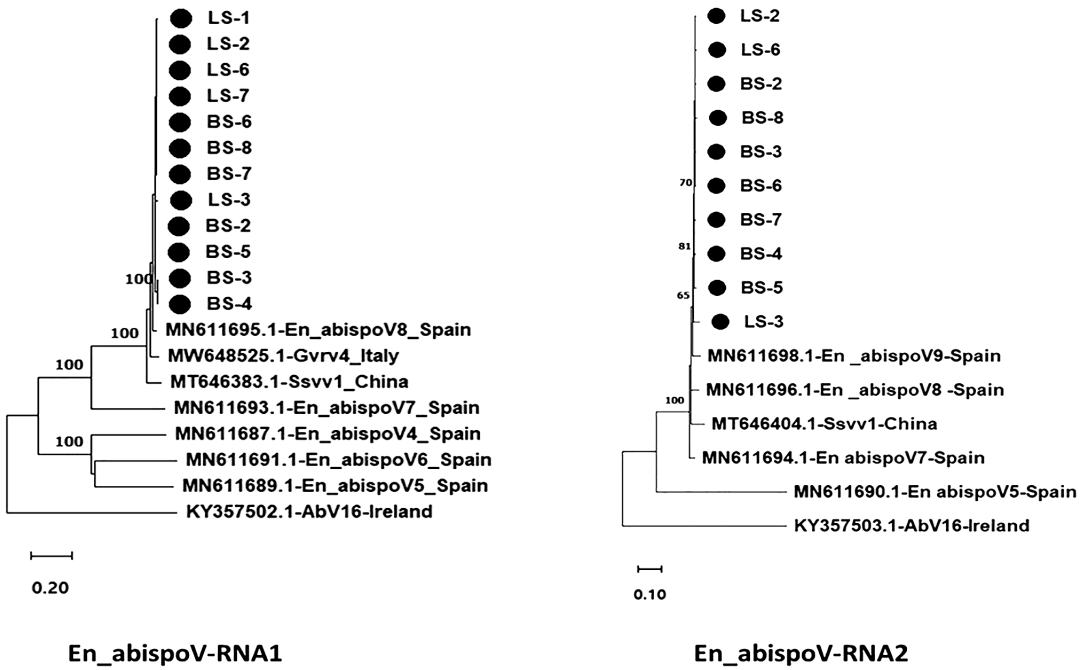

FIGURE 6
Maximum likelihood phylogram constructed with 1000 bootstrap replications for En_abispoV RNA1 and RNA 2 sequences with closely matched isolates obtained from GenBank. Nucleotide sequences are trimmed to equal lengths such as En_abispoV RNA1 with 1773 nt, and En_abispoV RNA2 with 1855 nt sequences. RNA1 isolates from sugar beet showed a close relationship with *Erysiphe necator-associated* abispo virus 8 isolate PMS7_214 (MN611695.1) from Spain followed by Grapevine-associated RNA virus 4 RNA-dependent RNA polymerase gene (MW648525.1) from Italy. In the case of RNA2, *Erysiphe necator*-associated abispo virus 8 isolate PMS7_153 (MN611696.1), *Erysiphe necator* associated abispo virus 9 isolate PMS8_99 (MN611698.1) and *Erysiphe necator* associated abispo virus 7 isolate PMS5_242 (MN611694.1) from Spain shared a close relationship with the sugar beet isolates. *Agaricus bisporus* virus-16 isolate AbV16-003 from Ireland shared a distant relationship with both the RNA1 and RNA2 sequences compared to all other isolates with less than 50% nt identities. • Marks denote isolates from this study.

numbers (PP739024 - PP739045). Phylogenetic analysis of the En_abispoV isolates identified in this study showed 43.80 -97.18% nt identities with the RNA1 of other related isolates that are used in the phylogenetic analysis. However, the RNA2 appears highly diverse sharing 32.60 - 94.58% identities with other related isolates (Figure 6). Among them, *Erysiphe necator*-associated abispo virus 8 isolate PMS7_214 (MN611695.1) from Spain showed 95.59% to 97.18% identities at the nt level with RNA1 sequences of this study. Further, the amino acid sequences of RdRp in RNA1 shared 98.54% to 99.68% similarities with the same isolate. In the case of RNA2, *Erysiphe necator*-associated abispo virus 7 isolate PMS5_242 (MN611694.1), *Erysiphe necator*-associated abispo virus 9 isolate PMS8_99 (MN611698.1), and *Erysiphe necator*-associated abispo virus 8 isolate PMS7_153 (MN611696.1) from Spain shared a close relationship with 91.86% to 94.58% nt identities and 98.84% to 99.82% similarities at the amino acids of replicase in RNA 2 (Figure 6; Supplementary Table 5). It is important to note that the RdRp in En_abispoV-RNA1 and the replicase in En_abispoV-RNA2 shared less than 35% aa similarity among the isolates identified in this study. *Sclerotinia sclerotiorum* virga-like virus 1 RNA1 (MT646383.1) and RNA2 (MT646404.1) shared 89.6% to 91.3% nt similarities with En_abispoV RNA1 and 2, respectively. *Agaricus bisporus* virus-16 isolate shared the least similarities with En_abispoV RNA1 and RNA2 with 43.8%-48.1% and 32.6%-45.0% nt identities, respectively (Figure 6).

4 Discussion

Meta-transcriptomic sequencing has dramatically increased our current knowledge of the natural diversity of viruses in several crops (Roossinck et al., 2015). The purpose of this study was to identify naturally inhabiting viruses in the roots and leaves of field-grown sugarbeet plants using a meta-transcriptomic approach. The sugarbeet samples analyzed in the study had hairy root symptoms resembling rhizomania or had leaf samples exhibiting a range of symptoms including leaf curling and yellowing that are reminiscent of virus yellows and curly top, known foliar viral diseases of sugarbeet. RNA-seq analyses revealed the occurrence and distribution of seven major sugarbeet infecting viruses that included BNYVV, BSBV, BSBMV, and BCTV; the recently discovered BvSatV isoforms; BvANV-1; and a new En_abispoV identified in this study.

Among the seven viruses, BNYVV was identified in all nine root libraries irrespective of the origin of the samples. However, the coverage across all four RNAs was low in the samples BS-7 and BS-8, which correlated to the mild rhizomania-like symptoms observed in these beet samples. The other soil-borne viruses that co-exist with

BNYVV, the BSBMV and BSBV, were also identified in samples in this study. BSBMV was detected in six root libraries and one of the leaf libraries, and all these samples originated from Minnesota and North Dakota sugarbeet growing fields. However, BSBMV was not detected in the root or leaf samples that were obtained from California, Colorado, and Idaho. The other soil-borne virus, BSBV, was primarily identified with high coverage in four root libraries, and with low coverage in BS-4, BS-7, and in the three leaf samples, revealing BSBV incidence in Idaho and Colorado, in addition to Minnesota and North Dakota. No sequencing reads representing BSBV were detected in the sample from California in this analysis.

BvSatV is a satellite virus that was first originally discovered from North Dakota and Minnesota sugarbeet production fields (Weiland et al., 2020). In this study, BvSat-1A and BvSat-1B, the two isoforms, were identified in Colorado, and Idaho, the two new locations of the western sugarbeet growing areas in the U.S. in addition to North Dakota and Minnesota. In fact, BvSatV was the second most dominant known virus as it was detected in 13 libraries from root and leaf samples that originated from Minnesota, North Dakota, Colorado, and Idaho, indicating the widespread occurrence of BvSatV in the U.S. Of note, recently, BSBV was found to serve as the helper virus for BvSatV replication (Weiland et al.,2024). Consistent with this, a correlation between the co-existence of BSBV and BvSatV was observed, supporting that BSBV is most likely a helper virus for BvSatV. However, it is also worth noting that in two leaf samples (LS-4 and LS-9), BvSatV was detected without the presence of BSBV; thus, the possible involvement of other viruses to serve as an alternative helper virus can not been excluded. HTS reads mapping to BVQ, and another soil-borne virus, *Beet black scorch virus* (*Betanecrovirus*) were not detected in any of the tested samples. Among the known foliar viruses, BCTV is the causal agent of curly top disease (Strausbaugh et al., 2017), and it was detected only in the sample from Idaho. Further, the viruses BChV, BWYV, and BYV that are associated with yellows disease (Hossain et al., 2021; Kozłowska-Makulska et al., 2009; Wintermantel, 2005) were undetectable in all the tested 18 libraries originating from across the U.S. Phylogenetic analysis revealed an overall low diversity among the BNYVV isolates identified in this study, and that these isolates showed high degree of similarity to the U.S. isolate of BNYVV in all the four RNA components (Weiland et al., 2020). The two isolates of BSBMV, a virus detected only in the U.S (Lee et al., 2001), and the two isolates from this study were randomly clustered with previously reported U. S. isolates. BSBV isolates of this study shared more than 98% homology for RNA1 to RNA3 with the previously reported U. S. (OP380963) and Brazilian (MH106715) isolates.

The newly identified En_abispoV was the most widespread virus sequence, next to BNYVV, detected among the identified viruses, and was represented in 14 samples that originated from Minnesota, Colorado, and North Dakota. Using HTS results, the nearly complete sequences of RNA1 and RNA2 of En_abispoV were assembled, which were confirmed using RT-PCR and Sanger sequencing. En_abispoV appears to be a new, as yet unclassified, virus that remains poorly characterized. The association of the virus with the fungus, *E. necator*, and the available virus-sequence information in GenBank comprise, to date, the sole documentation on this group of viruses. Taxonomically, these En_abispoV isolates are grouped under the "Unclassified Riboviria", where unclassified new or novel virus genomes that encode RNA-dependent RNA Polymerase (RdRp) or the RNA-dependent DNA Polymerase (RdDp) are included. As the name indicates, the genome structure of En_abispoV RNA1 and RNA2 resemble members of a mycovirus category with *E. necator* as the potential host. Several mycovirus-related RNA viruses other than the En_abispoV have been detected in *E. necator* (Pandey et al., 2018). However, a BLASTn search with *de novo* assembled contigs with specific criteria that included being more than 350 bp length, > 80% nucleotide identity, and > 80% coverage resulted in no contigs closely matching with the genomic fragments of fungus *Erysiphe necator* in any of the libraries analyzed in this study. In addition to aligning to En_abispoV, the assembled contigs matched with *Sclerotinia sclerotiorum* virga-like virus 1 (MT646383.1) in BLASTn analysis with 90% to 92% sequence similarities. The necrotrophic fungus *S. sclerotiorum* causes sclerotinia head and stalk rot and is one of the major production constraints of sunflower (*Helianthus annuus* L.) in the U.S. *Erysiphe necator* or its related species that cause powdery mildew, is a common disease of grapevine worldwide (Qiu et al., 2015). It is tempting to speculate that there was an existence of *E. batae*, and that the En_abispoV was associated with *E. batae*. In addition, phylogenetic analysis of En-abispoV RdRp showed 98.9% amino acid similarity with Grapevine-associated RNA virus 4 (MW648525.1) found in *Vitis vinifera* from Italian isolate, En_abispoV isolate 8, which is grouped under 'Unclassified Riboviria'. This study has identified several co-existing viruses including BNYVV, BSBMV, BSBV, BvSatV, and the newly characterized En_abispoV. In mixed infections, viruses can interact synergistically wherein the presence of one virus can enhance the replication and transmission of other viruses (Vanitharani et al., 2004). Consistent with this notion, BSBV was recently identified as the helper virus for BvSatV (Weiland et al., 2024). The identification of En_abispo virus may be due to the application of meta-transcriptomic analysis since mycoviruses often exist asymptomatically in their hosts. Hence, further research will be required to experimentally validate the interactions among co-existing viruses to elucidate the nature and mechanisms of these interactions.

The abispo virus terminology was introduced with a virus that was identified in *Agaricus bisporus*, the *Agaricus bisporus virus 16* (AbV16) with RNA1 containing the RdRP domain and RNA2 encoding a methyltransferase domain associated with brown cap mushroom disease (Deakin et al., 2017). The En_abispoV isolates of sugarbeet are unlikely to be related to AbV16 since these isolates shared less than 50% sequence identity with the RNA1 and RNA2 of the corresponding AbV16 components. Based on our study, we infer that the newly identified En_abispoV might have been transferred to sugarbeet from *E. necator* (syn. *Uncinula necator*) or *S. sclerotiorum*, or perhaps via soil carrying the fungi.

The meta-transcriptomic approach provides the opportunity to understand the occurrence of natural viromes under environmental conditions, which are underestimated when using specific practices for targeted sequencing approaches including culturing of pure cultures for pathogenic organisms (Roossinck et al., 2015). The agricultural practice of crop rotation provides an opportunity to dilute the plant-pathogen interactions, but it also offers new opportunities for novel adaptations. Evidence for the transfer of viruses between plants and fungi has been reported. For example, the acquisition of cucumber mosaic virus (CMV) by the phytopathogenic fungus *Rhizoctonia solani* from an infected plant as well as the ability of fungi to transmit the virus to the uninfected plants was reported (Andika et al., 2017). The replication of tobacco mosaic virus (TMV) was confirmed in phytopathogenic fungus *Colletotrichum falcatum* (Mascia et al., 2014). Similarly, *Magnaporthe oryzae*, the causal agent of the rice blast, was reported with virus infections from different families such as *Victorivirus*, *Partitivirus*, *Chrysovirus*, and *Tombusvirus* (Moriyama et al., 2018).

This study revealed the occurrence and distribution of sugarbeet-infecting viruses in the U.S. through a meta-transcriptomic approach followed by RT-PCR-based validation. Among the known sugarbeet-associated viruses, the geographical expansion of the BvSatV isoforms (BvSat-1A and BvSat-1B) was noticeable. Above all, we provide evidence for the identification of En_abispoV, a new virus naturally occurring in sugarbeet, which is prevalent across the country. In nature, virus adaptation to new hosts is influenced by holistic interactions among the host, insect vector, coexisting viruses, and environmental factors. The widespread occurrence of En-abispoV in sugarbeet needs further investigation to understand the host range and biology of the virus. These results set the baseline for further research to navigate towards understanding the biological significance of this virus for sugarbeet productivity.

Data availability statement

The datasets presented in this study can be found in online repositories. The names of the repository/repositories and accession number(s) can be found in the article/Supplementary Material.

Author contributions

CChi: Methodology, Formal Analysis, Validation, Writing – original draft. NW: Formal Analysis, Writing – review & editing. JW: Methodology, Writing – review & editing. ON: Methodology, Writing – review & editing. JH: Methodology, Writing – review & editing. MWB: Methodology, Writing – review & editing. CChu: Methodology, Writing – review & editing. AC: Methodology, Writing – review & editing. MK: Methodology, Writing – review & editing. MDB: Resources, Writing – review & editing. VR: Conceptualization, Funding acquisition, Investigation, Methodology, Project administration, Supervision, Writing – review & editing.

Funding

The author(s) declare that financial support was received for the research, authorship, and/or publication of this article. This research is supported by USDA–ARS Project 3060-21000-045-000-D and grants from the Sugarbeet Research and Education Board of Minnesota and North Dakota.

Acknowledgments

We thank Eric Rivera Santiago, USDA-ARS, for technical assistance.

Conflict of interest

The authors declare that the research was conducted in the absence of any commercial or financial relationships that could be construed as a potential conflict of interest.

Publisher's note

Author disclaimer

Mention of trade names or commercial products in this publication is solely for the purpose of providing specific information and does not imply recommendation or endorsement by the U.S. Department of Agriculture. USDA is an equal opportunity provider and employer.

Supplementary material

The Supplementary Material for this article can be found online at: https://www.frontiersin.org/articles/10.3389/fpls.2024.1429402/full#supplementary-material

References

Andika, I. B., Wei, S., Cao, C., Salaipeth, L., Kondo, H., and Sun, L. (2017). Phytopathogenic fungus hosts a plant virus: A naturally occurring cross-kingdom viral infection. *Proc. Natl. Acad. Sci.* 114, 12267–12272. doi: 10.1073/pnas.1714916114

Bankevich, A., Nurk, S., Antipov, D., Gurevich, A. A., Dvorkin, M., Kulikov, A. S., et al. (2012). SPAdes: a new genome assembly algorithm and its applications to single-cell sequencing. *J. Comput. Biol.* 19, 455–477. doi: 10.1089/cmb.2012.0021

Biancardi, E., McGrath, J. M., Panella, L. W., Lewellen, R. T., and Stevanato, P. (2010). "Sugarbeet," in *Root and tuber crops, Handbook of plant breeding*. Ed. J. Bradshow (Springer, New York), 173–219.

Bolger, A. M., Lohse, M., and Usadel, B. (2014). Trimmomatic: a flexible trimmer for Illumina sequence data. *Bioinformatics* 30, 2114–2120. doi: 10.1093/bioinformatics/btu170

Deakin, G., Dobbs, E., Bennett, J. M., Jones, I. M., Grogan, H. M., and Burton, K. S. (2017). Multiple viral infections in Agaricus bisporus-Characterisation of 18 unique RNA viruses and 8 ORFans identified by deep sequencing. *Sci. Rep.* 7, 2469. doi: 10.1038/s41598-017-01592-9

Duffus, J., Whitney, E., Larsen, R., Liu, H., and Lewellen, R. (1984). First report in western hemisphere of rhizomania of sugarbeet caused by beet necrotic yellow vein virus. *Plant Dis.* 68, 251.

Fujisawa, I., and Sugimoto, T. (1977). Transmission of beet necrotic yellow vein virus by Polymyxa betae. *Japanese J. Phytopathol.* 43, 583–586. doi: 10.3186/jjphytopath.43.583

German-Retana, S., Candresse, T., and Martelli, G. (1999). Closteroviruses (Closteroviridae). *Encyclopedia Virol.*, 266–273. doi: 10.1006/rwvi.1999.0053

Hall, T., Biosciences, I., and Carlsbad, C. (2011). BioEdit: an important software for molecular biology. *GERF Bull. Biosci.* 2, 60–61.

Hossain, R., Menzel, W., Lachmann, C., and Varrelmann, M. (2021). New insights into virus yellows distribution in Europe and effects of beet yellows virus, beet mild yellowing virus, and beet chlorosis virus on sugarbeet yield following field inoculation. *Plant Pathol.* 70, 584–593. doi: 10.1111/ppa.13306

Jo, Y., Choi, H., Kim, S.-M., Kim, S.-L., Lee, B. C., and Cho, W. K. (2017). The pepper virome: natural co-infection of diverse viruses and their quasispecies. *BMC Genomics* 18, 1–12. doi: 10.1186/s12864-017-3838-8

Jo, Y., Kim, S.-M., Choi, H., Yang, J. W., Lee, B. C., and Cho, W. K. (2020a). Sweet potato viromes in eight different geographical regions in Korea and two different cultivars. *Sci. Rep.* 10, 2588. doi: 10.1038/s41598-020-59518-x

Jo, Y., Lian, S., Chu, H., Cho, J. K., Yoo, S.-H., Choi, H., et al. (2018). Peach RNA viromes in six different peach cultivars. *Sci. Rep.* 8, 1844. doi: 10.1038/s41598-018-20256-w

Jo, Y., Yoon, Y. N., Jang, Y.-W., Choi, H., Lee, Y.-H., Kim, S.-M., et al. (2020b). Soybean viromes in the Republic of Korea revealed by RT-PCR and next-generation sequencing. *Microorganisms* 8, 1777. doi: 10.3390/microorganisms8111777

Kamitani, M., Nagano, A. J., Honjo, M. N., and Kudoh, H. (2019). A survey on plant viruses in natural Brassicaceae communities using RNA-seq. *Microb. Ecol.* 78, 113–121. doi: 10.1007/s00248-018-1271-4

Kozłowska-Makulska, A., Beuve, M., Syller, J., Szyndel, M. S., Lemaire, O., Bouzoubaa, S., et al. (2009). Aphid transmissibility of different European beet polerovirus isolates. *Eur. J. Plant Pathol.* 125, 337–341. doi: 10.1007/s10658-009-9474-7

Kwon, J., Kasai, A., Maoka, T., Masuta, C., Sano, T., and Nakahara, K. S. (2020). RNA silencing-related genes contribute to tolerance of infection with potato virus X and Y in a susceptible tomato plant. *Virol. J.* 17, 1–13. doi: 10.1186/s12985-020-01414-x

Lai, X., Wang, H., Wu, C., Zheng, W., Leng, J., Zhang, Y., et al. (2022). Comparison of potato viromes between introduced and indigenous varieties. *Front. Microbiol.* 13, 809780. doi: 10.3389/fmicb.2022.809780

Lee, L., Telford, E. B., Batten, J. S., Scholthof, K. B., and Rush, C. M. (2001). Complete nucleotide sequence and genome organization of Beet soilborne mosaic virus, a proposed member of the genus Benyvirus. *Arch. Virol.* 146, 2443–2453. doi: 10.1007/s007050170014

Li, H., and Durbin, R. (2009). Fast and accurate short read alignment with Burrows–Wheeler transform. *Bioinformatics* 25, 1754–1760. doi: 10.1093/bioinformatics/btp324

Mascia, T., Nigro, F., Abdallah, A., Ferrara, M., De Stradis, A., Faedda, R., et al. (2014). Gene silencing and gene expression in phytopathogenic fungi using a plant virus vector. *Proc. Natl. Acad. Sci.* 111, 4291–4296. doi: 10.1073/pnas.1315668111

Meunier, A., Schmit, J.-F., Stas, A., Kutluk, N., and Bragard, C. (2003). Multiplex reverse transcription-PCR for simultaneous detection of Beet necrotic yellow vein virus, Beet soilborne virus, and Beet virus Q and their vector Polymyxa betae Keskin on sugarbeet. *Appl. Environ. Microbiol.* 69, 2356–2360. doi: 10.1128/AEM.69.4.2356-2360.2003

Moriyama, H., Urayama, S.-i., Higashiura, T., Le, T. M., and Komatsu, K. (2018). Chrysoviruses in Magnaporthe oryzae. *Viruses* 10, 697. doi: 10.3390/v10120697

Pandey, B., Naidu, R. A., and Grove, G. G. (2018). Detection and analysis of mycovirus-related RNA viruses from grape powdery mildew fungus Erysiphe necator. *Arch. Virol.* 163, 1019–1030. doi: 10.1007/s00705-018-3714-0

Pecman, A., Kutnjak, D., Gutiérrez-Aguirre, I., Adams, I., Fox, A., Boonham, N., et al. (2017). Next generation sequencing for detection and discovery of plant viruses and viroids: Comparison of two approaches. *Front. Microbiol.* 8, 1998. doi: 10.3389/fmicb.2017.01998

Qiu, W., Feechan, A., and Dry, I. (2015). Current understanding of grapevine defense mechanisms against the biotrophic fungus (Erysiphe necator), the causal agent of powdery mildew disease. *Hortic. Res.* 2, 15020. doi: 10.1038/hortres.2015.20

Ramachandran, V., Wyatt, N., Rivera Santiago, E., Barth, H., Bloomquist, M., Weiland, J., et al. (2023a). First report of tomato bushy stunt virus naturally infecting sugarbeet in the United States. *Plant Dis.* 107, 1957. doi: 10.1094/PDIS-11-22-2530-PDN

Ramachandran, V., Wyatt, N., Rivera Santiago, E., Oliver, T., Neher., M., Weiland, J., et al. (2023b). First report of pepper yellow dwarf strain of Beet curly top virus and Spinach curly top Arizona virus in red table beet in Idaho, United States. *Plant Dis.* 107, 2571. doi: 10.1094/PDIS-12-22-2855-PDN

Roossinck, M. J., Martin, D. P., and Roumagnac, P. (2015). Plant virus metagenomics: advances in virus discovery. *Phytopathology* 105, 716–727. doi: 10.1094/PHYTO-12-14-0356-RVW

Rush, C. M., Liu, H. Y., Lewellen, R. T., and Acosta-Leal, R. (2006). The continuing saga of rhizomania of sugar beets in the United States. *Plant Dis.* 90, 4–15. doi: 10.1094/PD-90-0004

Saumet, A., and Lecellier, C.-H. (2006). Anti-viral RNA silencing: do we look like plants? *Retrovirology* 3, 1–11. doi: 10.1186/1742-4690-3-3

Strausbaugh, C. A., Eujayl, I. A., and Wintermantel, W. M. (2017). Beet curly top virus strains associated with sugarbeet in Idaho, Oregon, and a Western US Collection. *Plant Dis.* 101, 1373–1382. doi: 10.1094/PDIS-03-17-0381-RE

Tamada, T. (1999). "Benyvirus," in *Encyclopedia of virology*. Eds. R. G. Webster. and A. Granoff (Academic Press, London), 154–160.

Tamada, T., and Baba, T. (1973). Beet necrotic yellow vein virus from rizomania-affected sugarbeet in Japan. *Japanese J. Phytopathol.* 39, 325–332_321. doi: 10.3186/jjphytopath.39.325

Tamura, K., Stecher, G., and Kumar, S. (2021). MEGA11: molecular evolutionary genetics analysis version 11. *Mol. Biol. Evol.* 38, 3022–3027. doi: 10.1093/molbev/msab120

Tcherepanov, V., Ehlers, A., and Upton, C. (2006). Genome Annotation Transfer Utility (GATU): rapid annotation of viral genomes using a closely related reference genome. *BMC Genomics* 7, 1–10. doi: 10.1186/1471-2164-7-150

Teng, K., Chen, H., Lai, J., Zhang, Z., Fang, Y., Xia, R., et al. (2010). Involvement of C4 protein of beet severe curly top virus (family Geminiviridae) in virus movement. *PloS One* 5, e11280. doi: 10.1371/journal.pone.0011280

Vanitharani, R., Chellappan, P., and Fauquet, C. M. (2005). Geminiviruses and RNA silencing. *Trends Plant Sci.* 10, 144–151. doi: 10.1016/j.tplants.2005.01.005

Vanitharani, R., Chellappan, P., Pita, J. S., and Fauquet, C. M. (2004). Differential roles of AC2 and AC4 of cassava geminiviruses in mediating synergism and suppression of posttranscriptional gene silencing. *J. Virol.* 78, 9487–9498. doi: 10.1128/JVI.78.17.9487-9498.2004

Weiland, J. J., Bornemann, K., Neubauer, J. D., Khan, M. F., and Bolton, M. D. (2019). Prevalence and distribution of beet necrotic yellow vein virus strains in North Dakota and Minnesota. *Plant Dis.* 103, 2083–2089. doi: 10.1094/PDIS-02-19-0360-RE

Weiland, J. J., Sharma Poudel, R., Flobinus, A., Cook, D. E., Secor, G. A., and Bolton, M. D. (2020). RNAseq analysis of rhizomania-infected sugarbeet provides the first genome sequence of beet necrotic yellow vein virus from the USA and identifies a novel alphanecrovirus and putative satellite viruses. *Viruses* 12, 626. doi: 10.3390/v12060626

Weiland, J. J., Wyatt, N., Camelo, V., Spanner, R. E., Hladky, L. J., Ramachandran, V., et al. (2024). Beet soil-borne virus is a helper virus for the novel Beta vulgaris satellite virus 1A. *Phytopathology* 114, 1126–1136. doi: 10.1094/PHYTO-08-23-0299-KC

Wintermantel, W. M. (2005). Co-infection of Beet mosaic virus with beet yellowing viruses leads to increased symptom expression on sugarbeet. *Plant Dis.* 89, 325–331. doi: 10.1094/PD-89-0325

Wisler, G., Widner, J., Duffus, J., Liu, H.-Y., and Sears, J. (1997). A new report of rhizomania and other furoviruses infecting sugarbeet in Minnesota. *Plant Dis.* 81, 229–229. doi: 10.1094/PDIS.1997.81.2.229D

frontiers | Frontiers in Plant Science

TYPE Original Research
PUBLISHED 01 November 2024
DOI 10.3389/fpls.2024.1441145

OPEN ACCESS

EDITED BY
Chellappan Padmanabhan,
USDA APHIS PPQ Science and Technology, United States

REVIEWED BY
Jean Carlos Bettoni,
The New Zealand Institute for Plant and Food Research Ltd, New Zealand
Kishorekumar Reddy,
University of California, Davis, United States

*CORRESPONDENCE
Dag-Ragnar Blystad
dag-ragnar.blystad@nibio.no
Zhibo Hamborg
zhibo.hamborg@nibio.no

RECEIVED 30 May 2024
ACCEPTED 11 October 2024
PUBLISHED 01 November 2024

CITATION
Sapkota B, Trandem N, Fránová J, Koloniuk I, Blystad D-R and Hamborg Z (2024) Incidence of aphid-transmitted viruses in raspberry and raspberry aphids in Norway and experiments on aphid transmission of black raspberry necrosis virus.
Front. Plant Sci. 15:1441145.
doi: 10.3389/fpls.2024.1441145

Incidence of aphid-transmitted viruses in raspberry and raspberry aphids in Norway and experiments on aphid transmission of black raspberry necrosis virus

Bijaya Sapkota[1], Nina Trandem[1], Jana Fránová[2], Igor Koloniuk[2], Dag-Ragnar Blystad[1]* and Zhibo Hamborg[1]*

[1]Division of Biotechnology and Plant Health, Norwegian Institute of Bioeconomy Research, Ås, Norway, [2]Biology Centre CAS, Institute of Plant Molecular Biology, České Budějovice, Czechia

Raspberry (*Rubus idaeus* L.) is susceptible to aphid-borne viruses. We studied the incidence of four of them – black raspberry necrosis virus (BRNV), raspberry leaf mottle virus (RLMV), raspberry vein chlorosis virus (RVCV), and Rubus yellow net virus (RYNV) – in raspberry plants and aphids in and around Norwegian raspberry crops for three years (2019, 2021, and 2022). Most of the samples were from symptomatic plants. Applying RT-PCR, 274 leaf samples and 107 aphid samples were analyzed. All four viruses were found, but BRNV dominated: it was detected in 93% of the 178 leaf samples with virus and was the only virus that occurred more frequently as a single infection than in co-infections with the other viruses. The old cv. Veten had the highest virus incidence (97%) among the sampled plants, followed by uncultivated raspberry in the boundary vegetation (82%). All aphids identified were *Amphorophora idaei* and *Aphis idaei.* BRNV and/or RLMV was detected in 27% of the aphid samples. Notably, BRNV was detected in 30% of *A. idaei* samples, a species not known as a BRNV vector. In subsequent transmission experiments we found that although *A. idaei* can acquire BRNV within one hour, it did not transmit the virus to healthy raspberry plants. In contrast, *Am. idaei*, a known BRNV vector, was able to acquire the virus within one minute and transmit it within one hour of inoculation. Our study will improve the identification and management of BRNV.

KEYWORDS

***Rubus*, black raspberry necrosis virus, raspberry leaf mottle virus, Rubus yellow net virus, raspberry vein chlorosis virus**

1 Introduction

Red raspberry (*Rubus idaeus* L.), an economically important perennial crop, reached global production of 886538 tons in 2021 (FAO, 2022). Its popularity has increased significantly, especially in Europe and North America, due to its high nutritional, dietary and medicinal values. Norway is one of the raspberry producing countries in Europe, with an annual production of 1798 tons in 2021 (FAO, 2022). In Norway, the prime area for growing raspberries is in the western part, specifically within the fjord district of Sogn og Fjordane, now part of Vestland county (Bøthun and Heiberg, 2004). This region benefits from an ideal climate for raspberry production, contributing to its prominence in cultivation. Raspberry cv. Veten was the cornerstone cultivar for more than 30 years, mainly serving the processing industry with its robust characteristics (Haffner et al., 2002; Fotirić Akšić et al., 2022). However, the introduction of cv. Glen Ample in 1996 marked a significant shift, as this Scottish-bred variety supplanted cv. Veten due to its high yield with large fruit and excellent quality at high latitudes, flourishing even in the northern reaches of Brønnøysund in Nordland (65° N) (Heiberg et al., 2002; Bøthun and Heiberg, 2004). Recently, the cv. Glen Mor, bred by the James Hutton Institute in 2020, has raised the interest of Norwegian farmers, mainly due to its *Phytophthora* resistance (https://www.huttonltd.com/services/plant-varieties-breeding-licensing/raspberry/glen-mor).

Raspberry plants are vulnerable to a host of pathogens, particularly viruses (Martin et al., 2013). Till now, 24 plant viruses from different families and genera are known to infect raspberry (Tan et al., 2022; Koloniuk et al., 2023; Lenz et al., 2024). Among them, aphid-transmitted viruses, such as black raspberry necrosis virus (BRNV, *Sadwavirus rubi*), raspberry leaf mottle virus (RLMV, *Closterovirus macularubi*), and Rubus yellow net virus (RYNV, *Badnavirus reterubi*), are important and cause raspberry mosaic disease (RMD) when they occur as mixed infections (Converse, 1987; Alford, 2007). Yield losses due to the combined effect of these viruses in some red raspberry cultivars can be significant, ranging from 11 to 39% in different regions (Converse, 1963; Freeman and Stace-Smith, 1970). Individually, these viruses may not exhibit distinct symptoms in red raspberry (*R. idaeus* L.) cultivars (Jones and Jennings, 1980; Martin et al., 2013). For instance, BRNV may cause apical necrosis in shoots of the indicator species *R. henryi* and *R. occidentalis* (Jones and Jennings, 1980), while RLMV induces chlorotic leaf spots and mosaics in *R. idaeus* cv. Malling Landmark, and RYNV causes net-like chlorosis along veins in *R. occidentalis* cv. Munger (Stace-Smith, 1955a; Martin et al., 2013). Another aphid-borne virus, raspberry vein chlorosis virus (RVCV, genus *Rhabdovirus*), induces a yellow net pattern in most cultivars (Martin et al., 2013). The spread of viruses is often unintentionally facilitated by farmers, such as using infected planting material or overlooking slight symptoms, highlighting the importance of efficient detection and production of healthy planting material (Converse, 1987; Tatineni and Hein, 2023).

All viruses transmit efficiently through vegetative propagation techniques, with additional routes of transmission including carriers such as seeds, pollen, and insects such as aphids (Dietzgen et al., 2016). In Europe, the large European raspberry aphid, *Amphorophora idaei* (or *Am. rubi idaei*) is the primary vector transmitting BRNV, RLMV, and RYNV, while the small European raspberry aphid, *Aphis idaei* transmits RVCV (Martin et al., 2013; Tan et al., 2022).

Viral infections, facilitated by vector dispersal strategies, pose a significant challenge once established. The use of virus-free plant material is thus crucial for disease control (Wang et al., 2022a, Wang et al., 2022b; Bettoni et al., 2024). Studying virus occurrence and vector distribution on commercial farms is necessary to establish disease management strategies. The main objective of this study was to assess the relative distribution of aphid-transmitted viruses in symptomatic raspberry and aphids on such plants in commercial raspberry farms across the most important production area in Norway. The secondary objective was to evaluate the capability of *Am. idaei* and *A. idaei* as vectors for BRNV through aphid transmission experiments.

2 Materials and methods

2.1 Field survey and sample collection

Field sampling was carried out in June and July 2019, 2021, and 2022 in different counties in Norway (in 2020 the covid pandemic led to a break in the sampling). The sample sizes for different years and locations are listed in Table 1. The selected plantations were subjected to visual inspection and shoots of raspberry canes with leaves were collected. In the majority of cases, plants displaying virus symptoms were chosen. Additionally, asymptomatic samples with the presence of aphids were also included. A total of 274 samples of raspberry leaves were acquired, consisting predominantly of three cultivars – 'Glen Ample', 'Veten', and 'Glen Mor' - from open fields or polytunnels, and of non-cultivated raspberry plants of unknown variety found within the boundary vegetation of the plantations, referred to as "Wild" cultivars. Furthermore, some cultivated raspberry samples were labeled as "Others", signifying their unidentified cultivar name. Photographs were taken of all the samples collected to assist in the evaluation of leaf symptoms.

TABLE 1 Locations and number of raspberry leaf samples collected.

Sampling location	Sample size			
	2019	2021	2022	Total
Innlandet	8	0	0	8
Vestfold og Telemark	9	0	0	9
Viken	7	16	27	50
Vestland	39	68	83	190
Agder	0	11	6	17
Total	63	95	116	**274**

The sampling locations are the counties covering the most important raspberry growing areas in Norway, while the sample size indicates the number of raspberry samples collected in three different years (2019, 2021, and 2022).

In 2021 and 2022, any aphids colonizing the sampled leaves were also examined and a total of 107 aphid samples were collected over the two years. Morphological identification was conducted by examining random aphids from each collected sample under a stereo microscope (Lecia MZ72). Only morphologically identified *Am. idaei* and *A. idaei* were collected for molecular identification. The aphids were individually collected and placed in separate 2 ml Eppendorf tubes containing DNA/RNA Shield (Zymo Research, Irvine, CA, USA). For nymphs, 3-5 individuals were collected in a single tube, while for adults, the number was limited to 1-2 per tube.

2.2 RNA extraction

Raspberry leaf samples were ground into a fine powder using liquid nitrogen employing a mortar and pestle. Total RNA was then extracted from fresh young leaf tissues (50 mg) using the Norgen Plant/Fungi RNA kit (Norgen Biotek, Thorold, ON, Canada). Extraction was performed according to the manufacturer's instructions with some modifications, and then elution was performed in 50 µL of RNase-free water. DNase treatment was implemented on the column during the extraction process. In addition, plant samples infected with BRNV, RLMV, RYNV and RVCV and cultivated in the NIBIO greenhouse as positive controls were also subjected to a similar RNA extraction procedure. The amount of RNA was determined using a NanoDrop 1000b spectrophotometer (NanoDrop Technologies, Wilmington, DE, USA) and the extracted RNA was stored at a temperature of −80°C for future use.

Aphid samples collected in the DNA/RNA solution were processed by directly crushing them with a small glass rod and adding 600 µL of TRIzol reagent (Thermo Fisher Scientific, Waltham, MA, USA). The total RNA was extracted using a Direct-zol RNA Miniprep Kit (Zymo Research, CA, *USA*) according to the manufacturer's instructions. The purified RNA was then stored at −80°C.

2.3 RT-PCR and Sanger sequencing

The extracted total RNA was reverse transcribed (RT) using the Superscript IV Reverse Transcriptase kit (Invitrogen, Carlsbad, CA, USA) according to the manufacturer's guidelines. As an internal amplification control of the plant sample for amplification, RT-PCR was used to amplify mitochondrial NADH dehydrogenase *nad5* mRNA (Menzel et al., 2002). While internal controls of cytochrome c oxidase subunit I-COI (Folmer et al., 1994) were used for aphid samples. For the subsequent virus detection, only samples that passed the internal controls were included and carried out in a 25 µL reaction with Taq DNA polymerase (5U/µL) (InvitrogenTM, ThermoFisher Scientific, USA) according to the manufacturer's recommendations with 2 µL of cDNA. All primer sequences used in this study as well as their respective amplification conditions are listed in Table 2. As a part of quality control, reaction mixtures containing 2 µL of sterile water in place of the cDNA template were used as blank controls, and cDNA templates previously confirmed to be infected with the respective viruses were used as the virus-positive controls. The PCR programs applied to detect all the viruses were as follows: initial pre-denaturation step at 95°C for 2 minutes, followed by 35 cycles of denaturation at 95°C for 30 seconds, annealing at 47 to 60°C for 30 seconds, and extension at 72°C for 45 seconds. A final extension was performed at 72°C for 7 minutes. Each resulting PCR product (10 µL) was subjected to electrophoresis in a 1.2% agarose gel previously stained with SYBR safe DNA stain (Invitrogen, ThermoFisher Scientific, USA).

For aphid molecular identification, aphid samples amplified with COI primer were sent for Sanger sequencing (Eurofins Genomics, Norway). The purified PCR products were sequenced in both directions. The nucleotide sequences obtained from Sanger sequencing were analyzed using CLC Genomics Workbench 9.5.1 (Qiagen) and identified using the BLAST service against nr/nt database provided by the NCBI.

TABLE 2 All the primers used in this study.

Name of primer	Sequence (5′-3′)	Product size (bp)	Annealing temperature (Jones et al.)	Reference
Nad_F Nad_R	GATGCTTCTTGGGGCTTCTTGTT CTCCAGTCACCAACATTGGCATAA	181	50	(Menzel et al., 2002)
BRNV_1153 BRNV_1154	GCGCACTGAACCCAAGTTTA CAACATCGAATCCCTCAAGC	502	60	(McGavin et al., 2010)
RLMV_CPhF RLMV_CPhR	CGAAACTTYTACGGGGAAC CCTTTGAAYTCTTTAACATCGT	470	60	(Tzanetakis et al., 2007)
RYNV_1752 RYNV_1753	TCCAAAACCTCCCAGACCTAAAAC ATAATCGCAAAAGGCAAGCCAC	350	55	(Jones et al., 2002)
RVCV_3649 RVCV_3648	CCAACAAAGCTGATATWCCAG CCTCATCTAAGTARTCTTCCA	257	55	(Jones et al., 2019)
LCOI490 HCO2198	GGTCAACAAATCATAAAGATATTGG TAAACTTCAGGGTGACCAAAAAATCA	700	47	(Folmer et al., 1994)

2.4 Phylogenetic tree

A phylogenetic tree was made to study the genetic differences between two aphid species, *A. idaei* and *Am. idaei*. The sequences of these two species, along with closely related species and outgroups, were first aligned using multiple sequence alignment in Geneious Prime software. After that, the tree was generated using the Neighbor-Joining (NJ) method with the Tamura-Nei genetic distance model. To assess the robustness of the tree, bootstrap analysis was conducted with 1000 replicates. The outgroup for the analysis was set to *Empoasca decipiens* (GenBank Accession: OQ381266).

2.5 Aphid cultures

Colonies of *A. idaei* and *Am. idaei* were established as individual lines from overwintering eggs collected outdoors in the early spring in 2022 and subsequently tested for viruses. The aphids were kept on virus-free raspberry plants of cv. Glen Ample derived from tissue culture plants. The aphid cultures were maintained in net cages (70 x 50 x 50 cm) in a climate room at 18°C, 75% humidity, and a 16-h light/8-h dark cycle. All experiments were carried out under the same conditions in separate aphid net chambers, i.e., one cage per treatment.

2.6 Aphid transmission

Adult wingless aphids from tested BRNV-free colonies of *Am. idaei* and *A. idaei* were employed in the experiment. Starvation time was determined by not feeding the aphids for various periods of time up to two hours and then offering them a raspberry leaf to observe whether feeding commenced immediately or not using a Lecia MZ72 stereomicroscope. Based on this, the starvation time was set to one hour.

The aphid transmission experiment was carried based on methods from Halgren et al. (2007) and Koloniuk et al. (2023), with modifications. For the virus acquisition phase, aphids were allowed to feed on BRNV-infected leaves for different periods of time: 1 minute, 5 minutes, 1 hour, and 24 hours, with each acquisition group consisting of 13 aphids. Following this feeding period, three aphids were immediately tested for virus acquisition and a group of five aphids was carefully placed on the upper surfaces of each of two BRNV-free raspberry plants of raspberry cv. Ninni. The aphids were then placed for specific inoculation periods, including 5 minutes, 1 hour, 24 hours, and 48 hours (for *Am. idaei*) or 7 days (for *A. idaei)* as shown in Figure 1. Additionally, the experiment for *A. idaei* was repeated with three individual BRNV-free plants to verify the consistency and reproducibility of the transmission results. In total, five plants were applied for *A. idaei* transmission.

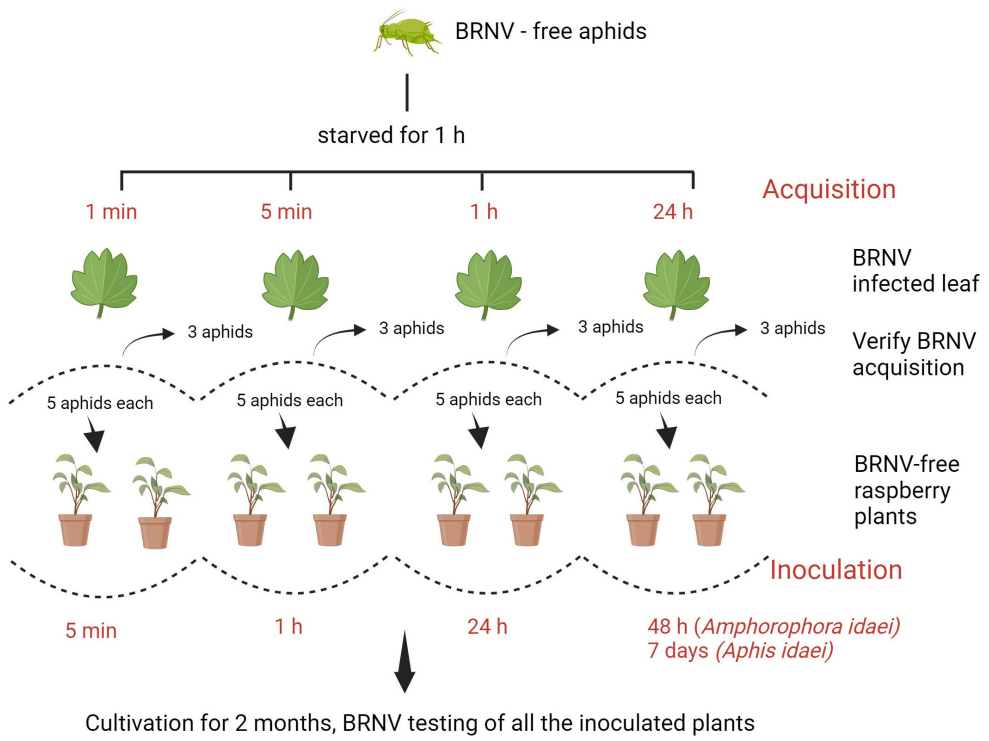

FIGURE 1
Schematic illustration of the assay for aphid-assisted transmission of black raspberry necrosis virus (BRNV) to raspberry plants. Created with BioRender.com.

2.7 Data analysis

Statistical analyses were performed with R-Studio software, using Microsoft Excel for graphical representation. The maps were created using the QGIS 3.24 software. For this purpose, Norway's shape file was obtained from Kartverket, the Norwegian mapping authority. The file was accessed via the following link: https://kartkatalog.geonorge.no/metadata/administrative-enheter-fylker/6093c8a8-fa80-11e6-bc64-92361f002671.

3 Results

3.1 Annual virus occurrence and geographical distribution

In 2019, out of 63 samples tested, 23 were found to be infected with one of the tested viruses. Notably, BRNV dominated with 22 cases, followed by RLMV (4) and RYNV (2). RVCV was detected in only one plant sample. All virus-infected samples were collected in Vestland County, with no occurrences in the other surveyed regions (Figure 2A).

In 2021, out of 95 tested leaf samples, 72 exhibited infections with one of the tested viruses. Once again, BRNV was predominant, found in 64 out of 95 samples, followed by RLMV (21) and RVCV (6). Interestingly, no instances of RYNV were detected this year. BRNV, RLMV, and RVCV were identified in samples from Vestland County, while BRNV and RVCV were also found in Viken and Agder Counties (Figure 2B).

In 2022, 83 out of 116 tested leaf samples displayed infection with one of the tested viruses. BRNV maintained its dominance with 79 cases, followed by RLMV (17) and RVCV (15). Additionally, RYNV was detected in 10 plant samples this year. Agder County exhibited the presence of only BRNV and RLMV, while Viken County had solely BRNV (Figure 2C). All mentioned viruses were identified in Vestland county including RYNV. The overall distribution of mentioned viruses in raspberry cultivars across different Norwegian counties (2019, 2021, and 2022) are tabulated in Supplementary Table S1.

3.2 Occurrence of single and mixed virus infections

In total, out of 274 collected samples, 178 samples exhibited either sole infection by a single virus or co-infections involving multiple tested viruses (Table 3). Upon analyzing the collective data spanning all three years, a clear pattern emerged, highlighting the substantial prevalence of BRNV, with an infection rate of 93.3% (166 out of 178). BRNV single infection accounted for a noteworthy 63.4% of the total infected samples, with 113 instances. Next in prevalence was mixed infections of BRNV and RLMV, constituting 16.2% of the total infected samples, amounting to 29 cases. In contrast, the single infection rate of the other aphid-borne viruses, namely RLMV, RYNV, and RVCV, was notably low (Table 3). Examining the co-infection dynamics, it was observed that the co-infection rate of BRNV with RLMV remained consistently high. Moreover, the survey unearthed instances of RMD, arising from concurrent infections of BRNV, RLMV, and RYNV. These instances were relatively scarce, constituting only 2.8% of the total infected samples, with a count of 5 cases (Table 3).

Most of the samples infected with BRNV had mosaic and vein clearing symptoms as shown in Figure 3A, while some others had no clear symptoms as in Figure 3C. Heavily BRNV-infected

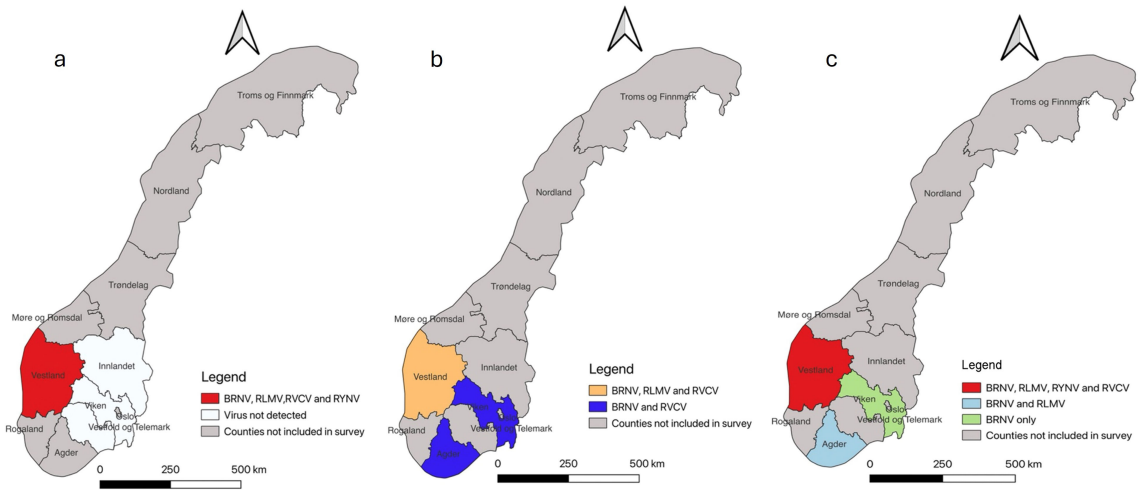

FIGURE 2
Map of Norway illustrating the surveillance area at county level and virus occurrences detected in each county. The gray color designates the counties not included in our study. **(A)** Survey results from 2019 reveal that all mentioned viruses were exclusively detected in Vestland County. **(B)** Survey results from 2021 indicate the presence of three different viruses in Vestland County (orange): BRNV, RLMV, and RVCV. In two other counties (blue), the detection of two viruses, BRNV and RVCV, is noted. **(C)** Survey results from 2022 indicate that all mentioned viruses were once again found exclusively in Vestland County. In Agder County (light blue), only BRNV and RLMV were detected, while in Viken (light green), only BRNV was present.

TABLE 3 Presence and incidence of detected raspberry viruses in a total of 274 raspberry samples.

Detected virus	No of RT-PCR positive samples	*Percentage (%) of positive samples in total number of infected samples
BRNV alone	113	63.4
RLMV alone	4	2.2
RYNV alone	3	1.6
RVCV alone	5	2.8
Single virus detected (total)	125	70.2
BRNV+RLMV	29	16.2
BRNV+RYNV	3	1.6
BRNV+RVCV	12	6.7
Co-infection with 2 viruses (total)	44	24.7
BRNV+RLMV+RYNV	5	2.8
BRNV+RLMV+RVCV	3	1.6
Co-infection with 3 viruses (total)	8	4.4
BRNV+RLMV+RYNV+RVCV	1	0.5
Co-infection with 4 viruses (total)	1	0.5

Total number of samples (n)=274, total infected samples=178.
*Relative occurrence, i.e., percentage derived by dividing the No of RT-PCR positive samples by No of Total infected samples (178).

raspberry cv. Glen Ample plants showed obvious reduced plant vigor with mosaic symptoms on leaves and symptoms spreading gradually to the neighbor plants in both sides (Figure 3B). The mixed infection of BRNV with other virus exhibited more intense symptoms (Figures 3D–G) varying from mosaic, yellowing, leaf curl, dwarf, and leaf malformation symptoms.

3.3 Virus infection and cultivars

All three cultivated cultivars ('Glen Ample', 'Glen Mor', and 'Veten'), along with the "Wild" and the "Others" category, demonstrated infection by at least one of the tested viruses (Figure 4). Notably, cv. Veten samples exhibited the highest infection rate, with 97% (31 out of 32 samples) infected. Following this, uncultivated raspberry samples ("Wild") showed an infection rate of 82% (50 out of 61 samples), and cv. Glen Mor of 58% (7 out of 12 samples). 'Glen Ample' exhibited a virus infection rate of 56% (70 out of 126 samples), and "Others" 52% (22 out of 42 samples). An analysis of virus infestation prevalence within these cultivars revealed that BRNV dominated across all cultivars (Figure 5). Notably, RYNV was not detected in the Veten and Glen Mor cultivars.

3.4 Aphid species distribution and virus infection

In total, 107 total RNA were extracted from collected aphid samples and checked with RT-PCR using COI primers before conducting virus diagnostics. Molecular identification of aphid species was performed on 13 and 76 aphid samples from 2021 and 2022, respectively. Specifically, only virus-infected aphids were molecularly identified in 2021, whereas all the COI-positive aphids were identified in 2022.

A total of 77 aphids were successfully molecularly identified, with 54 classified as *Am. idaei* and 23 as *A. idaei* (Supplementary Table S3 and Table 4). Amplicons of 575bp with 100% identity and 100% coverage were obtained for *A. idaei* (NCBI accession no. KF638947; 658 bp). Amplicons of 633 bp showed 100% identity and 100% coverage for large blackberry aphid, *Am. rubi* (NCBI accession no. JX507416; 668 bp). Based on the sampling host being raspberry, not blackberry, these amplicons were identified as large raspberry aphid, *Am. idaei*. These two sequences have been submitted to the NCBI GenBank: *Am. idaei* (accession no. PP265263) and *A. idaei* (accession no. PQ384946).

The phylogenetic tree (Figure 6) demonstrates a clear genetic distinction between *Am. idaei*, *A. idaei*, and other aphid species, regardless of whether they feed on raspberry plants. This provides molecular evidence for the accurate identification of the collected aphid samples. The phylogenetic relationships shown by the tree are well supported, with most bootstrap values being above 70%, indicating strong confidence in the evolutionary pathway. Here, the tree places *Am. idaei* (this study, GenBank Accession: PP265263) close to the previously available *Am. idaei* sequence (GenBank Accession: JF340095), due to the similarity between the two *Am. idaei* sequences. Both represent the same species, though the shorter sequence (JF340095, 453 bp) may not capture as much genetic variation as the longer sequence obtained in this study (633 bp). In this case, the 633 bp sequence of *Am. idaei* from this study (accession no. PP265263) offers an opportunity to refine these phylogenetic relationships for further study of aphids feeding on raspberry.

10.3389/fpls.2024.1441145

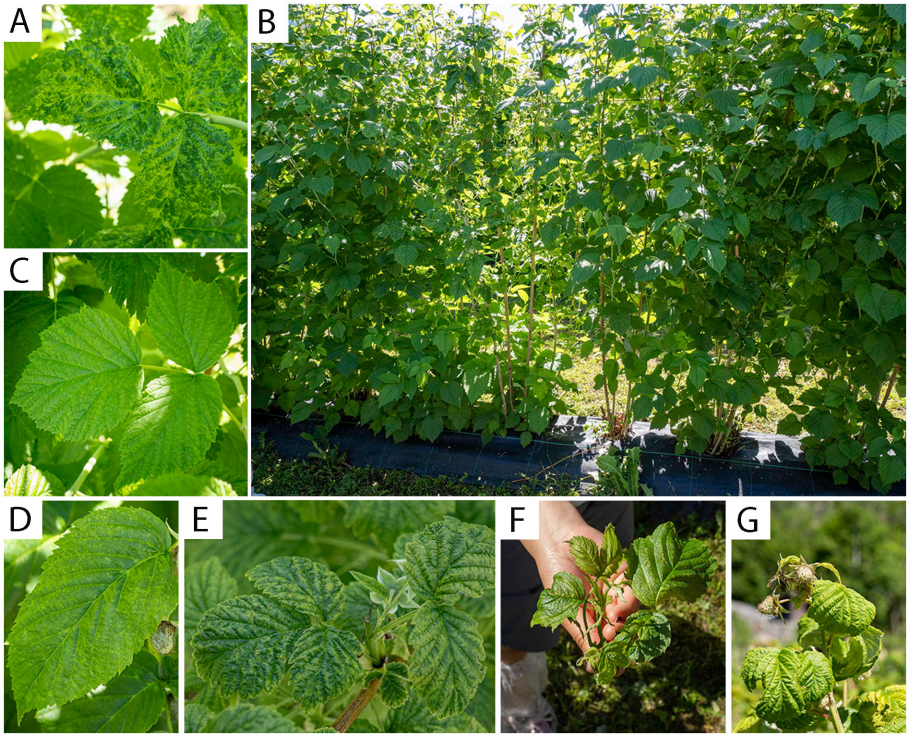

FIGURE 3
Virus-infected raspberry leaves and plants with diverse symptoms. **(A)** BRNV-infected raspberry cv. Glen Ample leaf with mosaic and vein clearing symptoms; **(B)** BRNV-infected raspberry cv. Glen Ample plants in a row: with heavy mosaic symptoms and reduced plant vigor in the middle of the row and random mosaic symptoms spreading to the neighbor plants in both sides; **(C)** BRNV-infected raspberry cv. Glen Ample leaf with no obvious symptoms; **(D)** BRNV and RLMV-infected raspberry cv. Veten leaf with yellow spot symptoms; **(E)** BRNV and RLMV-infected raspberry "wild" plant leaf with mosaic symptoms; **(F)** Raspberry "wild" plant shoot infected with BRNV, RLMV, RYNV and RVCV with yellowing, leaf curl, dwarf and leaf malformation symptoms; **(G)** Raspberry cv. Veten shoot with co-infection of BRNV, RLMV and RVCV (raspberry mosaic disease, RMD) with leaf curl and yellowing symptoms.

In total, one or more viruses were found in 27% of the aphid samples and BRNV was most common in both aphid species (Supplementary Table S2 and Table 4). No aphids were found positive for RVCV or RYNV. In the case of *Am. idaei*, out of the 54 total samples, 16 were found to be positive with BRNV only, 1 for RLMV only, and 5 for both BRNV and RLMV. Notably, 32 samples were free from the tested viruses. For *A. idaei*, comprising 23 samples, 6 were positive for BRNV only, 1 for both BRNV and RLMV, and 16 were free from the tested viruses. The overall distribution of the mentioned viruses in all 107 aphid samples collected in 2021 and 2022 are tabulated in Supplementary Table S2.

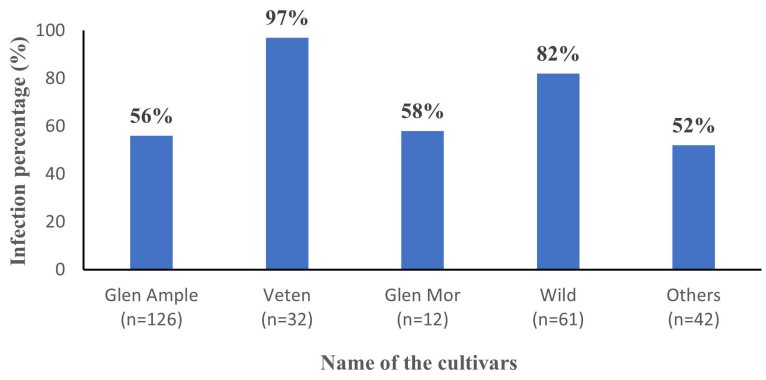

FIGURE 4
Average virus infection percentage of different cultivars (n= number of samples collected).

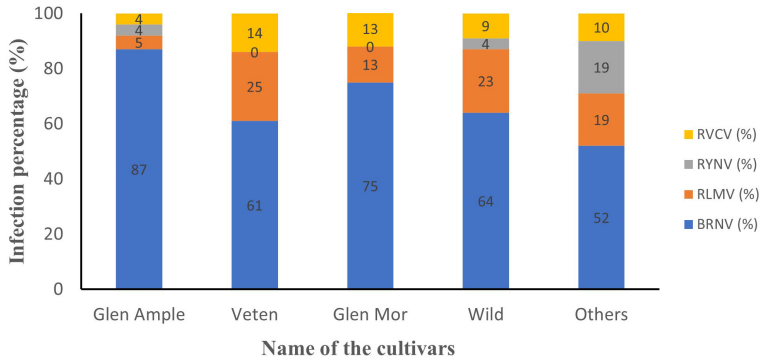

FIGURE 5
Infection percentage of different viruses within the cultivars. BRNV was dominant in all cultivars. RYNV was not detected in raspberry cv. Veten and cv. Glen Mor.

3.5 Transmission assay

The aphid cultures underwent initial screening for BRNV using RT-PCR, confirming their BRNV-free status. When feeding aphids with BRNV-infected raspberry leaves for 1 minute, 5 minutes, 1 hour, or 24 hours, *Am. idaei* consistently acquired BRNV and tested positive for BRNV in all the examined acquistion periods (Figure 7). Conversely, *A. idaei* aphids did not acquire BRNV after 1 min and 5 min (tested negative for BRNV) but demonstrated BRNV acquistion after 1 hour and 24 hours (tested positive for BRNV) (Figure 7). Notably, all BRNV-positive *Am. idaei* aphids tested negative for plant internal *nad5* control, ruling out the presence of plant debris inside the aphids. However, *A. idaei* were positive for plant internal *nad5* control after 24 hours of acquisition but tested negative after 1 hours of acquisition (Figure 8).

Subsequent testing of all inoculated plants for BRNV using RT-PCR, conducted two months after inoculation, revealed that none of the raspberry plants inoculated by *A. idaei* was positive for BRNV. In contrast, three raspberry plants inoculated by *Am. idaei* were positive for BRNV: two plants from 1- hour inoculation time and one plant from 48 hours (Figure 9, Table 5).

4 Discussion

4.1 Overview of virus occurrence and distribution in plants and aphids

In this investigation, our focus was on detecting four aphid-transmitted raspberry viruses. BRNV was the most common virus found in plant as well as aphid samples. The predominance of BRNV might be attributed to its efficient transmission by the aphid vector, *Am. idaei*, which acquires and transmits the virus to healthy plants within minutes (Stace-Smith, 1955b). In contrast, RLMV and RYNV exhibit longer acquisition and inoculation times in *Am. idaei*, and the same is the case for RVCV in *A. idaei* (Stace-Smith, 1955a, Stace-Smith, 1961; McMenemy et al., 2009). The high incidence of BRNV in raspberry growing area in Norway is corresponding to the previous survey in Finland (Susi et al., 2018).

Our study revealed a high percentage of co-infection occurrence of BRNV and RLMV both in plants and aphids, a trend aligning with reports of common co-infections in Europe (Converse, 1987). This co-infection is facilitated by the shared aphid vector and potentially also an attraction of the aphid vector to virus-infected plants within a short time window (McMenemy et al., 2012). Moreover, high co-infection rates are to be expected when mainly symptomatic plants are sampled, because BRNV, when found as a single infection, typically does not present symptoms on red raspberry (Stace-Smith, 1955b; Jones and Jennings, 1980). However, the high incidence of BRNV single infections in our study (41% of all our leaf samples) points to a presence of symptoms, and we observed mosaic and vein clearing symptoms on most of the Glen Ample leaf samples with BRNV single infection. None of these samples were found to be infected with either raspberry bushy dwarf virus or the raspberry leaf blotch virus, either. To fulfill Koch's postulates, transmission of BRNV to virus-free Glen Ample plants to induce similar symptoms should be further pursued. When BRNV was present with other examined viruses, i.e., as co-infections, the resulting symptoms were distinctive (Figure 3), as reported in earlier literature (Martin et al., 2013).

TABLE 4 Virus presence in molecularly identified aphid samples collected from raspberry fields.

Aphid species	Total tested samples	Positive with BRNV only	Positive with RLMV only	Positive with BRNV and RLMV	Total positive sample	Negative from tested viruses
Amphorophora idaei	54	16	1	5	22	32
Aphis idaei	23	6	0	1	7	16

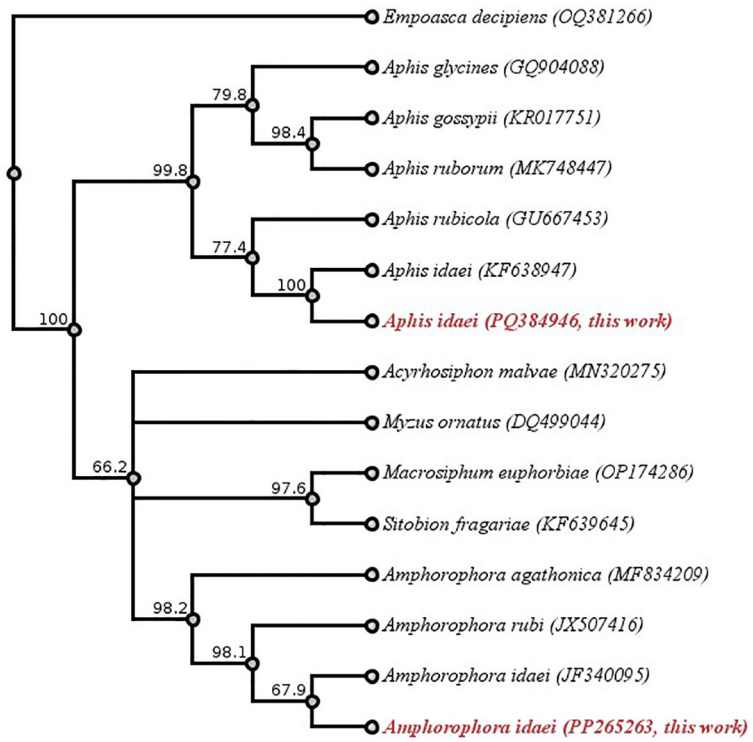

FIGURE 6
Phylogenetic tree based on COI sequence data for molecular identification of aphids. Species names and GenBank accession numbers are shown at the tips. Sequences highlighted in red, *Aphis idaei* (PQ384946) and *Amphorophora idaei* (PP265263), represent newly obtained sequences from this study. *Empoasca decipiens* (OQ381266) was applied as outgroup. Each branch of the tree contains a bootstrap value. Geneious version 2024.0 created by Biomatters. Available from https://www.geneious.com.

4.2 Virus infection and cultivars

Among the surveyed raspberry samples, 'Veten' exhibited the highest virus infection rate, followed by "wild" raspberries found in the semi-natural vegetation that frequently adjoins Norwegian raspberry crops. 'Veten' was prominent in Norway's raspberry industry for over 30 years, primarily grown for industrial use. However, over the past two decades, it has been replaced by 'Glen Ample' (Heiberg et al., 2002), a cultivar with a specific resistance gene, A1, which to a certain extent provides it with a defense against the important virus vector *Am. idaei* (McMenemy et al., 2009). This shift in cultivars must have forced *Am. idaei* populations to prefer the few 'Veten' crops left or remain on wild raspberry, resulting in an accumulation of virus infection in these plants. The proliferation of viral infections in "wild" raspberry is a point of concern. These plants may act as viral reservoirs for both pollen-transmitted raspberry viruses like raspberry bushy dwarf virus (not included in this study) and aphid-borne viruses like BRNV (Susi et al., 2018).

The presence of aphid-borne virus in more than half the leaf samples of the two cultivars with some resistance to *Am. idaei*, 'Glen Ample' and 'Glen Mor', highlights the importance of continued monitoring to reduce the risk of widespread virus transmission even

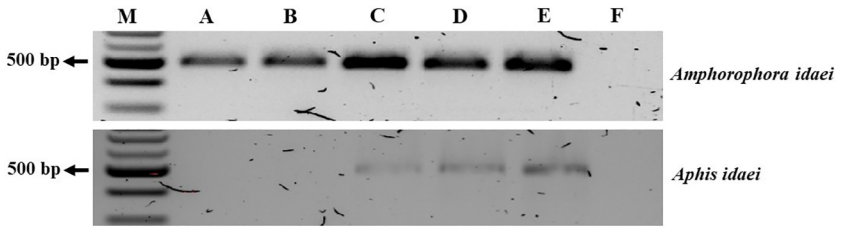

FIGURE 7
Gel picture of RT-PCR detection results for BRNV in collected aphids after different acquisition periods. From **(A–D)**: aphids collected after 1 min, 5 min, 1 h, and 24 h acquisition times, respectively; **(E)**: BRNV positive control; **(F)**: BRNV negative control; M: 100 bp ladder. The size of the targeted band for BRNV was 502 bp.

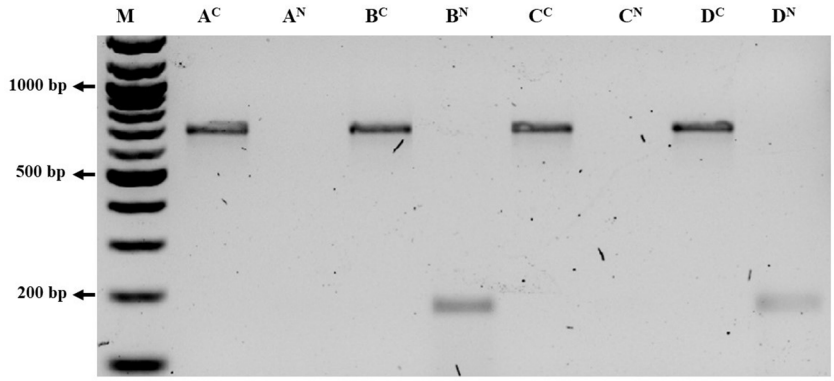

FIGURE 8
Gel picture of RT-PCR detection results of *Aphis idaei* after different acquisition period using COI and NAD primer. A^C and A^N: COI and NAD primer detection of aphids collected after 1 min respectively; B^C and B^N: COI and NAD primer detection of aphids collected after 5 min respectively. C^C and C^N: COI and NAD primer detection of aphids collected after 1 hours respectively. D^C and D^N: COI and NAD primer detection of aphids collected after 24 hours respectively; M: 100 bp ladder. The size of the targeted band for COI was 700 bp and the size of the targeted band for NAD was 181 bp. Aphids in all acquisition time were positive for COI primer but NAD returned positive for the samples of 5 minute and in 24 hours only.

in resistant cultivars and to avoid relying on one method of virus management. *Am. idaei* has been found on 'Glen Ample' in Norway since 2015 (Trandem et al., 2015) and was also found in this study; indeed, *Am. idaei* for the transmission experiments was reared on 'Glen Ample' without problems. Our study thus aligns with McMenemy et al. (2009), who reported that the *Am. idaei* resistance conferred by the A1 gene had been broadly overcome by other biotypes of the aphid in Scotland, resulting in a notable surge in the occurrence of viruses transmitted by this vector. Two of the viruses known to be transferred by *Am. idaei*, BRNV and RLMV, were also found on newly established 'Glen Mor' plants with no obvious virus-like symptoms in our study. However, as the sample size was low and no *Am. idaei* was collected on these plants, we do not know if the viruses came with the planting materials or transmitted by aphids after planting.

4.3 Aphid species and BRNV transmission assay

Eight different aphids have been reported sucking on raspberries and transmitting different viruses, i.e., *Am. idaei*, *Am. rubi*, *Am. agathonica*, *A. idaei*, *A. rubicola*, *Macrosiphum euphorbiae, Sitobion fragariae, and Myzus ornatus* (Tan et al., 2022). Two of them, i.e., *Am. idaei* and *A. idaei*, were confirmed by combining morphological and molecular identification in this study. This result showed the dominance of *Am. idaei* and *A. idaei* in Norwegian raspberry; they are by far the two most common aphids in European raspberry (Gordon et al., 1997; McMenemy et al. (2009). The absence of the other six aphids in our samples are explainable: *Am. rubi* is typically associated with blackberry (Alford, 2007), *Am. agathonica* and *A. rubicola* are specific in North America (Blackman and Eastop, 2000; Martin et al., 2013) and the others have alternative hosts and are only occasionally observed on raspberry plants (Gordon et al., 1997; Tan et al., 2022).

It should be mentioned that identifying aphids feeding on raspberry based solely on sequence of COI fragments obtained by PCR is insufficient. Initially, all *Amphorophora* on *Rubus* were grouped as a single species, *Amphorophora rubi* (Kaltenbach). Further studies based on host-plant transfers and morphological studies determined that there were two distinct species: *Amphorophora idaei*, which feeds only on red raspberry, and *Amphorophora rubi*, which feeds only on blackberry (Börner, 1939; Blackman et al., 1977). Therefore, combining host information with morphological and molecular data is crucial for

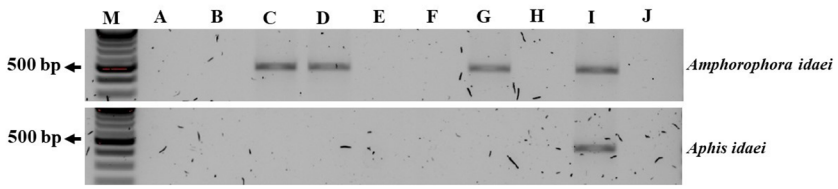

FIGURE 9
Gel picture of RT-PCR detection results for BRNV in raspberry plants after 2 months of treating BRNV infected aphids in different inoculation periods. From **(A–H)**: raspberry plants tested for BRNV after two month of different inoculation time where, **(A, B)**: plants inoculated for 5 minutes; **(C, D)**: plants inoculated for 1 hours; **(E, F)**: plants inoculated for 24 hours and **(G, H)**: inoculated for 48 hours with *Am. idaei* and 7 days with *A. idaei*. Here, **(I)**: BRNV positive control; **(J)**: BRNV negative control; **(M)**: 100 bp ladder. The size of the targeted band for BRNV was 502 bp.

TABLE 5 Summary of results from BRNV transmission assay with two aphid species.

Aphid species	Acquisition period	RT-PCR test of aphid after acquisition	Inoculation period	RT-PCR test of plants after inoculation	Number of infected plants
Amphorophora idaei	1 min.	Pos.	5 min	Neg.	0/2
	5 min	Pos.	1 h	Pos.	2/2
	1 h	Pos.	24 h	Neg.	0/2
	24 hr	Pos.	48 h	Pos.	1/2
Aphis idaei	1 min	Neg.	5 min	Neg.	0/5
	5 min	Neg.	1 h	Neg.	0/5
	1 h	Pos.	24 h	Neg.	0/5
	24 h	Pos.	7 days	Neg.	0/5

"Pos." means RT-PCR positive result and "Neg." means RT-PCR negative result.

accurate aphid identification. The newly submitted COI sequence of *Am. idaei* from this study (accession no. PP265263) may contribute to more precise molecular identification for future studies on aphids feeding on raspberry.

In the transmission experiments, we found that *Am. idaei* can acquire and transmit BRNV within a remarkably short period, one minute for acquisition and within one hour for inoculation. These results correspond with the earlier research of Stace-Smith (1955b), who observed that this aphid required 15 minutes for virus acquisition and around 2 minutes for transmission. Such behavior was reviewed and classified as a semi-persistent type of virus transmission by McMenemy et al. (2009) and was partially observed in our experiment, although the acquisition time in our study was notably shorter, within 1 minute. This discrepancy in acquisition time could be due to the sensitivity of our RT-PCR methodology, which can detect lower virus concentrations than the traditional indicator-plant based methods used by Stace-Smith (1955b). Furthermore, our experiments revealed that virus transmission was not observed within 5 minutes but only became apparent after 1 hour. It is crucial to recognize that aphid behavior significantly influences transmission rates, and transmission is not always guaranteed, as noted by Stace-Smith (1955b). Additionally, the limited sample size in our study, with only 2 plants per treatment, may have contributed to the absence of observed transmission within the 5-minute inoculation period.

For the transmission experiment with *A. idaei*, the aphids acquired BRNV within 1 hour, but transmission to healthy raspberry plants could not be confirmed. Interestingly, *A. idaei* tested positive for the plant internal *nad*5 control after 24 hours of acquisition but tested negative after just 1 hour of acquisition. This suggests uncertainty in the ability of *A. idaei* to effectively acquire BRNV. The virus uptake by the aphid could be through the gut region or hemocoel, whereas transmission is likely hindered by multiple barriers (Lightle et al., 2012). For persistent or circulative mode of transmission, the virus must be retained in the aphid's salivary gland and for non-persistent transmission, it would require a certain level of specificity, such as protein interactions, for the virus to bind to the aphid's stylet (Lightle et al., 2012; Abhinash et al., 2023). In our case, the virus may not be able to reach the salivary glands which should be investigated comprehensively to fully understand the underlying mechanisms of transmission.

5 Conclusion

Our study focused on the occurrence and distribution of aphid transmitted viruses on various raspberry cultivars in Norway. The results consistently identified BRNV as the most prevalent virus across all year, constituting 93% of total infected samples. Notably, BRNV was most common as a single infection, followed by mixed infection with RLMV, which is the second most prevalent virus. Other viruses like RVCV and RYNV were considerably less common. Observation revealed distinct mosaic patterns and vein clearing symptoms with BRNV single infection that intensified in co-infections with other viruses. This information could assist farmers in early detection of viral infections.

Virus identification in aphid samples and transmission experiments further elucidated the dynamics of BRNV with aphids. *A. idaei* demonstrated the ability to acquire BRNV within an hour but did not transmit it, in contrast to *Am. idaei*, which rapidly acquired and transmitted the virus within the same timeframe. These findings highlight the intricate nature of aphid-virus interactions and emphasize the urgent need for effective management practices. The observed infection rates across different cultivars underscore the necessity for enhanced surveillance and the adoption of virus-free plant materials as a crucial management strategy. Our study lays a foundation for future research and development of integrated control measures, ensuring the sustainability of raspberry production in the face of evolving viral threats and changing climatic conditions.

Data availability statement

The datasets presented in this study can be found in online repositories. The names of the repository/repositories and accession number(s) can be found in the article/Supplementary Material.

Ethics statement

The manuscript presents research on animals that do not require ethical approval for their study.

Author contributions

BS: Data curation, Formal analysis, Investigation, Methodology, Validation, Visualization, Writing – original draft, Writing – review & editing, Software. NT: Investigation, Writing – original draft, Writing – review & editing, Supervision. JF: Writing – original draft, Writing – review & editing, Funding acquisition, Project administration. IK: Funding acquisition, Writing – original draft, Writing – review & editing, Software. D-RB: Funding acquisition, Writing – original draft, Writing – review & editing, Conceptualization, Investigation, Project administration, Supervision. ZH: Conceptualization, Funding acquisition, Investigation, Project administration, Supervision, Writing – original draft, Writing – review & editing, Data curation, Formal analysis, Methodology, Resources, Validation, Visualization, Software.

Funding

The author(s) declare financial support was received for the research, authorship, and/or publication of this article. The research leading to these results has received funding from the EEA Grants and the Technology Agency of the Czech Republic within the KAPPA Programme (TO01000295). The Norwegian Institute of Bioeconomy Research (NIBIO) also received funding from the Research Council of Norway (Contract No. 342631/L10). Additional support was also obtained from the Czech Academy of Sciences (RVO60077344).

Acknowledgments

The authors would like to thank extension officers from Norwegian Agriculture Extension Service (Norsk Landbruksrådgiving SA, NLR) for sample collections. We also thank Dr. Stuart MacFarlane from James Hutton Institute for providing the source of positive controls grown within NIBIO´s greenhouse facilities.

Conflict of interest

The authors declare that the research was conducted in the absence of any commercial or financial relationships that could be construed as a potential conflict of interest.

Publisher's note

All claims expressed in this article are solely those of the authors and do not necessarily represent those of their affiliated organizations, or those of the publisher, the editors and the reviewers. Any product that may be evaluated in this article, or claim that may be made by its manufacturer, is not guaranteed or endorsed by the publisher.

Supplementary material

The Supplementary Material for this article can be found online at: https://www.frontiersin.org/articles/10.3389/fpls.2024.1441145/full#supplementary-material

References

Abhinash, B., Shreya, K., Markad Ajinkya, B., Meenakshi, R., and Seweta, S. (2023). Mechanism of arthropod-mediated transmission of plant viruses - A review. *J. Advanced Zoology* 44, 38–52. doi: 10.17762/jaz.v44is6.1960

Alford, D. V. (2007). *Pests of fruit crops: a color handbook* (London, UK: Elsevier).

Bettoni, J. C., Wang, M. R., Li, J. W., Fan, X., Fazio, G., Hurtado-Gonzales, O. P., et al. (2024). Application of biotechniques for *in vitro* virus and viroid elimination in pome fruit crops. *Phytopathology* 114, 930–954. doi: 10.1094/PHYTO-07-23-0232-KC

Blackman, R., Eastop, V., and Hills, M. (1977). Morphological and cytological separation of Amphorophora Buckton (Homoptera: Aphididae) feeding on European raspberry and blackberry (Rubus spp.). *Bull. Entomological Res.* 67, 285–296. doi: 10.1017/S000748530001110X

Blackman, R. L., and Eastop, V. F. (2000). Aphids on the world's crops: an identification and information guide. Second Edition. (West Sussex, England: John Wiley & Sons Ltd). 466 pp.

Börner, C. (1939). Neue Gattungen und Arten der mitteleuropäischen Aphidenfauna. *Arbeiten über physiologische und angewandte Entomologie aus Berlin-Dahlem* 6 (1), 75-83.

Bøthun, M., and Heiberg, N. (2004). Satsing på økologisk bringebær (Production of organic raspberries in Norway). *Norsk Frukt og bær* 7, 16–18.

Converse, R. H. (1963). Influence of heat-labile components of the raspberry mosaic complex on growth and yield of red raspberries. *Phytopathology* 53, 1.

Converse, R. H. (1987). Virus diseases of small fruits. USDA Agricultural Handbook No 631. 277 ss. Washington D.C., USA.

Dietzgen, R., Mann, K., and Johnson, K. (2016). Plant virus–insect vector interactions: current and potential future research directions. *Viruses* 8, 303. doi: 10.3390/v8110303

FAO (2022). *FAOSTAT statistical database* (Rome: Food and Agriculture Organisation of the United Nations).

Folmer, O., Black, M., Hoeh, W., Lutz, R., and Vrijenhoek, R. (1994). DNA primers for amplification of mitochondrial cytochrome C oxidase subunit I from diverse metazoan invertebrates. *Mol. Mar. Biol. Biotechno.* 3 (5), 294–9.

Fotirić Akšić, M., Nešović, M., Ćirić, I., Tešić, Ž., Pezo, L., Tosti, T., et al. (2022). Chemical fruit profiles of different raspberry cultivars grown in specific Norwegian agroclimatic conditions. *Horticulturae* 8, 765. doi: 10.3390/horticulturae8090765

Freeman, J., and Stace-Smith, R. (1970). Effects of raspberry mosaic viruses on yield and growth of red raspberries. *Can. J. Plant Sci.* 50, 521–527. doi: 10.4141/cjps70-099

Gordon, S., Woodford, J., and Birch, A. (1997). Arthropod pests of Rubus in Europe: pest status, current and future control strategies. *J. Hortic. Sci.* 72, 831–862. doi: 10.1080/14620316.1997.11515577

Haffner, K., Rosenfeld, H. J., Skrede, G., and Wang, L. (2002). Quality of red raspberry *Rubus idaeus* L. cultivars after storage in controlled and normal atmospheres. *Postharvest Biol. Technol.* 24, 279–289. doi: 10.1016/S0925-5214(01)00147-8

Halgren, A., Tzanetakis, I. E., and Martin, R. R. (2007). Identification, Characterization, and Detection of Black raspberry necrosis virus. *Phytopathology®* 97, 44–50. doi: 10.1094/phyto-97-0044

Heiberg, N., Standal, R., and Måge, F. (2002). Evaluation of red raspberry cultivars in Norway. *Acta Hortic*. 585, 199-202. doi: 10.17660/ActaHortic.2002.585.31

Jones, A., and Jennings, D. (1980). Genetic control of the reactions of raspberry to black raspberry necrosis, raspberry leaf mottle and raspberry leaf spot viruses. *Ann. Appl. Biol.* 96, 59–65. doi: 10.1111/j.1744-7348.1980.tb04769.x

Jones, A. T., McGavin, W. J., Geering, A. D. W., and Lockhart, B. E. L. (2002). Identification of Rubus yellow net virus as a distinct badnavirus and its detection by PCR in *Rubus* species and in aphids. *Ann. Appl. Biol.* 141, 1–10. doi: 10.1111/j.1744-7348.2002.tb00189.x

Jones, S., McGavin, W., and MacFarlane, S. (2019). The complete sequences of two divergent variants of the rhabdovirus raspberry vein chlorosis virus and the design of improved primers for virus detection. *Virus Res.* 265, 162–165. doi: 10.1016/j.virusres.2019.03.004

Koloniuk, I., Fránová, J., Přibylová, J., Sarkisova, T., Špak, J., Tan, J. L., et al. (2023). Molecular characterization of a novel enamovirus infecting raspberry. *Viruses* 15, 2281. doi: 10.3390/v15122281

Lenz, O., Koloniuk, I., Sarkisová, T., Čmejla, R., Valentová, L., Rejlová, M., et al. (2024). Molecular characterization of a novel rubodvirus infecting raspberries. *Viruses* 16, 1074. doi: 10.3390/v16071074

Lightle, D. M., Dossett, M., Backus, E. A., and Lee, J. C. (2012). Location of the mechanism of resistance to Amphorophora agathonica (Hemiptera: Aphididae) in red raspberry. *J. Economic Entomology* 105, 1465–1470. doi: 10.1603/ec11405

Martin, R. R., MacFarlane, S., Sabanadzovic, S., Quito, D., Poudel, B., and Tzanetakis, I. E. (2013). Viruses and virus diseases of *Rubus*. *Plant Dis.* 97, 168–182. doi: 10.1094/PDIS-04-12-0362-FE

McGavin, W., McMenemy, L., and MacFarlane, S. (2010). The complete sequence of a UK strain of black raspberry necrosis virus. *Arch. Virol.* 155, 1897–1899. doi: 10.1007/s00705-010-0807-9

McMenemy, L. S., Hartley, S. E., MacFarlane, S. A., Karley, A. J., Shepherd, T., and Johnson, S. N. (2012). Raspberry viruses manipulate the behaviour of their insect vectors. *Entomologia Experimentalis Applicata* 144, 56–68. doi: 10.1111/j.1570-7458.2012.01248.x

McMenemy, L. S., Mitchell, C., and Johnson, S. N. (2009).). Biology of the European large raspberry aphid, *Amphorophora idaei:* its role in virus transmission and resistance breakdown in red raspberry. *Agric. For. Entomology* 11, 61–71. doi: 10.1111/j.1461-9563.2008.00409.x

Menzel, W., Jelkmann, W., and Maiss, E. (2002). Detection of four apple viruses by multiplex RT-PCR assays with coamplification of plant mRNA as internal control. *J. Virological Methods* 99, 81–92. doi: 10.1016/S0166-0934(01)00381-0

Stace-Smith, R. (1955a). Studies on rubus virus diseases in British Columbia: i. rubus yellow-net. *Can. J. Bot.* 33, 269–274. doi: 10.1139/b55-020

Stace-Smith, R. (1955b). Studies on Rubus Virus Diseases in British Columbia: II. Black raspberry necrosis. *Can. J. Bot.* 33, 314–322. doi: 10.1139/b55-027

Stace-Smith, R. (1961). Studies on rubus virus diseases in British Columbia: vii. raspberry vein chlorosis. *Can. J. Bot.* 39, 559–565. doi: 10.1139/b61-045

Susi, H., Rajamäki, M. L., Artola, K., Jayaraj-Mallika, F. R., and Valkonen, J. P. T. (2018). Molecular detection and characterisation of black raspberry necrosis virus and raspberry bushy dwarf virus isolates in wild raspberries. *Ann. Appl. Biol.* 173, 97–111. doi: 10.1111/aab.12438

Tan, J. L., Trandem, N., Fránová, J., Hamborg, Z., Blystad, D.-R., and Zemek, R. (2022). Known and potential invertebrate vectors of raspberry viruses. *Viruses* 14, 571. doi: 10.3390/v14030571

Tatineni, S., and Hein, G. L. (2023). Plant viruses of agricultural importance: current and future perspectives of virus disease management strategies. *Phytopathology®* 113, 117–141. doi: 10.1094/phyto-05-22-0167-rvw

Trandem, N., Eklo, T., and Vintland, A. (2015). Stor bringebærbladlus (Amphorophora idaei) oppdaget i 'Glen Ample'. (Large European raspberry aphid discovered in 'Glen Ample'). Norsk Frukt og Bær 18, 13.

Tzanetakis, I. E., Halgren, A., Mosier, N., and Martin, R. R. (2007). Identification and characterization of Raspberry mottle virus, a novel member of the Closteroviridae. *Virus Res.* 127, 26–33. doi: 10.1016/j.virusres.2007.03.010

Wang, M. R., Bi, W. L., Bettoni, J. C., Zhang, D., Volk, G. M., and Wang, Q. C. (2022a). Shoot tip cryotherapy for plant pathogen eradication. *Plant Pathol.* 71, 1241–1254. doi: 10.1111/ppa.13565

Wang, M. R., Hamborg, Z., Ma, X. Y., Blystad, D. R., and Wang, Q. C. (2022b). Double-edged effects of the cryogenic technique for virus eradication and preservation in shallot shoot tips. *Plant Pathol.* 71, 494–504. doi: 10.1111/ppa.13466

frontiers | Frontiers in Plant Science

TYPE Methods
PUBLISHED 21 November 2024
DOI 10.3389/fpls.2024.1443815

OPEN ACCESS

EDITED BY
Chellappan Padmanabhan,
USDA APHIS PPQ Science and Technology, United States

REVIEWED BY
Dongmei Chen,
Hangzhou Dianzi University, China
Md Ashraful Haque,
Indian Council of Agricultural Research (ICAR), India
Shivaranjani Baruah,
Cornell University, in collaboration with reviewer KG

*CORRESPONDENCE
Kun Liang
liangkun@tust.edu.cn

RECEIVED 04 June 2024
ACCEPTED 17 October 2024
PUBLISHED 21 November 2024

CITATION
Zhang X, Liang K and Zhang Y (2024) Plant pest and disease lightweight identification model by fusing tensor features and knowledge distillation.
Front. Plant Sci. 15:1443815.
doi: 10.3389/fpls.2024.1443815

Plant pest and disease lightweight identification model by fusing tensor features and knowledge distillation

Xiaoli Zhang, Kun Liang* and Yiying Zhang

College of Artificial Intelligence, Tianjin University of Science & Technology, Tianjin, China

Plant pest and disease management is an important factor affecting the yield and quality of crops, and due to the rich variety and the diagnosis process mostly relying on experts' experience, there are problems of low diagnosis efficiency and accuracy. For this, we proposed a Plant pest and Disease Lightweight identification Model by fusing Tensor features and Knowledge distillation (PDLM-TK). First, a Lightweight Residual Blocks based on Spatial Tensor (LRB-ST) is constructed to enhance the perception and extraction of shallow detail features of plant images by introducing spatial tensor. And the depth separable convolution is used to reduce the number of model parameters to improve the diagnosis efficiency. Secondly, a Branch Network Fusion with Graph Convolutional features (BNF-GC) is proposed to realize image super-pixel segmentation by using spanning tree clustering based on pixel features. And the graph convolution neural network is utilized to extract the correlation features to improve the diagnosis accuracy. Finally, we designed a Model Training Strategy based on knowledge Distillation (MTS-KD) to train the pest and disease diagnosis model by building a knowledge migration architecture, which fully balances the accuracy and diagnosis efficiency of the model. The experimental results show that PDLM-TK performs well in three plant pest and disease datasets such as Plant Village, with the highest classification accuracy and F1 score of 96.19% and 94.94%. Moreover, the model execution efficiency performs better compared to lightweight methods such as MobileViT, which can quickly and accurately diagnose plant diseases.

KEYWORDS

image classification, spatial tensor, knowledge distillation, light weighting, graph convolutional neural networks

1 Introduction

The variety of crops grown in countries around the world is large and intensive, and according to the world food and agriculture statistical yearbook released by the Food and Agriculture Organization of the United Nations (FAO) in 2023, the global agricultural economy reached $3.7 trillion and employed a population of approximately 873 million people, which accounts for 27% of the global labor force (FAO, 2023). On average, more than 40% of natural losses in agricultural production are caused by plant pests and diseases each year, resulting in a global economic loss of more than 220 billion dollars (FAO, 2022). Thus, once a crop is infested with pests and diseases, it is very easy to cause widespread infection of crops, which seriously affects crop yields and restricts the development of agricultural productivity. However, traditional identification of plant pests and diseases is usually done by experienced plant pathologists or farmers to diagnose the type of leaf pests and diseases. This not only requires a lot of time and effort, but also the process is subjective and limited, which makes it difficult to accurately determine the type of disease and thus leads to the aggravation of plant pests and diseases (Sajitha et al., 2024). Therefore, how to quickly and accurately identify the types of plant pests and diseases is the crucial to ensure the safety and stability of agricultural production, and its research has important theoretical significance and application value.

With the continuous development of smart agriculture and artificial intelligence technology, scholars combined with computer vision related theories to carry out research on plant pest and disease recognition methods. Especially, the research on intelligent plant image recognition based on machine vision and deep learning has achieved better practical results (Rimal et al., 2023). Machine vision methods usually use traditional image processing algorithms or manually designed feature classifiers, which mainly rely on the distinguishing features of different pests and diseases to design the recognition scheme, and are widely used in crop pest detection and classification (Thakuria et al., 2023). However, plant images collected in the natural environment are easily interfered by factors such as light in the environment, which leads to errors in the detection results and inaccurate classification (Zheng and Zhang, 2022). At the same time, with the increasing variety of plant diseases, it is difficult to construct suitable classifiers to distinguish approximate representations by means of manual feature selection. Therefore, traditional machine vision-based pest and disease detection methods are difficult to achieve effective recognition results (Ali et al., 2024). With the continuous development of deep learning in recent years, network models represented by multilayer convolutional neural network (CNN) and attention mechanism have achieved effective results in plant pest and disease recognition (Math and Dharwadkar, 2022). Deep learning based plant pest and disease recognition technique is automated to extract global and contextual features of pest and disease images compared to traditional recognition methods mainly using supervised learning (Roxa et al., 2023). It avoids manual selection of features but extracts richer feature information through autonomous learning, which can cope with diverse crop environments (Sharma et al., 2022). And it can handle massive image data with strong robustness and high accuracy (Shamsul Kamar et al., 2023). In order to further improve the accuracy and training efficiency of the model, techniques such as KD and migration learning are usually combined to fine-tune the parameters of the model to achieve knowledge migration (Khan et al., 2022). Although the above methods can effectively promote the construction of smart agriculture, with the increasing types of plant pests and diseases, as well as the limitations of hardware equipment in the actual application scenarios, there are still some problems that affect the efficiency and accuracy of plant pests and diseases recognition (Manavalan, 2022). 1) The complex structure and large number of parameters of the deep neural network greatly affect the recognition efficiency of the model. 2) The lightweight network model is difficult to mine and fuse the key features, which leads to information loss and thus reduces the accuracy of the model. To address the above problems, we proposed a Plant pest and Disease Lightweight identification Model by fusing Tensor features and Knowledge distillation (MTS-KD) to realize accurate and efficient diagnosis of multiple plant pests and diseases. The specific contributions are as follows.

- Constructed Lightweight Residual Blocks based on Spatial Tensor (LRB-ST). Enhanced the perception and extraction of shallow detail features of plant images by introducing spatial tensor, and reduced the number of model parameters by using depth-separable convolution to improve the diagnostic efficiency.
- Proposed Branch Network Fusion with Graph Convolutional features (BNF-GC). The image super-pixel segmentation was realized by using spanning tree clustering based on pixel features, and the graph convolution neural network was used to extract correlation features to improve the diagnostic accuracy.
- Designed Model Training Strategy based on Knowledge Distillation (MTS-KD). Train the pest and disease diagnosed model by building a knowledge migration architecture, fully balancing the accuracy of the model with the diagnosis efficiency.

The sections of this paper are organized as follows, section 2 focus on introducing and analyzing the current research related to plant pest and disease diagnosis. Section 3 focus on the method proposed in this paper. Section 4 describes the qualitative and quantitative analysis of this paper's method with other image classification methods to verify the accuracy of the method for plant pest and disease diagnosis. Section 5 discusses the convergence of the method and the configuration of each module to fully justify the method in terms of model construction and parameter selection. Finally, section 6 gives a summary and future research.

2 Related work

In order to fully utilize computer or artificial intelligence techniques to assist in pest control, machine learning and deep learning based methods have been proposed for plant image

recognition (Cetiner, 2022). While improving the accuracy of more plant pest and disease recognition, it also focuses on lightweight design to improve the diagnostic efficiency. It effectively solves the problem that traditional crop pest and disease image recognition methods rely heavily on manual feature extraction and have poor generalization ability for image recognition in complex backgrounds (Rustia et al., 2022).

The application of machine learning in pest recognition has significantly enhanced the efficiency of pest control. Zhao et al. (2022) and Johari et al. (2022) proposed a multi-step plant adversity recognition method based on hyperspectral imaging and continuous wavelet analysis, used k-mean clustering and support vector machine algorithms to detect abnormal regions of tea tree leaves, and used the random forest algorithm to construct the tea tree discriminant model. Motie et al. (2023) extracted and analyzed spectral vegetation features and used support vector machine (SVM) to classify wheat diseased plants. Bhandari et al. (2023) implemented EfficientNetB5 with a tomato leaf disease (TLD) dataset without any segmentation, and the model achieved high accuracy. Catalkaya et al. (2024) established a KASP (Kompetitive Allele-Specific PCR) analysis method for plant pest identification by designing two forward primers and one reverse primer to enhance the identification accuracy of the algorithm. Pansy and Murali (2023) proposed an unmanned aerial imaging remote sensor for spatio-temporal resolution identification of mango pests and diseases using fuzzy C-mean clustering for diseased leaves and pests, respectively. Despite the deep mining of plant image features, to further enhance the recognition and accuracy, Aldakheel et al. (2024) and Subbaian et al. (2024) applied the YOLOv4 algorithm to plant leaf disease detection. And data enhancement techniques such as histogram equalization and level flipping were used to improve the dataset and effectively enhance the accuracy of plant image disease classification. Zhu et al., 2023 proposed a data evaluation method based on martingale distance and entropy to address the problem of lack of labeling data in intelligent pest identification. This method can filter high value data, thus achieving effective pest recognition performance with small data size. Chodey and Shariff (2023) proposed a Self-Improving Tephritid Swarm Optimization Algorithm (SITSA) to train a pest detection model by selecting the optimal weights and designing a grey scale covariance matrix based feature extraction method to segment the image. Nandhini and Brindha (2024) proposed a new data enhancement technique and feature fusion technique that fuses multi-scale features from global feature extraction network and visual regeneration network to improve accuracy as well as robustness. Although the efficiency of plant pest and disease recognition has been substantially improved, the recognition effect still needs to be improved. This is due to the fact that traditional machine learning methods usually need to select features manually, and their feature representation capability is relatively limited to fully capture the complex structure and information in the image.

Deep learning currently possesses robust feature representation capabilities, enabling it to automatically extract essential semantic information from plant disease and pest images. Li et al. (2024) proposed an interactive bilinear Transformer network, which utilizes fine-grained recognition techniques to realize the types of garden plant diseases. Xia et al. (2023) and Zhang et al. (2023) proposed a pest classification method based on Convolutional Neural Network (CNN) and improved Vision Transformer model, which extracts the features of the objects at different scales and fine-grains, to address the problems of low efficiency of pest classification methods, which are not adapted to large-scale environments. Wei et al. (2022) proposed a multi-scale feature fusion based crop pest classification method (MFFNet), which obtains the deep feature information of pest images through multiple convolutional operations to accurately recognize and classify crop pests. Liu et al. (2024) and Yu et al. (2022) proposed a plant pest type recognition method based on YOLOv5 by introducing modules such as hierarchical classification and attention mechanism, respectively, which effectively avoided the problems of time-consuming, laborious, and inaccurate manual classification. Xiao et al. (2022), on the other hand, combined hyperspectral imaging with deep learning, which designed a spectral feature extraction module through one-dimensional convolution and attention mechanism between spectral channels, effectively utilizing spectral information to improve detection accuracy. On this basis, Cheng et al. (2022) used to recognize the category of tomato diseases in images by fine-tuning the pre-trained model. Qiang et al. (2023) proposed a dual backbone network based pest detection method for citrus leaves in response to the problem that pests on the surface of plants are difficult to distinguish due to their small size and camouflage, which utilizes a single-shot multi-box detector improved by a dual backbone network to enhance the detection accuracy. Dai et al. (2024) and Li et al. (2024) proposed similar deep information feature fusion networks extracting and fusing relevant features from different network layers, respectively, while fusing contextual information at different scales using pyramid-squeezed attention (PSA) to produce better pixel-level attention for improved localization of plant disease areas. Ishengoma et al. (2022) proposed a hybrid convolutional neural network (CNN) model. It was also combined with Unmanned Aerial Vehicle (UAV) technology to build a parallel architecture using two separate models (i.e., VGG 16 and InceptionV3) to realize the identification of plant diseases in large areas. Shafik et al. (2023) proposed an enhanced Convolutional Neural Network (CNN) along the use of Long Short Term Memory (LSTM) using Majority Voting Integrated Classifier for plant disease and pest recognition.

Plant pest and disease identification methods based on artificial intelligence not only enhance the accuracy of disease type identification but also advance agricultural automation and intelligence, helping to mitigate losses caused by pests and diseases. Machine learning-based methods struggle to efficiently extract potential critical features and often require substantial manual labeling efforts. Although deep neural network architectures improve accuracy, they significantly increase model complexity, presenting challenges in parameter training and practical deployment (Li et al., 2023). This complexity results in longer training times and demands greater computational resources, limiting recognition efficiency, particularly in real-time applications. Additionally, the intricacies of hyperparameter tuning and the risk of overfitting pose significant obstacles for practitioners, especially in resource-constrained environments. Although lightweight network

models have been proposed to address these issues, fewer parameters often struggle to capture key features in large image datasets. Additionally, noise and other interference present in the images are challenging to filter effectively. These disturbances can obscure important features that are critical for accurate identification of plant pests and diseases. Therefore, how to balance the accuracy and efficiency of plant pest and disease diagnosis methods remains to be solved.

3 Methodology

3.1 Model framework

In order to improve the efficiency and accuracy of plant pest and disease diagnosis, we constructed a classification model applied to plant pest and disease diagnosis based on a deep learning network architecture, combined with model compression and training methods to achieve accurate identification of various categories of plant pest and disease classes.

The PDLM-TK model comprises three primary components, as shown in Figure 1. First, a Lightweight Residual Blocks based on Spatial Tensor (LRB-ST) network is designed, which integrates multiple spatial tensors to extract semantic information from plant disease images progressively, from the initial to the final layers. The input plant disease and pest images undergo initial downsampling, followed by four sequential layers of LRB-ST, to capture advanced semantic information about the disease. Next, the Branch Network Fusion with Graph Convolutional features (BNF-GC) is introduced to deeply mine and fuse different levels of residual block features using graph convolution. BNF-GC applies a graph convolutional neural network to the output of each LRB-ST layer, focusing on localized pest and disease information to guide classification. Finally, a Model Training Strategy based on Knowledge Distillation (MTS-KD) is implemented. This strategy utilizes the plant pest and disease dataset to train a teacher network, enabling knowledge transfer to the student network. KD is performed during the student network's training using the target dataset.

The number of network layers and parameters of PDLM-TK are presented in Table 1. PDLM-TK primarily consists of four LRB-STs and BNF-GC as the main feature extraction structure, with a fully connected multi-classification network appended at the end for pest and disease type recognition. Among these, LRB-ST is primarily responsible for extracting key features from pest and disease images, while BNF-GC focuses on mining the correlation features between image regions, thereby achieving a balance between global and local image features. Plant pest and disease images are downsampled through preliminary convolution and pooling layers. Subsequently, feature maps at various levels are deeply mined by LRB-ST and BNF-GC, respectively. It is important to note that LRB-ST utilizes Depth-Separable Convolution (DSC), whereas BNF-GC performs feature extraction using Graph Convolution Network (GCN). The number of output feature map channels for each LRB-ST corresponds to the output feature vector size of BNF-GC. MTS-KD, in turn, is based on PDLM-TK, which serves as the student network for knowledge distillation. The remaining sections of this chapter provide a detailed description of each of these modules.

3.2 Lightweight residual blocks based on spatial tensor

With the continuous stacking of network layers, the high-level semantic features embedded in images are continuously mined and acquired, but the shallow image semantic features are also easily lost. These features play a crucial role in constructing more complex representations, especially in plant pest and disease recognition, where the texture of some leaves and the color change of damaged areas have a great impact on the final classification results. The residual network enhances the model's perception of small changes

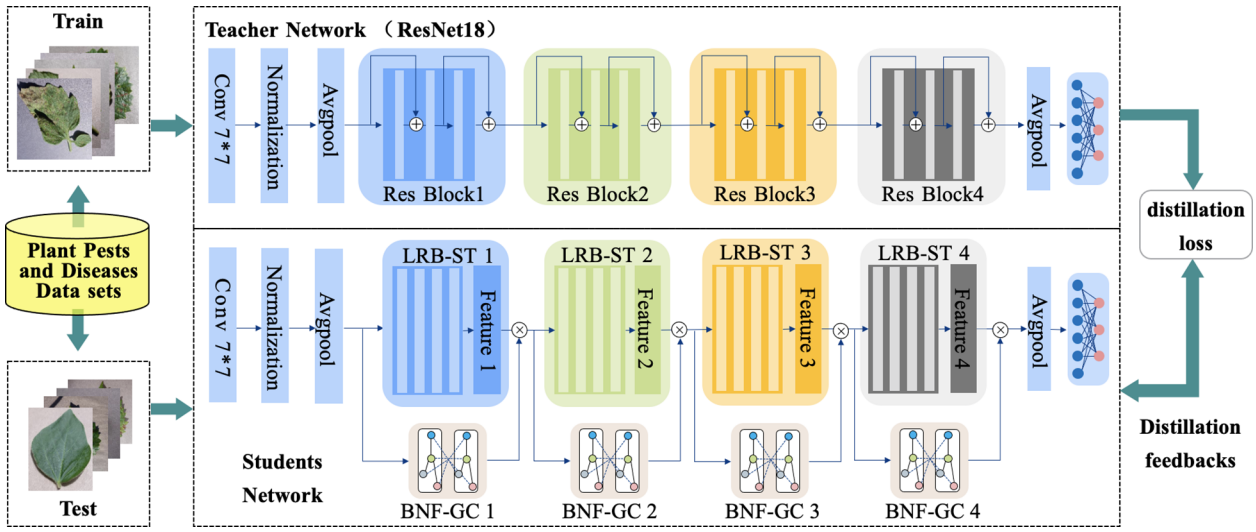

FIGURE 1
General framework diagram of PDLM-TK.

TABLE 1 Network layers and parameters of PDLM-TK.

Layer Name	Conv_1	LRB-ST _1	LRB-ST _2	LRB-ST _3	LRB-ST _4	Conv_2
		BNF-GC_1	BNF-GC _2	BNF-GC _3	BNF-GC _4	
Output Size	112*112	56*56	28*28	14*14	7*7	1*1
		64	128	256	512	
Structure	7*7, 64, stride 2, 3*3, maxpool, stride 2	$\begin{Bmatrix} 3\star3,\ 64 \\ 3\star3,\ 64 \end{Bmatrix}\star2$	$\begin{Bmatrix} 3\star3,\ 128 \\ 3\star3,\ 128 \end{Bmatrix}\star2$	$\begin{Bmatrix} 3\star3,\ 256 \\ 3\star3,\ 256 \end{Bmatrix}\star2$	$\begin{Bmatrix} 3\star3,\ 512 \\ 3\star3,\ 512 \end{Bmatrix}\star2$	average, 512, softmax
		(4,25,32)	(4,16,32)	(4,9,32)	(4,4,32)	
Params[K]	9.41	31.97	90.15	225.09	1,120	494

The bolded text represents the type and the values represent the best results.

in the input image more effectively by enhancing the underlying semantics. Aiming at the problem that it is difficult to effectively capture and transfer feature information of different dimensions in residual networks, we propose LRB-ST. The principle is shown in Figure 2. The semantic information of different dimensions in the input feature graph is mined by defining a trainable spatial tensor. And it is fused with the underlying data as a way to enhance the feature mining ability of the classification model. Meanwhile, in order to improve the classification efficiency of the model, Depthwise Separable Convolution (DSC) is used to replace the traditional convolution operation to reduce the number of model parameters. The specific steps are as follows.

Firstly, the spatial tensor P_{xy} is defined to extract the residual block features. For the input layer i feature block $Block_i$, the spatial tensor P_{xy} is defined according to its input size, which is fused by multiplying with the feature maps of each channel of $Block_i$ on the original residual connection. The computational procedure is shown in Equation 1. Where DSW represents the depth separable convolution and σ represents the normalization and activation operation on the features.

$$Block_i' = \sigma(DSW(Block_i)) + P_{xy} * Block_i \quad (1)$$

Secondly, depth-separable convolution is used to reduce the number of parameters. Feature extraction is achieved by depth convolution and pointwise convolution, and the input block feature $Block_i$ is stacked with the feature fusion result in Equation 1 on an element-by-element basis to obtain the fused feature $Block_i'$ after two depth-separable convolutions and normalized activation. After that, the feature $Block_{i+1}$ of the residual block is output through the same two depth-separable convolution and used for the calculation of the next residual block. As shown in Equation 2.

$$Block_{i+1} = Block_i' + \sigma(DSW(Block_i')) \quad (2)$$

The overall structure of the LRB-ST is depicted in Figure 2, comprising two feature superposition processes and one downsampling operation. This study adopts the ResNet18 architecture to facilitate the deep feature extraction of plant pest and disease image data by superimposing four LRB-STs as the backbone network. This approach enables the model to focus on features across different levels while ensuring the effective transmission of deep semantic information. Furthermore, it effectively reduces the number of model parameters, thereby enhancing the classification efficiency of model.

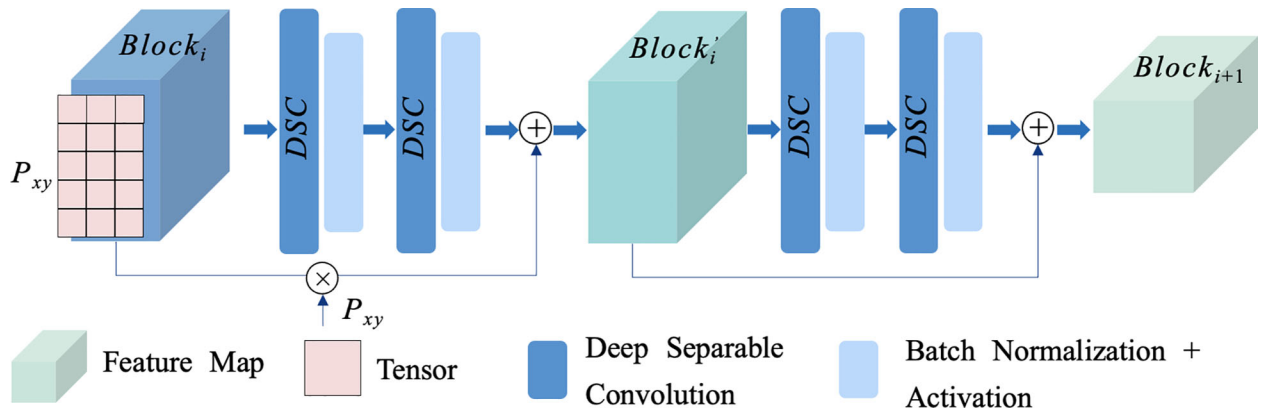

FIGURE 2
Schematic diagram of LRB-ST.

3.3 Branch network fusion with graph convolutional features

Since there are factors such as background and noise in the plant image data besides the target region, and the use of deep learning-based classification model can extract key features, but it is still difficult to avoid interference by redundant information, which in turn affects the results of plant pest and disease diagnosis. In order to improve the robustness of the model and mine the correlation features of different regions in the image, we propose BNF-GC, the principle of which is shown in Figure 3.

BNF-GC mainly uses super-pixel segmentation to effectively reduce image complexity and extract potential regional features, which can effectively improve the classification performance of the model. Meanwhile, the graph convolutional neural network is used to mine the intrinsic correlation of different regions, which further improves the accuracy of pest and disease diagnosis.

Step1: Construct plant disease image spanning tree $ST(v, e, w)$. Map the plant image feature data into an undirected graph G and represent it as $G = (V, E)$. Where each pixel point represents a node in the undirected graph and two neighboring pixel points form an edge $e(v_i, v_j)$. Where the weights w of the edges are jointly determined by the coordinates $v_i(x_i, y_i)$ and pixel values p_i of the pixel points. The distance between nodes is normalized according to the size of the image $M \times N$ and fused with the normalized pixel value features as the weight of each node pixel. The calculation process is shown in Equation 3.

$$w = \sqrt{[(x_i - x_j)^2 + (y_i - y_j)^2]/(M^2 + N^2)} + p_i/255 \tag{3}$$

Step2: Aggregate the nodes in the region to form a super-pixel segmented image. The nodes are aggregated to form different segmentation regions R according to the minimum spanning tree method. The maximum weight $Max(w_i)$ on the minimum spanning tree in a segmented region indicates the degree of intra-class variation of its internal nodes, while the minimum weight $Min(w_i)$ between different regions represents its inter-class variation. Therefore, the regions that meet the condition $Max(w_i) \le Min(w_i)$ are merged, after which the inter and intra-class differences are re-compared until the expected number of segmented regions is reached and then stopped, and finally the plant pest image $Seg(R_1, R_2, R_3, \cdots R_n)$ containing multiple aggregated regions is obtained. The calculation process is shown in Equation 4.

$$Seg(R_i) = \begin{cases} \sum_{i \in R} R_i(w_i) & Max(w_i) \le Min(w_i) \\ R_i(w_i) & other \end{cases} \tag{4}$$

Step3: Calculate the feature terms of each segmentation region of the superpixel map $Seg(s_1, s_2, s_3, \cdots s_n)$. Since the image in each segmentation region contains rich semantic information, this paper selects the pixel mean value p_i, the region center coordinate (cx_i, cy_i) and the number of included pixel points c_i in the segmentation region as the superpixel point feature $s_i(p_i, cx_i, cy_i, c_i)$ of each segmentation region. And the feature values of each region are normalized for subsequent feature mining respectively. The calculation process is shown in Equations 5–7.

$$p_i = \frac{1}{n}\sum_{j=0}^{n} p_j \quad j \in R_i \tag{5}$$

$$(cx_i, cy_i) = \left(\frac{1}{m}\sum_{i=0}^{m} c_i, \frac{1}{n}\sum_{i=0}^{n} cy_i\right) \quad m, n \in R_i \tag{6}$$

$$c_i = count(R_i) \tag{7}$$

Step4: Construct graph convolutional neural network GCN to mine local correlation information. According to the dimension of

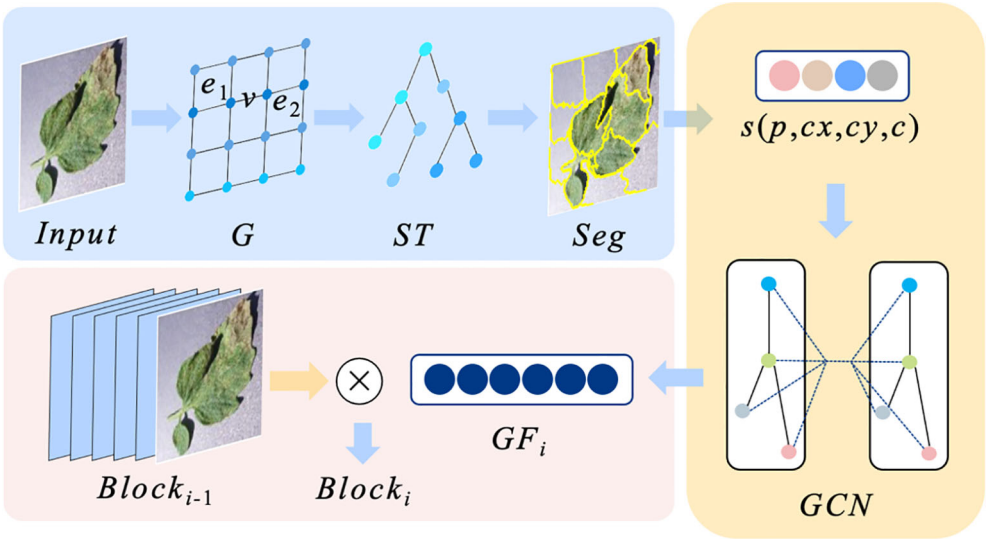

FIGURE 3
Schematic diagram of BNF-GC.

image features in the segmented region, construct the graph convolution neural network GCN_i corresponding to the ith residual block, and then mine the regional correlation through multi-layer graph convolution computation to get the feature vector GF_i. Finally, the correlation features are multiplied with the output feature map $Block_{i-1}$ of the previous residual block to generate the fusion $Block_i$, which is used for the feature computation of the next residual block. The computation process is shown in Equations 8 and 9.

$$GF_i = GCN_i(s_i) \tag{8}$$

$$Block_i = Block_{i-1} * GF_i \tag{9}$$

The BNF-GC module creates a graph convolutional network branching structure for deep mining of residual block features, which effectively realizes regional relevance feature extraction for plant pest and disease image data. The module enhances the classification performance of the model by enhancing the deep fusion of the underlying semantic information, which emphasizes the main features of the target region and effectively avoids the interference of the background and other information.

3.4 Model training strategy based on knowledge distillation

Although existing publicly available datasets contain more images of plant pests and diseases, the lightweight model proposed in this paper contains fewer parameters, which makes it difficult to capture the rich features of the dataset. Especially when the dataset is limited or noisy, it is difficult for the model to learn the implicit knowledge by using only the dataset training. In this regard, this paper proposes MTS-KD, as shown in Figure 4. The ResNet18 network is used as the backbone network of the teacher model, and the prediction results and soft labels of the teacher model are used to guide the training of the student model. This approach effectively enhances the model's learning capacity and improves its generalization ability, which helps mitigate the significant bias present in the plant dataset. As a result, the model's training efficiency is improved without compromising its high accuracy.

During the training process of the model through MTS-KD, the plant pest and disease images were first categorized according to the training set and test set. After that, they were fed into both teacher-student models for forward computation. The Softmax classification result produced by the teacher model under high temperature T is used as soft label S_L.

The student model produces the same prediction results after going through the training based on KD. In this case, the Softmax output at the same temperature T condition is L_s, while the prediction result produced at $T = 1$ is L_h. L_s in MTS-KD uses Kullback-Leibler Divergence to calculate the relative difference between the predictions of the teacher-student models. In turn, L_h uses the cross-entropy loss function to calculate the difference between the results predicted by the student model and the real pest label. Afterwards, the losses of these two components are summed up as the total model loss for optimization and training of the parameters. Where the loss function formulas for L_s and L_h are shown in Equations 10 and 11.

$$L_s = -\sum_{i=0}^{N} s_i^T \log(t_i^T) \tag{10}$$

$$L_h = -\sum_{i=0}^{N} l_i \log(t_i^1) \tag{11}$$

Where N is the number of total categories in the dataset. t_i^T refers to the value that the teacher model predicts as i after Softmax at temperature T. t_i^1 represents the true label prediction result of the teacher model at temperature 1. Similarly, s_i^T refers to the value of T predicted by the student model at temperature i, and l_i represents the value of the ith true label in the total number of categories N. The two calculations are shown in Equation 12.

$$p_i^T = \frac{\exp(P_i/T)}{\sum_N \exp(P_N/T)} \tag{12}$$

p_i^T in Equation 12 can be used to calculate the predictions for the teacher model and the student model, respectively. Therefore, the total loss L_t is defined as shown in Equation 13. Loss weights are

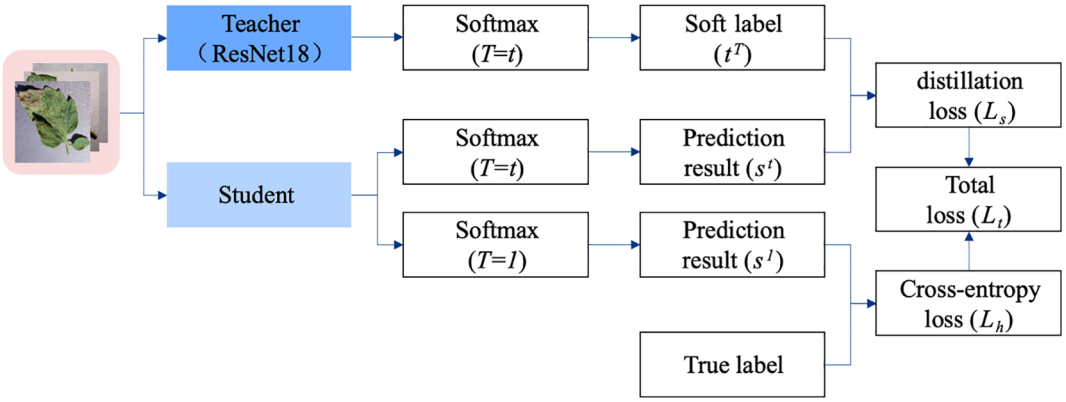

FIGURE 4
Framework diagram of MTS-KD.

employed to balance the influence between soft targets and hard targets from the teacher model during the training process of the student model. In the context of plant pest and disease identification, it is particularly important to emphasize the knowledge derived from the teacher model for training the student network. Where λ is the loss weight for student model training, and $(1-\lambda)$ is the loss weight for prediction layer distillation.

Model parameter optimization is guided by the Knowledge Distillation (KD) training strategy, which facilitates the transfer of knowledge from the teacher model to the student model. This innovative approach allows the student model to more effectively replicate the feature extraction capabilities of the teacher model, thereby enhancing its ability to grasp complex patterns and nuances in the input images. Furthermore, this knowledge transfer not only improves the classification and recognition performance of the student model but also contributes to training efficiency. When compared to training from scratch, the student model is able to converge to optimal performance levels more quickly and requires less time and resources. Consequently, the implementation of KD not only enhances the capabilities of student models but also simplifies the overall training process, establishing it as a compelling strategy for improving the effectiveness of artificial intelligence in plant pest and disease identification.

4 Experimental analysis

4.1 Experimental environment and dataset

For the configuration of the experimental environment, the input plant pest and disease image data were randomly clipped into (3, 512, 512) size inputs. The experiments are based on PyTorch 1.11.0 deep learning framework and the operating system of the experimental environment is Ubuntu 20.04. We implement the model code using Python 3.9 programming language and the GPU hardware platform is used with 2 pieces of RTX3080.Adam is chosen as the model optimizer. The batch of input images is 8 at a time. The learning rate is initially set to 0.01, and the number of iterations for model training is set to 120. All models are trained from scratch to ensure the fairness of the comparison results. The configuration of specific parameters is shown in Table 2.

To evaluate the effectiveness of the proposed method, two plant datasets, Ai Challenger (AI Challenge, 2018), Plant Village (Hughes and Salathé, 2015), and an insect dataset, IP102 (Wu et al., 2019), are selected in this paper. The Ai Challenger plant disease identification dataset is shown in Figure 5A, which includes 31,718 plant leaf images with 61 categories, including 10 species such as apple and 27 pests. Plant Village dataset is shown in Figure 5B, which is labelled by crop pathologists and contains 54309 images with 13 species and 26 crop disease categories. IP102 is a field-constructed large-scale dataset used for pest identification and is shown in Figure 5C. It has a total of 75,222 images containing 102 common pests with an average of 737 samples per class. Some images of plant pests and diseases in the three datasets are shown in Figure 5. The experimental datasets were divided according to the 8:2 training and testing sets.

4.2 Comparative models and evaluation metrics

In order to demonstrate the superiority of the proposed method, the experiment uses five lightweight classification models such as ShuffleNet-V2 (Ma et al., 2018), MobileNet-V3-Large (Howard et al., 2020), EfficientNet B1 (Tan and Le, 2019), MobileViT-S (Mehta and Rastegari, 2022) and Inception v3 (Szegedy et al., 2015) to carry out comparison experiments with PDLM-TK. Since this study belongs to the task of pest and disease image classification, the various models are quantitatively evaluated using Precision (P), Recall (R) and F1 score (F1). And the confusion matrix is drawn according to its evaluation results to visualize the correct classification of the models in each category and realize the visual evaluation of the model performance. Its calculation is shown in Equations 13–15.

$$Precision = \frac{TP}{TP + FP} \tag{13}$$

$$Recall = \frac{TP}{TP + FN} \tag{14}$$

$$F1 = \frac{2 \times Precision \times Recall}{Precision + Recall} \tag{15}$$

Where *TP* is the correct image pest category, the number of images that the model correctly predicts as positive instances. *FP* is the false positive instances of the image, the number of images that the model incorrectly categorizes as positive instances. *TN* is the number of images that the model correctly predicted as other pest and disease types. *FN* denotes the number of images that the model incorrectly predicted as other categories when categorizing the correct category.

Considering the large number of pest and disease categories in the plant and insect datasets used, in order to evaluate the

TABLE 2 Configuration table of experimental environment and parameters.

Experimental environment	Configuration	Model parameters	Configuration
GPU	RTX3080(10 GB) * 2	optimizer	Adam
OS	Ubuntu 20.04	Batch_size	8
Deep Learning Framework	PyTorch 1.11.0	lr	0.01
programming language	Python 3.9	epoch	120

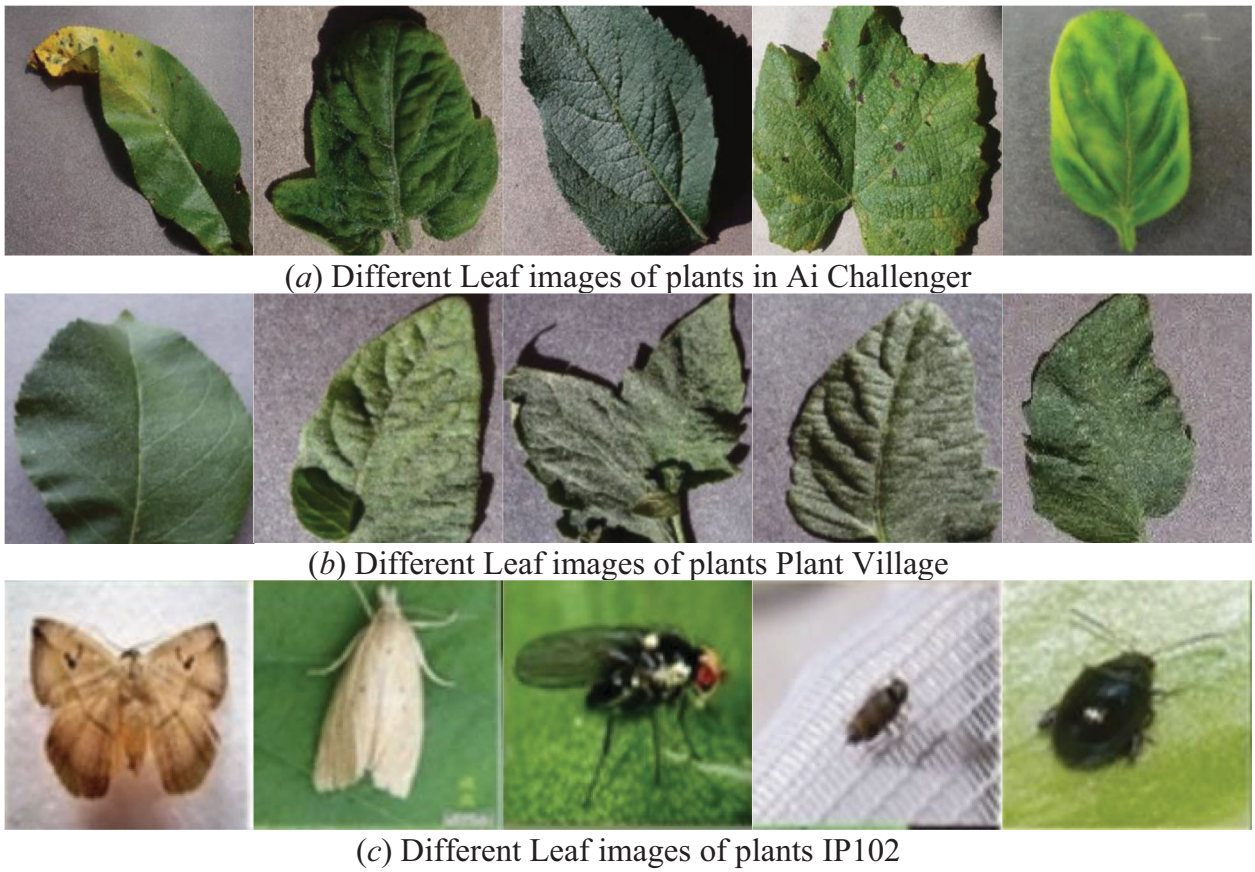

FIGURE 5
Selected images from the three datasets used for the experiment. As shown in Figures **(A, B)** are five plant leaves from the Ai Challenger and Plant Village datasets, respectively, and the five images in Figure **(C)** are plant insects from the IP102 dataset.

diagnostic performance of the proposed methods more comprehensively, the experimental evaluation was statistically analyzed using the Top1 accuracy rate (the accuracy rate of the pest category ranked No. 1 in the model diagnostic results in accordance with the actual results) and the Top5 accuracy rate, respectively.

At the same time, in order to evaluate the diagnostic efficiency of the models, the experiments not only analyzed the performance of the above six models in the three indexes of Acc, P and F1, but also evaluated the number of parameters and the amount of floating-point calculations (GFLOPs) included in the models. In general, the larger the number of parameters included in the model, the lower its training and execution efficiency, and the larger the amount of floating point calculations, the slower the model diagnosis speed.

4.3 Quantitative effectiveness evaluation of plant pest and disease diagnostics

The results of the evaluation of Top1 accuracy of six models on three plant pest and disease datasets are shown in Table 3. The comparison shows that multiple models have the best classification results on the Plant Village dataset. The reason for this is analyzed to be due to the fact that this dataset contains fewer types of pests and diseases as compared to the other two, and therefore the models classify better on this dataset with less difference in the amount of data. The PDLM-TK method achieved the best P, exceeding the best EfficientNet B1 model by 1.82%, but slightly lower in R and F1 values. This is due to the fact that the composite scaling strategy used by EfficientNet can well utilize the feature extraction ability of the convolutional layer to form a more complete deep learning model network structure. PDLM-TK performs even better on the other two datasets, exceeding the other models by an average of 2.54%, 1.22% and 1.86% on P, R and F1. The experimental results effectively demonstrate the effectiveness of the PDLM-TK method proposed in this paper in plant pest and disease diagnosis. Specifically, the method not only achieves high classification accuracy across various datasets but also showcases superior efficiency compared to traditional approaches.

In order to evaluate the comprehensive classification performance of the methods and avoid the error that exists in using only Top1 accuracy, as shown in Table 4, the evaluation results of Top5 accuracy of various models on the three plant diseases and pests datasets are shown in Table 3. According to the experimental results, it can be seen that it is in line with the Top1 accuracy assessment, and the Top5 accuracy assessment results of each model are more accurate compared to the Top1 accuracy. Meanwhile, the PDLM-TK method performed better in classifying pests and diseases on multiple datasets compared to other methods.

TABLE 3 Evaluation results of Top1 accuracy for various models.

DataSet	Metrics	Model					
		ShuffleNet-V2	MobileNet-V3-Large	EfficientNet B1	MobileViT-S	Inception v3	PDLM-TK
Ai Challenger	P	86.74	83.21	87.93	82.93	90.42	**92.64**
	R	83.12	81.13	85.10	80.79	87.51	**89.32**
	F1	84.89	82.16	86.49	81.85	88.94	**90.95**
Plant Village	P	90.13	87.20	94.36	92.12	93.62	**95.44**
	R	89.64	85.42	**92.03**	87.48	88.16	90.57
	F1	89.88	86.30	**93.18**	89.74	90.81	92.94
IP102	P	77.75	75.46	78.52	72.13	80.02	**82.87**
	R	72.61	73.60	71.37	70.03	78.46	**79.10**
	F1	75.09	74.52	74.77	71.06	79.23	**80.94**

The bolded text represents the type and the values represent the best results.

The highest P, R and F1 values were found on the Ai Challenger and IP102 datasets, and the R and F1 values on the Plant Village dataset were higher than the Inception v3 optimal model by 2% and 0.82, respectively. This shows that our proposed PDLM-TK can realize the diagnosis of plant pests and diseases in a more comprehensive and accurate way.

4.4 Plant pest and disease diagnosis effect visualization and analysis

As shown in Figure 6, the average accuracy histograms of methods such as PDLM-TK on the three plant pest and disease datasets are shown. Analyzing along the direction of the dataset, it can be seen from the height of the histogram that the three colors of the bar represented by PDLM-TK have the highest average on the three datasets. This proves that its combined performance is better on both Top1 and Top5 assessment methods. Meanwhile, according to the column height performance of different models, it can be seen that the heights of the columns of the three colors of PDLM-TK are closer to each other. This indicates that the method has stronger classification accuracy and stability for plant pest and disease images, and can realize more accurate pest and disease diagnosis.

In order to further observe the performance of each model on the test set of plant pests and diseases in a more intuitive way, we utilize the confusion matrix to present the test set classification results of each model. The confusion matrix can be taken in the form of a matrix to summarize the real and predicted categories, and to observe the differences that exist in the prediction results for the classification of different categories. Due to the large number of labels and samples in the plant pest and disease dataset, the numbers in it are no longer displayed, and the performance of each model is only observed and analyzed through the model classification results. Each square in the horizontal and vertical axes of the confusion matrix represents the category corresponding to plant pests and diseases, and the color of each square corresponds to the number of images classified into that region. The darker the

TABLE 4 Evaluation results of Top5 accuracy for various models.

DataSet	Metrics	Model					
		ShuffleNet-V2	MobileNet-V3-Large	EfficientNet B1	MobileViT-S	Inception v3	PDLM-TK
Ai Challenger	P	89.34	87.11	90.32	85.13	95.71	**96.19**
	R	85.31	84.16	88.49	82.13	91.60	**93.72**
	F1	87.28	85.61	89.40	83.60	93.61	**94.94**
Plant Village	P	94.30	90.16	94.55	93.63	**95.79**	95.20
	R	90.31	88.02	89.90	89.08	90.16	**92.26**
	F1	92.26	89.08	92.17	91.30	92.89	**93.71**
IP102	P	80.13	80.35	82.43	76.64	83.42	**85.51**
	R	76.48	78.31	79.60	74.33	80.02	**80.69**
	F1	78.26	79.32	80.99	75.47	81.68	**83.03**

The bolded text represents the type and the values represent the best results.

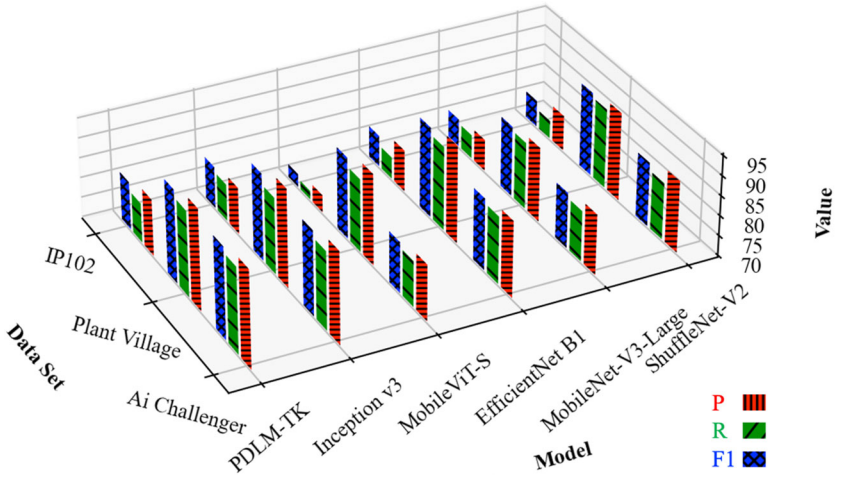

FIGURE 6
Histogram of Top1 and Top5 average accuracy of various models on three datasets.

color on the diagonal represents the more images that are classified correctly.

The confusion matrix for each model's classification prediction for the test set portion of the Ai Challenger dataset is shown in Figure 7. From the distribution of squares of different colors in the confusion matrix, it can be seen that the MobileNet-V3-Large and MobileViT-S models have more uniform diagnosis results for different categories of plant pests and diseases, which is mainly manifested by the similar colors of the squares on the diagonal line, but their classification effect is lower than that of the MobileNet-V3-Large and Inception v3 models. Inception v3 has a better classification effect on some kinds of plant pest and disease images, but there is a phenomenon of misclassification of some categories, which is mainly reflected in the lighter color of the squares in the middle of the diagonal of some categories. The confusion matrix corresponding to the PDLM-TK method has a more uniform and saturated color distribution on the diagonal, which shows that its classification effect is more stable.

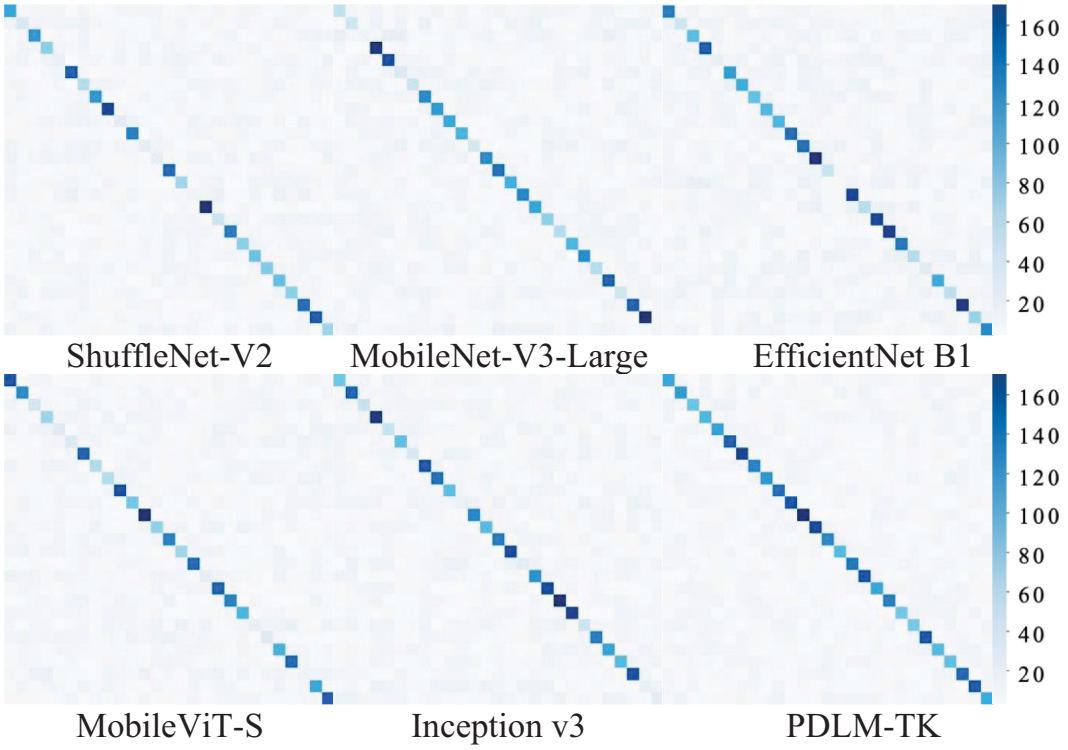

FIGURE 7
Confusion matrix of different methods on Ai Challenger dataset.

The confusion matrix of each model for classifying images on Plant Village test set is shown in Figure 8, which is a richer dataset with fewer disease categories. As shown by the color and distribution of diagonal squares, the methods have better classification results. Especially, the two methods, Inception v3 and EfficientNet B1, have the majority of dark-colored squares on the diagonal. The MobileNet-V3-Large method has multiple light-colored squares compared to the two, indicating a partial misclassification. While PDLM-TK has the darkest colored squares compared to the other methods and all of them are distributed on diagonal. It can be fully demonstrated that PDLM-TK has strong classification performance for plant pest disease image diagnosis.

According to the confusion matrix distribution shown in Figure 9, it can be seen that the models are slightly less effective than the other two datasets in classifying insects in the IP102 dataset. The reason is due to the large number of insect species contained in this dataset, and the lightweight classification models are difficult to balance multiple critical features. Among them, two models, EfficientNet B1 and Inception v3, have better classification effects than the other models and can basically realize the discrimination of multiple types of insects. The PDLM-TK method proposed in this paper has the best classification performance compared to the other models because it trains the model by KD, which has a strong feature capturing ability despite the small number of model parameters. In summary, the validation of the plant leaf and insect datasets demonstrates that the PDLM-TK method is able to accurately realize plant pest and disease diagnosis.

5 Discussion

5.1 Evaluation of model stability and efficiency

Plant pest and disease diagnosis should not only have high accuracy, but also the stability and efficiency of the model is equally important, which is related to the classification effect and diagnosis quality in the practical application of agriculture. Therefore, in this paper, several models are trained on Ai Challenger using the same experimental environment, and their loss functions are plotted as line graphs for analysis. At the same time, the models are ranked according to the number of parameters they contain and their actual execution efficiency, and are compared and analyzed in the form of a table.

As shown in Figure 10, the change process of loss when the six methods are trained on the IP102 dataset is shown. From the fluctuation of the folded line, it can be seen that the PDLM- TK method proposed in this paper converges rapidly in the first 20 iteration loops and decreases steadily with the growth of the number of iterations. Notably, after the 110th iteration, the models exhibited stability. While the other methods exhibit similar fold convergence processes, their fluctuations are more

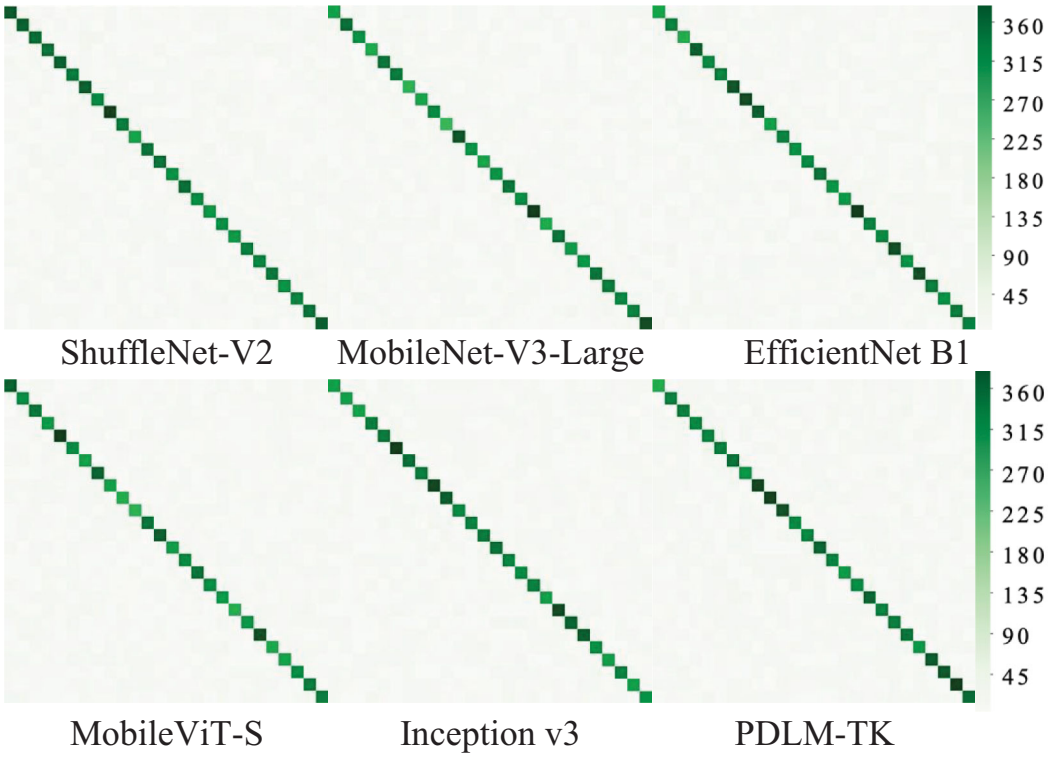

FIGURE 8
Confusion matrix for different methods on the Plant Village dataset.

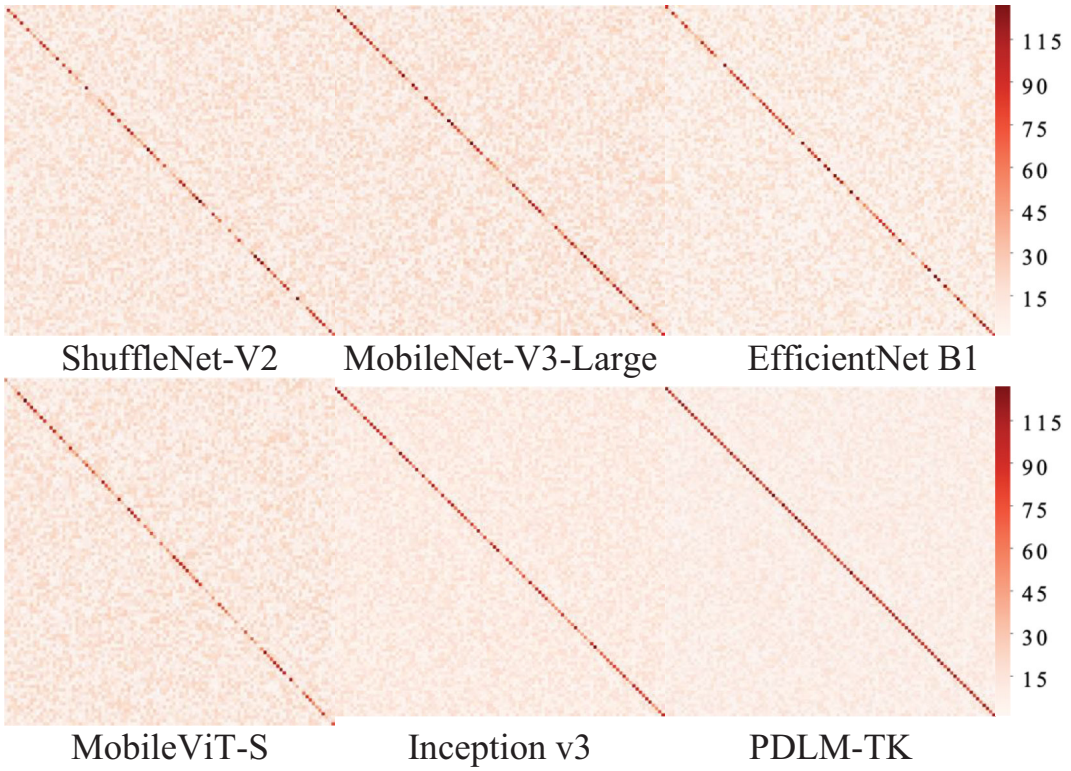

FIGURE 9
Confusion matrix for different methods on the IP102 dataset.

pronounced, and their final converged values are higher. This clearly demonstrates that the method proposed in this paper is more stable and achieves faster convergence.

To evaluate the actual running efficiency of each model, this paper uses GFLOPs and Params metrics to measure the execution speed of the models. As shown in Table 5, EfficientNet B1 has the smallest amount of computation, and PDLM-TK is only 0.1 behind it in the second place. As shown by the parameter count, PDLM-TK contains the least number of parameters, followed by MobileNet-V3-Large. Combining the evaluation indexes such as the accuracy of each method, the PDLM-TK method achieves higher accuracy through less time, and is able to better balance the efficiency and accuracy of the model, compared to other models both in diagnostic accuracy and efficiency.

5.2 Assessment of KD effectiveness in teacher networks

As presented in Table 6, the evaluation results of the Top1 accuracy for PDLM-TK when different teacher networks were utilized across three plant pest and disease datasets are shown.

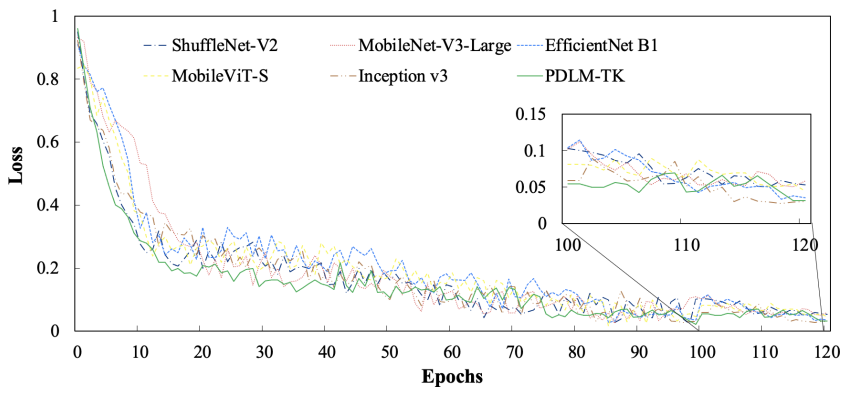

FIGURE 10
Loss curves for various methods on the IP102 dataset.

TABLE 5 Statistical results of parameters and computational efficiency from various models.

Metrics	ShuffleNet-V2	MobileNet-V3-Large	EfficientNet B1	MobileViT-S	Inception v3	PDLM-TK
GFLOPs	0.56	0.23	**0.6**	1.75	9.62	0.7
Params[M]	5.6	4.3	6.6	5.1	24.7	**1.97**

The bolded text represents the type and the values represent the best results.

The comparison indicates that using ResNet18 as the teacher network yielded superior overall results, surpassing the ImageNet model by 0.63, 1.14, and 0.9 in the P, R, and F1 metrics, respectively. This improvement is attributed to the structural similarities between PDLM-TK's backbone, which is derived from the residual blocks of ResNet. It can thus be concluded that knowledge migration is more effective when the chosen teacher network has a similar model structure, enhancing the effectiveness of the KD process.

5.3 Network grad-CAM visualization

To better assess the PDLM-TK model's ability to learn the characteristics of plant pests and diseases, we predicted a portion of the test set data for each disease and visualized the results using Grad-CAM. The visualization outcomes are presented in Figure 11. In this study, the last layer of the PDLM-TK model was selected as the feature visualization layer, with the heat map superimposed on the original image. The Figure 11A displays the original plant pest images, while the Figure 11B shows the weighted visualization results..

Upon examining the visualization results, we observed that the PDLM-TK model not only accurately predicted the classification of each disease but also successfully identified the key regions corresponding to various plant disease locations or pests. Additionally, it was noted that the model paid less attention to irrelevant and complex backgrounds surrounding the diseased leaves, instead concentrating on the characterization of disease features and pests during the feature selection process.

5.4 Ablation experiment

Based on the existing plant disease and pest classification model structure we designed the PDLM-TK model, which contains several modules to realize feature extraction, mining and model training respectively. Among them, residual blocks integrating multiple LRB-STs are designed to enhance the deep extraction of semantic features of different dimensions and to improve the model classification accuracy, which extracts the semantic information of different channels in plant disease images layer by layer. For the redundant information interference in the image, we proposed BNF-GC, which deeply mines the residual block features by graph convolution in order to focus on the disease features. We utilize the plant pest and disease dataset to train the teacher network and construct MTS-KD to realize knowledge transfer to the student network. To fully evaluate the main role played by each module, we designed ablation experiments based on the architecture of unused modules (Basic). Finally, they are evaluated and analyzed on Ai Challenger using P, R and F1 respectively.

As shown in Table 7 for the results of the ablation experiments of each module. "✓" stands for the blocks being selected, in the first four sets of experiments the Basic model (ResNet18) without several modules has the lowest evaluation scores, while the effect of using MTS-KD is higher than the other two types of modules. This proves that each module plays a role in improving the model classification effect, especially the effect of MTS-KD improves the model classification performance more. From the experimental results of groups 5 to 7, it can be seen that BNF-GC and MTS-KD have the best R when they are paired together, which is higher than the effect of group 8 when multiple modules are used at the same time, but it is slightly lower in terms of P and F1 values. The reason for this is that the BNF-GC module is able to better balance the feature information between different levels, but due to the similarity of some plant pests and diseases in terms of the types of performance, it is difficult to distinguish the real categories by only emphasizing the attention to the same representations, which leads to the easy occurrence of the misclassification phenomenon. With the addition of LRB-ST enables the multilayer channel semantic information to be better mined, which is used to enhance the model's capture of plant pest and disease characteristics for each category. Therefore, a combination of multiple evaluation indexes leads to the best classification performance of the PDLM-TK method incorporating the three modules.

TABLE 6 Top1 accuracy evaluation results of different teacher networks.

Teacher Networks	P		R		F1	
	ResNet18	ImageNet	ResNet18	ImageNet	ResNet18	ImageNet
Ai Challenger	92.64	91.27	89.32	88.36	90.95	89.79
Plant Village	95.44	96.62	90.57	90.77	92.94	93.60
IP102	82.87	81.13	79.10	76.43	80.94	78.71
Average	**90.31**	89.67	**86.33**	85.18	**88.27**	87.37

The bolded text represents the type and the values represent the best results.

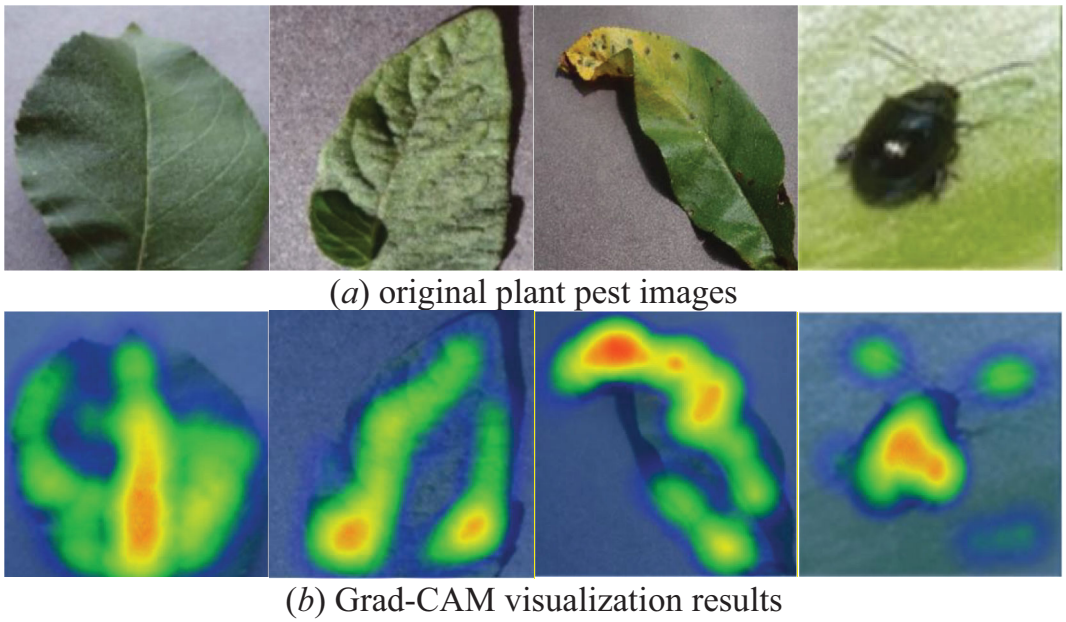

FIGURE 11
Plant disease and pest images used Grad-CAM visualization results, figure **(A)** shows the plant leaves in the dataset and figure **(B)** shows the results visualized using Grad-CAM.

6 Conclusion

To address the issues of low efficiency and accuracy in plant pest and disease diagnosis, the capabilities of tensor and graph deep learning in feature mining are fully utilized. The model network structure is optimized by integrating knowledge distillation (KD) and other techniques, resulting in the proposal of a Plant Pest and Disease Lightweight Identification Model (PDLM-TK) that fuses tensor features and KD. First, a lightweight residual block based on spatial tensor is constructed to enhance the perception and extraction of shallow detail features of plant images by introducing spatial tensor, and depth separable convolution is used to reduce the number of model parameters to improve the diagnostic efficiency. Secondly, a branching network incorporating graph convolutional features is proposed to realize image super-pixel segmentation by using spanning tree clustering based on pixel features, and graph convolutional neural network is used to extract correlation features to improve diagnostic accuracy. Finally, a model training strategy based on KD is designed to train the pest and disease diagnosis model by building a knowledge migration architecture, which fully balances the accuracy and diagnosis efficiency of the model.

In order to verify the diagnostic performance of the model in plant diseases and pests, we carried out experiments on three plant disease and pest datasets, including Plant Village, and the results proved that PDLM-TK had the best performance in terms of classification accuracy and efficiency, and was able to realize fast and accurate diagnosis of plant diseases. Although the method

TABLE 7 Evaluation results of ablation experiments.

No.	Blocks				Metrics		
	Basic	LRB-ST	BNF-GC	MTS-KD	P	R	F1
1	✓				76.43	73.21	74.79
2	✓	✓			82.64	80.3	81.45
3	✓		✓		83.22	79.67	81.41
4	✓			✓	85.34	81.27	83.26
5	✓	✓	✓		86.42	83.13	84.74
6	✓		✓	✓	92.35	**89.47**	90.89
7	✓	✓		✓	91.42	88.74	90.06
8	✓	✓	✓	✓	**92.64**	89.32	**90.95**

The bolded text represents the type and the values represent the best results.

achieves better plant disease and pest classification results, the performance of the model in the face of some small-sample disease and pest datasets remains to be examined, and in the future, we can further increase the number of disease and pest species as well as datasets with different sample set sizes for testing, so as to further enhance the model's value for practical application. In the subsequent study, we will further integrate real farming environments within the experimental field, collect data on a variety of plant diseases and pests, and assess the model's performance in varied deployment settings and on smaller-scale farmland.

Data availability statement

The datasets presented in this study can be found in online repositories. The names of the repository/repositories and accession number(s) can be found in the article/supplementary material.

Ethics statement

The studies involving humans were approved by Tianjin University of Science and Technology. The studies were conducted in accordance with the local legislation and institutional requirements. The participants provided their written informed consent to participate in this study. The animal studies were approved by Tianjin University of Science and Technology. The studies were conducted in accordance with the local legislation and institutional requirements. Written informed consent was obtained from the owners for the participation of their animals in this study.

Author contributions

XZ: Writing – review & editing, Conceptualization, Methodology, Project administration. KL: Writing – review & editing, Conceptualization, Methodology. YZ: Writing – original draft, Conceptualization, Methodology.

Funding

The author(s) declare that financial support was received for the research, authorship, and/or publication of this article. This work was supported in part by the National Natural Science Foundation of China (No. 62377036).

Conflict of interest

The authors declare that the research was conducted in the absence of any commercial or financial relationships that could be construed as a potential conflict of interest.

Publisher's note

References

AI Challenge (2018). *Classification data set of diseases and insect pests*. Available online at: https://aistudio.baidu.com/datasetdetail/76075. (Accessed Oct. 29, 2024).

Aldakheel, E. A., Zakariah, M., and Alabdalall, A. H. (2024). Detection and identification of plant leaf diseases using YOLOv4. *Front. Plant Sci.* 15, 1355941. doi: 10.3389/fpls.2024.1355941

Ali, M. A., Sharma, A. K., and Dhanaraj, R. K. (2024). Heterogeneous features and deep learning networks fusion-based pest detection, prevention and controlling system using IoT and pest sound analytics in a vast agriculture system. *Comput. Electric. Eng.* 116, 109146. doi: 10.1016/j.compeleceng.2024.109146

Bhandari, M., Shahi, T. B., Neupane, A., and Walsh, K. B. (2023). BotanicX-AI: identification of tomato leaf diseases using an explanation-driven deep-learning model. *Joournal Imaging* 9, 53. doi: 10.3390/jimaging9020053

Catalkaya, M., Goknur, A., and Devran, Z. (2024). Rapid identification of Meloidogyne hapla by KASP assay. *Crop Prot.* 178, 106600. doi: 10.1016/j.cropro.2024.106600

Cetiner, H. (2022). Citrus disease detection and classification using based on convolution deep neural network. *Microprocess. Microsys.* 95, 104687. doi: 10.1016/j.micpro.2022.104687

Cheng, H.-H., Dai, Y.-L., Lin, Y., Hsu, H., Lin, C., Huang, J., et al. (2022). Identifying tomato leaf diseases under real field conditions using convolutional neural networks and a chatbot. *Comput. Electron. Agric.* 202, 107365. doi: 10.1016/j.compag.2022.107365

Chodey, M. D., and Shariff, C. N. (2023). Pest detection via hybrid classification model with fuzzy C-means segmentation and proposed texture feature. *Biomed. Signal Process. Control* 84, 104710. doi: 10.1016/j.bspc.2023.104710

Dai, G., Tian, Z., Fan, J., Sunil, C., and Dewi, C. (2024). DFN-PSAN: Multi-level deep information feature fusion extraction network for interpretable plant disease classification. *Comput. Electron. Agric.* 216, 108481. doi: 10.1016/j.compag.2023.108481

FAO (2022). *FAO's Plant Production and Protection Division* (Rome: FAO). doi: 10.4060/cc2447en

FAO (2023). *World Food and Agriculture – Statistical Yearbook 2023* (Rome: FAO). doi: 10.4060/cc8166en

Howard, A., Sandler, M., Chu, G., Chen, B., Tan, M., Wang, W., et al. (2020). "Searching for mobileNetV3," in *2019 IEEE/CVF International Conference on Computer Vision*. 1314–1324 (Seoul, Korea: IEEE). doi: 10.1109/ICCV.2019.00140

Hughes, D. P., and Salathé, M. (2015). An open access repository of images on plant health to enable the development of mobile disease diagnostics. 1–13. Available at: https://arxiv.org/abs/1511.08060.

Ishengoma, F. S., Rai, I. A., and Ngoga, S. R. (2022). Hybrid convolution neural network model for a quicker detection of infested maize plants with fall armyworms using UAV-based images. *Ecol. Inf.* 67, 101502. doi: 10.1016/j.ecoinf.2021.101502

Johari, S. N. A. M., Khairunniza-Bejo, S., Shariff, A. R. M., Husin, N., Brasi, M., and Kamarudin, N. (2022). Identification of bagworm (Metisa plana) instar stages using hyperspectral imaging and machine learning techniques. *Comput. Electron. Agric.* 194, 106739. doi: 10.1016/j.compag.2022.106739

Khan, A. I., Quadri, S. M. K., Banday, S., and Shah, J. (2022). Deep diagnosis: A real-time apple leaf disease detection system based on deep learning. *Comput. Electron. Agric.* 198, 107093. doi: 10.1016/j.compag.2022.107093

Li, D., Zhang, C., Li, J., Li, M., Huang, M., and Tang, Y. (2024). MCCM: multi-scale feature extraction network for disease classification and recognition of chili leaves. *Front. Plant Sci.* 15, 1367738. doi: 10.3389/fpls.2024.1367738

Li, R., Shang, Z., Zheng, C., Li, H., Liang, Q., and Cui, Y. (2023). Efficient distributional reinforcement learning with kullback-leibler divergence regularization. *Appl. Intel.* 53, 24847–24863. doi: 10.1007/s10489-023-04867-z

Li, Y., Ma, L., and Sun, N. (2024). A bilinear transformer interactive neural networks-based approach to fine-grained recognition and protection of plant diseases for gardening design. *Crop Prot.* 180, 106660. doi: 10.1016/j.cropro.2024.106660

Liu, Y., Li, X., Fan, Y., Liu, L., and Shao, L. (2024). Classification of peanut pod rot based on improved YOLOv5s. *Front. Plant Sci.* 15, 1364185. doi: 10.3389/fpls.2024.1364185

Ma, N., Zhang, X., Zheng, H.-T., and Sun, J. (2018). "ShuffleNet V2: Practical guidelines for efficient cnn architecture design," in *Proceedings of the European Conference on Computer Vision (ECCV)*, New York. 122–138 (ACM).

Manavalan, R. (2022). Towards an intelligent approaches for cotton diseases detection: A review. *Comput. Electron. Agric.* 200, 107255. doi: 10.1016/j.compag.2022.107255

Math, R. M., and Dharwadkar, N. (2022). Early detection and identification of grape diseases using convolutional neural networks. *J. Plant Dis. Prot.* 129, 521–532. doi: 10.1007/s41348-022-00589-5

Mehta, S., and Rastegari, M. (2022). MobileViT: Light-weight, general-purpose, and mobile-friendly vision transformer. 1–26. Available at: https://arxiv.org/abs/2110.02178.

Motie, J. B., Saeidirad, M. H., and Jafarian, M. (2023). Identification of Sunn-pest affected (Eurygaster Integriceps put.) wheat plants and their distribution in wheat fields using aerial imaging. *Ecol. Inf.* 76, 102146. doi: 10.1016/j.ecoinf.2023.102146

Nandhini, C., and Brindha, M. (2024). Visual regenerative fusion network for pest recognition. *Neural Comput. Appl.* 36, 2867–2882. doi: 10.1007/s00521-023-09173-w

Pansy, D. L., and Murali, M. (2023). UAV hyperspectral remote sensor images for mango plant disease and pest identification using MD-FCM and XCS-RBFNN. *Environ. Monit. Assess.* 195, 1120. doi: 10.1007/s10661-023-11678-9

Qiang, J., Liu, W., Li, X., Guan, P., Du, Y., Liu, B., et al. (2023). Detection of citrus pests in double backbone network based on single shot multibox detector. *Comput. Electron. Agric.* 212, 108158. doi: 10.1016/j.compag.2023.108158

Rimal, K., Shah, K. B., and Jha, A. K. (2023). Advanced multi-class deep learning convolution neural network approach for insect pest classification using TensorFlow. *Int. J. Environ. Sci. Technol.* 20, 4003–4016. doi: 10.1007/s13762-022-04277-7

Roxa, Z., Phoofolo, M. W., Dawuda, P. M., Molapo, S., and Majoro, L. (2023). Identification and prevalence of ticks on Merino sheep in Lesotho. *Trop. Anim. Health Prod.* 55, 70. doi: 10.1007/s11250-023-03492-9

Rustia, D. J. A., Chiu, L.-Y., Lu, C.-Y., Wu, Y., and Chen, S. (2022). Towards intelligent and integrated pest management through an AIoT-based monitoring system. *Pest Manage. Sci.* 78, 4288–4302. doi: 10.1002/ps.v78.10

Sajitha, P., Andrushia, A. D., and Anand, N. (2024). A review on machine learning and deep learning image-based plant disease classification for industrial farming systems. *J. Ind. Inf. Integr.* 38, 100572. doi: 10.1016/j.jii.2024.100572

Shafik, W., Tufail, A., Liyanage, C. D. S., and Apong, R. (2023). Using a novel convolutional neural network for plant pests detection and disease classification. *J. Sci. Food Agric.* 103, 5849–5861. doi: 10.1002/jsfa.v103.12

Shamsul Kamar, N. A., Abd Rahim, S. K., Ambrose, A. A., Awing, N., and Samdin, Z. (2023). Pest and disease incidence of coniferous species in Taman Saujana Hijau, Putrajaya urban park, Malaysia. *J. Forest. Res.* 34, 2065–2077. doi: 10.1007/s11676-023-01644-z

Sharma, R. P., Ramesh, D., Pal, P., Tripathi, S., and Kumar, C. (2022). IoT-enabled IEEE 802.15.4 WSN monitoring infrastructure-driven fuzzy-logic-based crop pest prediction. *IEEE Internet Things J.* 9, 3037–3045. doi: 10.1109/JIOT.2021.3094198

Subbaian, S., Balasubramanian, A., Marimuthu, M., Chandrasekaran, S., and Muthusaravanan, G. (2024). Detection of coconut leaf diseases using enhanced deep learning techniques. *J. Intel. Fuzzy Syst.* 46, 5033–5045. doi: 10.3233/JIFS-233831

Szegedy, C., Vanhoucke, V., Ioffe, S., Shlens, J., and Wojna, Z. (2015). Rethinking the inception architecture for computer vision. *arXiv: 1512.00567*. Available at: http://arxiv.org/abs/1512.00567.

Tan, M., and Le, Q. V. (2019). "EfficientNet: rethinking model scaling for convolutional neural networks," in *International Conference on Machine Learning*, Long Beach, CA, USA. 6105–6114, LR.

Thakuria, D., Chaliha, C., Dutta, P., Sinha, S., and Uzir, P. (2023). Citrus Huanglongbing (HLB): Diagnostic and management options. *Physiol. Mol. Plant Pathol.* 125, 102016. doi: 10.1016/j.pmpp.2023.102016

Wei, D., Chen, J., Luo, T., and Wang, Z. (2022). Classification of crop pests based on multi-scale feature fusion. *Comput. Electron. Agric.* 194, 106736. doi: 10.1016/j.compag.2022.106736

Wu, X., Zhan, C., Lai, Y.-K., Cheng, M., and Yang, J. (2019). "IP102: A large-scale benchmark dataset for insect pest recognition," in *2019 IEEE/CVF Conference on Computer Vision and Pattern Recognition (CVPR)*. 8779–8788.

Xia, W., Han, D., Li, D., Wu, Z., Han, B., Wang, J., et al. (2023). An ensemble learning integration of multiple CNN with improved vision transformer models for pest classification. *Ann. Appl. Biol.* 182, 144–158. doi: 10.1111/aab.v182.2

Xiao, Z., Yin, K., Geng, L., Wu, J., Zhang, F., Liu, Y., et al. (2022). Pest identification via hyperspectral image and deep learning. *Signal Image Video Process.* 16, 873–880. doi: 10.1007/s11760-021-02029-7

Yu, Y., Sun, T., and Yan, J. (2022). Improved YOLOv5 network for agricultural pest detection. *Fourteenth Int. Conf. Graphics Image Process. (ICGIP 2022).* 12705, 1270507. doi: 10.1117/12.2680747

Zhang, Y., Li, M., Zhou, B., et al (2023). Automatic cotton spider mites' damage grading algorithm for depth residual network based on transfer learning. *Comput. Electron. Agric.* 212, 108070. doi: 10.1016/j.compag.2023.108070

Zhao, X., Zhang, J., Huang, Y., Tian, Y., and Yuan, L. (2022). Detection and discrimination of disease and insect stress of tea plants using hyperspectral imaging combined with wavelet analysis. *Comput. Electron. Agric.* 193, 106717. doi: 10.1016/j.compag.2022.106717

Zheng, Z., and Zhang, C. (2022). Electronic noses based on metal oxide semiconductor sensors for detecting crop diseases and insect pests. *Comput. Electron. Agric.* 197, 106988. doi: 10.1016/j.compag.2022.106988

Zhu, L., Li, Z., and Hu, S. (2023). Efficient data-centric pest images identification method based on Mahalanobis entropy for intelligent agriculture. *J. Electron. Imaging* 32, 1–13. doi: 10.1117/1.JEI.32.5.052406

Frontiers in Plant Science

Cultivates the science of plant biology and its applications

The most cited plant science journal, which advances our understanding of plant biology for sustainable food security, functional ecosystems and human health.

Discover the latest Research Topics

See more →

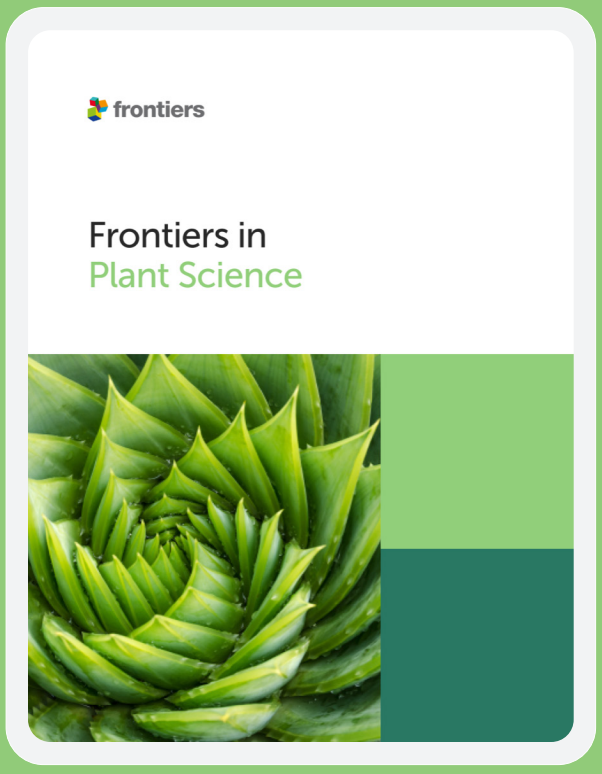

Frontiers

Avenue du Tribunal-Fédéral 34
1005 Lausanne, Switzerland
frontiersin.org

Contact us

+41 (0)21 510 17 00
frontiersin.org/about/contact